

UNCLASSIFIED

AD NUMBER

AD839015

LIMITATION CHANGES

TO:

Approved for public release; distribution is unlimited.

FROM:

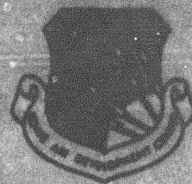
Distribution authorized to DoD only;
Administrative/Operational Use; AUG 1968. Other requests shall be referred to Rome Air Development Center, Rome, NY. Pre-dates formal DoD distribution statements. Treat as DoD only.

AUTHORITY

RADC ltr 10 Feb 1972

THIS PAGE IS UNCLASSIFIED

RADC-TR-68-180
Final Report



EXPANDED LITTLE IDA - EXPERIMENTAL RESULTS

R. W. Swanson

T. C. Matsumoto

D. T. Olmsted

General Electric Company

TECHNICAL REPORT NO. RADC-TR- 68-180

August 1968

EACH TRANSMITTAL OF THIS DOCUMENT
OUTSIDE THE DEPARTMENT OF DEFENSE
MUST HAVE PRIOR APPROVAL OF RADC
(EMASA), GAFB, N.Y.
THE DISTRIBUTION OF THIS DOCUMENT
IS LIMITED UNDER THE U. S. MUTUAL
SECURITY ACTS OF 1949

Rome Air Development Center
Air Force Systems Command
Griffiss Air Force Base, New York

AD 839015

When US Government drawings, specifications, or other data are used for any purpose other than a definitely related government procurement operation, the government thereby incurs no responsibility nor any obligation whatsoever; and the fact that the government may have formulated, furnished, or in any way supplied the said drawings, specifications, or other data is not to be regarded, by implication or otherwise, as in any manner licensing the holder or any other person or corporation, or conveying any rights or permission to manufacturer, use, or sell any patented invention that may in any way be related thereto.

This document may be reproduced to satisfy official needs of U.S. Government agencies.

Do not return this copy. Retain or destroy.

**Best
Available
Copy**

EXPANDED LITTLE IDA - EXPERIMENTAL RESULTS

R. W. Swanson

T. C. Matsumoto

D. T. Olmsted

General Electric Company

**EACH TRANSMITTAL OF THIS DOCUMENT
OUTSIDE THE DEPARTMENT OF DEFENSE
MUST HAVE PRIOR APPROVAL OF RADC
(EMASA), GAFB, N.Y. 13440**

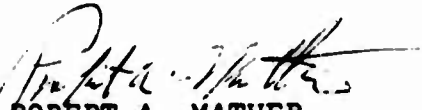
FOREWORD

This final report on experimental results was prepared by the General Electric Company, Advance Development Engineering, Heavy Military Electronics Department, Syracuse, New York, under Contract AF 30(602)-3946, Project 5582, Task 558202, with Rome Air Development Center, Griffiss Air Force Base, New York. The General Electric project manager for this effort was Ross M. Chapman. Mr. Robert A. Mather, EMASA, was the RADC Project Engineer.

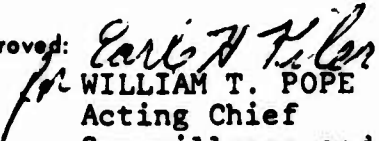
This technical documentary report represents the efforts of a number of contributors who had an important part in writing various parts of this document. The editorial and overall technical responsibility for this report was assigned to Roger W. Swanson. Individual contributors include Stephen G. Engle, John M. Jeffords, Paul H. Kirchner, T.C. Matsumoto, Gary R. Nelson, Donald T. Olmsted, Joseph A. Reeve, and Roger W. Swanson.

This Technical Report has been reviewed and is approved.

Approved:


ROBERT A. MATHER
Contract Engineer

Approved:


WILLIAM T. POPE
Acting Chief
Surveillance and
Control Division

FOR THE COMMANDER:


IRVING J. GABELMAN
Chief, Advanced Studies Group

ABSTRACT

This final report -- Experimental Results -- describes the work performed on U. S. Air Force Contract AF 30(602)-3946 in the area of data reduction and data analysis of the experimental measurements from the mode reliability, mode loss, spectrum, azimuth of arrival, and noise/interference experiments. The Expanded Little IDA Program has been a continuation, as well as an expansion, of the effort previously carried out under U. S. Air Force Contract AF 30(602)-3360 to investigate the characteristics of ionospherically propagated HF signals. The long term objective of these studies is to provide more accurate estimates of the major environmental factors needed for improved over-the-horizon radar system design. A separate final report is being issued covering the instrumentation that has been employed to meet the requirements of this program.

This report begins with a description of how the experimental results can be applied to the system design of over-the-horizon radars of the backscatter type and discusses the subject of confidence limits for the experimental measurements. Experimental results gathered for the mode reliability experiment over the Coco Solo (Canal Zone) to Stockbridge/Starr Hill (New York) path from December 1965 to August 1967 and over the Thule (Greenland) to Stockbridge/Starr Hill path from December 1966 through May 1967 are presented on a seasonal basis. The relationship of the excess loss for 2E propagation over the Coco Solo path with the ratio f/MUF is reviewed.

The coherence times obtained from the spectrum experiment for various modes of propagation existing over the Coco Solo path and Thule path are discussed. Some initial experimental results using the modified azimuth of arrival equipment are presented. Data collected during 1967 on the two ARN-2 noise receiving sets located at Starr Hill are provided, as well as some initial results using the noise/interference receiver.

EVALUATION

A very important area of interest to those concerned with surveillance and control systems is the concept of over-the-horizon radars and the problems peculiar to those radars. A considerable amount of effort has been expended by the Air Force over the past several years to prove the feasibility of the OHD concept. In spite of the significant efforts in the equipment and technique areas and although the concept of OHD has been proven feasible, many serious uncertainties still exist about the propagation medium, i.e. the ionosphere.

The objective of this particular effort was to collect, reduce and analyze the propagation data required for the design and operation of over-the-horizon backscatter radars. The major experiments that were to be performed were mode availability and reliability, frequency aperture availability, mode loss, azimuth of arrival fluctuations, spectrum broadening and noise/interference statistics. These experiments were to be conducted over paths covering a variety of geographic areas encompassing the full gamut of possible environmental conditions that could be expected to be experienced by future OTH radars.

The paths that were established were Thule, Greenland to Starr Hill, New York; Keflavik, Iceland to Starr Hill; and Panama Canal Zone to Starr Hill.

Unfortunately, this program was beset by many technical and logistical difficulties during the design and implementation phase. As a result, only a limited amount of data were collected over the Panama to Starr Hill and Thule to Starr Hill paths and no data were collected on the Iceland to Starr Hill path. The data that were collected were limited to mode loss, mode reliability, aperture availability and spectrum information.

A follow-on program, (Environmental Studies for OHD) has been implemented and is now underway. Data are presently being collected on all experiments and over all three propagation paths.


ROBERT A. MATHER
Contract Engineer

TABLE OF CONTENTS

<u>Section</u>	<u>Title</u>	<u>Page</u>
I	INTRODUCTION	1
II	SYSTEM UTILIZATION	5
	1. The Implications of OHR Defense Missions on the ELIDA Experiments	5
	2. Experimental Confidence	26
	a. Background	26
	b. Usable Mode Probability	30
III	MODE RELIABILITY EXPERIMENT	37
	1. Introduction	37
	2. Summary of Observations by Season	39
	a. Coco Solo to Stockbridge/Starr Hill	39
	b. Thule to Stockbridge/Starr Hill	78
	3. Mode Availability -- Coco Solo to Stockbridge/Starr Hill . . .	93
	4. Mode Availability -- Thule to Stockbridge/Starr Hill	125
	5. Frequency Aperture Availability -- Coco Solo to Stockbridge/ Starr Hill	135
	6. Frequency Aperture Availability -- Thule to Stockbridge/ Starr Hill	171
	7. MOF-JF Availability -- Coco Solo to Stockbridge/Starr Hill . .	181
	8. MOF-JF Availability -- Thule to Stockbridge/ Starr Hill	217
	9. Downtime -- Coco Solo to Stockbridge/Starr Hill	227
	10. Statistical Summary	229
	a. Mode Availability	229
	b. Frequency Aperture Availability	236
	c. MOF-JF Availability	243
	11. The Effects of Solar Disturbances on Propagation as Observed Over the Coco Solo Path	249
	a. Introduction	249
	b. Comparisons of Natural Factors and Recorded Signals . .	250
IV	MODE LOSS EXPERIMENT	277

TABLE OF CONTENTS (continued)

<u>Section</u>	<u>Title</u>	<u>Page</u>
V	SPECTRUM EXPERIMENT	281
	1. Introduction	281
	2. Equipment and Experimental Procedures	283
	3. Data Reduction and Processing	284
	a. Format and Handling	284
	b. Computer Program	285
	4. Results	285
	a. Coco Solo to Central New York Path	285
	b. Thule to Starr Hill Path	285
	c. Discussion of Results	289
	d. Discussion of Sources of Error	293
	5. Integration Considerations for Over-the Horizon Radars Utilizing Spectrum Results	295
	a. Introduction	295
	b. Some Useful Analytical Results	296
	c. Use of Integration in a Typical OHR Application	297
VI	AZIMUTH OF ARRIVAL EXPERIMENT	303
	1. Introduction	303
	2. Discussion of Measurements	304
VII	NOISE/INTERFERENCE EXPERIMENT	323
	1. Introduction	323
	2. Experiment Design Considerations	323
	a. Experimental Objective	323
	b. Experimental Motivation	323
	c. Information Needs	325
	d. Instrumentation Configuration	325
	3. Noise Measurements with ARN-2 Receivers	327
	a. Measurement Technique	327
	b. Data Output Format	329
	c. Results	329

TABLE OF CONTENTS (concluded)

<u>Section</u>	<u>Title</u>	<u>Page</u>
VIII	CONCLUSIONS	385
	1. Mode Reliability Experiment	385
	2. Mode Loss Experiment	386
	3. Spectrum Experiment	388
	4. Azimuth of Arrival Experiment	389
	5. Noise/Interference Experiment	389
	a. Noise Measurements with ARN-2	389
	b. Noise/Interference Measurements	390
IX	ABBREVIATIONS AND SYMBOLS	393
	APPENDIX I	395
	Transformation of Probability Density Functions for $Z = XY$	
	APPENDIX II	397
	Computation of Probability Convolutions	
	APPENDIX III	401
	Numerical Calculation of Confidence Limits	
	APPENDIX IV	405
	Coco Solo LPV Antenna Patterns	
	APPENDIX V	417
	Geographical Data on ELIDA Field Sites	
	REFERENCES AND BIBLIOGRAPHY	419

LIST OF ILLUSTRATIONS

<u>Figure</u>	<u>Title</u>	<u>Page</u>
1	Dominant Mode Existence	10
2	Cumulative Probability Function of $10 \log_{10} (L_p L_1 NF)$	12
3	Diurnal Variation of Median 1F2 JF for Winter Months	14
4	Statistical Behavior of Daily JF's About the Median JF.....	16
5	Cumulative Probability of the Normalized Frequency Aperture	17
6	Cumulative Distribution of Excess Loss	18
7	Cumulative Distribution of Spectral Bandwidth.....	19
8	Distribution of Temporal Correlation (Amplitude and Phase)	20
9	Probability Density Function for Relative Receive Polarization (Horizontal/Vertical)	21
10	Probability Density Function for Normalized Cross-Correlation Between Horizontal and Vertical Receive Polarizations	22
11	Cumulative Probability of Short Term Signal Level Relative to Median	23
12	Probability Density of Normalized Time Auto- Correlation for Received Signal Level	24
13	Median Azimuth of Arrival Diurnal Behavior	24
14	Probability Density of Azimuth of Arrival for Daylight Hours	25
15	Cumulative Probability of Noise/Interference Level at 80 to 90 percent of 2000-nmi 1F2 JF	25
16	Probability Density Function	28
17	Usable Mode Confidence/Level vs. Number of Samples	34
18	Summary of 2E Mode Observations, Coco Solo Path, Winter 1966	40
19	Summary of 2E Mode Observations, Coco Solo Path, Spring 1966	42
20	Summary of 2E Mode Observations, Coco Solo Path, Summer 1966	43
21	Summary of 2E Mode Observations, Coco Solo Path, Autumn 1966	44

LIST OF ILLUSTRATIONS (continued)

<u>Figure</u>	<u>Title</u>	<u>Page</u>
22	Summary of 2E Mode Observations, Coco Solo Path, Winter 1967	45
23	Summary of 2E Mode Observations, Coco Solo Path, Spring 1967	46
24	Summary of 2E Mode Observations, Coco Solo Path, Summer 1967	47
25	Summary of 1F2 Mode Observations, Coco Solo Path, Winter 1966	48
26	Summary of 1F2 Mode Observations, Coco Solo Path, Spring 1966	49
27	Summary of 1F2 Mode Observations, Coco Solo Path, Summer 1966	50
28	Summary of 1F2 Mode Observations, Coco Solo Path, Autumn 1966	51
29	Summary of 1F2 Mode Observations, Coco Solo Path, Winter 1967	52
30	Summary of 1F2 Mode Observations, Coco Solo Path, Spring 1967	53
31	Summary of 1F2 Mode Observations, Coco Solo Path, Summer 1967	54
32	Summary of N Mode Observations, Coco Solo Path, Winter 1966	55
33	Summary of N Mode Observations, Coco Solo Path, Spring 1966	56
34	Summary of N Mode Observations, Coco Solo Path, Summer 1966	57
35	Summary of N Mode Observations, Coco Solo Path, Autumn 1966	58
36	Summary of N Mode Observations, Coco Solo Path, Winter 1967	59
37	Summary of N Mode Observations, Coco Solo Path, Spring 1967	60
38	Summary of N Mode Observations, Coco Solo Path, Summer 1967	61
39	Summary of 2F2 Mode Observations, Coco Solo Path, Winter 1966	62

LIST OF ILLUSTRATIONS (continued)

<u>Figure</u>	<u>Title</u>	<u>Page</u>
40	Summary of 2F2 Mode Observations, Coco Solo Path, Spring 1966	63
41	Summary of 2F2 Mode Observations, Coco Solo Path, Summer 1966	64
42	Summary of 2F2 Mode Observations, Coco Solo Path, Autumn 1966	65
43	Summary of 2F2 Mode Observations, Coco Solo Path, Winter 1967	66
44	Summary of 2F2 Mode Observations, Coco Solo Path, Spring 1967	67
45	Summary of 2F2 Mode Observations, Coco Solo Path, Summer 1967	68
46	Summary of 2E _s Mode Observation, Coco Solo Path, Winter 1967	69
47	Summary of 2E _s Mode Observation, Coco Solo Path, Spring 1967	70
48	Summary of 2E Mode Observation, Thule Path, Winter 1967 ...	79
49	Summary of 2E Mode Observation, Thule Path, Spring 1967 ...	80
50	Summary of 1F2 Mode Observation, Thule Path, Winter 1967 ..	81
51	Summary of 1F2 Mode Observation, Thule Path, Spring 1967 ..	82
52	Summary of N Mode Observation, Thule Path, Winter 1967 ...	83
53	Summary of N Mode Observation, Thule Path, Spring 1967 ...	84
54	Summary of 2F2 Mode Observation, Thule Path, Winter 1967 ..	85
55	Summary of 2F2 Mode Observation, Thule Path, Spring 1967 ..	86
56	Summary of 2E _s Mode Observation, Thule Path, Winter 1967 ..	87
57	Summary of 2E _s Mode Observation, Thule Path, Spring 1967 ..	88
58	2E Mode Availability, Coco Solo Path, Winter 1966	92
59	2E Mode Availability, Coco Solo Path, Spring 1966	94
60	2E Mode Availability, Coco Solo Path, Summer 1966	96
61	2E Mode Availability, Coco Solo Path, Autumn 1966	97
62	2E Mode Availability, Coco Solo Path, Winter 1967	98
63	2E Mode Availability, Coco Solo Path, Spring 1967	99
64	2E Mode Availability, Coco Solo Path, Summer 1967	100
65	1F2 Mode Availability, Coco Solo Path, Winter 1966	101

LIST OF ILLUSTRATIONS (continued)

<u>Figure</u>	<u>Title</u>	<u>Page</u>
66	1F2 Mode Availability, Coco Solo Path, Spring 1966	102
67	IF2 Mode Availability, Coco Solo Path, Summer 1966	103
68	IF2 Mode Availability, Coco Solo Path, Autumn 1966	104
69	IF2 Mode Availability, Coco Solo Path, Winter 1967	105
70	IF2 Mode Availability, Coco Solo Path, Spring 1967	106
71	IF2 Mode Availability, Coco Solo Path, Summer 1967	107
72	N Mode Availability, Coco Solo Path, Winter 1966	108
73	N Mode Availability, Coco Solo Path, Spring 1966	109
74	N Mode Availability, Coco Solo Path, Summer 1966	110
75	N Mode Availability, Coco Solo Path, Autumn 1966	111
76	N Mode Availability, Coco Solo Path, Winter 1967	112
77	N Mode Availability, Coco Solo Path, Spring 1967	113
78	N Mode Availability, Coco Solo Path, Summer 1967	114
79	2F2 Mode Availability, Coco Solo Path, Winter 1966	115
80	2F2 Mode Availability, Coco Solo Path, Spring 1966	116
81	2F2 Mode Availability, Coco Solo Path, Summer 1966	117
82	2F2 Mode Availability, Coco Solo Path, Autumn 1966	118
83	2F2 Mode Availability, Coco Solo Path, Winter 1967	119
84	2F2 Mode Availability, Coco Solo Path, Spring 1967	120
85	2F2 Mode Availability, Coco Solo Path, Summer 1967	121
86	2E _S Mode Availability, Goco Solo Path, Spring 1967	122
87	2E _S Mode Availability, Coco Solo Path, Summer 1967	123
88	2E Mode Availability, Thule Path, Winter 1967	124
89	2E Mode Availability, Thule Path, Spring 1967	126
90	1F2 Mode Availability, Thule Path, Winter 1967	127
91	1F2 Mode Availability, Thule Path, Spring 1967	128
92	N Mode Availability, Thule Path, Winter 1967	129
93	N Mode Availability, Thule Path, Spring 1967	130
94	2F2 Mode Availability, Thule Path, Winter 1967	131
95	2F2 Mode Availability, Thule Path, Spring 1967	132
96	2E _S Mode Availability, Thule Path, Winter 1967	133
97	2E _S Mode Availability, Thule Path, Spring 1967	134

LIST OF ILLUSTRATION (continued)

<u>Figure</u>	<u>Title</u>	<u>Page</u>
98	2E Frequency Aperture Availability, Coco Solo Path, Winter 1966.	136
99	2E Frequency Aperture Availability, Coco Solo Path, Spring 1966.	138
100	2E Frequency Aperture Availability, Coco Solo Path, Summer 1966.	139
101	2E Frequency Aperture Availability, Coco Solo Path, Autumn 1966.	140
102	2E Frequency Aperture Availability (MHz), Coco Solo Path, Winter 1967.	141
103	2E Frequency Aperture Availability (MHz), Coco Solo Path, Spring 1967.	142
104	2E Frequency Aperture Availability (MHz), Coco Solo Path, Summer 1967.	143
105	1F2 Frequency Aperture Availability (MHz), Coco Solo Path, Winter 1966.	144
106	1F2 Frequency Aperture Availability (MHz), Coco Solo Path, Spring 1966.	145
107	1F2 Frequency Aperture Availability (MHz), Coco Solo Path, Summer 1966.	146
108	1F2 Frequency Aperture Availability (MHz), Coco Solo Path, Autumn 1966.	147
109	1F2 Frequency Aperture Availability (MHz), Coco Solo Path, Winter 1967.	148
110	1F2 Frequency Aperture Availability (MHz), Coco Solo Path, Spring 1967.	149
111	1F2 Frequency Aperture Availability (MHz), Coco Solo Path, Summer 1967.	150
112	N Frequency Aperture Availability (MHz), Coco Solo Path, Winter 1966.	151
113	N Frequency Aperture Availability (MHz), Coco Solo Path, Spring 1966.	152
114	N Frequency Aperture Availability (MHz), Coco Solo Path, Summer 1966.	153
115	N Frequency Aperture Availability (MHz), Coco Solo Path, Autumn 1966.	154
116	N Frequency Aperture Availability (MHz), Coco Solo Path, Winter 1967.	155

LIST OF ILLUSTRATION (continued)

<u>Figure</u>	<u>Title</u>	<u>Page</u>
117	N Frequency Aperture Availability (MHz), Coco Solo Path, Spring 1967	156
118	N Frequency Aperture Availability (MHz), Coco Solo Path, Summer 1967	157
119	2F2 Frequency Aperture Availability (MHz), Coco Solo Path, Winter 1966	158
120	2F2 Frequency Aperture Availability (MHz), Coco Solo Path, Spring 1966	159
121	2F2 Frequency Aperture Availability (MHz), Coco Solo Path, Summer 1966	160
122	2F2 Frequency Aperture Availability (MHz), Coco Solo Path, Autumn 1966	161
123	2F2 Frequency Aperture Availability (MHz), Coco Solo Path, Winter 1967	162
124	2F2 Frequency Aperture Availability (MHz), Coco Solo Path, Spring 1967	163
125	2F2 Frequency Aperture Availability (MHz), Coco Solo Path, Summer 1967	164
126	2Es Frequency Aperture Availability (MHz), Coco Solo Path, Summer 1966	165
127	2Es Frequency Aperture Availability (MHz), Coco Solo Path, Autumn 1966	166
128	2Es Frequency Aperture Availability (MHz), Coco Solo Path, Winter 1967	167
129	2Es Frequency Aperture Availability (MHz), Coco Solo Path, Spring 1967	168
130	2Es Frequency Aperture Availability (MHz), Coco Solo Path, Summer 1967	169
131	2E Mode Frequency Aperture Availability, Thule Path, Winter 1967	170
132	2E Mode Frequency Aperture Availability, Thule Path, Spring 1967	172
133	1F2 Mode Frequency Aperture Availability, Thule Path, Winter 1967	173
134	1F2 Mode Frequency Aperture Availability, Thule Path, Spring 1967	174
135	N Mode Frequency Aperture Availability, Thule Path, Winter 1967	175
136	N Mode Frequency Aperture Availability, Thule Path, Spring 1967	176

LIST OF ILLUSTRATION (continued)

<u>Figure</u>	<u>Title</u>	<u>Page</u>
137	2F2 Mode Frequency Aperture Availability, Thule Path, Winter 1967. . . .	177
138	2F2 Mode Frequency Aperture Availability, Thule Path, Spring 1967. . . .	178
139	2E _g Mode Frequency Aperture Availability, Thule Path, Winter 1967. . . .	179
140	2E Mode Frequency Aperture Availability, Thule Path, Spring 1967. . . .	180
141	2E Mode MOF Availability, Coco Solo Path, Winter 1966.	182
142	2E Mode MOF Availability, Coco Solo Path, Spring 1966.	184
143	2E Mode MOF Availability, Coco Solo Path, Summer 1966.	185
144	2E Mode MOF Availability, Coco Solo Path, Autumn 1966.	186
145	2E Mode MOF Availability, Coco Solo Path, Winter 1967.	187
146	2E Mode MOF Availability, Coco Solo Path, Spring 1967.	188
147	2E Mode MOF Availability, Coco Solo Path, Summer 1967.	189
148	1F2 Mode JF Availability, Coco Solo Path, Winter 1966.	190
149	1F2 Mode JF Availability, Coco Solo Path, Spring 1966.	191
150	1F2 Mode JF Availability, Coco Solo Path, Summer 1966.	192
151	1F2 Mode JF Availability, Coco Solo Path, Autumn 1966.	193
152	1F2 Mode JF Availability, Coco Solo Path, Winter 1967.	194
153	1F2 Mode JF Availability, Coco Solo Path, Spring 1967.	195
154	1F2 Mode JF Availability, Coco Solo Path, Summer 1967.	196
155	N Mode MOF Availability, Coco Solo Path, Winter 1966.	197
156	N Mode MOF Availability, Coco Solo Path, Spring 1966.	198
157	N Mode MOF Availability, Coco Solo Path, Summer 1966.	199
158	N Mode MOF Availability, Coco Solo Path, Autumn 1966.	200
159	N Mode MOF Availability, Coco Solo Path, Winter 1967.	201
160	N Mode MOF Availability, Coco Solo Path, Spring 1967.	202
161	N Mode MOF Availability, Coco Solo Path, Summer 1967.	203
162	2F2 Mode JF Availability, Coco Solo Path, Winter 1966.	204
163	2F2 Mode JF Availability, Coco Solo Path, Spring 1966.	205
164	2F2 Mode JF Availability, Coco Solo Path, Summer 1966.	206
165	2F2 Mode JF Availability, Coco Solo Path, Autumn 1966.	207
166	2F2 Mode JF Availability, Coco Solo Path, Winter 1967.	208
167	2F2 Mode JF Availability, Coco Solo Path, Spring 1967.	209
168	2F2 Mode JF Availability, Coco Solo Path, Summer 1967.	210
169	2E _g Mode MOF Availability, Coco Solo Path, Summer 1966.	211

LIST OF ILLUSTRATION (continued)

<u>Figure</u>	<u>Title</u>	<u>Page</u>
170	2E _g Mode MOF Availability, Coco Solo Path, Autumn 1966	212
171	2E _g Mode MOF Availability, Coco Solo Path, Winter 1967	213
172	2E _g Mode MOF Availability, Coco Solo Path, Spring 1967	214
173	2E _g Mode MOF Availability, Coco Solo Path, Summer 1967	215
174	2E Mode MOF Availability, Thule Path, Winter 1967	216
175	2E Mode MOF Availability, Thule Path, Spring 1967	218
176	1F2 Mode JF Availability, Thule Path, Winter 1967	219
177	1F2 Mode JF Availability, Thule Path, Spring 1967	220
178	N Mode MOF Availability, Thule Path, Winter 1967	221
179	N Mode MOF Availability, Thule Path, Spring 1967	222
180	2F2 Mode JF Availability, Thule Path, Winter 1967	223
181	2F2 Mode JF Availability, Thule Path, Spring 1967	224
182	2E _g Mode MOF Availability, Thule Path, Winter 1967	225
183	2E _g Mode MOF Availability, Thule Path, Spring 1967	226
184	Mean Mode Availability, Coco Solo Path	230
185	2E Mode Availability, Coco Solo Path	232
186	1F2 Mode Availability, Coco Solo Path	233
187	N Mode Availability, Coco Solo Path	234
188	2F2 Mode Availability, Coco Solo Path	235
189	Mean 90 Percent Available Aperture, Coco Solo Path.	236
190	2E Mode Mean Aperture, Coco Solo Path	238
191	1F2 Mode Mean Aperture, Coco Solo Path	239
192	N Mode Mean Aperture, Coco Solo Path.	240
193	2F2 Mode Mean Aperture, Coco Solo Path	241
194	Mean 90 Percent MOF-JF, Coco Solo Path	242
195	2E Mode MOF, Coco Solo Path.	244
196	1F2 Mode JF, Coco Solo Path	246
197	N Mode MOF, Coco Solo Path	247
198	2F2 Mode JF, Coco Solo Path	248
199	Natural Factors, October 1966	275
200	Natural Factors, May 1967	276
201	Loss Nomenclature	278
202	Excess Loss VS. f/MOF for 2E Mode at 11.3 MHz (No. of Points 431, Daytime Only)	280
203	Data Collection for the Spectrum Experiment	282

LIST OF ILLUSTRATION (continued)

<u>Figure</u>	<u>Title</u>	<u>Page</u>
204	One-Way Signal Coherence Time for Various Modes, Coco Solo to Starr Hill and Stockbridge Paths	286
205	Comparison of One-Way Signal Coherence Values for Various Modes, Coco Solo to Starr Hill and Stockbridge Sites . .	287
206	Comparison of Coherence for 2E and 1F2 Modes During Aurora, Coco Solo to Starr Hill Path	288
207	Coherence Time Occurrence for 2E and 1F2 Modes, Thule to Starr Hill Path	290
208	Signal Coherence Time for 2E Mode, Coco Solo and Thule to Starr Hill Paths	292
209	Signal Processing Gain vs. Number of Pulses Integrated	298
210	Coherent Integration Loss for a 40-prf Radar due to Signal Decorrelation	300
211	Optimum Length of Coherently Processed Train as a Function of the Ratio of Pulse Repetition Period to the 3-dB Width of the Signal Autocorrelation Function	302
212	AOA Records for 2 January 1968 around 1330 EST	311
213	AOA Record for 2 January 1968 around 1405 EST	312
214	AOA Record for 3 January 1968 around 1425 EST	313
215	AOA Record for 3 January 1968 around 1550 EST	314
216	AOA Record for 3 January 1968 around 1850 EST	315
217	AOA Record for 4 January 1968 around 1220 EST	316
218	AOA Record for 4 January 1968 around 1250 EST	317
219	AOA Record for 14 February 1968 after 0930 EST	318
220	AOA Record for 14 February 1968 around 1010 EST	319
221	AOA Record for 14 February 1968 around 1040 EST	320
222	AOA Record for 14 February 1968 around 1100 EST	321
223	AOA Record for 14 February 1968 around 1135 EST	322
224	Noise/Interference Experiment Instrumentation Representation	326
225	ARN-2 Receiver Output Format	330
226	Season Median Noise Power, Omnidirectional Antenna Starr Hill, Winter 1967	331
227	Season Median Noise Power, Omnidirectional Antenna, Starr Hill, Spring 1967	332
228	Season Median Noise Power, Omnidirectional Antenna, Starr Hill, Summer 1967	334

LIST OF ILLUSTRATION (continued)

<u>Figure</u>	<u>Title</u>	<u>Page</u>
229	Season Median Noise Power, Omnidirectional Antenna Starr Hill, Autumn 1967	335
230	Monthly Median Noise Power, Omnidirectional Antenna Starr Hill, March 1967	336
231	Monthly Median Noise Power, Omnidirectional Antenna Starr Hill, April 1967	338
232	Monthly Median Noise Power, Omnidirectional Antenna Starr Hill, May 1967	339
233	Monthly Median Noise Power, Omnidirectional Antenna Starr Hill, June 1967	340
234	Monthly Median Noise Power, Omnidirectional Antenna Starr Hill, July 1967	341
235	Monthly Median Noise Power, Omnidirectional Antenna Starr Hill, August 1967	342
236	Season Noise Power Deciles, Omnidirectional Antenna Starr Hill, Winter 1967	343
237	Season Noise Power Deciles, Omnidirectional Antenna Starr Hill, Spring 1967	344
238	Season Noise Power Deciles, Omnidirectional Antenna Starr Hill, Summer 1967	345
239	Monthly Noise Power Deciles, Omnidirectional Antenna Starr Hill, March 1967	346
240	Monthly Noise Power Deciles, Omnidirectional Antenna Starr Hill, May 1967	347
241	Monthly Noise Power Deciles, Omnidirectional Antenna Starr Hill, June 1967	348
242	Monthly Noise Power Deciles, Omnidirectional Antenna Starr Hill, July 1967	349
243	Monthly Noise Power Deciles, Omnidirectional Antenna Starr Hill, August 1967	350
244	Monthly Median Noise Power, Directional Antenna Starr Hill, June 1967	360
245	Monthly Median Noise Power, Directional Antenna Starr Hill, August 1967	362
246	Monthly Median Noise Power, Directional Antenna Starr Hill, September 1967	363

LIST OF ILLUSTRATION (concluded)

<u>Figure</u>	<u>Title</u>	<u>Page</u>
247	Median Noise Power, Directional Antenna Relative to Omnidirectional Antenna Starr Hill, 1967.....	364
248	N/I Receiver Output Format, 90 Percent of MUF	366
249	N/I Receiver Output Format, 80 Percent of MUF	368
250	N/I Receiver Output Format, 70 Percent of MUF	369
251	N/I Receiver Output Format, 50 Percent of MUF	370
252	N/I Receiver Summary Statistics	372
253	Interference Level vs. Frequency	373
254	Noise/Interference Power for North Horizontal Antenna, Autumn 1967, Daytime	374
255	Noise/Interference Power for North Horizontal Antenna, Autumn 1967, Nighttime	376
256	Noise/Interference Power for North Vertical Antenna, Autumn 1967, Daytime	377
257	Noise/Interference Power for North Vertical Antenna, Autumn 1967, Nighttime	378
258	Noise/Interference Power for South Vertical Antenna, Autumn 1967, Daytime	379
259	Noise/Interference Power for South Vertical Antenna, Autumn 1967, Nighttime	380
260	Predicted MUF, September and October 1967.....	382
261	Diurnal Variations of Interference Level, SV Antenna	382
262	Cumulative Distribution Curves of Noise and Interference	383
263	Equiprobable Value Approximation to Continuous Distribution	399
264	LPV Antenna Gain Pattern, 9.104 MHz	406
265	LPV Antenna Gain Pattern, 11.399 MHz	408
266	LPV Antenna Gain Pattern, 13.989 and 16.459 MHz	409
267	LPV Antenna Gain Pattern, 19 MHz	410
268	LPV Antenna Gain Pattern, 22 MHz	411
269	LPV Antenna Gain Pattern, 26.1 MHz	412
270	LPV Antenna Gain Pattern, 30 MHz	413
271	Combined Antenna Patterns for Mode Loss Experiment at 11.3 MHz..	414
272	Combined Antenna Patterns for Mode Loss Experiment at 16.6 MHz..	414
273	Combined Antenna Patterns for Mode Loss Experiment at 22.3 MHz..	415

LIST OF TABLES

<u>Section</u>	<u>Title</u>	<u>Page</u>
I	Relationship between Environmental Experiments and OHR System Considerations	5
II	Mode Availability, Coco Solo Path, December 1965 - January 1966	71
III	Mode Availability, Coco Solo Path, March 1967	72
IV	Mode Availability, Coco Solo Path, April 1967	73
V	Mode Availability, Coco Solo Path, May 1967	74
VI	Mode Availability, Coco Solo Path, June 1967	75
VII	Mode Availability, Coco Solo Path, July 1967	76
VIII	Mode Availability, Coco Solo Path, August 1967	77
IX	Mode Availability, Thule Path, March 1967	89
X	Mode Availability, Thule Path, April 1967	90
XI	Mode Availability, Thule Path, May 1967	91
XII	Downtime	228
XIII	Natural Factors, December 1965	253
XIV	Natural Factors, January 1966	254
XV	Natural Factors, February 1966	255
XVI	Natural Factors, March 1966	256
XVII	Natural Factors, April 1966	259
XVIII	Natural Factors, May 1966	260
XIX	Natural Factors, June 1966	261
XX	Natural Factors, July 1966	262
XXI	Natural Factors, August 1966	263
XXII	Natural Factors, September 1966	264
XXIII	Natural Factors, October 1966	265
XXIV	Natural Factors, November 1966	266
XXV	Natural Factors, December 1966	269
XXVI	Natural Factors, January 1967	270
XXVII	Natural Factors, February 1967	271
XXVIII	Natural Factors, March 1967	272
XXIX	Natural Factors, April 1967	273
XXX	Natural Factors, May 1967	274
XXXI	ARN-2 Receiver Characteristics	328

LIST OF TABLES (concluded)

<u>Section</u>	<u>Title</u>	<u>Page</u>
XXXII	Log Deviation in Decibels Below F_a , February 1967	351
XXXIII	Voltage Deviation in Decibels Below F_a , February 1967	351
XXXIV	Log Deviation in Decibels Below F_a , March 1967	352
XXXV	Voltage Deviation in Decibels Below F_a , March 1967	352
XXXVI	Log Deviation in Decibels Below F_a , April 1967	353
XXXVII	Voltage Deviation in Decibels Below F_a , April 1967	353
XXXVIII	Log Deviation in Decibels Below F_a , May 1967	354
XXXIX	Voltage Deviation in Decibels Below F_a , May 1967	354
XL	Log Deviation in Decibels Below F_a , June 1967	355
XLI	Voltage Deviation in Decibels Below F_a , June 1967	356
XLII	Log Deviation in Decibels Below F_a , July 1967	357
XLIII	Voltage Deviation in Decibels Below F_a , July 1967	357
XLIV	Log Deviation in Decibels Below F_a , August 1967	358
XLV	Voltage Deviation in Decibels Below F_a , August 1967	359
XLVI	Coco Solo LPV Measurements	406
XLVII	Geographical Information on the ELIDA Field Sites	417

SECTION I

INTRODUCTION

This final technical documentary report -- Experimental Results -- reviews the work performed on Air Force Contract AF 30(602)-3946, under the supervision of the Rome Air Development Center (RADC), in the area of data reduction and data analysis of the experimental measurements. This program has been a continuation, as well as an expansion, of the effort previously carried out under Contract AF 30(602)-3360 (also directed by RADC) to determine the characteristics of ionospherically propagated high frequency (HF) signals. The long term objective of the Expanded Little IDA program is to provide more accurate estimates of major environmental factors needed for improved system design of over-the-horizon radars (OHR) of the backscatter type. This is the final in a series of technical documentary reports issued covering the work being performed on this contract; the previous reports (references 1 through 7) were devoted to either the new equipment being furnished or the experimental results. The new instrumentation that has been being designed, built, delivered, and employed to meet the requirements of this program has been described in references 1, 3, 5, and 7. Reference 7 is another final report on this program and contains a detailed description of the equipment employed.

Overall and detailed descriptions of the five major experiments that have been conducted on this expanded program are provided in reference 2. These are the Mode Reliability Experiment, the Mode Loss Experiment (including signal characteristics), the Spectrum Experiment, the Azimuth of Arrival Experiment and the Noise/Interference Experiment. Basically, the objective of the mode reliability experiment is to determine the "availability" of the lower order dominant modes (such as 1F2, 2F2, 2E, and N) for 2000-nmi paths. Similarly, the goal of the mode loss experiment is to determine the losses associated with these same modes and other significant signal characteristics such as polarization sensitivity. The spreading and the signal coherence for various propagated modes are obtained from the results of the spectrum experiment. The azimuth experiment is intended to measure the azimuthal angular statistical characteristics of these same signals. Inherent to the design of any communications or radar system is the noise level with which it must contend. For this reason, an experiment has been conducted to more precisely determine the noise and

interference environment in which an OHR system must operate. Results for a number of the above experiments have been reported in detail in references 2, 4, and 6.

To conduct these experiments, three remote transmitting sites have been installed that are approximately 2000 nmi (3704 km) from a receiving site located in central New York. (Appendix V contains a tabulation of the more precise values of distance and also bearing between the various sites of interest.) The remote sites have been situated so that measurements may be made on HF paths that pass through the auroral zone and extend into the tropics. A site at Coco Solo, Canal Zone -- which was previously employed on the Little IDA Program -- was in operation for most of the program, permitting the collection of data on HF signals transmitted over a 2000-nmi north/south path. This is an example of a temperate/tropical path approximately parallel to the earth's magnetic field. A second remote site, at Thule, Greenland, became operational during the latter part of the program and was employed to obtain data on 2000-nmi HF signals that pass through the auroral zone. In order to adequately sample in the northern region of interest, a third distant site was installed at Keflavik, Iceland, which permits a more detailed experimental study of propagation effects near the outer edge of the auroral zone. This also represents a 2000-nmi path from the central New York receiving site which was located at the RADC Starr Hill Test Annex at the completion of this program. Until the beginning of March 1967, the receiving site had been situated at the RADC Stockbridge facility, approximately 40 km south of Starr Hill.

The utilization of the experimental data gathered on this program for improved OHR system design and for the determination of OHR performance is discussed. From the basic radar range equation, key parameters and relationships that should be established from the experimental measurements are pointed out. One of major importance is the correspondence between propagation loss and the noise/interference level. How the actual data might be grouped for presentation of the information is also described with a number of examples given. Of major concern to an endeavor of this type are the confidence limits that should be associated with the experimental measurements. This matter is discussed in considerable detail with an example provided of the number of samples needed to obtain a certain measurement accuracy with a certain level of confidence.

The experimental results collected over the Coco Solo to Stockbridge/Starr Hill path for the mode reliability experiment from December 1965 to August 1967 are discussed in considerable detail in Section II. Also included are mode reliability results for the Thule to Stockbridge/Starr Hill path from December 1966 through May 1967. The information for this experiment is derived from oblique soundings made over these paths. The modes of propagation that have received the most attention are the 2E, 1F2, N, 2F2, and (recently) the 2E_g. The data are presented on a seasonal basis. Some of this information was presented in references 2, 4, and 6 on a monthly basis. The measured hourly mode availability for each of the dominant modes is shown, as is their frequency aperture and MOF or JF availabilities for probabilities of occurrence of 90, 50, and 25 percent assuming that the particular mode in question exists. The data base for this experiment will be reviewed on a seasonal basis indicating the number of samples available as a function of time of day for each of the dominant modes. The percentage of time that various combinations of modes are not available on the Coco Solo path is presented; it is pointed out that every time measurements were taken at least one of the following modes was available: 2E, 1F2, and 2F2. A statistical summary of the various mode reliability results is provided on a seasonal basis dividing a 24-hour day into three major time periods: daytime, nighttime, and dusk. This section of the report concludes with a discussion of an investigation to relate various mode reliability results to different natural factors such as solar flares and magnetic disturbances.

The additional loss term developed in reference 4 to describe the "excess" loss measured for the 2E mode of propagation over the Coco Solo path has been modified; the resulting equation is presented in Section IV. Further analysis of the mode loss measurements has been performed using the data collected over the Coco Solo path between February 1966 and February 1967. A comparison between the loss term mentioned above and a compilation of the 2E measurements is made which indicates very good agreement.

Signal coherence data obtained on the spectrum experiment for the period 23 September 1966 through 7 July 1967 are presented in this report. The Coco Solo to central New York data are available for this entire period, while Thule to Starr Hill data are available for the period 26 April through 7 July 1967. System configuration

changes since the last experimental* report are also discussed. The coherent integration loss factor, L_1 , associated with coherently integrating a received pulse train of partially incoherent pulses is discussed and used to show that the definition of signal coherence as numerically equal to one-half the half-amplitude width of the normalized signal autocorrelation function is indeed an adequate and desirable measure of signal coherence. Results for the processing gain obtained using various types of signal integration for an example OHR system are also discussed.

Initial results were obtained during the early part of 1968 for the azimuth of arrival experiment using transmissions from the Coco Solo site. As described in reference 5, the use of two separate receivers for this experiment has been discontinued. Instead, both signals from the two arrays that comprise the interferometer are being time multiplexed through one receiver. These first findings for this experiment are presented in Section VI.

The noise/interference experiment is discussed in Section VII, starting with a review of the experimental design considerations including the objective for this experiment and the basic equipment configurations employed for this task. This experiment can be broken down into two parts: one concerned with atmospheric noise measurements obtained using two ARN-2 noise measuring receivers furnished by ESSA, and a second with noise/interference (N/I) data collected over the range from 4 to 39 MHz using a specially built dual-channel receiver. The methods of measurement employed with these two types of receivers are described as well as the resulting output format for the data. The results obtained using the ARN-2 receivers over a period of eight months are presented. These were obtained from measurements made using both the standard whip antenna and the directional antennas located at the RADC Starr Hill Test Annex. Results of measurements made from mid-September to mid-October using the N/I dual channel receiver are also included.

Conclusions based upon the experimental results are contained in this report for the five major experiments conducted on the Expanded Little IDA program.

* Reference 6

SECTION II

SYSTEM UTILIZATION

1. THE IMPLICATIONS OF OHR DEFENSE MISSIONS ON THE ELIDA EXPERIMENTS

Experiments on the HF environment as related to the utilization of over-the-horizon radar for various defense missions can best be categorized as follows:

1. Those that relate primarily to OHR systems' performance reliability, and
2. Those that primarily affect the specific design of the OHR system.

The first type involves those environmental factors which primarily influence the reliability with which an OHR can perform its mission. The second type provides environmental information that primarily affects the design of the total system and/or individual radars. Obviously, the second type are related to the first, but their primary utility is for design purposes. Key environmental experiments are categorized according to the above criterion in Table I.

TABLE I
RELATIONSHIP BETWEEN ENVIRONMENTAL EXPERIMENTS
AND OHR SYSTEM CONSIDERATIONS

EXPERIMENT	TYPE*
MODE RELIABILITY	
Mode Availability	P
Mode MOF-JF Availability	D
Frequency Aperture Availability	D, P
MODE LOSS	
Loss	P, D
Polarization	D
Fading Characteristics	D

*The order indicates the priority of utility. P signifies performance, D - design.

TABLE I (concluded)

MODE SPECTRUM	
Coherent Integration Time	P, D
Clutter Rejection	P, D
AZIMUTH OF ARRIVAL	
Tracking Accuracy	D, P
NOISE/INTERFERENCE	
Noise Characteristics (Both atmospheric and interference)	P, D
Clear Channel Availability	D, P
Interference Characteristics	D

Concerning experiments related to performance (type P), a useful performance measure is:

$$\begin{aligned}
 \text{Radar Reliability} &= P \text{ (one or more usable modes)} \\
 &= P (A \text{ or } B \text{ or } C \text{ or } D) \\
 &= 1 - P (\bar{A}, \bar{B}, \bar{C}, \text{ and } \bar{D})
 \end{aligned}
 \tag{1}$$

where A, B, C, and D describe the 1F2, 2F2, 2E, and N mode usabilities and "not" A (\bar{A}), etc., imply that the respective mode is not usable.

From an experimental standpoint, it is convenient to collect data on the "dominant mode" (x) observed to exist at a particular time and assume that, when mode x is not usable neither are any of the other dominant modes available.* Then, by proper

* The dominant mode is that mode identified by the experiment operator in real time as being the strongest, stable, lowest order mode existing at a particular time as determined from an oblique sounding along with an experience factor. From experience on the Coco Solo path, the dominant modes are the 2E, 1F2, and 2F2 with the occurrence and reliability of the N and 2E_s modes not as good. For the purposes of this analysis, four dominant modes will be considered as indicated above.

manipulation of the data collected, $P(\bar{A}, \bar{B}, \bar{C}, \text{ and } \bar{D})$ can be determined, presented statistically for the data collection period, and extrapolated to other time frames and geographical regions.

It is assumed that the probability that there are no usable modes can be formed as follows:

$$\begin{aligned}
 P(\bar{A}, \bar{B}, \bar{C}, \text{ and } \bar{D}) &= P(\bar{x}) \\
 &= P(x \text{ does not exist or } \text{SNR} < M \text{ when } x \text{ exists}) \\
 &= P(x \text{ does not exist}) + P(\text{SNR} < M \text{ when } x \text{ exists}) \\
 &= P(x \text{ does not exist}) + P(\text{SNR} < M) P(x)
 \end{aligned} \tag{2}$$

where

1. x is the dominant mode,
2. Existence implies that the mode is visible in the sounder output with a minimum frequency aperture,
3. Mode existence and signal-to-noise ratio (SNR) have been assumed to be mutually exclusive, and
4. M is the minimum acceptable SNR based on known system parameters.

$P(x \text{ does not exist}) = 1 - P(x \text{ exists})$ can be determined from mode reliability data collected using the oblique sounding records. For x to exist at a particular measurement time, at least one mode of the four (A , B , C , or D) must exist with a frequency aperture of at least 1 MHz. The 1-MHz lower limit on aperture requirement is based on considerations of mode stability, clear channel availability, and mode identification.

Turning next to the significance of SNR on the usability of mode x , consider the radar range equation:

$$\begin{aligned}
 \text{SNR} &= \frac{P_T G_T G_R T \lambda^3 \sigma}{(4\pi)^3 R^4 K T_0 N F L_s L_p L_i} \\
 &= \frac{k}{L_p L_i N F} \geq M \text{ for satisfactory performance}
 \end{aligned} \tag{3}$$

where

k is a constant involving all the system constants such as average power (P_T), combined antenna gain (G_T, G_R), integration time (T), range (R), target cross section (σ), system loss (L_s), etc.

L_p is the propagation loss over and above two-way spreading loss $\left[\frac{1}{R^4}\right]$,

L_i is coherent integration loss associated with the signal spectrum,

NF is the system noise factor (re kT_0) involving man-made, galactic, and atmospheric noise

Equation (2) requires knowledge of P (SNR < M when x exists) =

$$P \left[\frac{k}{L_p L_i NF} < M \text{ when } x \text{ exists} \right]$$

$$P \left[\frac{1}{L_p L_i NF} < \frac{M}{k} \text{ when } x \text{ exists} \right] \quad (4)$$

$$P \left[L_p L_i NF > n \text{ when } x \text{ exists} \right]$$

where

$$n = \frac{k}{M} \quad (5)$$

Since L_p , L_i , and NF are not known to be independent, the measurement of these parameters should be combined for each measurement time to form a single factor.

The statistical behavior of this factor is the quantity that must be measured as a function of time of day, season, ionospheric state, etc., and extrapolated to other time frames (SSN's) and geographical locations (bearings). Since the losses, L_p and L_i , can be measured only at one frequency at a time, the actual measurement may not be at the optimum frequency; thus, it will be necessary to use a "bootstrap" technique, where

the collected data are used to determine the optimum frequency (for example, a particular fraction of the dominant mode MOF or JF). Having found the optimum frequency relationship experimentally, the collected loss data can be adjusted to the optimum frequency. Since the clear channel noise level is measured at various fractions of the MOF or JF, the correct noise levels will be available to use with the adjusted loss measurement. By proper execution of key experiments along with appropriate data reduction and analysis, it should be possible to extract the desired statistic.

The following figures are examples of the type of experimental output that are desired. The measured existence of a dominant mode as a function of time of day, for winter, $\overline{SSN} = 70$, and a particular path is shown in Figure 1. The cumulative probability function of $10 \log_{10} \frac{L_p L_i}{P_i} NF$ for particular hours of the day, season, \overline{SSN} , and path is shown in Figure 2. Figures such as these are desirable for all measurement conditions (seasons, \overline{SSN} , etc.). The method for extrapolating these data to other time frames (\overline{SSN}) and geographical locations is also necessary so that the system designer can evaluate hypothesized OHR systems.

Referring to the experimental breakdown discussed previously, it may be seen that frequency aperture availability and clear channel availability contribute to the OHR system performance in a secondary fashion. An attempt was made to account for their influence by requiring that at least a 1-MHz frequency aperture exist on a particular mode in order that it be classed as existing at a particular measurement time. This assumption simplifies the radar reliability relationship to a manageable form in terms of the experimental requirements. A somewhat optimistic assumption will be made that the lowest noise level measured to exist on any 4-kHz channel in the particular 1-MHz subband under examination using the noise/interference experiment is used for the "NF" term of Equation (4). From another viewpoint, this assumption maybe considered conservative because an interference level is employed to determine the operating noise level for an OHR system rather than using atmospheric noise (as reported in reference 8, for instance). While the percentage of channels that approaches the true atmospheric/galactic noise level is of interest from a system design standpoint, it is not essential to the radar performance relationship. Further, requiring at least a 1-MHz frequency aperture on a particular mode insures that the mode is minimally stable; i.e., small electron density changes in the ionosphere should not "knockout" the mode. It is doubtful that an operational radar could take

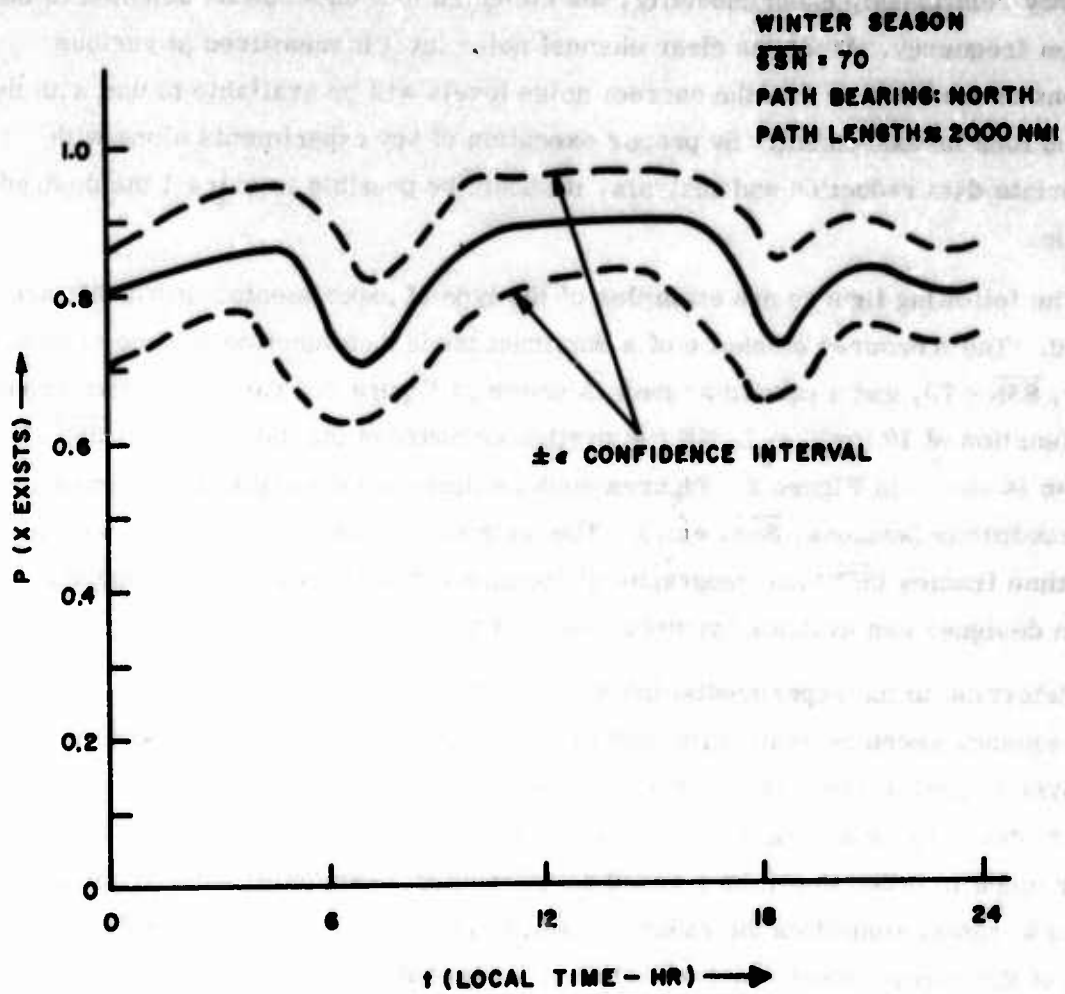


Figure 1. Dominant Mode Existence

advantage of modes with smaller frequency apertures, as they would be too time variant. In consideration of these factors, it appears reasonable (and legitimate) to require at least a 1-MHz aperture on each mode and use the lowest noise level measured (which may be man-made, galactic, or atmospheric noise) in the appropriate 1-MHz subband.

Proper attention must be given to certain of the environmental factors in the OHR design in order that the measured and/or predicted reliabilities may be achieved. A good example of such a factor is the mode MOF or JF availability. The system designer must have valid information on the range of expected operating frequencies in order to specify the required radar frequency range. This is best provided with information on the diurnal behavior of the monthly median MOF or JF for each mode, together with the respective statistical distributions about these medians for each month (or season, whichever is more applicable). Figures 3 and 4 depict the type of data and format that would be useful to the system designer. Figure 3 depicts the diurnal characteristics of the median JF for the 1F2 mode under certain conditions, and Figure 4 depicts the cumulative probability function of the random variable, JF, normalized to the median value for the JF. As shown, the diurnal characteristics have been grouped into three time blocks (day, night, transitional); however, the validity of any such grouping must be confirmed from the collected data. It should be mentioned that such a grouping has been employed to analyze the mode reliability results as discussed later in this report.

Frequency aperture availability was previously discussed as it relates to the radar performance; however, it also may influence system design. The design influence may occur in at least two ways: the "quasi-instantaneous" operating bandwidth, and the frequency scheduling of multiple radars making up the total OHR system. In regard to the first, some knowledge of the available operating frequency aperture is necessary to specify the frequency bandwidth over which the radar must be prepared to select clear channels, set up, and operate in a "quasi-instantaneous" fashion. "Quasi" is used to denote the fact that the transmitted waveform does not require this instantaneous bandwidth; rather, the radar must be capable of setting up and operating in any portion of this bandwidth in a relatively short time (i.e., a small amount of time for switching may be tolerable). With regard to the second point, it is most likely that many essentially independent radars will be collocated to provide surveillance of a given portion of the total threat region. To the extent that

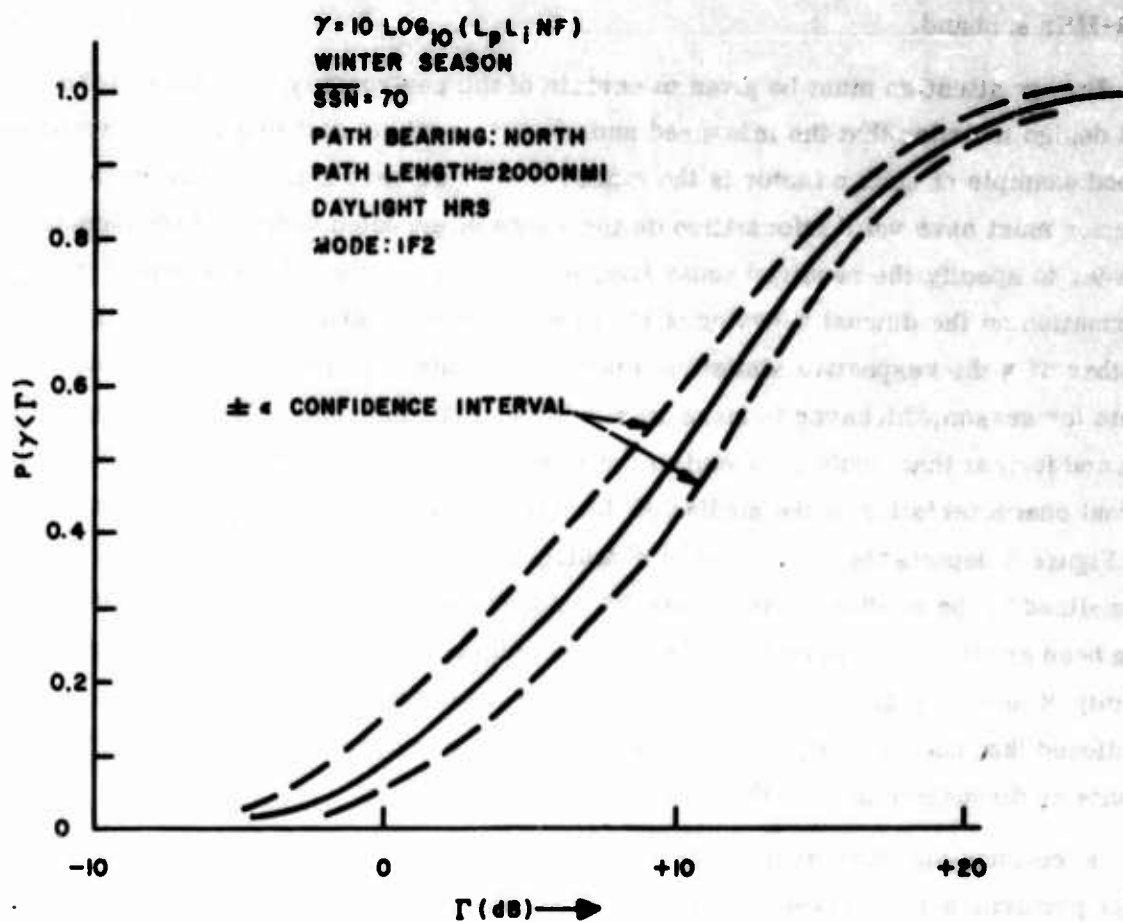


Figure 2. Cumulative Probability Function of $10 \log_{10}(L_p L_1 NF)$

ionospheric conditions are similar over several of the paths used by the different radars, suitable attention must be given to frequency scheduling to prevent cross-radar-jamming. In this context, then, knowledge of the available frequency aperture is important to the system designer. For the same reason, the number of "clear channels" available in a given band is important information. The type of frequency aperture availability information that would be useful is shown in Figure 5.

The mode loss and spectrum experiments have been assumed to relate primarily to performance; however, for obvious reasons, they also relate rather directly to system design. The propagation loss and coherent integration loss (from the spectrum experiment) in conjunction with the noise level and other factors such as range, target cross section, etc., are essential to the specification of the required "radiated" energy ($G_T G_R P_T$) for the radar. They are also useful in establishing target signal levels that the receiver/signal processing will have to handle, thereby in part establishing the necessary gain, dynamic range, and linear operating range for this equipment. The information from the spectrum experiment is also useful in assessing the accuracy to be expected in target velocity measurement, clutter spectral properties for clutter filtering, and temporal coherent integration times.

Examples of useful formats are shown in Figures 6, 7, and 8. The cumulative distribution functions conveniently summarize the mode loss and spectrum/temporal coherence data for system design usage. Grouping the data according to limited f/JF or f/MOF regions for the various modes, as shown in Figure 6, is used only as an example of what may be necessary to account for any frequency dependence.

The polarization characteristics of the energy arriving over the horizon from the extended ranges has implications on the design both of the OHR antenna and signal processing. In the event that the received energy for a particular mode shows a consistent preference for one polarization, it is logical to take this into account in the antenna design. Likewise, if there is no long term polarization preference, but the fading between the two receive polarizations is decorrelated or negatively correlated, diversity reception techniques can be used to advantage to improve detection and tracking performance. The type of information and format that would be useful to the OHR system designer to assess this particular effect is shown in Figures 9 and 10. The data grouping indicated (winter months, \overline{SSN} , daylight hours, etc.) is only used for convenience; the actual experimental data must be used to determine the final grouping.

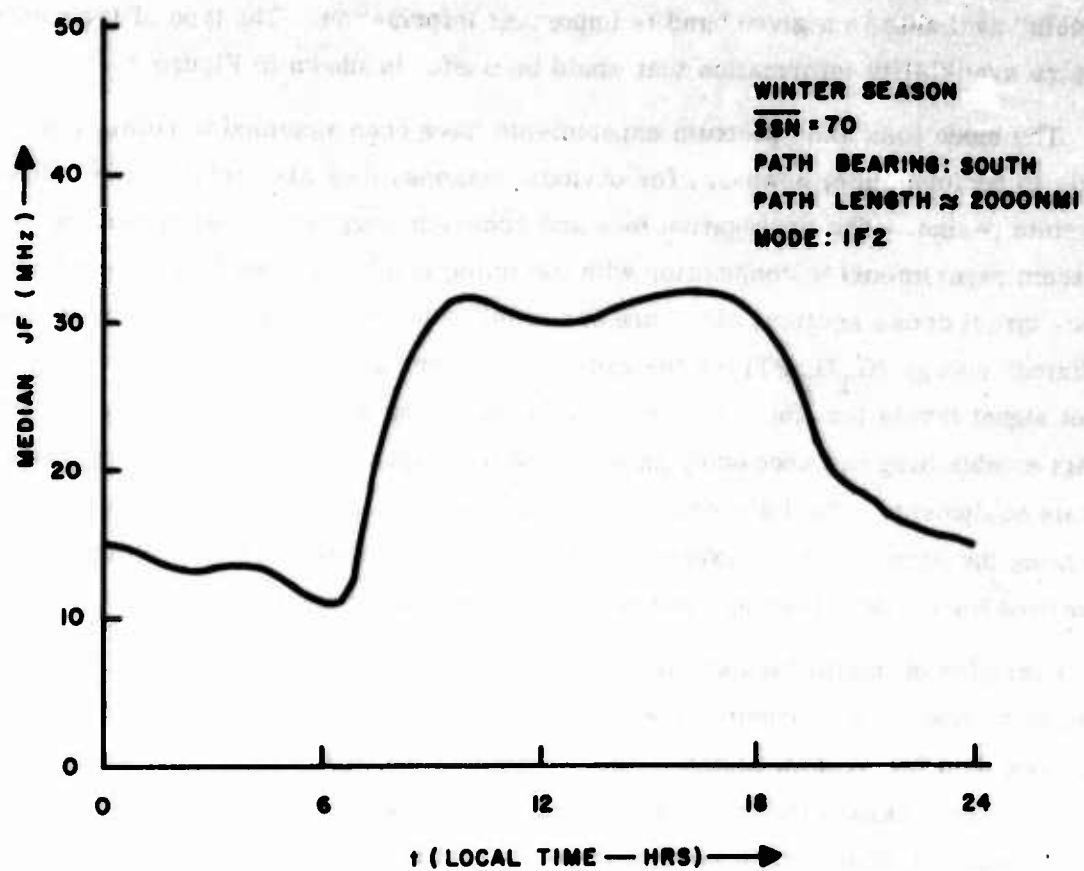


Figure 3. Diurnal Variation of Median IF2 JF for Winter Months

In a similar manner, the signal level fading characteristics are essential to proper system design. Figures 11 and 12 are examples of the type of experimental information that is desirable. The measured cumulative probability function of signal level for a particular class of received signals which would be useful in assessing the effect of expected signal strength variations about the median is shown in Figure 11. The probability density of the temporal autocorrelation $[p(\tau_0) = 0.5]$ of the received signal level (magnitude only, not phase) for a particular mode, etc., is shown in Figure 12. This latter information is useful in the design of an OHR system which must operate in a search mode such that "scan-to-scan" target correlation is important.

The azimuth of arrival of the various modes has implications on both design and performance. In a search type OHR, that scans over the region of interest, knowledge of off-great-circle-path propagation is important in the specification of the antenna beamwidths and scanning geometry/schedule, as well as for determining the basic positional accuracy that OHR targets can be measured at the extended ranges. The type of information and format that would be useful for assessing the effects of off-great-circle-path propagation is shown in Figures 13 and 14.

In addition to the effects on system performance, the noise/interference characteristics at frequencies required for illumination of the extended ranges across the threat region of interest can have a significant effect on system design. The actual noise levels and interference levels/distributions are necessary to specify the receiver noise figure, dynamic range, and linear operating range. The statistics on clear channel availability can have significant effects on the geographical deployment and scan scheduling of the individual radars that make up to a total OHR network. The type of information that would be useful to account for the noise/interference effects in the system design is shown in Figure 15.

In the above discussion, typical examples of the type of data that would be useful have been described. The particular temporal, seasonal, etc., groupings used were intended only as examples; the actual groupings will depend on actual data. Once the most effective groupings have been identified, the data should be analyzed accordingly and the results presented for all conditions during the data collection period (i.e., seasons, times of day, paths, etc.). Likewise, the necessary relationships for extrapolating the results to other time frames (SSN's) and paths (geographic/geomagnetic positions in the threat region) are desirable.

$$x = \frac{\text{IF2 JF}}{\text{MEDIAN IF2JF}} - 1$$

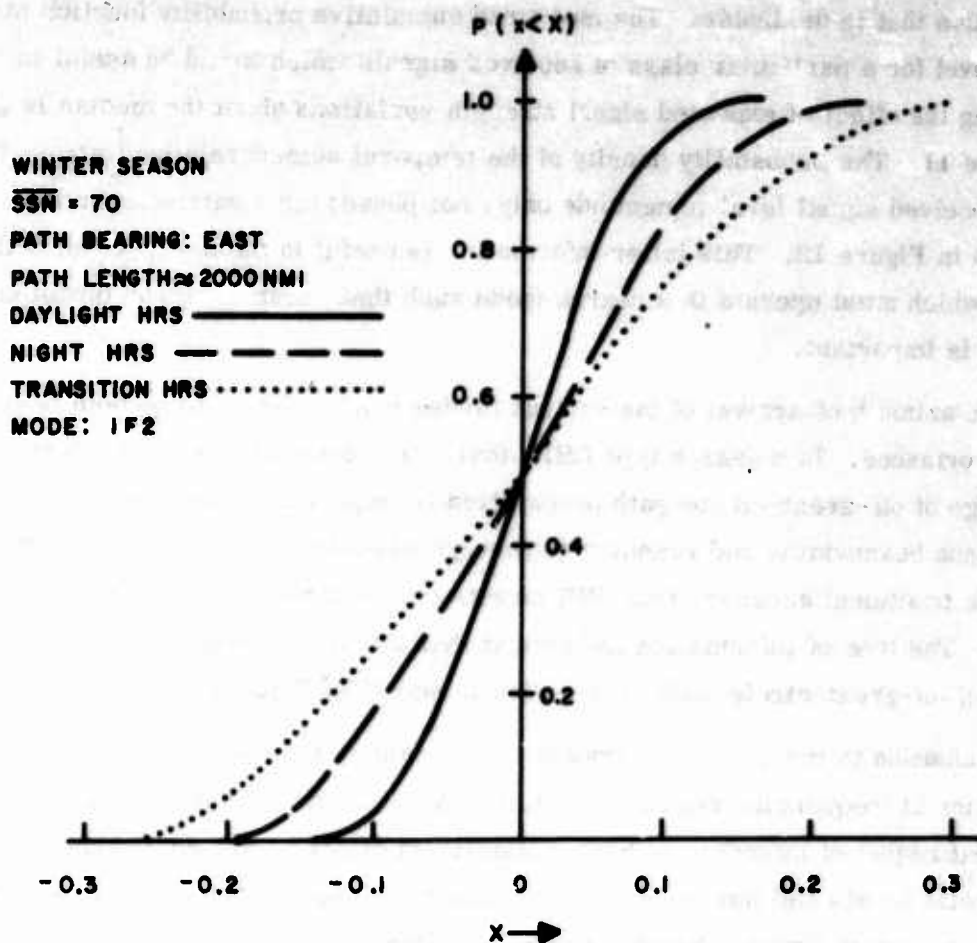


Figure 4. Statistical Behavior of Daily JF's About the Median JF

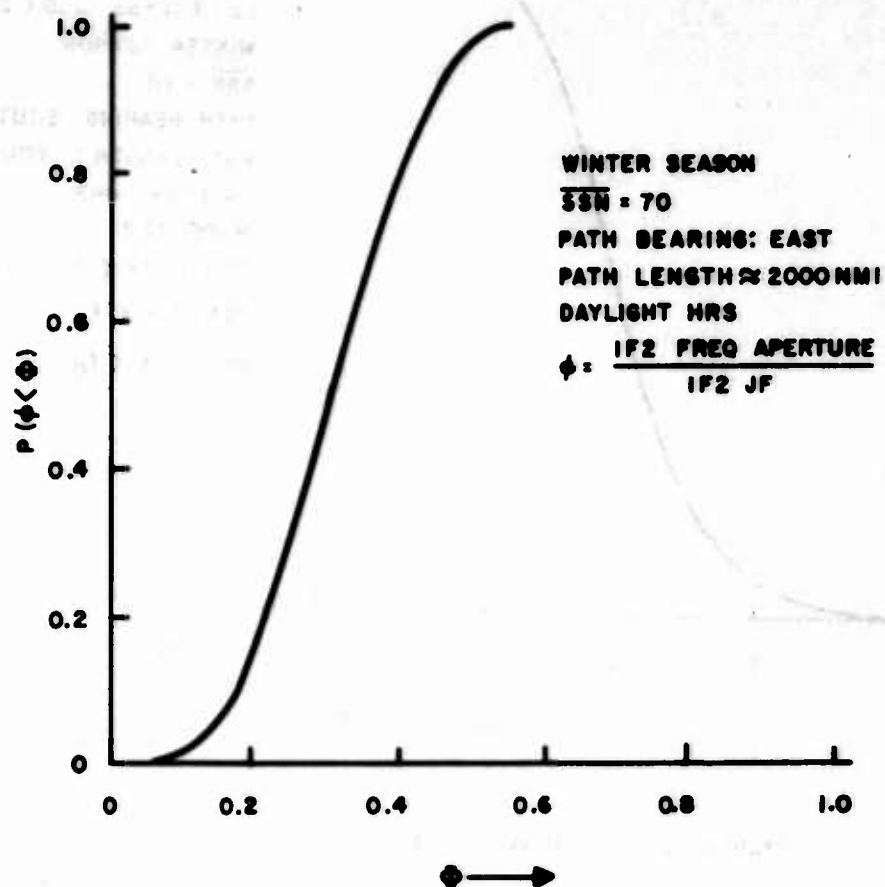


Figure 5. Cumulative Probability of the Normalized Frequency Aperture

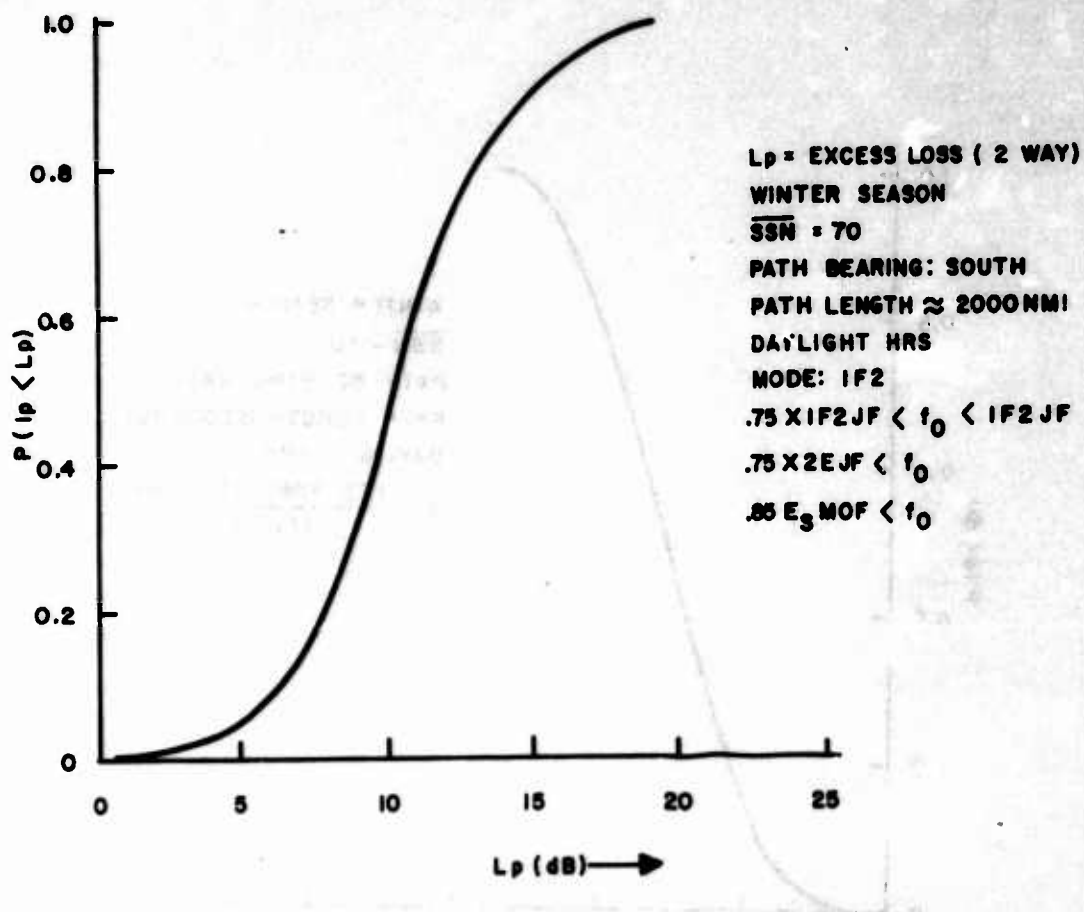


Figure 6. Cumulative Distribution of Excess Loss

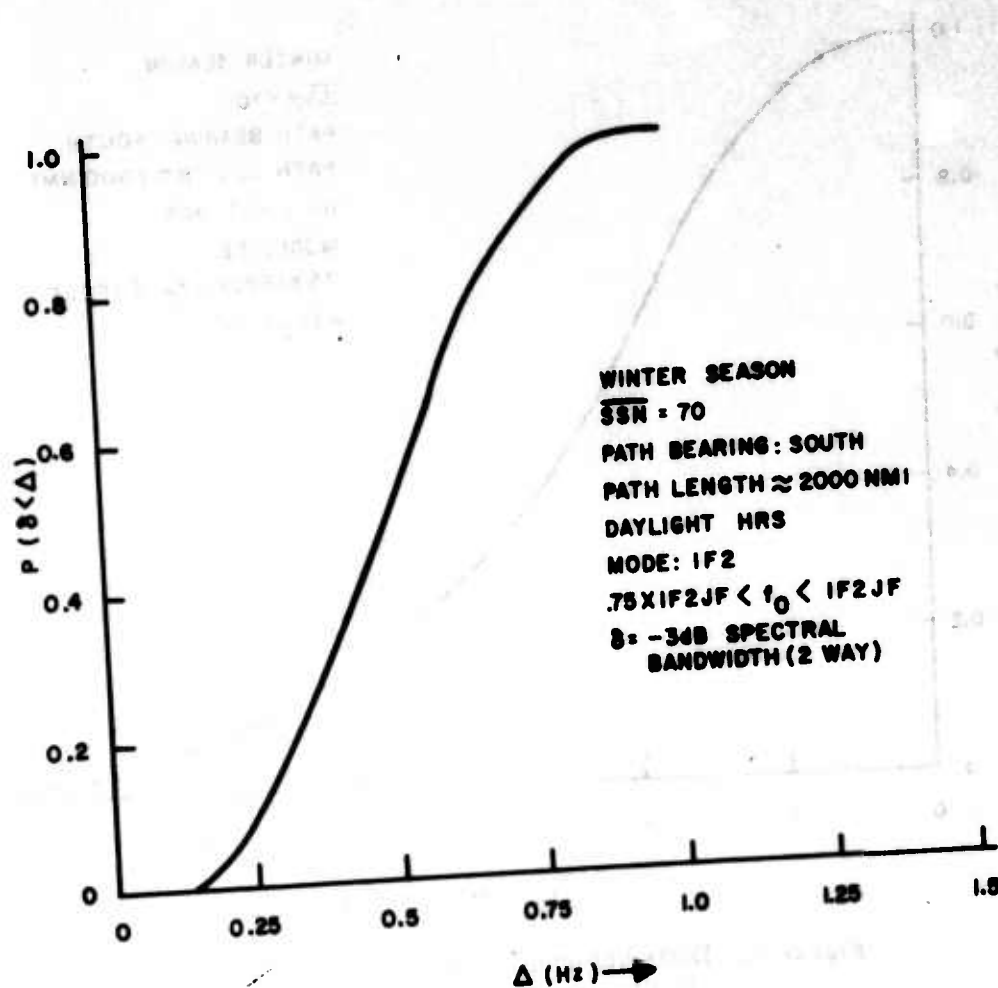


Figure 7. Cumulative Distribution of Spectral Bandwidth

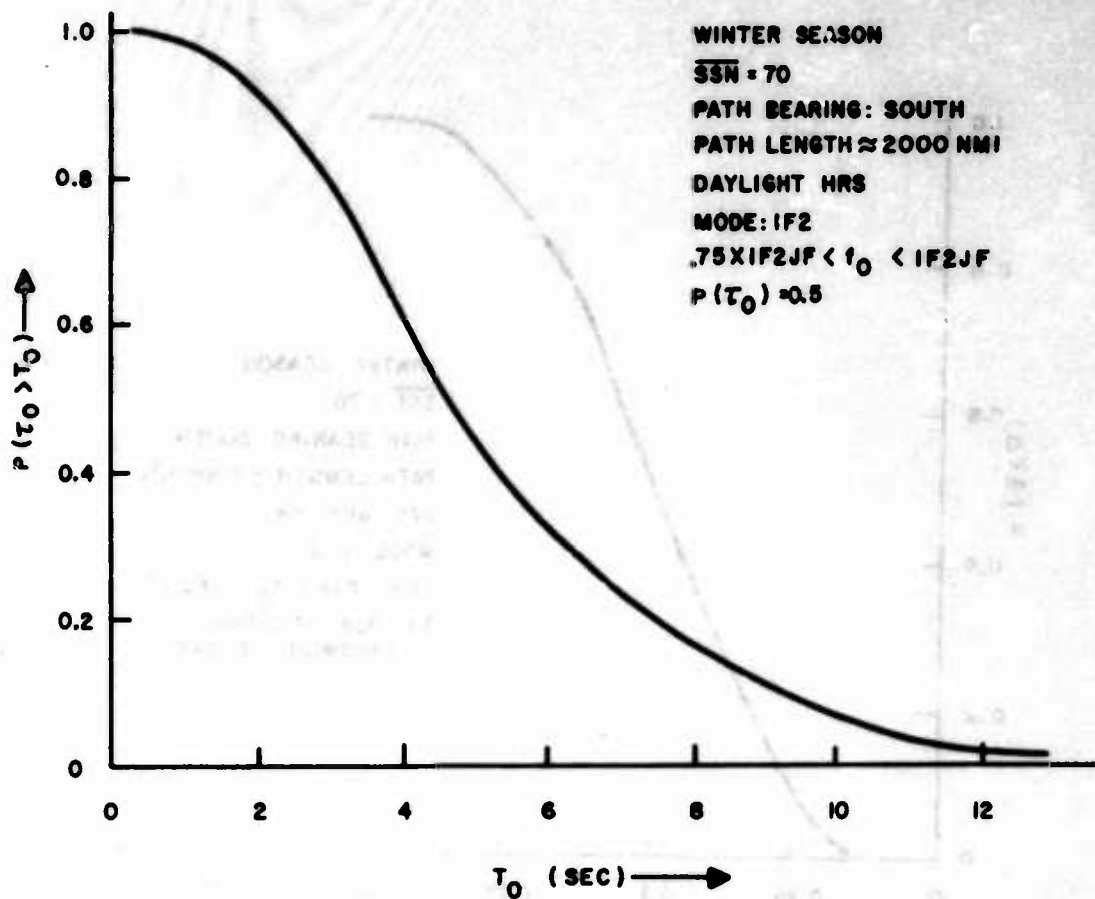


Figure 8. Distribution of Temporal Correlation (Amplitude and Phase)

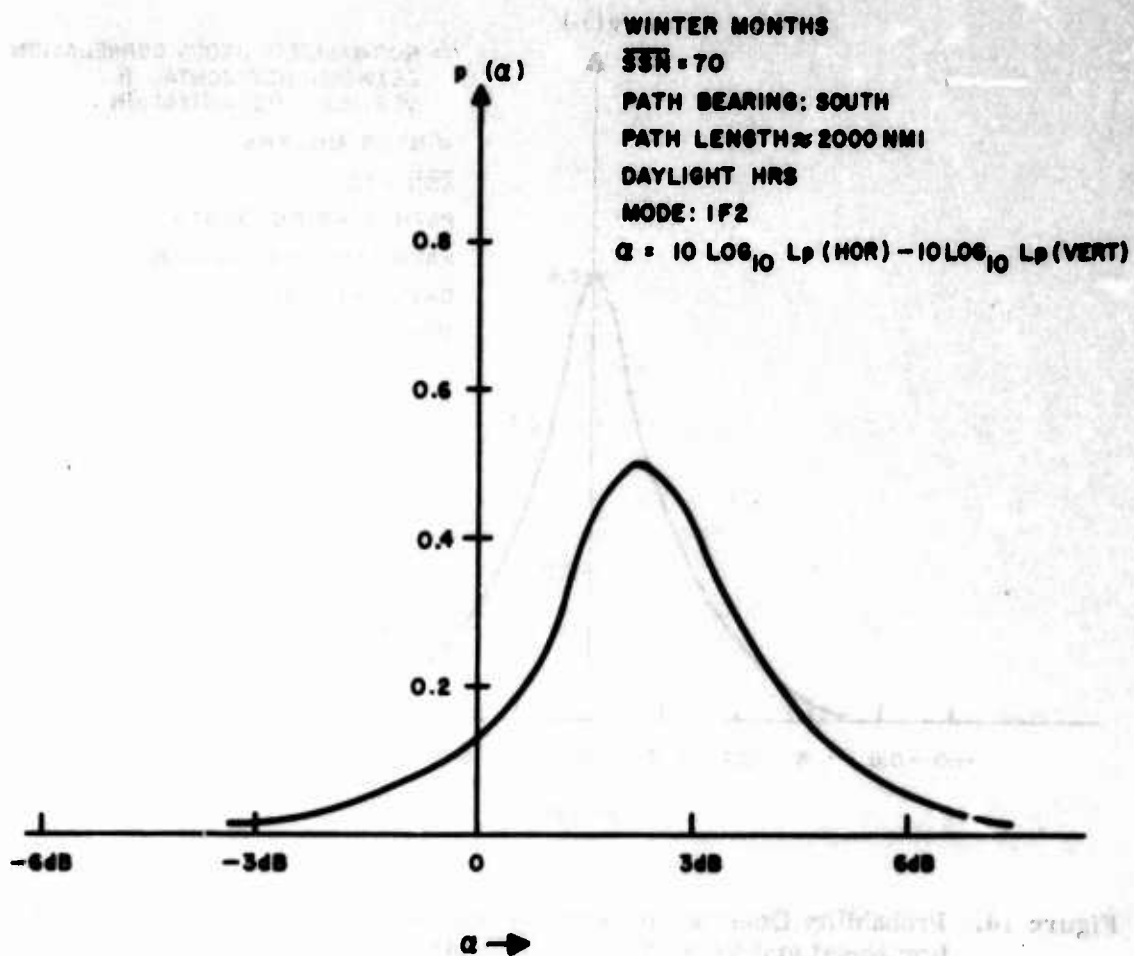


Figure 9. Probability Density Function For Relative Receive Polarization (Horizontal/Vertical)

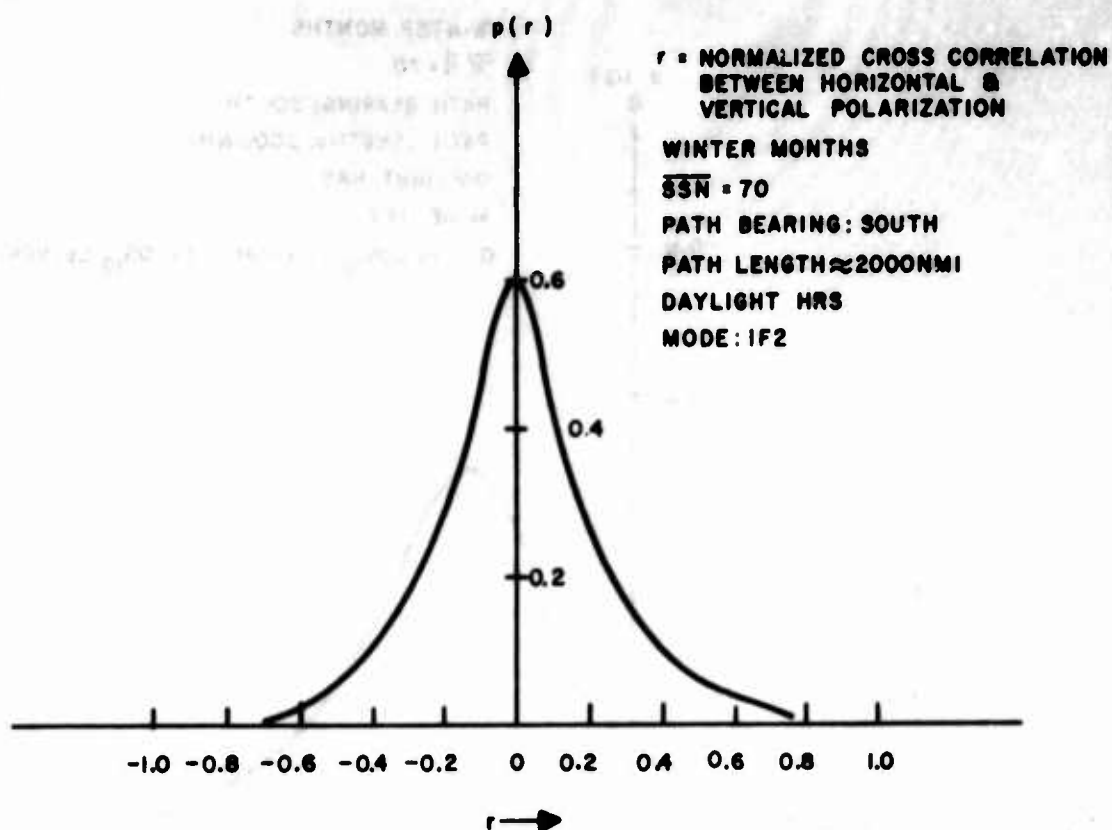


Figure 10. Probability Density Function for Normalized Cross-Correlation Between Horizontal and Vertical Receive Polarizations

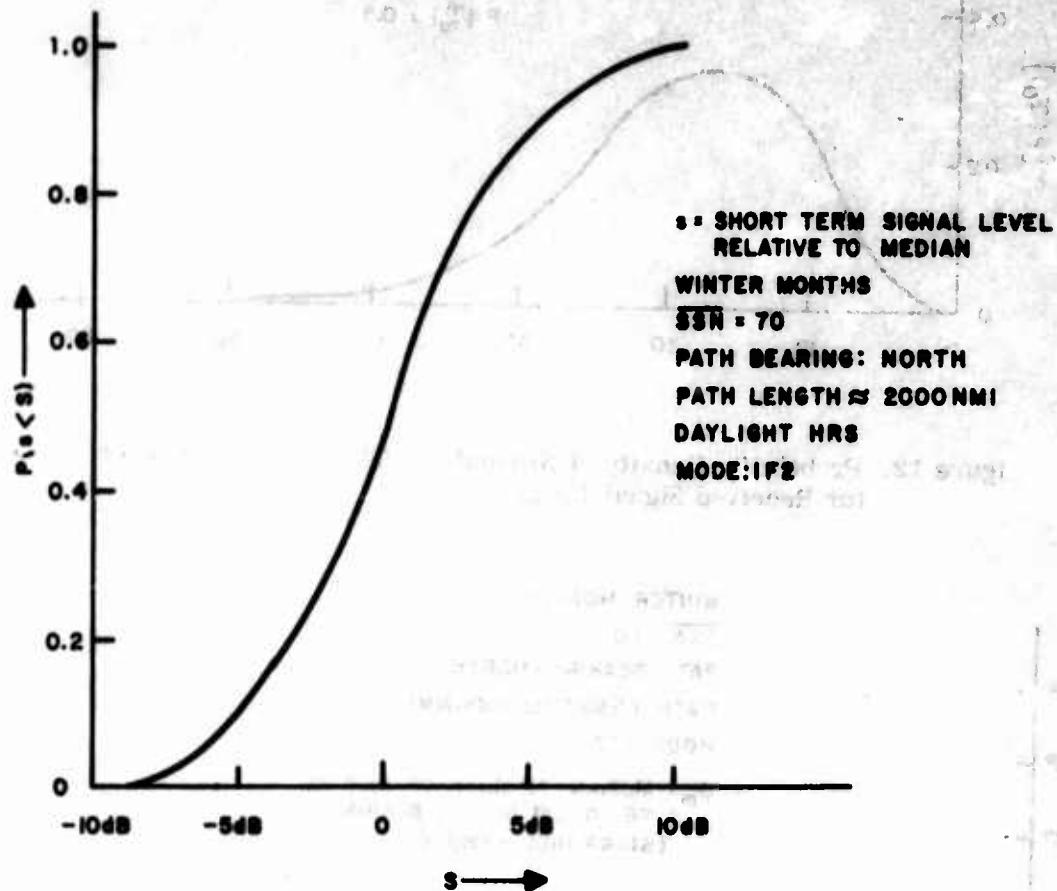


Figure 11. Cumulative Probability of Short Term Signal Level Relative to Median

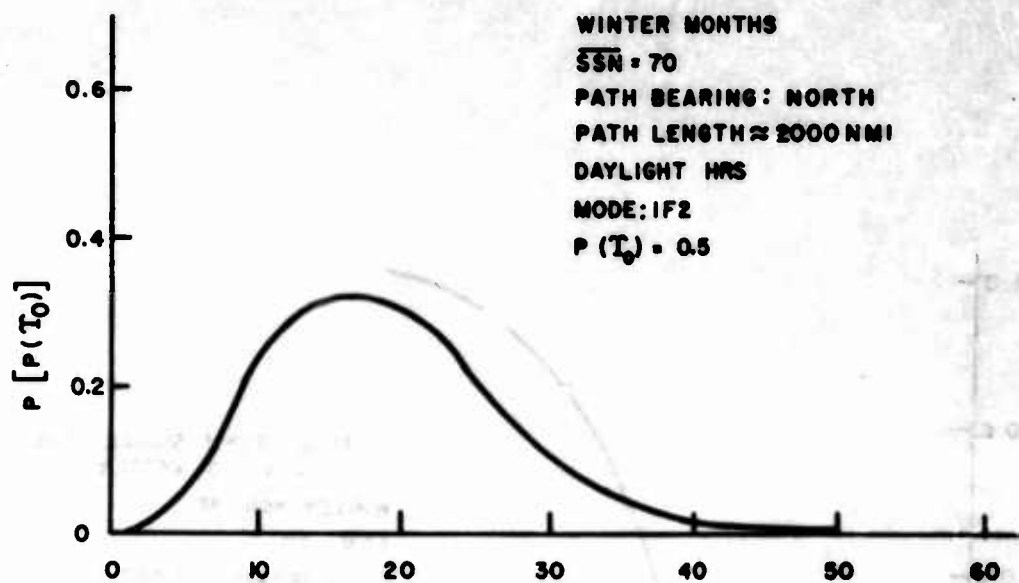


Figure 12. Probability Density of Normalized Time Autocorrelation for Received Signal Level

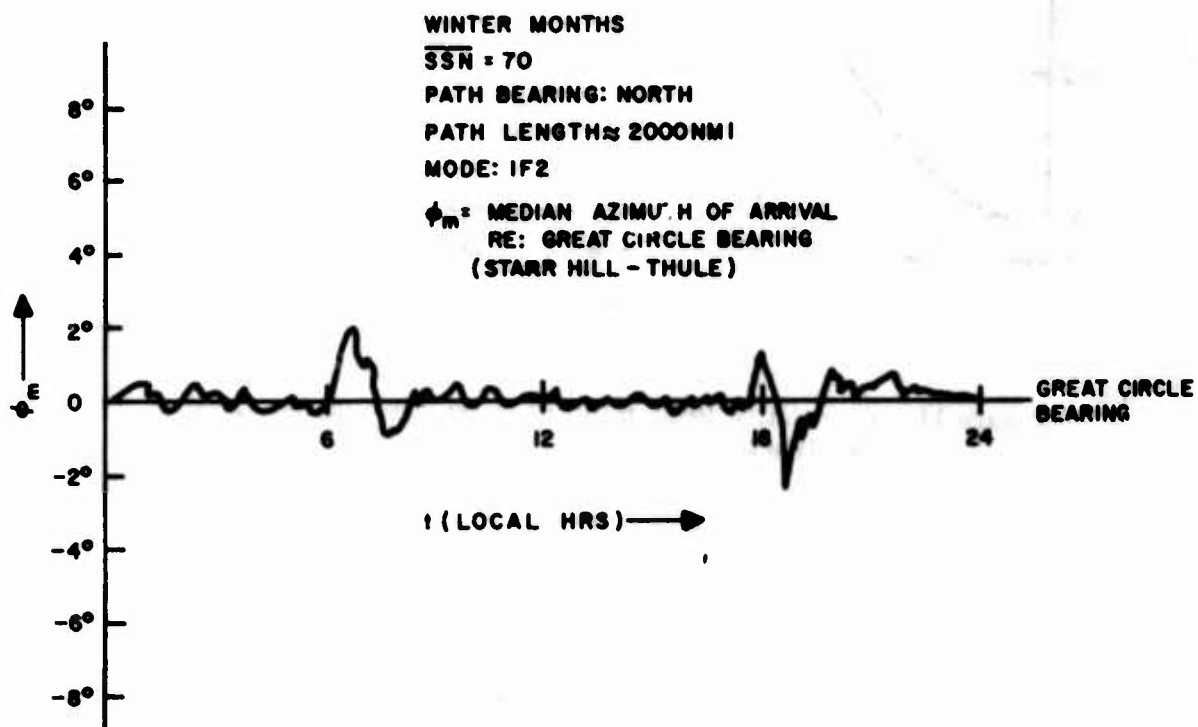


Figure 13. Median Azimuth of Arrival Diurnal Behavior

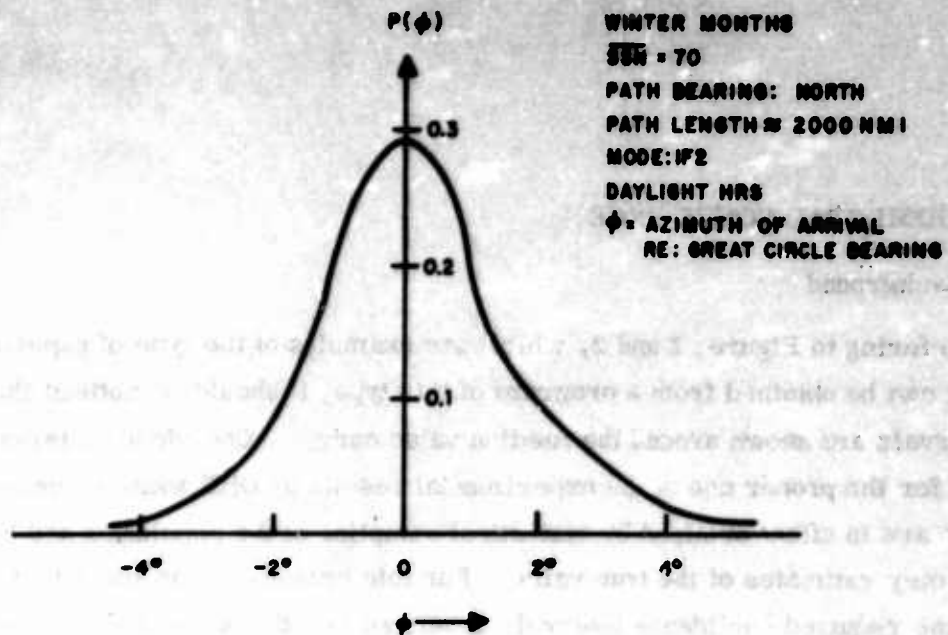


Figure 14. Probability Density of Azimuth of Arrival for Daylight Hours

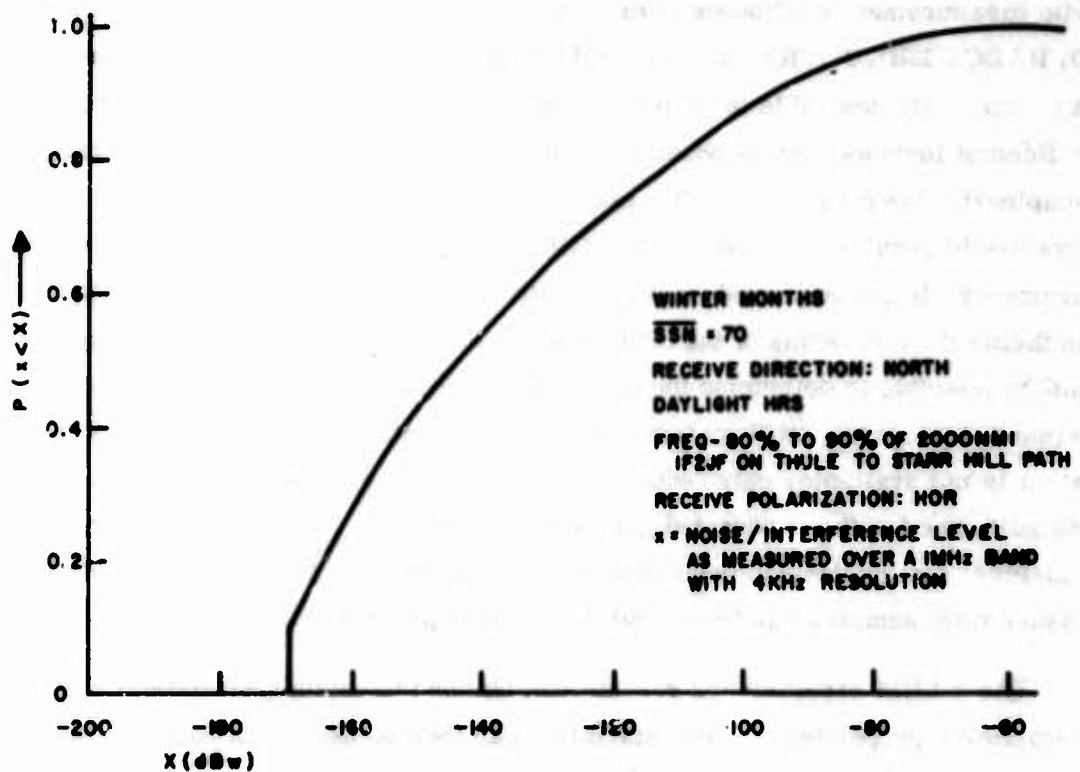


Figure 15. Cumulative Probability of Noise/Interference Level at 80 to 90 percent of 2000-nmi 1F2 JF

2. EXPERIMENTAL CONFIDENCE

a. Background

Referring to Figures 1 and 2, which are examples of the type of experimental output that can be obtained from a program of this type, it should be noticed that confidence intervals are shown around the median value curves. Confidence intervals are necessary for the proper use of the experimental results by OHR system designers, since the results are in effect obtained by statistical sampling of the population and hence represent only estimates of the true value. For this reason, it was important to establish the required confidence intervals/levels so that the planned experiments could be properly conducted; i.e., scheduled to provide an adequate data sample. It was felt that this information should logically come from the system planners, deployment strategists, gaming theorists, etc.; hence, individuals in several organizations were contacted in connection with the ELIDA Program for their views on realistic measurement confidence intervals/levels. The organizations contacted were RAND, RADC, ESD, MITRE, and GE (HMED and TEMPO). The general opinion was that it is obviously desirable to keep the confidence interval as small as possible and the confidence level as high as possible consistent with reasonable experimental cost and complexity; however, no specific numbers were given. To provide specific numbers would require knowledge of the OHR system's cost sensitivity relative to the parameters being measured, together with the cost relationships of the experiments themselves in terms of the confidence intervals/levels. With this information it would be possible to determine the optimum experiment in terms of total cost (experimental program, OHR system, and its operation); however, since this information is not available, only "educated guesses" can be made at this time. To provide guidance for these educated guesses, an analysis of expected confidence interval/level for the desired environmental parameter as a function of the number of measurement samples has been conducted and is presented here.

The ELIDA experimental results can be used to obtain a statistical measure of key ionospheric properties. These statistics can then be used to predict the operating performance of OHR systems, as well as influence their design as much as possible. Since sampling techniques are utilized to obtain the experimental data bank, a brief review of sampling theory is given here, followed by an analysis of the expected effects.

The statistics of the parameter to be estimated can be described by the probability density function of the parameter, a typical example of which is shown in Figure 16. The probability that the random variable, x , will fall in the interval x_1 to x_2 is given by the area under the curve from x_1 to x_2 . If the probability density is known, then the mean, variance, etc., as well as the interval probabilities can be calculated. From the ELIDA experiments, samples of random variables with generally unknown probability densities or populations will be obtained; hence, it will be necessary to estimate the population statistics.

The samples that have been taken of the ionospheric properties are often combined to yield the average or mean of that property. The best estimator of the average is the sum of the samples divided by the number of samples or

$$\text{Sample mean} = M = \frac{1}{N} \sum_{i=1}^N x_i \quad (6)$$

The mean found by Equation (6) is called the sample mean. How closely the sample mean estimates the true mean is a function of the number of measurements and the population of the random variable. The Chebyshev inequality can be used to measure the error between the true and sample means.* This inequality is useful here because it can be used regardless of the population from which the random variable comes; however, it provides only an upper limit on the expected error. This results in a conservative measure of error. The Chebyshev inequality is given by

$$P \left[|M - M_x| \geq \epsilon \right] \leq \frac{S_x^2}{2\epsilon^2} \quad (7)$$

where $P[] = \text{Probability of } []$

$M = \text{sample mean}$

$M_x = \text{actual mean of the parameter}$

$\epsilon = \text{any positive number}$

$S_x^2 = \text{sample variance, and is given by}$

$$S_x^2 = \frac{1}{N-1} \sum_{i=1}^N (x_i - M)^2 \quad (8)$$

* Reference 9, p. 79.

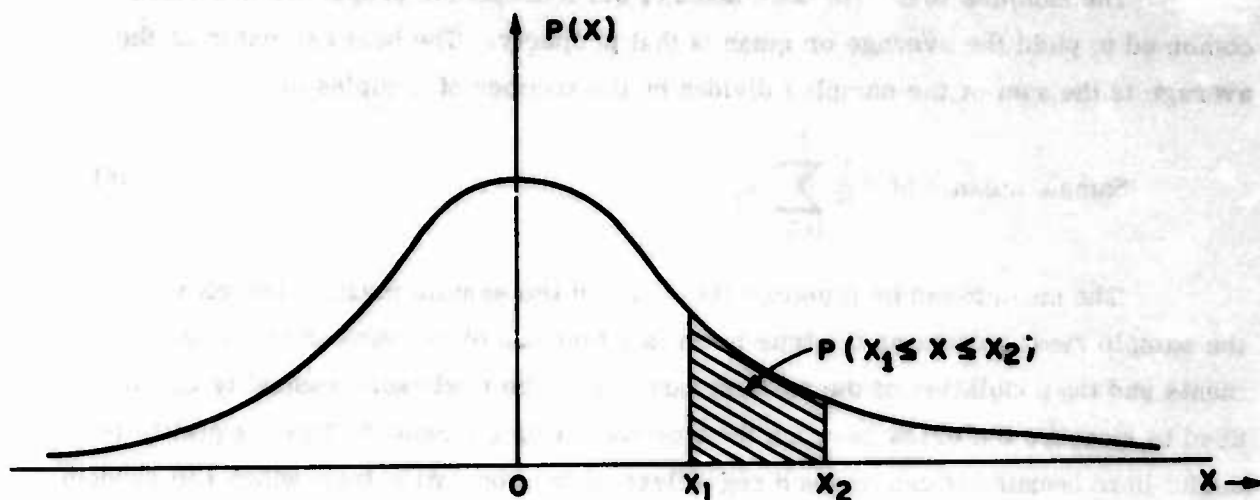


Figure 16. Probability Density Function

If the population variance (σ_x^2) is known, then the sample variance can be replaced by $\frac{\sigma_x^2}{N}$.

A confidence factor in the estimate can be calculated if certain statistics of the population are known; for instance, if many samples of the population are taken and these samples are separated in groups, the distribution of the sample means of these groups will be distributed in a gaussian fashion. If the population variance is known, then the variance of the distribution of sample means (S_m^2) is given by

$$S_m^2 = \frac{\sigma_x^2}{N} \quad (9)$$

where N is the number of samples used to determine the sample mean. Equation (9) can be substituted into Equation (7) to obtain the upper limit on the expected error if the variance of the population is known; however, this method provides an unrealistically high error. Since the sample means will be gaussian distributed with variance given by Equation (9), more precise means of calculating the accuracy of the estimation can be made by use of confidence intervals.

Suppose that a sample of N measurements of a random variable is made and the sample mean, M , is calculated; also, let the population variance of the random variable, σ_x^2 , be known. Because the distribution of sample means is known to be gaussian with mean M_x (the mean of the random variable) and variance $\frac{\sigma_x^2}{N}$ then a confidence interval on the sample mean can be calculated; e.g.,

$$M - 1.64 \frac{\sigma_x}{\sqrt{N}} \leq M_x \leq M + 1.64 \frac{\sigma_x}{\sqrt{N}} \quad (10)$$

with 90 percent confidence. Other confidence factors can be found in tables of the normal curve (Ref. 10). If the variance of the population is not known, the sample variance can be used in Equation (10) with a resulting approximate confidence. The absolute confidence cannot be calculated, but an upper bound can be found by use of the Chebyshev inequality.

b. Usable Mode Probability

The probability that there will be at least one usable mode can be defined as

$$P(\text{usable mode}) = 1 - P(\text{no usable mode})$$

where $P(\bar{x}) = P(\text{no usable mode})$

$$= P(x \text{ does not exist}) + P(\text{SNR} < M) P(x \text{ exists}) \quad (11)$$

x is defined as the dominant mode, and

M is the minimum acceptable SNR based on known system parameters.

Note that, since either the mode exists or it does not, it follows that

$$P(x \text{ does not exist}) + P(x \text{ exists}) = 1 \quad (12)$$

$$P(\bar{x}) + P(x) = 1$$

The probability that the dominant mode does not exist and the probability that the SNR is less than the minimum acceptable level if the dominant mode does exist are found by sampling the HF environment with experiments. Since experimental data are used to estimate the above quantities, there will be estimation errors as discussed previously. To compute this type of error, the terms on the right-hand side of Equation (11) will be handled separately.

The probability that the dominant mode does not exist, $P(x \text{ does not exist})$, is a fixed number for a given set of ionospheric conditions. When the experiment to determine the dominant mode availability is conducted, two outcomes are possible: the dominant mode exists or the dominant mode does not exist. Such a random variable has a Bernoulli probability distribution (Ref. 10). Repeating the experiment for similar ionospheric conditions will result in N samples from which the sample probability that the dominant mode does not exist, $\hat{P}(x \text{ does not exist})$, will be determined. The $\hat{}$ indicates the sample value or estimate of the true quantity. The desired estimate is readily given by

$$\hat{P}(\bar{x}) = \hat{P}(x \text{ does not exist}) = \frac{\text{number of times dominant mode not available}}{\text{number of trials}}$$

Recalling the background discussion, the confidence interval for the true value,

$P(\bar{x})$ can be found as follows if the population variance ($\sigma_{\bar{x}}^2$) is known

$$\hat{P}(\bar{x}) - k \frac{\sigma_{\bar{x}}}{\sqrt{N}} \leq P(\bar{x}) \leq \hat{P}(\bar{x}) + k \frac{\sigma_{\bar{x}}}{\sqrt{N}} \quad (13)$$

where

$\hat{P}(\bar{x})$ = estimate that the dominant mode does not exist

$P(\bar{x})$ = true probability that the dominant mode does not exist

$\sigma_{\bar{x}}$ = standard deviation of the population

k is the factor related to the percent confidence desired; e.g.

k	Confidence Level (percent)
0.25	60
0.52	70
0.84	80
1.28	90
1.96	95

If the population standard deviation is not known, the sample standard deviation can be used to give approximate confidence limits which are reasonably good for large N . In the subject Bernoulli case, the population variance ($\sigma_{\bar{x}}^2$) is a function of the parameter to be estimated and is given by

$$\sigma_{\bar{x}}^2 = P(\bar{x}) [1 - P(\bar{x})] \quad (14)$$

Substituting Equation (14) into (13) yields

$$k \sqrt{\frac{P(\bar{x}) [1 - P(\bar{x})]}{N}} > |P(\bar{x}) - \hat{P}(\bar{x})| \quad (15)$$

Equation (15) can be solved for the true probability that the dominant mode does not exist, $P(\bar{x})$, and results in the following expression for the confidence limits $P(\bar{x})$.

$$\begin{aligned} \frac{1}{1 + k^2/N} \left[\hat{P}(\bar{x}) + \frac{k^2}{2N} - k \sqrt{\frac{\hat{P}(\bar{x}) [1 - \hat{P}(\bar{x})]}{N} - \frac{k^2}{4N^2}} \right] \\ \leq P(\bar{x}) \leq \\ \frac{1}{1 + k^2/N} \left[\hat{P}(\bar{x}) + \frac{k^2}{2N} + k \sqrt{\frac{\hat{P}(\bar{x}) [1 - \hat{P}(\bar{x})]}{N} + \frac{k^2}{4N^2}} \right] \end{aligned} \quad (16)$$

If N is large, the distribution of $P(\bar{x})$ approaches gaussian by virtue of the central limit theorem, and the above table of k versus confidence level may be used directly with but small error to give the desired confidence interval for $P(\bar{x})$.

c. Confidence Limits for $\hat{P}(\text{SNR} < M)$

The method just described to obtain confidence limits for $P(\bar{x})$ can be used to obtain confidence limits for $P(\text{SNR} < M)$, and $P(x \text{ exists})$. These three confidence intervals must be combined, using Equation (11) to obtain the total confidence interval on P (usable mode). The procedure is to combine the distribution of the individual probabilities, $\hat{P}(\bar{x})$, $\hat{P}(\text{SNR} < M)$ and $\hat{P}(x \text{ exists})$, and obtain the distribution of \hat{P} (usable mode).

From Equations (11) and (12),

$$\begin{aligned}\hat{P}(\text{usable mode}) &= \\ &\hat{P}(\bar{x}) + \hat{P}(\text{SNR} < M) \hat{P}(x \text{ exists}) \\ &= 1 - \hat{P}(x \text{ exists}) + \hat{P}(\text{SNR} < M) \hat{P}(x \text{ exists})\end{aligned}\quad (17)$$

The probability estimates on the right-hand side of Equation (17) are gaussian distributed.

The distribution of $\hat{P}(\text{SNR} < M) \hat{P}(x \text{ exists})$ involves the product of two random variables and is derived in Appendix I. Before substituting appropriate values into the expression derived in Appendix I, some simplifying definitions will be made.

Let

$$\begin{aligned}P_1 &= P(\text{SNR} < M) \\ \hat{P}_1 &= \text{estimate of } P_1 \\ \sigma_1 &= \text{standard deviation of } P_1 \text{ given by } \sqrt{P_1 \{1 - P_1\}} \\ P_2 &= P(x \text{ exists}) \\ \hat{P}_2 &= \text{estimate of } P_2 \\ \sigma_2 &= \text{standard deviation of } P_2 \text{ given by } \sqrt{P_2 \{1 - P_2\}}\end{aligned}$$

Then, the density function of $\hat{Z} = \hat{P}_1 \hat{P}_2$ is

$$\frac{1}{2\pi \sigma_1 \sigma_2} \int_0^1 \frac{1}{\hat{P}_1} e^{-\frac{1}{2} \left[\frac{\hat{P}_1 - P_1}{\sigma_1} \right]^2 - \frac{1}{2} \left[\frac{\hat{Z}/\hat{P}_1 - P_2}{\sigma_2} \right]^2} d\hat{P}_1 \quad (18)$$

The density function of $\hat{P}(x \text{ exists})$ is gaussian with mean = $P(x \text{ exists})$ and standard deviation = $\sqrt{P(x \text{ exists}) \{1 - P(x \text{ exists})\}}$.

The density function of $\hat{P}(\text{usable mode})$ is found from the densities of $\hat{P}(x \text{ exists})$ and $P_z(Z)$ given by Equation (18). The final form will not be given here, as it is rather unwieldy and shows no further information. Suffice it to say that the two random variables are combined by convolving their individual density functions.

As experimental data become available in the future, the density of $\hat{P}(\text{usable mode})$ can be found by numerically combining the individual densities. The technique for doing this is discussed in Appendix II.

The Chebyshev inequality -- Equation (7) -- can be used to give an indication of the desired confidence interval for various confidence levels. The needed parameters are the sample mean, the sample variance, and the desired confidence interval (ϵ). The form of the inequality for the probability of a usable mode is

$$P \left[\left| \hat{P}(\text{usable mode}) - P(\text{usable mode}) \right| \geq \epsilon \right] \leq \frac{S_x^2}{N \epsilon^2}$$

The sample variance of the probability of a usable mode can be obtained by applying the delta process to Equation (17). This involves taking the implicit derivative of Equation (17), squaring the result, and taking the expected value. The implicit derivative is

$$\begin{aligned} \delta \hat{P}(\text{usable mode}) = & \\ - \delta \hat{P}(x \text{ exists}) + \hat{P}(\text{SNR} < M) \delta \hat{P}(x \text{ exists}) & \\ + \hat{P}(x \text{ exists}) \delta \hat{P}(\text{SNR} < M) & \end{aligned}$$

In squaring the above equation and taking the expected value of the result, it should be noted that the cross terms will be zero, since it will be assumed that $\hat{P}(x \text{ exists})$ and $\hat{P}(\text{SNR} < M)$ are independent. The remaining terms which define the variance of $\hat{P}(\text{usable mode})$ are

$$\begin{aligned} \sigma^2_{\hat{P}(\text{usable mode})} = S_x^2 = & \\ \left[1 + \hat{P}(\text{SNR} < M) \right] \sigma^2_{\hat{P}(x \text{ exists})} & \\ + \hat{P}(x \text{ exists}) \sigma^2_{\hat{P}(\text{SNR} < M)} & \end{aligned} \quad (19)$$

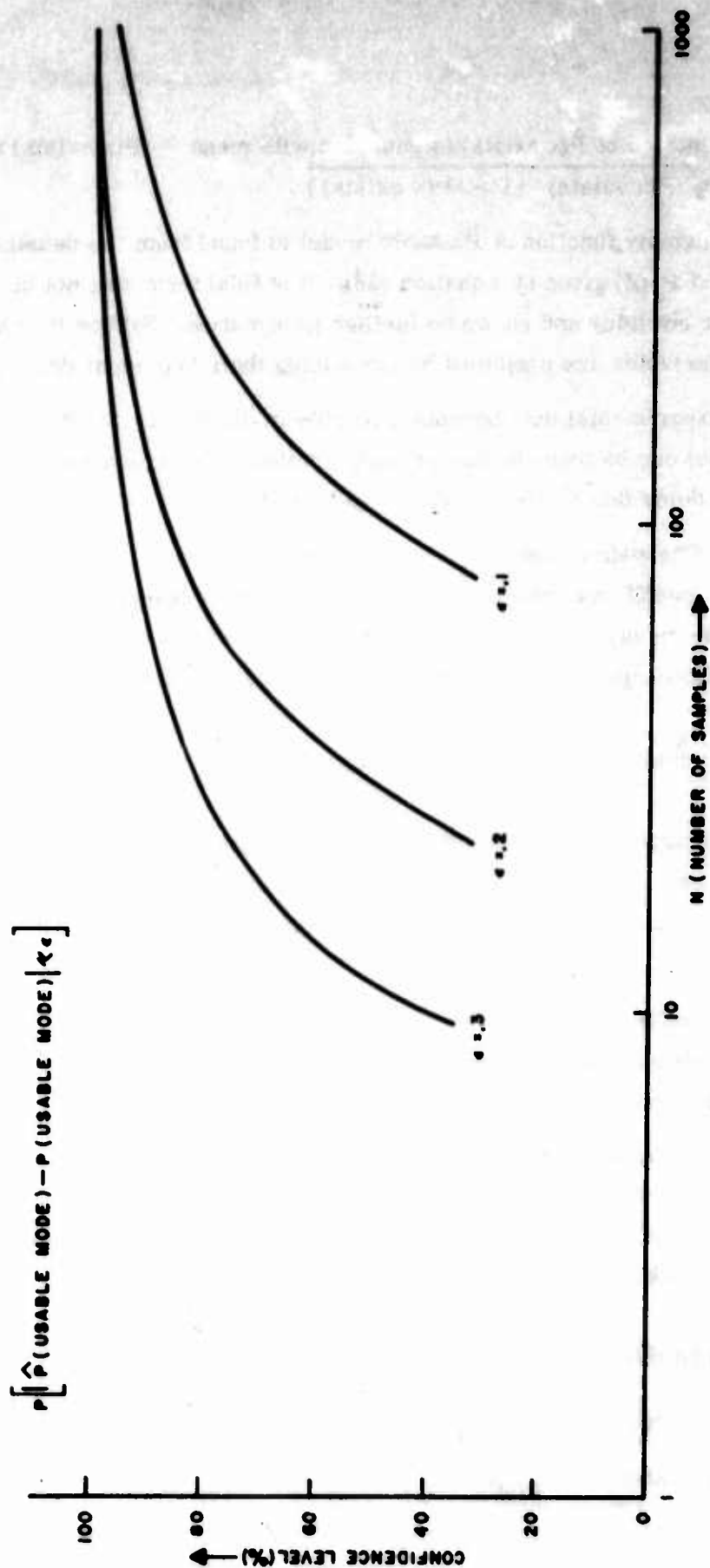


Figure 17. Usable Mode Confidence/Level vs. Number of Samples

Some numerical results can be obtained if the variances in Equation (19) are replaced by the population variances of Bernoulli-type probabilities. This yields

$$S_x^2 = \{1 + \hat{P}(\text{SNR} < M)\} \hat{P}(x \text{ exists}) \{1 - \hat{P}(x \text{ exists})\} + \hat{P}(x \text{ exists}) \hat{P}(\text{SNR} < M) \{1 - \hat{P}(\text{SNR} < M)\} \quad (20)$$

The final expression is obtained by substituting the above into the Chebyshev inequality and is as follows

$$P \left[\left| \hat{P}(\text{usable mode}) - P(\text{usable mode}) \right| \geq \epsilon \right] \leq \frac{1}{N\epsilon^2} \left\{ \left[1 + \hat{P}(\text{SNR} < M) \right] \hat{P}(x \text{ exists}) \left[1 - \hat{P}(x \text{ exists}) \right] + \hat{P}(x \text{ exists}) \hat{P}(\text{SNR} < M) \left[1 - \hat{P}(\text{SNR} < M) \right] \right\} \quad (21)$$

A form of Equation (21) is plotted in Figure 17 parametric in ϵ , the confidence interval. The equation gives the probability that the difference between the estimate, $\hat{P}(\text{usable mode})$, and the actual value, $P(\text{usable mode})$, will be greater than or equal to ϵ ; however, it is more convenient to consider the probability that the difference between the estimate and actual value will be less than or equal to ϵ , so this has been done in plotting Figure 17. This confidence is plotted as a function of the number of samples with ϵ (the confidence interval) as a parameter. A typical example shows that about 260 samples are required to give an interval of ± 0.1 ($\epsilon = 0.1$) with a confidence of 80 percent. This means that the actual mode usability, $\hat{P}(\text{usable mode})$, can be expected to fall within ± 0.1 (10 percent) of the measured mode usability, $P(\text{usable mode})$, with 80 percent confidence. The details for calculating the confidence limits are given in Appendix III.

In using Figure 17 it should be remembered that the Chebyshev inequality was used so that the resulting confidence interval represents the ultimate bounds on the actual value; i. e., these results are pessimistic. When information on the statistics (actual or estimates) of the measured parameters is obtained, the confidence interval can be reduced.

SECTION III

MODE RELIABILITY EXPERIMENT

1. INTRODUCTION

The characteristics and availability of the first-order modes provide a basis for determination of the best modes and frequencies to use for OHR applications and the reliabilities that may be expected within the bounds of a wide range of environmental parameters. Among these parameters are time of day, month, and sunspot number; location in the equatorial, midlatitude, or polar region; paths that are east-west within these zones or north-south within or across from one zone to another; and natural factors such as flares and magnetic storms that effectively modify the ionosphere.

Data assembled in a form adequate for consideration in this study have been gathered on a 2000-nmi south-north path from a site located in the equatorial zone to a midtemperate zone site (Coco Solo (Canal Zone) to Central New York State) and from a polar location (Thule, Greenland) to the same receiving area. Approximately 21 months of data are included in this report from the first path (December 1965 to August 1967) and six months on the latter path (December 1966 to May 1967). These data were gathered at a time starting shortly after the sunspot minimum had been reached; thus, at this writing, variations across the 11-year sunspot cycle will have to be determined on the basis of the available propagation literature in addition to the trends of the measurement data reported in this document.

The oblique propagation modes that have appeared to be most useful on the paths mentioned above are the one-hop F2 (1F2), the two-hop F2 (2F2), and the two-hop E (2E). A hybrid of one E-layer reflection and one F-layer reflection -- the N mode -- appears to frequently fill a vacancy at the low frequency end of the 1F2 mode and as such has received full consideration. An M mode, consisting of two F2-layer reflections and one reflection from the top of the E layer at the midpath, may sometimes be used, but has been available such a small percentage of the time that complete analysis of this mode has not been conducted. For the latter portion of the observation period, the two-hop sporadic-E mode (2E_s) has been included. This is generally not a dependable mode for operating purposes, but does sometimes indicate the presence of an LOF cutoff for other modes.

The sources of the basic information used in these investigations are oblique ionograms taken over the indicated paths. For a clearer understanding of the indicated availabilities, the equipment limitations with respect to propagation and ambient factors should also be considered. Equipment sensitivity and ambient noise levels are such that the measured availability of signals and values of MOF-JF are usually independent of the equipment and wholly dependent on propagation conditions. On the other hand, the LOF, with the exception of E-layer cutoff, depends on a number of factors such as transmitter power, antenna to equipment coupling losses, antenna gains, total receiving system noise figure, and ambient noise level at the receiving site.

For the purposes of this investigation, the following division of the year into four seasons was made. This division is the same as that employed for reporting the characteristics of atmospheric noise in CCIR Report 322 (Ref. 8).

SEASON	MONTHS
Winter	December, January, February
Spring	March, April, May
Summer	June, July, August
Autumn	September, October, November

In the sections to follow on the Mode Reliability Experiment, the data base for this experiment will be reviewed on a seasonal basis indicating the number of samples available as a function of time of day for each of the dominant modes: 2E, 1F2, N, 2F2, and 2E_g. Hourly mode availability tables are provided for those months that this information is not already available in earlier reports (Refs. 4 and 6).

The mode availability for the Coco Solo path is next presented on a seasonal basis for the dominant modes, covering a period of seven seasons. The Thule mode availability results are then described for two seasons. This is followed by a discussion of the frequency aperture availability and MOF-JF availability for both the Coco Solo and Thule paths. The percentage of time that various combinations of modes are not available on the Coco Solo path is reviewed, pointing out that at any

time when measurements were taken at least one of the following modes was available: 2E, 1F2, and 2F2. A statistical summary of the various mode reliability results is provided on a seasonal basis dividing a 24-hour day into three major time periods: daytime, nighttime, and dusk. This part of the report concludes with a discussion of an investigation to relate various mode reliability results to different natural factors such as solar flares and magnetic disturbances.

2. SUMMARY OF OBSERVATIONS BY SEASON

a. Coco Solo to Stockbridge/Starr Hill

A graphical hourly summary of observations and signals (modes) seen for the mode reliability experiment has been prepared on a seasonal basis. These are shown for the Coco Solo to Stockbridge/Starr Hill path in Figures 18 through 47 for the five dominant modes: 2E, 1F2, N, 2F2 and 2E_s. These graphs serve in effect as a means of quickly indicating the approximate data base for the seasonal information presented in this section, and also as an approximate indication of the mode availability in that this is equal to the number of signals seen divided by the number of observations made that would permit seeing a mode on a given ionogram. For example, for the winter of 1966 for the 2E mode (Figure 18), we note minimum observations of eight and minimum signals seen of seven; also maximum observations and signals seen of eighteen. For the 2E mode in the spring of 1966 (Figure 19), nighttime observations are about the same as for winter, and the number of signals seen are much less than the observations at night, but in the daytime there are a large number of observations and signals are seen with what would be almost perfect availability.

Nighttime observations for the summer of 1966 (Figure 20) are still about the same, but midday observations are slightly greater in number. The same holds for autumn of 1966 (Figure 21), but it is noted that the signals seen are much fewer than previously noted. The maximum daytime observations at noon in autumn ran as high as 50. They are slightly less in the winter of 1967 (Figure 22) and the further drop in the spring of 1967 (Figure 23) in number of observations is due to the move to the new receiving site during this period. It is obvious that a similar, but not necessarily exactly the same, number of observations were obtained for the other modes. While the information for each of these modes was taken from the same ionogram, various factors prevented adequate observation of all modes at the same time. Chief among

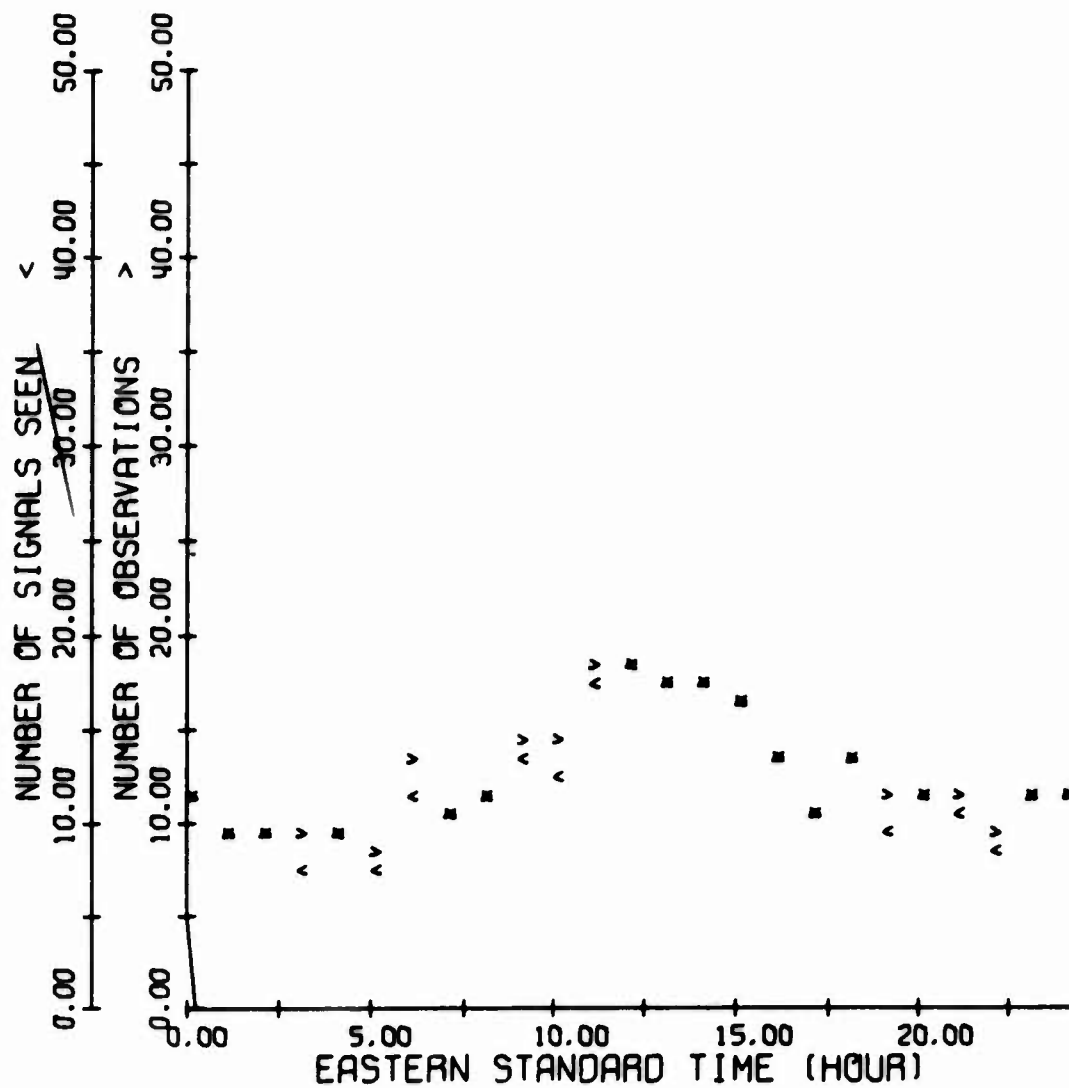


Figure 18. Summary of 2E Mode Observations, Coco Solo Path, Winter 1966

these were problems in photography, and high noise/interference levels at the lower frequencies which prevented observation of the high order modes. These graphical summaries provide a composite of the data previously included in the hour, day, month mode tables contained in the interim reports published on this program (Refs. 4 and 6) and in Tables II through VIII. These later tables cover the months of December 1965 and January 1966, and the period from March through August 1967; with the ones published earlier they form a complete set of the basic mode availability information.

Tables II through VIII provide a summary, by day and hours, of all data collected during the periods mentioned above. In turn, this provides the basis for all mode availability information. The rows represent the hours from 0100 to 2400 EST or 0100 to 2400 GMT as indicated, while the columns represent the dates for which data are available. The heading 8 2 stands for August 2. In each of the entries the number "1" stands for propagation (signal observed) by the 2E mode for the hour and date in question, "2" stands for the 1F2 mode, "3" the N mode, "4" the 2F2 mode, and "0" indicates no signal observed via a particular mode for this hour and date. A blank where a number should appear indicates that the ionogram for the hour and date in question could not be satisfactorily interpreted to determine if this particular mode is present or not. For sporadic-E propagation, the number "5" indicates that the $2E_s$ mode is present. No "0" representation is used to show the absence of the $2E_s$ mode when it could have been observed on the ionogram record; hence, all blank spaces in the 5 column are assumed to be 0's. This was done on the assumption that only a small amount of $2E_s$ propagation would be present. It is noted that these tables, in effect, are truth tables and provide a convenient reference for other plots and tabulations of this mode availability information.

It is noted that no graphical summary of observations for the $2E_s$ mode is included until the spring of 1967, while $2E_s$ data reduction began in the summer of 1966. Some question existed during this time with respect to their inclusion and, hence, to the method of handling the $2E_s$ data. There is still some question as to the identification of the $2E_s$ mode, but full consideration as a mode begins with spring of 1967. There is a quite small availability of the mode during these months (Figure 46). For the summer of 1967 (Figure 47) a more nearly equal day/night observation exists and more signals were also seen.

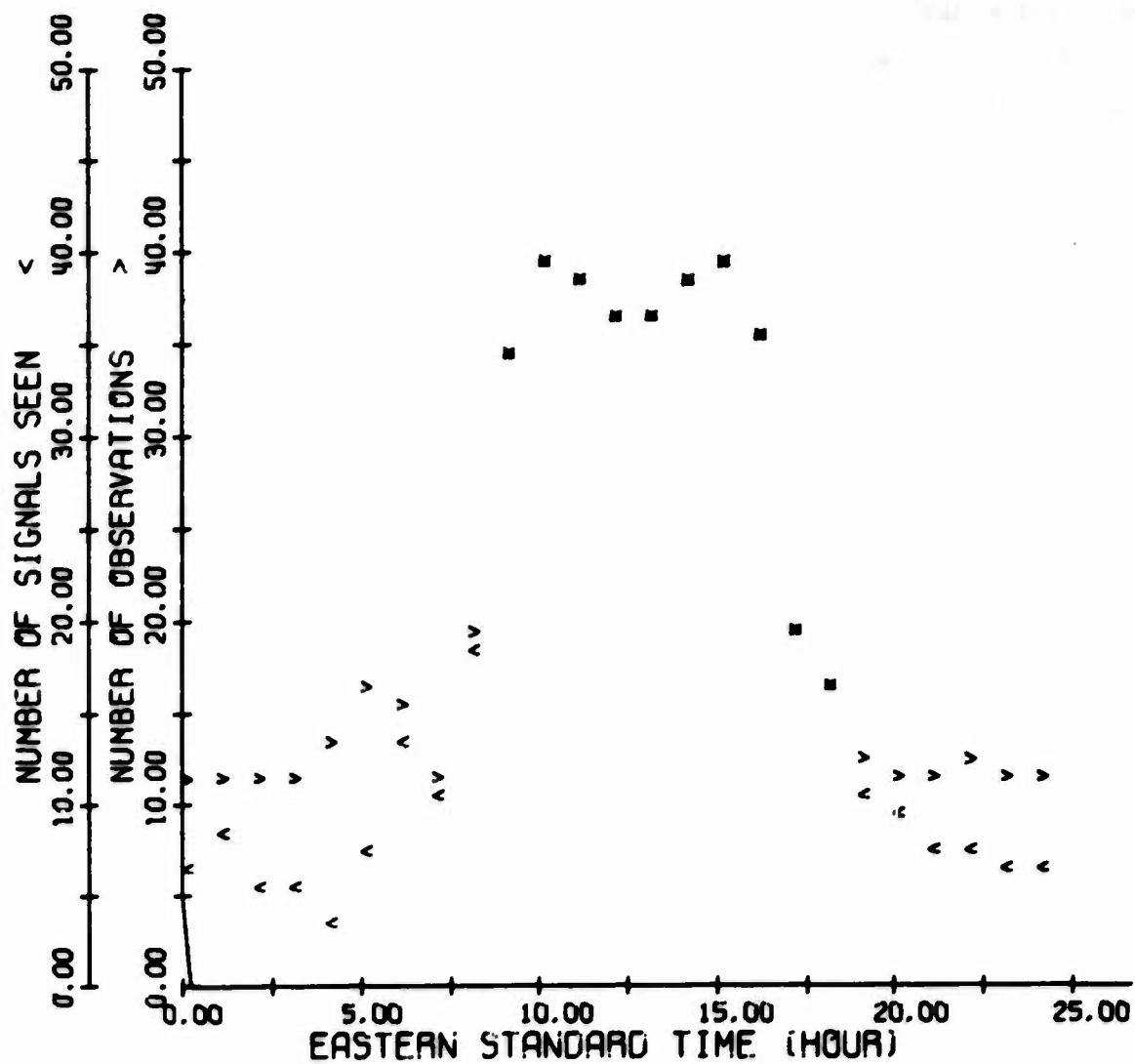


Figure 19. Summary of 2E Mode Observations, Coco Solo Path, Spring 1966

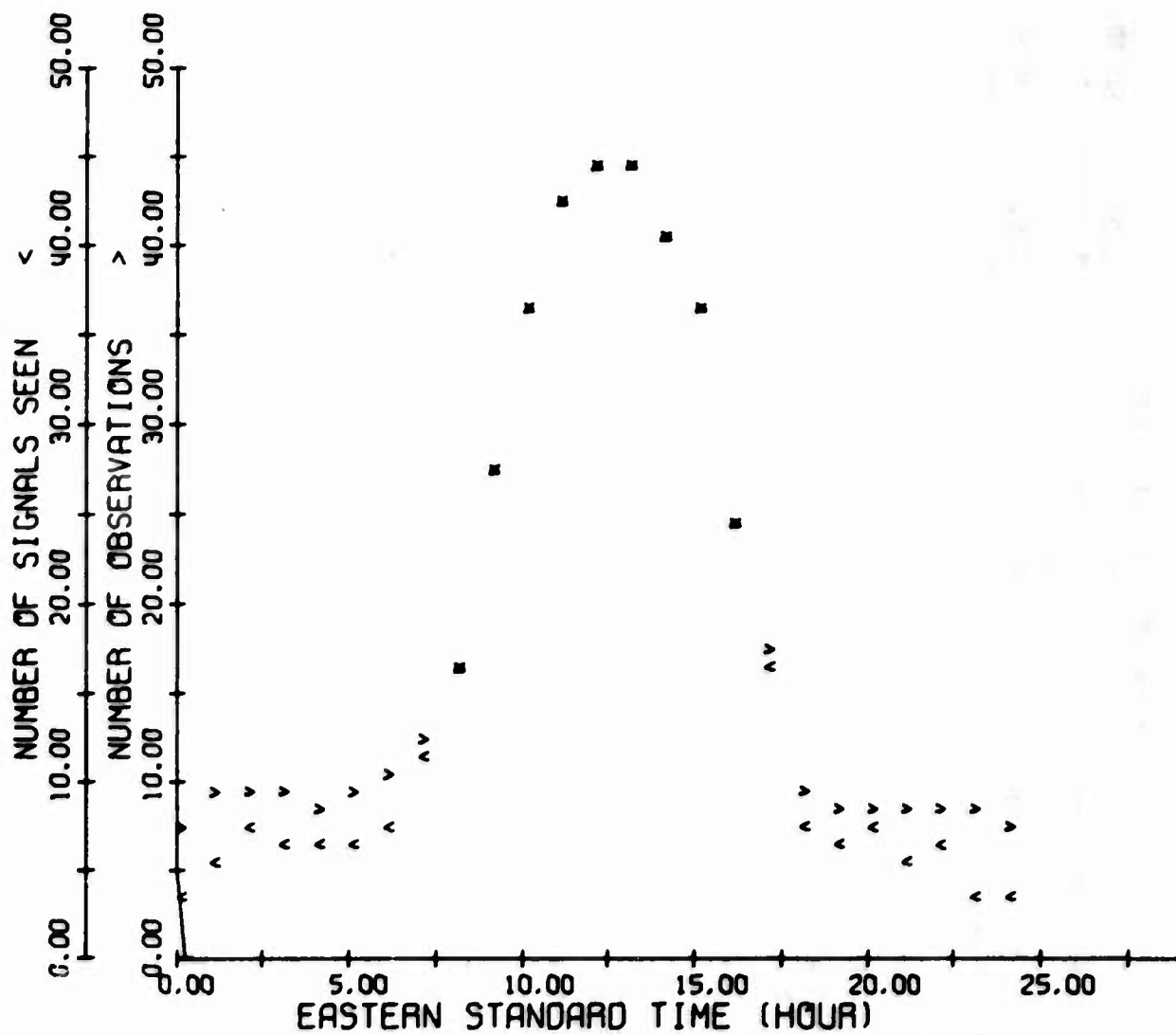


Figure 20. Summary of 2E Mode Observations, Coco Solo Path, Summer 1966

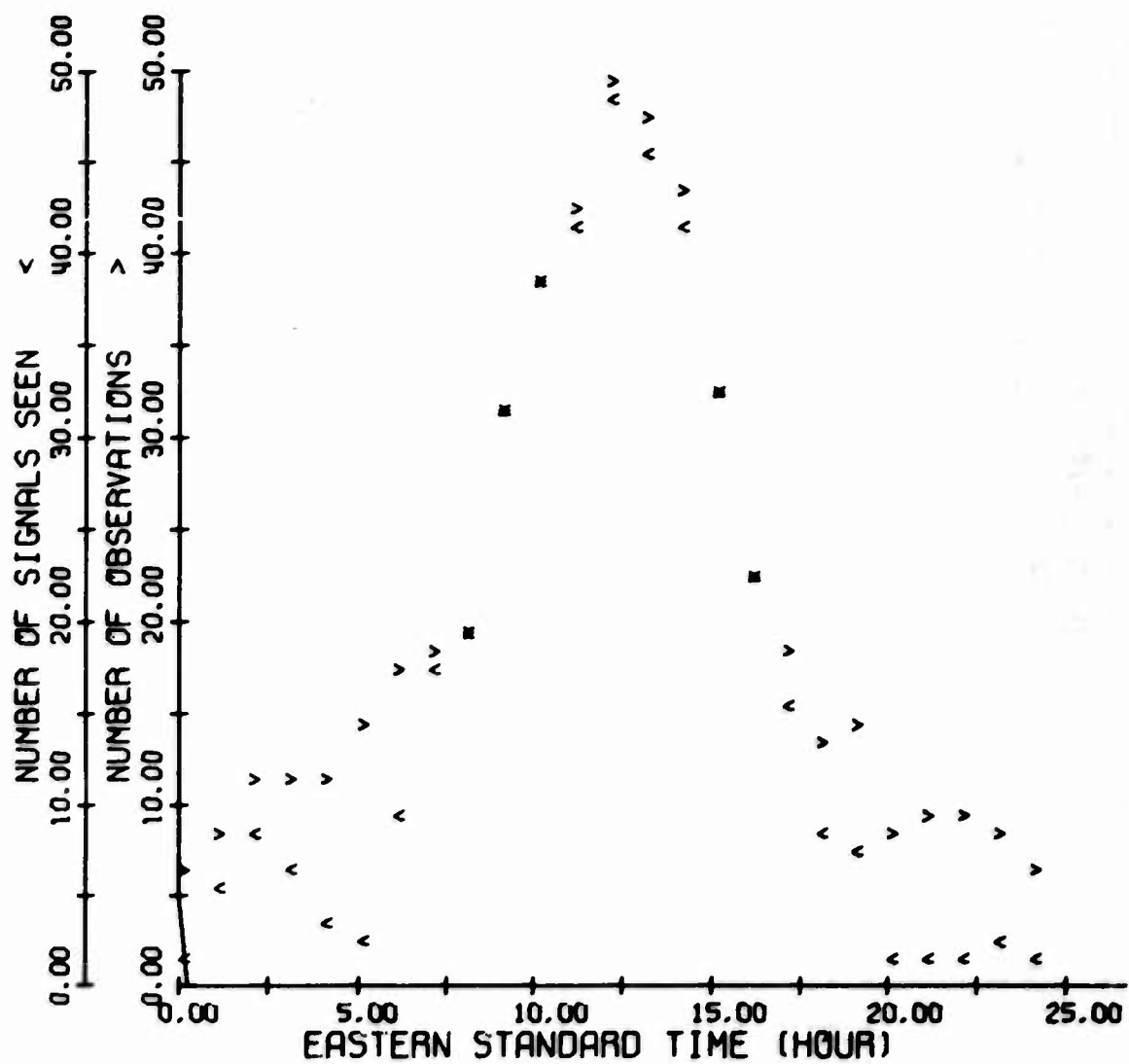


Figure 21. Summary of 2E Mode Observations, Coco Solo Path, Autumn 1966

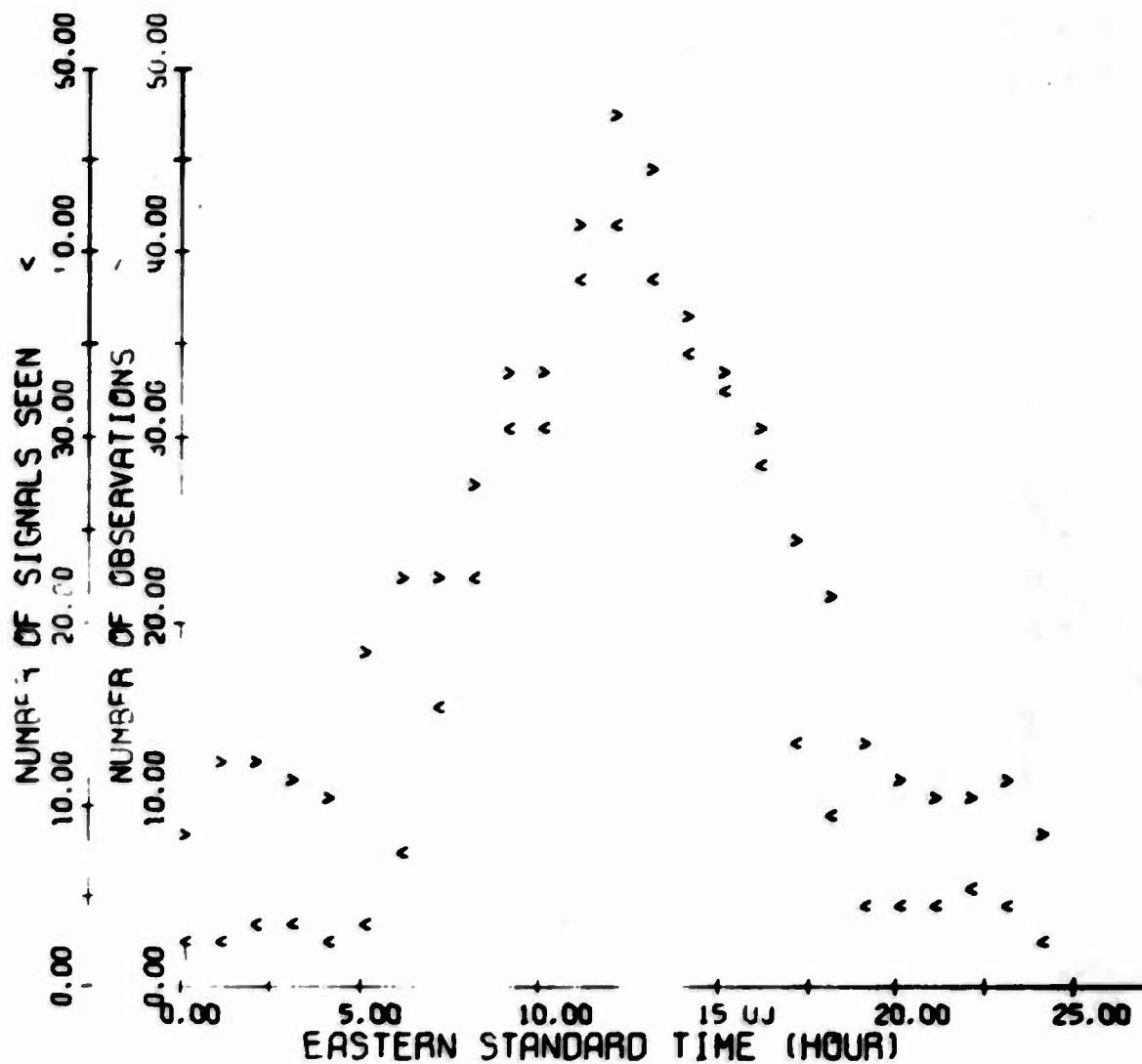


Figure 22. Summary of 2E Mode Observations, Coco Solo Path, Winter 1967

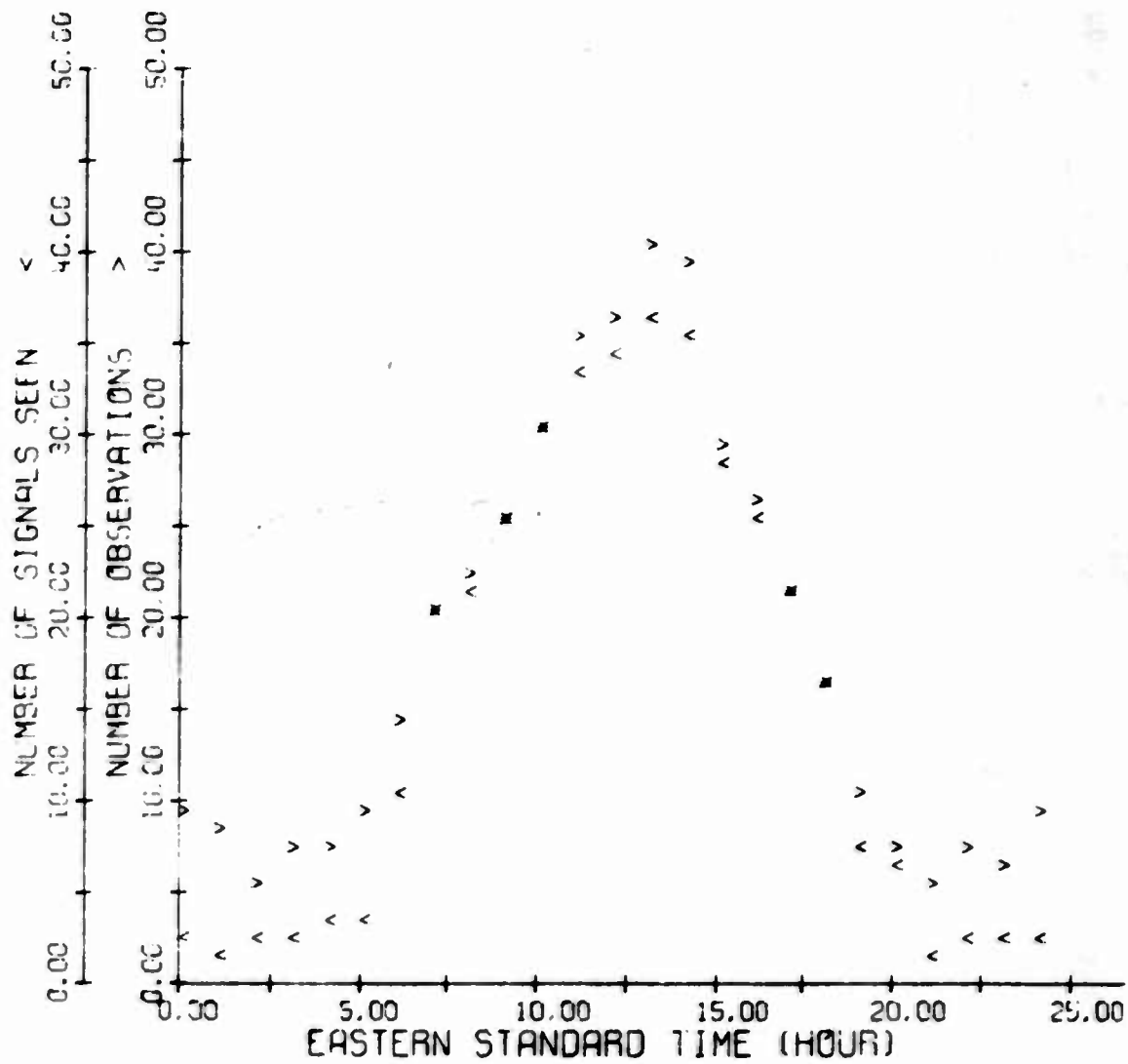


Figure 23. Summary of 2E Mode Observations, Coco Solo Path, Spring 1967

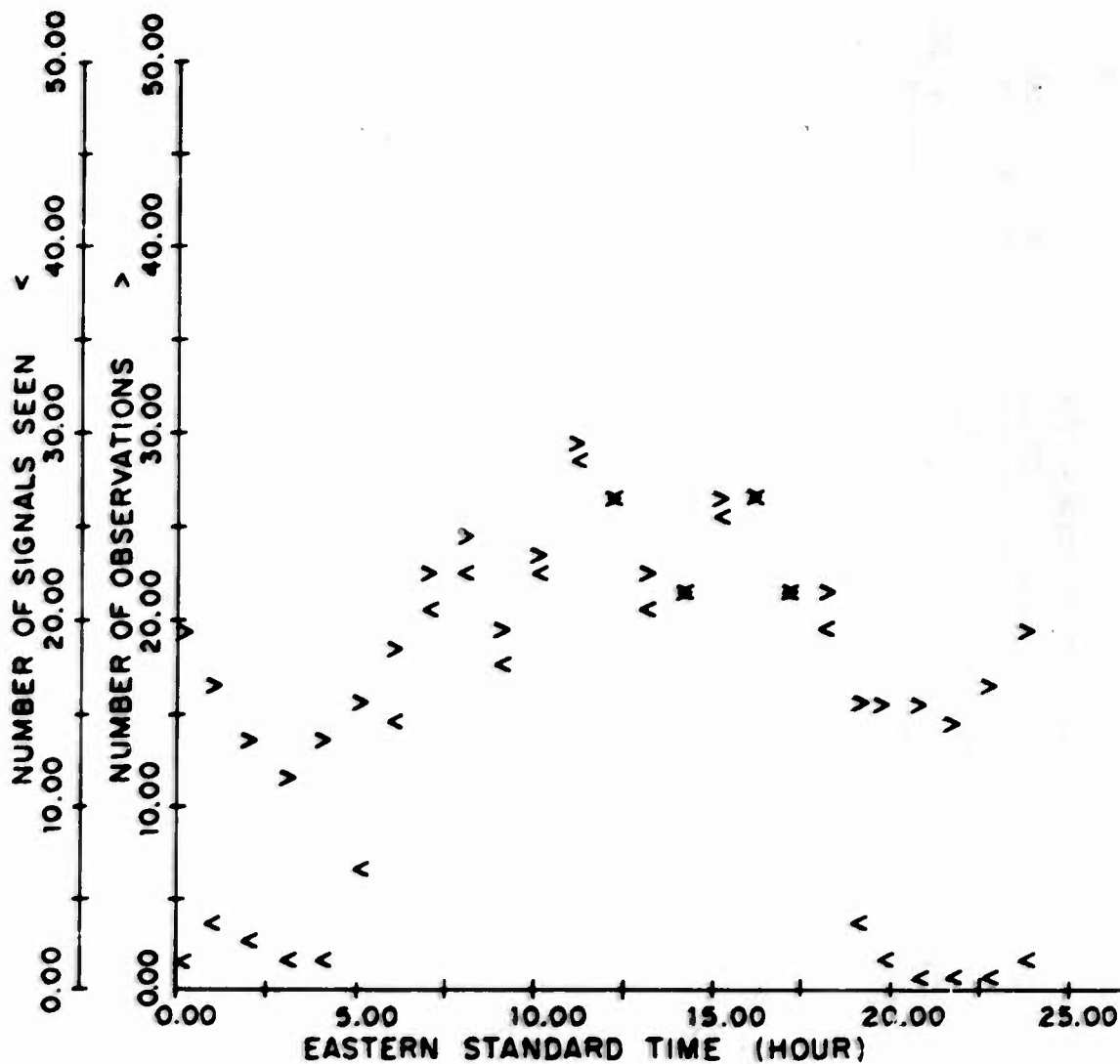


Figure 24. Summary of 2E Mode Observations, Coco Solo Path, Summer 1967

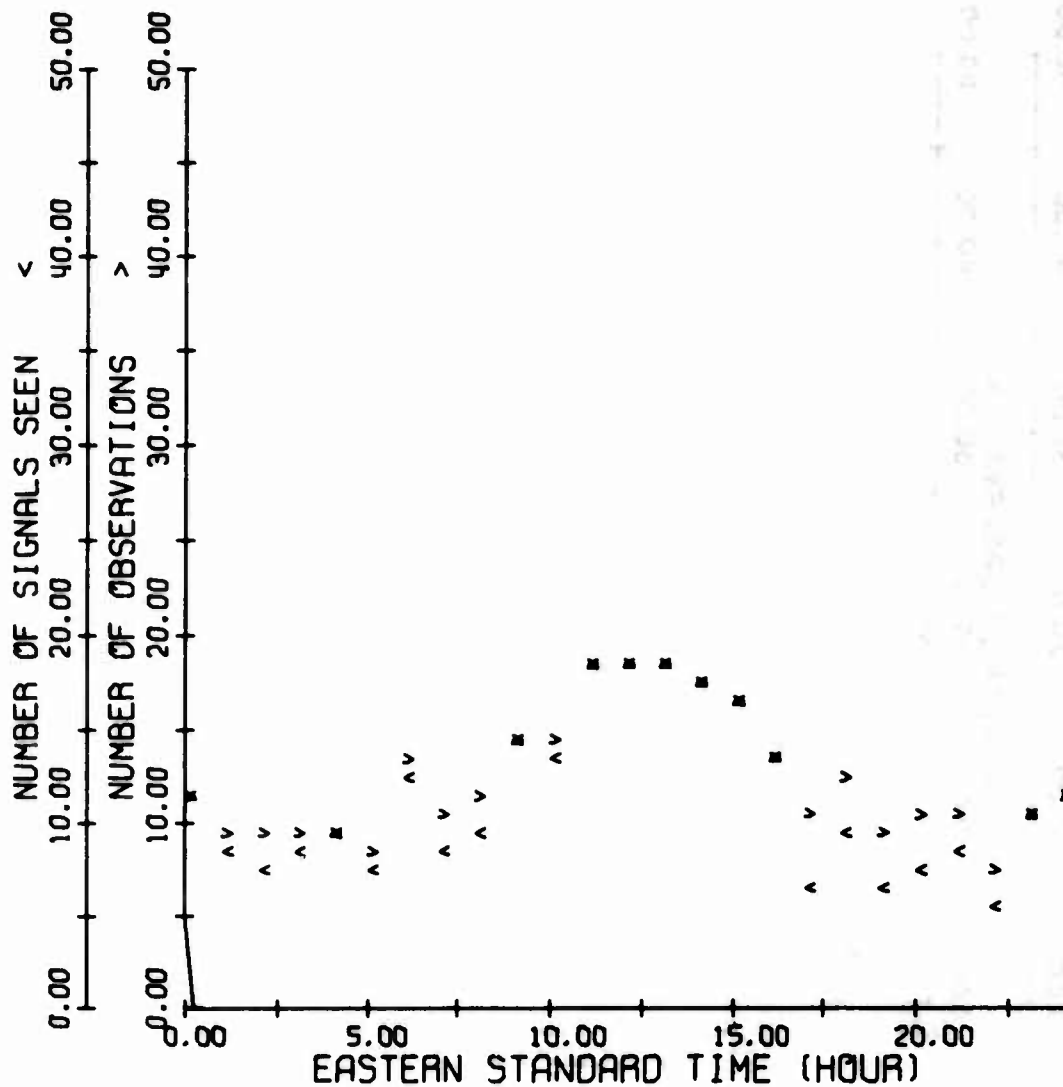


Figure 25. Summary of 1F2 Mode Observations, Coco Solo Path, Winter 1966

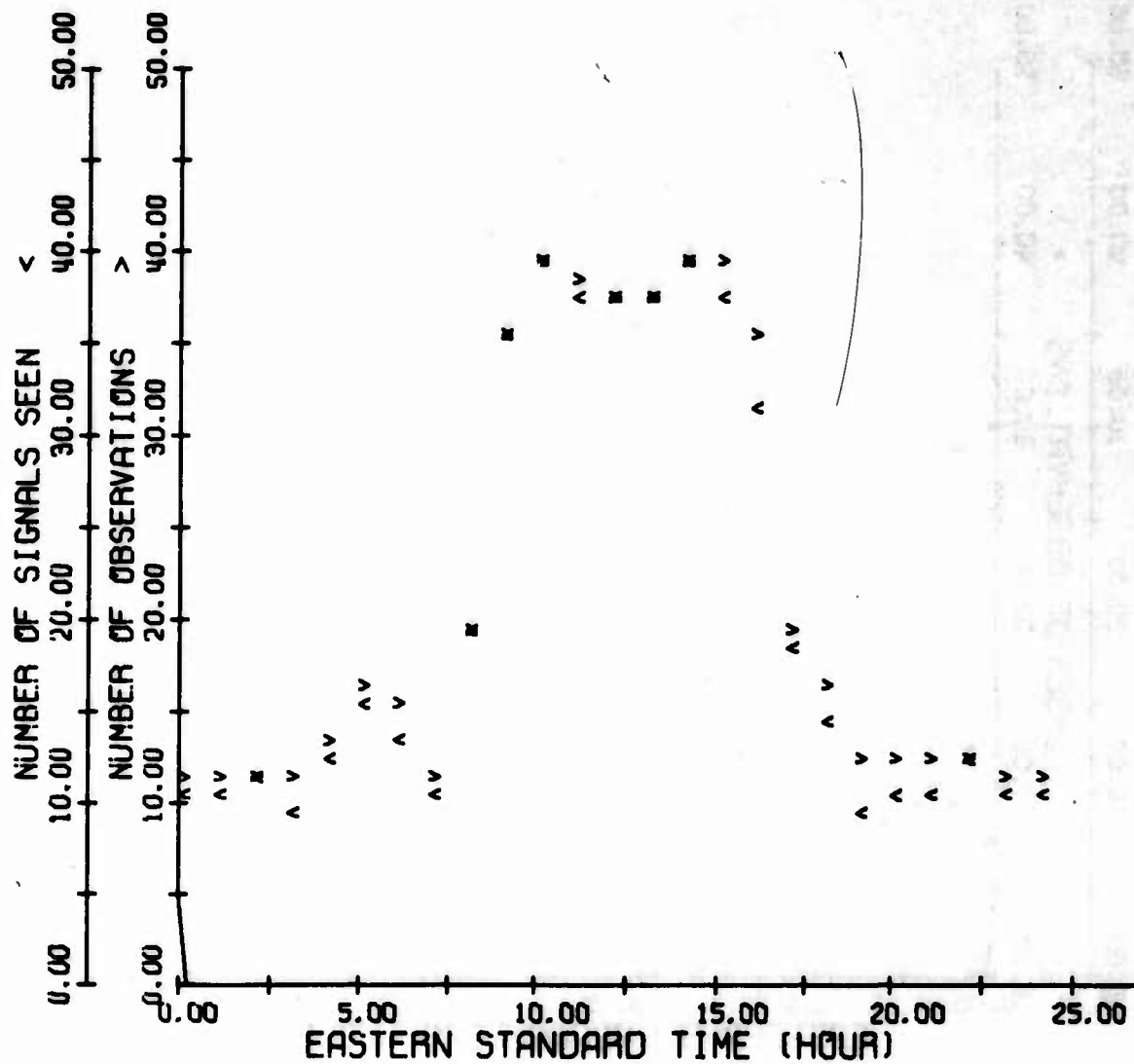


Figure 26. Summary of 1F2 Mode Observations, Coco Solo Path, Spring 1966

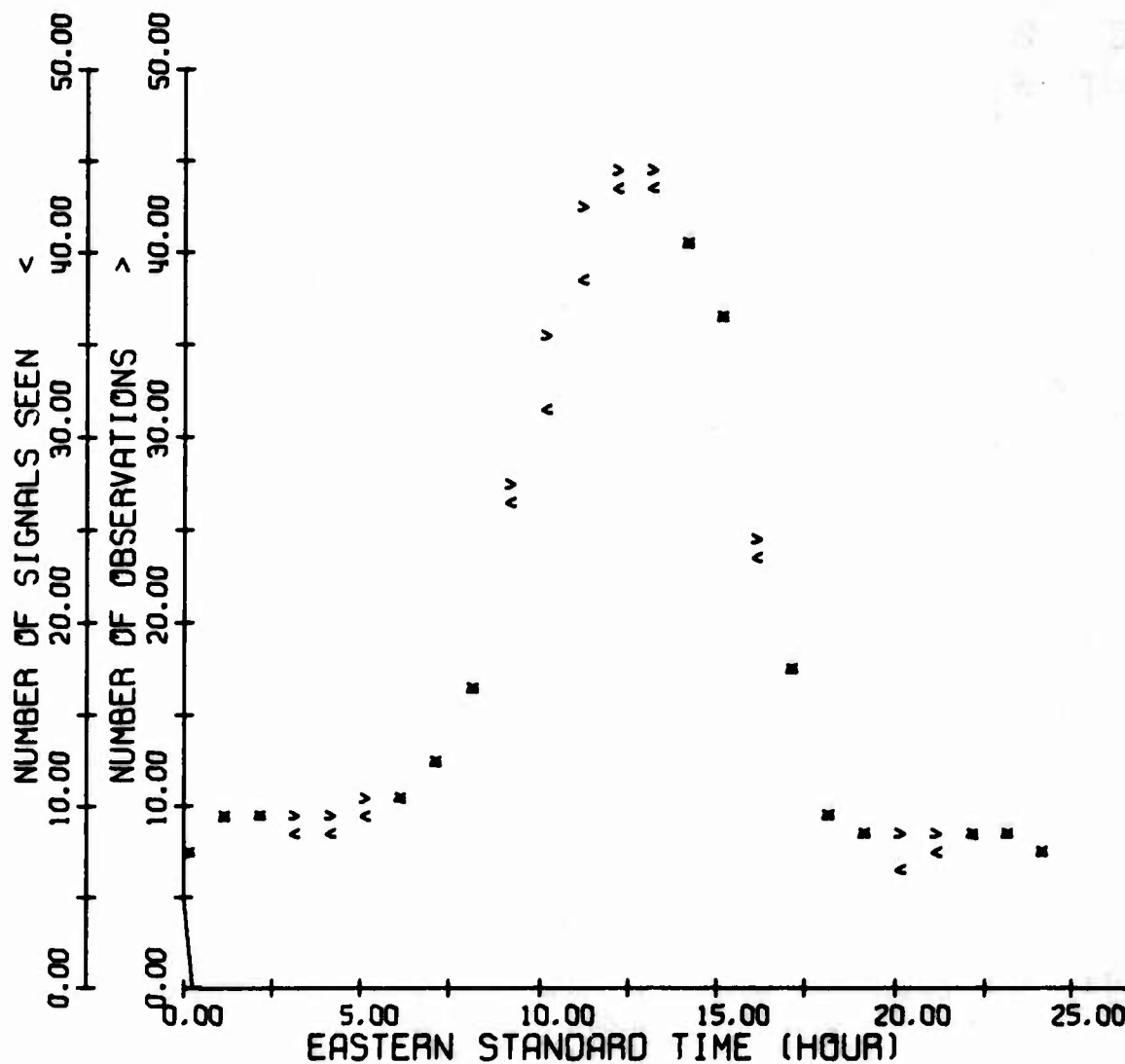


Figure 27. Summary of 1F2 Mode Observations, Coco Solo Path, Summer 1966

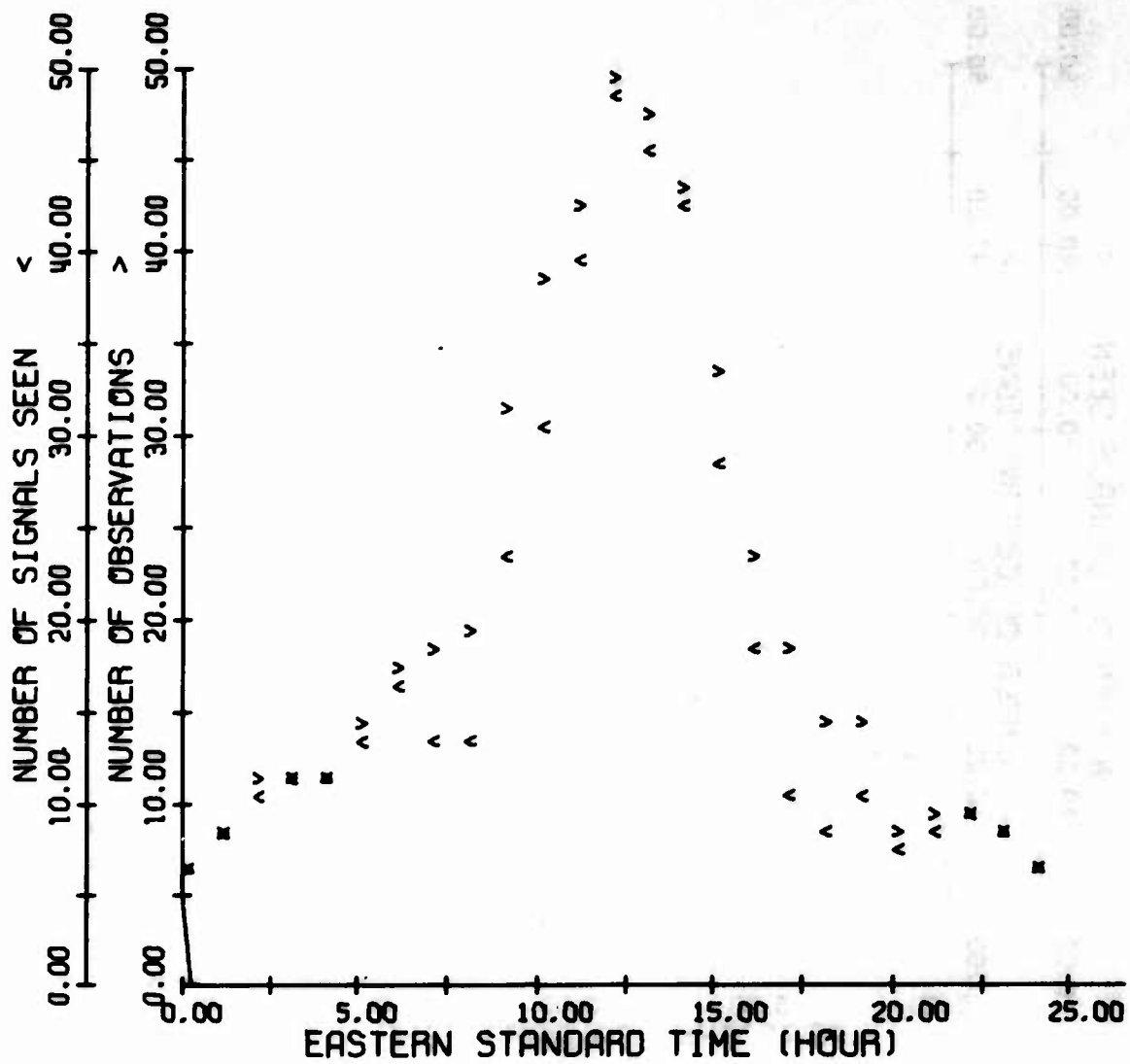


Figure 28. Summary of 1F2 Mode Observations, Coco Solo Path, Autumn 1966

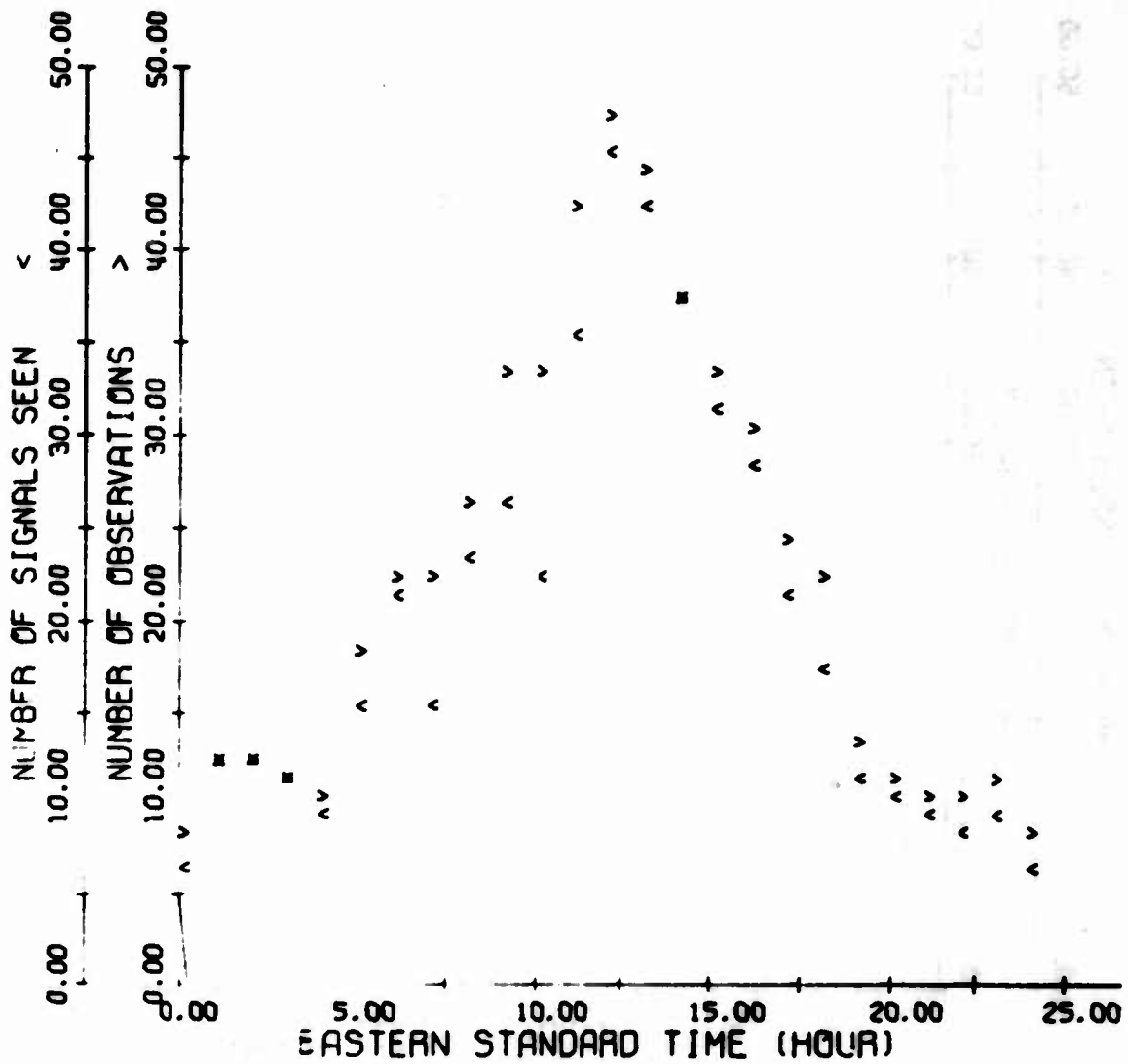


Figure 29. Summary of 1F2 Mode Observations, Coco Solo Path, Winter 1967

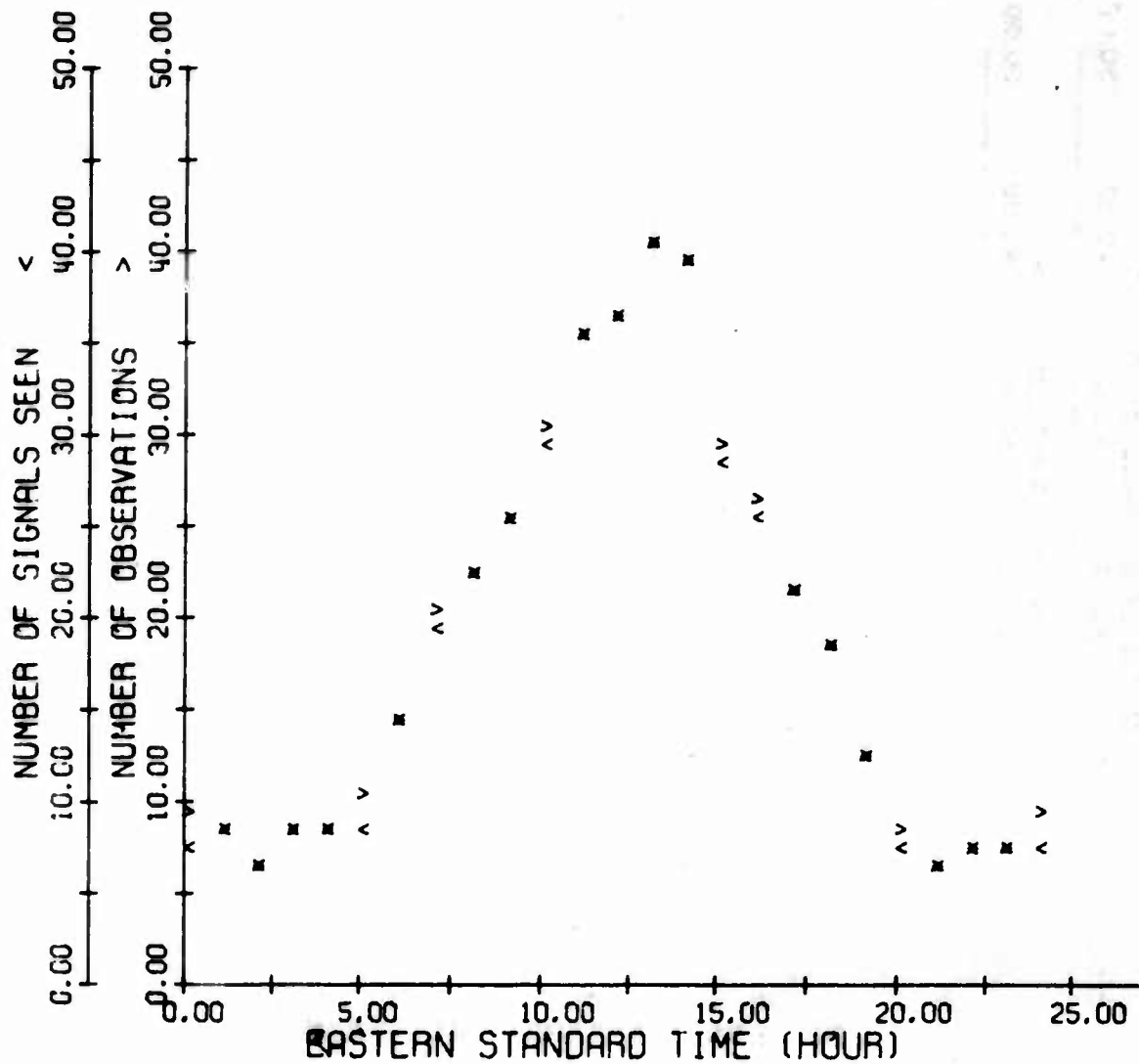


Figure 30. Summary of 1F2 Mode Observations, Coco Solo Path, Spring 1967

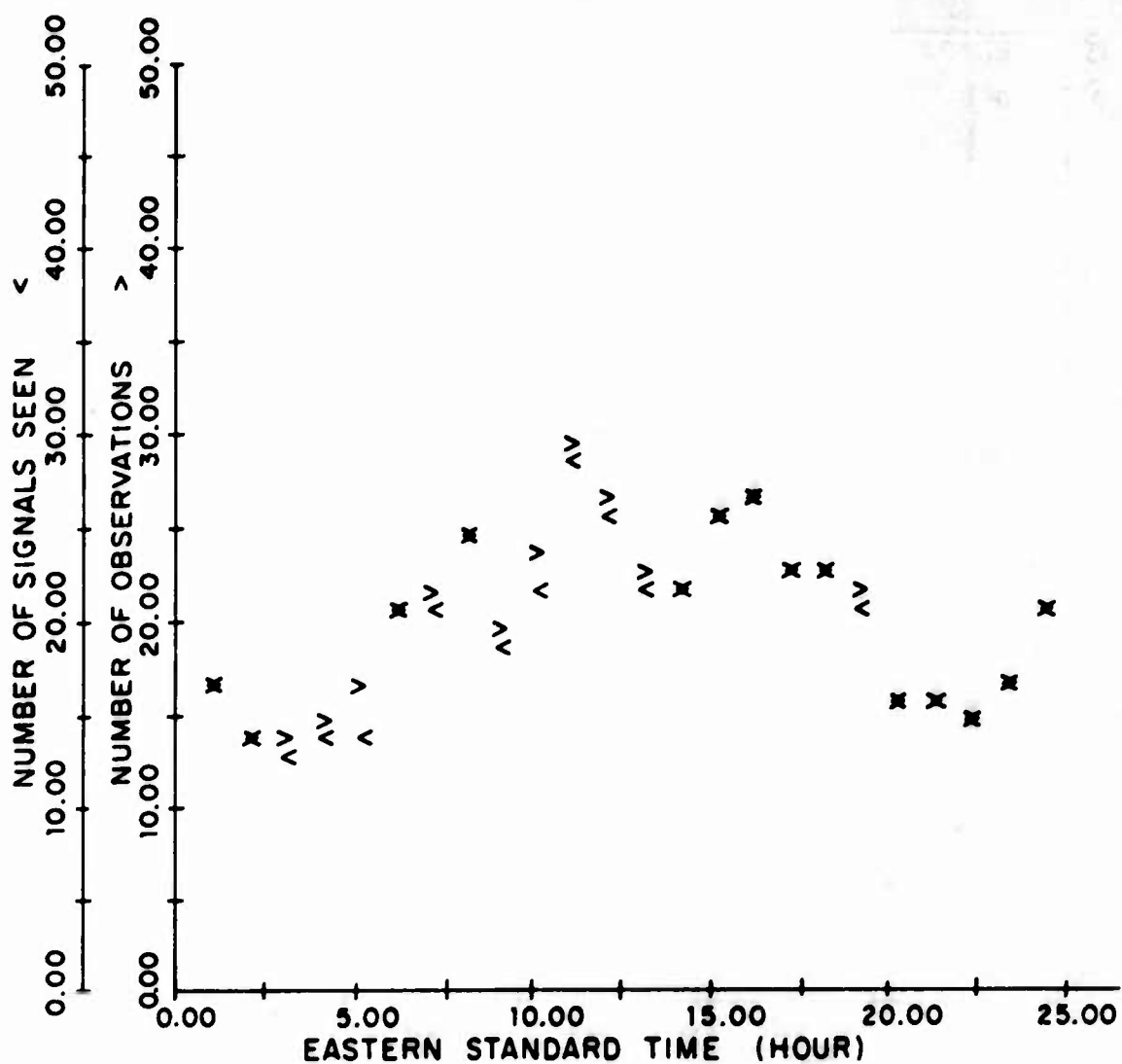


Figure 31. Summary of 1F2 Mode Observations, Coco Solo Path, Summer 1967

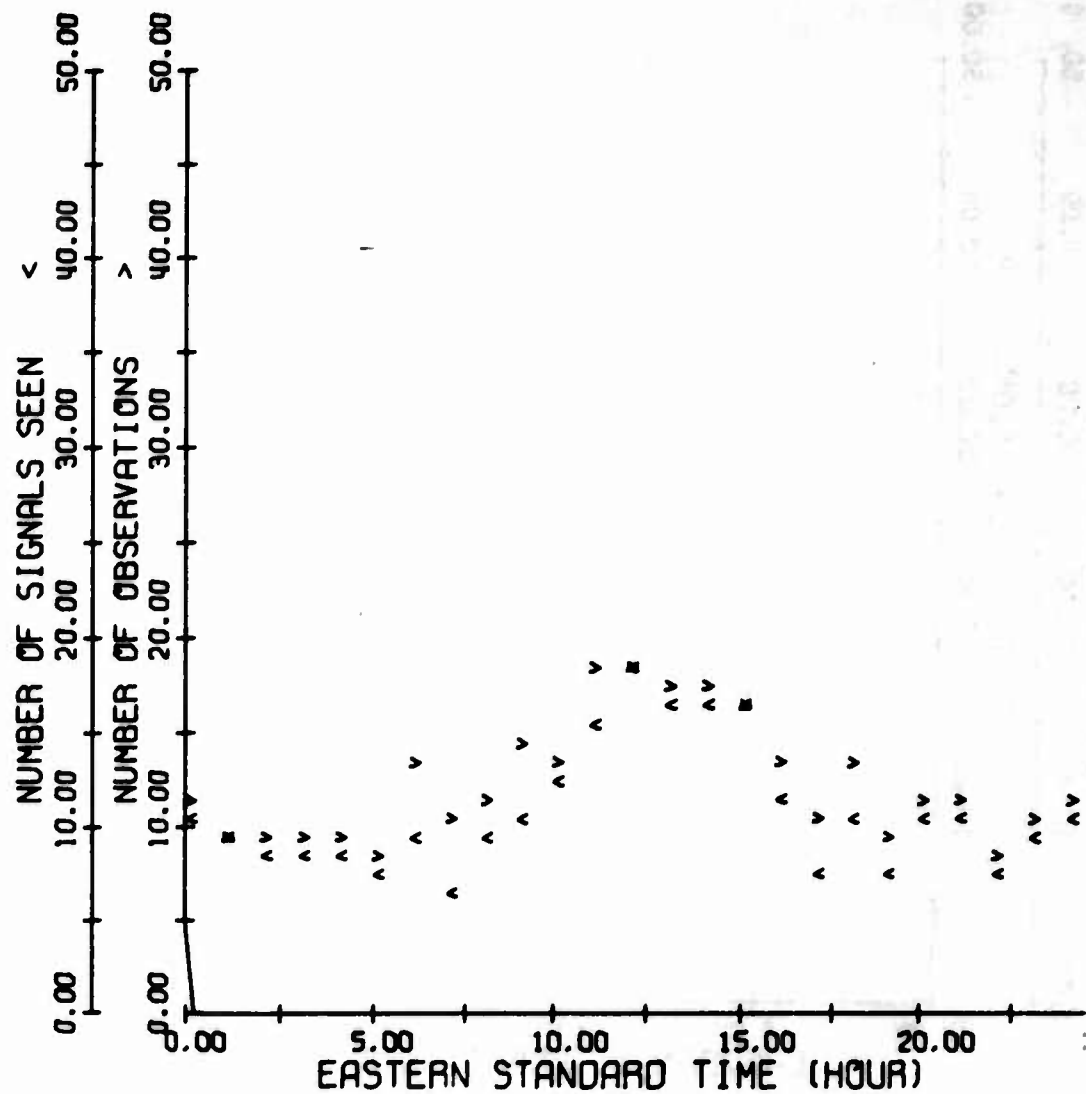


Figure 32. Summary of N Mode Observations, Coco Solo Path, Winter 1966

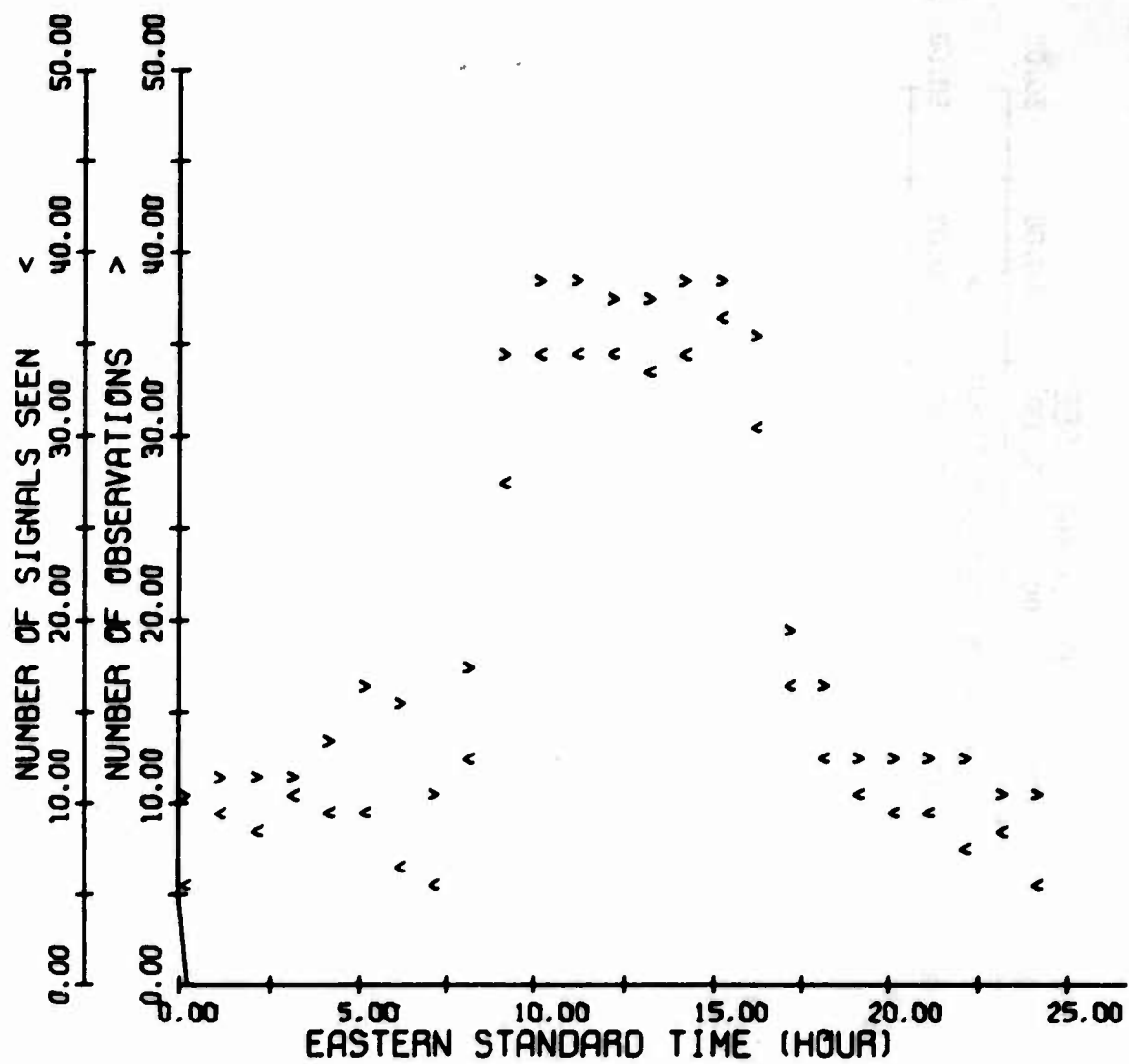


Figure 33. Summary of N Mode Observations, Coco Solo Path, Spring 1966

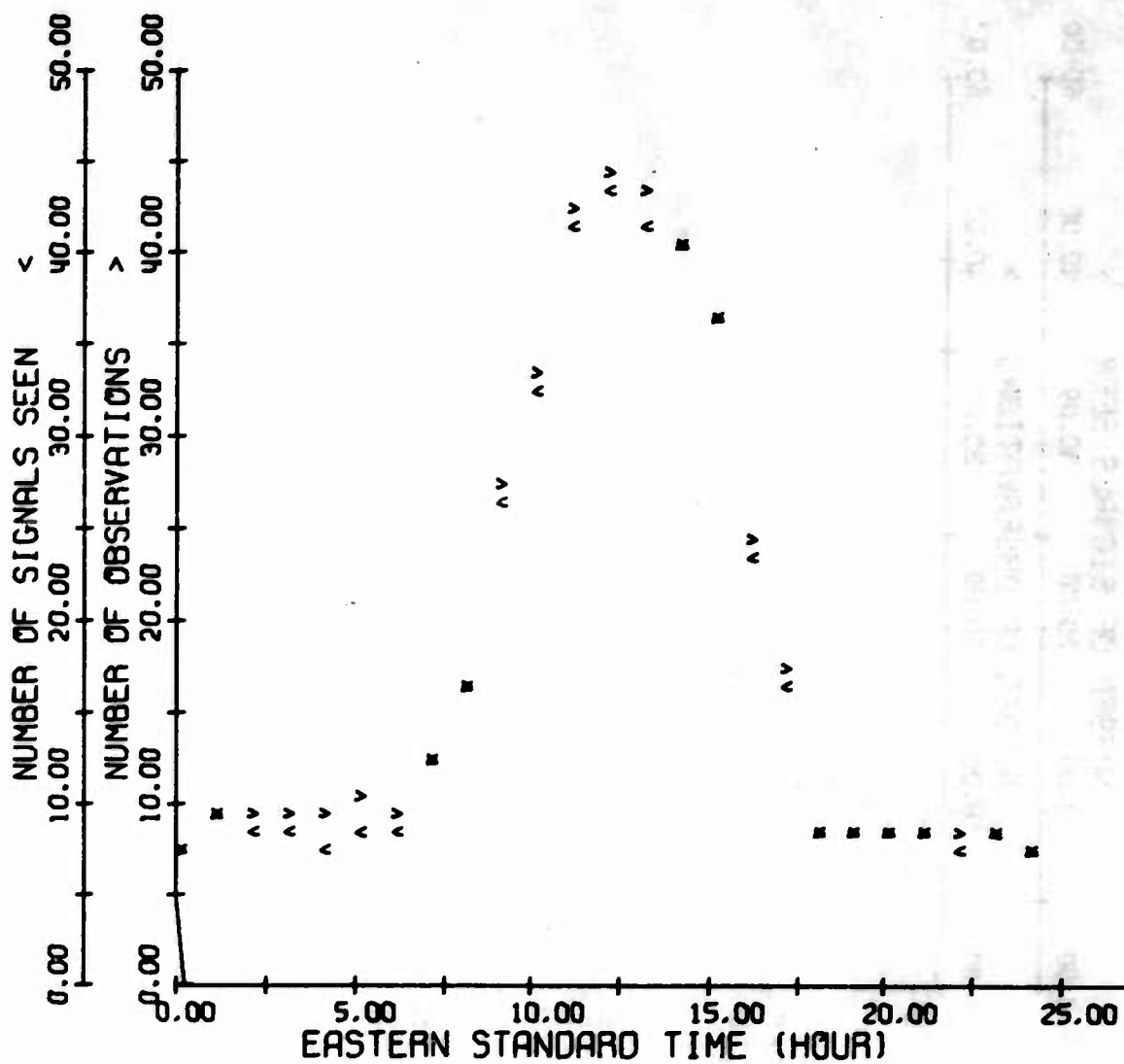


Figure 34. Summary of N Mode Observations, Coco Solo Path, Summer 1966

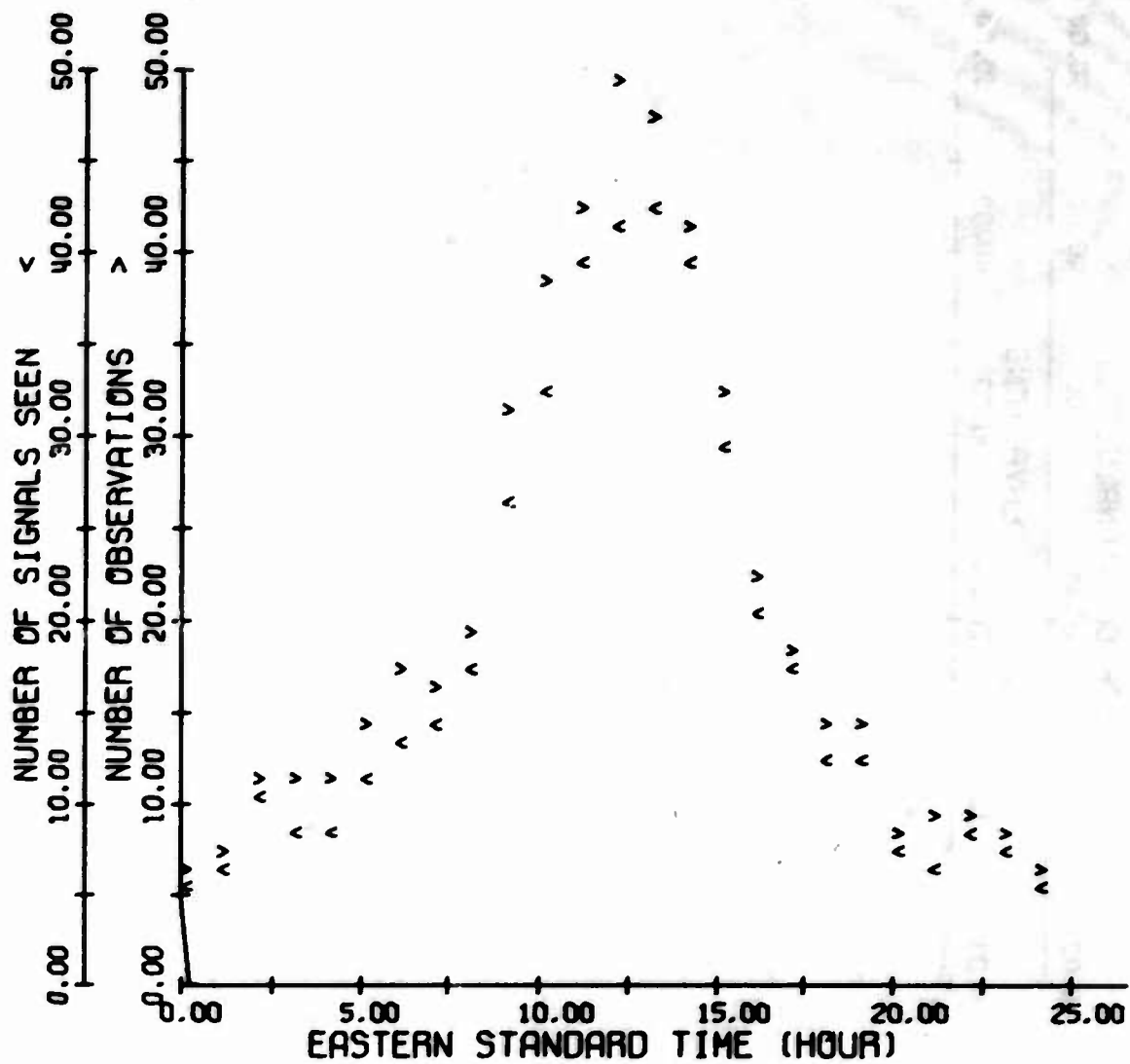


Figure 35. Summary of N Mode Observations, Coco Solo Path, Autumn 1966

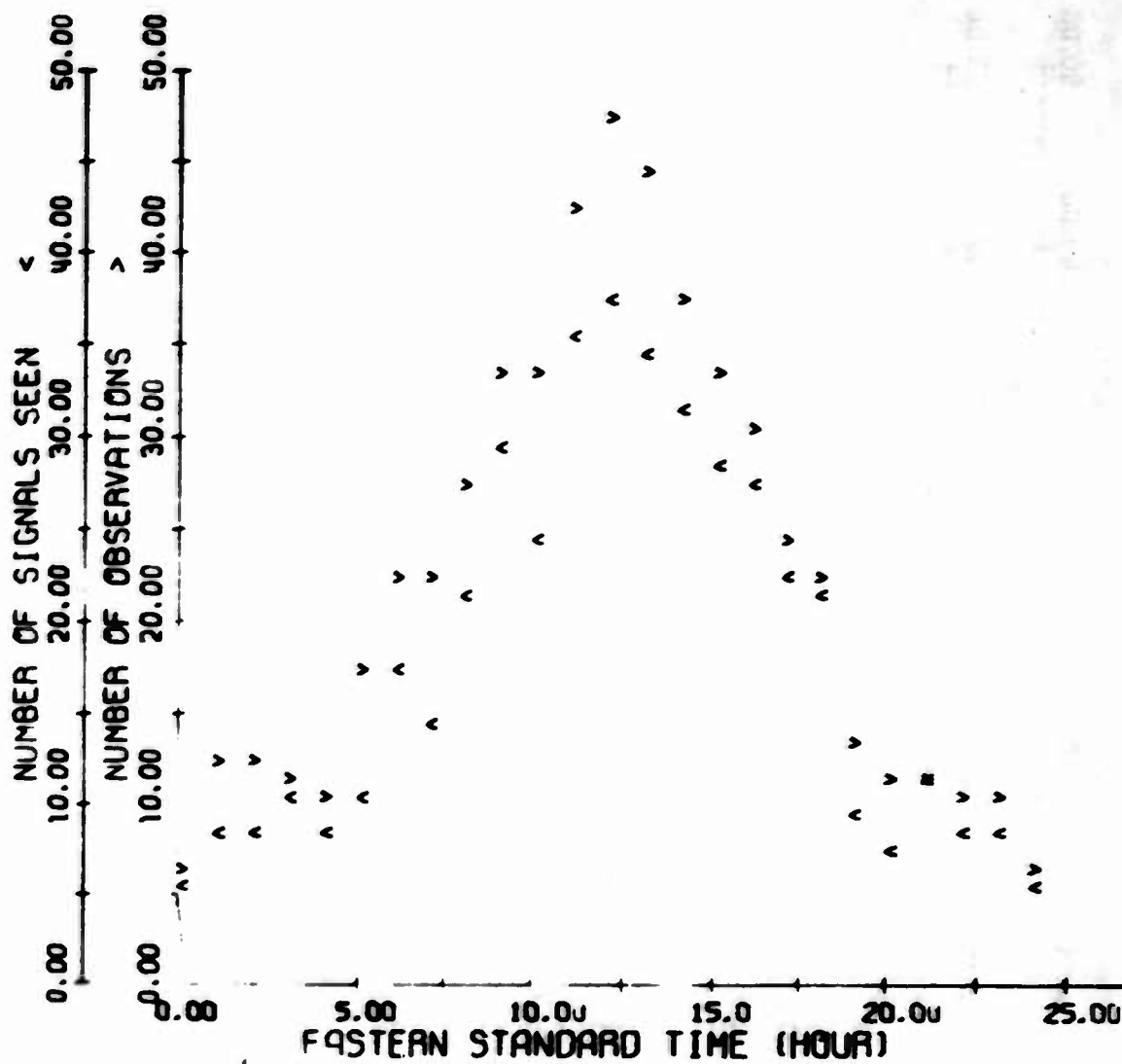


Figure 36. Summary of N Mode Observations, Coco Solo Path, Winter 1967

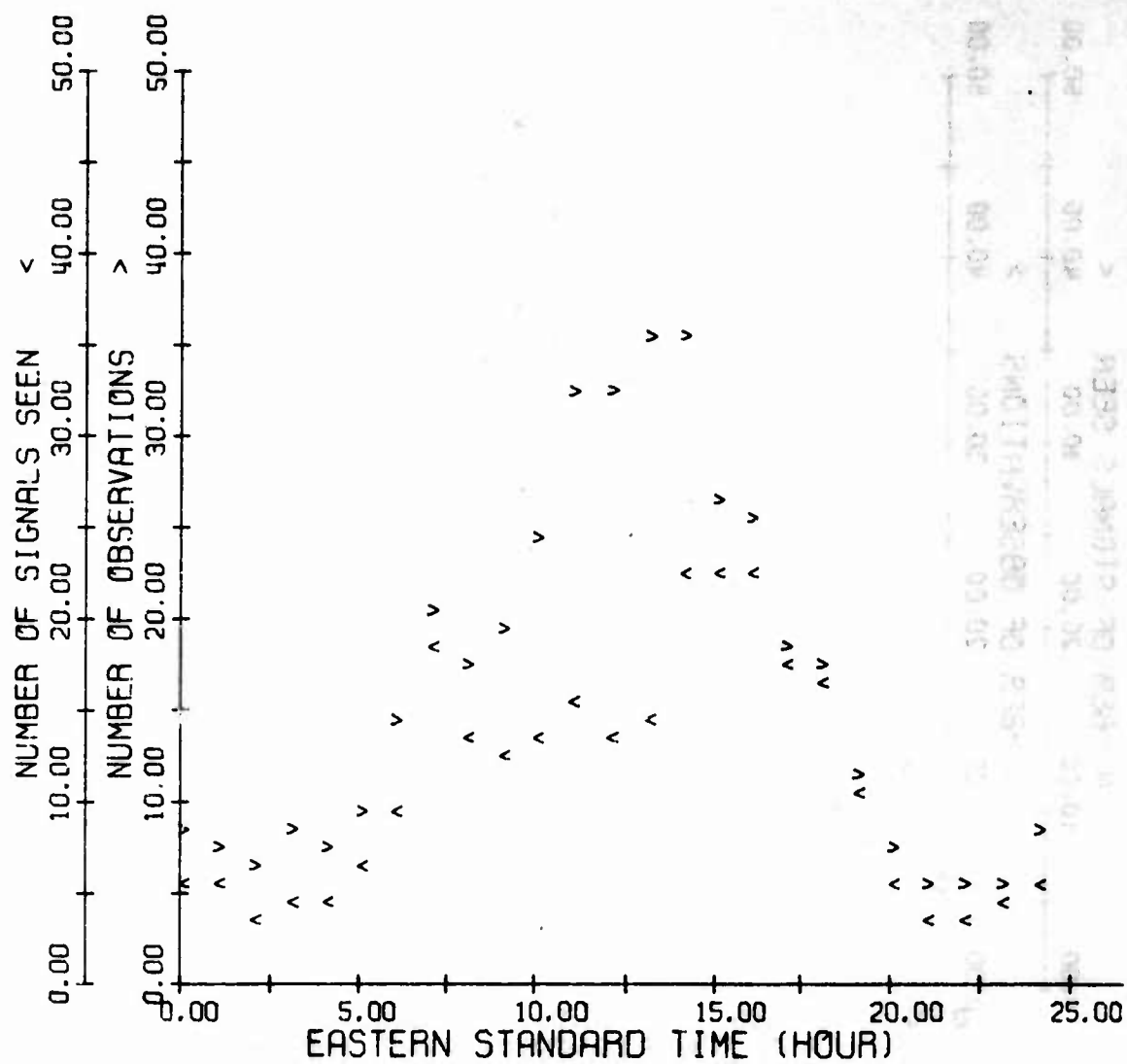


Figure 37. Summary of N Mode Observations, Coco Solo Path, Spring 1967

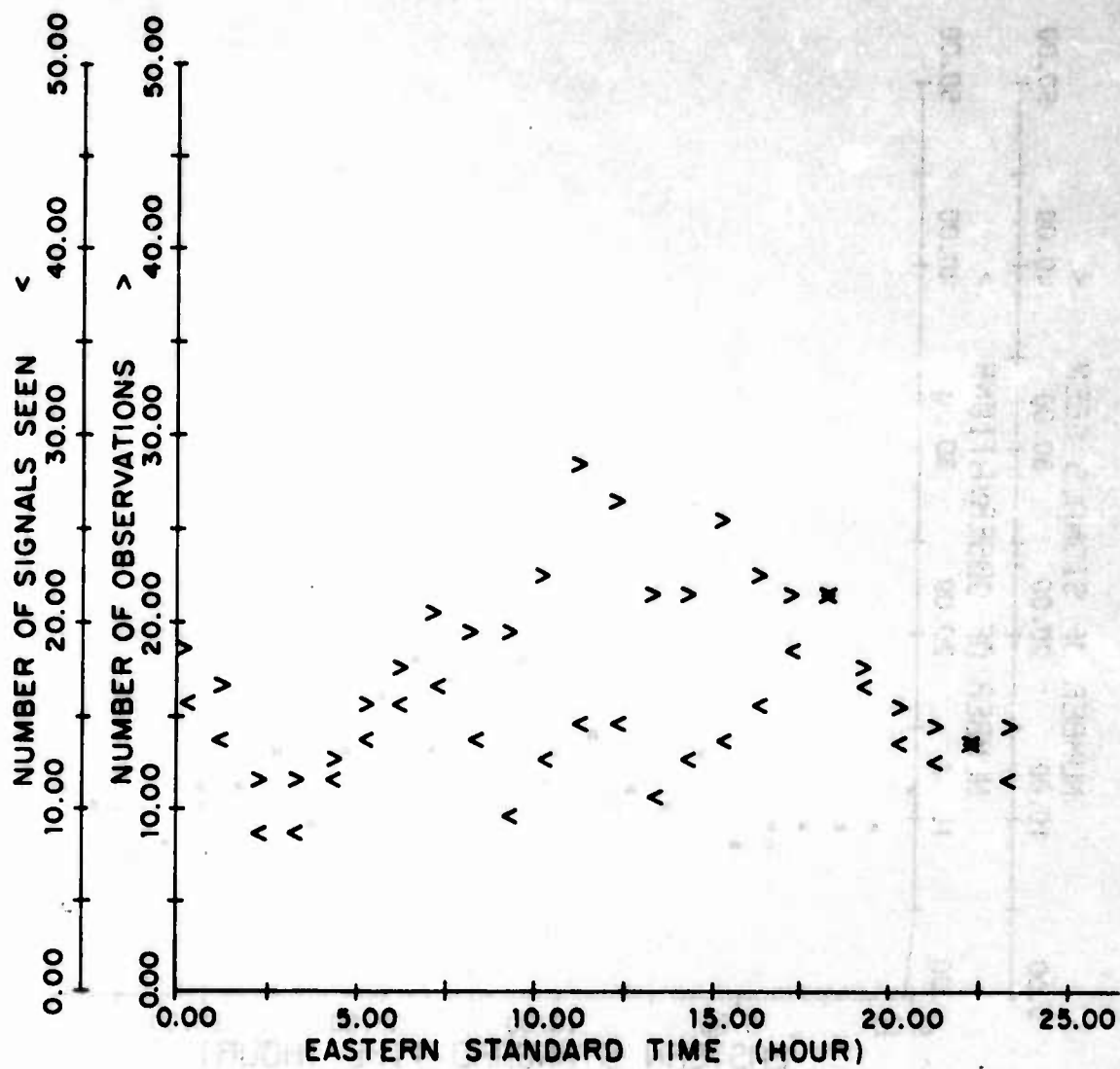


Figure 38. Summary of N Mode Observations, Coco Solo Path, Summer 1967

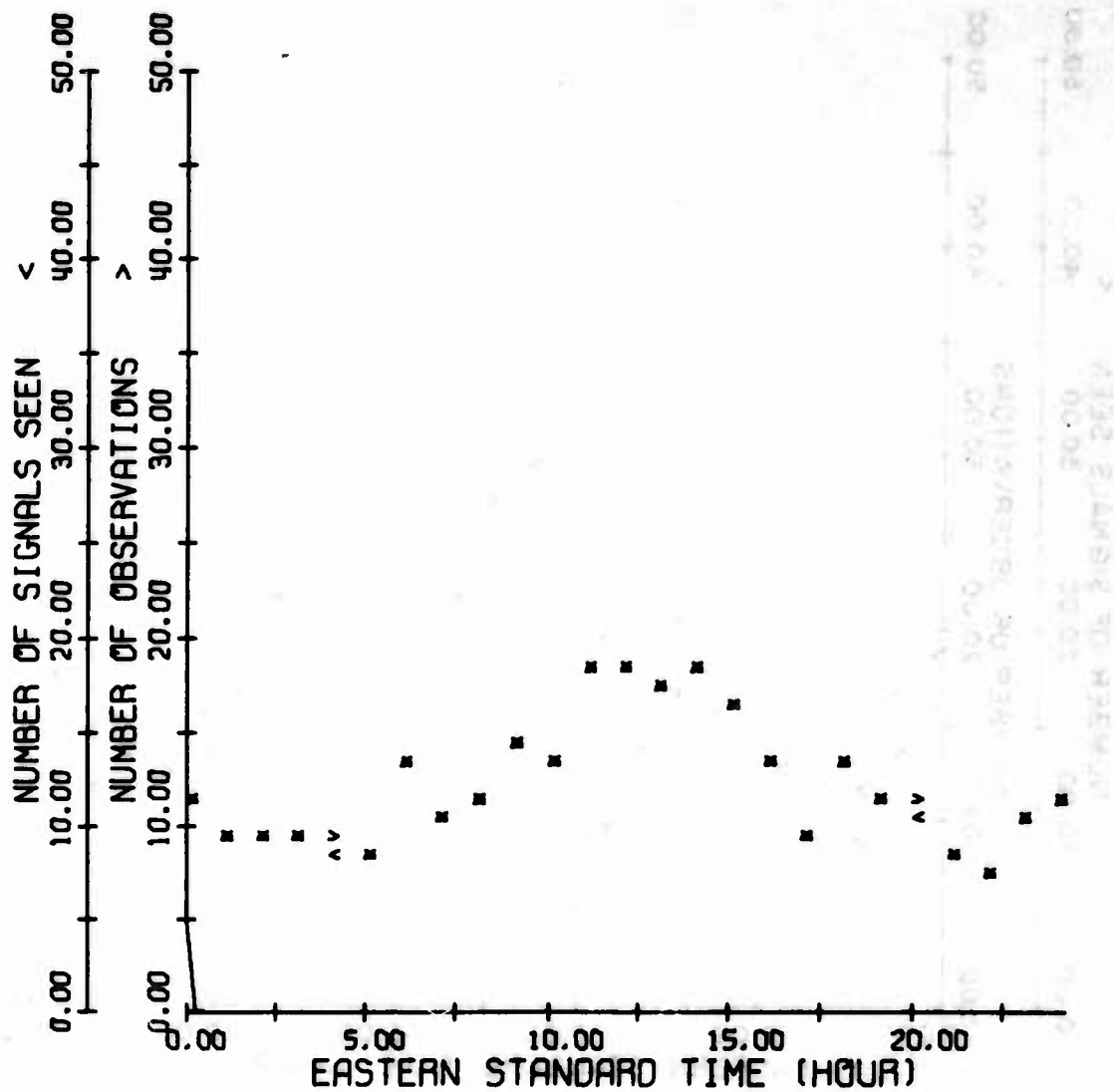


Figure 39. Summary of 2F2 Mode Observations, Coco Solo Path, Winter 1966

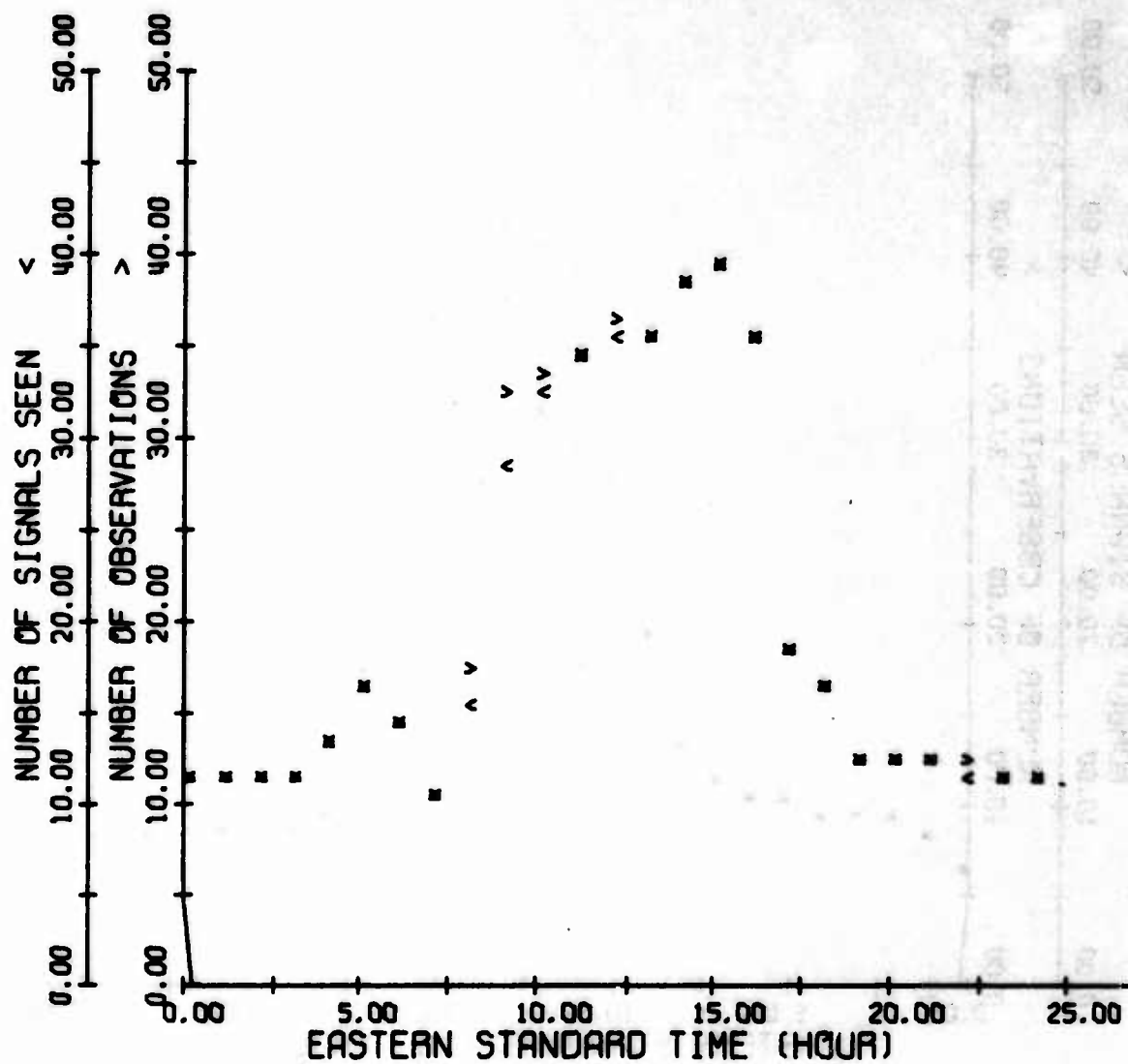


Figure 40. Summary of 2F2 Mode Observations, Coco Solo Path, Spring 1966

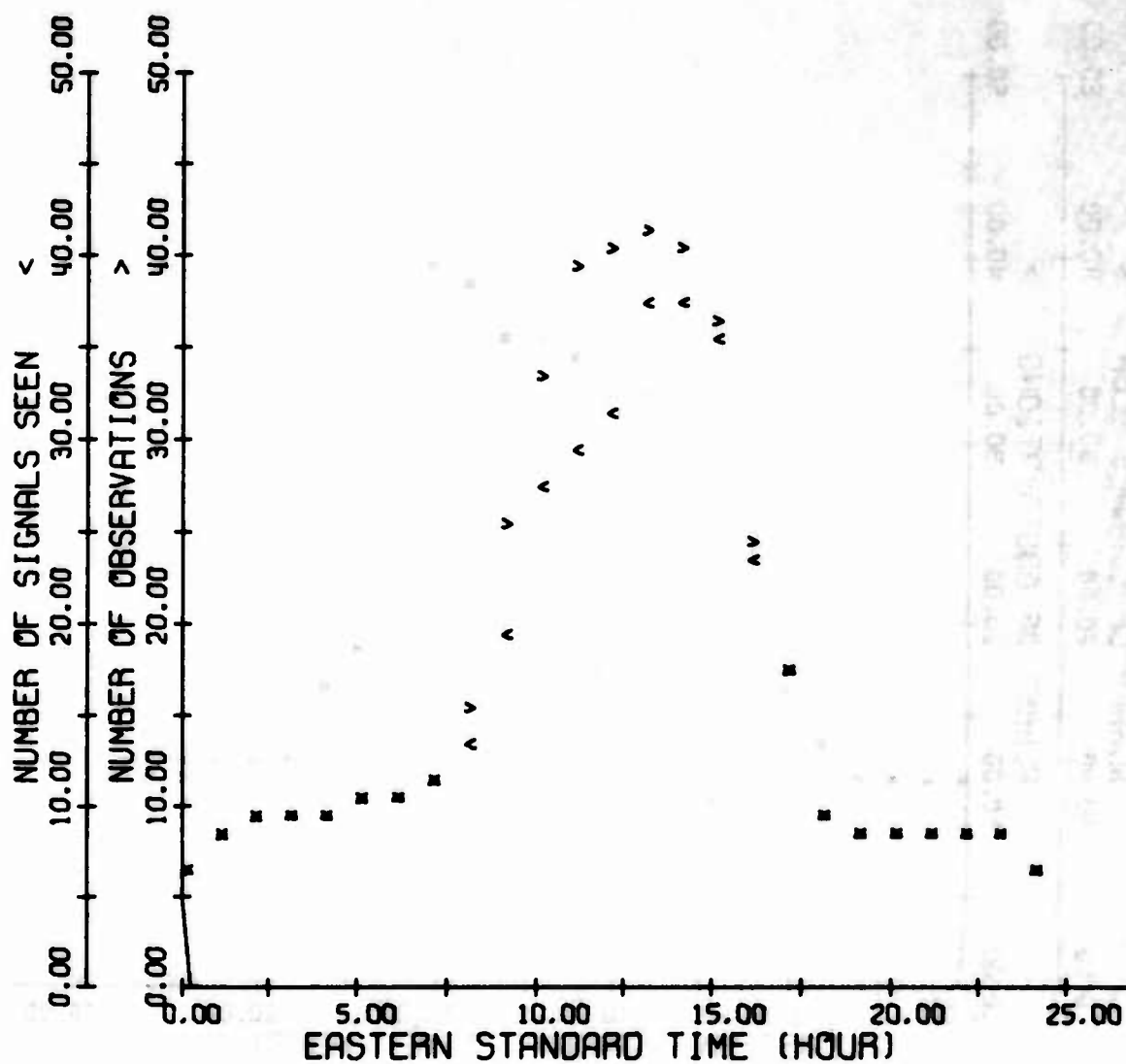


Figure 41. Summary of 2F2 Mode Observations, Coco Solo Path, Summer 1966

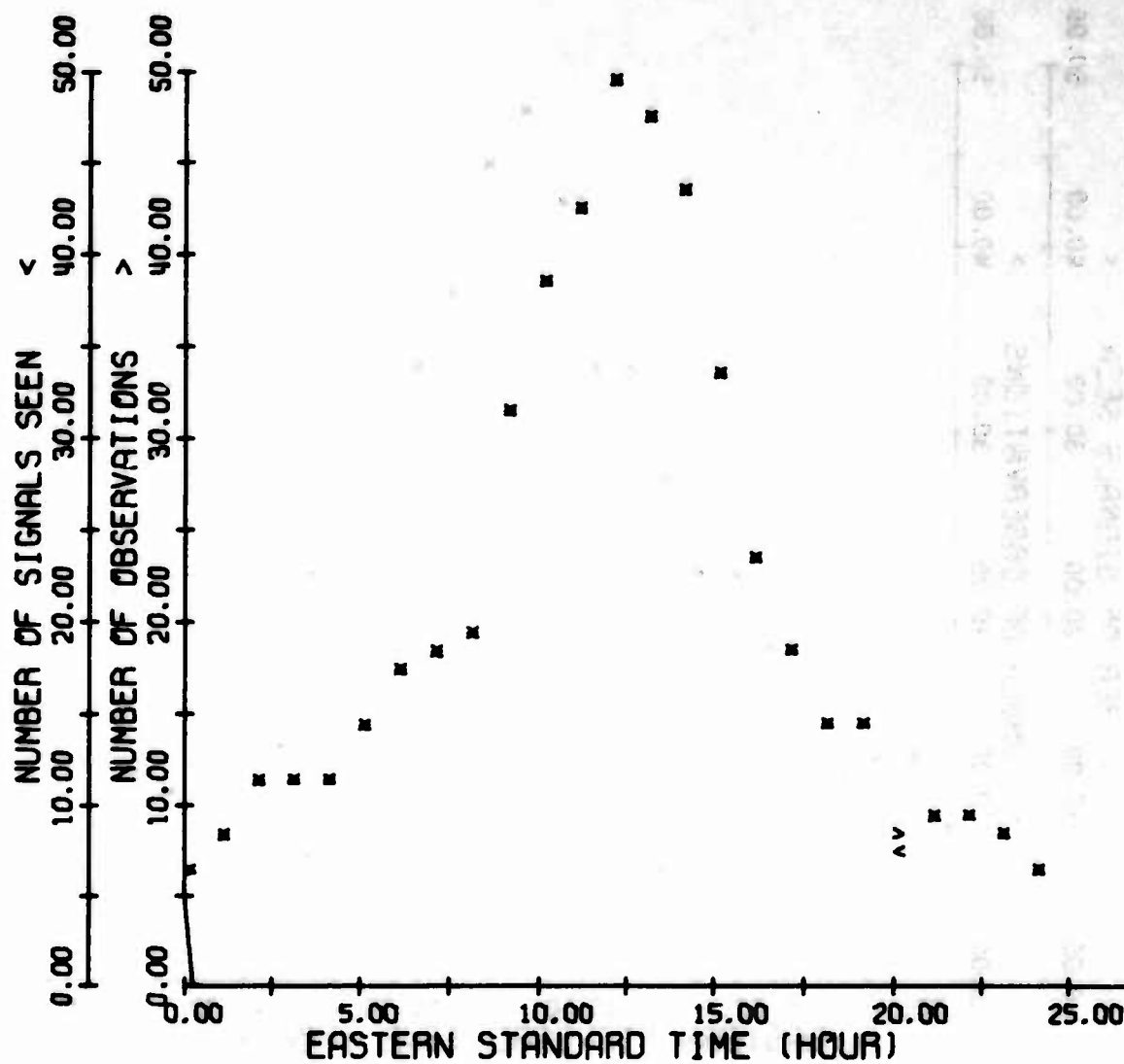


Figure 42. Summary of 2F2 Mode Observations, Coco Solo Path, Autumn 1966

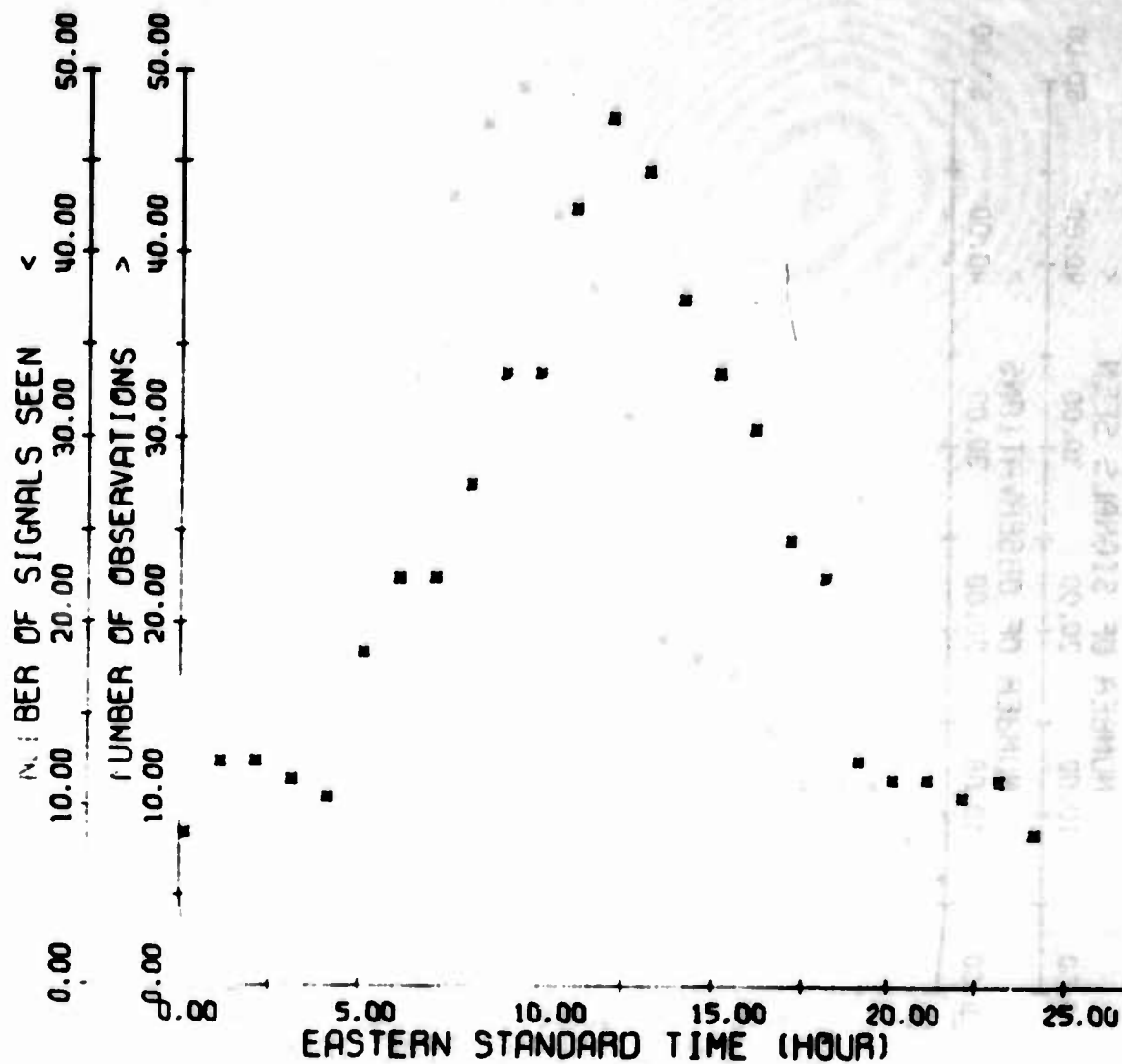


Figure 43. Summary of 2F2 Mode Observations, Coco Solo Path, Winter 1967

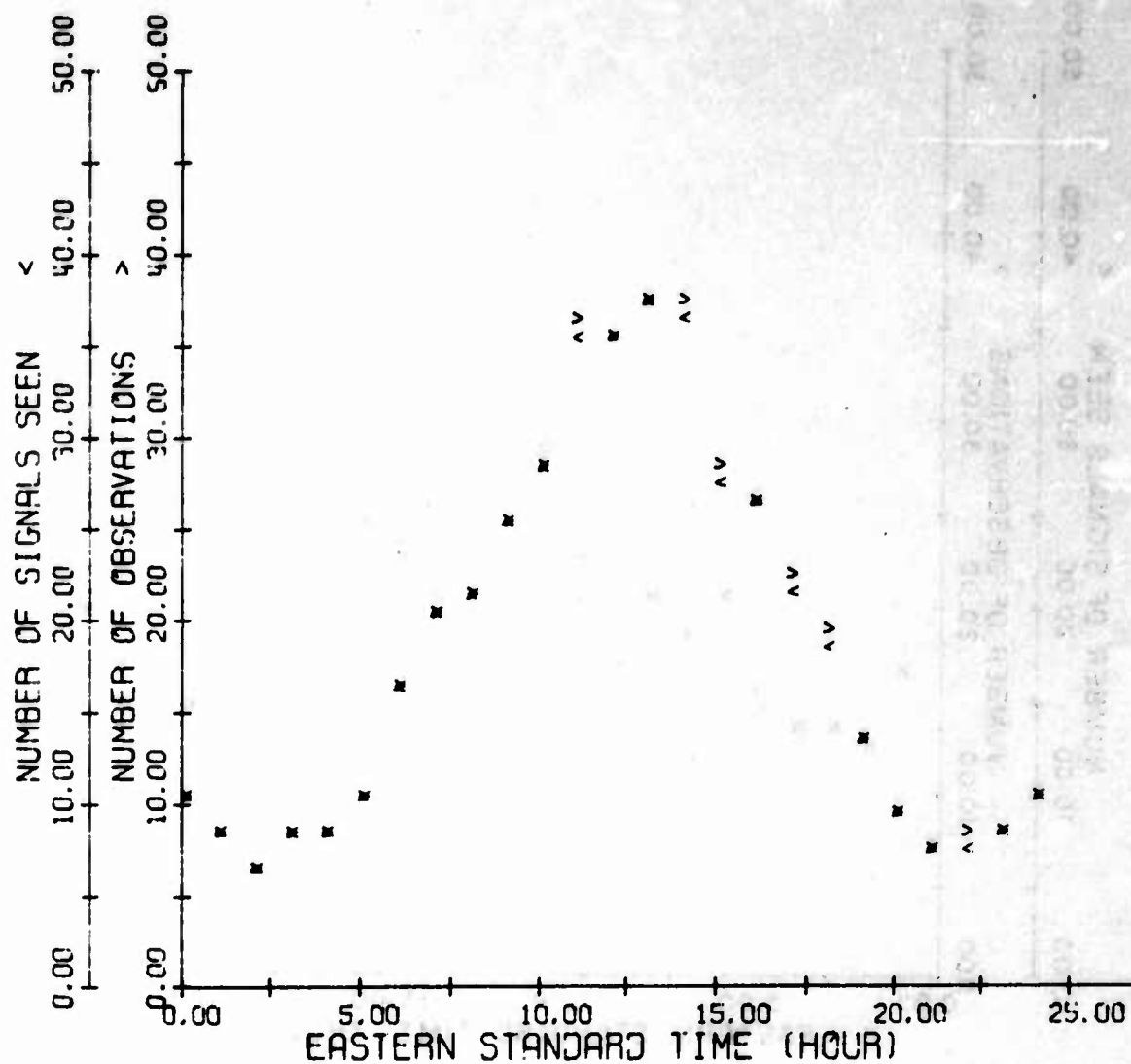


Figure 44. Summary of 2F2 Mode Observations, Coco Solo Path, Spring 1967

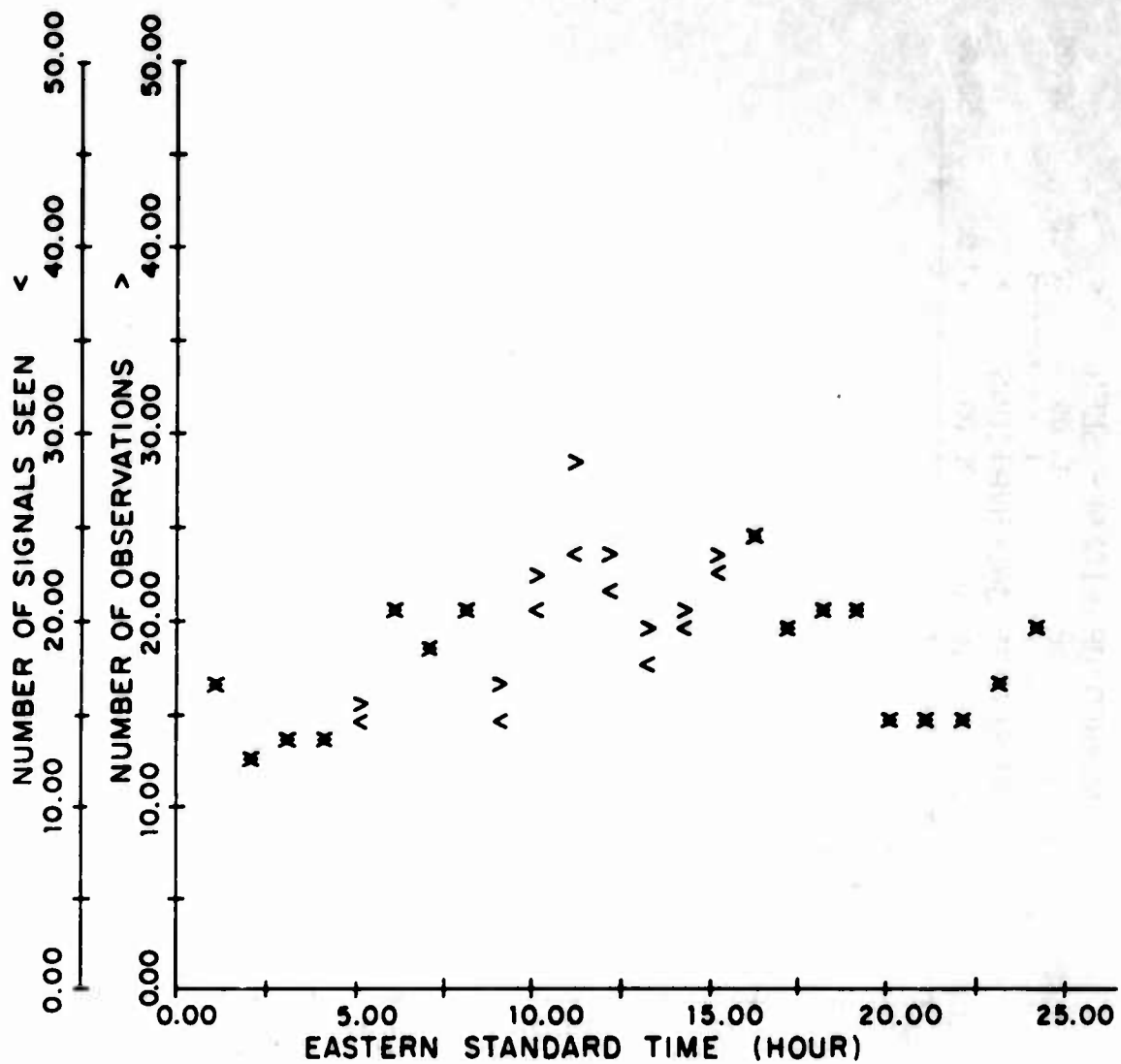


Figure 45. Summary of 2F2 Mode Observations, Coco Solo Path, Summer 1967

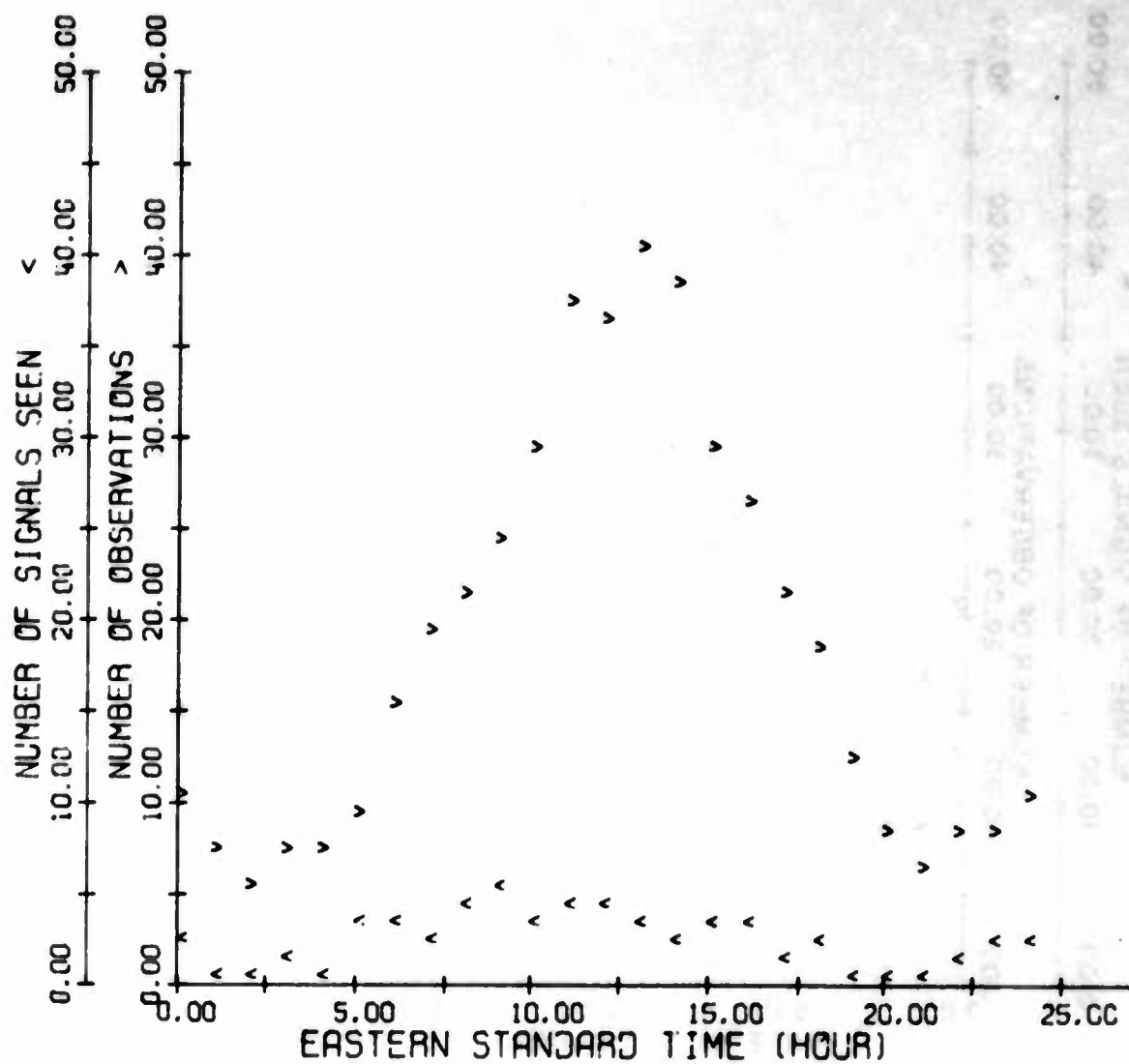


Figure 46. Summary of 2E Mode Observations, Coco Solo Path, Winter 1967

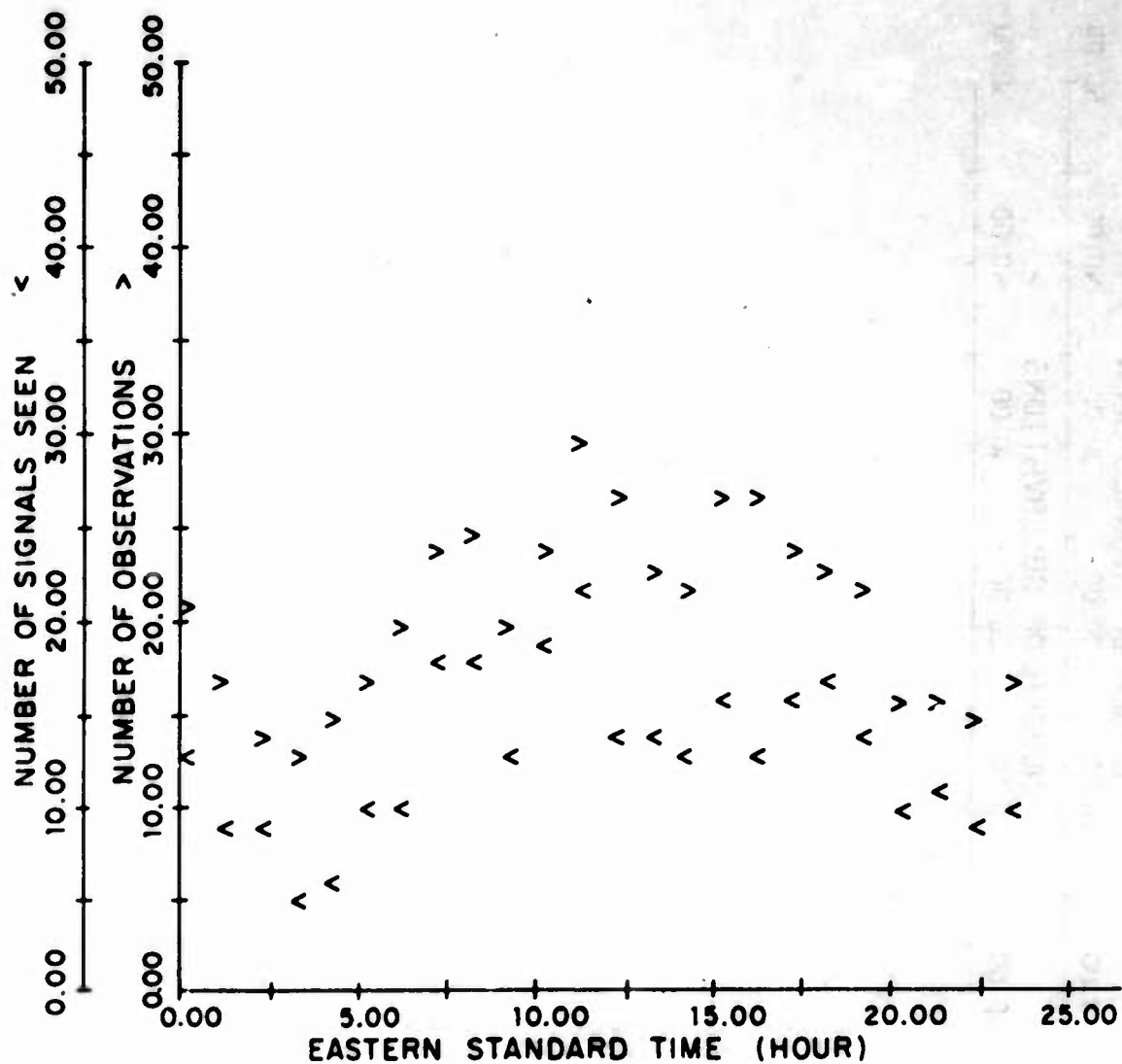


Figure 47. Summary of 2E Mode Observations, Coco Solo Path, Spring 1967

TABLE I

2

TABLE III

MODE AVAILABILITY, COCO SOLO PATH, MARCH 1967

MT	3 16	3 17	3 20	3 21	3 22	3 23	3 24	3 27	3 28	3 29	3 30	3 31
1					02040							
2					2040							
3					02040							
4					02 40							
5					00 40							
6				02040	2 40							
7				12340	12340				12340			
8				12340	12340	12040			12340			
9				12340	12040	12040	12040	12340	12040			
10				12340	12040	12040		12340	12040	12040		
11	12340				2030	12040	12040	12040	12040	12040	040	
12	12040	12040				12040	12040	12040	12040	12040	12340	
13	12040	12040				12340	12040	12040	12040	12040	12040	12040
14	12340	12340	12040		12340	12340	12340	12340		12040	12340	12040
15	12340	12340	12040		12340	12340		12340		12340	12040	
16	02340	12340	12340		12340	12340		12340		12340		
17	4		12 40			12340		12340		12340		
18	4		12 40					1240		12040		
19	4		2 40							02040		
20	4									02040		
21	4									02040		
22	0 40									02040		
23	0 40									12340		
24	0 40			02040						12040		

Availabilities of 2E, 1F2, N, 2F2, and 2E_s are presented in this order for each date and time indicated.

- 1 = Signal observed via the 2E mode for this hour and date.
- 2 = Signal observed via the 1F2 mode for this hour and date.
- 3 = Signal observed via the N mode for this hour and date.
- 4 = Signal observed via the 2F2 mode for this hour and date.
- 5 = Signal observed via the 2E_s mode for this hour and date.
- 0 = No signal observed via this mode for this hour and date.
- (blank) = No valid data for this mode for this hour and date.

TABLE IV

MODE AVAILABILITY, COCO SOLO PATH, APRIL 1967

DAY	4	4	4	5	4	6	4	7	4	10	4	11	4	12	4	13	4	14	4	17	4	18	4	19	4	20	4	21	4	24	4	25	4	26	4	28		
1					02340																			00340											02340			
2					02040																																	
3					02040																			00340												2340		
4					02040																			12340												2340		
5					02040																			12340												2040		
6				12040	02040																			12340	12340								1	40	12340			
7				12340	12040																			12340	12340									12340	12040			
8				12340	12040									12	0									12340	12340								12	40	02040			
9				12040										12340	12340									12	40	12340			12040	12	40	12	40	12340				
10										12040	12040	12340	12	40	12340	12340	12040	12040	12040	12040	12040	12040	12040	12040	12040	12040	12040	12040	12040	12040	12040	12040	12040	12040	12040	12040		
11	02040									12040	12	40	12040	12340	12	40	12340	12040	12040									12040	12040	12340	12340	12040	12	40	12340			
12	02040									12040	12340	12040	12040	12040	12340	12040	12040	12040	12340									12040	12340	12040	12	40	12340					
13	02040	12340	020	0						12040	12340	12	40	12040	12040	12040	12040	12340	12340									12	0	12040	12340	12340	12040					
14	02040	12340	02040	1204	12340					12040	12340	12340	12040						12340								12340	12340					12	40	12340			
15	02340		12340	12340	12040								12340					12340								12340	12340	12340							12340			
16			12340	12340	12340								12340					12340								12340	12340	12340										
17	12340		12340		12340								12340					12340								12340		12340										
18			12340		2340								12340					12340								12340		12340										
19			12340										12340					12340								12340		2340										
20			12040										2340													12340												
21			2	40									00340													12340												
22			2	40									00340													12340												
23			2	40									00340													2	40											
24			02340	10340																																2340		

Availabilities of 2E, 1F2, N, 2F2, and 2E₂ are presented in this order for each date and time indicated.

- 1 = Signal observed via the 2E mode for this hour and date.
- 2 = Signal observed via the 1F2 mode for this hour and date.
- 3 = Signal observed via the N mode for this hour and date.
- 4 = Signal observed via the 2F2 mode for this hour and date.
- 5 = Signal observed via the 2E₂ mode for this hour and date.
- 0 = No signal observed via this mode for this hour and date.
- (blank) = No valid data for this mode for this hour and date.

TABLE V

MODE AVAILABILITY, COCO SOLO PATH, MAY 1967

MODE	1	2	3	4	5	6	7	8	9	10	11	12	13	14	15	16	17	18	19	20	21	22	23	24	25	26	27	28	29	30
1										0240														02 40	1					12340
2										0240														12340	2					12340
3										0240														12340	3					12340
4										0240														12340	4					12340
5		0240								12340	0240													12340	5					02340
6		12340	12340							12340	0240													12340	6					02340
7		12340	12340							12340	12340													12340	7					12340
8		12 40								12340	12340													12340	8					12340
9		12 40								12340	12340													12340	9					12340
10		12 40								12340	12340													12340	10					12340
11		12340								12340	12340													12340	11					12340
12		12340								12340	12340													12340	12					12340
13		12 40								12340	12340													12340	13					12340
14		12 40								12340	12340													12340	14					12340
15		0240	12340	12340						12340	12340													12340	15					020000
16		12340								12340	12340													12340	16					12 0
17		12340								12340	12340													12340	17					10040
18		12340								12340	12340													12340	18					12340
19		12340								12340	12340													12340	19					12340
20		12340								12340	12340													12340	20					12 40
21		12340								12340	12340													12340	21					21
22		12340								12340	12340													12340	22					02000
23		12340								12340	12340													12340	23					02340
24		12340								12340	12340													12340	24					00000

TABLE VI
MODE AVAILABILITY, COCO SOLO PATH, JUNE 1967

CODE	0	1	2	3	4	5	6	7	8	9	0	1	2	3	4	5	6	7	8	9	0	1	2	3	4	5	6	7	8	9	0	
1			02345							12340						02340							02340							023 9	023 0	
2			02345							02345						02345							02340								02 9	02340
3			02345						3	02 45						02340							02 40								02340	02 45
4			02345							02345						02340							02 40									02 45
5			02345							02345						12340							02340								02340	
6										02340						12340							02340								12345	
7										02340						12345							02340								02345	
8										02340						12340							02340								02345	
9										02340						12343							02340								02345	
10										12340 12340						12345							123 9 02340								12345	
11										12340 12345						12345							12340 12340								12345	
12										12345 12345						12345 12345							12 40 123 0								12345	
13										12345 12345						12 45 12345							12340 12 0								12345	
14										120 5 12345						120 0 12345							12340 12340								120 5	
15										12000 12345						12345 12345 12 45							12345								12005	12045
16										12005 12345 12345						12340 12340 12345 12345 12340 12 40 12340							12005							12005	12045	
17										12005 12345						12340 12340 12340 12340 12340 12340 12340 12340							12005							12005	12045	
18										12005 12345						12340 12340 12340 120 0 12 5							12005							12005	12045	
19										12305 12345						12345 12340 12340 12345							12345							12040	12040	
20										12340						12340 12340 12340 12345							12340 000 0 1 0 5 12345							12040	12040	
21										12340						12340 12340 12 0							12340 000 0 1 0 5 12345							12 0 12045		
22										12340						12340							12340 1 9								123 0	
23										12340						123 9							12340 12 40								12345	
24										12340						02340							02 40								02340	

TABLE VII
MODE AVAILABILITY, COCO SOLO PATH, JULY 1967

	7	8	9	10	11	12	13	14	15	16	17	18	19	20	21	22	23	24	25	26	27	28	29	30	31
1																									
2																									
3																									
4																									
5																									
6																									
7																									
8																									
9																									
10																									
11																									
12																									
13																									
14																									
15																									
16																									
17																									
18																									
19																									
20																									
21																									
22																									
23																									
24																									

TABLE VIII

77

b. Thule to Stockbridge/Starr Hill

Measurements on the Thule path were not started until the winter of 1967. At this time the path extended from Thule to Stockbridge. The receiving station was transferred to the RADC Starr Hill Test Annex at the end of the winter. This represented only a small change in distance, from 3732 km to 3696 km. The graphical hourly summaries of observations for the Thule path are shown in Figures 48 through 57. Chiefly noted in these observations is that during the winter, there was roughly no 2E mode seen at any time. The same applies to the two-hop sporadic E mode. The N mode also represents next to nothing in the winter time. In fact, only the F reflected modes appear to be of any consequence at this time. The small quantity of data available leaves validity of any conclusions concerning the winter Thule data somewhat in doubt. Somewhat better observational conditions are noted in the spring for all modes after the move had been made to the Starr Hill receiving location. Due to the small amount of data available for the summer of 1967 on the Thule path, none are included in this report.

In addition to the figures mentioned above, Tables IX, X, and XI are provided for the Thule path which are in the same form as those described for the Coco Solo path. These tables, together with those contained in reference 6, form a complete set of this type of information for the Thule path.

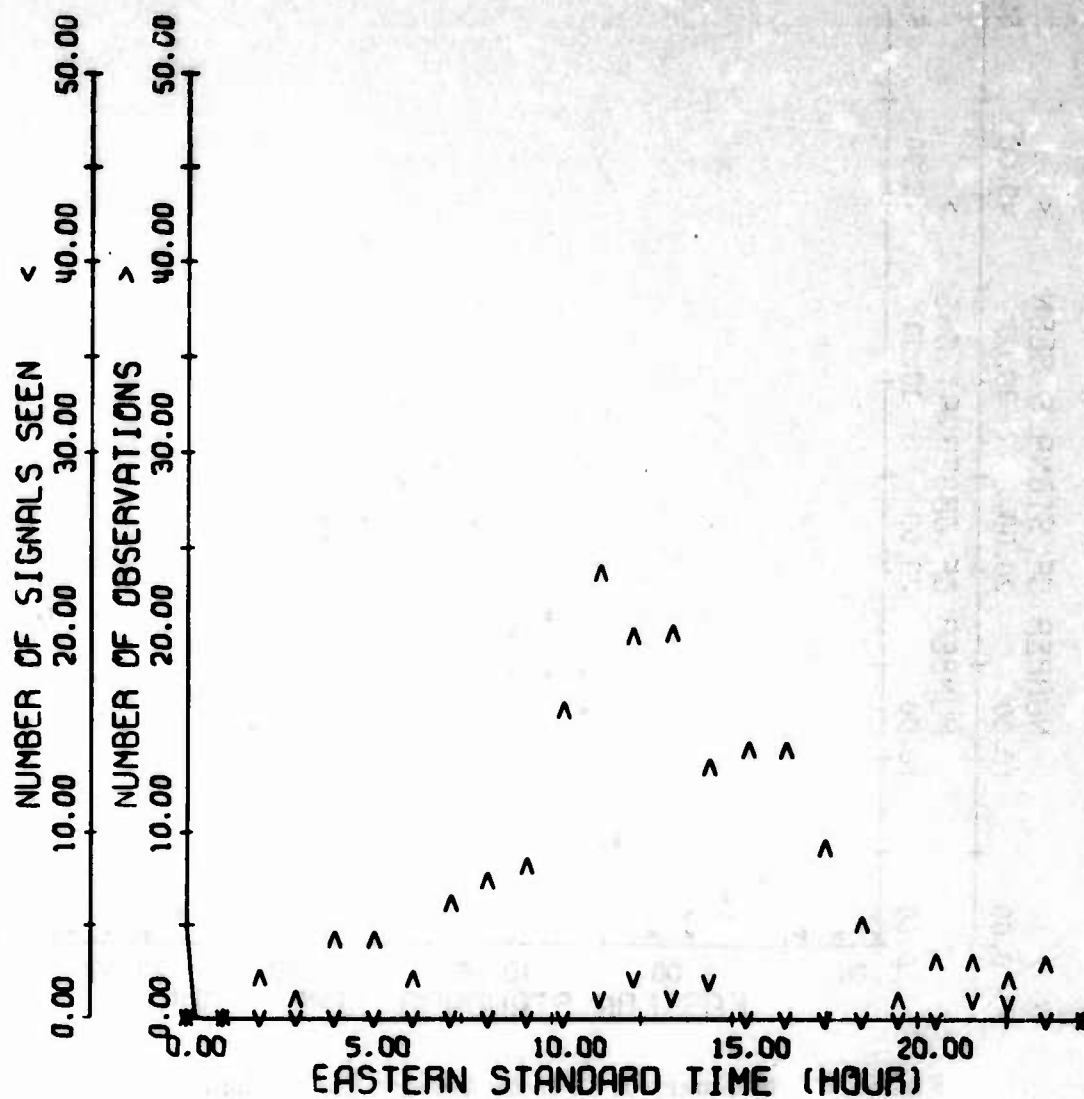


Figure 48. Summary of 2E Mode Observations, Thule Path, Winter 1967

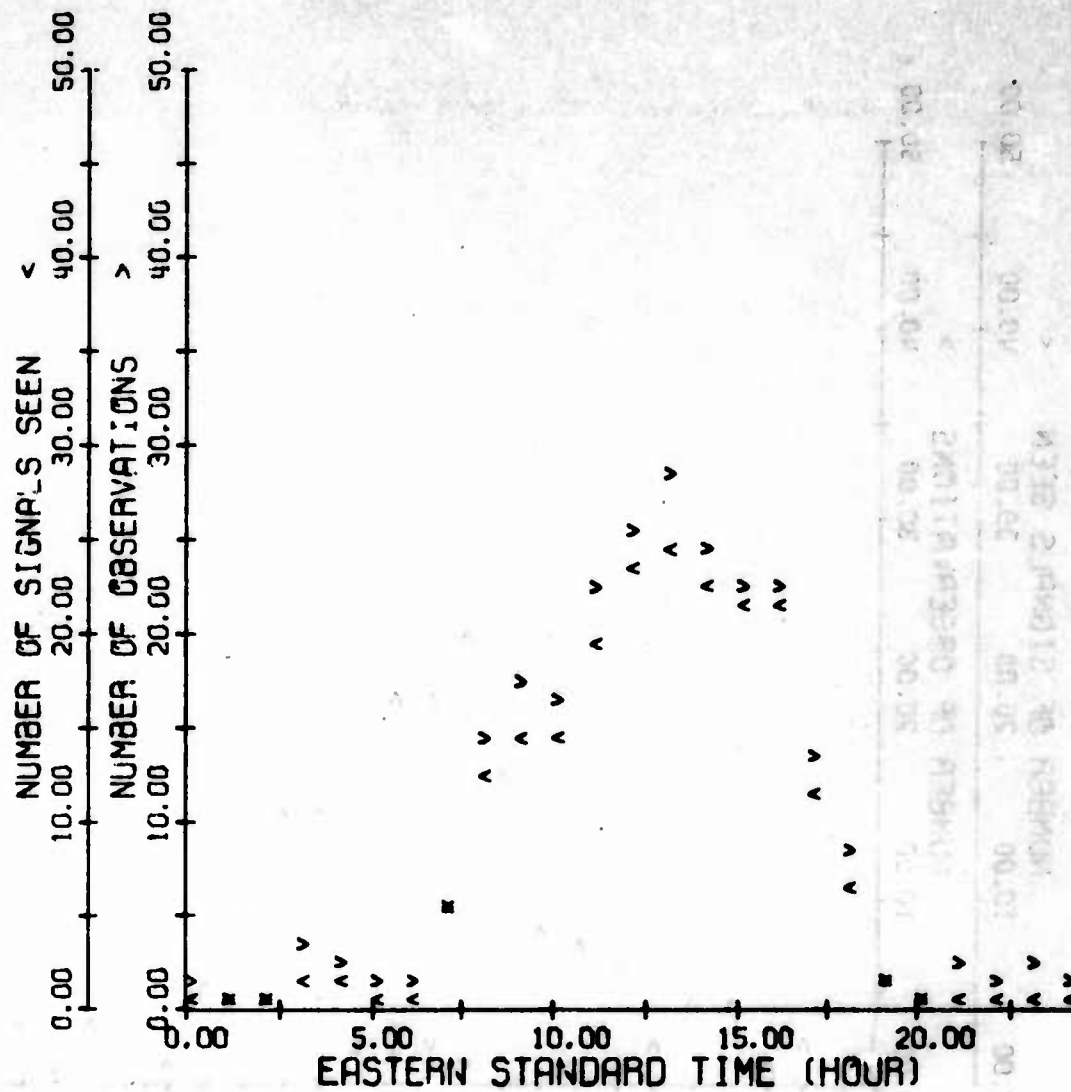


Figure 49. Summary of 2E Mode Observations, Thule Path, Spring 1967

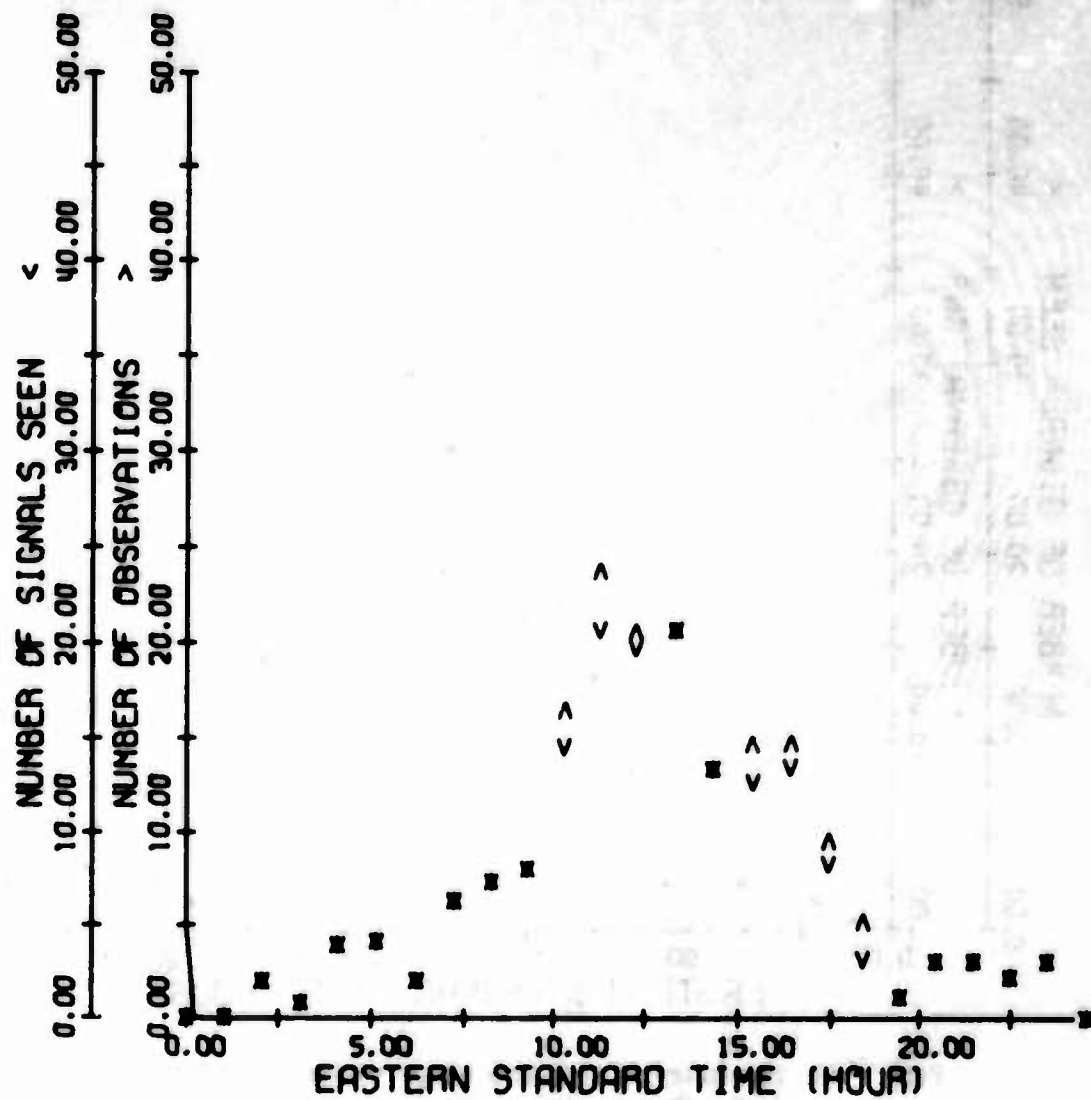


Figure 50. Summary of 1F2 Mode Observations, Thule Path, Winter 1967

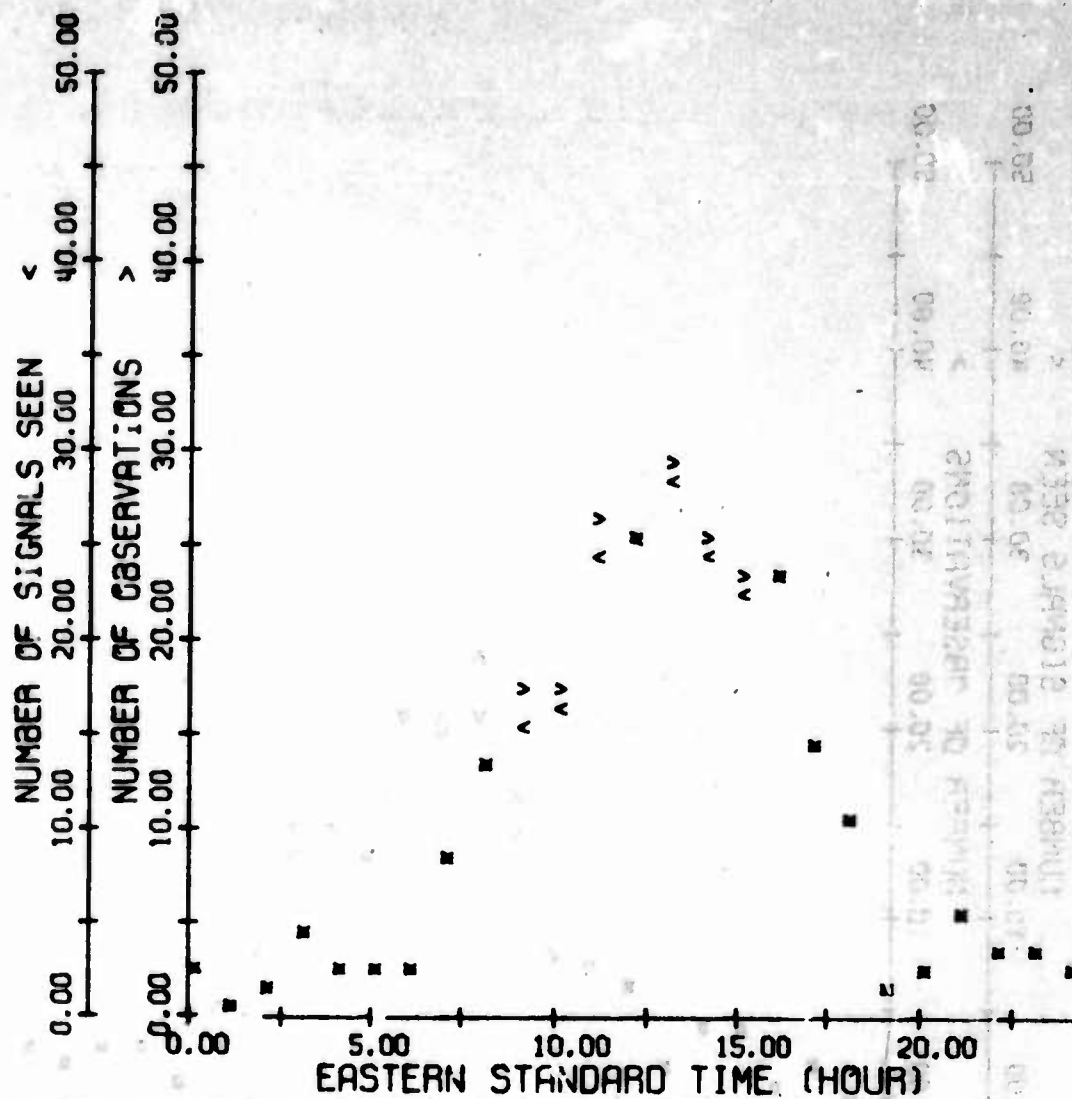


Figure 51. Summary of 1F2 Mode Observations, Thule Path, Spring 1967

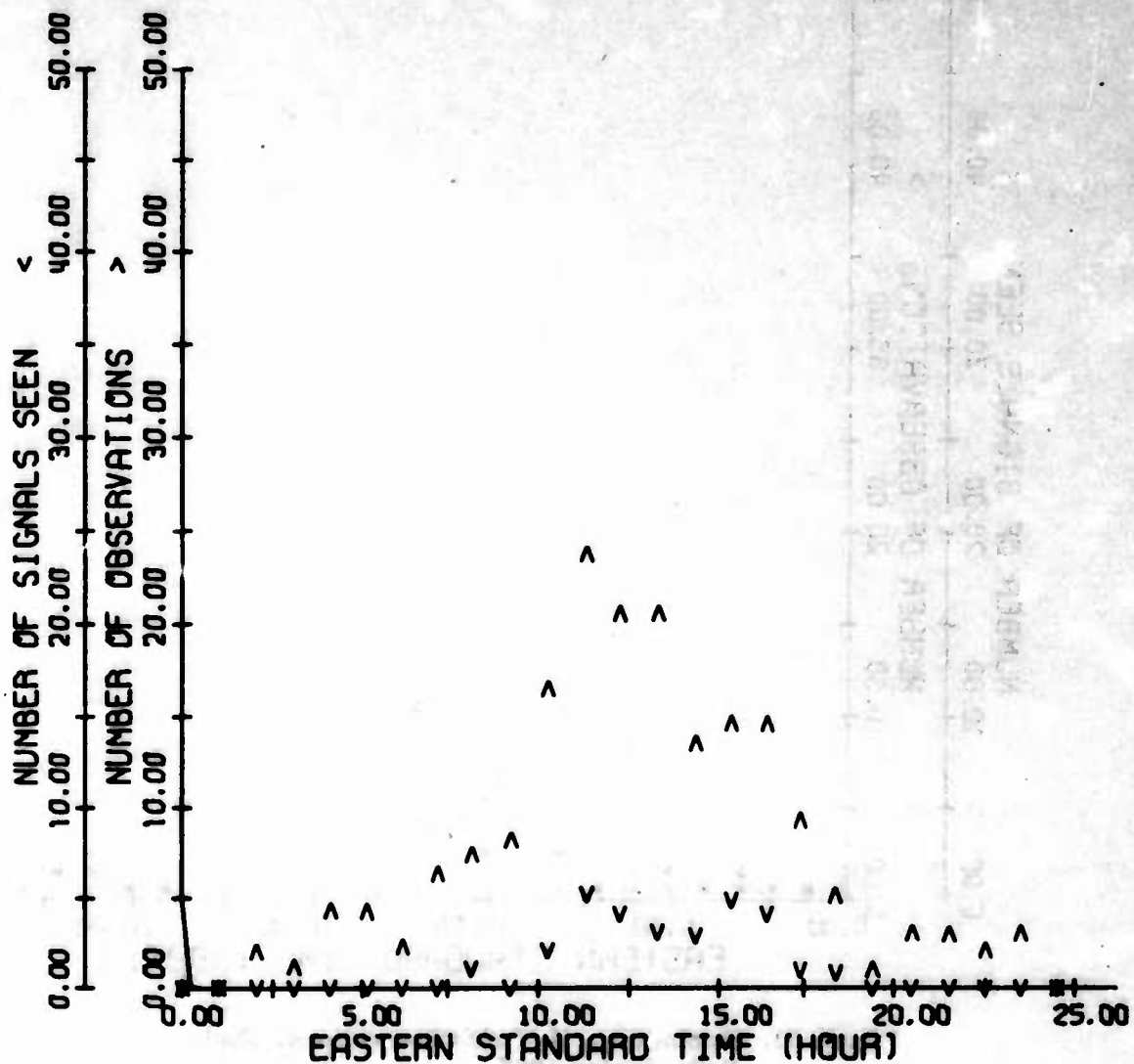


Figure 52. Summary of N Mode Observations, Thule Path, Winter 1967

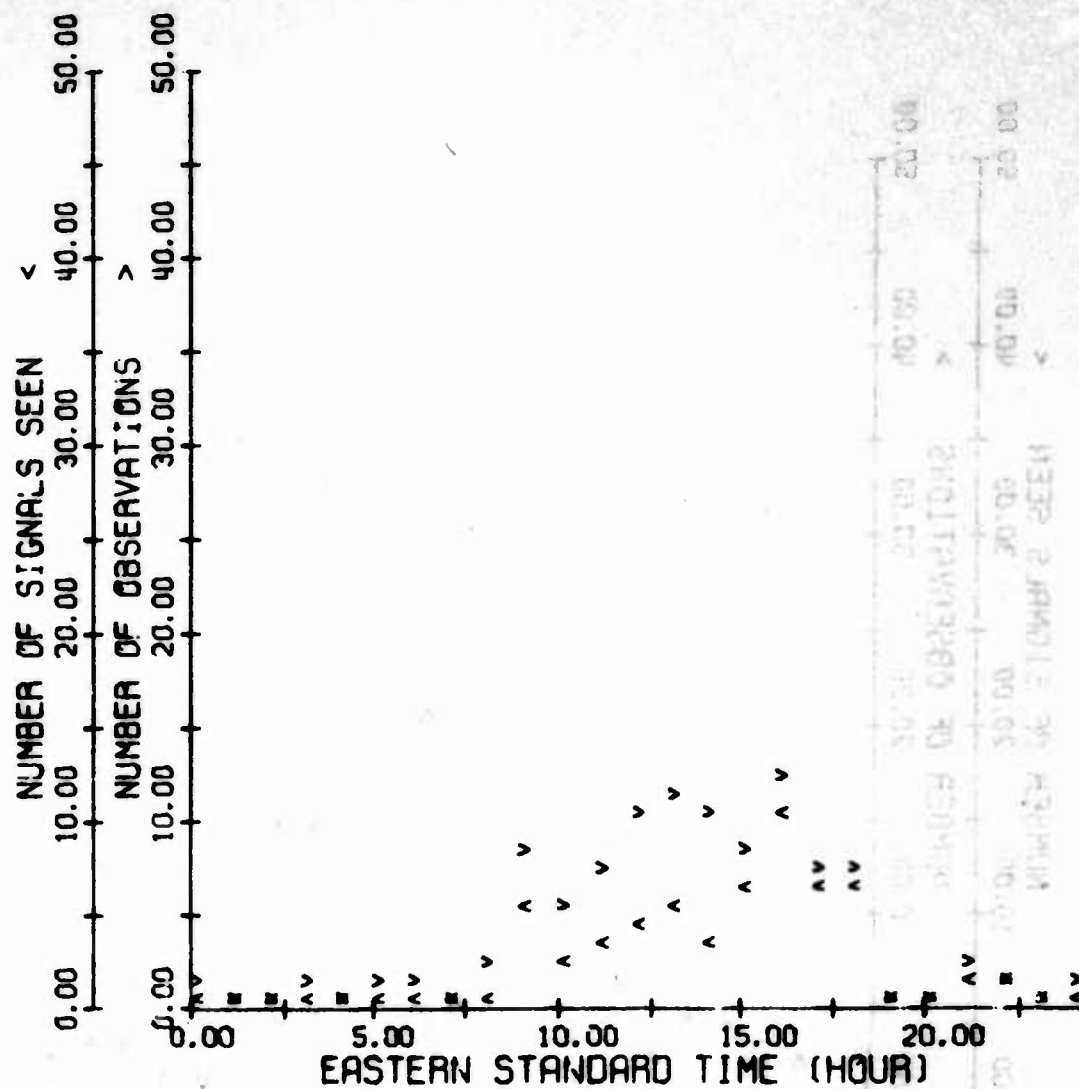


Figure 53. Summary of N Mode Observations, Thule Path, Spring 1967

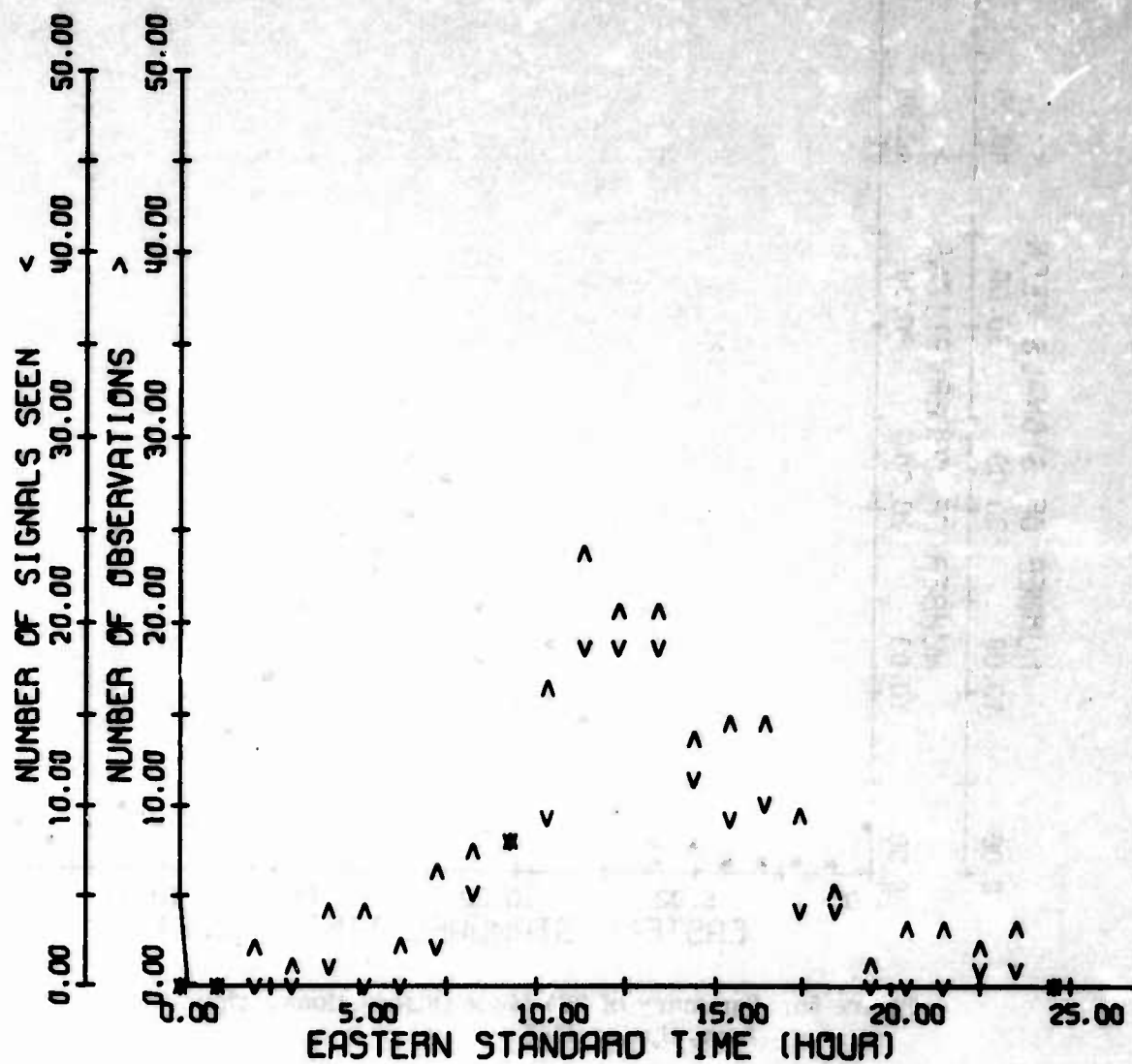


Figure 54. Summary of 2F2 Mode Observations, Thule Path, Winter 1967

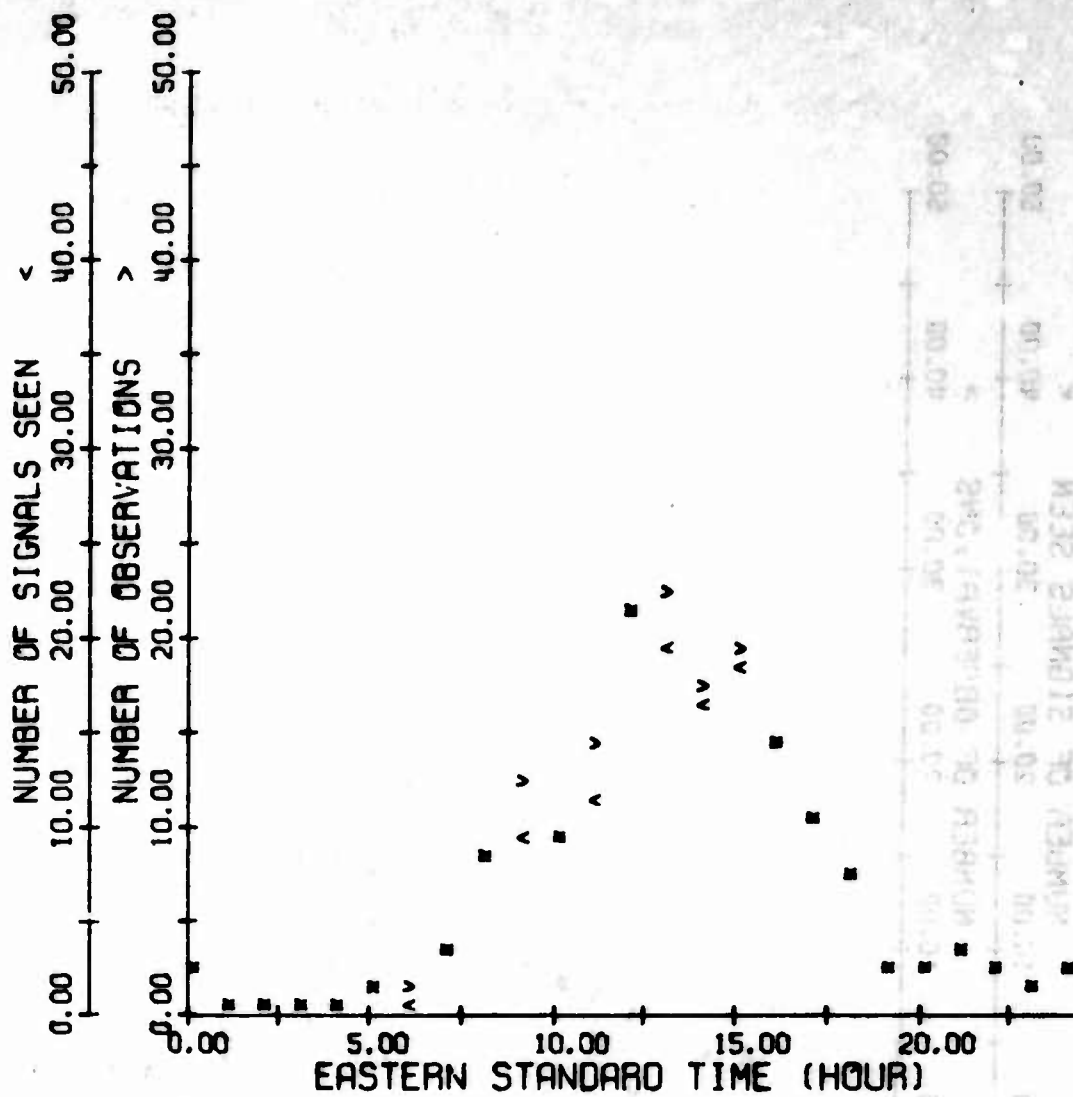


Figure 55. Summary of 2F2 Mode Observations, Thule Path, Spring 1967

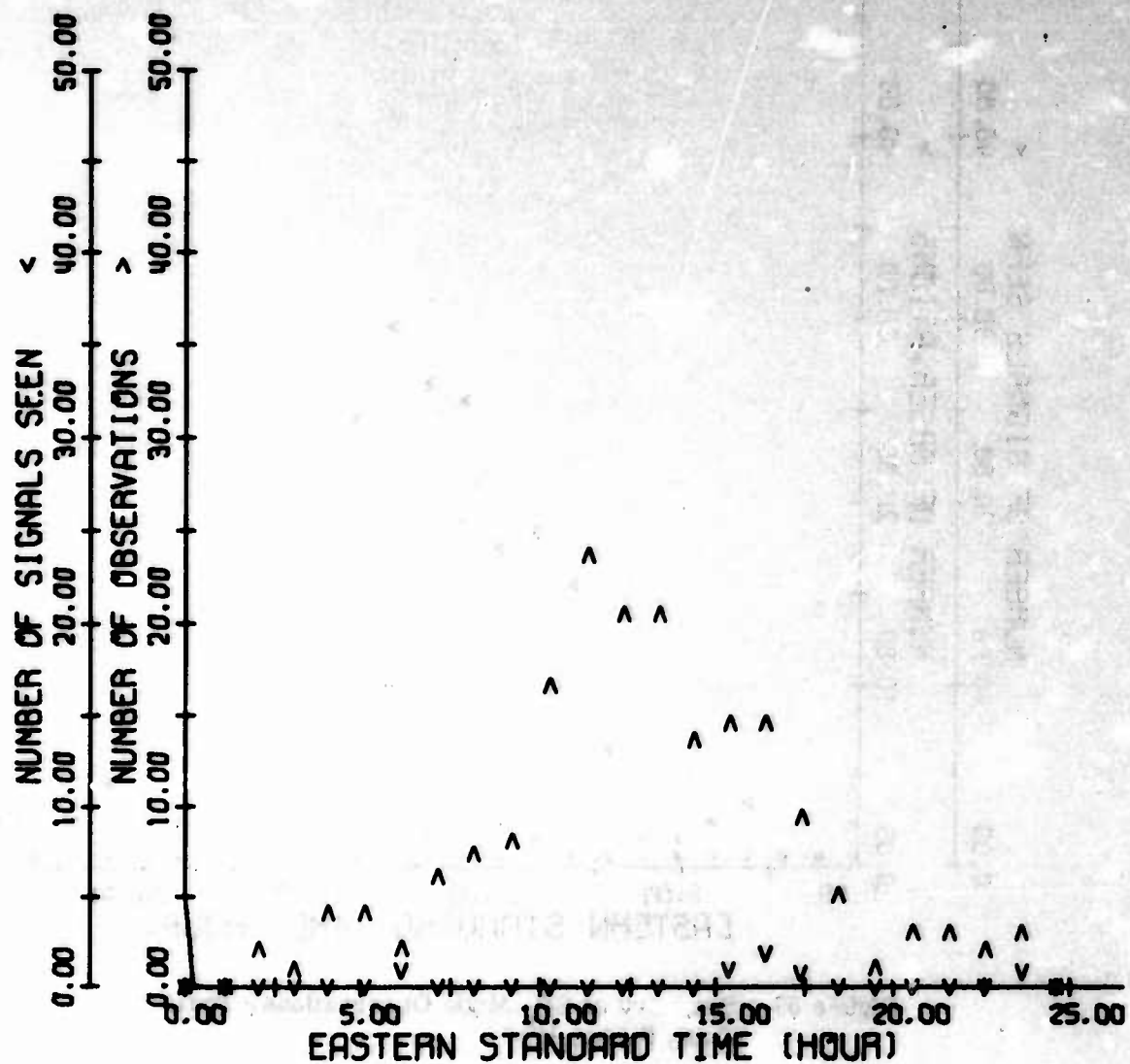


Figure 56. Summary of 2E Mode Observations, Thule Path, Winter 1987

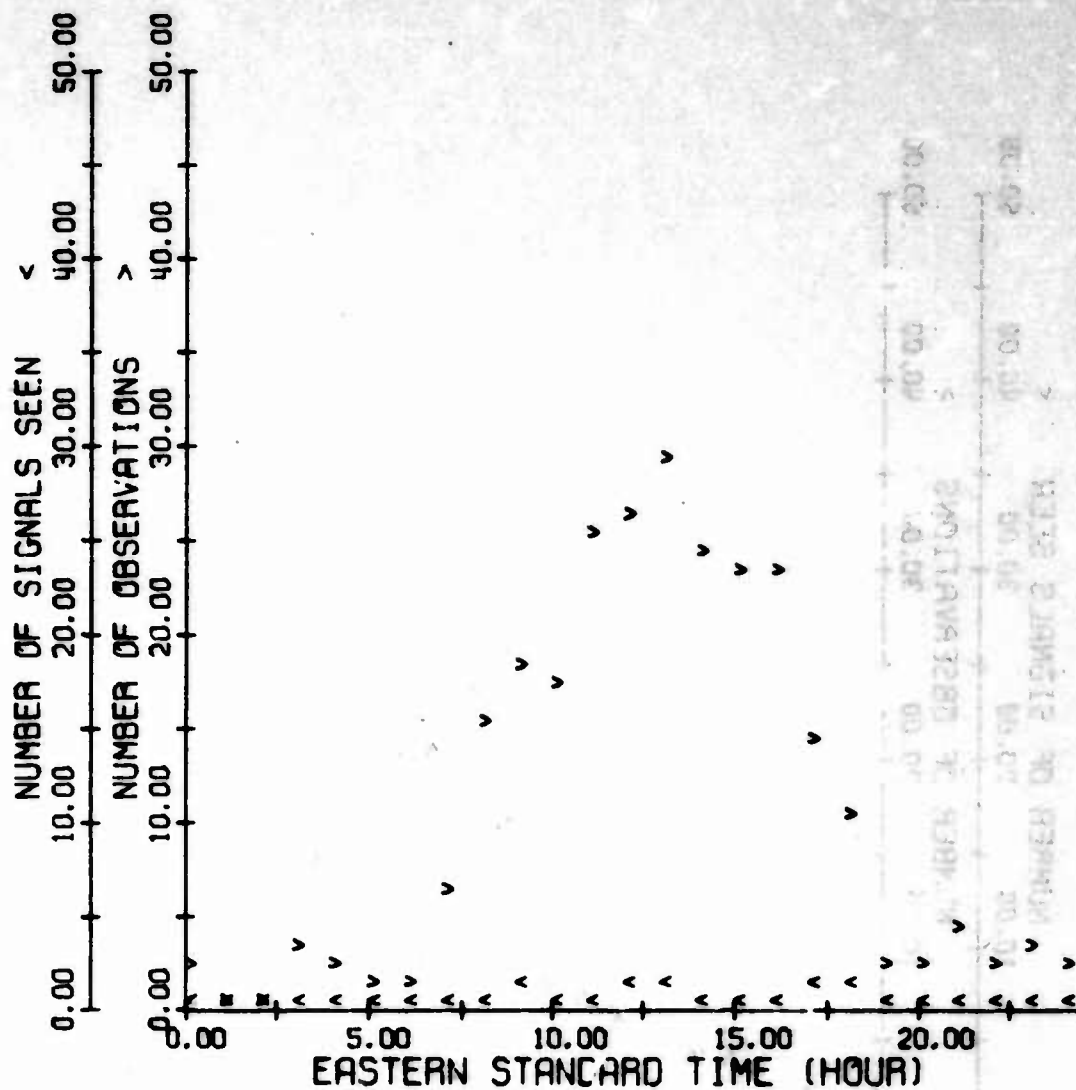


Figure 57. Summary of 2E Mode Observations, Thule Path, Spring 1967

TABLE IX
MODE AVAILABILITY, THULE PATH, MARCH 1967

MODE	3 16	3 17	3 22	3 23	3 24	3 27	3 28	3 29	3 30
1									
2									
3									
4									
5									
6									
7							2 40		
8						02040	2 40		
9			0		12 40		120 0		
10			12 0						
11	02040		2 0						
12	02040		12 0		2 40				
13	02040	2 0	12 0	12040	12040			2 40	
14	02040	2 0	12 0	12040	12 40	12040			
15	02040	12040	12040	12040		12040			
16	02040		2 40	12040		12040			
17						2 40			
18						2240		2 0	
19								1 40	
20									
21	2							02 40	
22	2							2 40	
23	2 0							02 40	
24									0200

Availabilities of 2E, 1F2, N, 2F2, and 2E_s are presented in this order for each date and time indicated.

- 1 = Signal observed via the 2E mode for this hour and date.
- 2 = Signal observed via the 1F2 mode for this hour and date.
- 3 = Signal observed via the N mode for this hour and date.
- 4 = Signal observed via the 2F2 mode for this hour and date.
- 5 = Signal observed via the 2E_s mode for this hour and date.
- 0 = No signal observed via this mode for this hour and date.
- (blank) = No valid data for this mode for this hour and date.

TABLE X
MODE AVAILABILITY, THULE PATH, APRIL 1967

DAY	4	5	6	7	8	9	10	11	12	13	14	15	16	17	18	19	20	21	22	23	24	25	26	27	28	29	30
1																											
2																120 0											
3																1 0											
4																											
5																											
6																											
7															12 0								11 0				
8									12 0						1 0								12 40				
9									12340 12 0						12 0								02000 12 0 12340				
10									02040 12040 12340						12 0 12 0								2 0 1 0 12 40				
11									120 0 123 0 12 40 10000 12 0 12 0 12 0												12 0 2 0 12 40 12040 12 40						
12									120 0 12040 12040 12 40 12 40 12 0 12 40												12 0 1 0 12 40 12340 12 40						
13									02000 120 0 12040 12 40 12040 12 0												12 0 1 0 12 40 12 40						
14									12 0 12 0 120 0 12 40 12040 120 0												12 40 12 40						
15									12 0 12 40 12 40 12 40 12 0												4 12 0 12 0 12 40						
16									12 0 12040 12340 12 40												123 0 12 0 12 0 12 0						
17									12340 02340 12340 12340												02040 12 0						
18									12340 02040 12340 12340												02340						
19									2 40																		
20									2 40																		
21									020 0												2340						
22									02340																		
23									02 0																		
24									02 40																		

Availabilities of 2E, 1F2, N, 2F2, and 2E_u are presented in this order for each date and time indicated.

- 1 = Signal observed via the 2E mode for this hour and date.
- 2 = Signal observed via the 1F2 mode for this hour and date.
- 3 = Signal observed via the N mode for this hour and date.
- 4 = Signal observed via the 2F2 mode for this hour and date.
- 5 = Signal observed via the 2E_u mode for this hour and date.
- 0 = No signal observed via this mode for this hour and date.
- (blank) = No valid data for this mode for this hour and date.

TABLE XI

MODE AVAILABILITY, THULE PATH, MAY 1967

DAY	1	2	3	4	5	6	7	8	9	10	11	12	13	14	15	16	17	18	19	20	21	22	23	24
1																								
2																								
3																								
4																								
5																								
6																								
7																								
8																								
9																								
10																								
11																								
12																								
13																								
14																								
15																								
16																								
17																								
18																								
19																								
20																								
21																								
22																								
23																								
24																								

Availabilities of 2E, 1F2, N, 2F2, and 2E_g are presented in this order for each date and time indicated.

- 1 = Signal observed via the 2E mode for this hour and date.
- 2 = Signal observed via the 1F2 mode for this hour and date.
- 3 = Signal observed via the N mode for this hour and date.
- 4 = Signal observed via the 2F2 mode for this hour and date.
- 5 = Signal observed via the 2E_g mode for this hour and date.
- 0 = No signal observed via this mode for this hour and date.
- (blank) = No valid data for this mode for this hour and date.

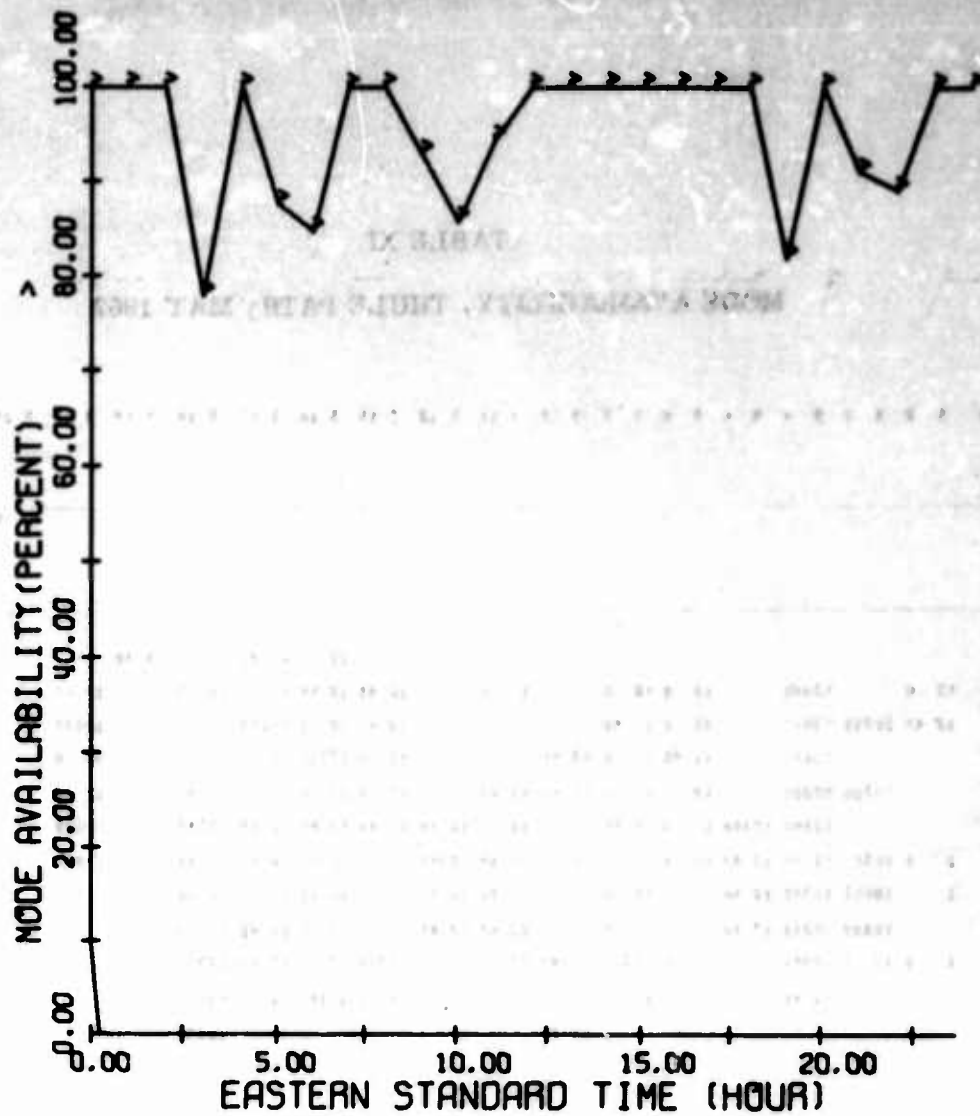


Figure 58. 2E Mode Availability, Coco Solo Path, Winter 1966

3. MODE AVAILABILITY -- COCO SOLO TO STOCKBRIDGE/STARR HILL

The hourly mode availability results obtained on the Coco Solo to Stockbridge path and later from Coco Solo to Starr Hill will be presented in this section on a seasonal basis, rather than on a monthly basis which has generally been done in the past (Refs. 2, 4, and 6). The 2E mode shown in Figures 58 - 64 provides quite characteristic daytime mode availability, but for the winter of 1966 and the spring of 1966 it has a greater nighttime availability than is realistic. The reason for this is that the 2E_s and the standard 2E modes were lumped together as the 2E mode availability during these periods. This procedure was used into the first month of summer 1966 providing a higher nighttime 2E mode availability than is generally realistic. The first full season in which the 2E_s mode was considered separately, or rather an attempt made to remove it, was autumn of 1966, where there is a considerable amount of nighttime E shown, particularly in the after-midnight hours. Whether this is nocturnal E or sporadic-E propagation is questionable at this time. During the winter and spring of 1967 the daytime 2E mode availability remains quite standard, but again the question of whether the nighttime E is a nocturnal 2E mode or a sporadic 2E mode still exists. During the summer of 1967 the good daytime 2E mode availability lags the sunrise and lasts until almost midnight. An attempt has been made to remove all sporadic-E modes, particularly during the winter, spring, and summer of 1967 (Figures 86 and 87). As a quick summary, the daytime 2E mode availability is quite good, but the nighttime 2E mode availability (as expected) is quite poor.

The seasonal 1F2 mode availability on the Coco Solo to Central New York path is presented in Figures 65 - 71. There has been some blocking at night in the winter of 1966, probably from sporadic-E, although that was not fully identified at the time. The results for spring of 1966 are somewhat more consistent -- the summer is a little higher and autumn falls away quite radically in the forenoon and afternoon hours. The mode availabilities for winters of 1966 and 1967 are somewhat different during the hours around noontime in that the 1F2 mode has less than 100 percent availability in the winter of 1967, whereas it was 100 percent for the winter of 1966. There has been a considerable increase in sunspot activity during this 12-month period (from a SSN of 28 for January 1966 to SSN of 73 for January 1967); however, the spring of 1967 has the best 1F2 mode availability (Figures 65 - 71). The results for the summer of 1967 do not differ much from those for the summer of 1966.

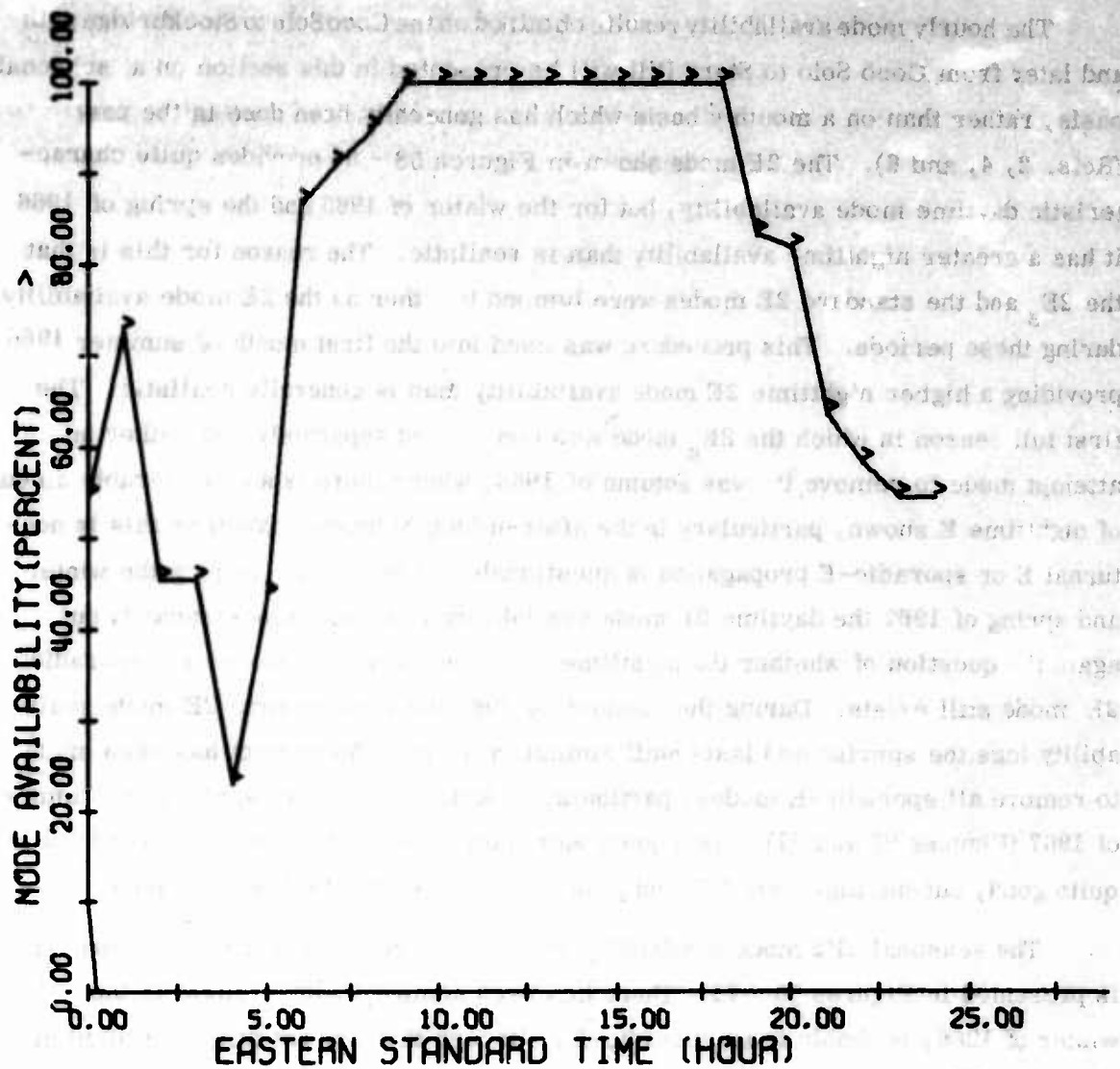


Figure 59. 2E Mode Availability, Coco Solo Path, Spring 1966

The N mode (Figures 72 - 78) shows its usual erratic character: during the summer of 1966 its mode availability is quite good; the worst N mode availability shows up in the spring and summer of 1967.

The 2F2 mode (Figures 79 - 85) has the best overall mode availability of all the modes considered, and is the best on a seasonal basis for the winter of 1967, with 100 percent mode availability at all times. Unfortunately, its use is tempered by its lower junction frequency compared to the 1F2 mode.

The best information on sporadic-E propagation (Figures 86 and 87) or the $2E_s$ mode is shown for the spring of 1967; interestingly enough, availability exists during both daytime and nighttime. The summer of 1967 shows a quite high incidence of this mode. Note also that the sporadic-E layer probably has a much greater nuisance value to the other modes of propagation than as a means of propagation itself.

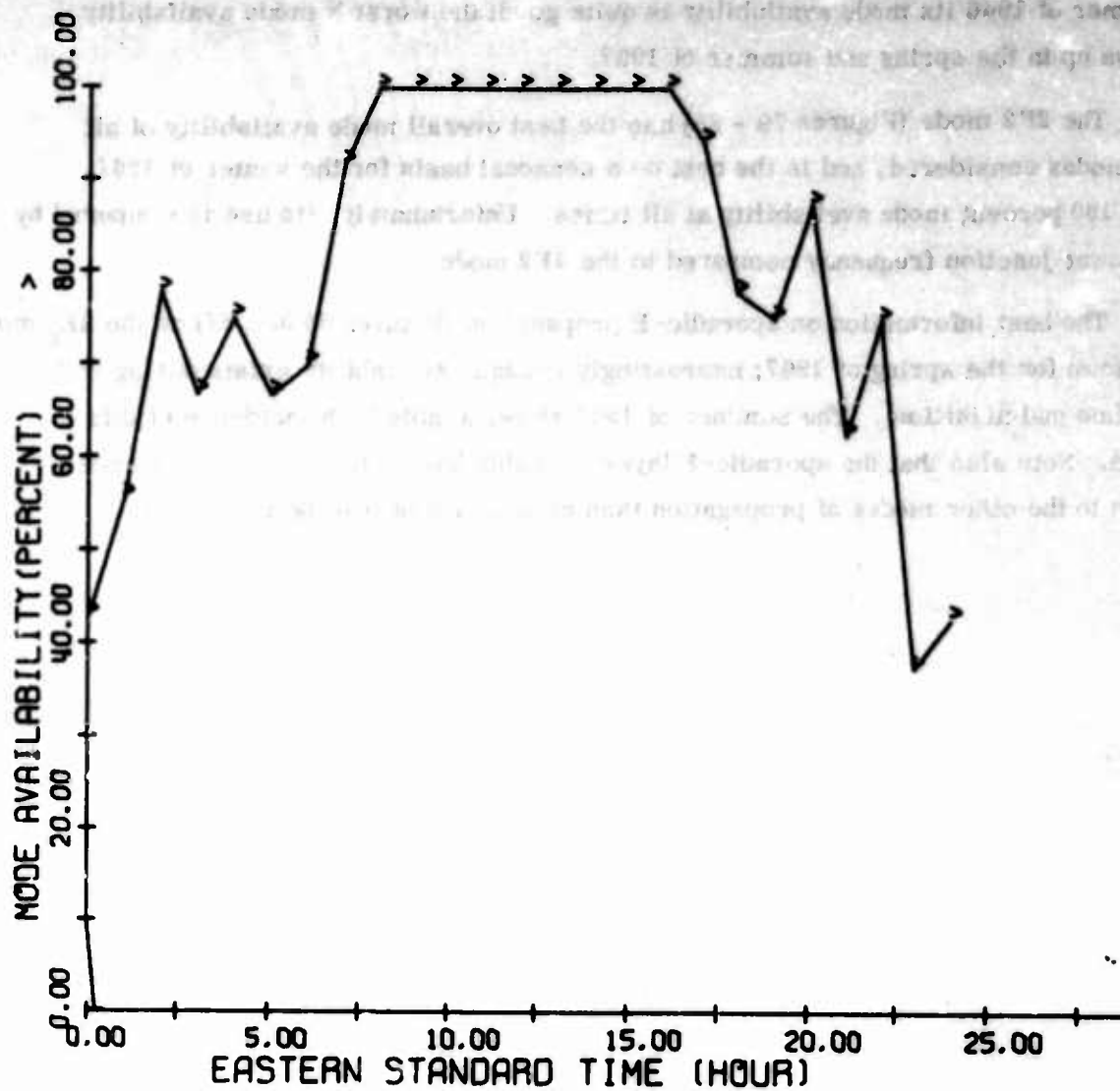


Figure 60. 2E Mode Availability, Coco Solo Path, Summer 1966

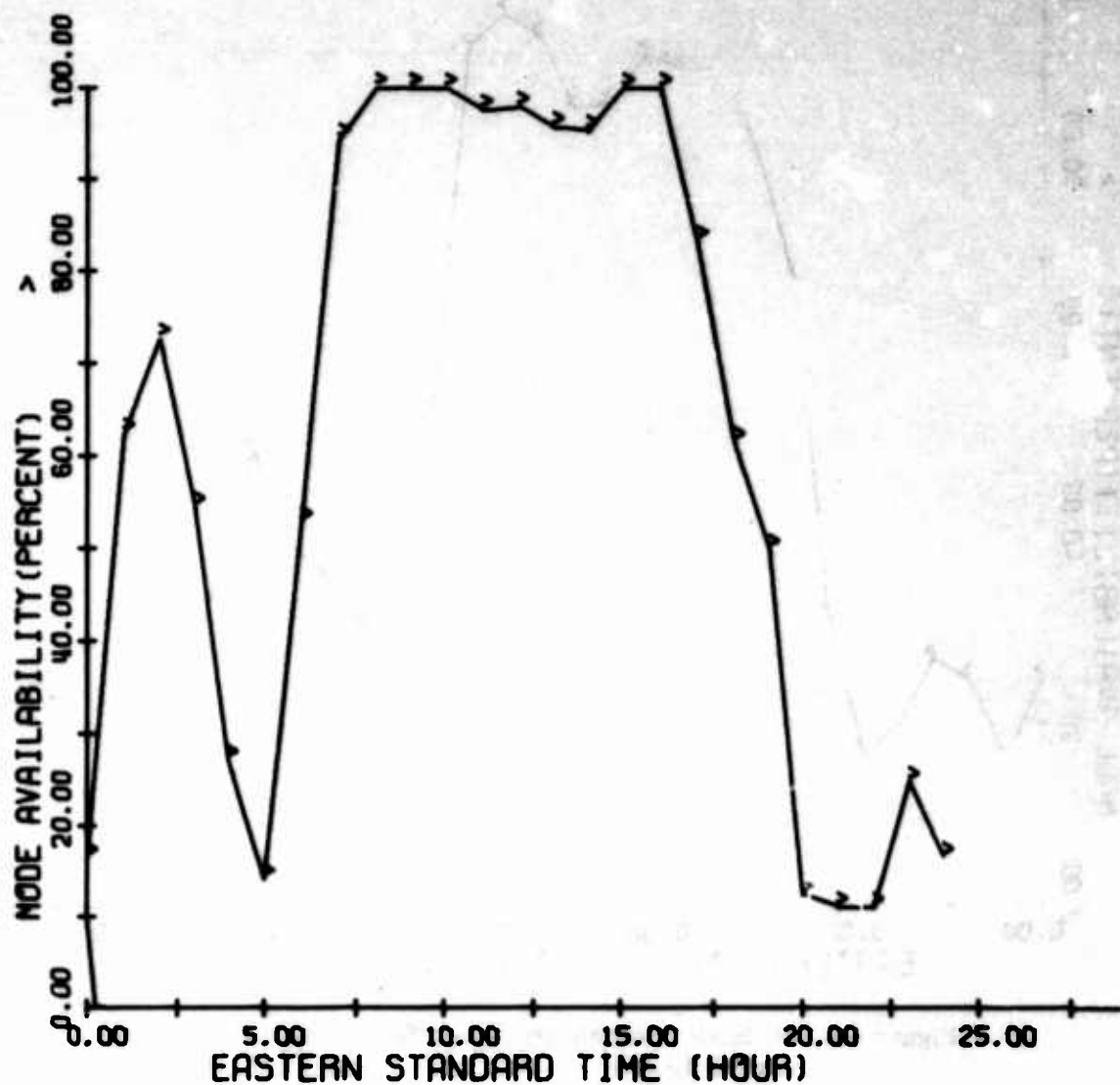


Figure 61. 2E Mode Availability, Coco Solo Path, Autumn 1966

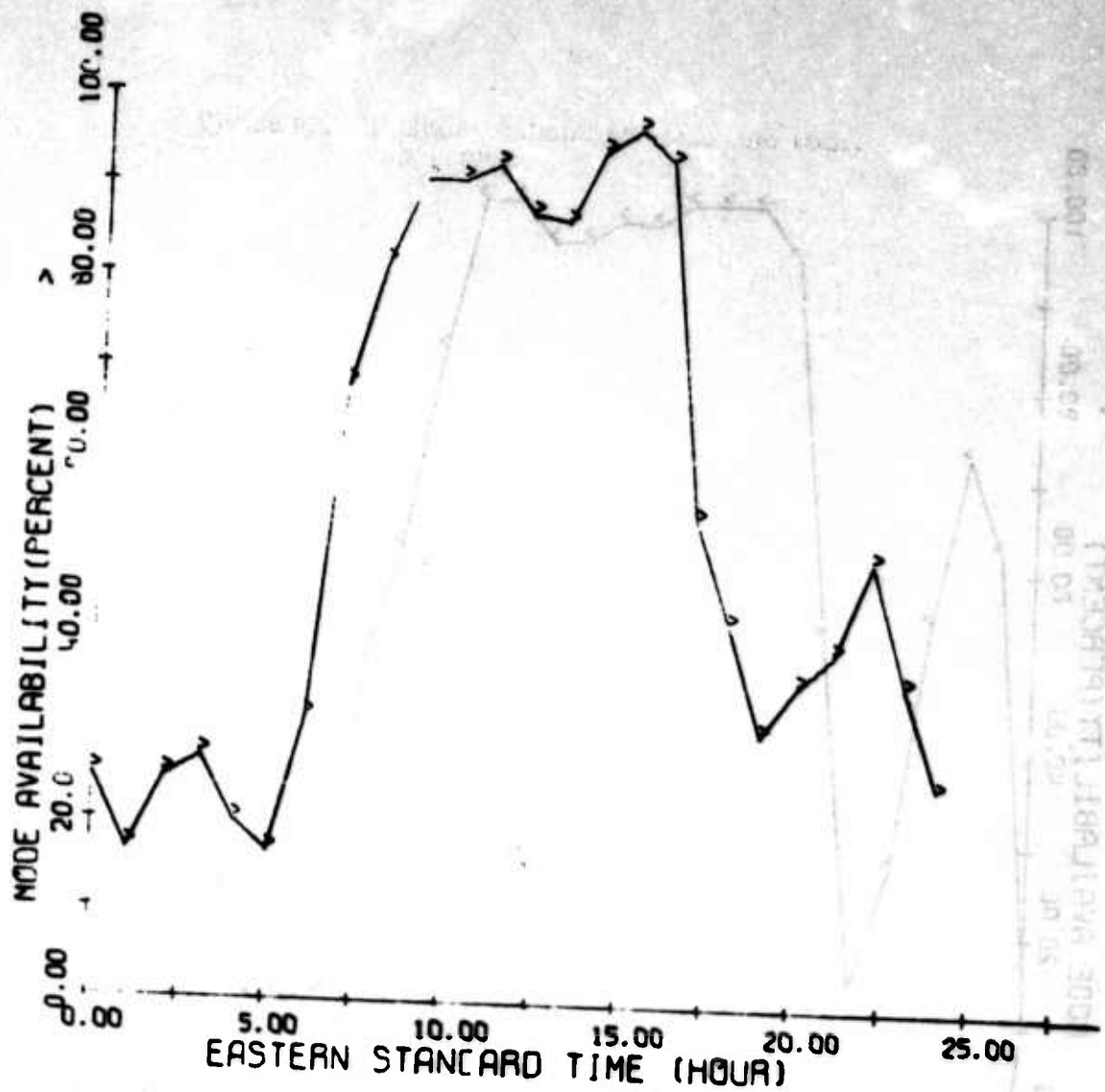


Figure 62. 2E Mode Availability, Coco Solo Path, Winter 1967

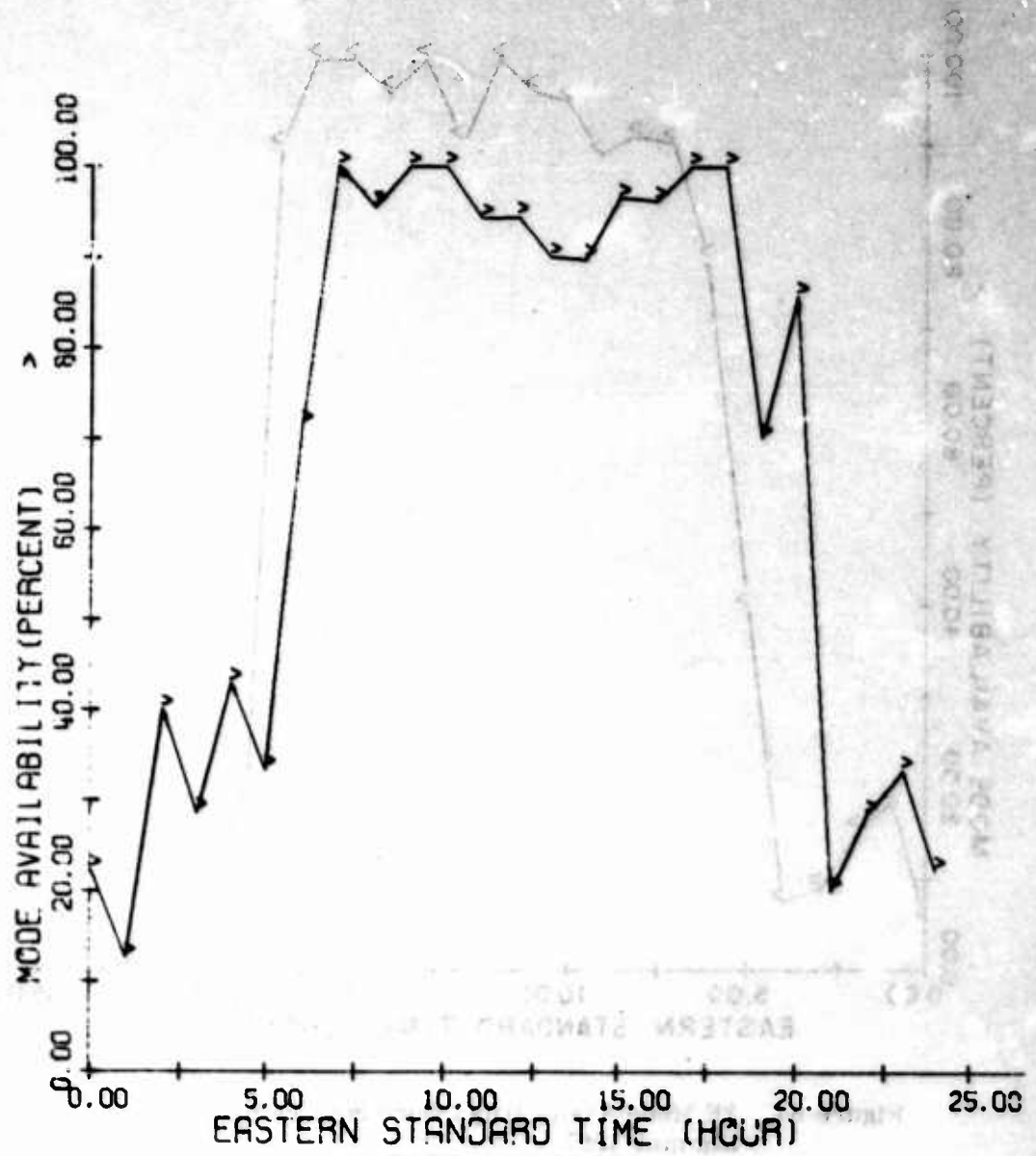


Figure 63. 2E Mode Availability, Coco Solo Path, Spring 1967

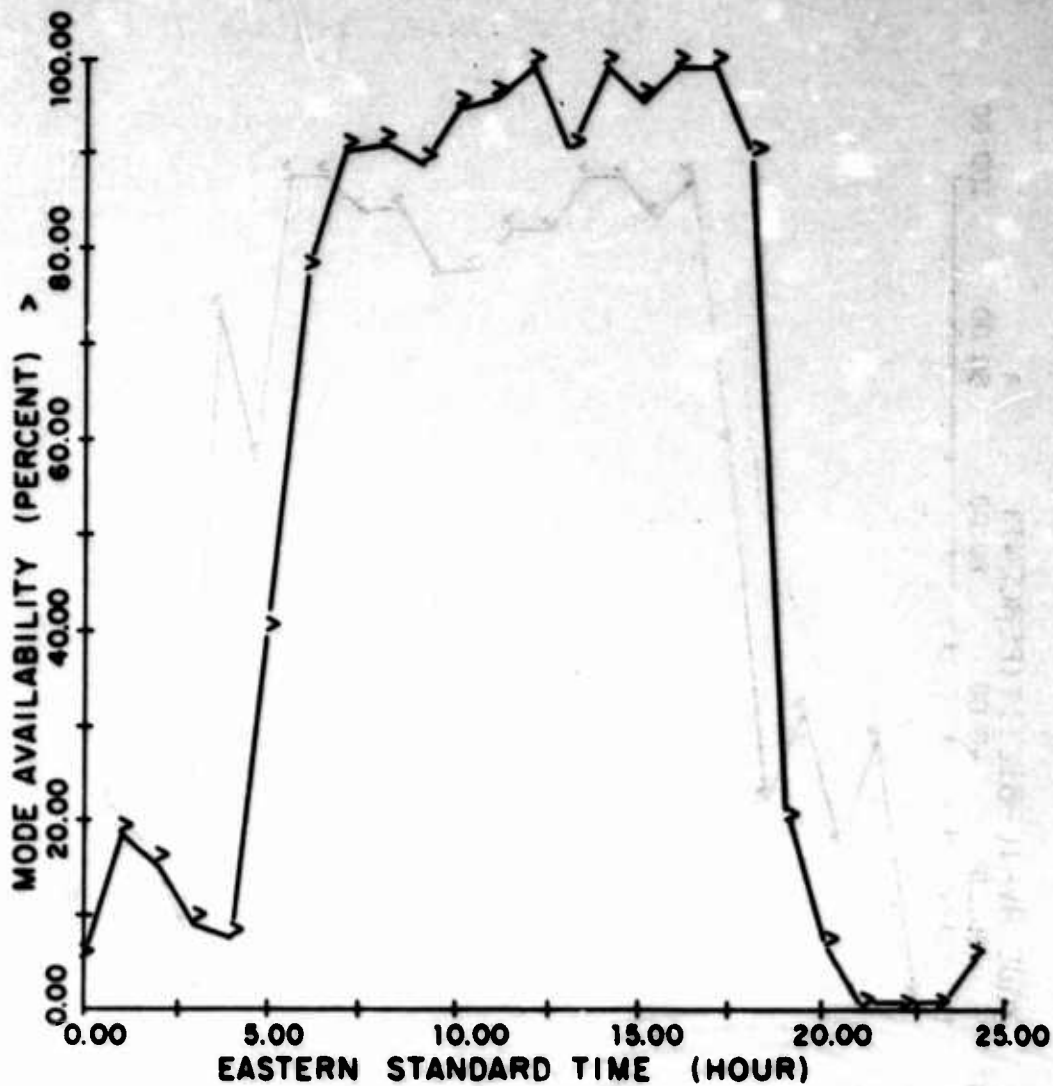


Figure 64. 2E Mode Availability, Cozo Solo Path, Summer 1967

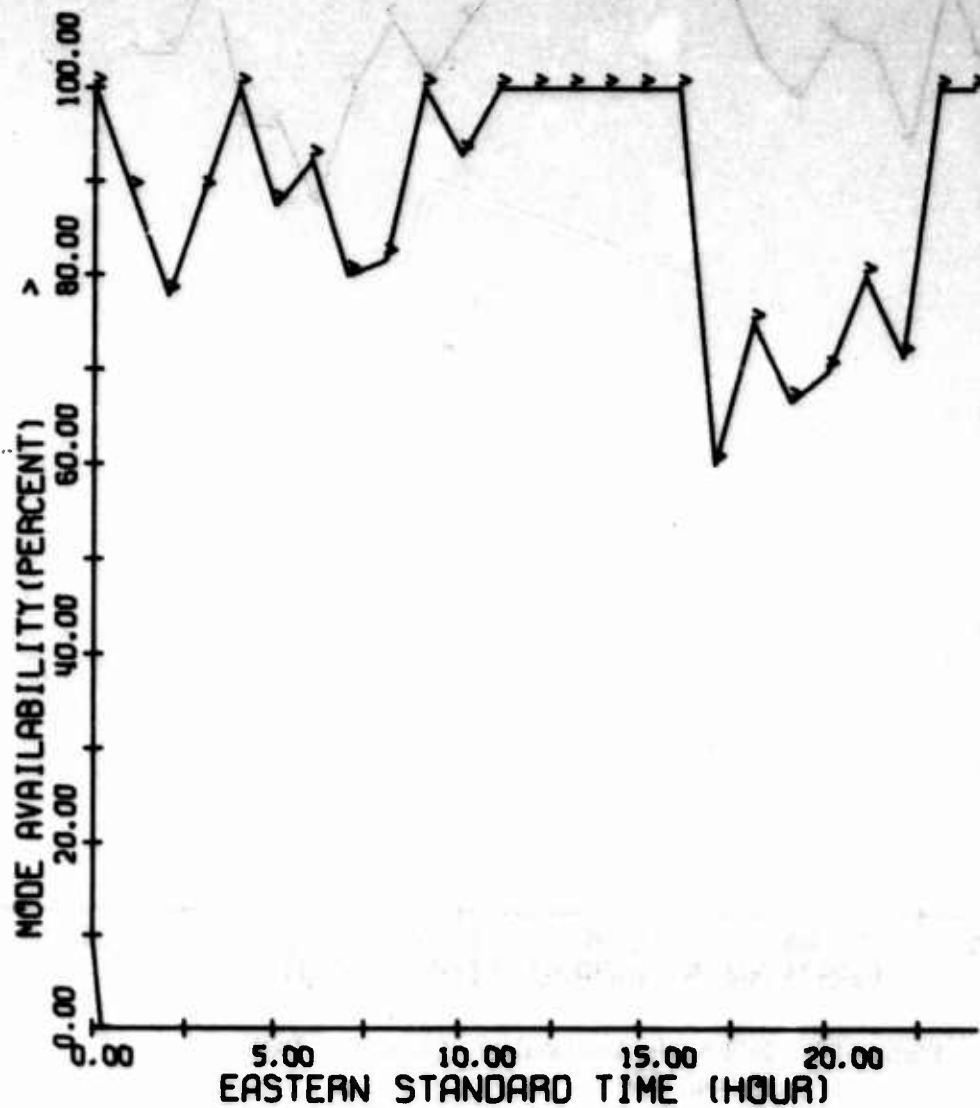


Figure 65. 1F2 Mode Availability, Coco Solo Path, Winter 1966

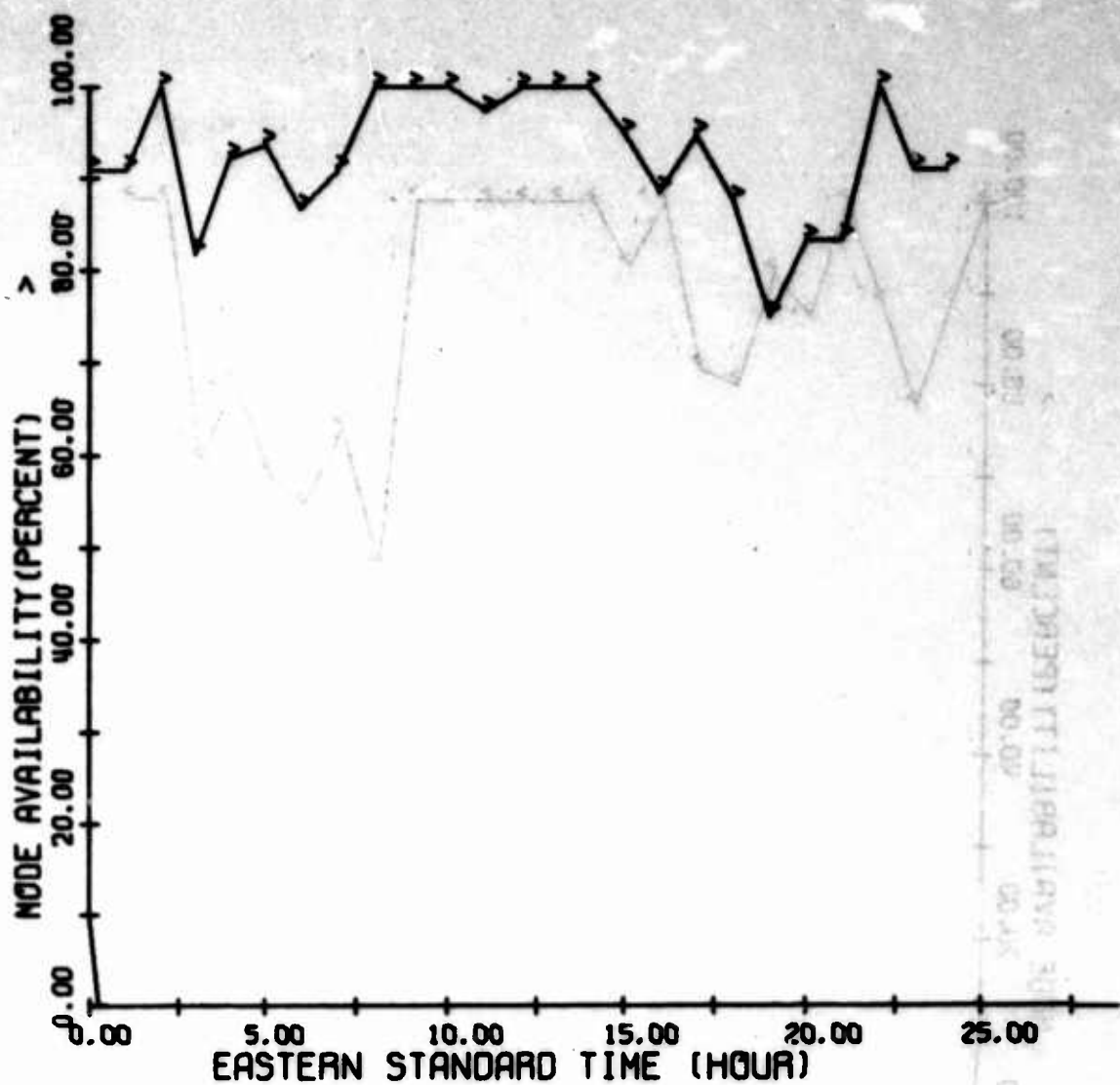


Figure 66. 1F2 Mode Availability, Coco Solo Path, Spring 1966

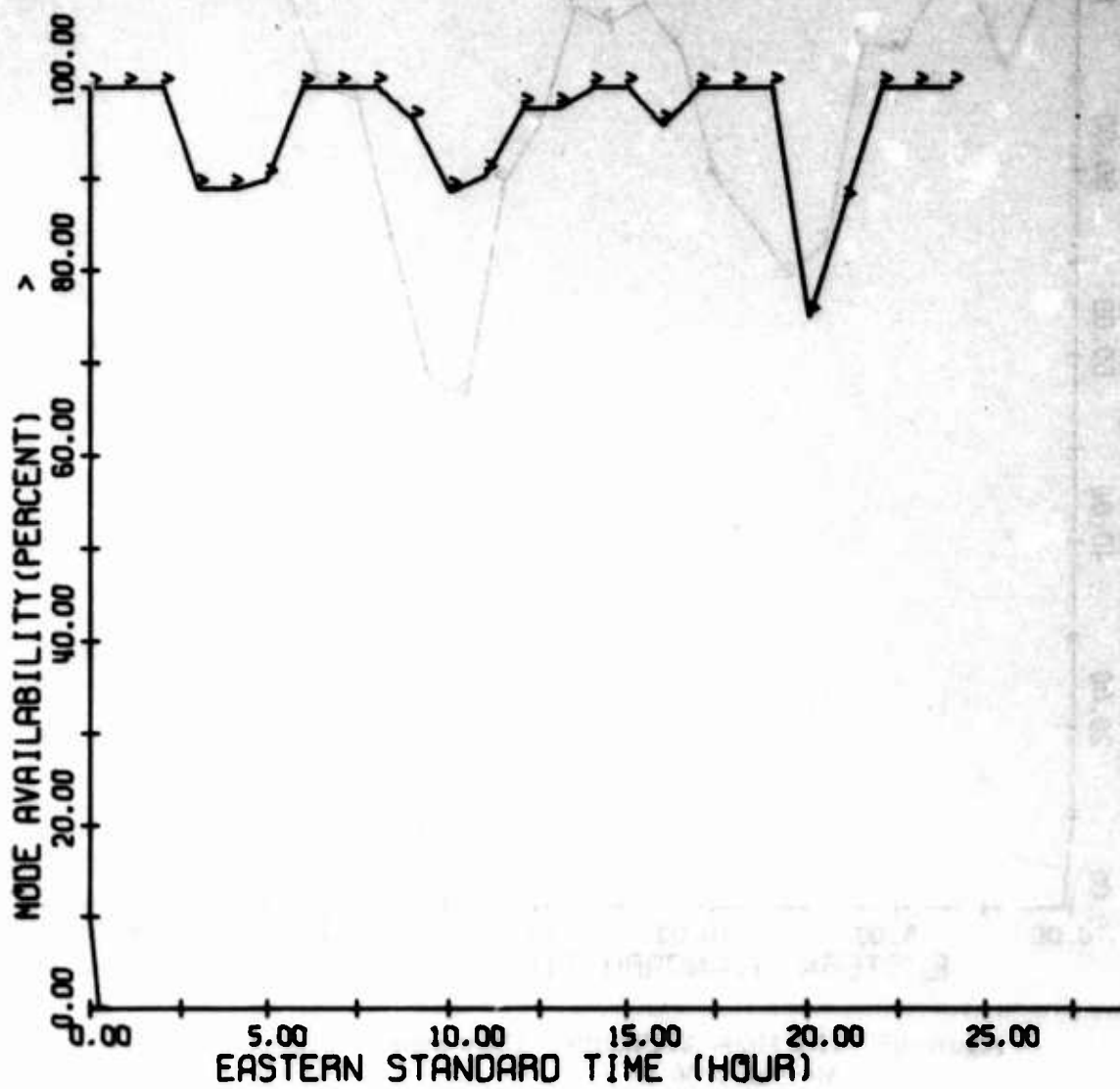


Figure 67. 1F2 Mode Availability, Coco Solo Path, Summer 1966

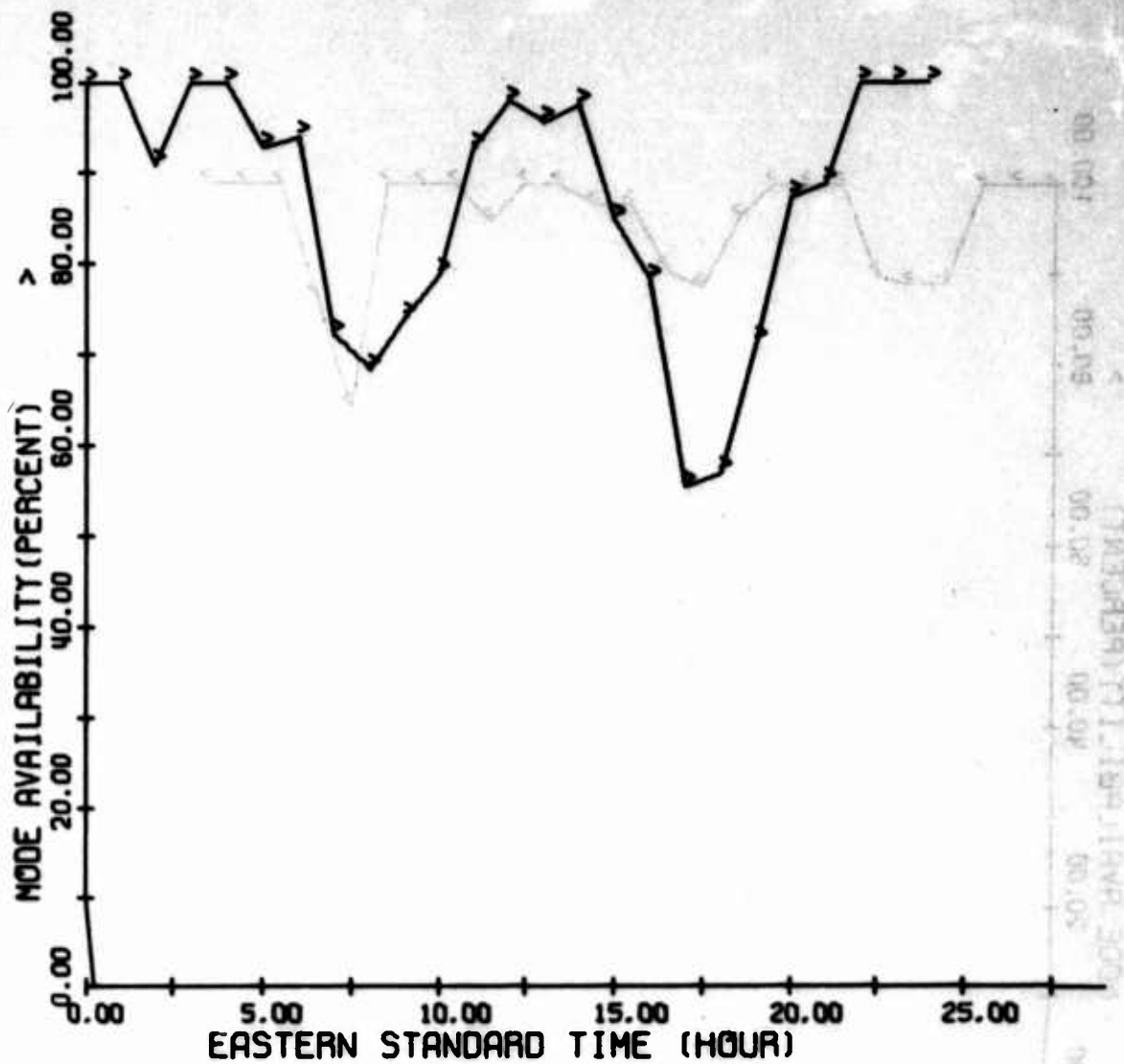


Figure 68. 1F2 Mode Availability, Coco Solo Path, Autumn 1966

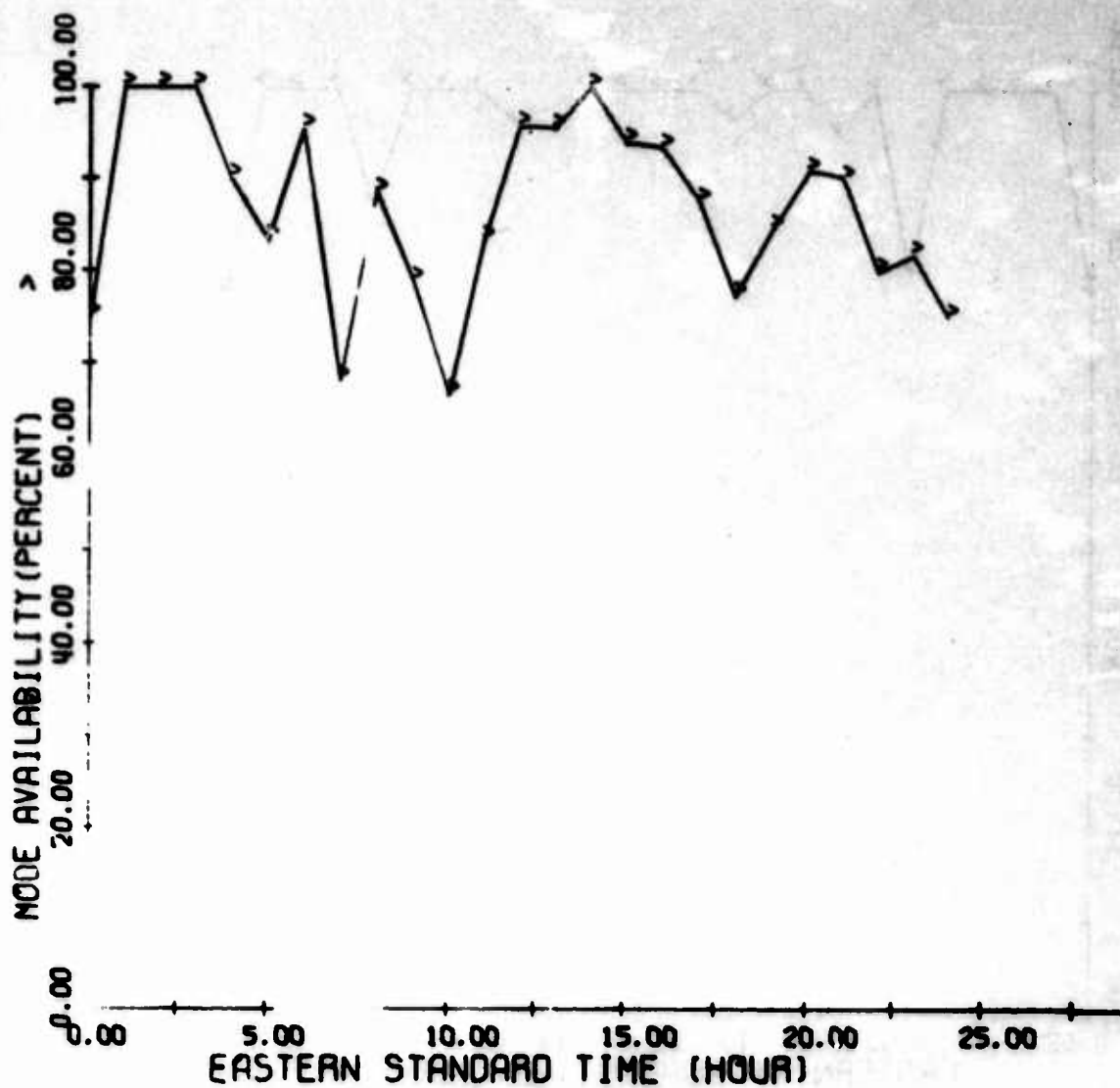


Figure 69. 1F2 Mode Availability, Coco Solo Path, Winter 1967

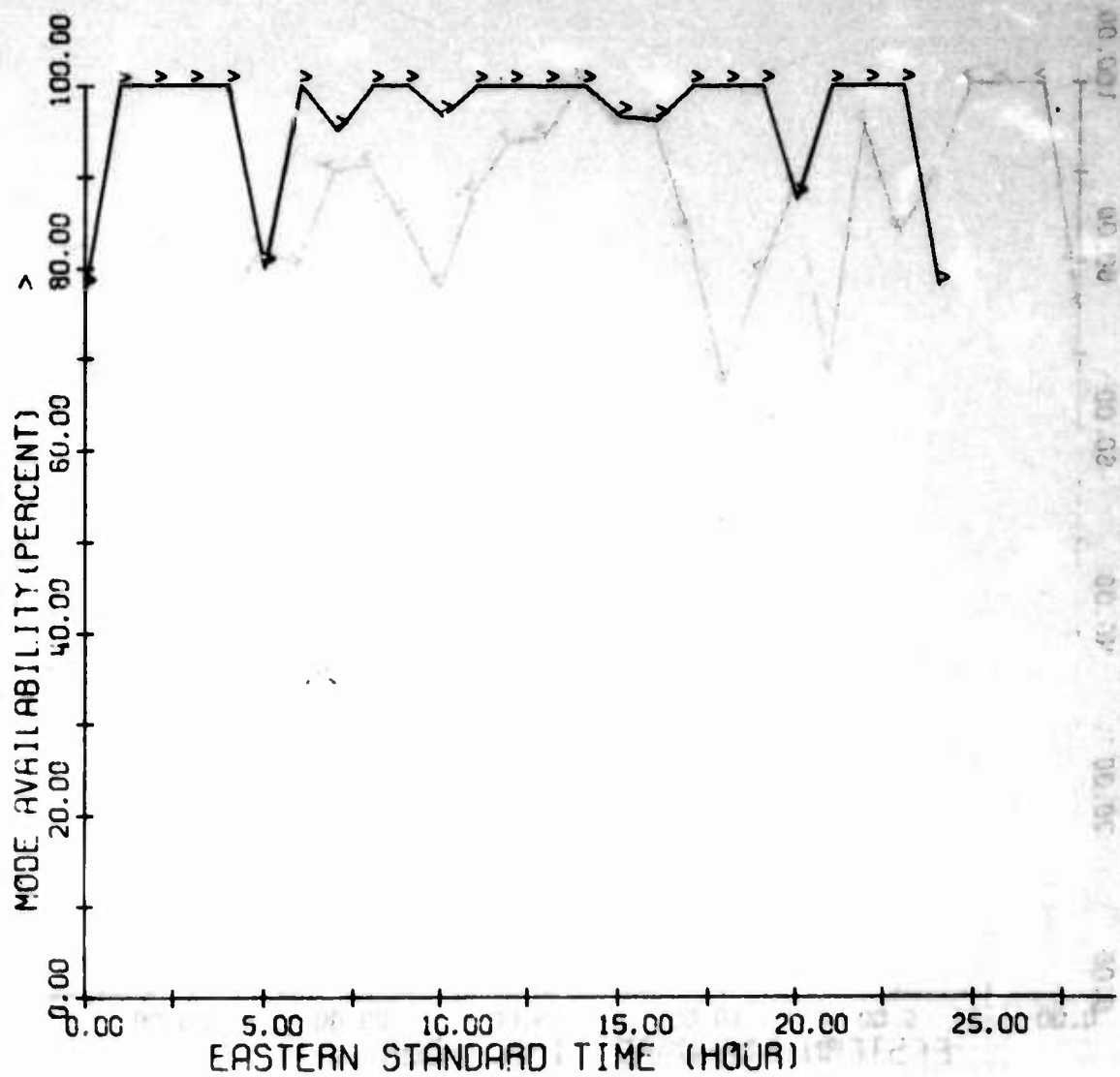


Figure 70. 1F2 Mode Availability, Coco Solo Path, Spring 1967

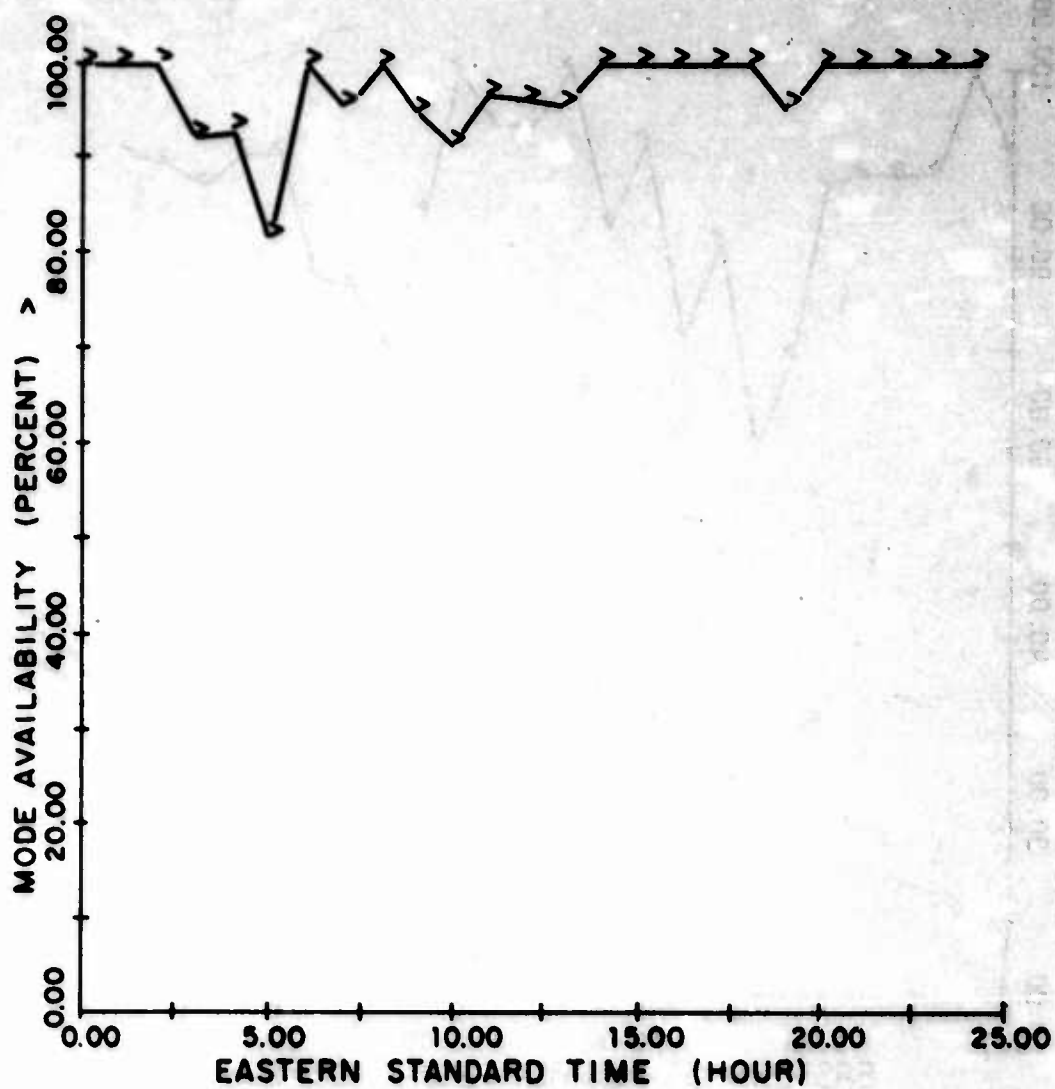


Figure 71. 1F2 Mode Availability, Coco Solo Path, Summer 1967

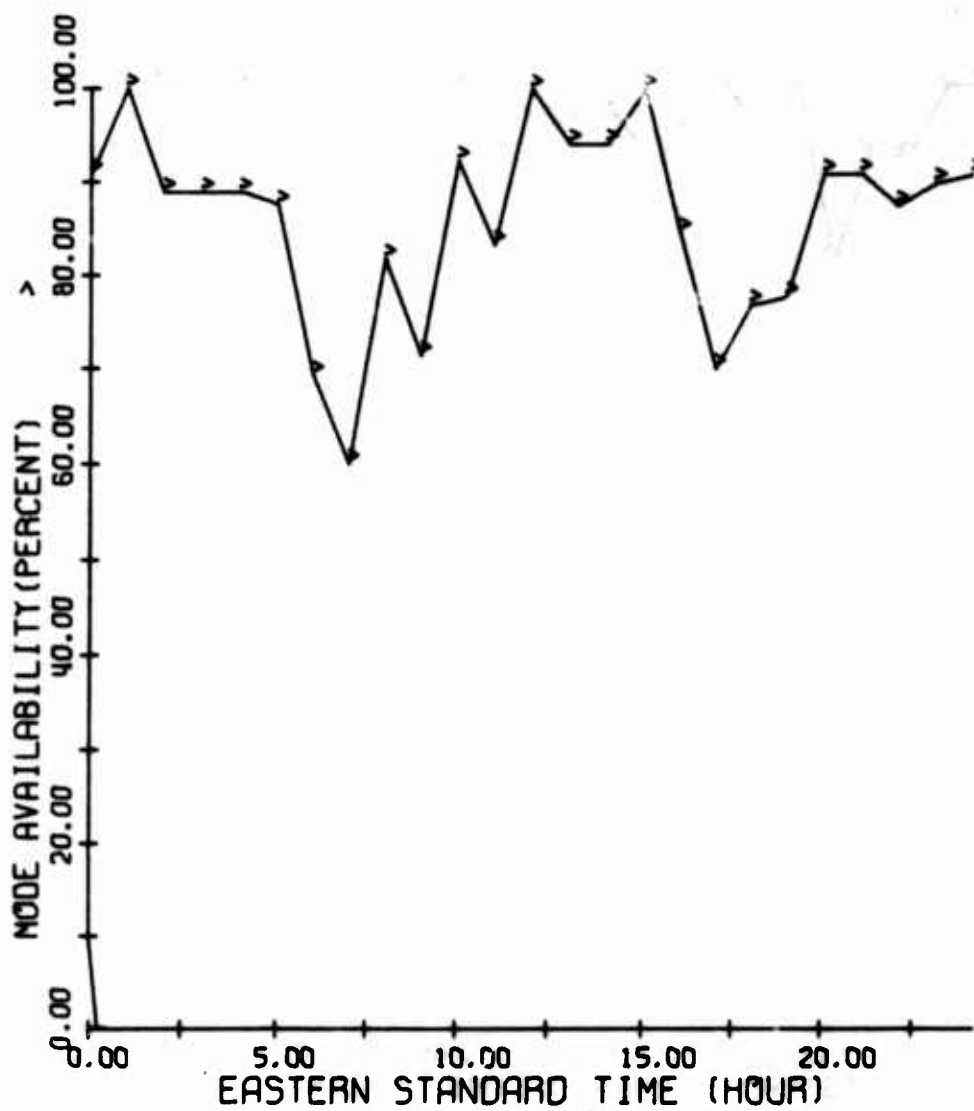


Figure 72. N Mode Availability, Coco Solo Path, Winter 1966

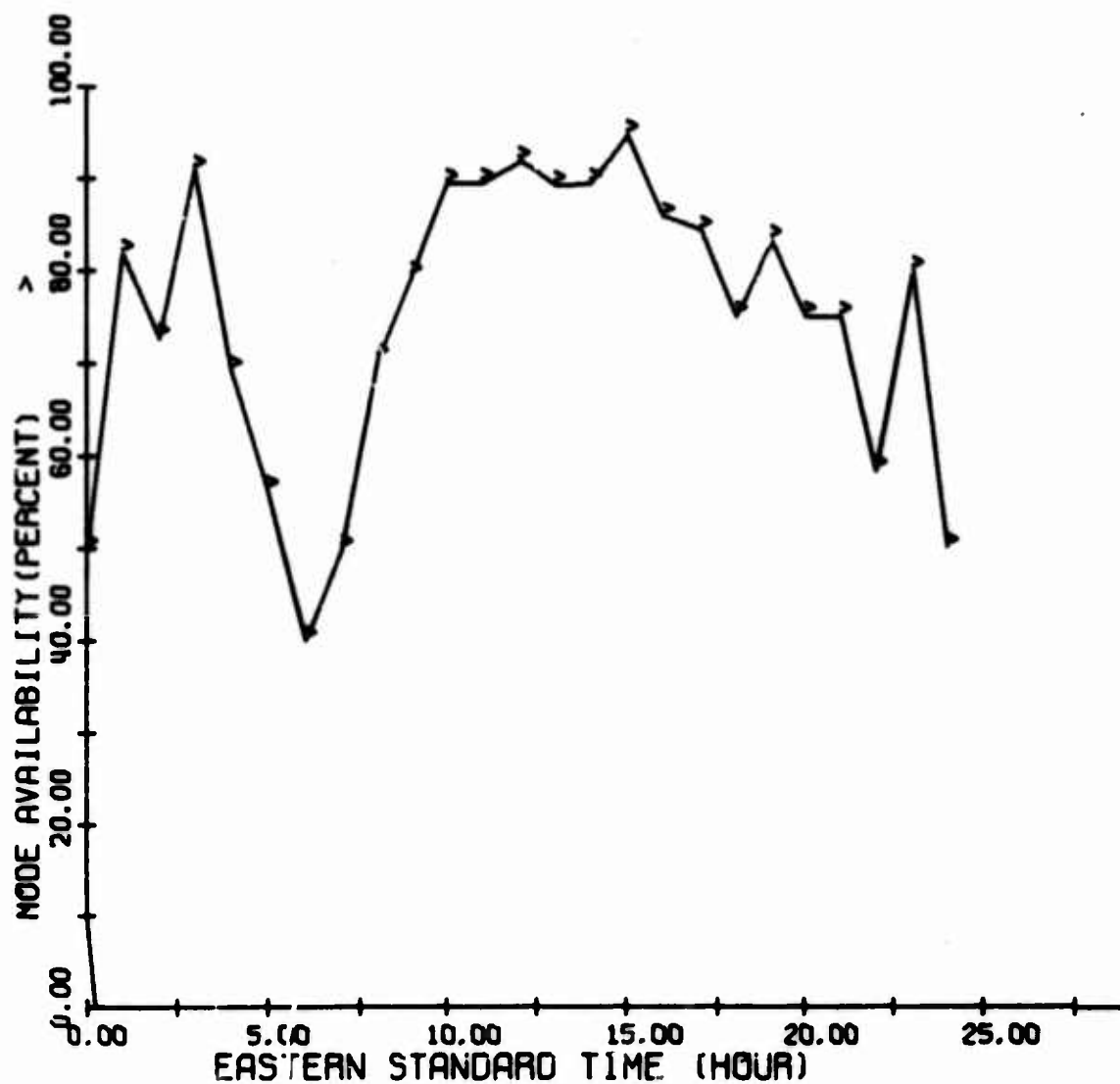


Figure 73. N Mode Availability, Coco Solo Path,
Spring 1966

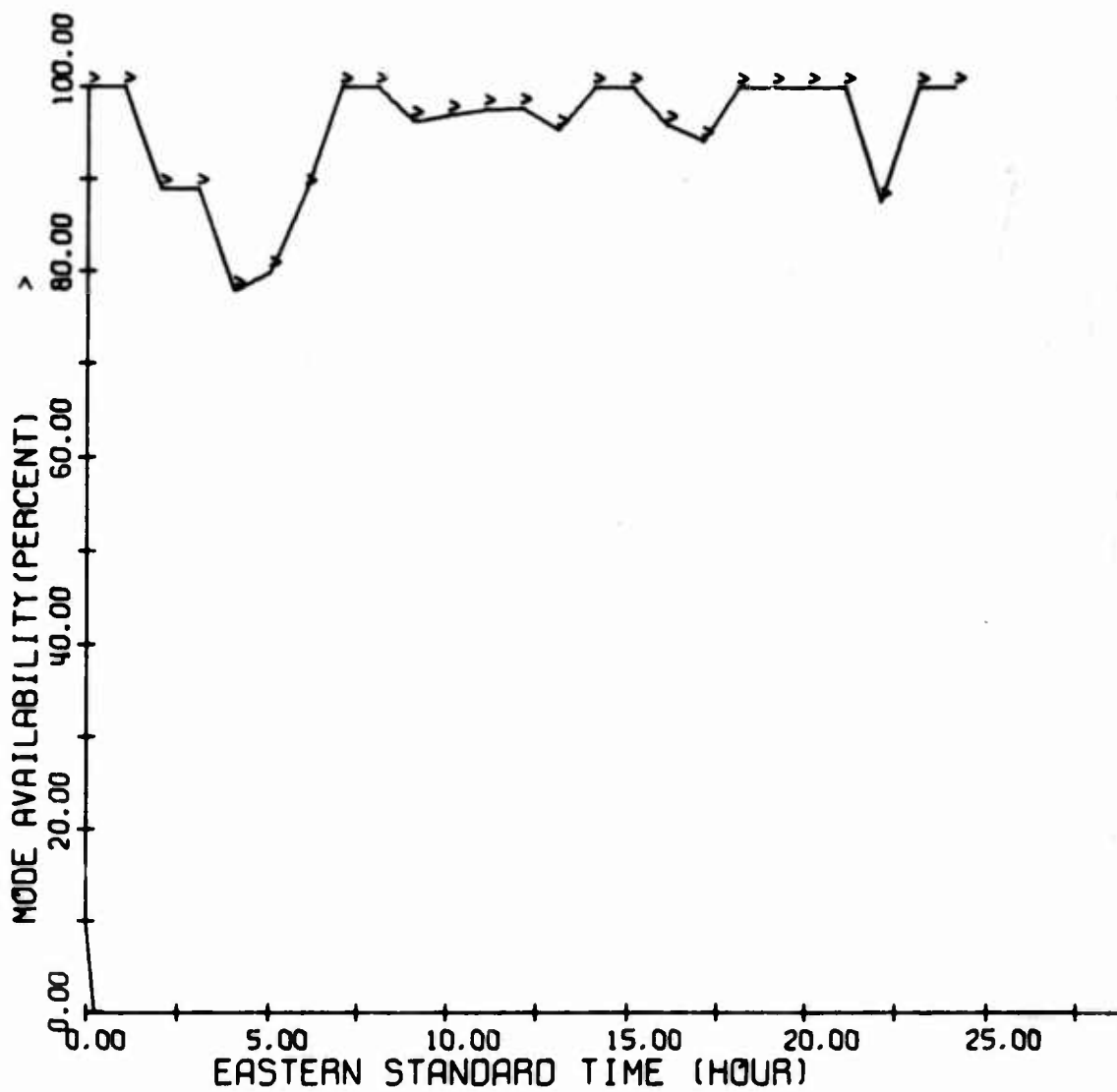


Figure 74. N Mode Availability, Coco Solo Path, Summer 1966

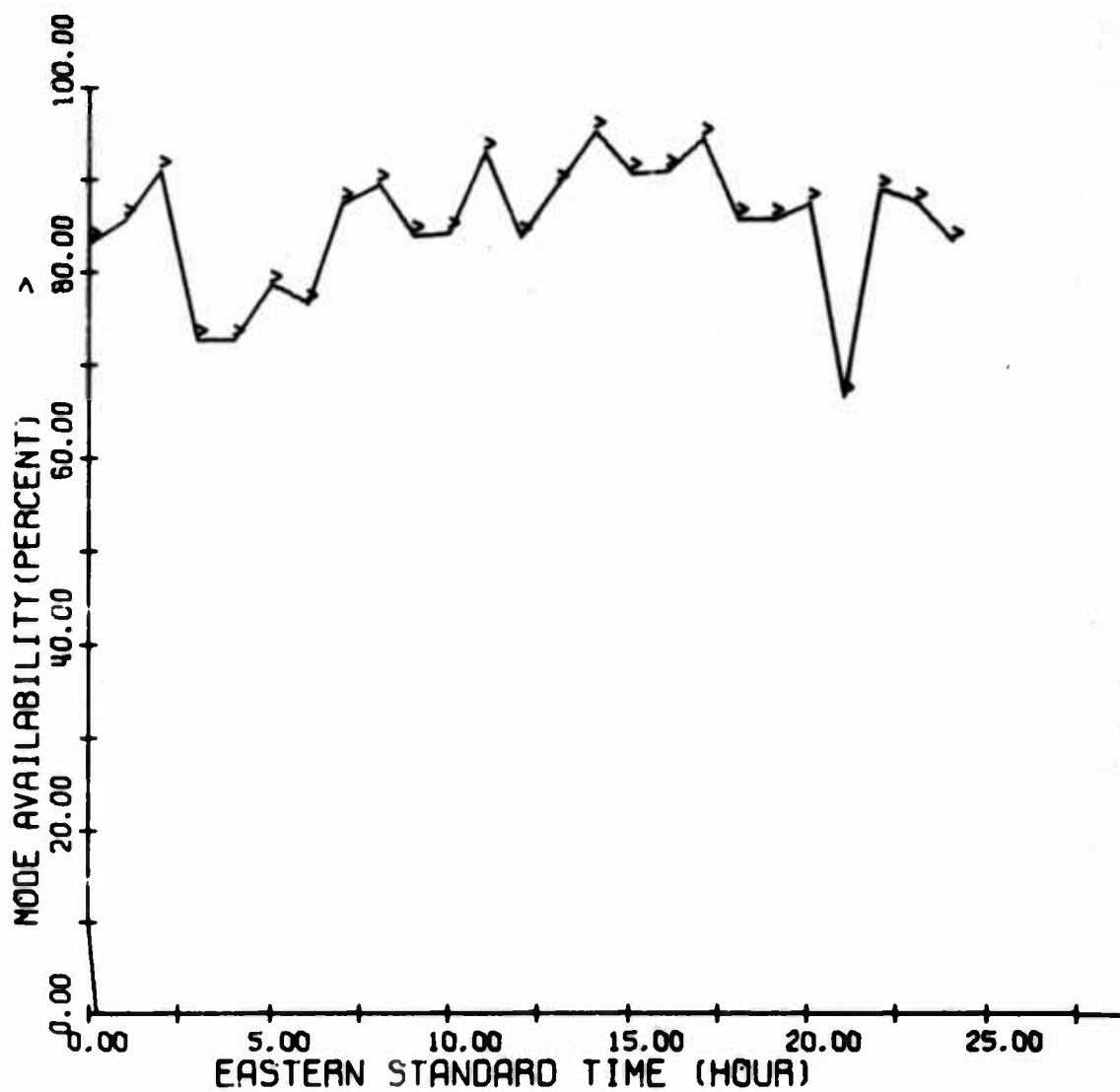


Figure 75. N Mode Availability, Coco Solo Path, Autumn 1966

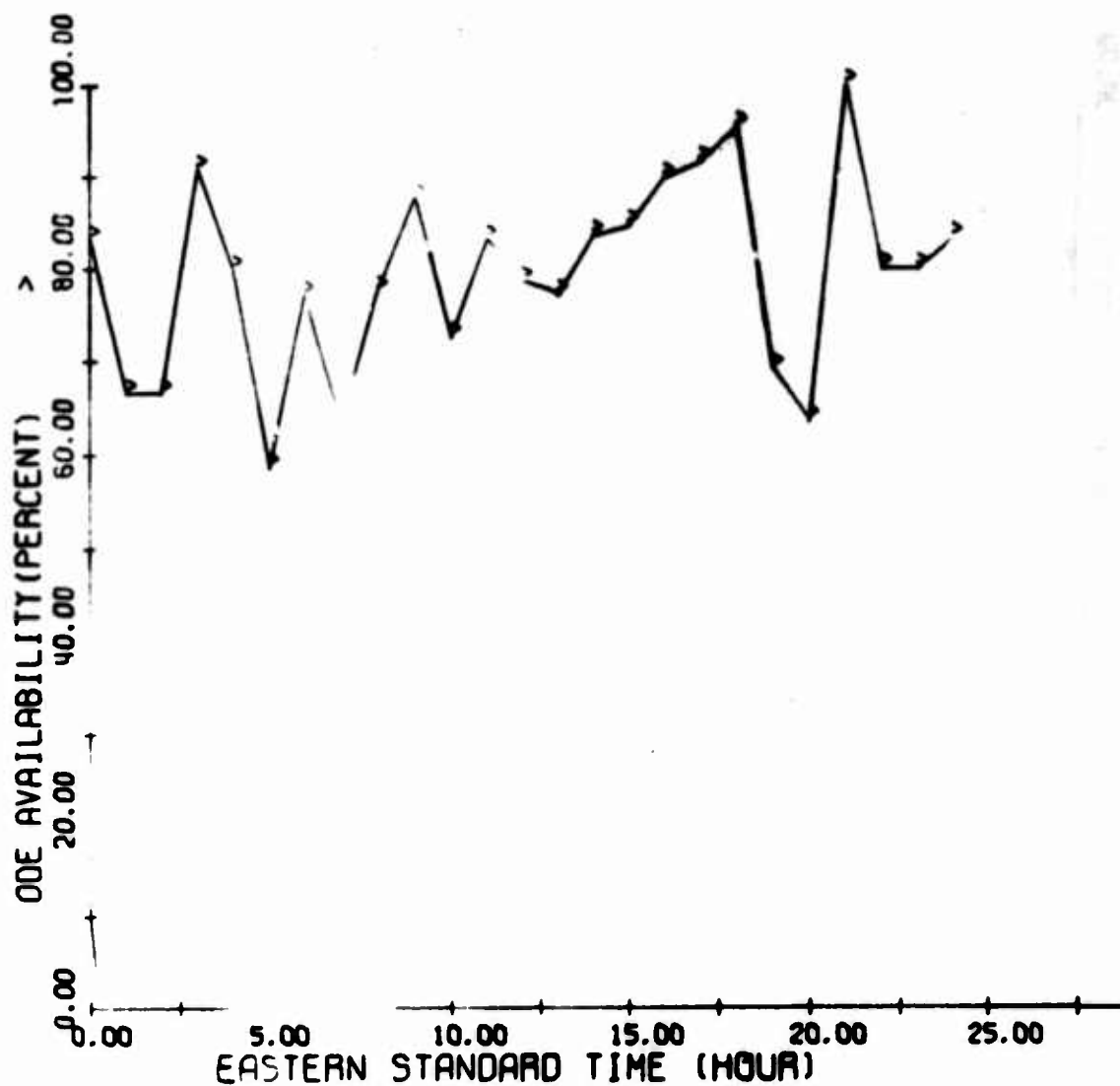


Figure 76. N Mode Availability, Coco Solo Path,
Winter 1967

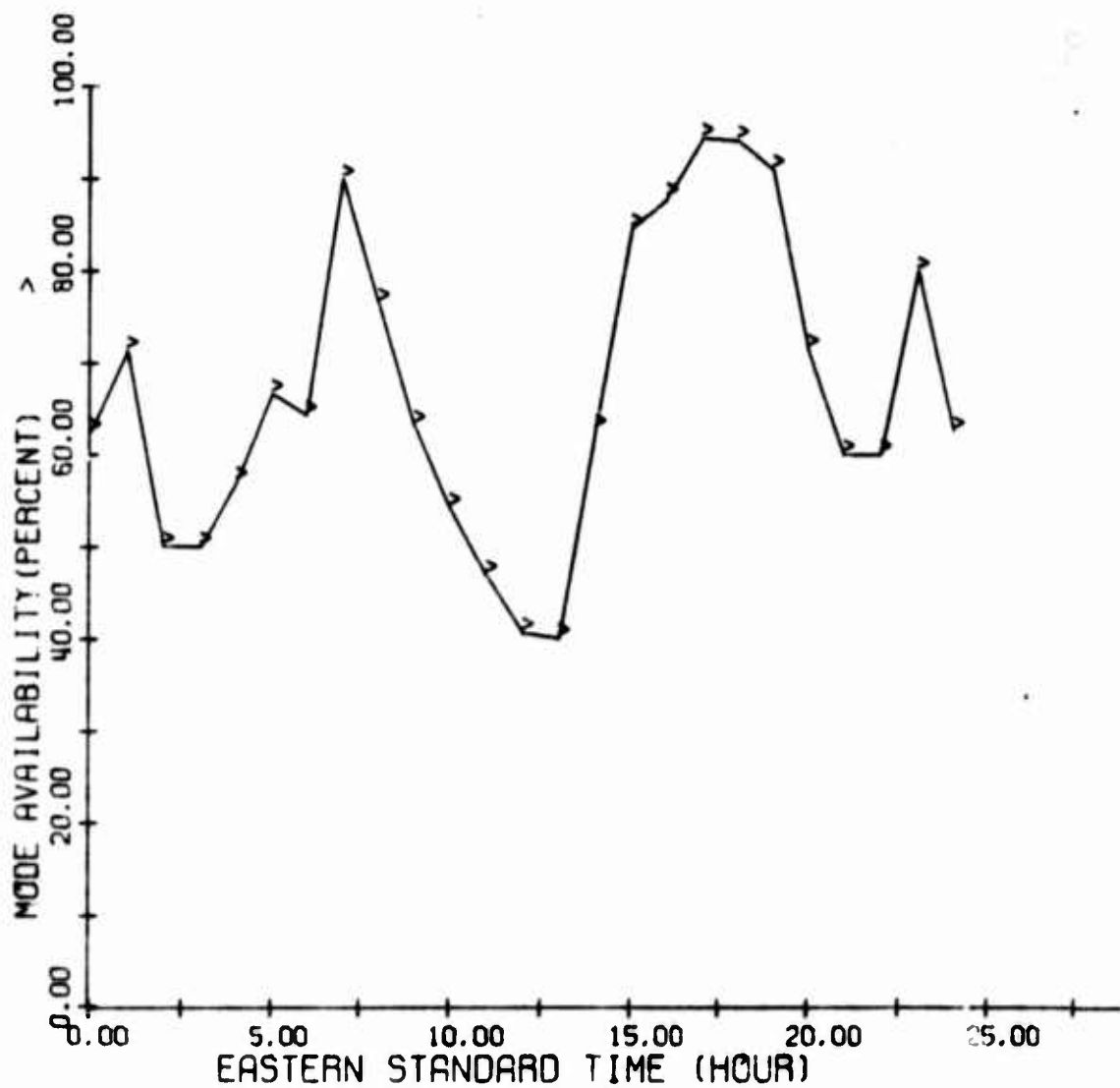


Figure 77. N Mode Availability, Coco Solo Path, Spring 1967

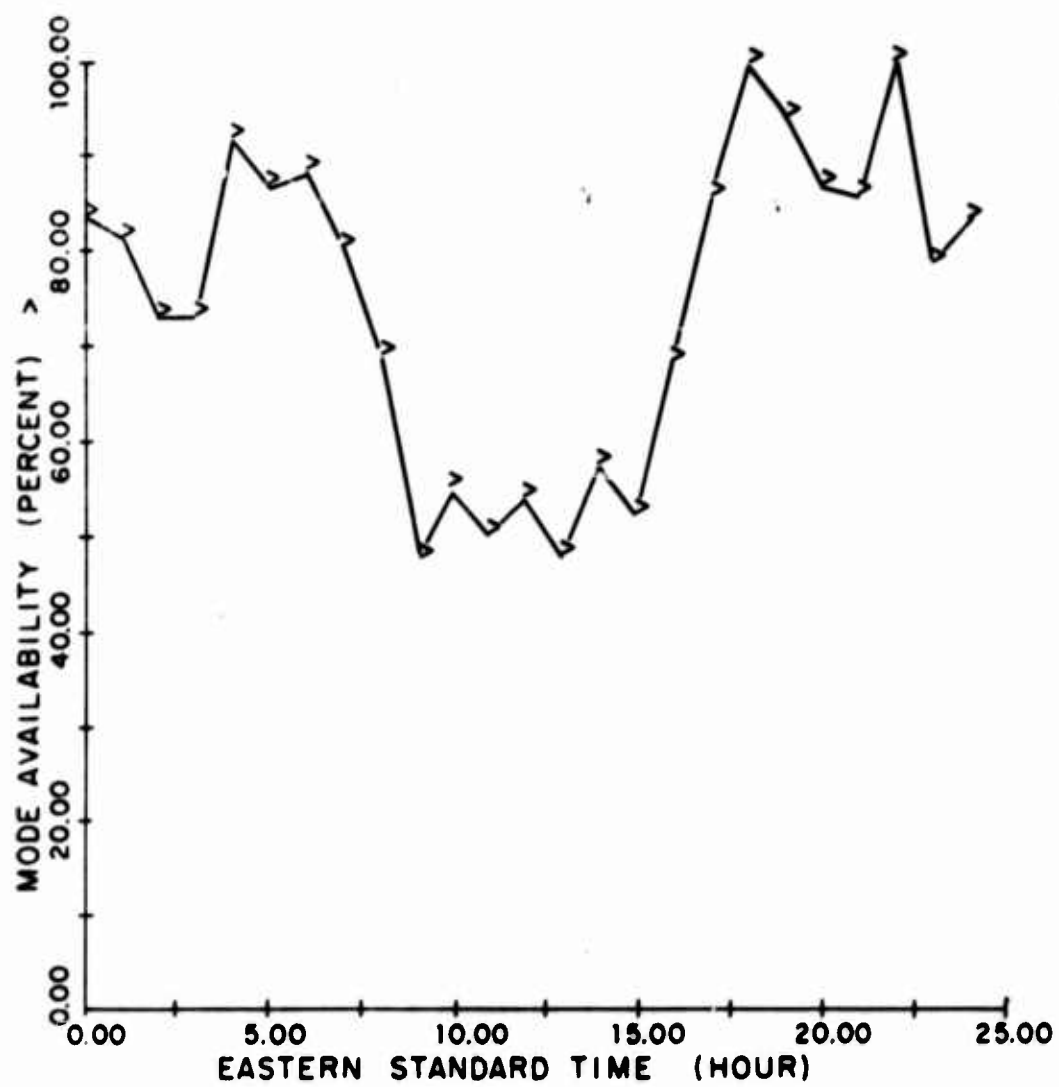


Figure 78. N Mode Availability, Coco Solo Path, Summer 1967

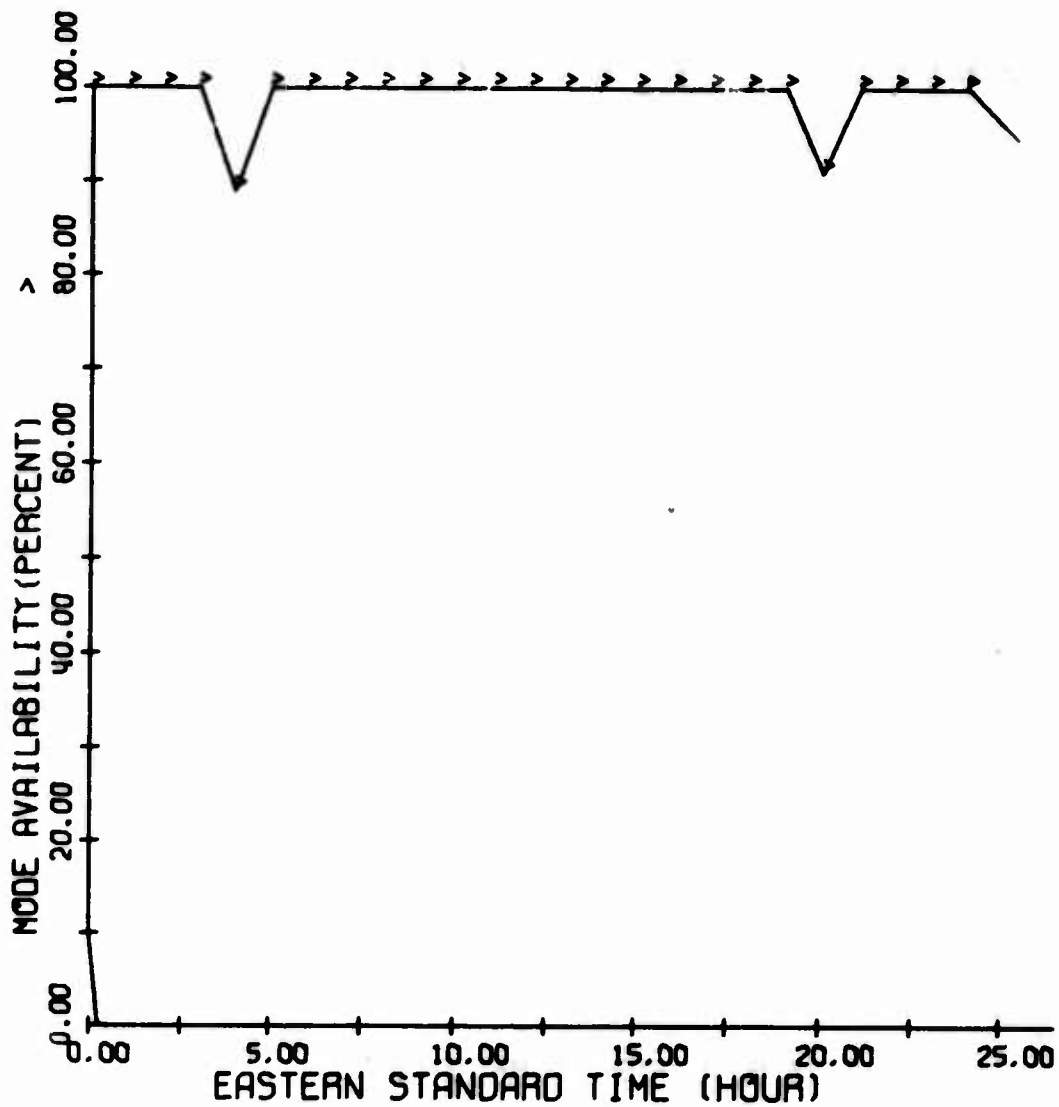


Figure 79. 2F2 Mode Availability, Coco Solo Path, Winter 1966

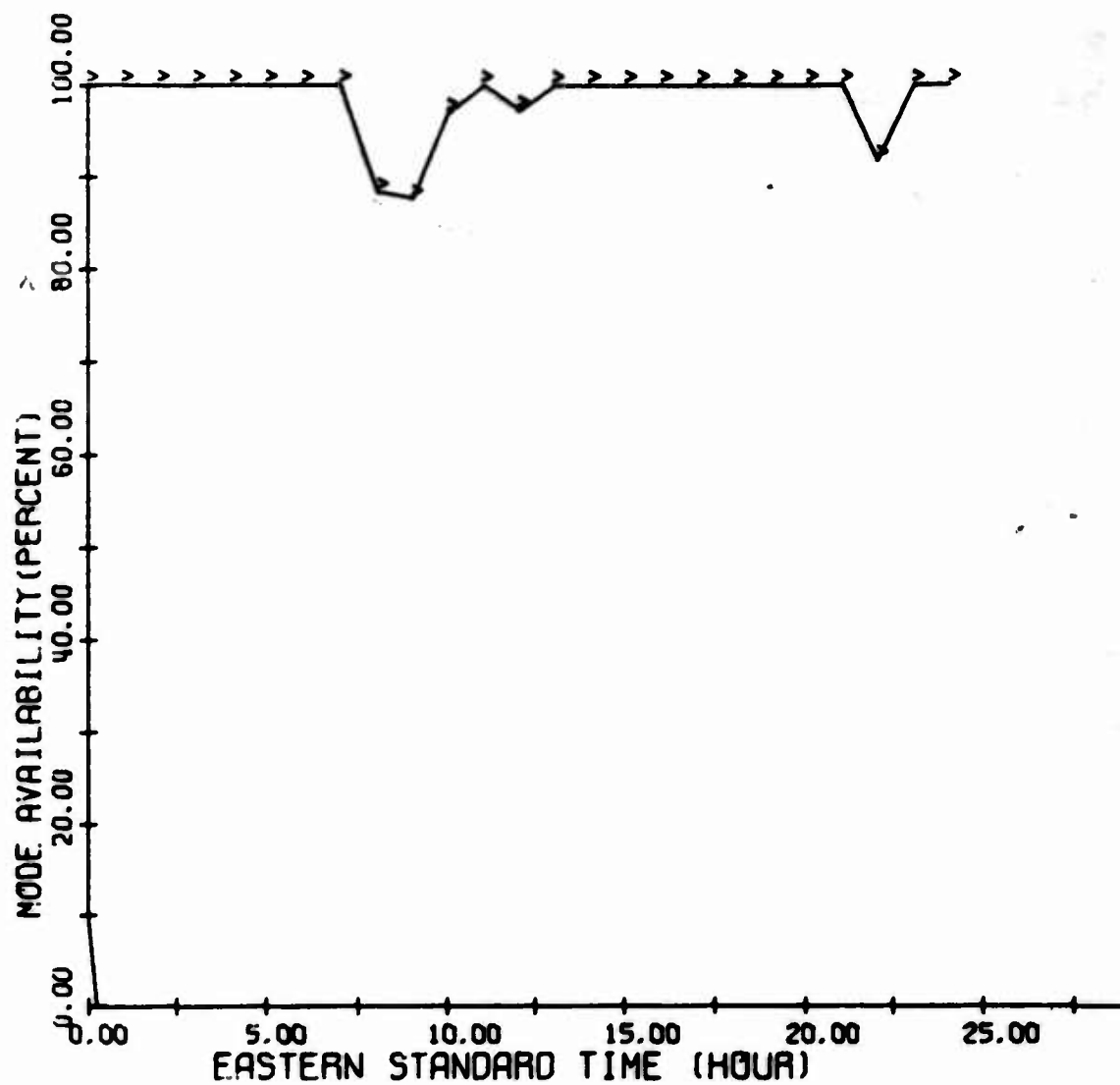


Figure 80. 2F2 Mode Availability, Coco Solo Path, Spring 1966

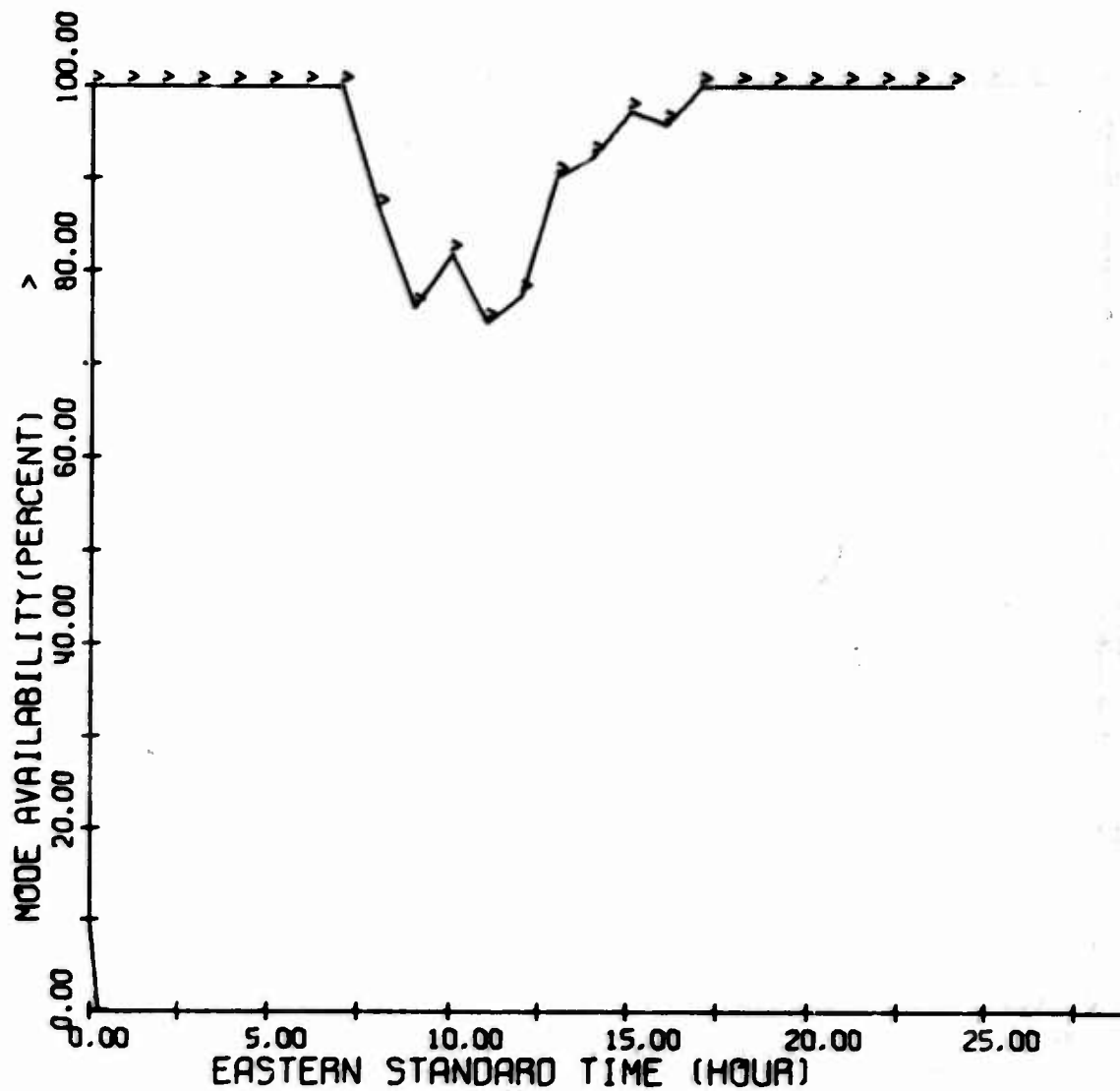


Figure 81. 2F2 Mode Availability, Coco Solo Path, Summer 1966

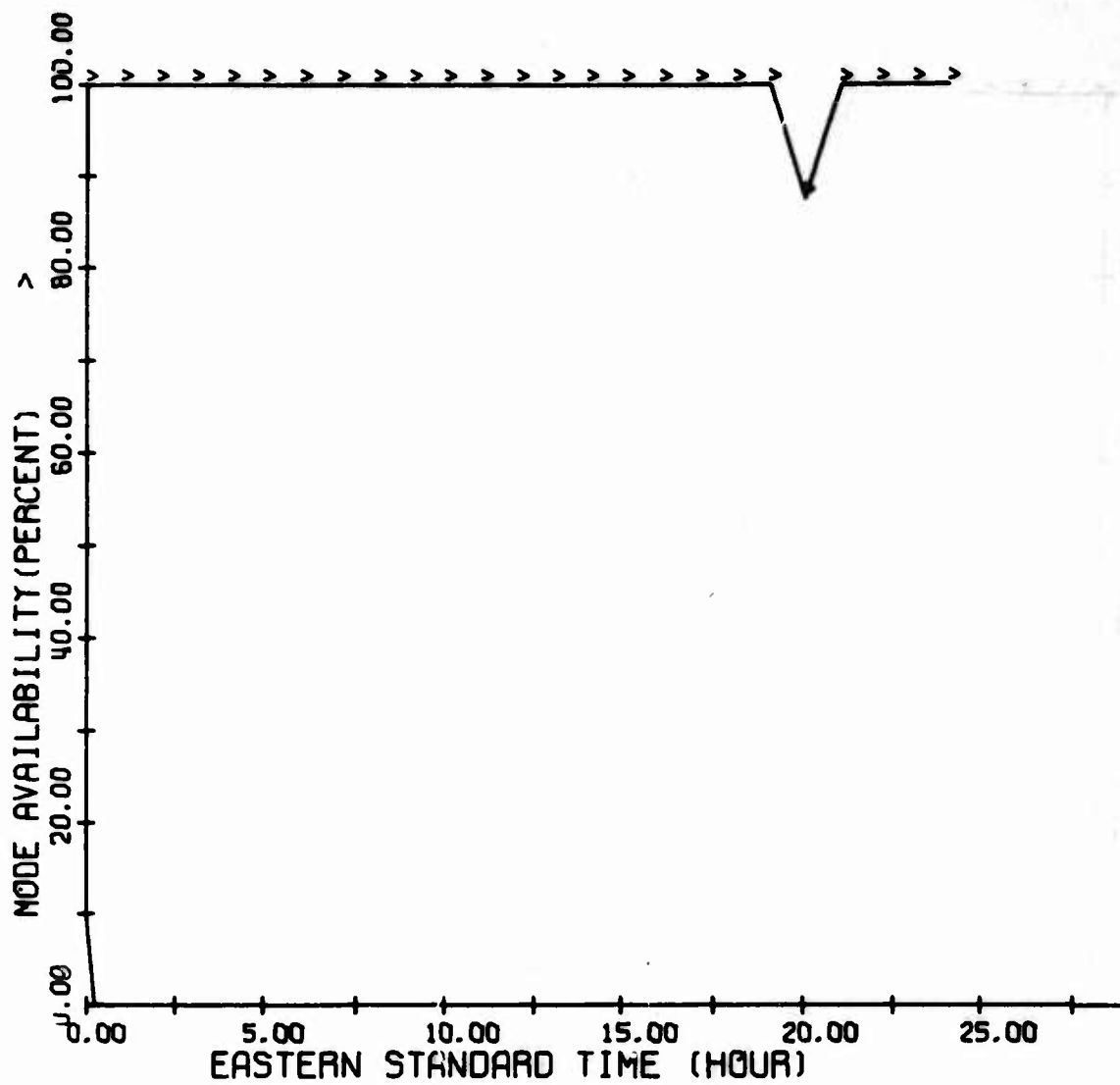


Figure 82. 2F2 Mode Availability, Coco Solo Path,
Autumn 1966

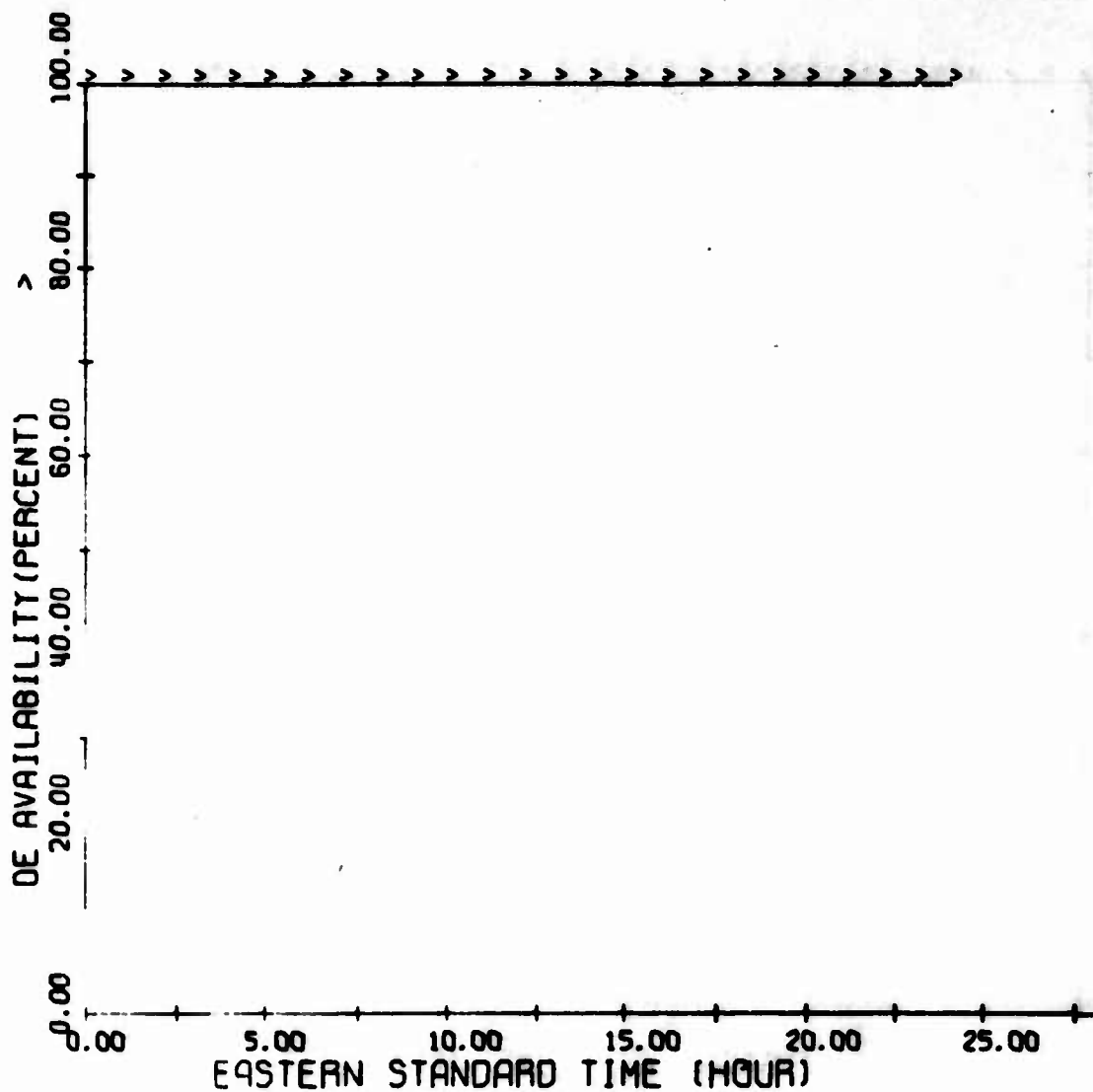


Figure 83. 2F2 Mode Availability, Coco Solo Path, Winter 1967

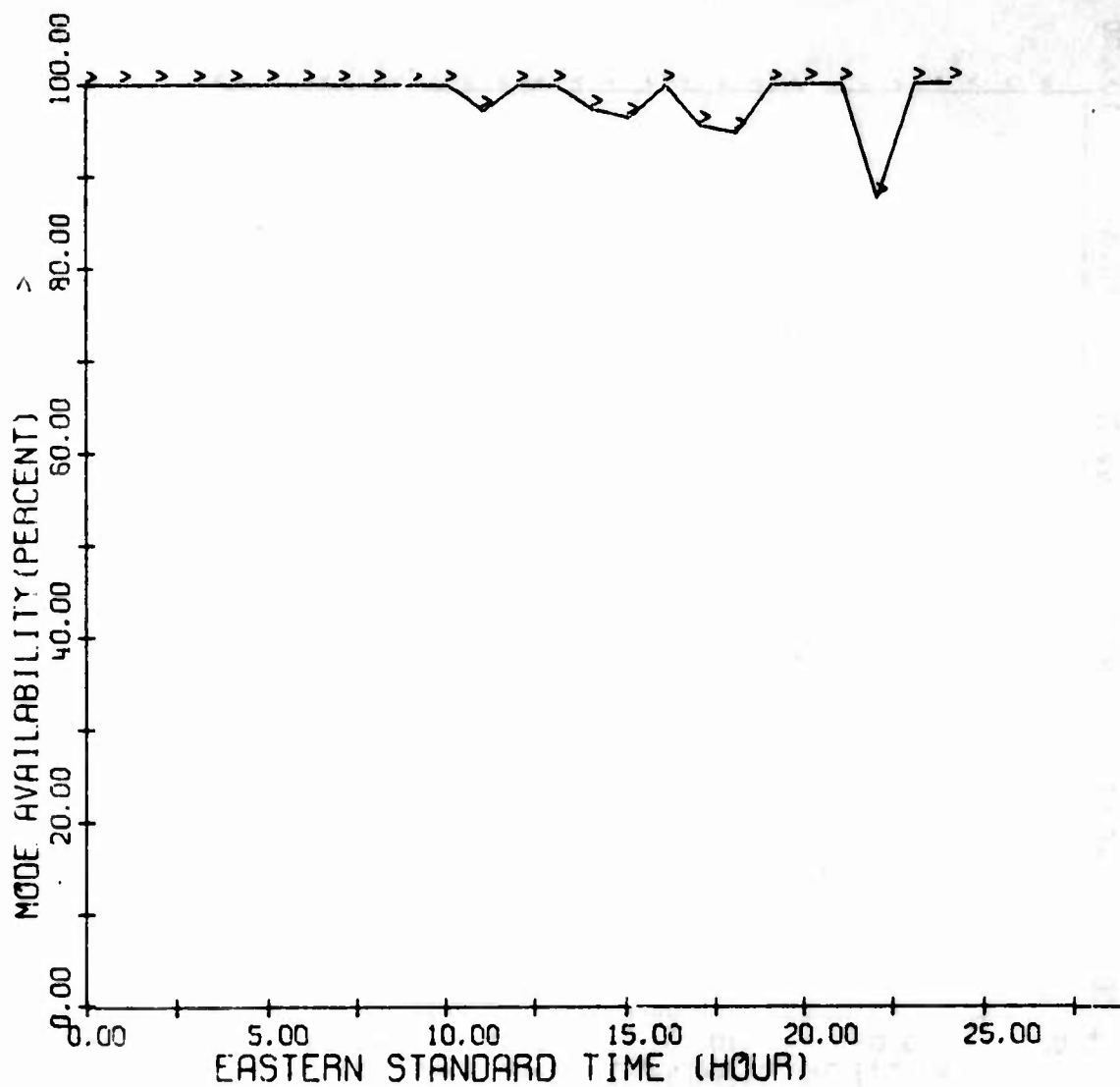


Figure 84. 2F2 Mode Availability, Coco Solo Path, Spring 1967

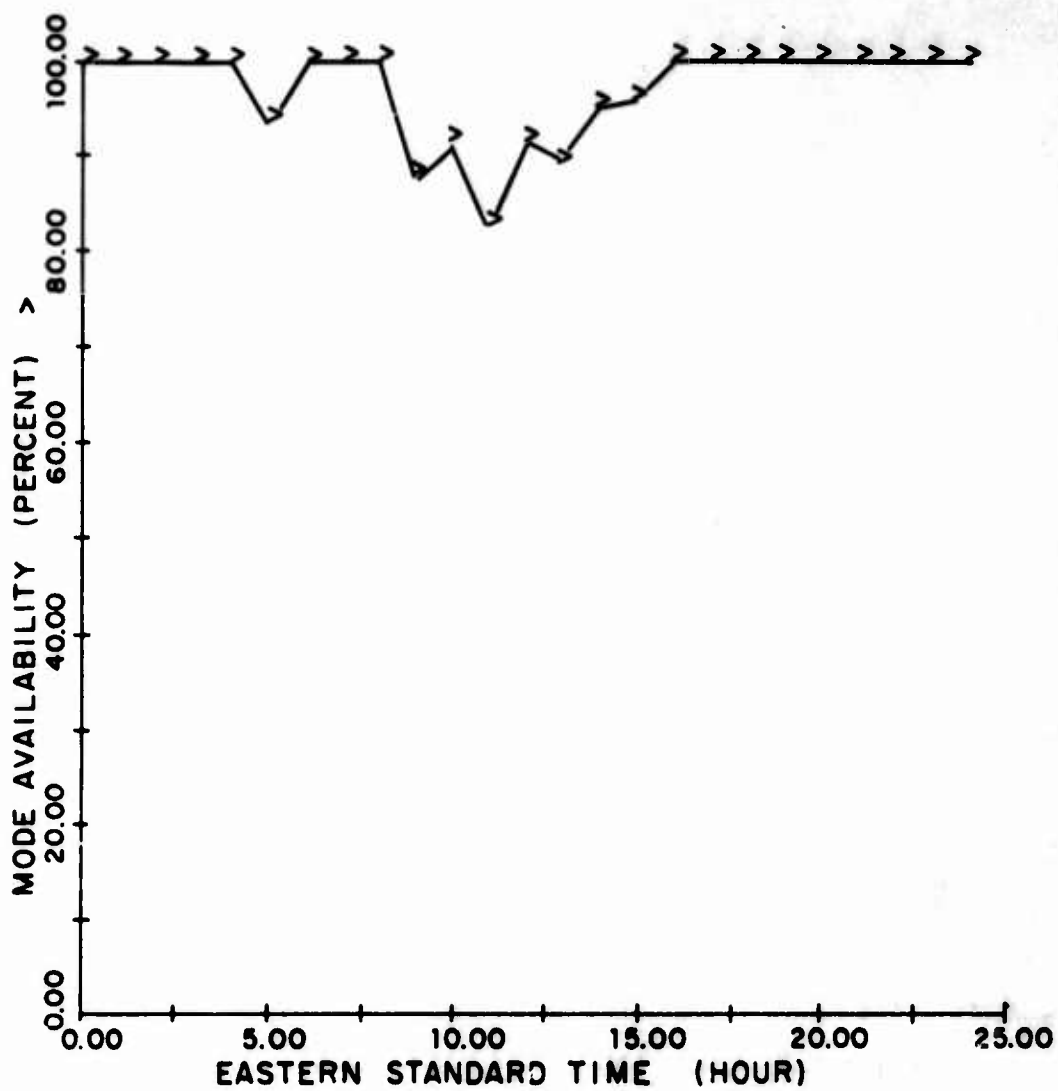


Figure 85. 2F2 Mode Availability, Coco Solo Path, Summer 1967

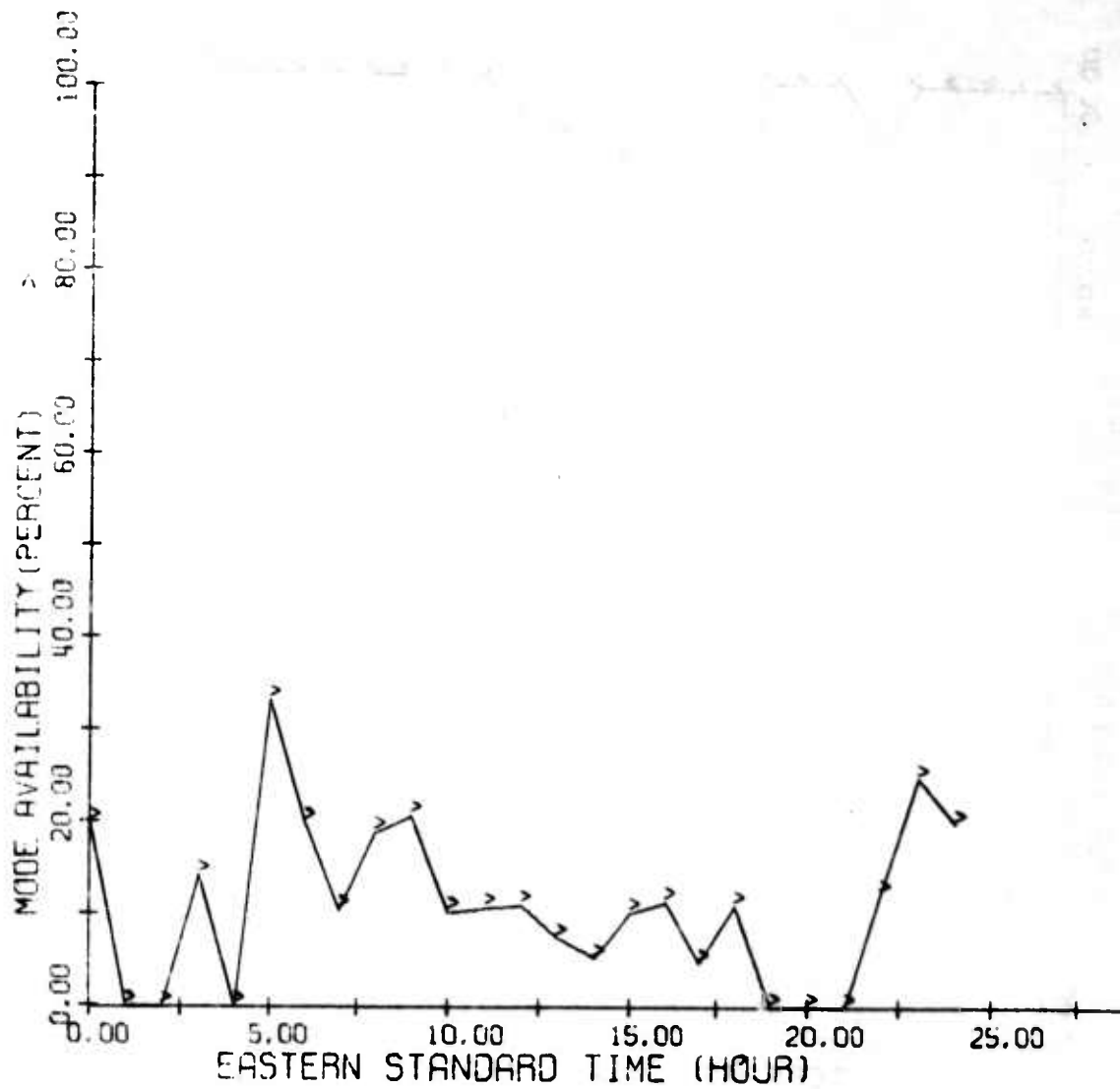


Figure 86. 2E_s Mode Availability, Coco Solo Path,
Spring 1967

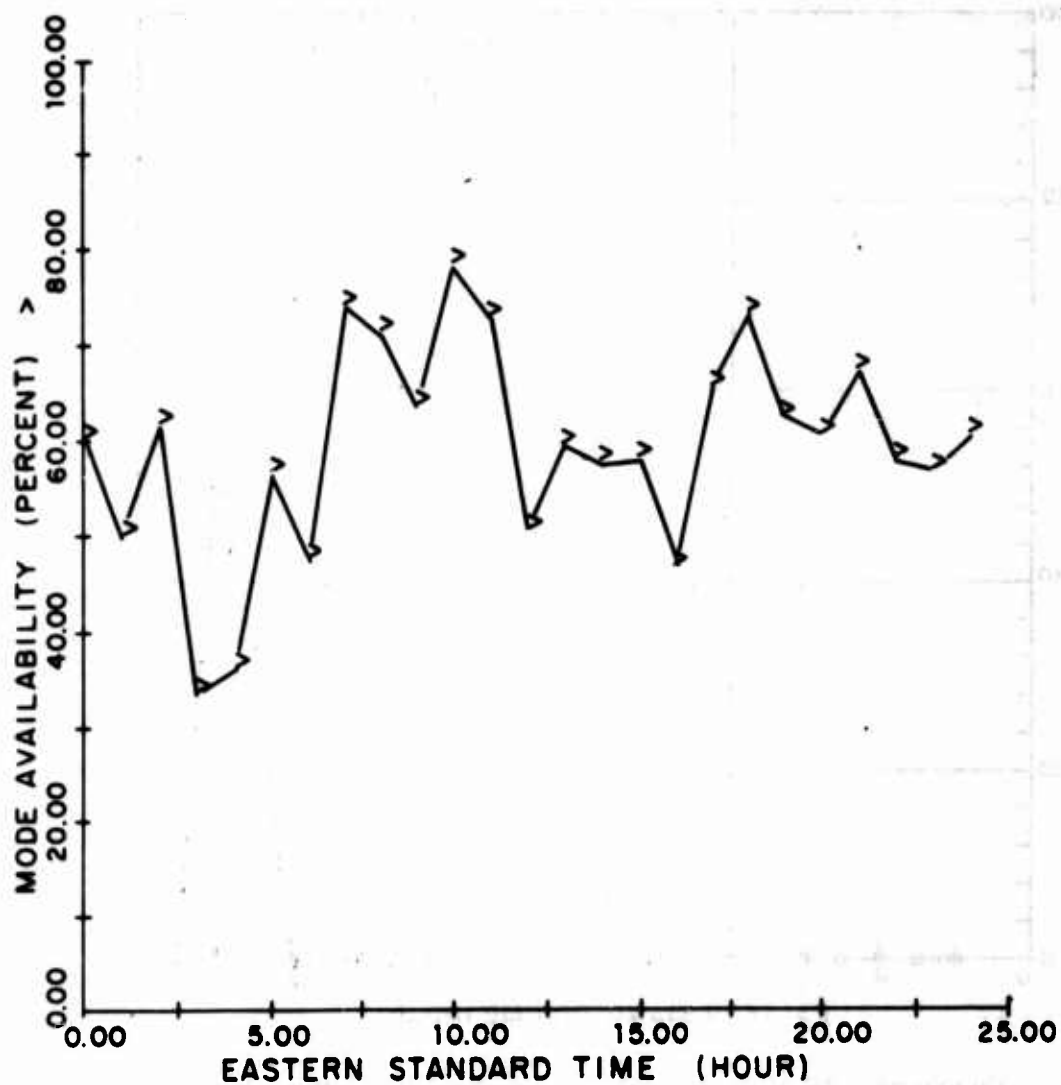


Figure 87. 2E Mode Availability, Coco Solo Path, Summer 1967

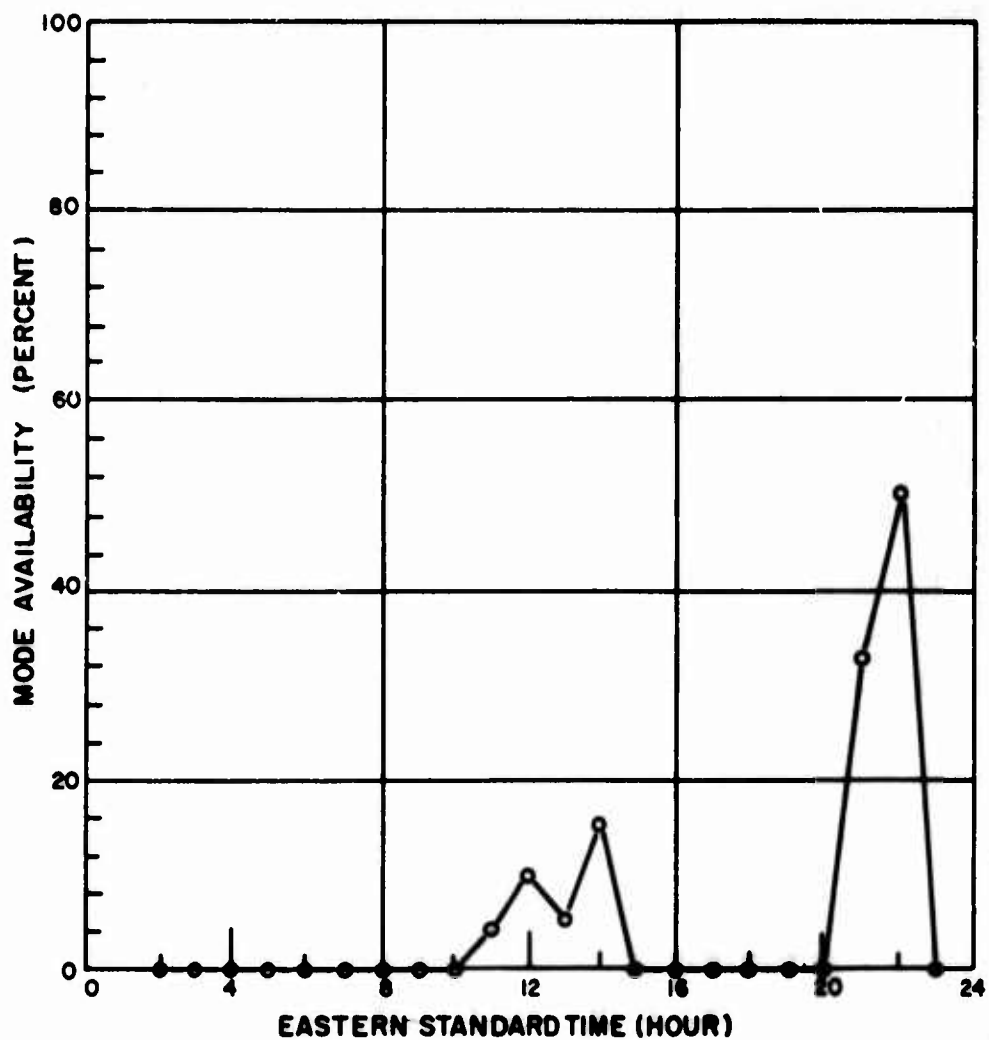


Figure 88. 2E Mode Availability, Thule Path, Winter 1967

4. MODE AVAILABILITY -- THULE TO STOCKBRIDGE/STARR HILL

Reference to the summary of observation (Figures 48 - 57) indicates that the data base for the Thule path in the winter of 1967 is very small. It is again noted that no data on the Thule path existed before this date. Actually, the Thule to Stockbridge path was run during the winter of 1967 while the Thule to Starr Hill path did not begin until the spring of 1967.

Regardless of the data base, it is surprising to note the very small percentage of 2E mode availability (Figure 88 and 89) in the daytime during the winter of 1967 and particularly to note that the daytime mode availability was the poorest and the nighttime was best. The results for spring of 1967, however, on the Thule to Starr Hill path indicate a more normal 2E mode availability.

The 1F2 mode availability (Figures 90 and 91) on the other hand, for the winter of 1967 showed, even with the small data base, 100 percent 1F2 mode availability at night, and fair availability for daytime and transitional periods. Some predictions calculated for this period are shown with the measured values and conform quite well at night and are not too unrealistic in the daytime. The 1F2 mode availability for the spring of 1967 is again 100 percent at night and quite good in the daytime.

The N mode (Figures 92 and 93) as might be expected, was slightly better than the 2E mode for the winter, but is still a very poor mode with nothing at night, and quite low availabilities in the daytime. In the spring, it improved slightly during the daylight hours and shows some availability during the transitional period.

The 2F2 mode availability (Figures 94 and 95) for the winter of 1967 is the poorest of any 2F2 measurements that have been made. Predictions for this period were for 100 percent mode availability throughout, but only the daytime availability was near this level. During the spring of 1967 the early nighttime 2F2 mode availability was 100 percent, but the daytime was somewhat erratic. During the winter of 1967 the 2E_g mode availability (Figures 96 and 97) was spotty, but had some high values. During the spring of 1967 its availability is almost negligible.

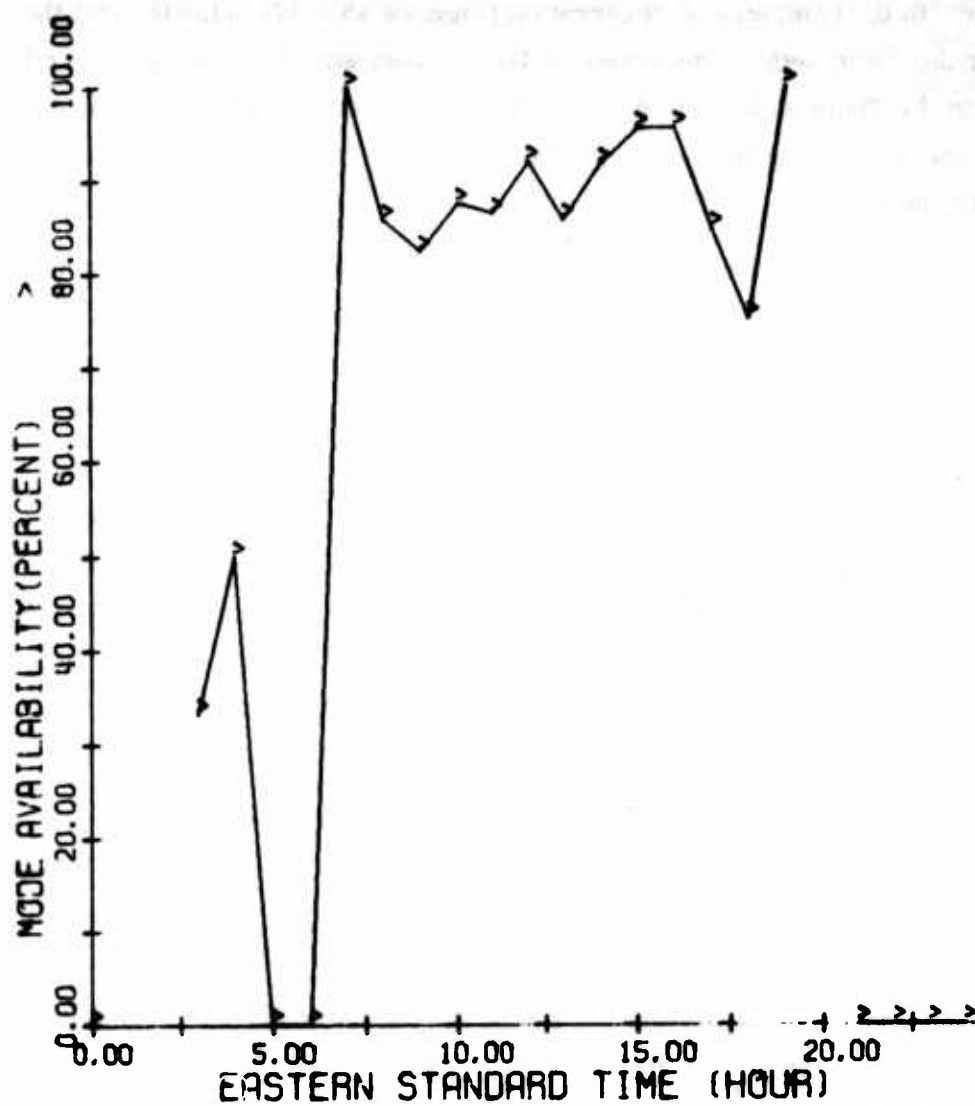


Figure 89. 2E Mode Availability, Thule Path, Spring 1967

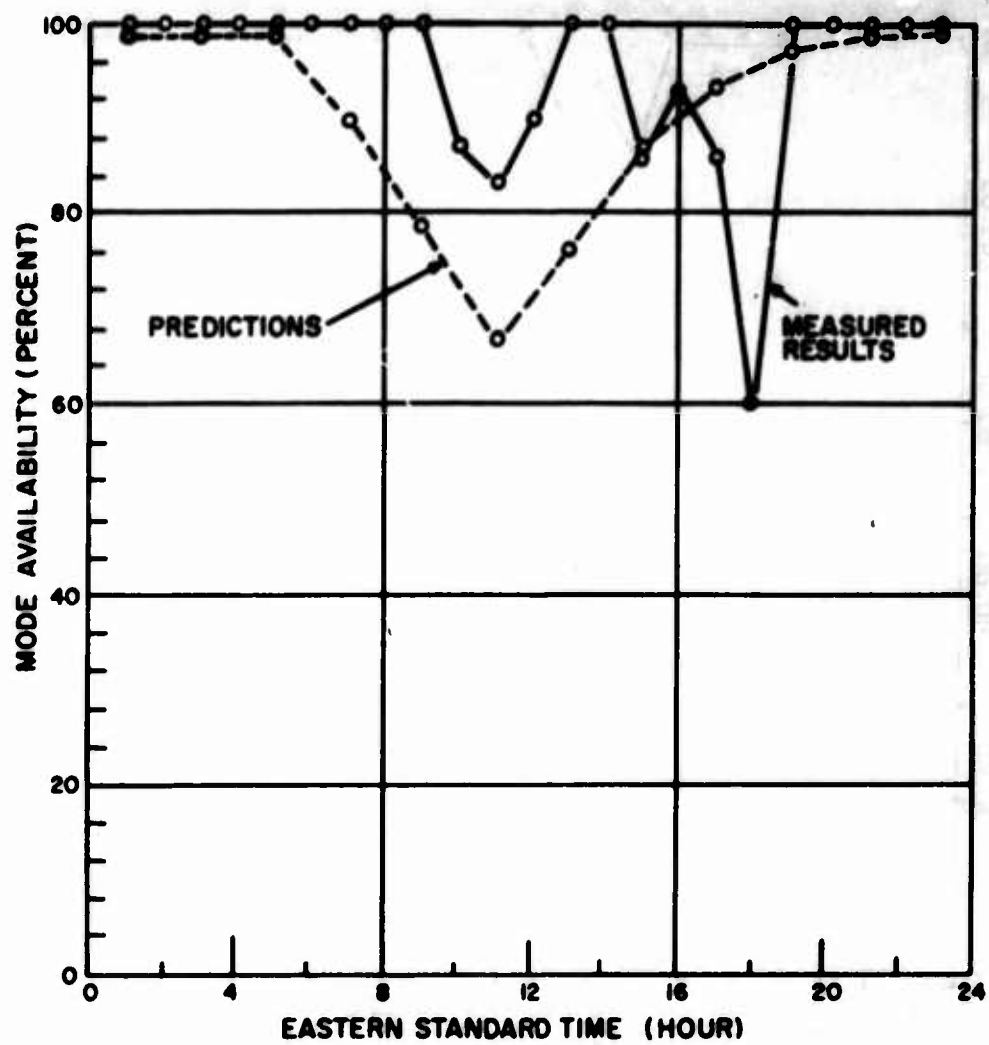


Figure 90. 1F2 Mode Availability, Thule Path, Winter 1967

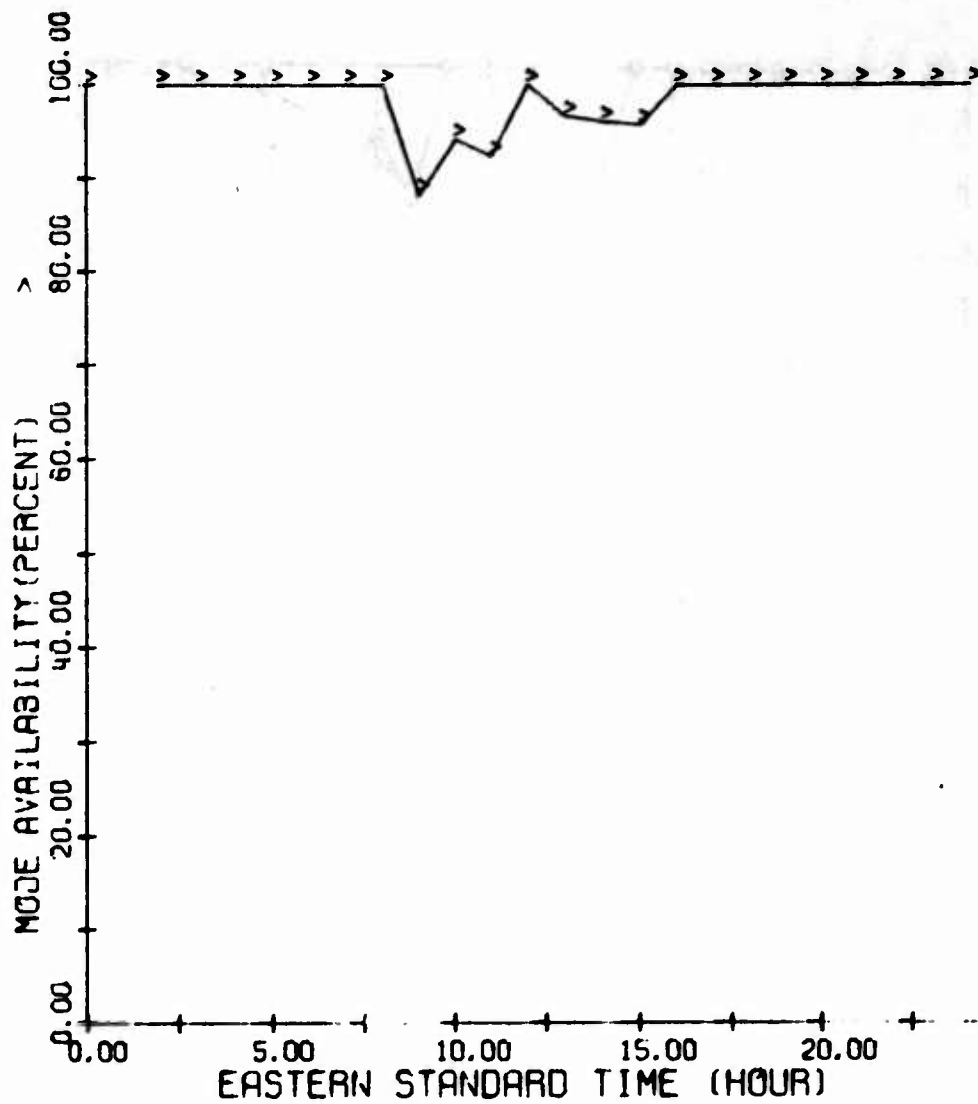


Figure 91. 1F2 Mode Availability, Thule Path, Spring 1967

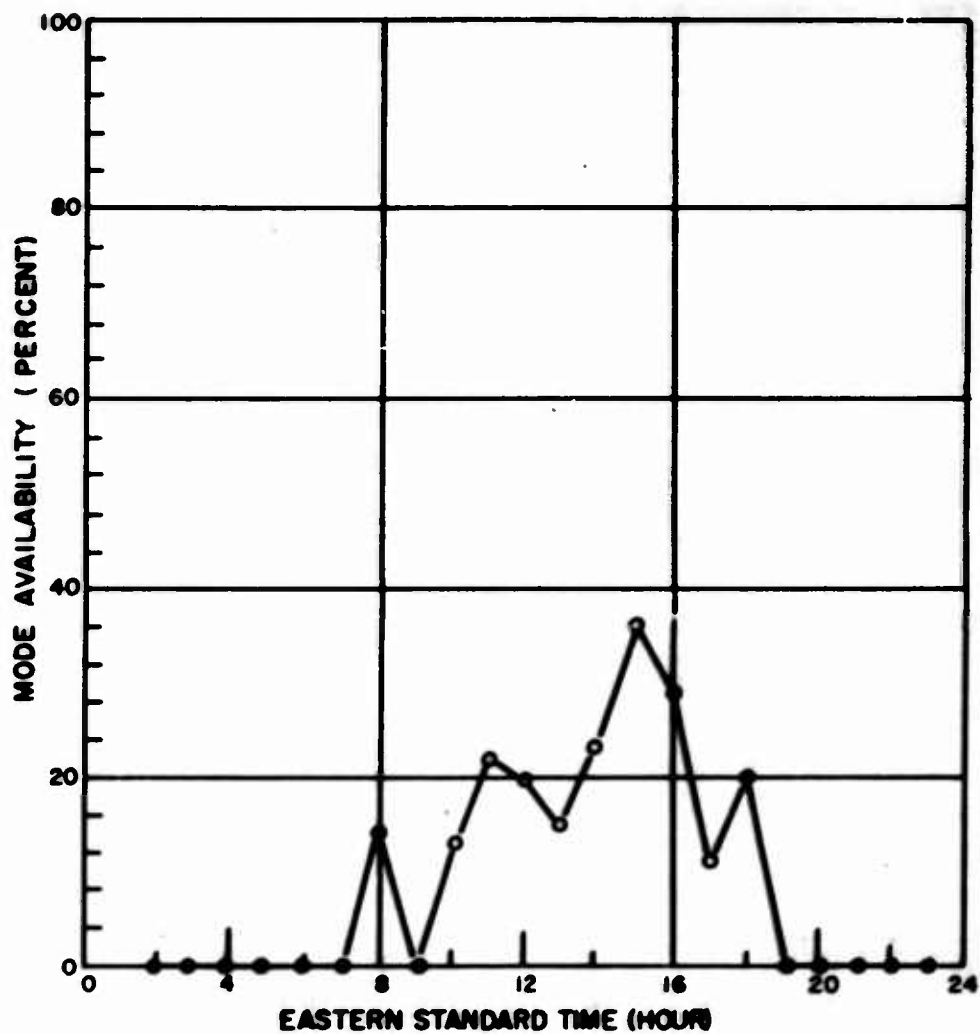


Figure 92. N Mode Availability, Thule Path, Winter 1967

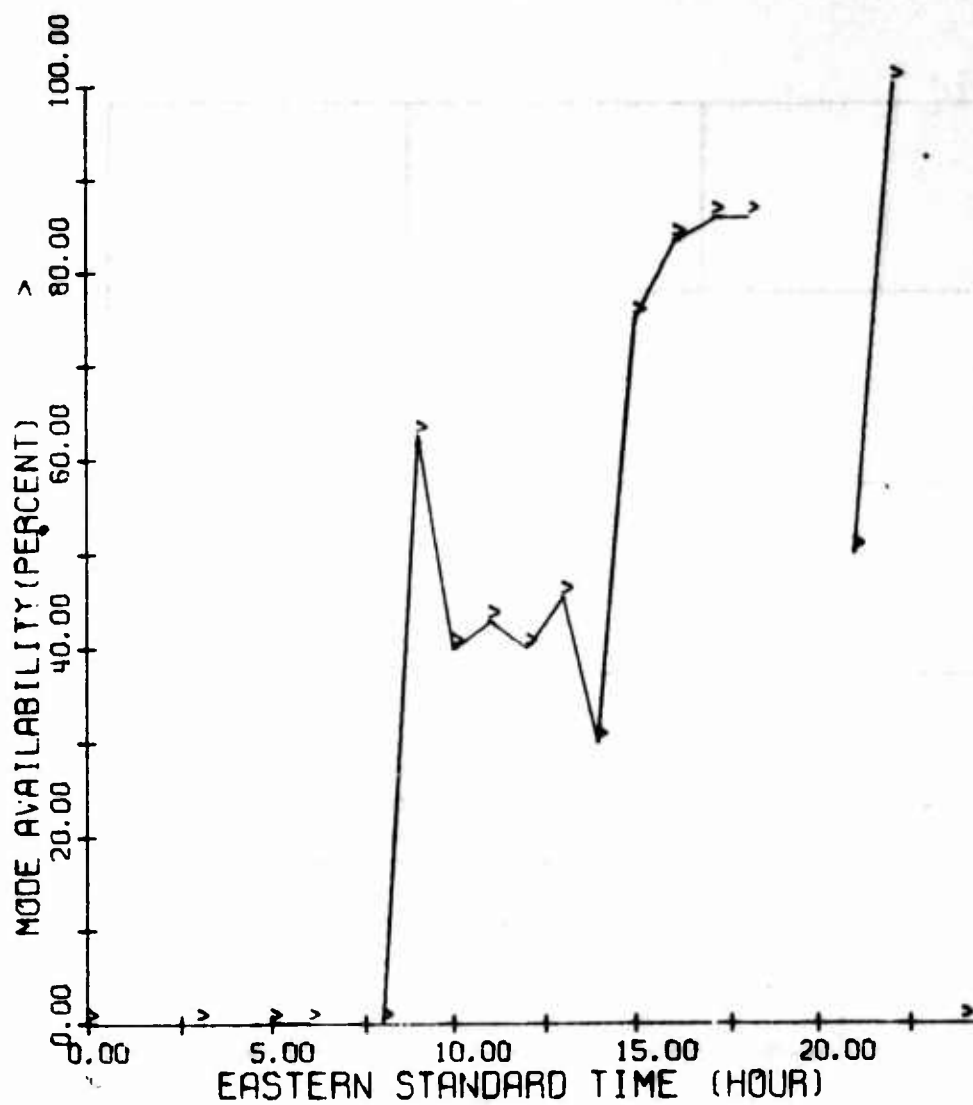


Figure 93. N Mode Availability, Thule Path, Spring 1967

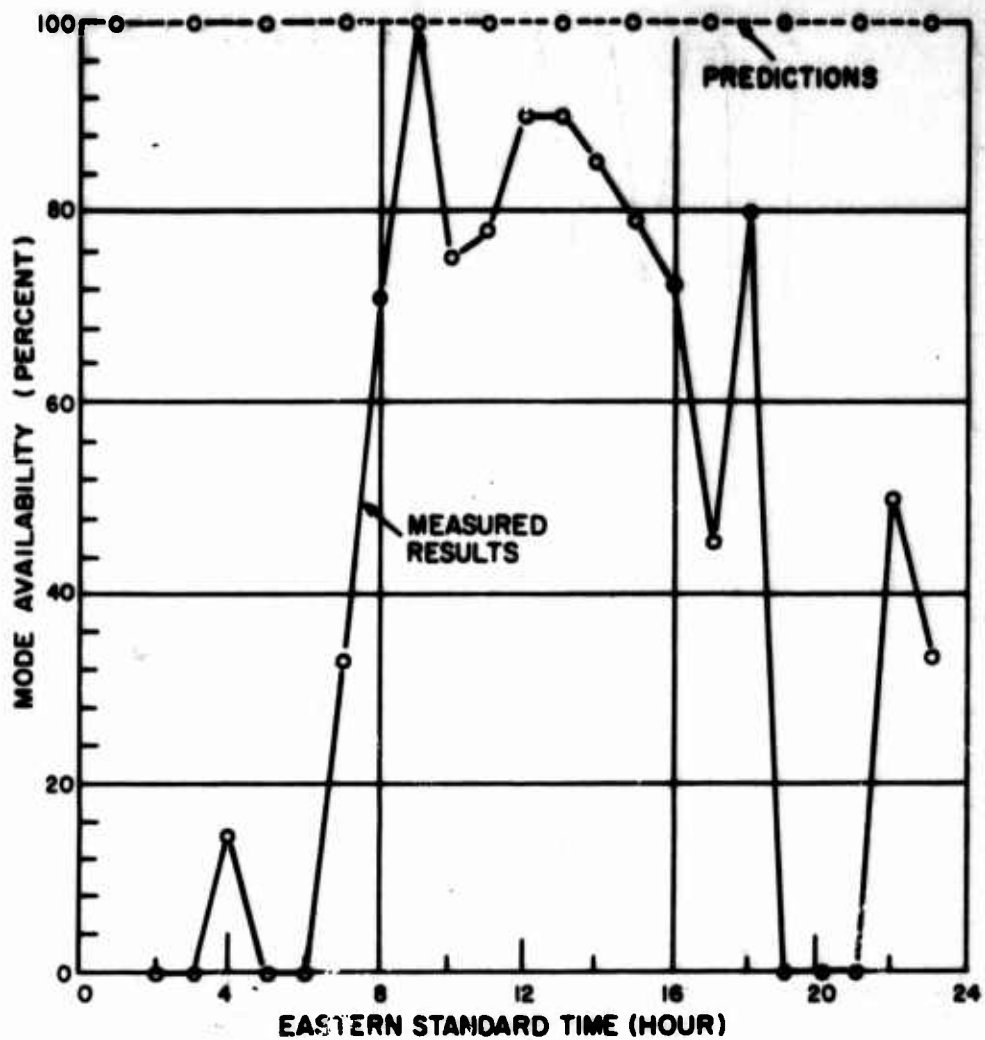


Figure 94. 2F2 Mode Availability, Thule Path, Winter 1967

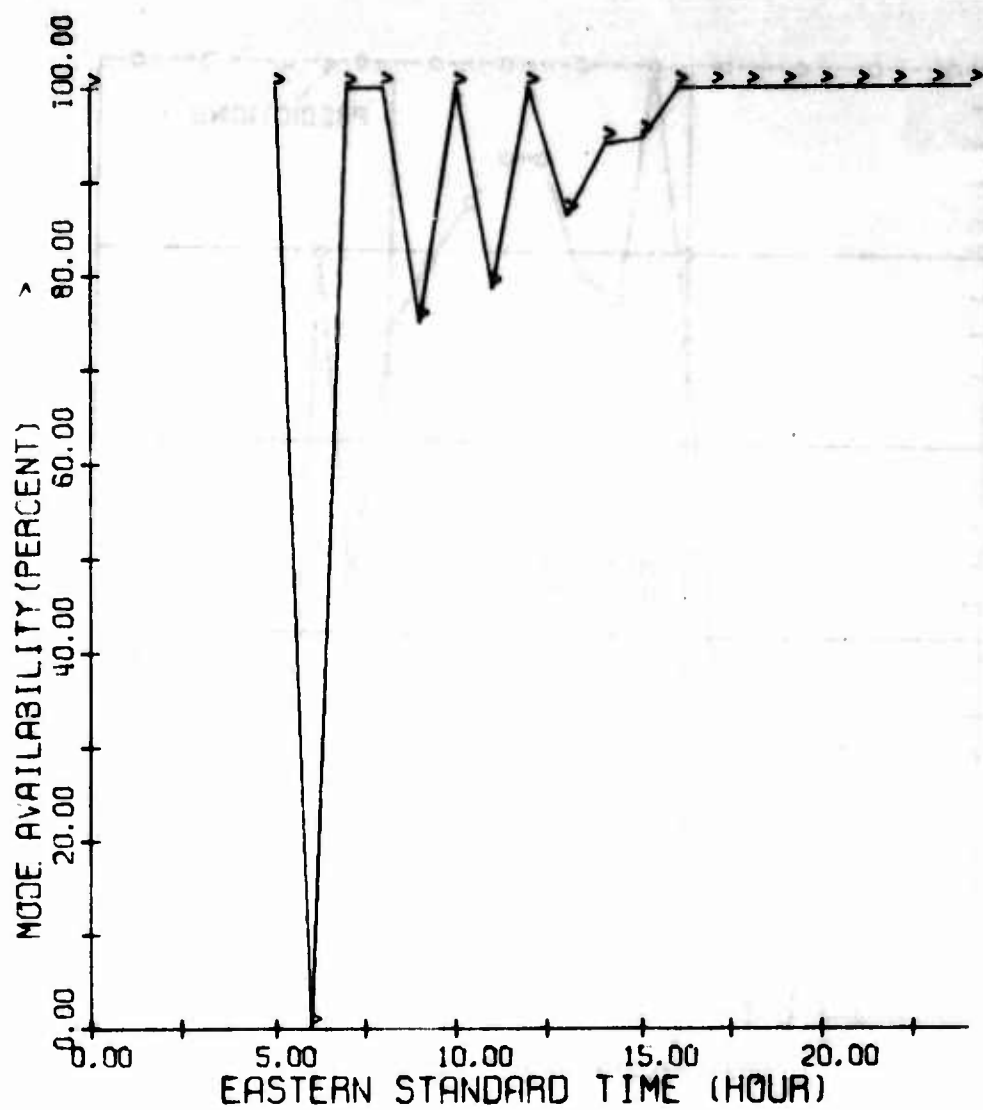


Figure 95. 2F2 Mode Availability, Thule Path, Spring 1967

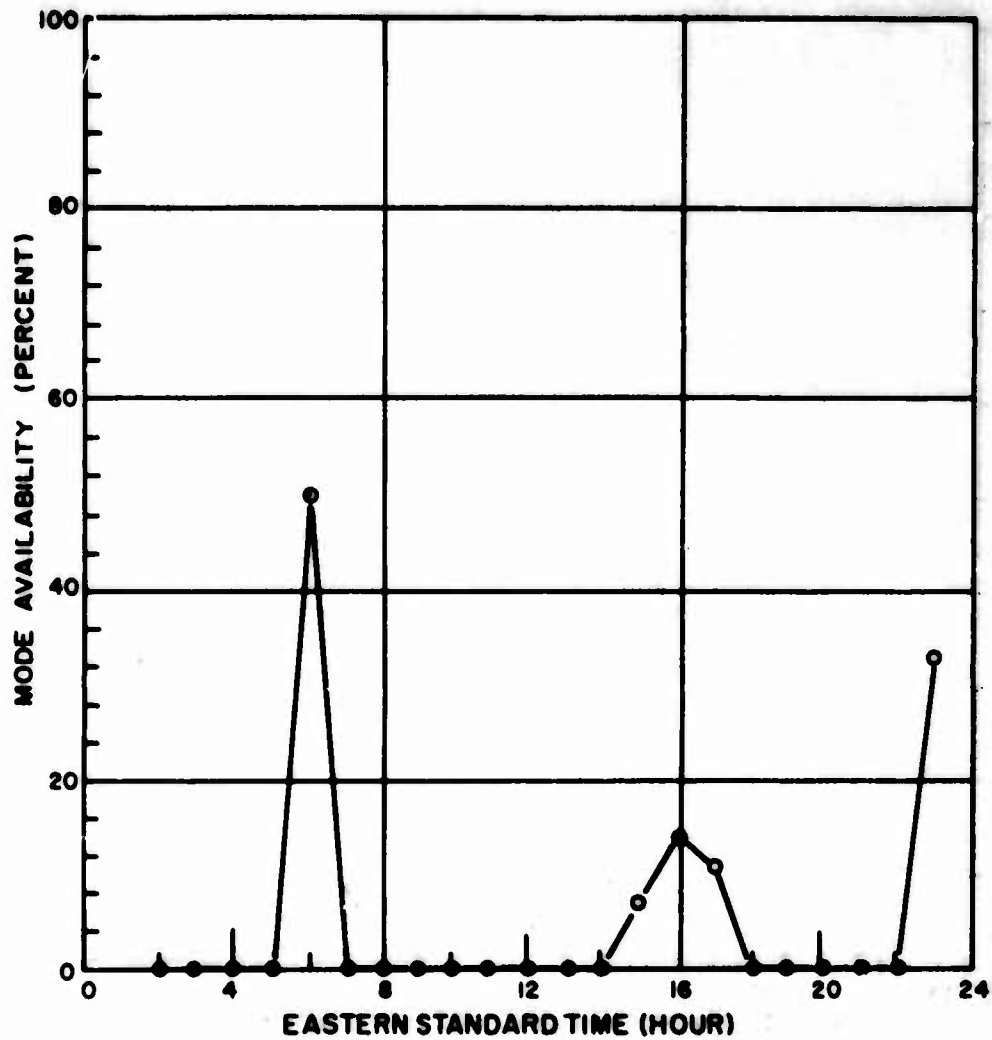


Figure 96. $2E_8$ Mode Availability, Thule Path, Winter 1967

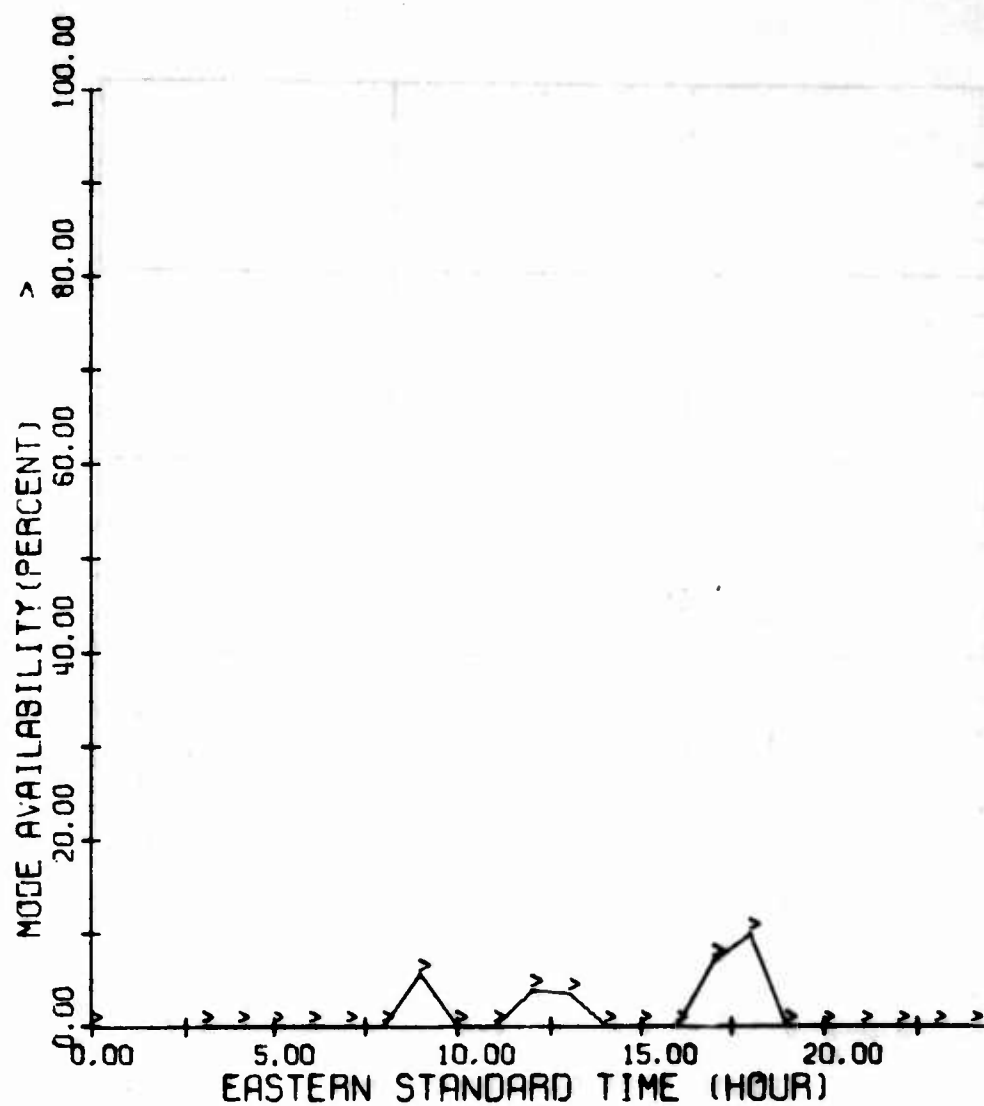


Figure 97. 2E_s Mode Availability, Thule Path, Spring 1967

5. FREQUENCY APERTURE AVAILABILITY -- COCO SOLO TO STOCKBRIDGE/ STARR HILL

As it has been stated in earlier reports (Refs. 2, 4, and 6) on the mode reliability experiment, the frequency aperture availability has been measured from the MOF or JF down to the first major break in the trace of the mode in the ionogram, which thereby has been declared as the LOF. The frequency aperture thus derived is the total usable frequency aperture for a given mode and does not include sketchy sections of the frequency aperture that might otherwise be indicated. Although these apertures are generally small, they usually exceed 1-MHz 90 percent of the time, and for lower percentages of the time are much larger. In general, the following description of the results obtained on the Coco Solo path will refer to the 90 percent frequency aperture availability only. In the winter of 1966 for the 2E mode (Figures 98 - 104) the 90 percent aperture drops to the 1-MHz point in several spots and reaches a maximum of 4 MHz. Spring 1966 is consistently even lower at the 90 percent level, while summer 1966 daytime values reach 3 and 4 MHz, but nighttime values are down to 1-MHz. The results for the summer of 1967 are not as good as for the summer of 1966. The 1-MHz nighttime values continue in the summer of 1966; for the fall of 1966 daytime maximums are on the order of 2 or 3 MHz. The same holds true for the results during the winter of 1967, with some small pickup at nighttime for the spring.

The 1F2 frequency apertures (Figures 105 - 111) produce almost the same sequence as discussed above for the 2E mode on the Coco Solo path: low at night; slightly higher in the daytime in the winter of 1966; in the spring some small daytime improvement and one higher spot at 2000 EST. The level for the summer of 1966 achieves highs of 4 and 5 MHz and again drops to a low of 1 MHz. The results for the summer of 1967 do not match very closely to those obtained in the summer of 1966. The autumn of 1966 values range from nighttime levels of 1 or 2 MHz to daytime values as high as 4 MHz. The winter 1967 values are consistently on the order of 2 MHz, except in midafternoon, and the results for the spring of 1967 have some highs that are greater than 5 MHz in the daytime with nighttime values of 2 MHz.

The N mode frequency aperture (Figures 112 - 118) runs consistently low during the winter and spring of 1966; the summer nighttime frequency aperture is the highest

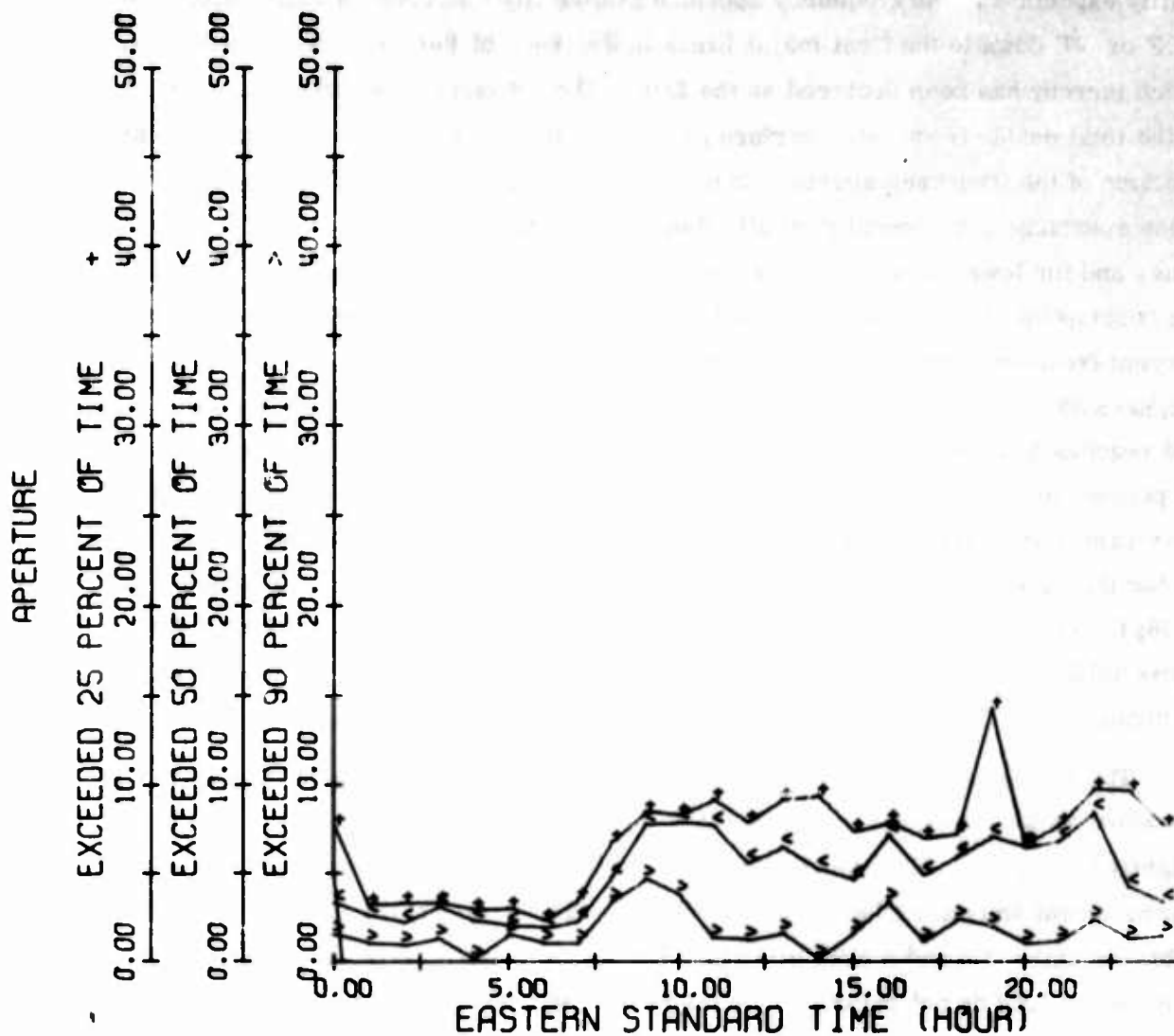


Figure 98. 2E Frequency Aperture Availability (MHz), Coco Solo Path, Winter 1966

and the daytime values are the lowest. The frequency aperture for autumn of 1966 has consistently low values with one spotty higher value, and the same is true for the winter of 1967. The frequency aperture for the spring of 1967 has its highest value in the early morning hours.

The frequency aperture for the 2F2 mode (Figures 119 - 125) runs slightly higher than the other modes with the morning and afternoon values the best for winter and spring of 1966. The afternoon values are the best for the summer of 1966, and the morning and afternoon values are again the highest for the fall 1966. In the winter of 1967 considerably higher daytime values were measured; for summer of 1967 the lowest is again during the day. The spring of 1967 shows a very adequate value for the frequency aperture in early morning; that is, from midnight on, and late afternoon and evening.

The frequency aperture for the $2E_g$ mode is shown in Figures 126 - 130. The best way to describe its frequency aperture is that it is somewhat erratic throughout, and it is quite low during many of the seasons covered for this mode.

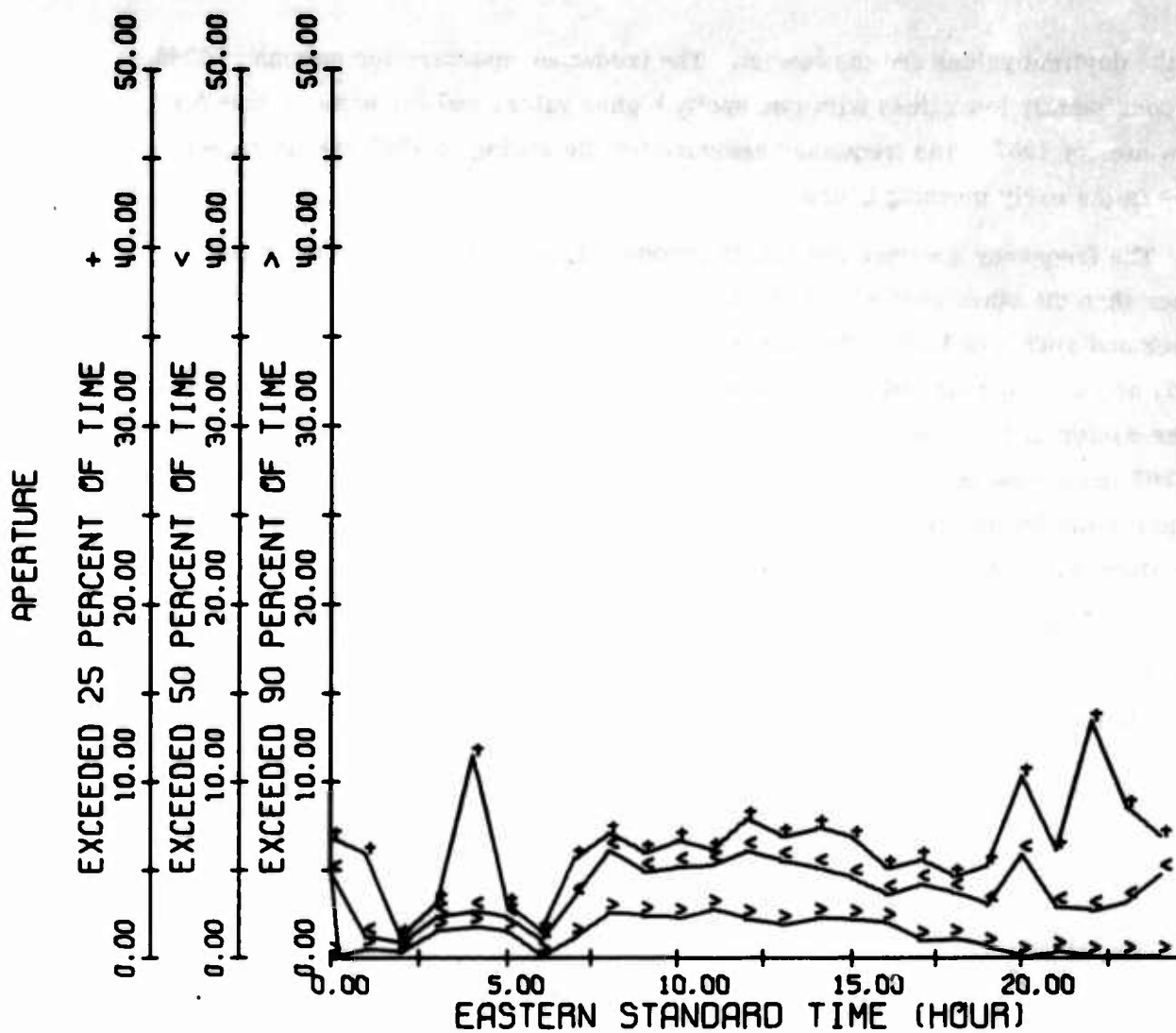


Figure 99. 2E Frequency Aperture Availability (MHz), Coco Solo Path, Spring 1966

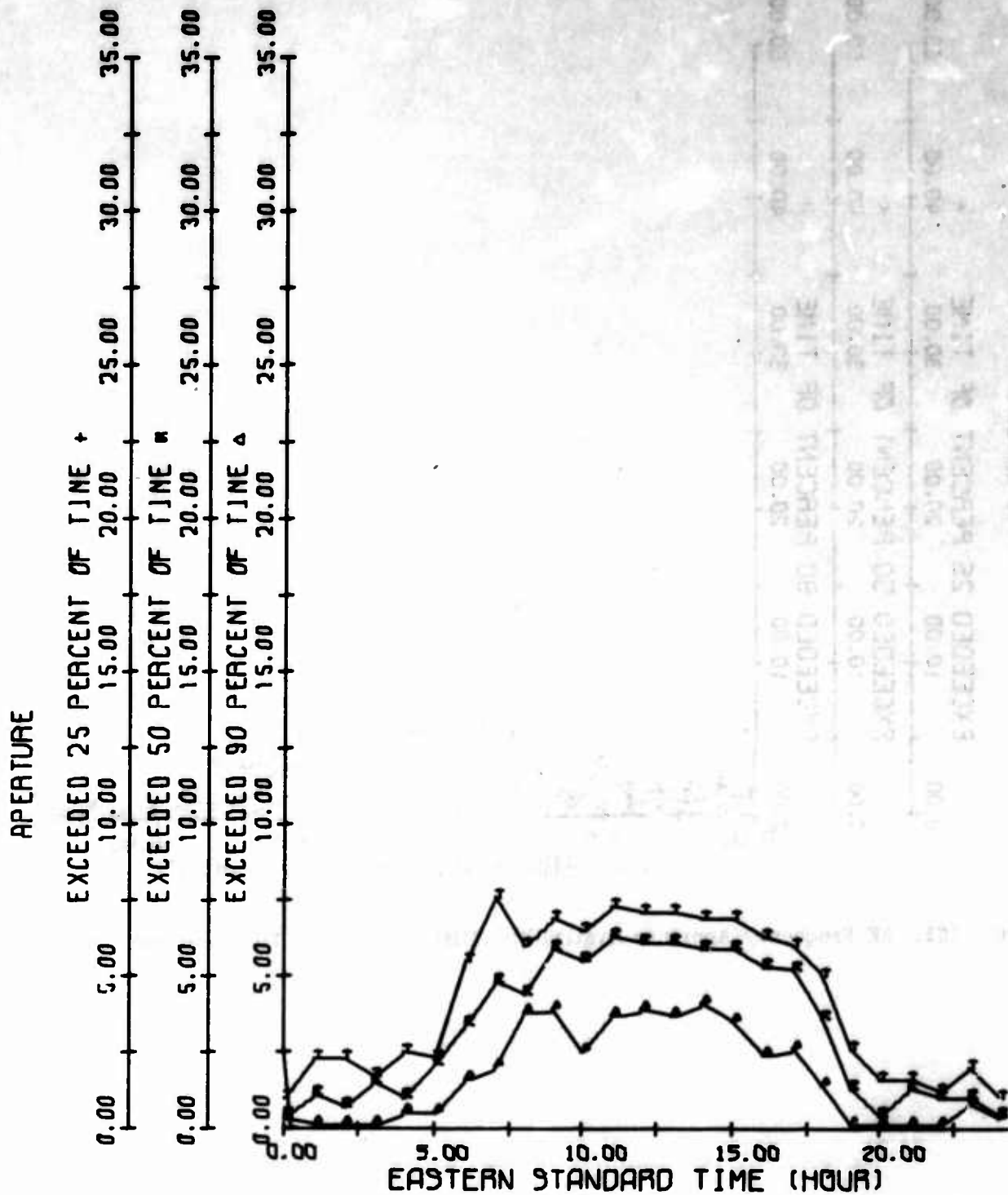


Figure 100. 2E Frequency Aperture Availability (MHz), Coco Solo Path, Summer 1966

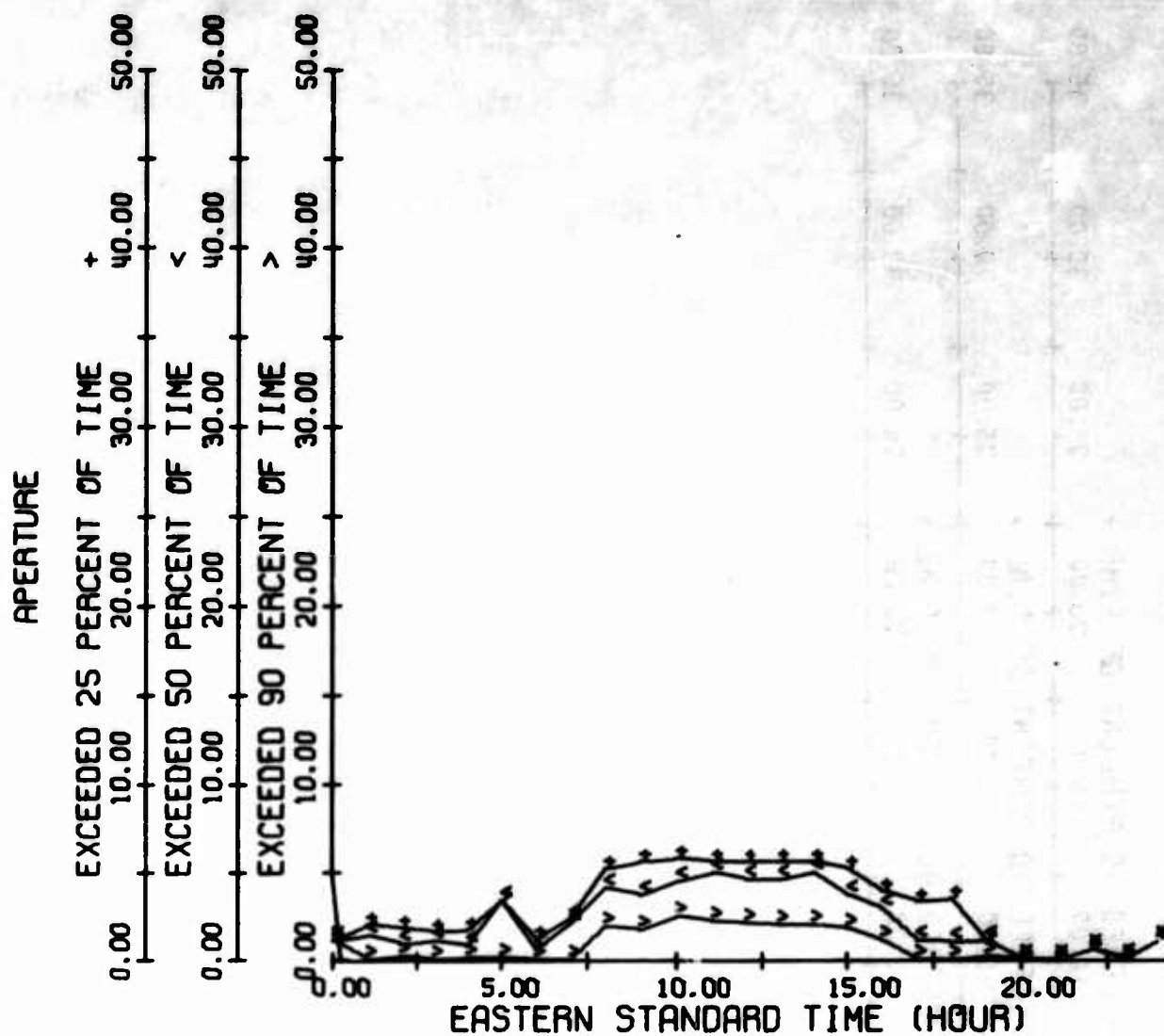


Figure 101. 2E Frequency Aperture Availability (MHz), Coco Solo Path, Autumn 1966

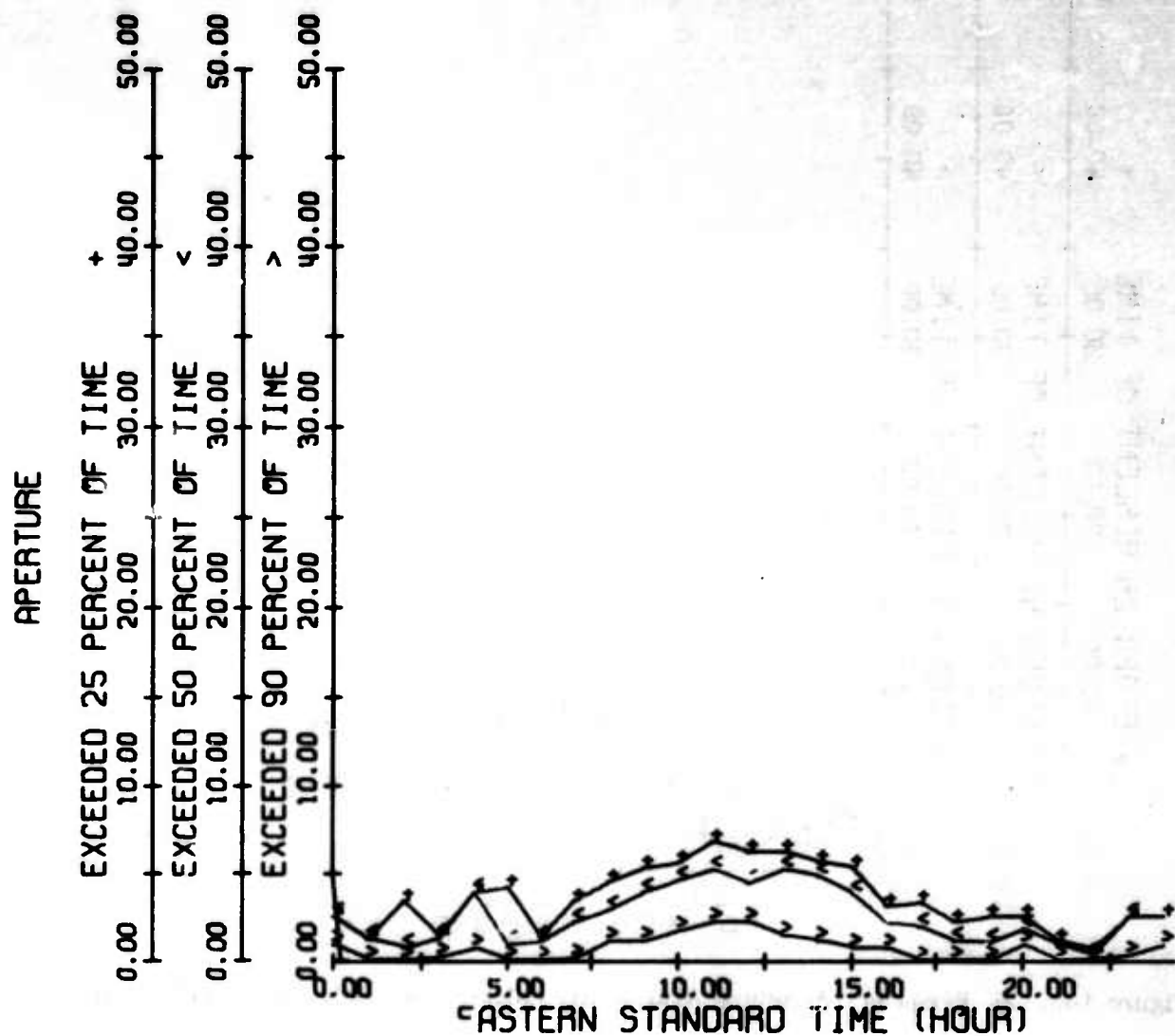


Figure 102. 2E Frequency Aperture Availability (MHz), Coco Solo Path, Winter 1967

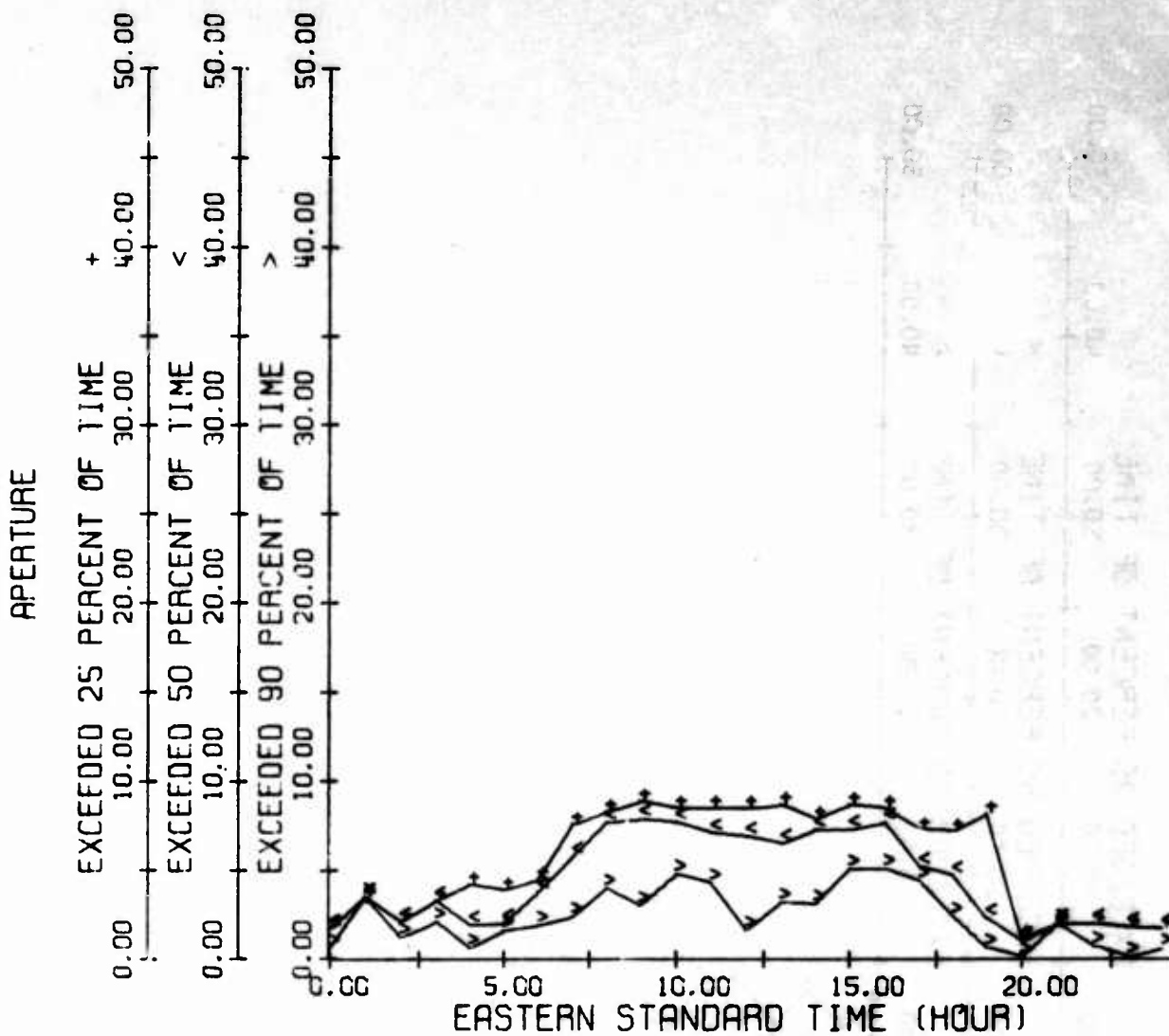


Figure 103. 2E Frequency Aperture Availability (MHz), Coco Solo Path, Spring 1967

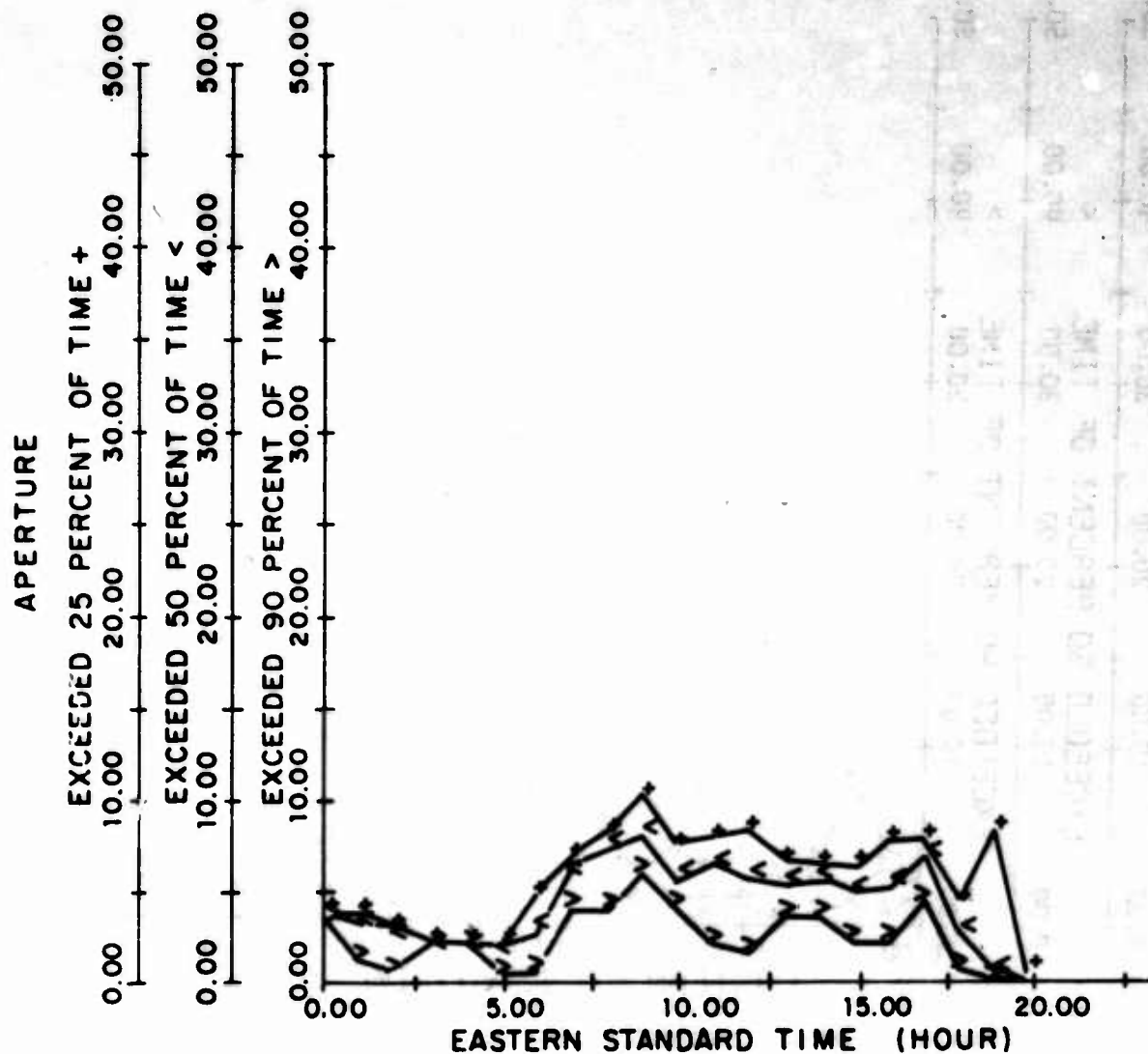


Figure 104. 2E Frequency Aperture Availability (MHz), Coco Solo Path, Summer 1967

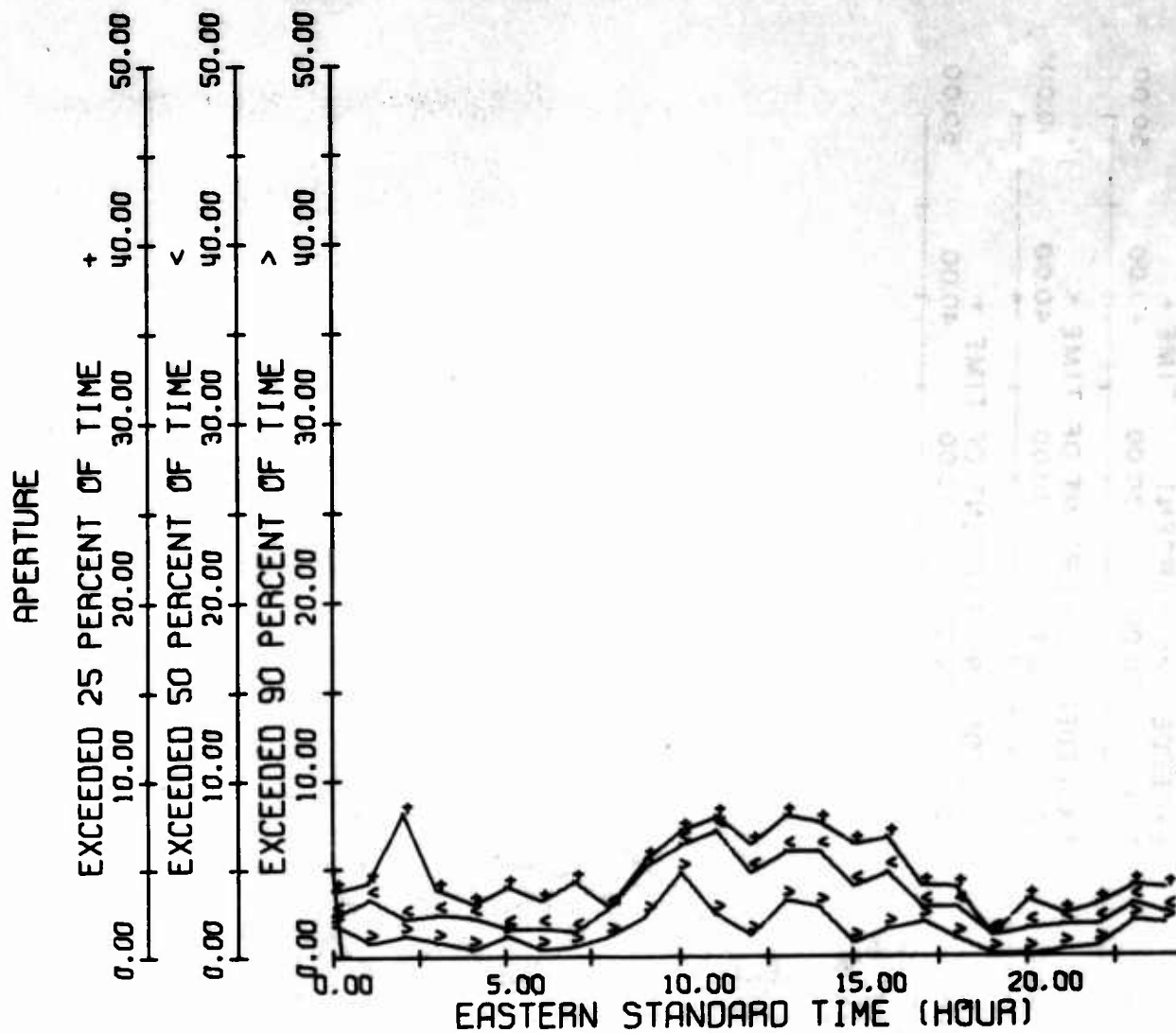


Figure 105. 1F2 Frequency Aperture Availability (MHz), Coco Solo Path, Winter 1966

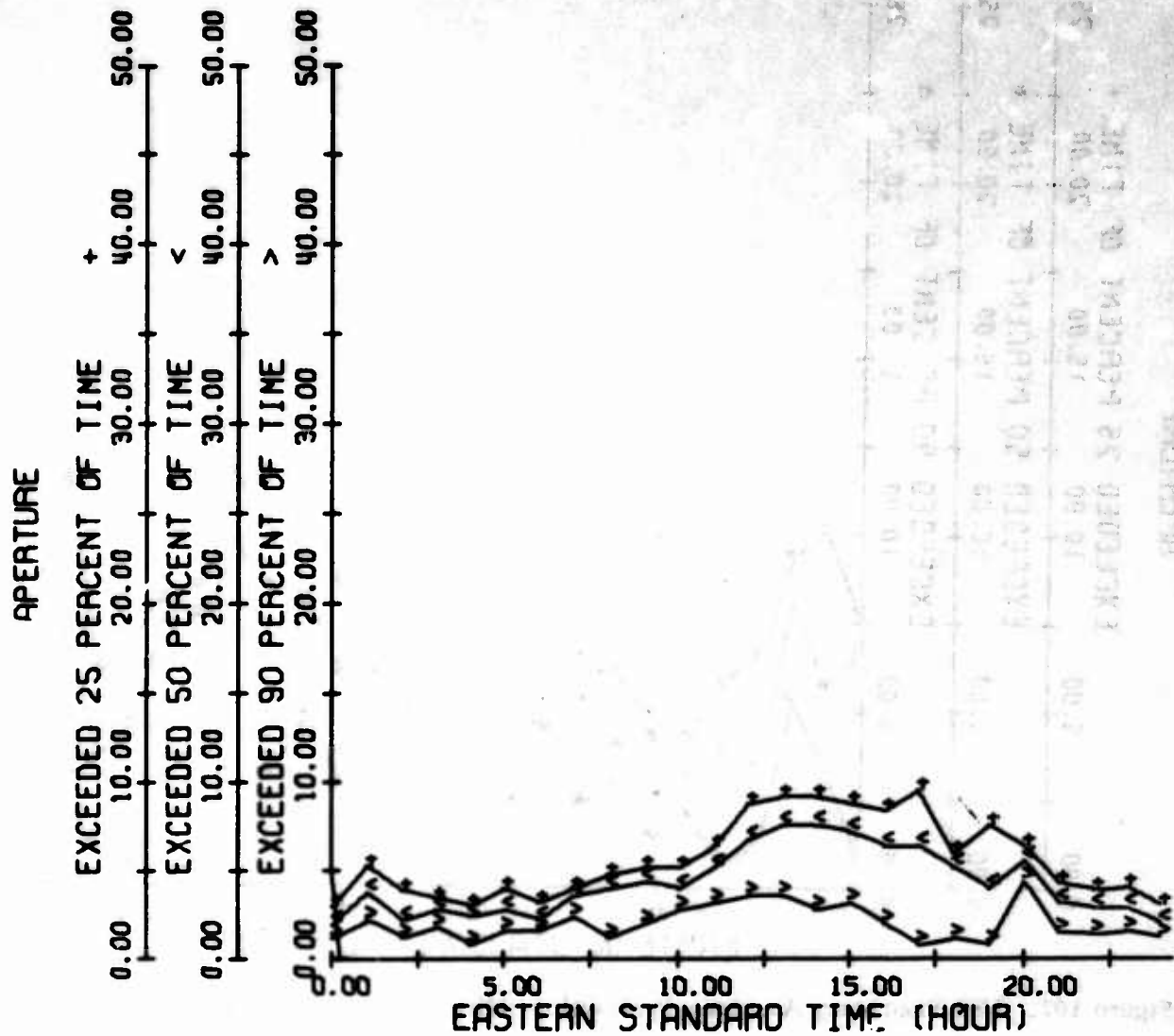


Figure 106. 1F2 Frequency Aperture Availability (MHz), Coco Solo Path, Spring 1966

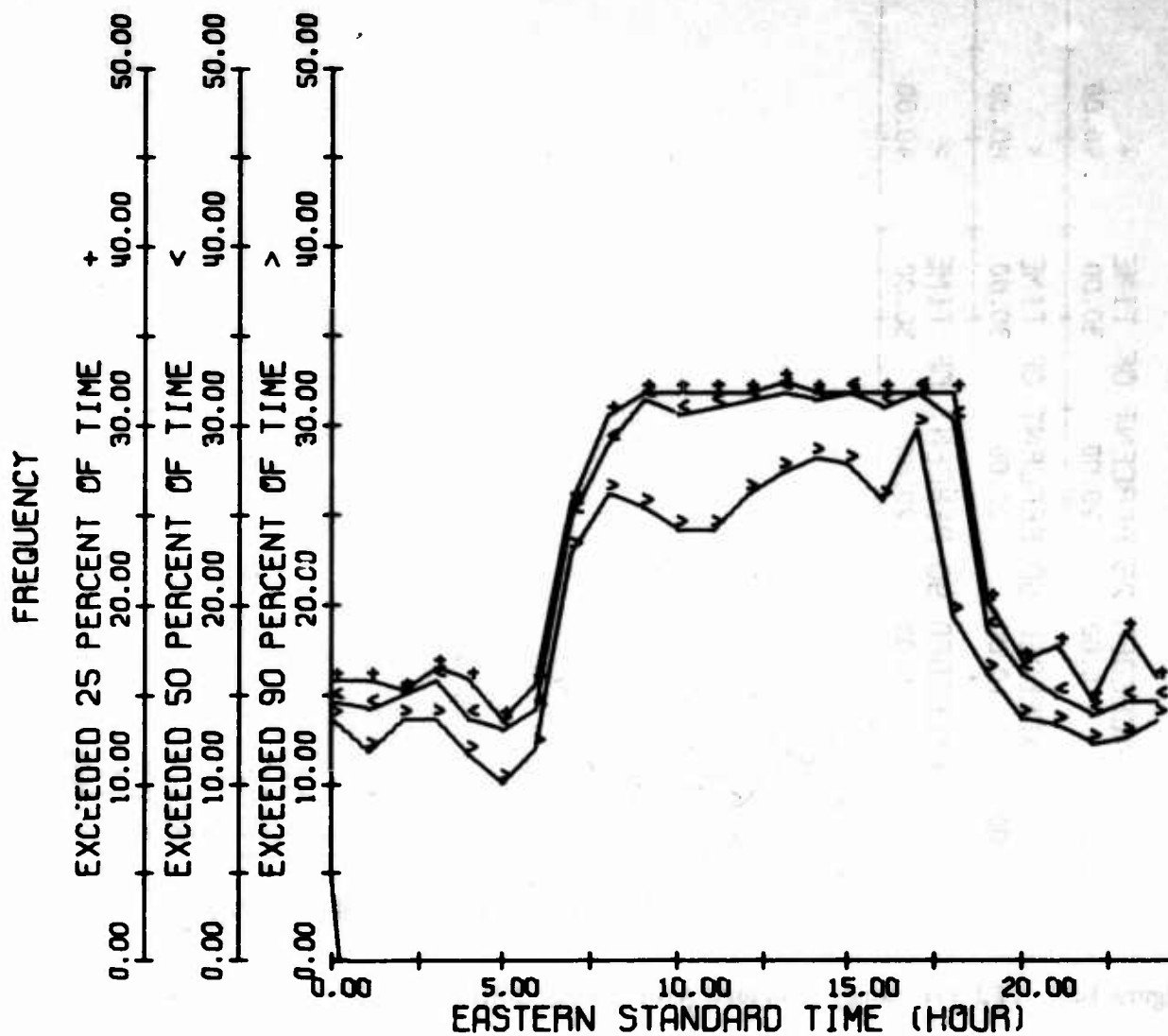


Figure 108. 1F2 Frequency Aperture Availability (MHz), Coco Solo Path, Autumn 1966

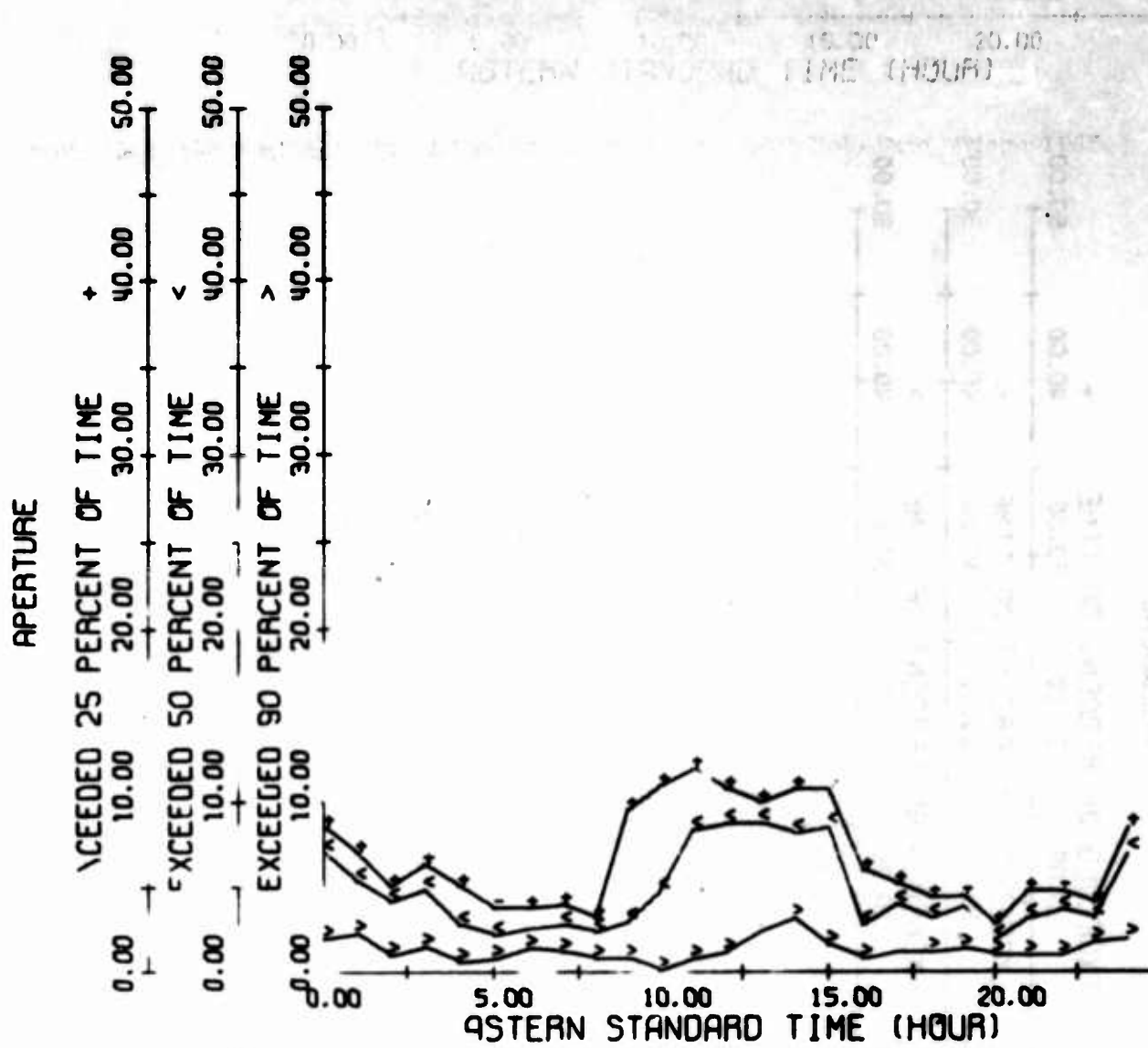


Figure 109. 1F2 Frequency Aperture Availability (MHz), Coco Solo Path, Winter 1967

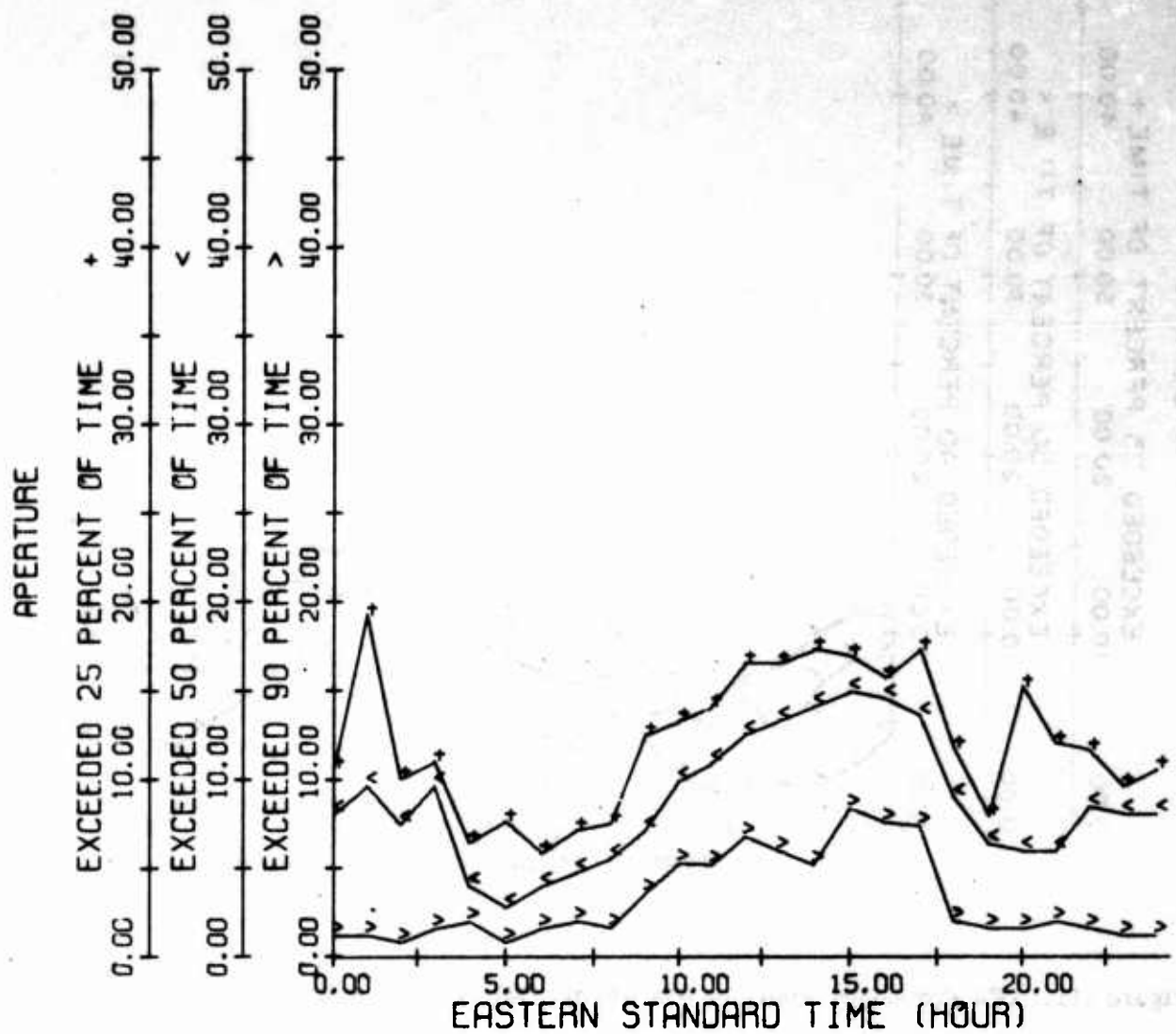


Figure 110. 1F2 Frequency Aperture Availability (MHz), Coco Solo Path, Spring 1967

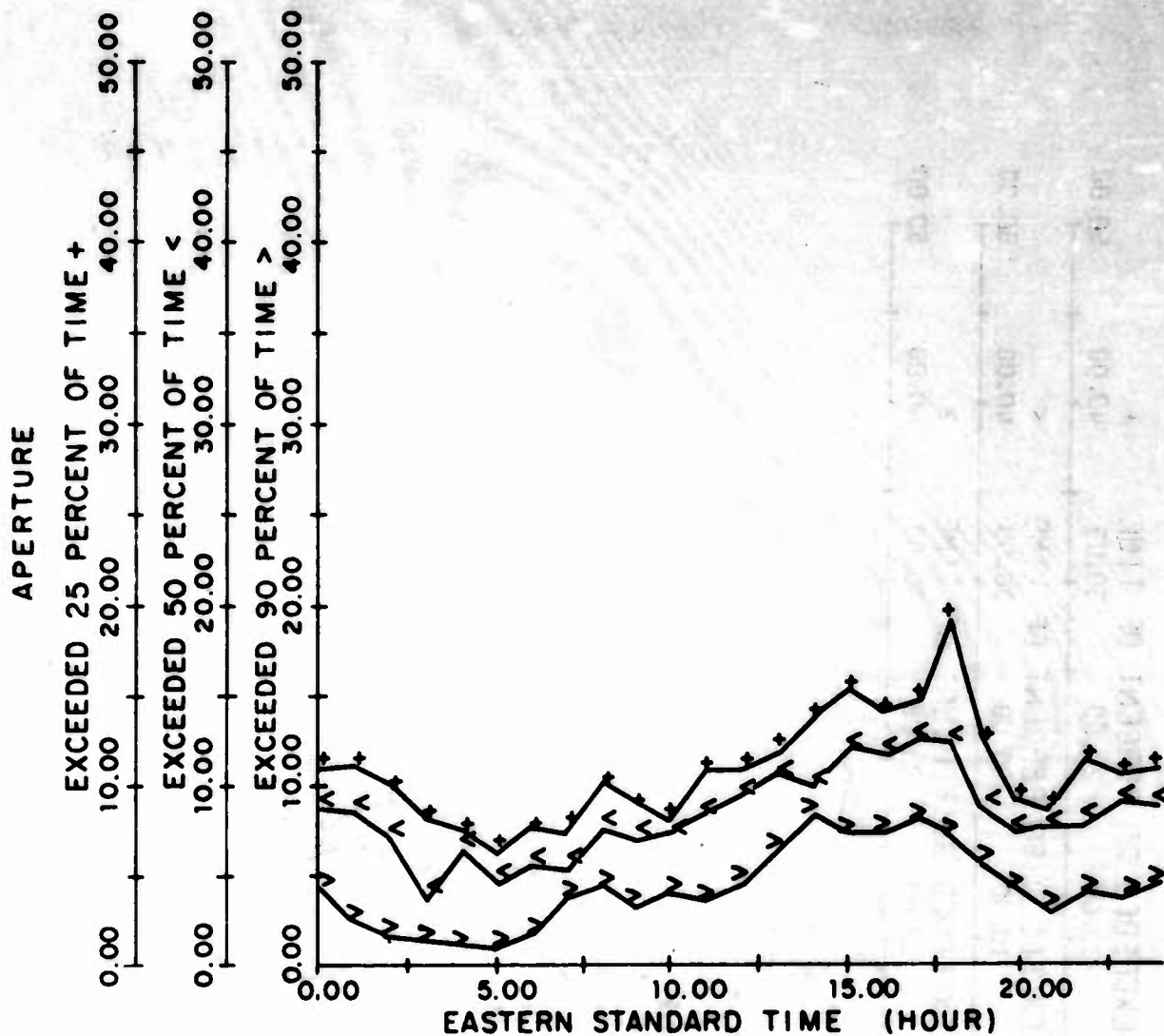


Figure 111. 1F2 Frequency Aperture Availability (MHz), Coco Solo Path, Summer 1967

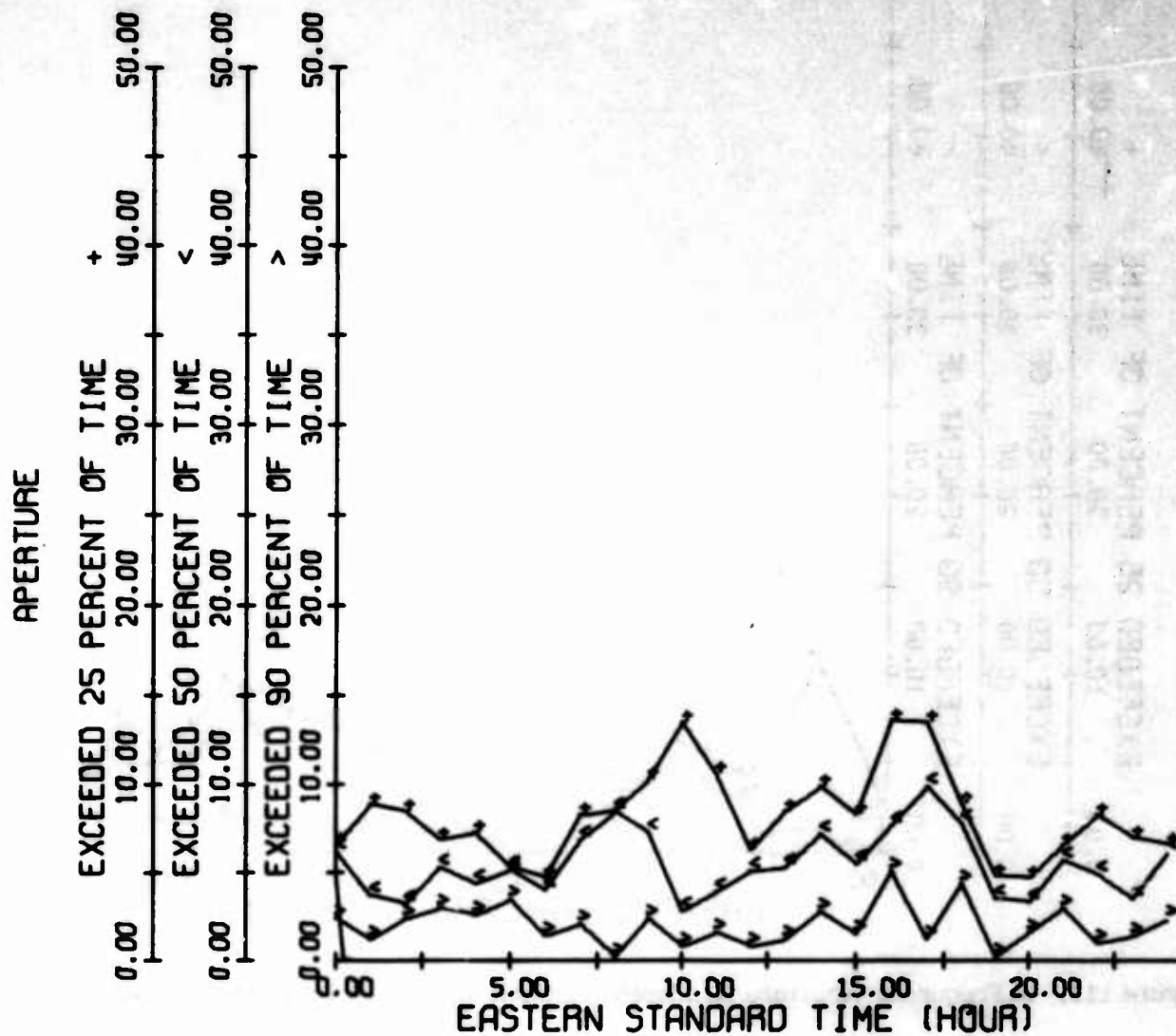


Figure 112. N Frequency Aperture Availability (MHz), Coco Solo Path, Winter 1966

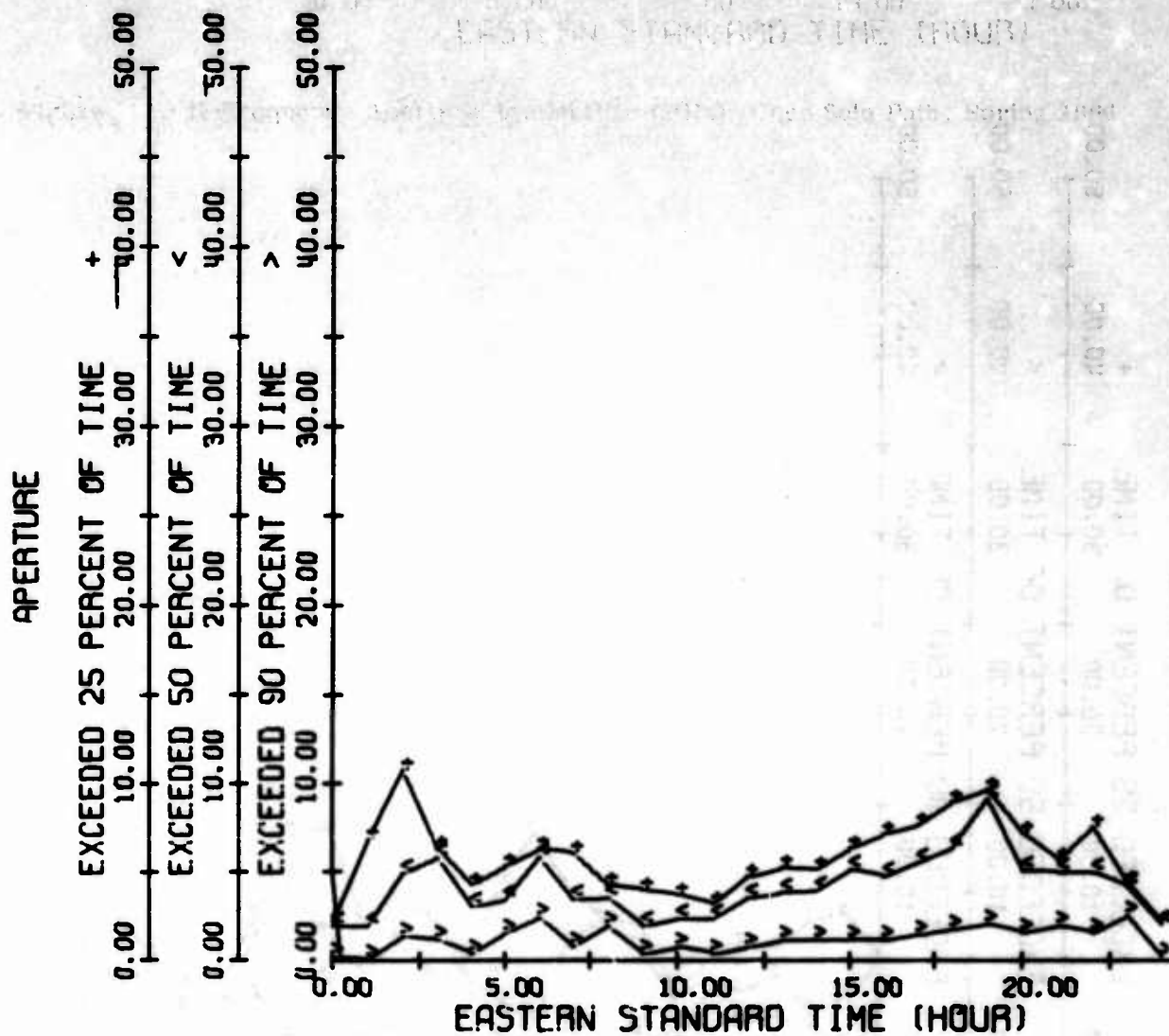


Figure 113. N Frequency Aperture Availability (MHz), Coco Solo Path, Spring 1966

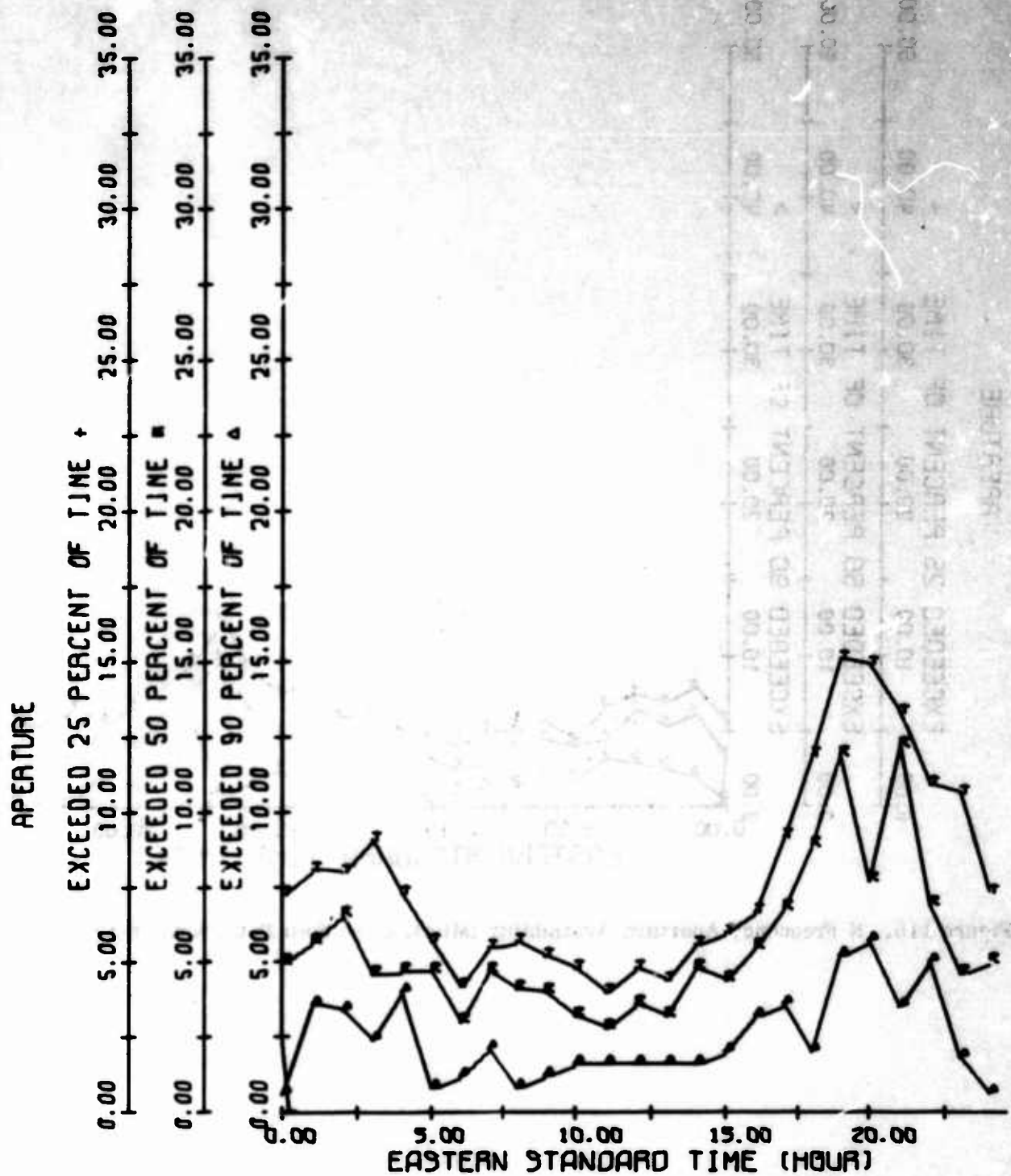


Figure 114. N Frequency Aperture Availability (MHz), Coco Solo Path, Summer 1966

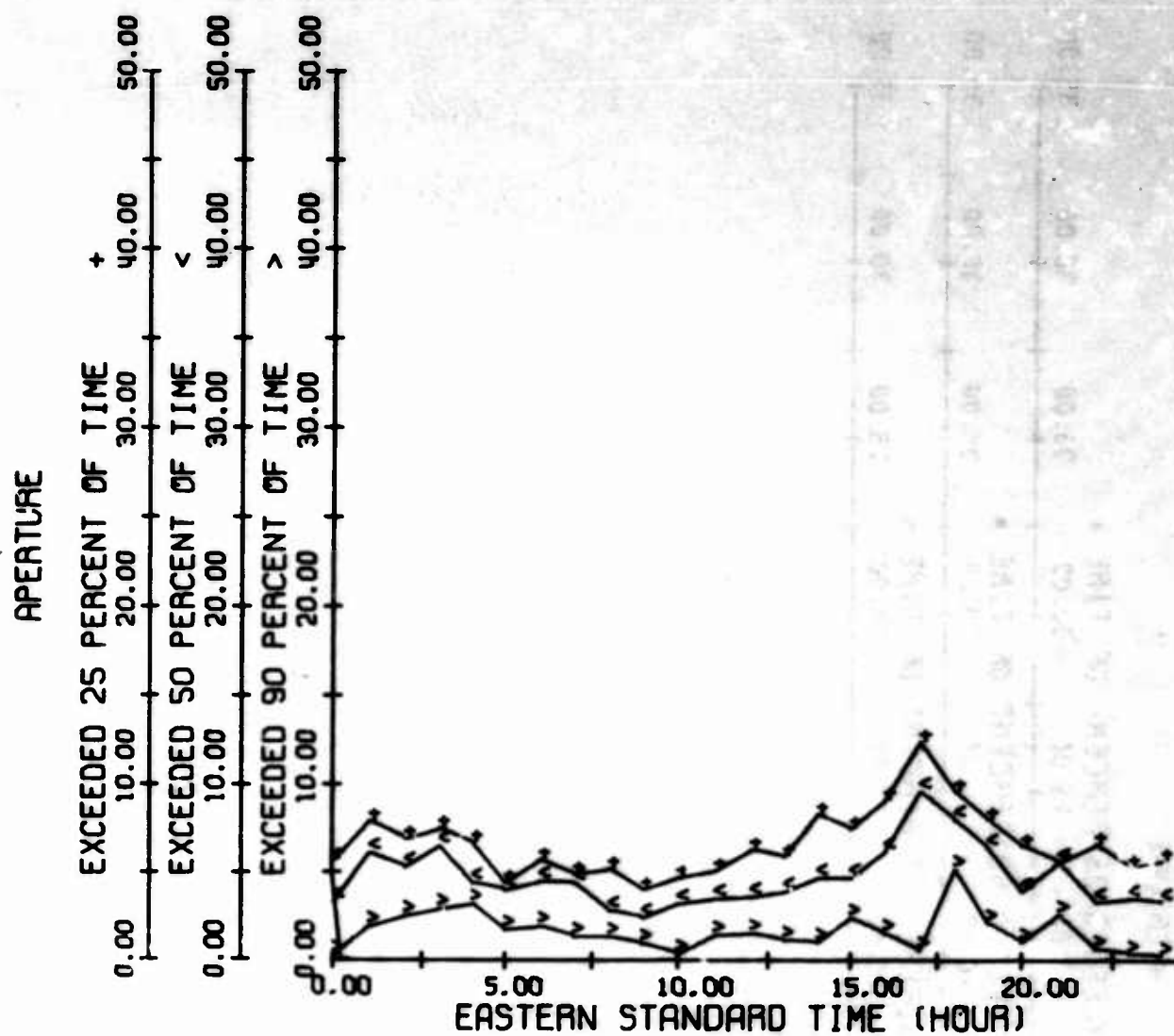


Figure 115. N Frequency Aperture Availability (MHz), Coco Solo Path, Autumn 1966

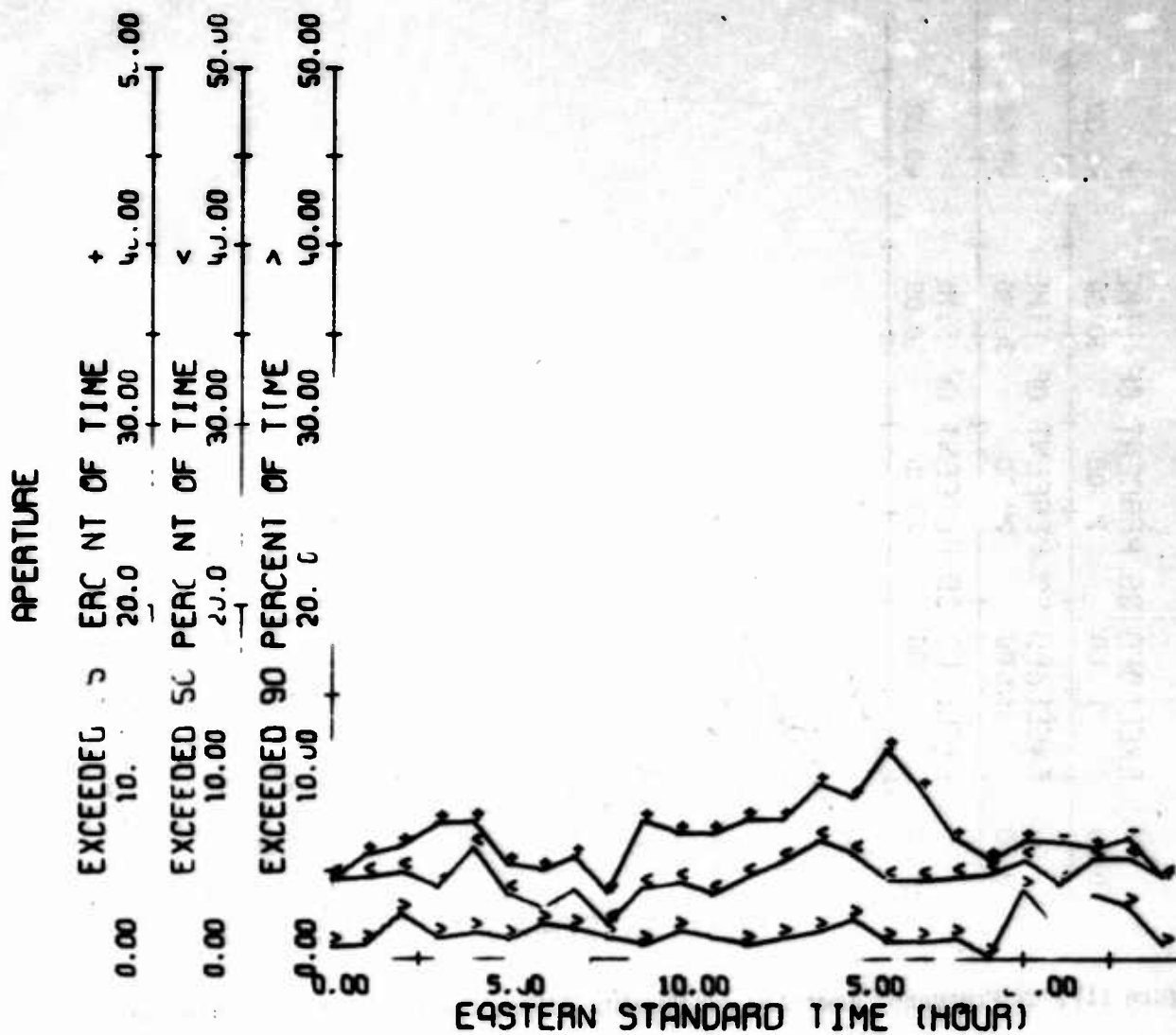


Figure 116. N Frequency Aperture Availability (MHz), Coco Solo Path, Winter 1967

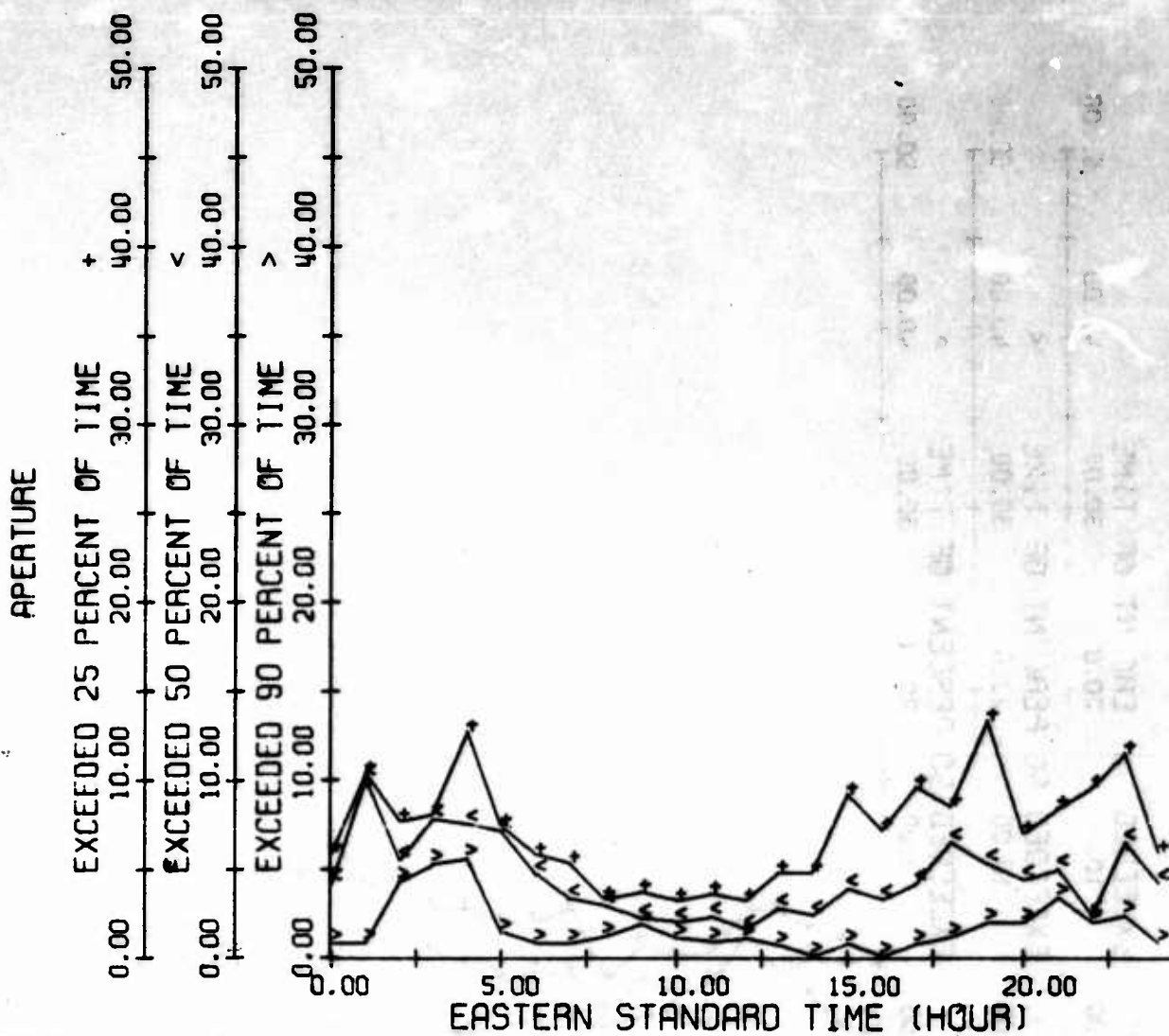


Figure 117. N Frequency Aperture Availability (MHz), Coco Solo Path, Spring 1967

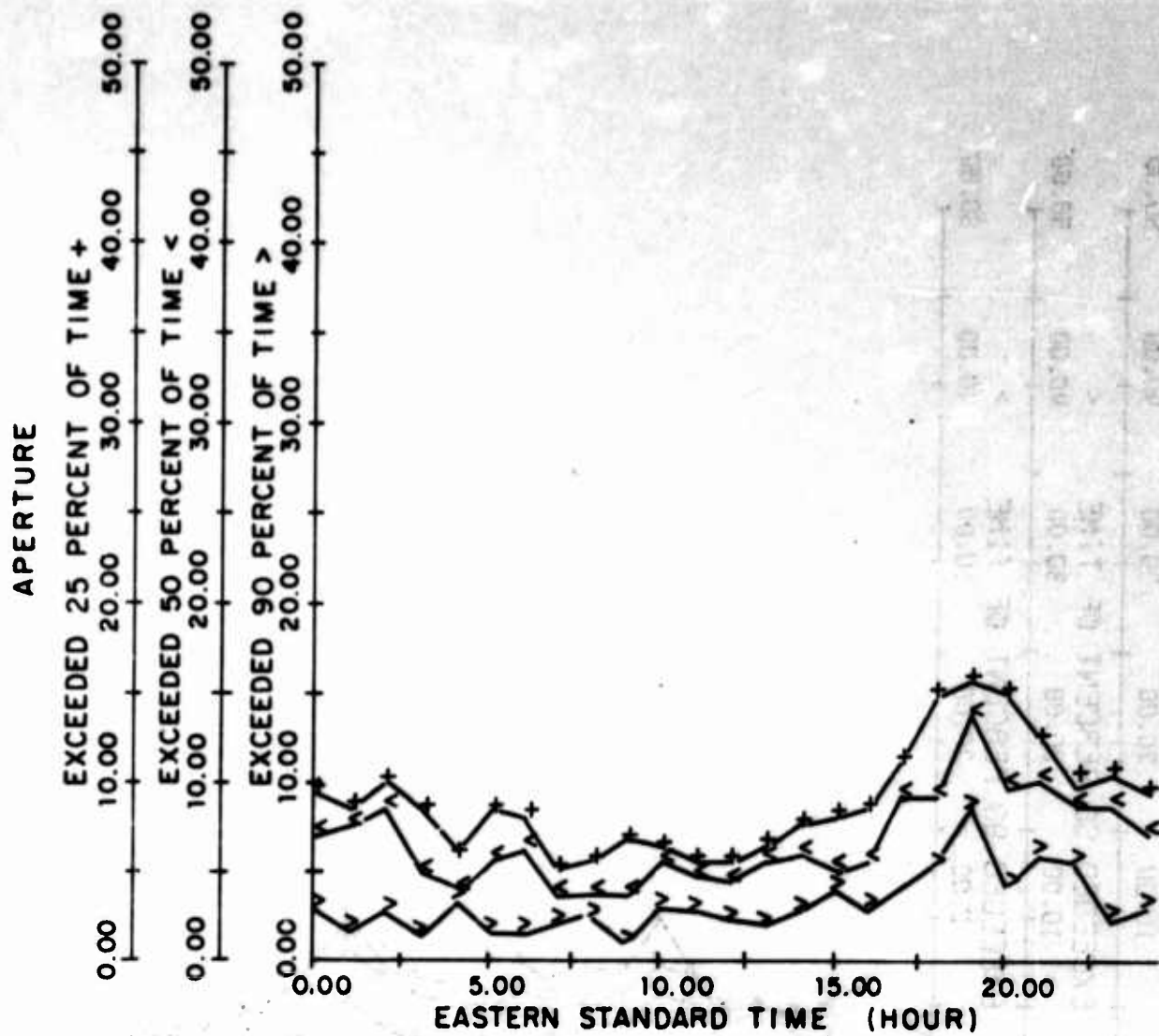


Figure 118. N Frequency Aperture Availability (MHz), Coco Solo Path, Summer 1967

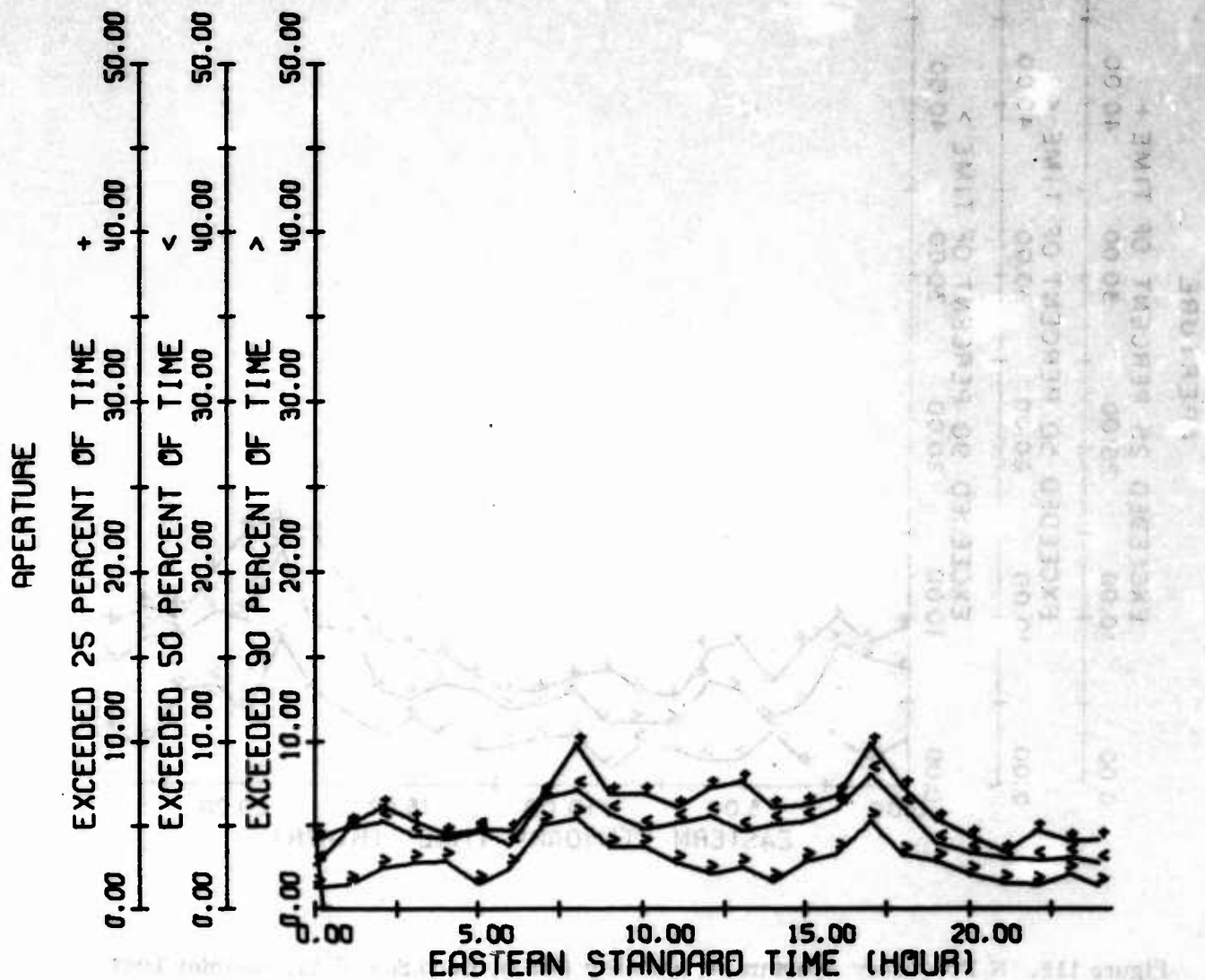


Figure 119. 2F2 Frequency Aperture Availability (MHz), Coco Solo Path, Winter 1966

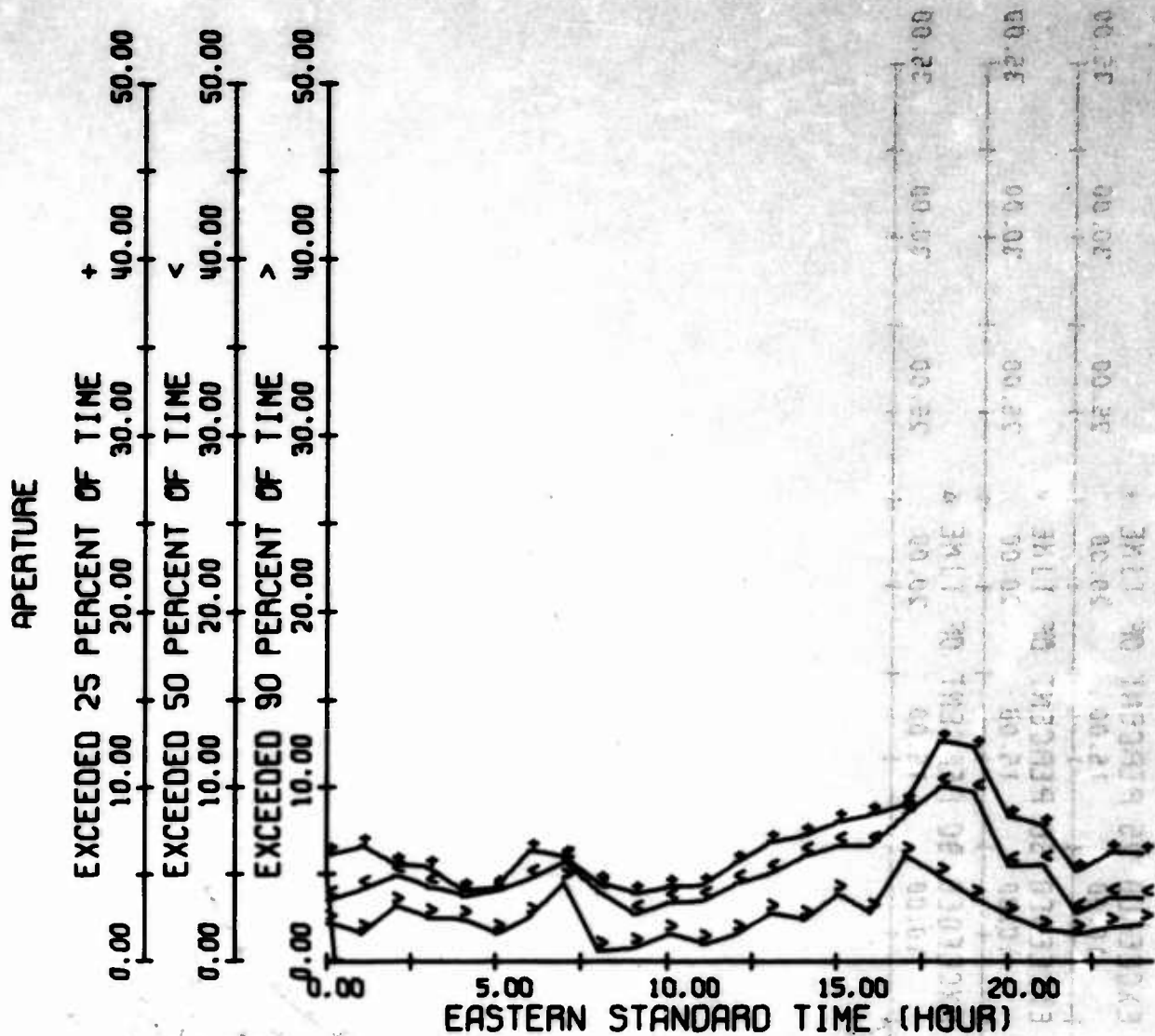


Figure 120. 2F2 Frequency Aperture Availability (MHz), Coco Solo Path, Spring 1966

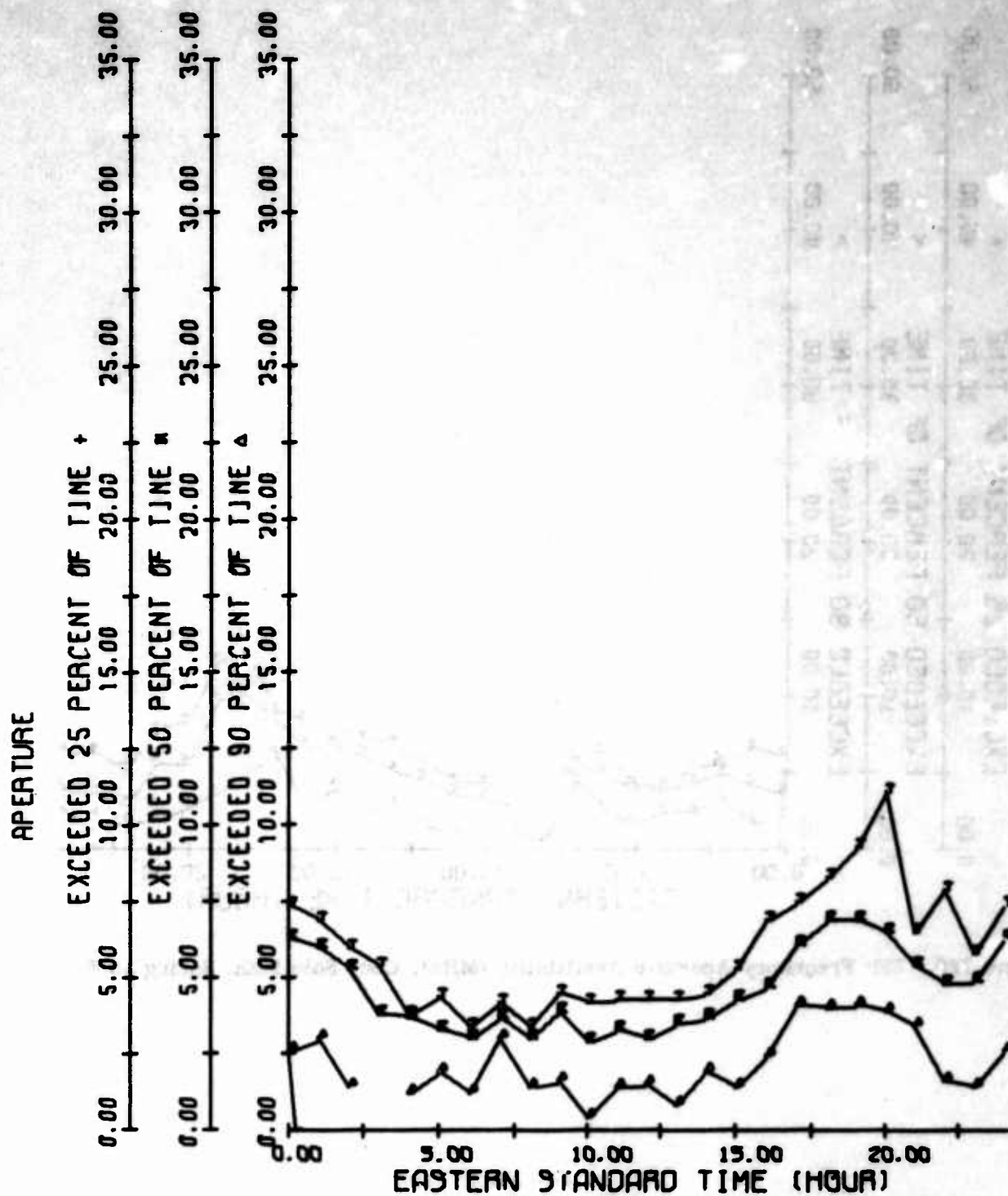


Figure 121. 2F2 Frequency Aperture Availability (MHz), Coco Solo Path, Summer 1966

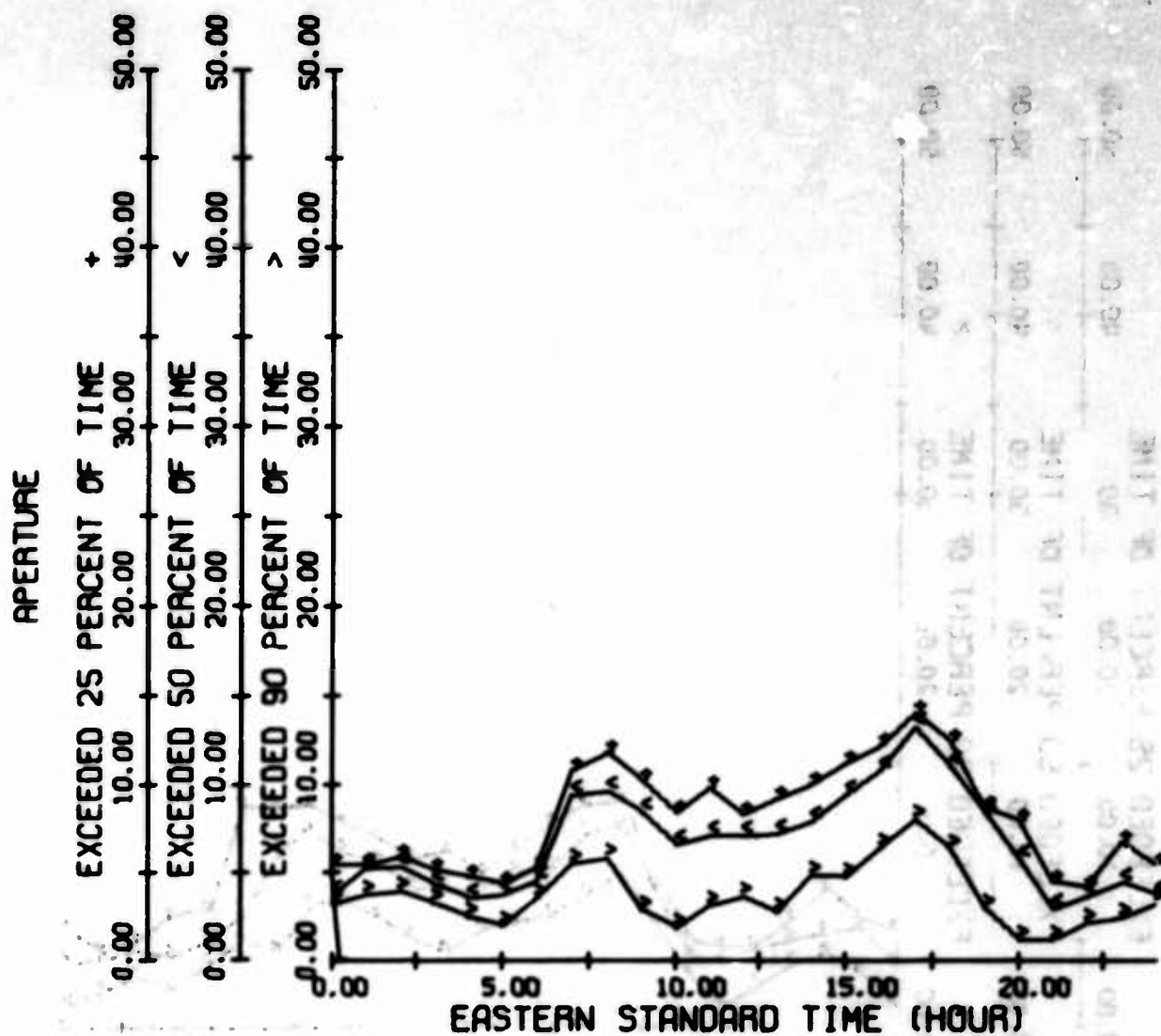


Figure 122. 2F2 Frequency Aperture Availability (MHz), Coco Solo Path, Autumn 1966

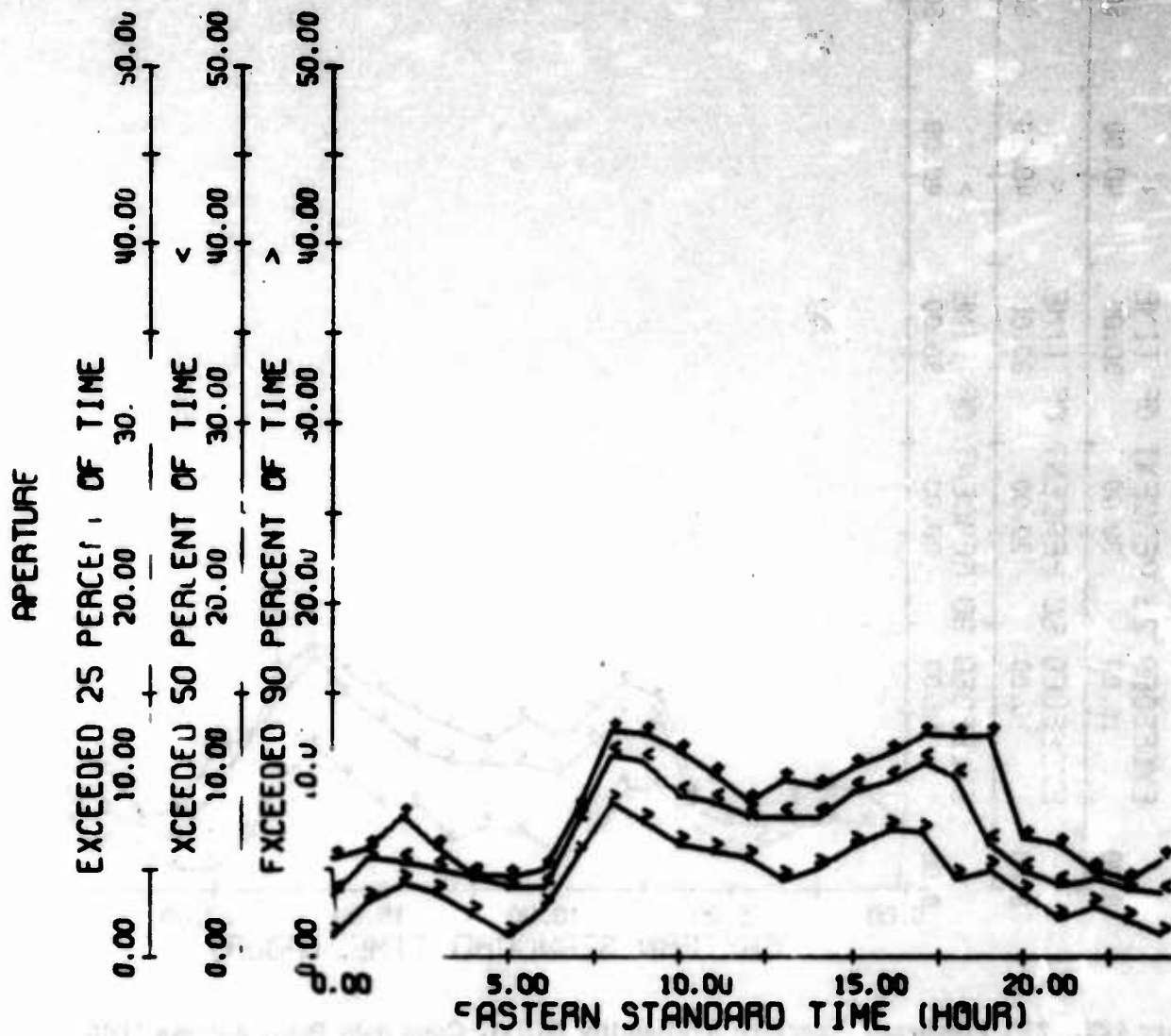


Figure 123. 2F2 Frequency Aperture Availability (MHz), Coco Solo Path, Winter 1967

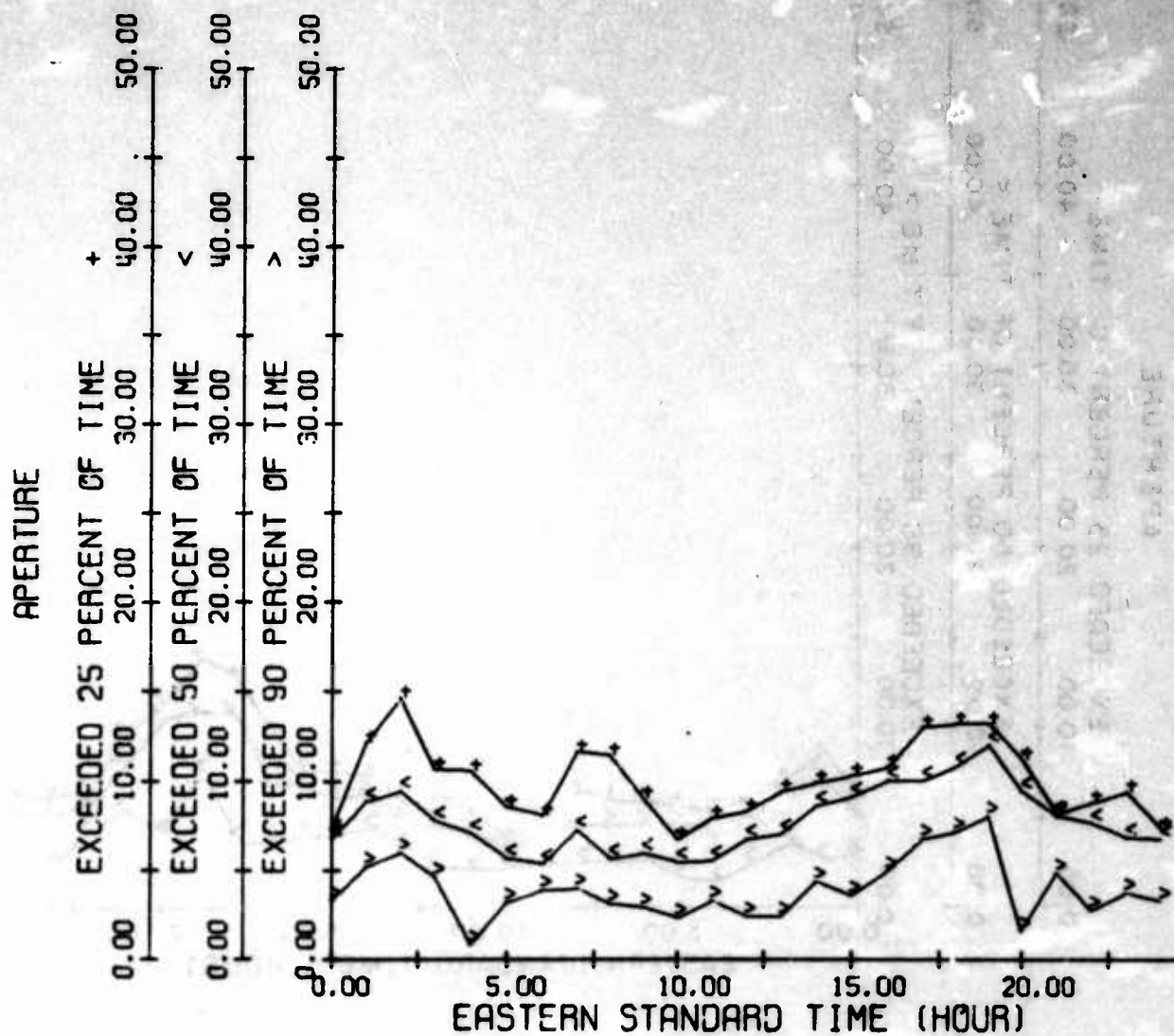


Figure 124. 2F2 Frequency Aperture Availability (MHz), Coco Solo Path, Spring 1967

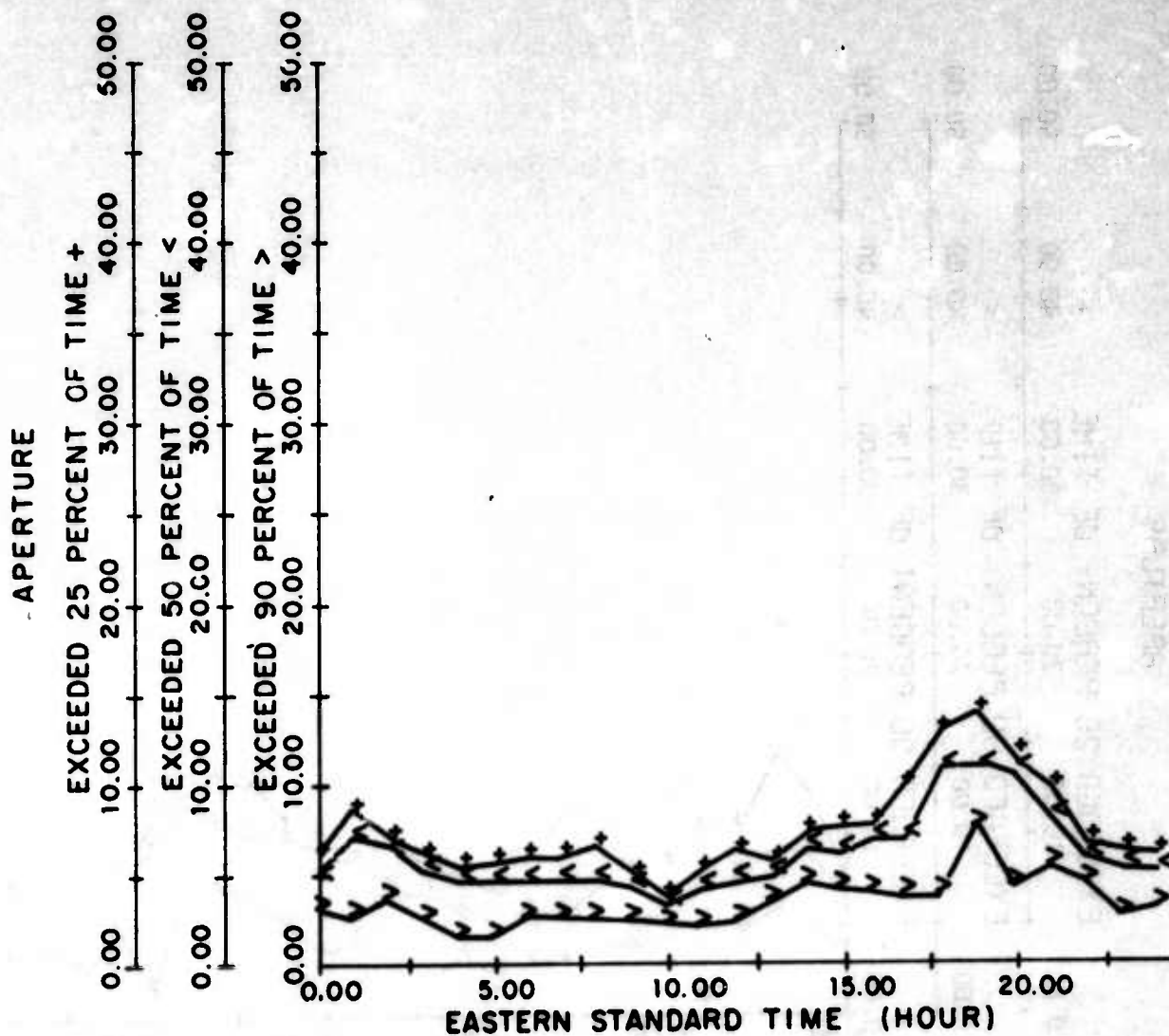


Figure 125. 2F2 Frequency Aperture Availability (MHz), Coco Solo Path, Summer 1967

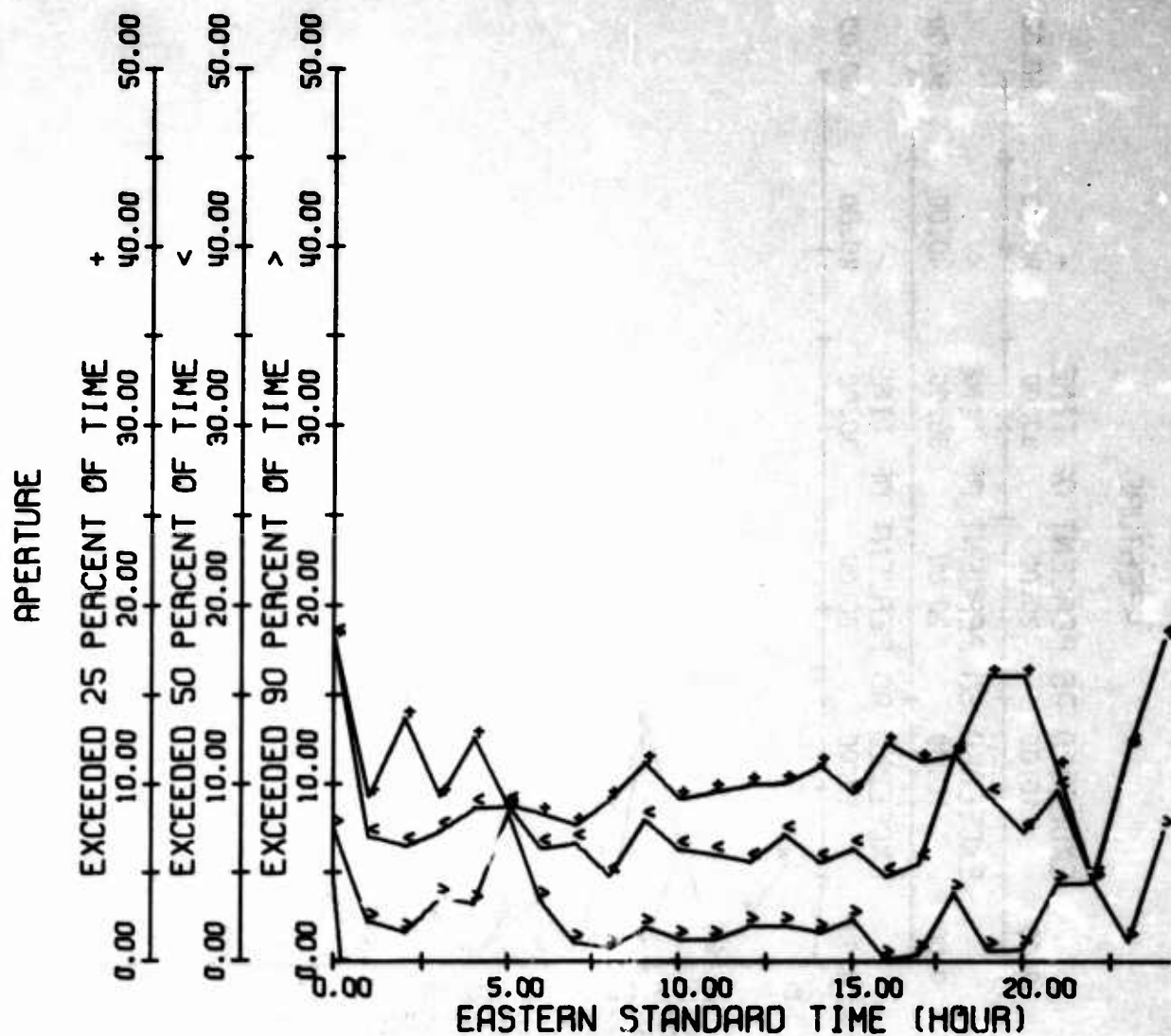


Figure 126.2E_g Frequency Aperture Availability (MHz), Coco Solo Path, Summer 1966

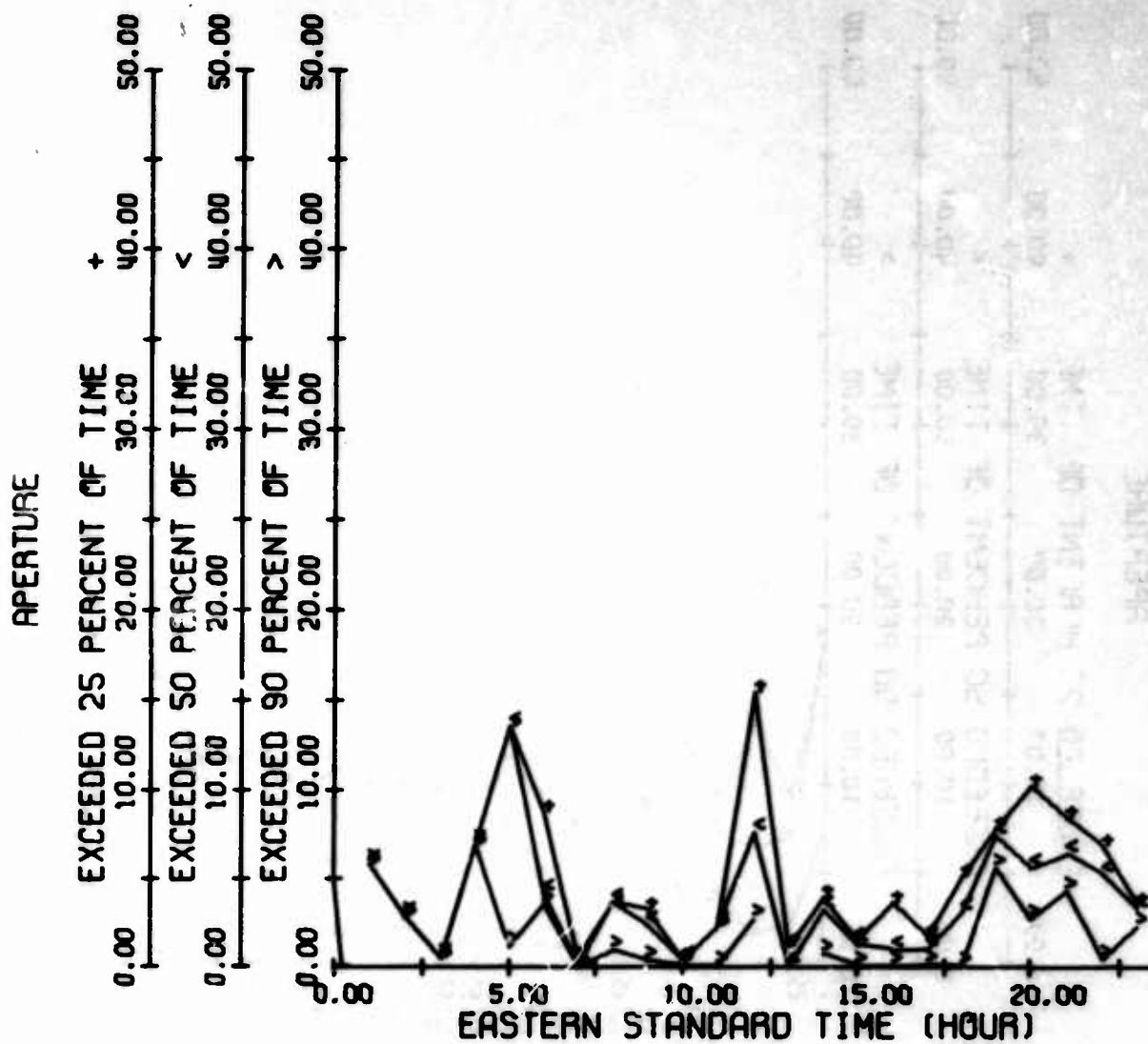


Figure 127. $2E_8$ Frequency Aperture Availability (MHz), Coco Solo Path, Autumn 1966

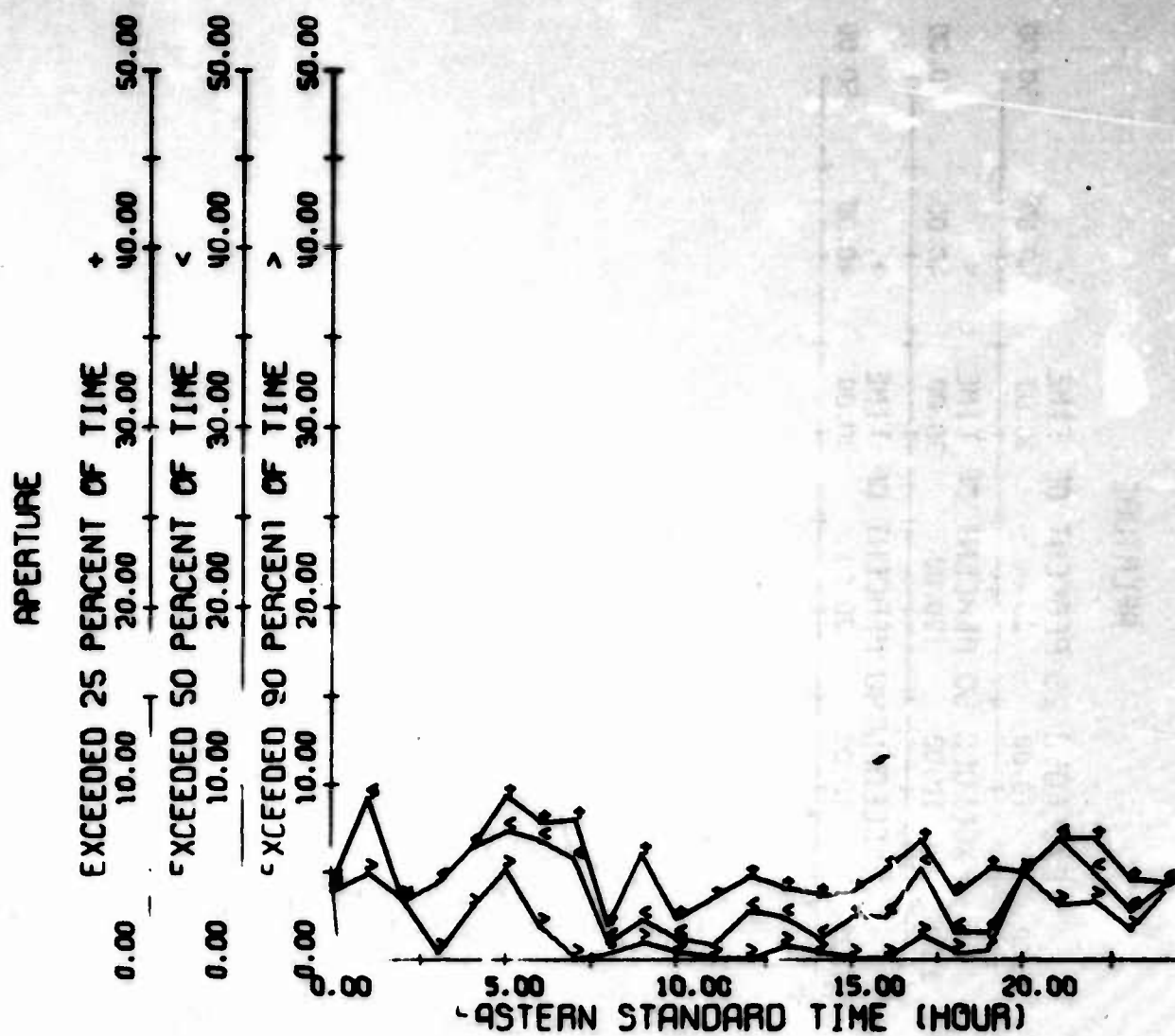


Figure 128. 2E₉ Frequency Aperture Availability (MHz), Coco Solo Path, Winter 1967

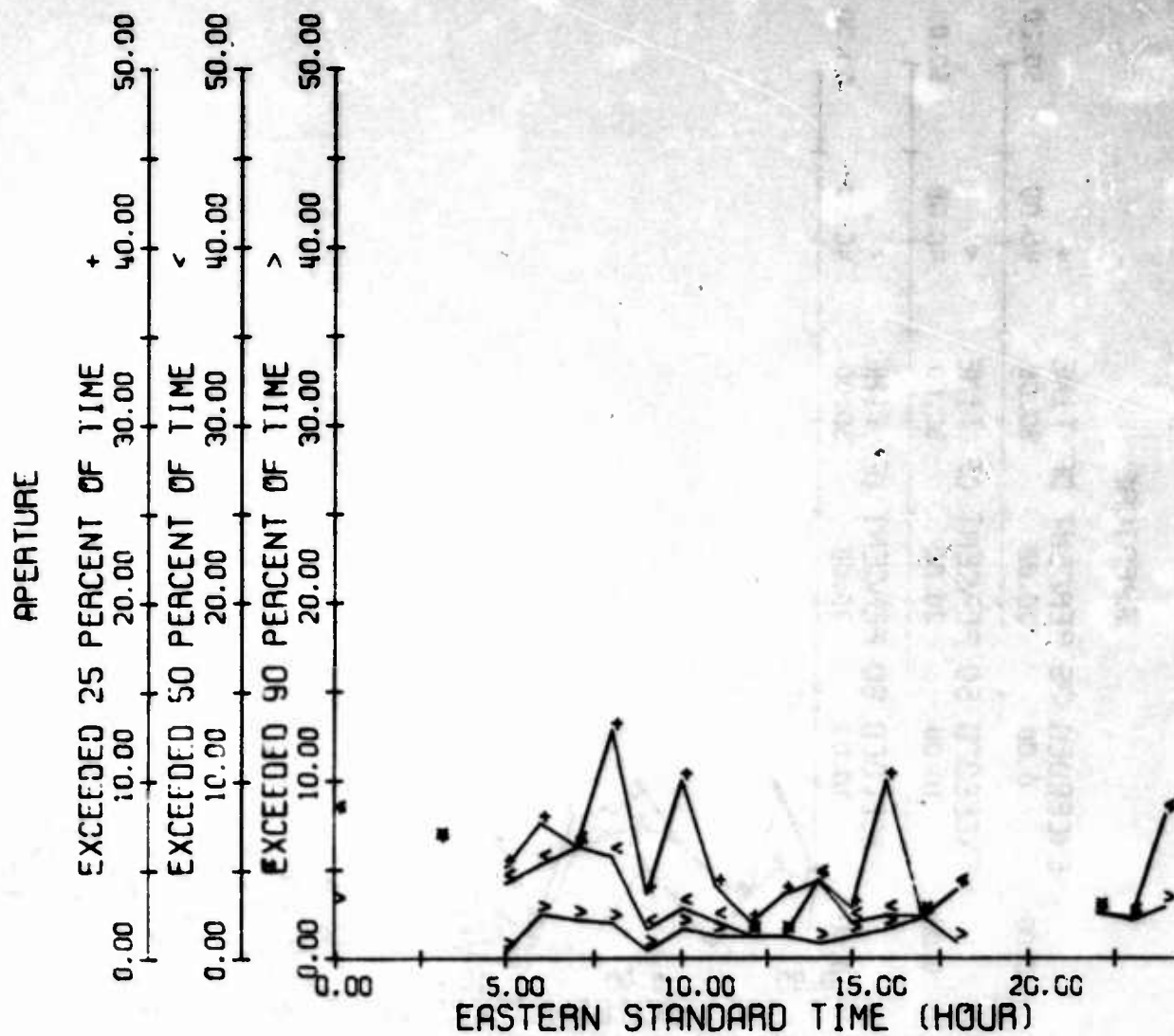


Figure 129.2E_s Frequency Aperture Availability (MHz), Coco Solo Path, Spring 1967

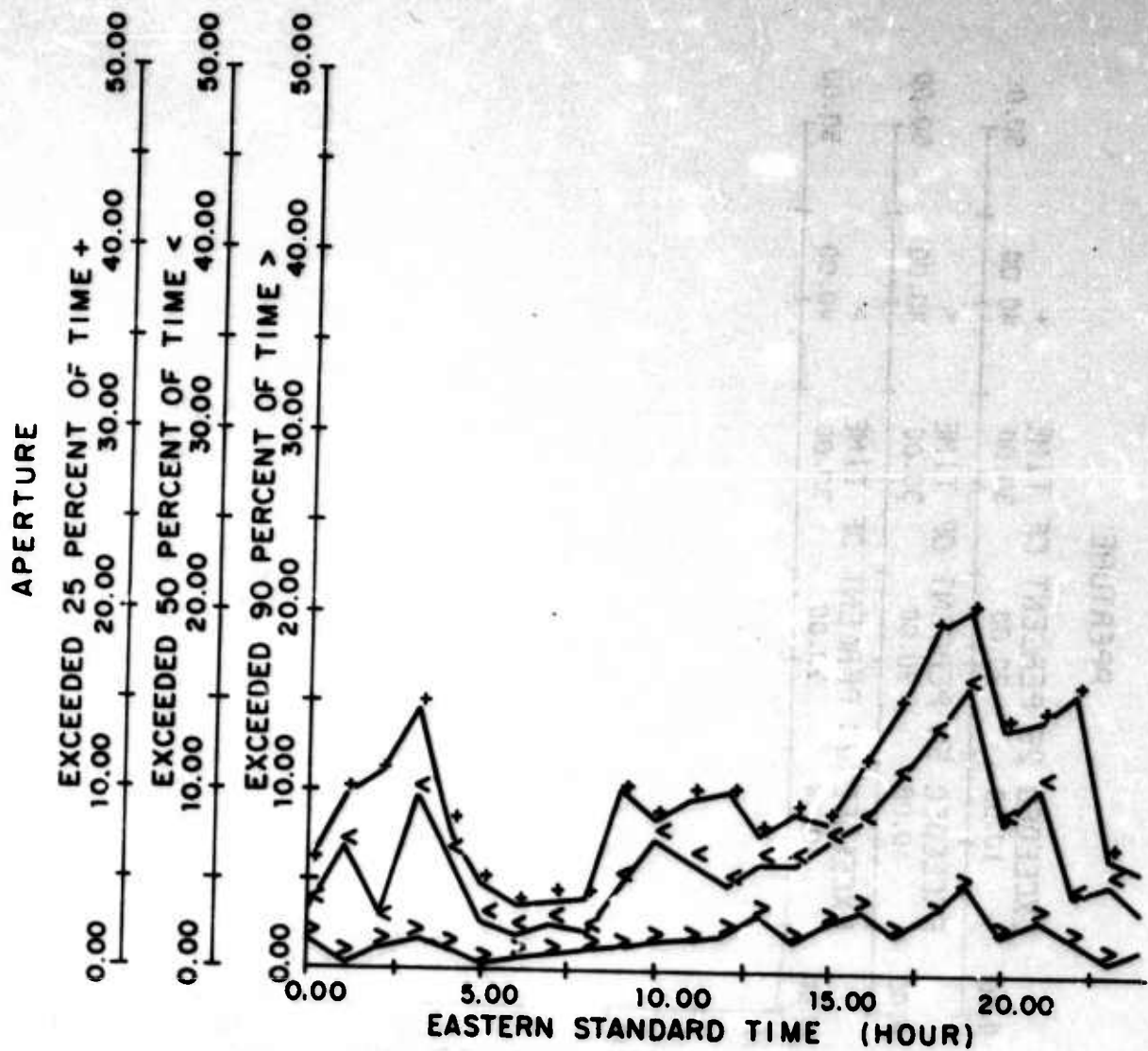


Figure 130. $2E_s$ Frequency Aperture Availability (MHz), Coco Solo Path, Summer 1967

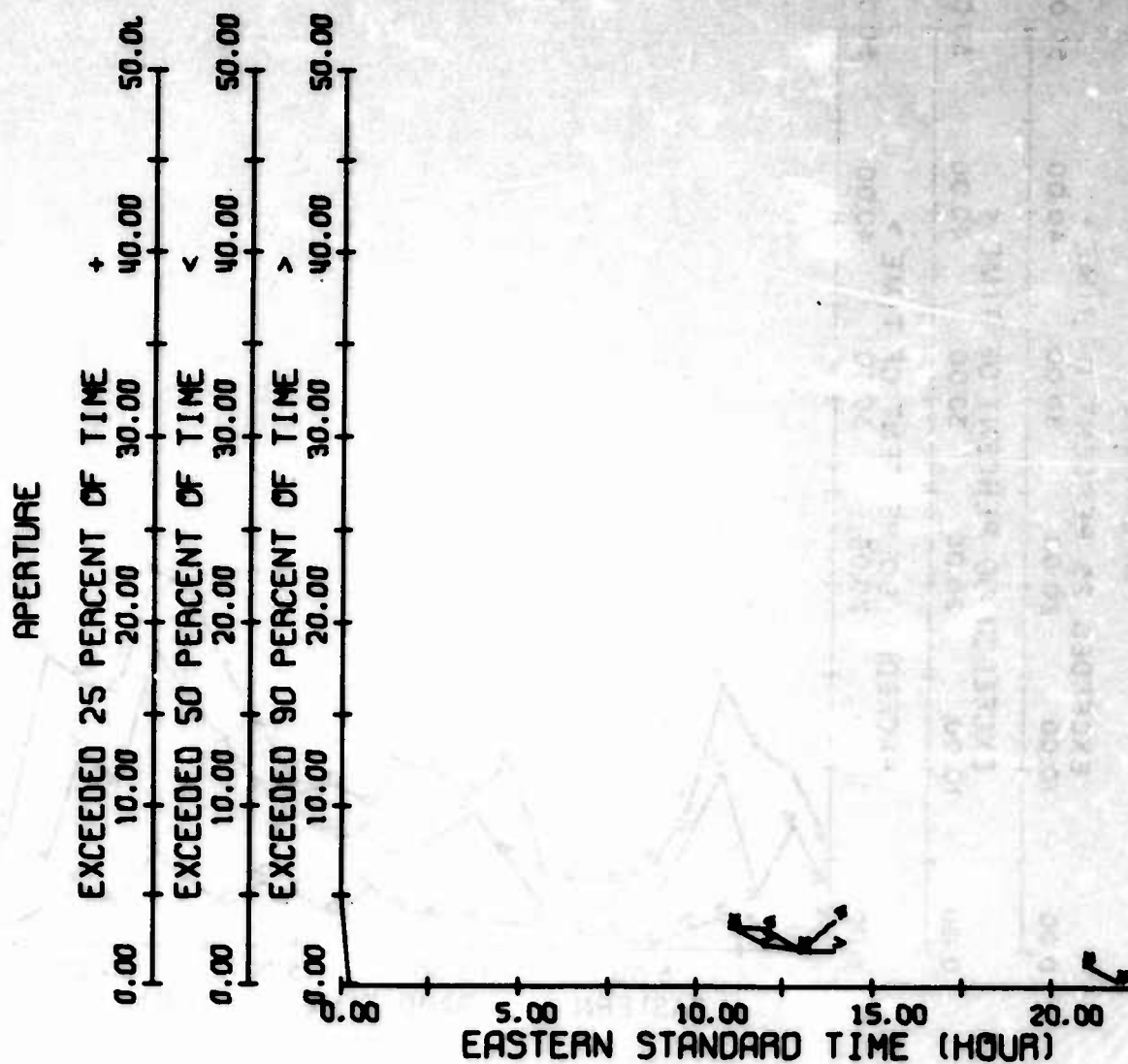


Figure 131. 2E Mode Frequency Aperture Availability, Thule Path, Winter 1967

6. FREQUENCY APERTURE AVAILABILITY -- THULE TO STOCKBRIDGE/ STARR HILL

In the following, only the results for the winter of 1967 and the spring of 1967 are available for the Thule path. The winter of 1967 results are from measurements on the Thule to Stockbridge path; in the spring, from Thule to Starr Hill. The difference in distances is slight. For the 2E mode (Figures 131 and 132) only a few bits of data exist for winter, but during the daytime hours the apertures are satisfactory. More adequate data are available for the spring, but again only daytime hours show a good frequency aperture availability. Apertures for the 1F2 mode (Figures 133 and 134) are satisfactory for both seasons, being slightly higher in the late afternoon and nights. The N mode frequency aperture for the winter of 1967 (Figures 135 and 136) is satisfactory, but for the spring is very poor. The 2F2 mode frequency aperture also was slightly better for the winter than for the spring (Figures 137 and 138). The 2E_g frequency aperture data for both seasons are quite sketchy (Figures 139 and 140).

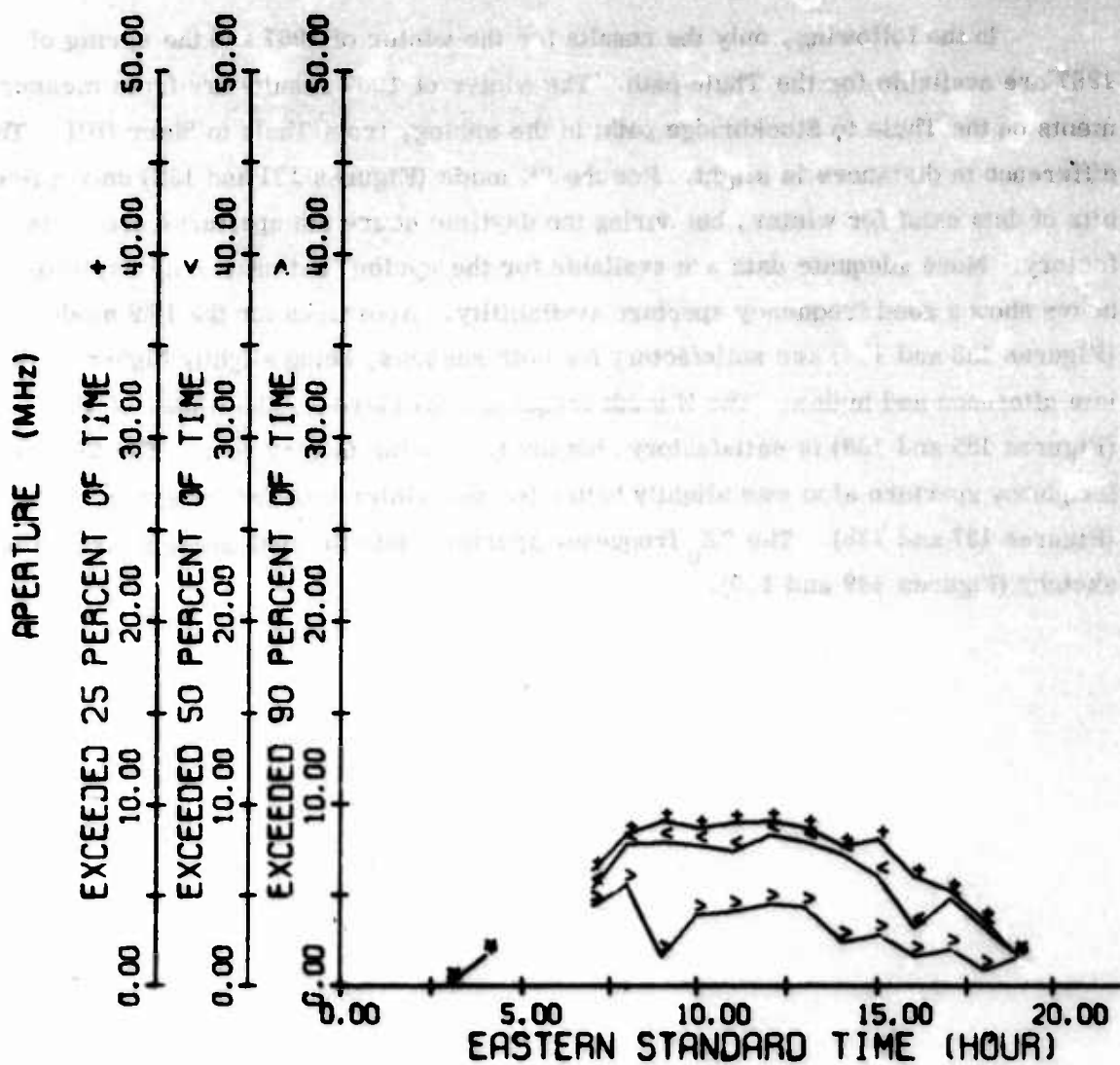


Figure 132. 2E Mode Frequency Aperture Availability, Thule Path, Spring 1967

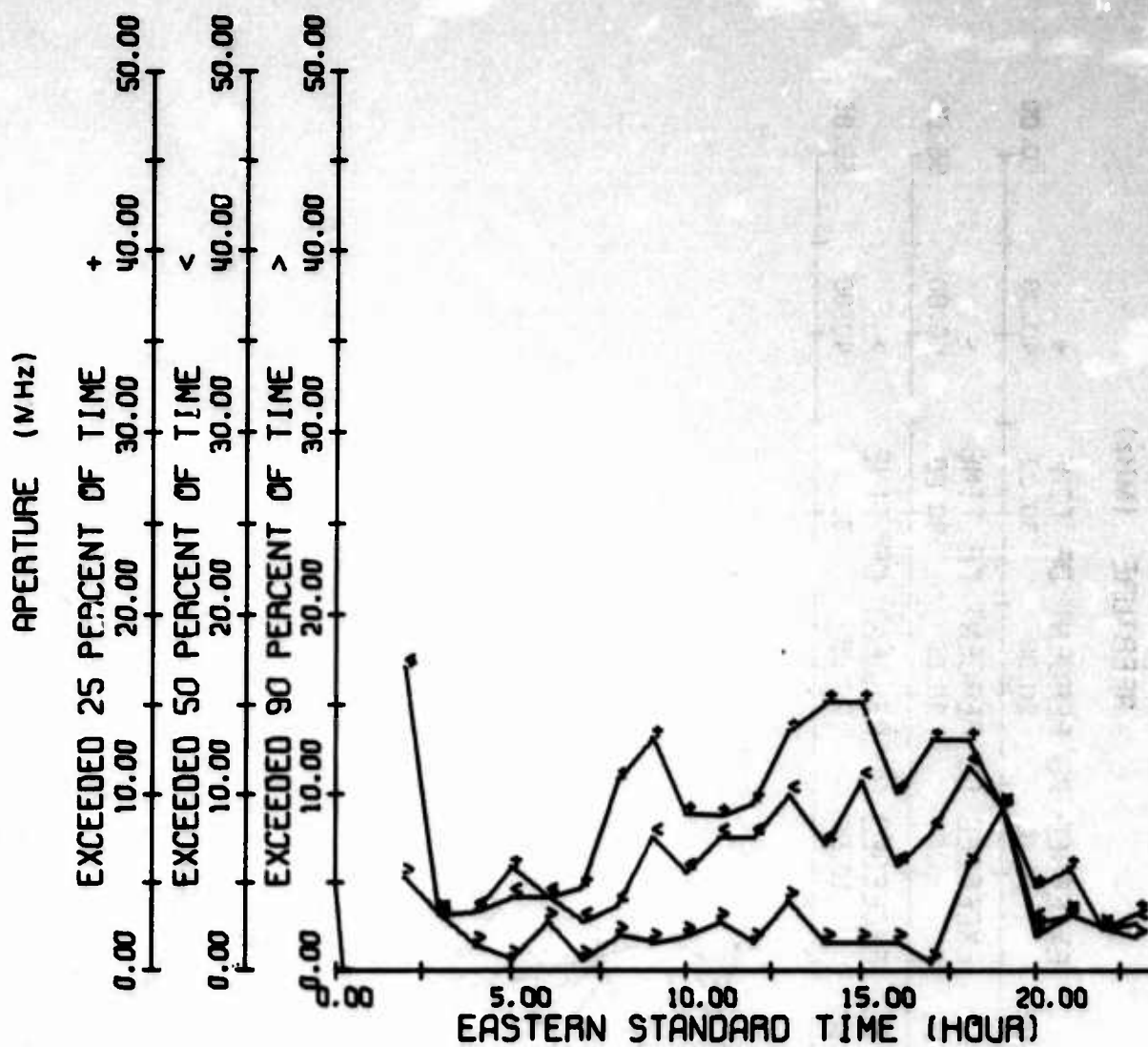


Figure 133. 1F2 Mode Frequency Aperture Availability, Thule Path, Winter 1967

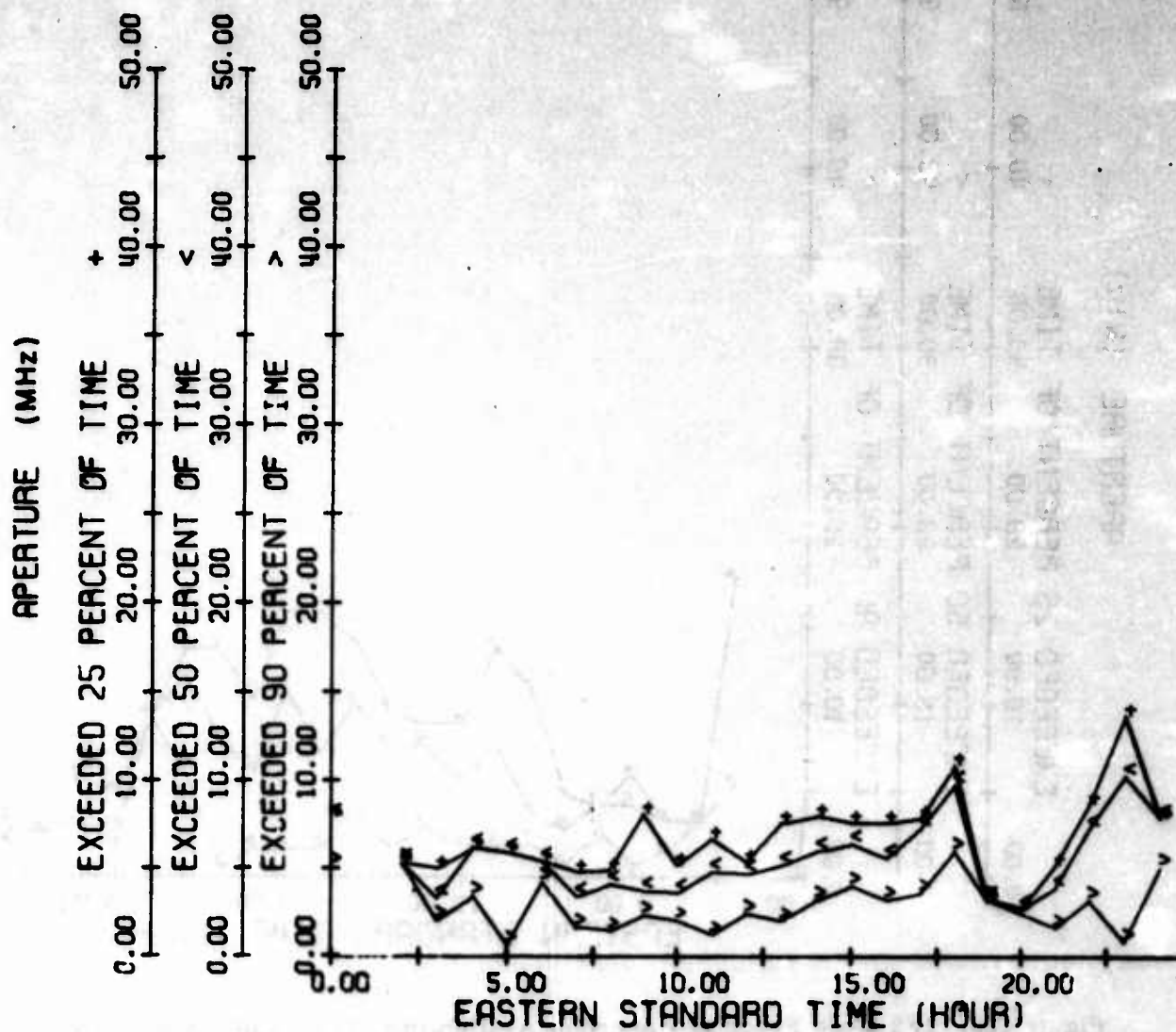


Figure 134. 1F2 Frequency Aperture Availability, Thule Path, Spring 1967

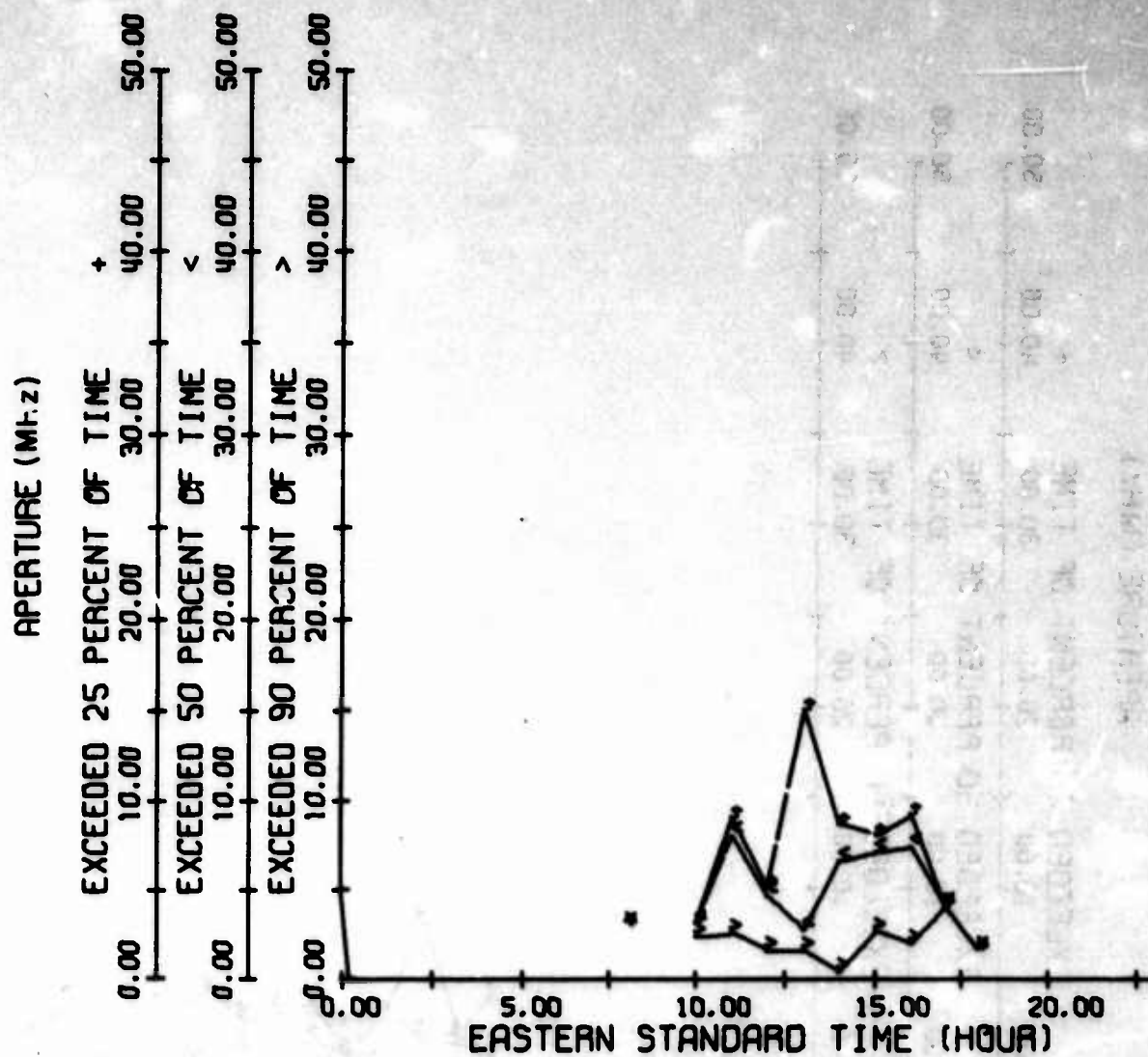


Figure 135. N Mode Frequency Aperture Availability, Thule Path, Winter 1967

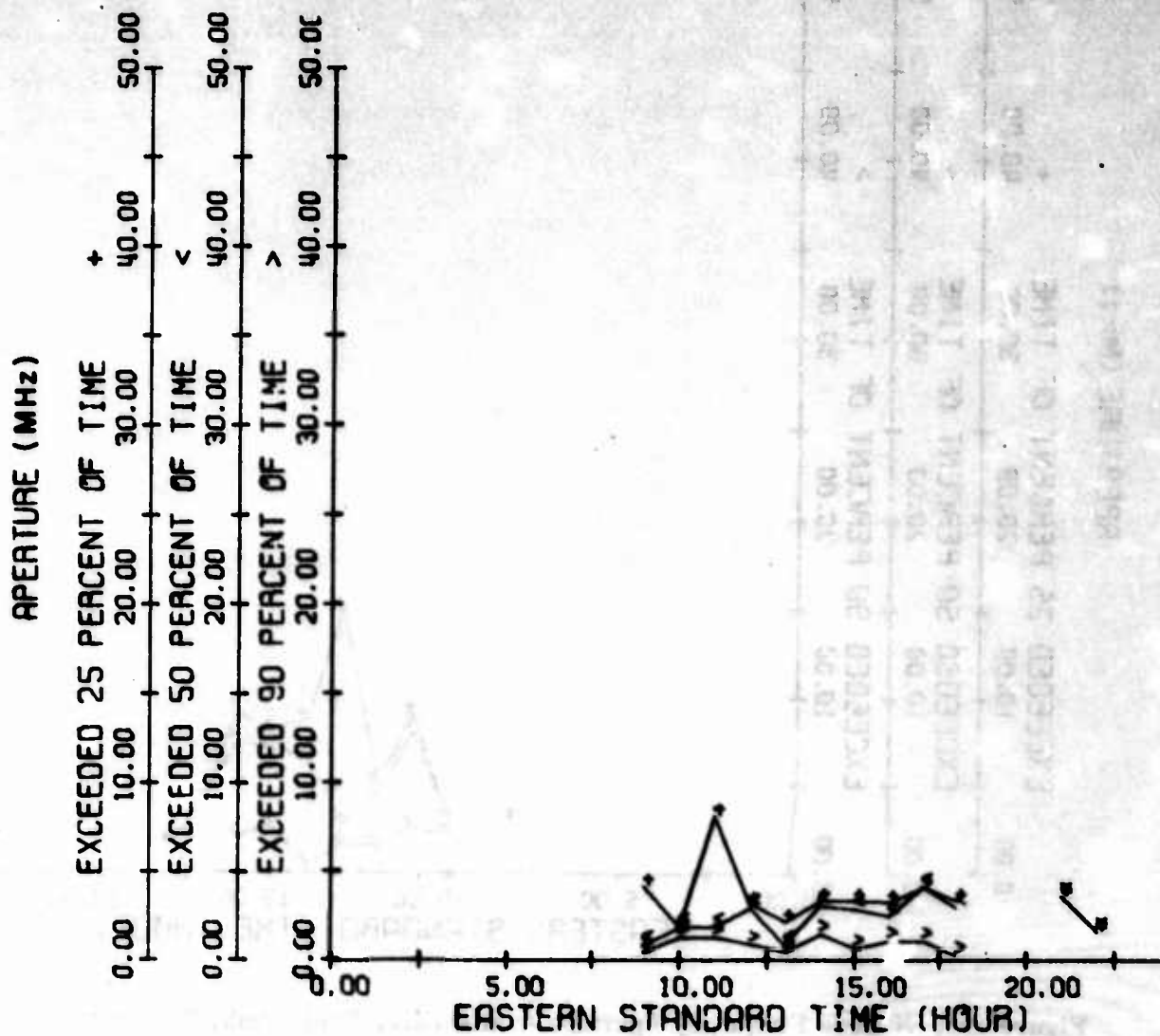


Figure 136. N Mode Frequency Aperture Availability, Thule Path, Spring 1967

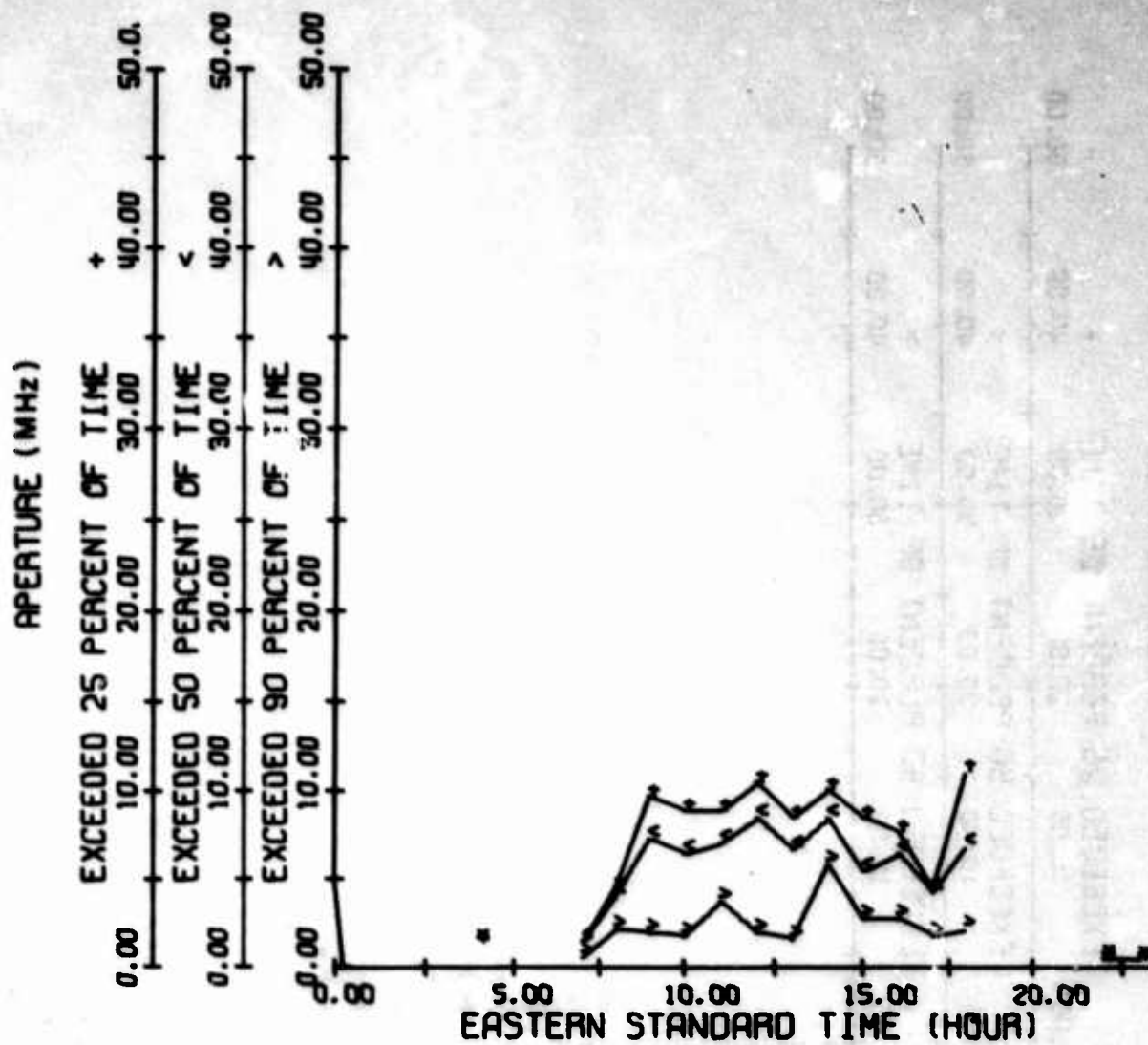


Figure 137. 2F2 Mode Frequency Aperture Availability, Thule Path, Winter 1967

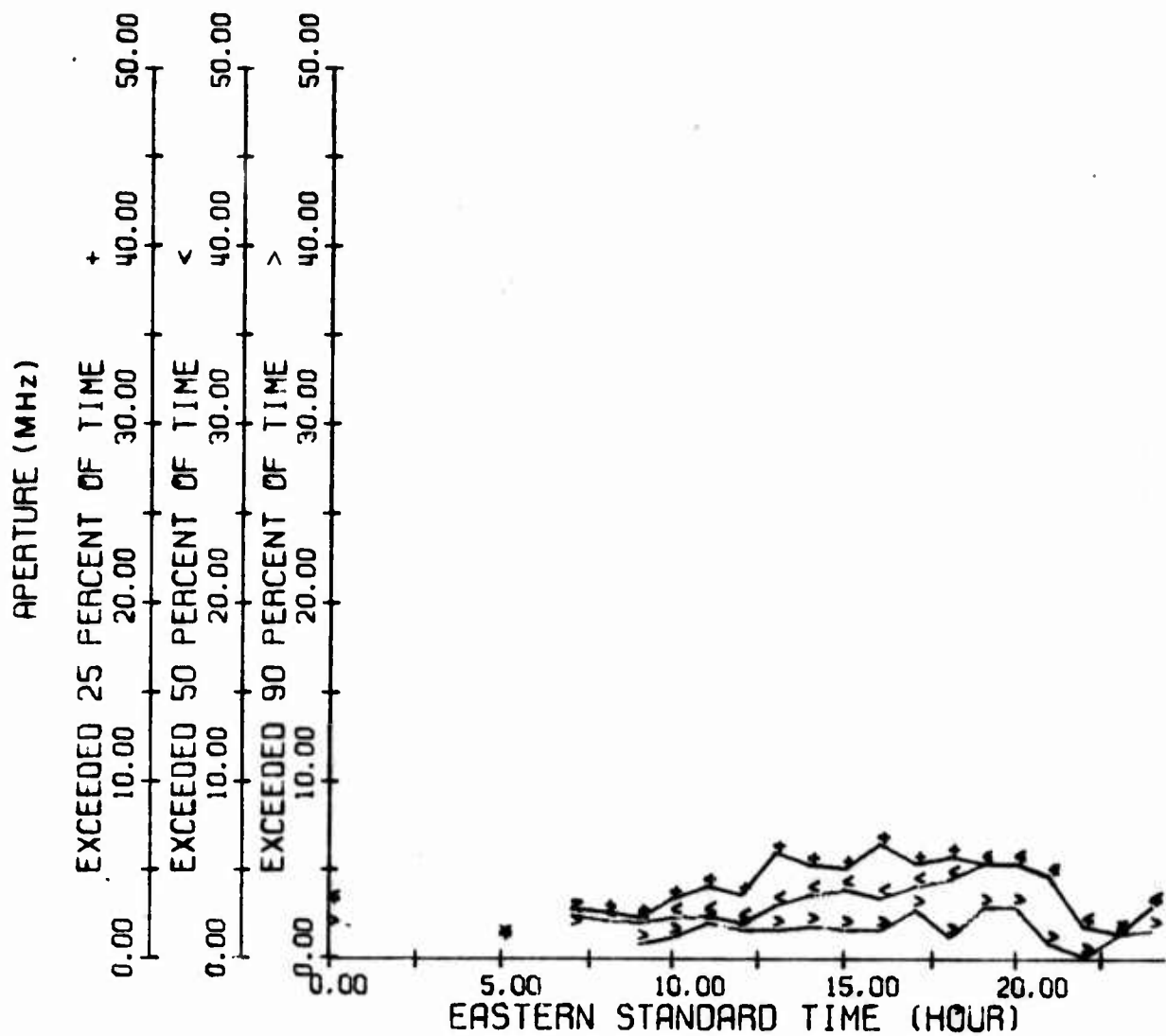


Figure 138. 2F2 Mode Frequency Aperture Availability, Thule Path, Spring 1967

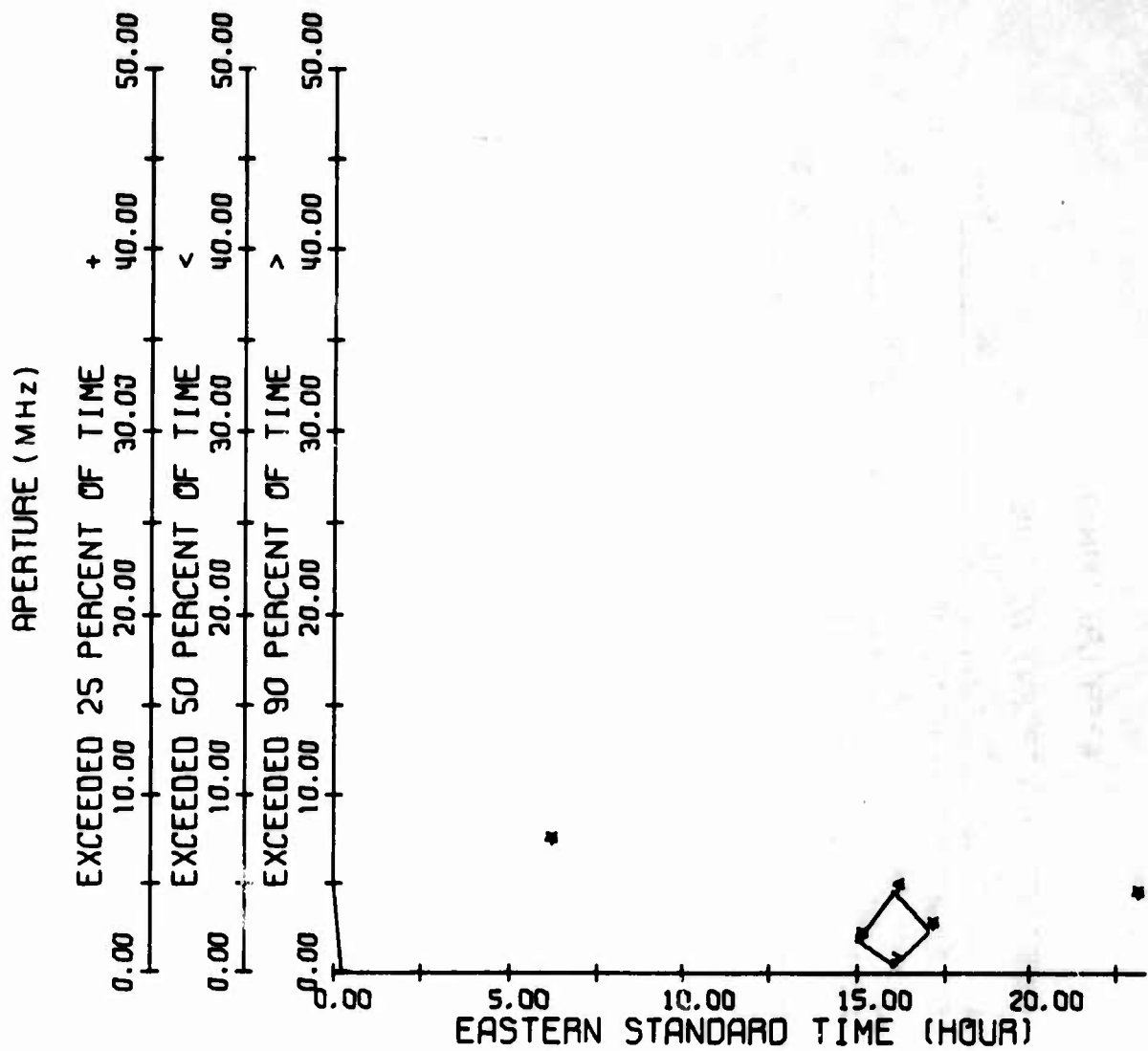


Figure 139. $2E_g$ Mode Frequency Aperture Availability, Thule Path, Winter 1967

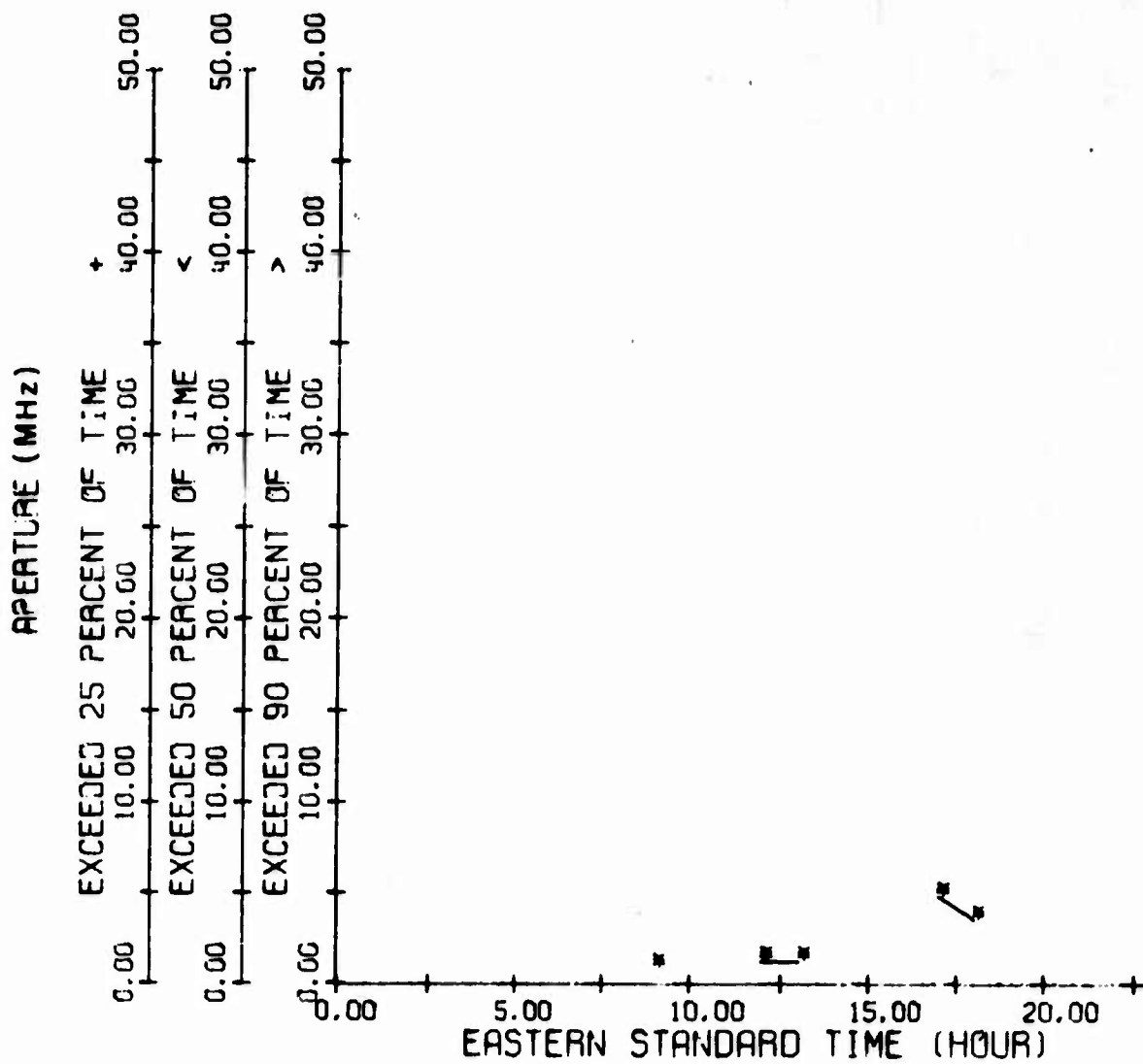


Figure 140. 2E_s Mode Frequency Aperture Availability, Thule Path, Spring 1967

7. MOF-JF AVAILABILITY -- COCO SOLO TO STOCKBRIDGE/STARR HILL

The seasonal MOF-JF availability results for the Coco Solo path which cover the period from winter 1966 to summer 1967 (seven seasons) are presented in this section. The 2E mode (Figures 141 - 147) MOF availability ranges from about 5 MHz at night to about 14 MHz in daytime for the 90 percent availability level in the winter of 1966, roughly the same for the spring of 1966, and picking up to about 17 MHz at about midday in the summer of 1966. In the autumn of 1966 the MOF has dropped back to 15 MHz maximum, which it holds for the winter of 1967; but in the spring of 1967 extends to about 15 MHz throughout the day, rather than reaching this as a peak value.

The 1F2 mode (Figures 148 - 154) JF availability ranges from a low of about 10 MHz at sunrise and sunset in the winter of 1966 to slightly higher at other times of the night, and to a peak in the daytime of about 25 MHz for 90 percent availability. There is some drop in the spring of 1966 at various times and a tendency for the highest values to occur late in the day. This is noted more strongly in the results for the summer of 1966, where the values range from an absolute minimum of about 10 MHz to a maximum of about 23 MHz. In the autumn of 1966 the minimum value is still 10 MHz during the night but the maximum value for 90 percent JF availability was about 28 MHz. In the winter of 1967 night values run about 11 and 12 MHz. In daytime there is a long stretch of (about) 30 MHz values. There is a drop in the 90 percent JF availability at the peak values in the spring of 1967 with somewhat erratic maximums showing up slightly less than 30 MHz; however, at this point the maximum for the 25 percent JF availability is almost 40 MHz.

The N mode MOF availability (Figures 155 - 161) is consistently good throughout in an erratic sort of fashion, but is quite a bit lower than the 1F2 mode JF availability.

The 2F2 mode JF availability (Figures 162 - 168) is consistently lower than that for the 1F2 mode as would be expected; however, there are some trends with 2F2 results that are worth noting. In the winter of 1966 and in the winter of 1967 the JF availabilities for this mode for all three percentages of JF availability are quite uniform and quite close together, with the highest frequency availability occurring during the early daylight hours. Also for winter 1967 the frequency availability in general is about 5 MHz higher during the daytime compared to the results for winter 1966. Higher daylight frequencies are noted for spring in both 1966 and 1967

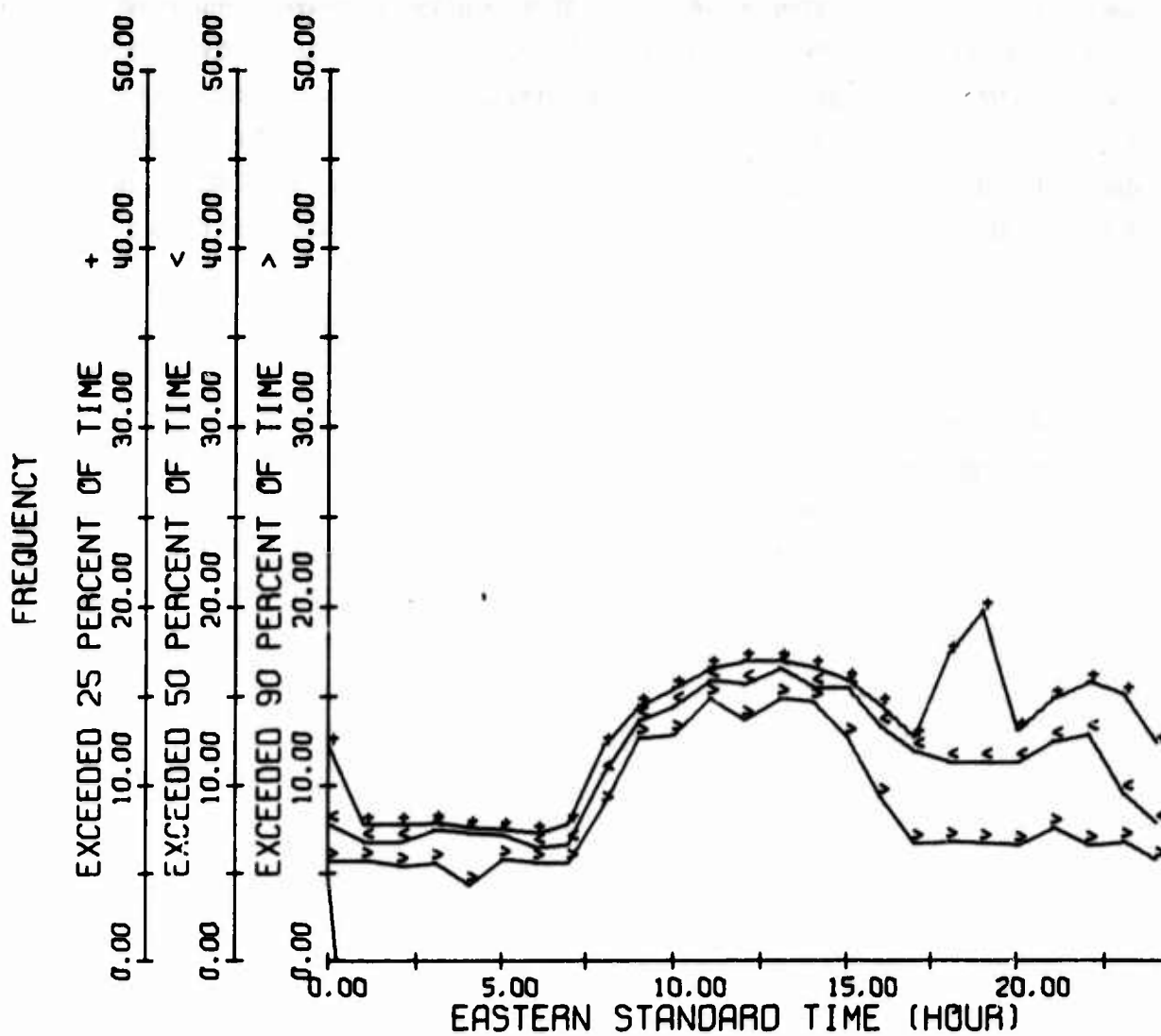


Figure 141. 2E Mode MOF Availability, Cocc Solo Path, Winter 1966

in the afternoon rather than in the morning (as during the winter), and a considerable amount of uniformity has been lost. In the summer of 1966 the whole picture "leans" toward a later part of the day insofar as when the highest frequency occurs; also, the spread between the maximum and minimum values for the JF availability is the least for this season. In the autumn this still holds, but the trend is slipping back in the direction of wintertime.

The $2E_s$ mode (Figures 169 - 173) was not recorded separately from the 2E mode until the summer of 1966. With the exception of the spring of 1967, when there are a considerable number of hours missed entirely, the frequency availabilities of the $2E_s$ mode would be very misleading; in fact, they look about as good as those for the N mode. Only by reference to the data base is it possible to recognize the lack of usefulness of the $2E_s$ mode.

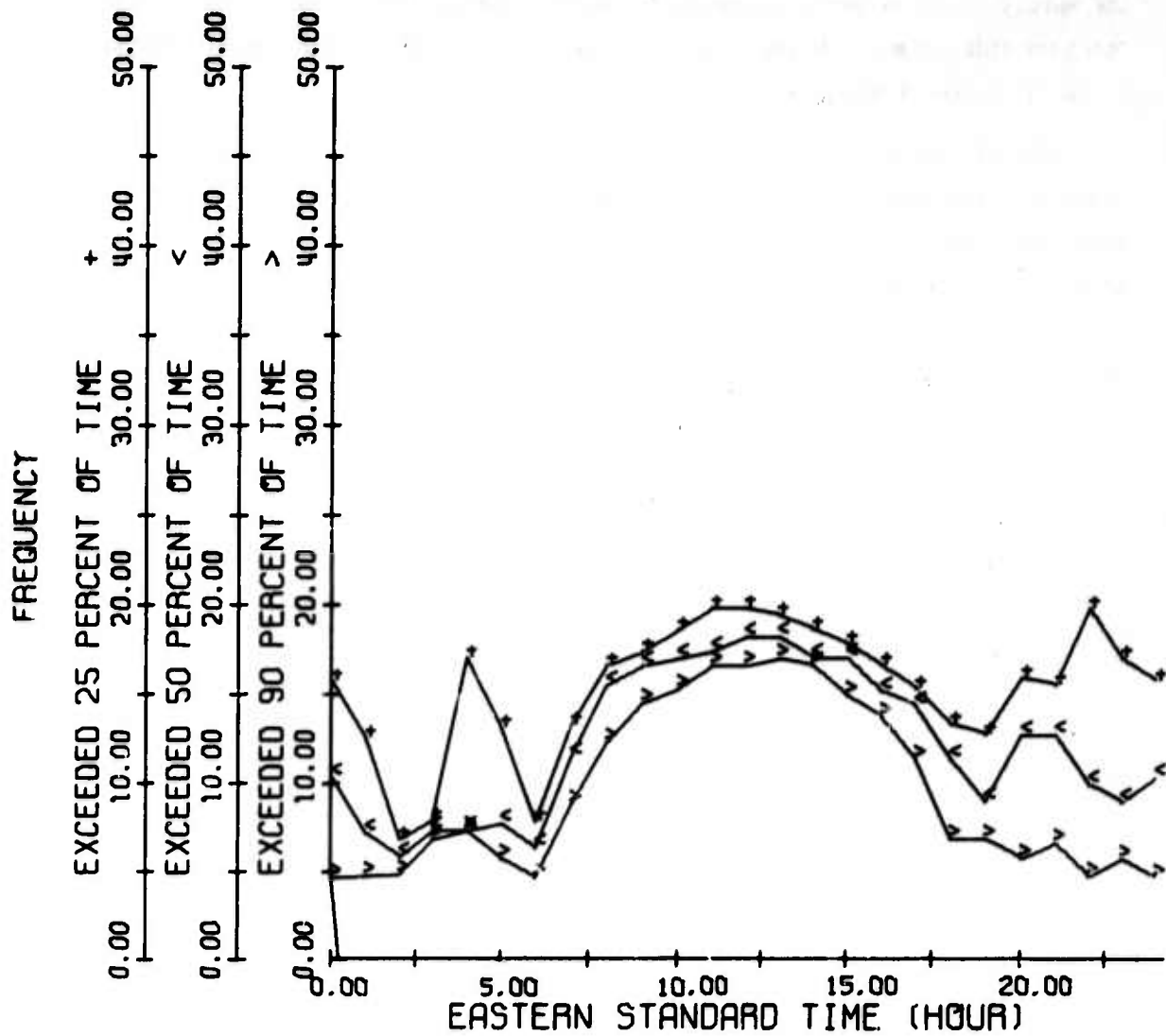


Figure 142. 2E Mode MOF Availability, Coco Solo Path, Spring 1966

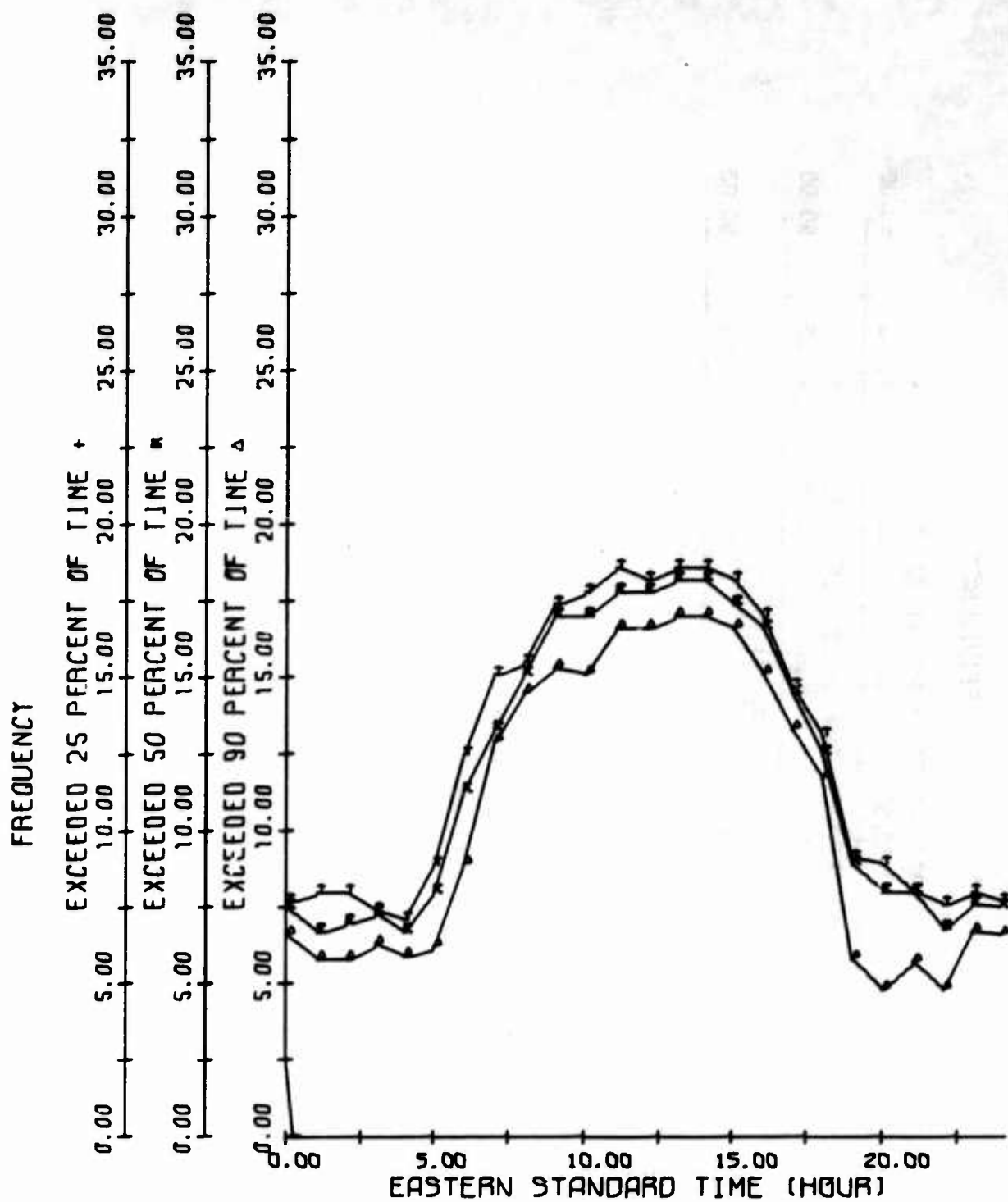


Figure 143. 2E Mode MOF Availability, Coco Solo Path, Summer 1966

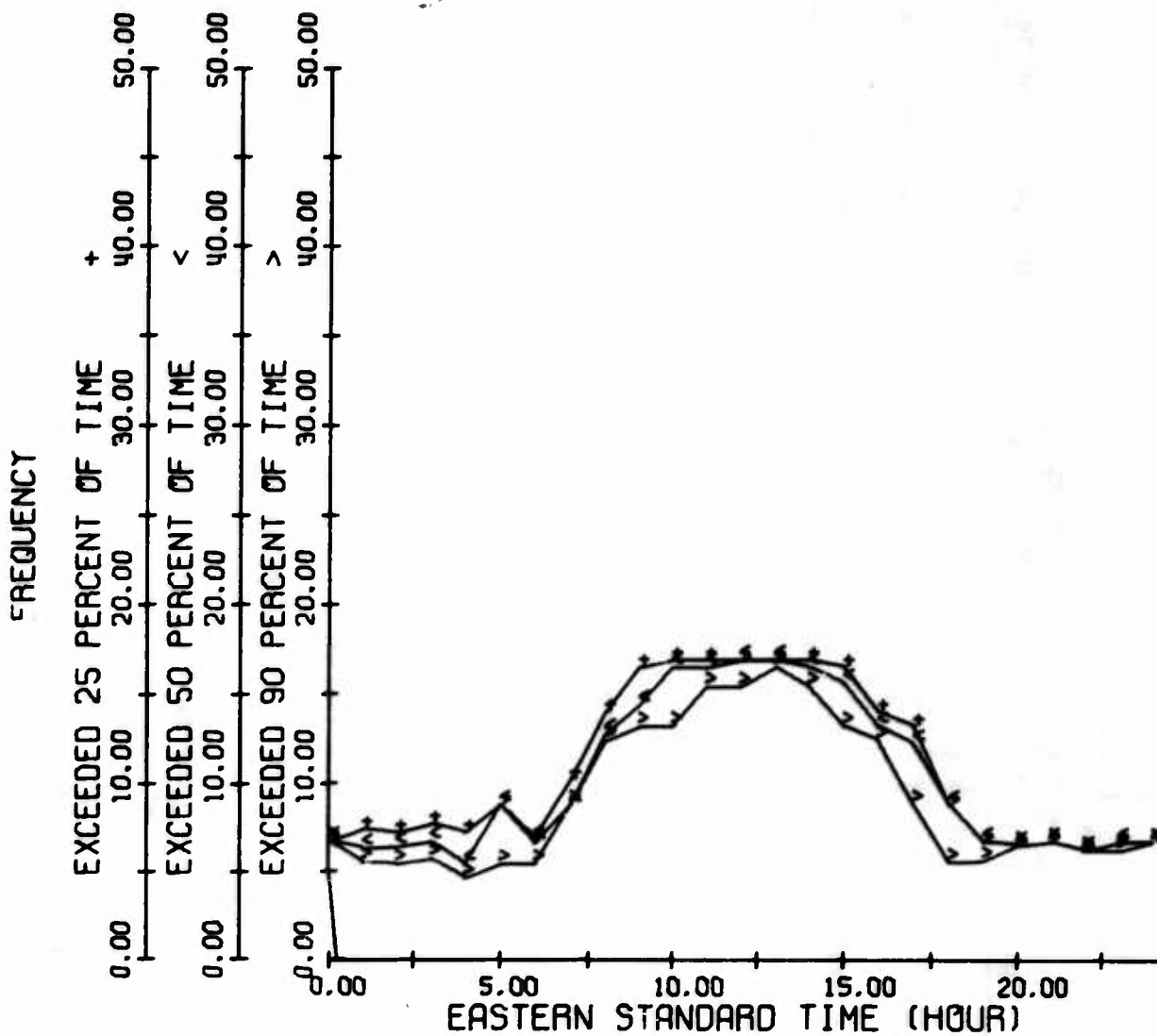


Figure 144. 2E Mode MOF Availability, Coco Solo Path, Autumn 1966

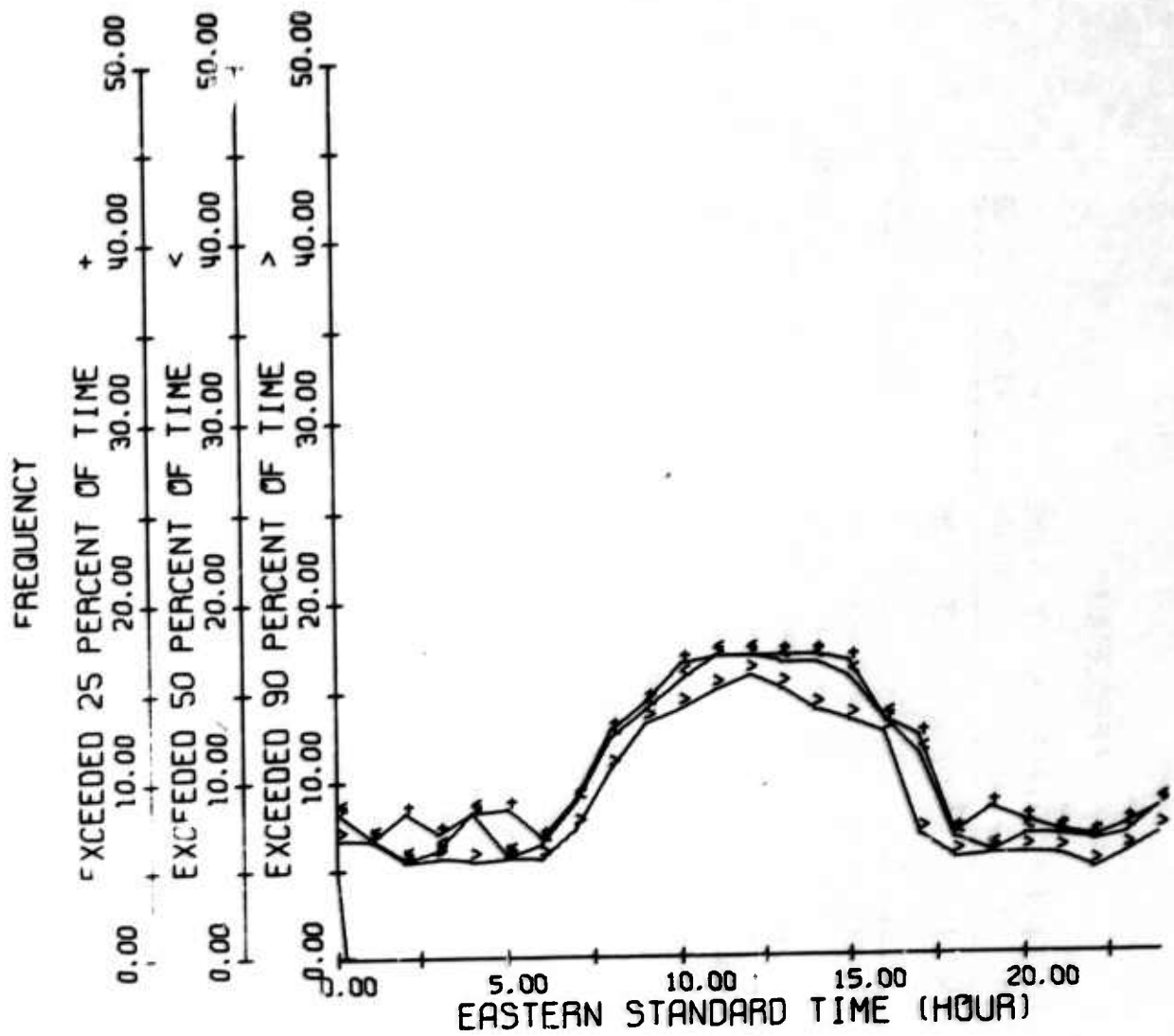


Figure 145. 2E Mode MOF Availability, Coco Solo Path, Winter 1967

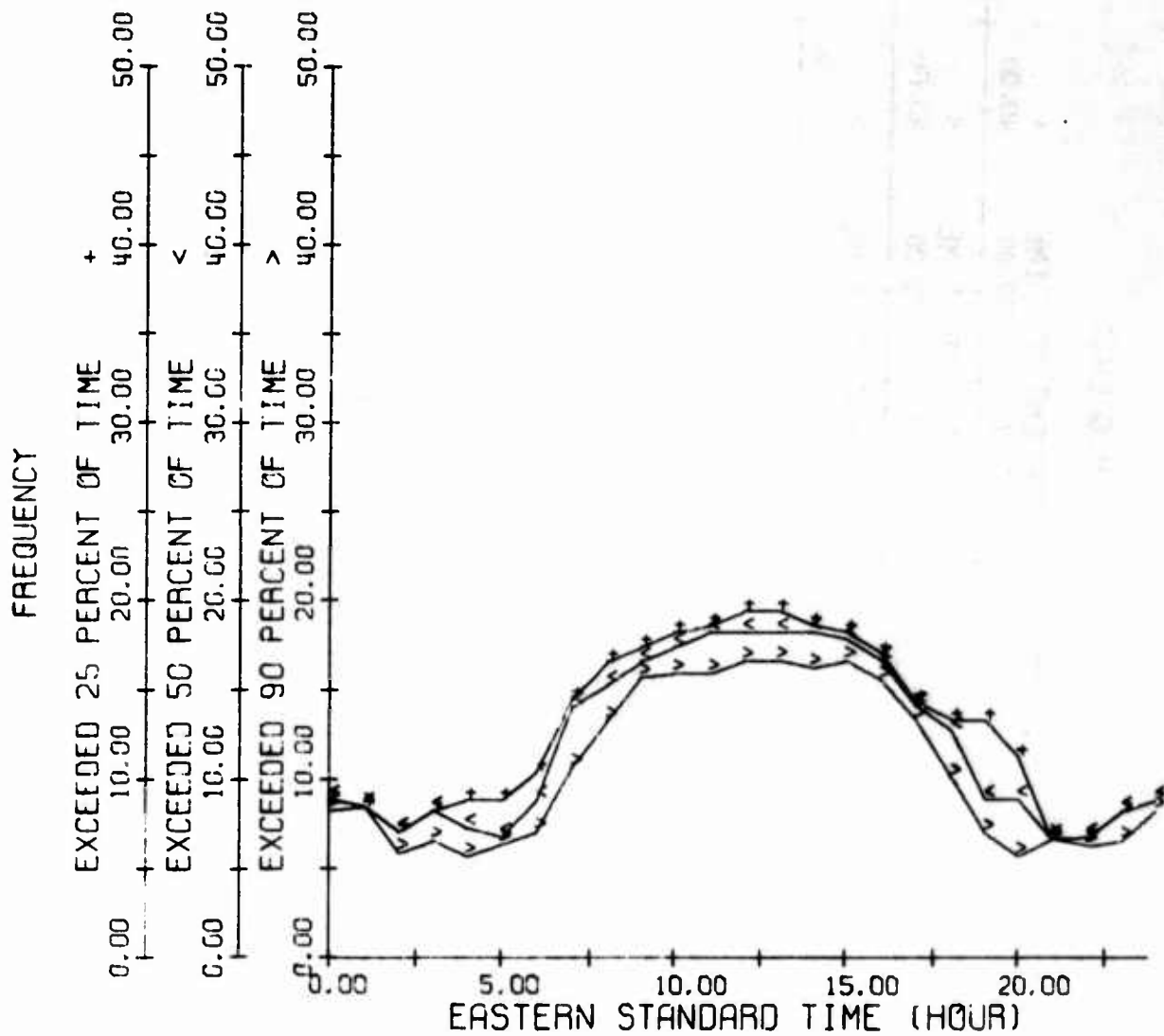


Figure 146. 2E Mode MOF Availability, Coco Solo Path, Spring 1967

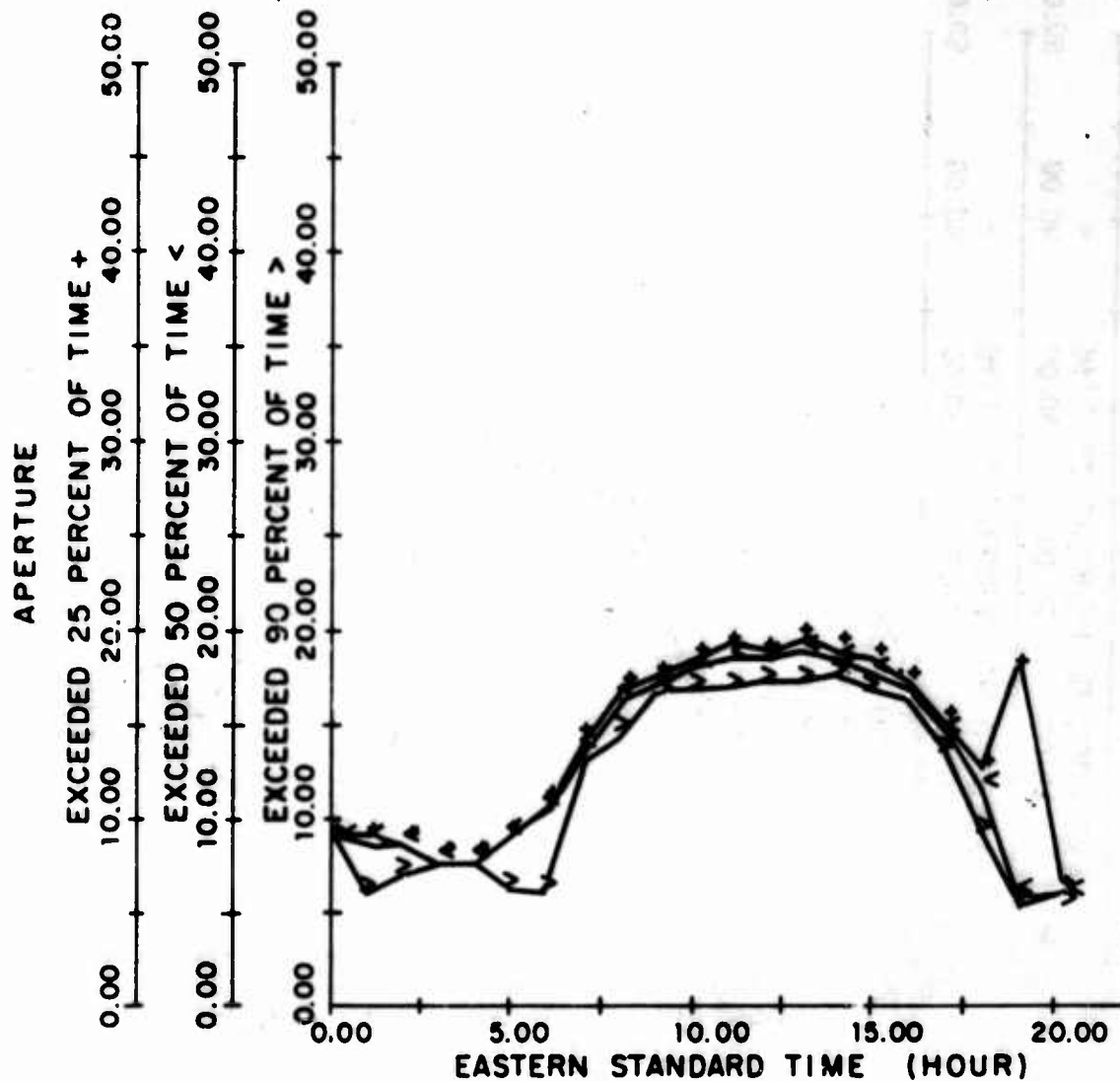


Figure 147. 2E Mode MOF Availability, Coco Solo Path, Summer 1967

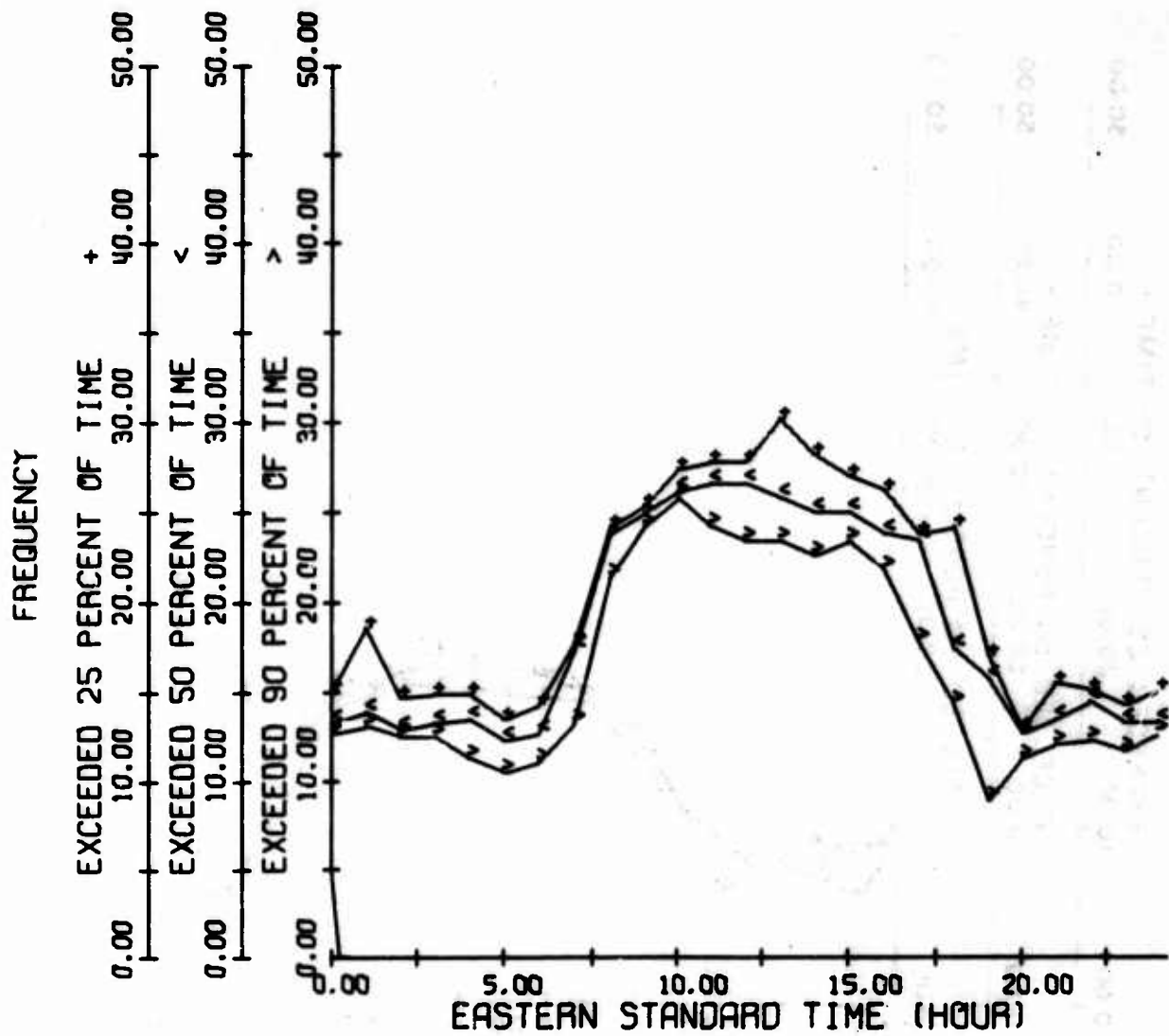


Figure 148. 1F2 Mode JF Availability, Coco Solo Path, Winter 1966

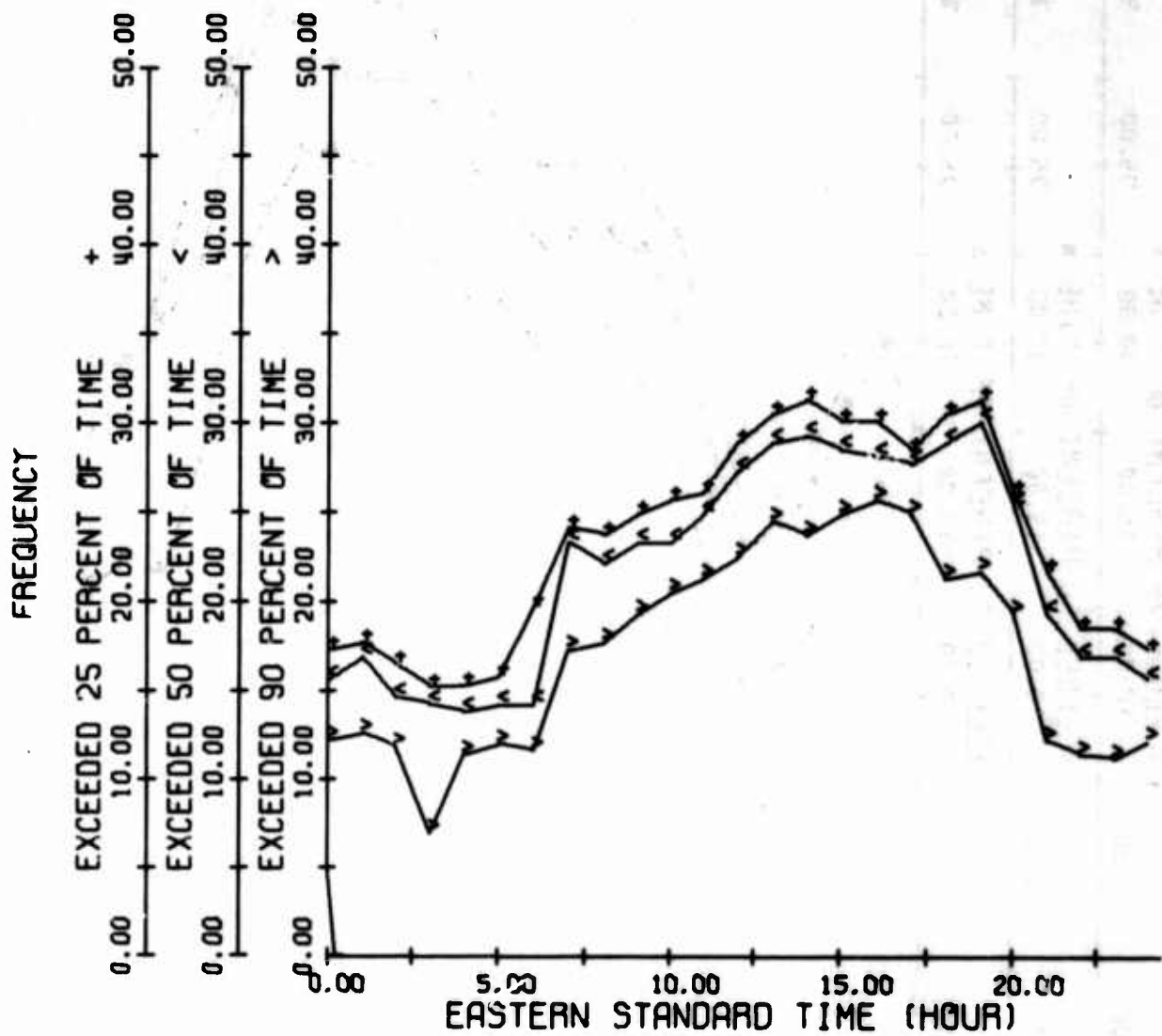


Figure 149. 1F2 Mode JF Availability, Coco Solo Path, Spring 1966

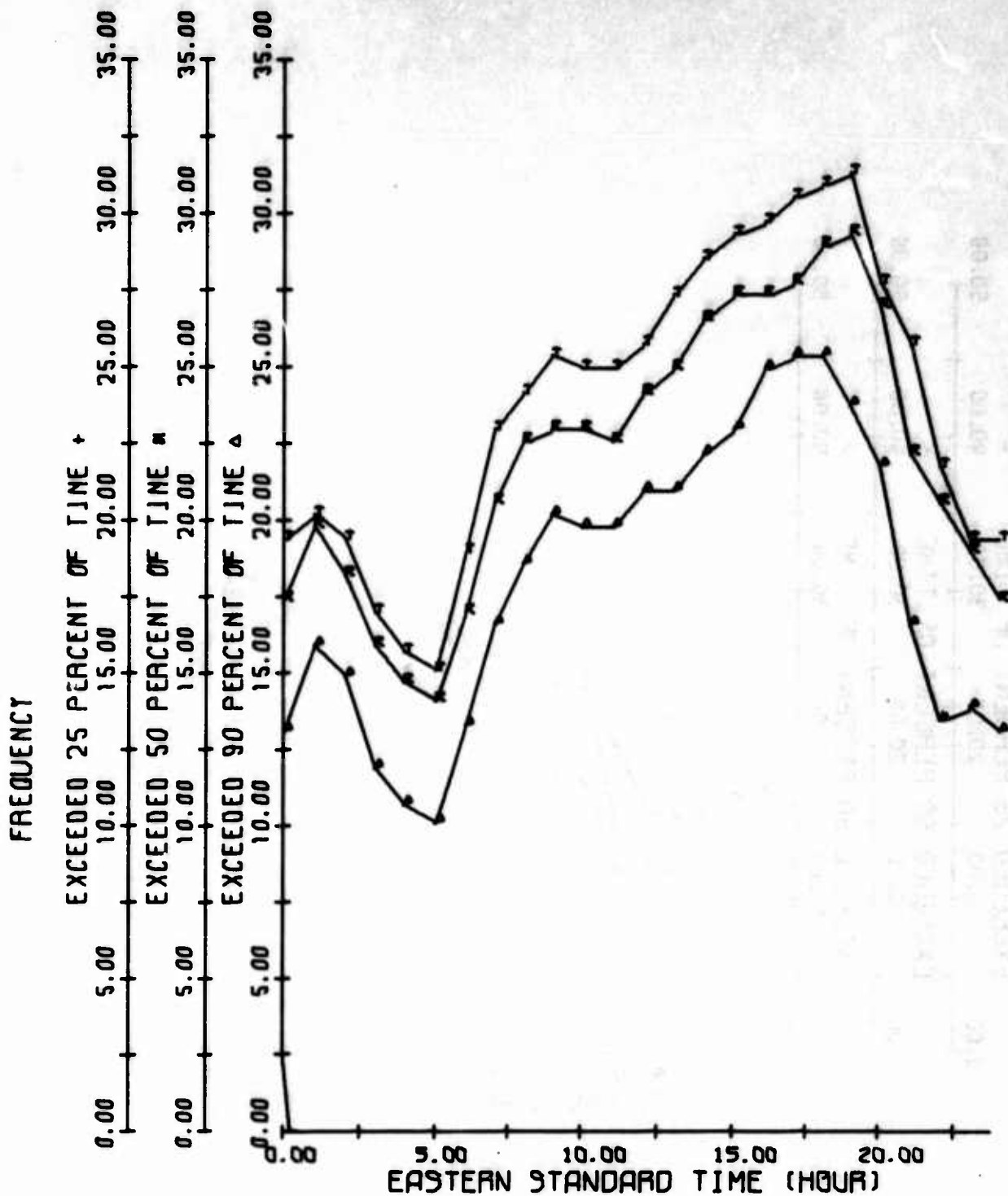


Figure 150. 1F2 Mode JF Availability, Coco Solo Path, Summer 1966

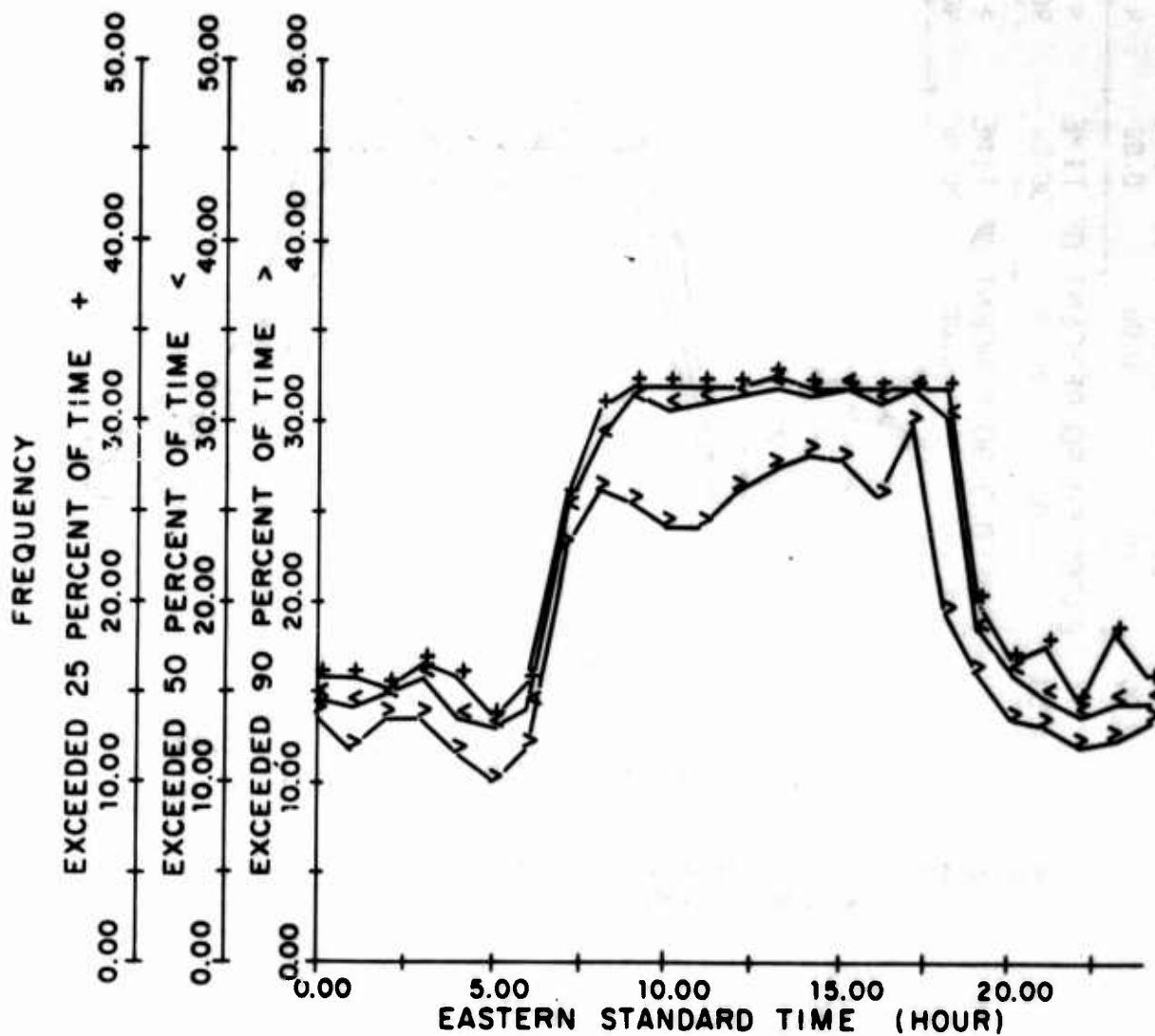


Figure 151. 1F2 Mode JF Availability, Coco Solo Path, Autumn 1966

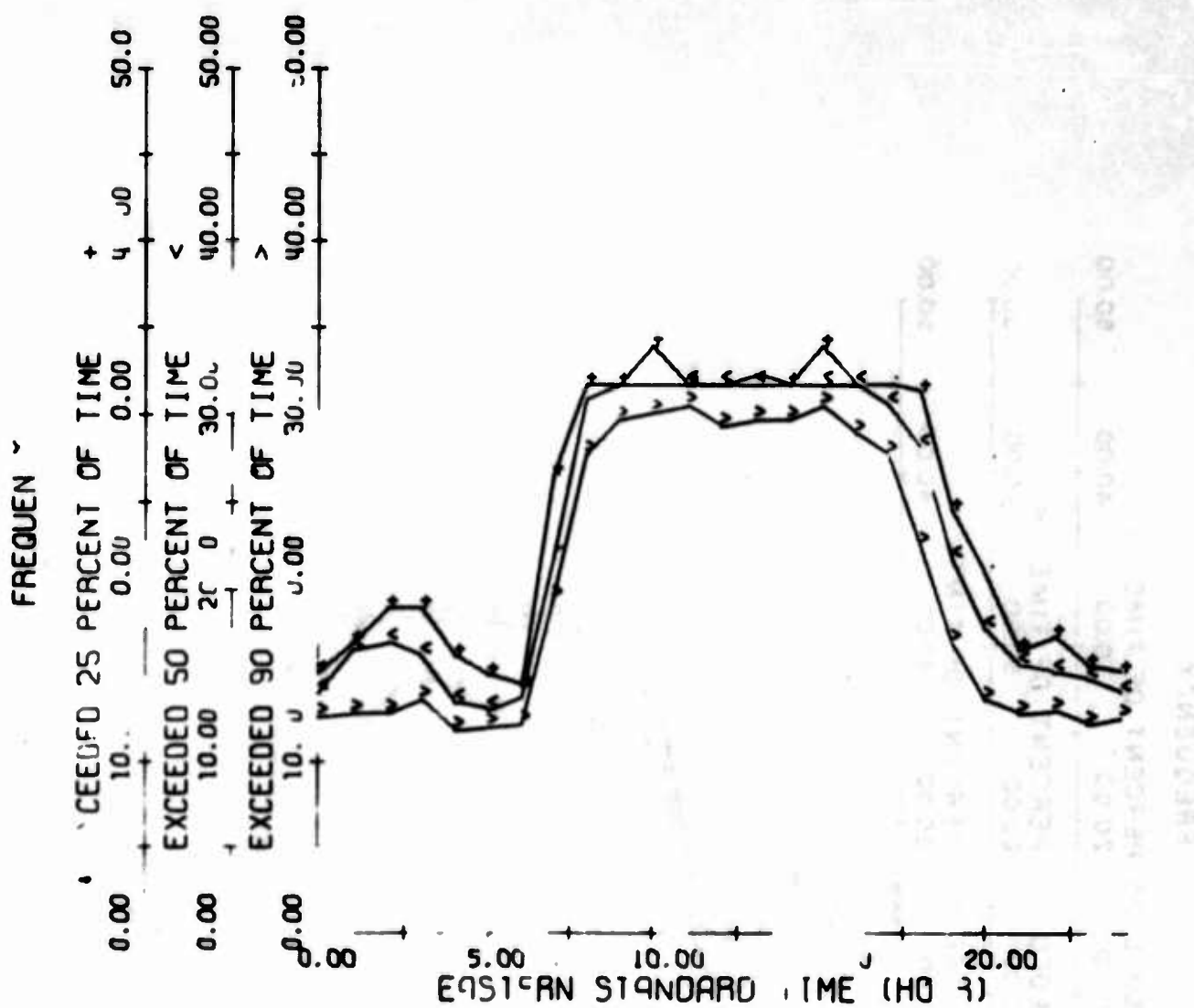


Figure 152. 1F2 Mode JF Availability, Coco Solo Path, Winter 1967

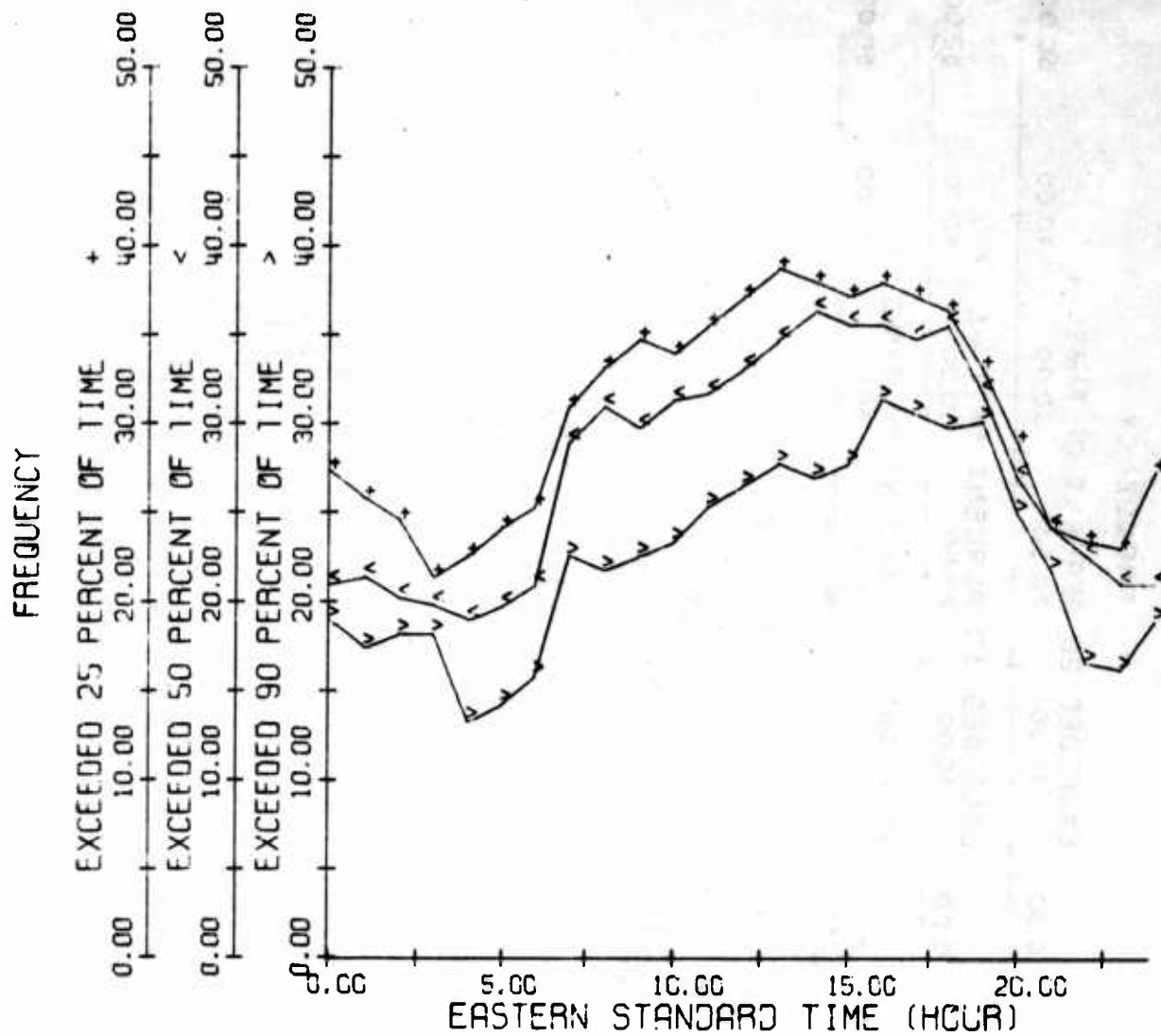


Figure 153. 1F2 Mode JF Availability, Coco Solo Path, Spring 1967

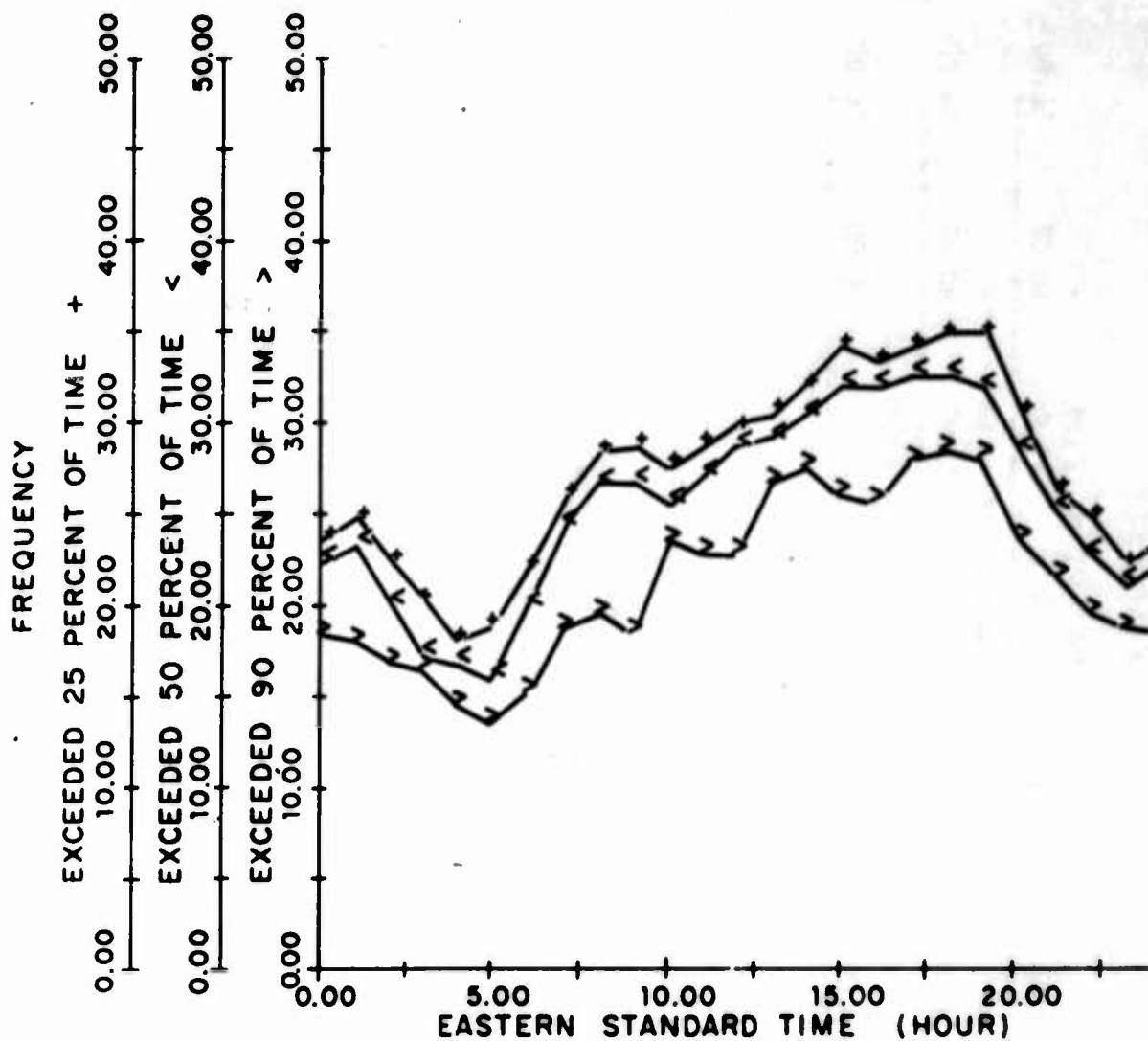


Figure 154. 1F2 Mode JF Availability, Coco Solo Path, Summer 1967

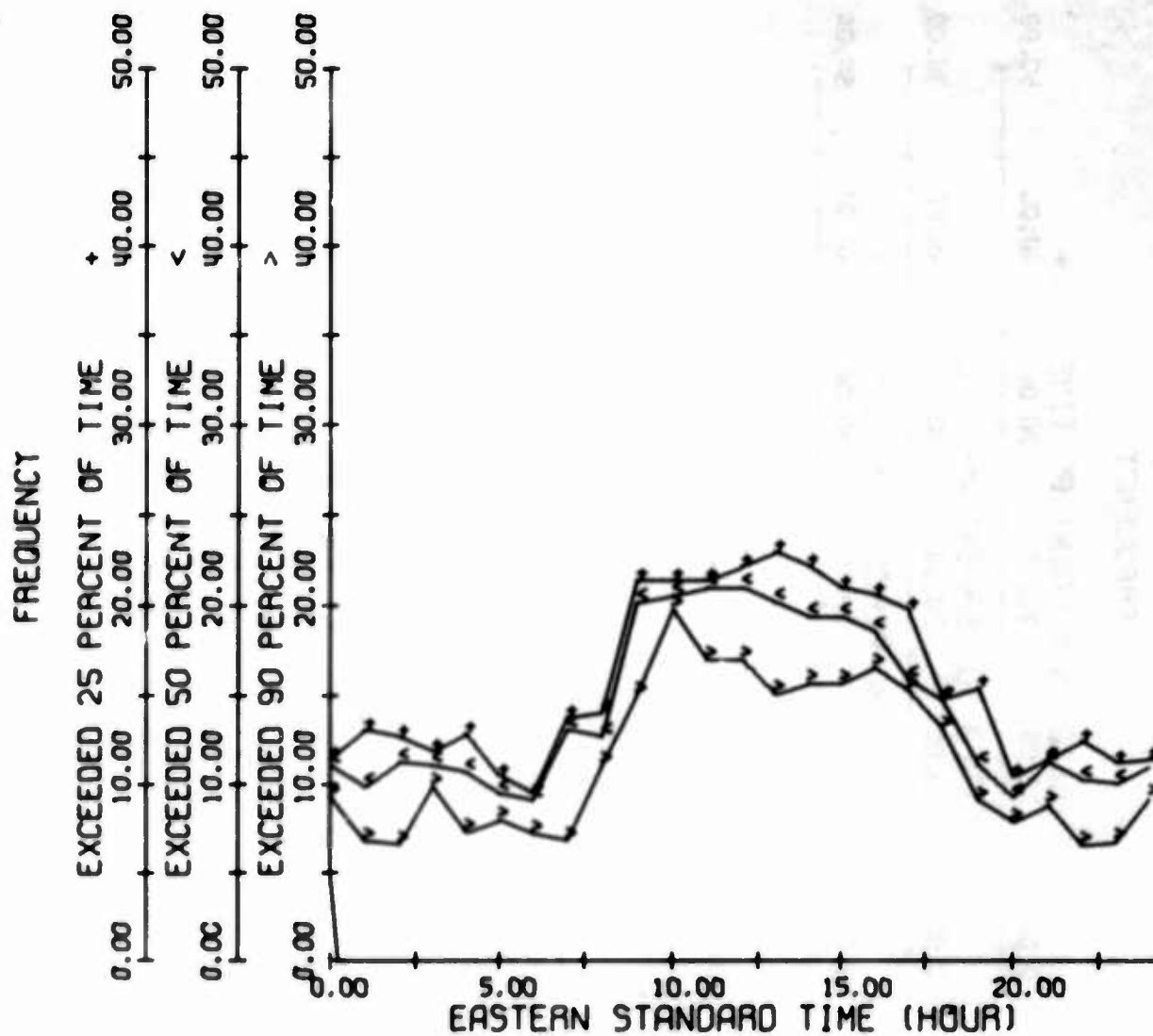


Figure 155. N Mode MOF Availability, Coco Solo Path, Winter 1966

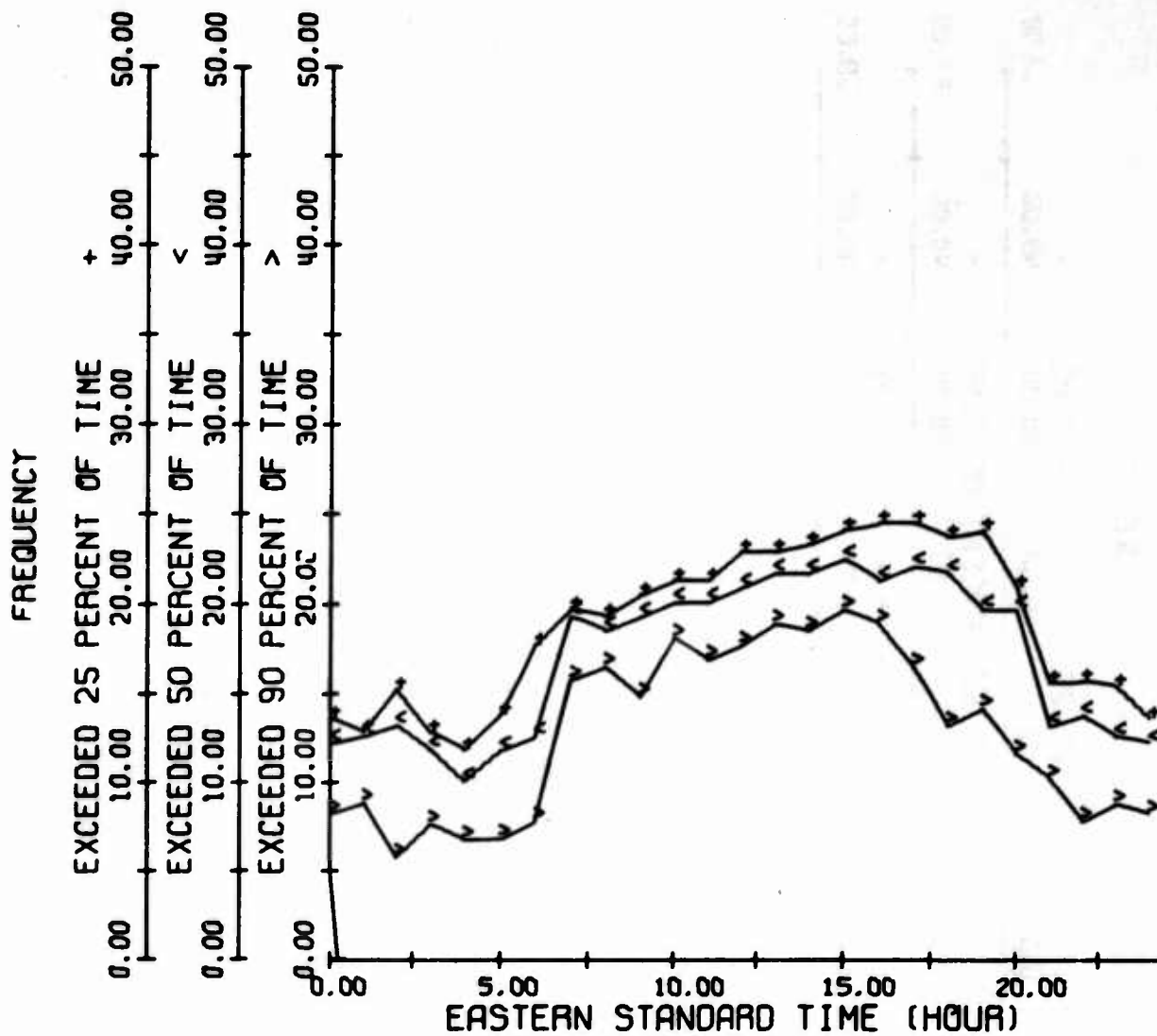


Figure 156. N Mode MOF Availability, Coco Solo Path, Spring 1966

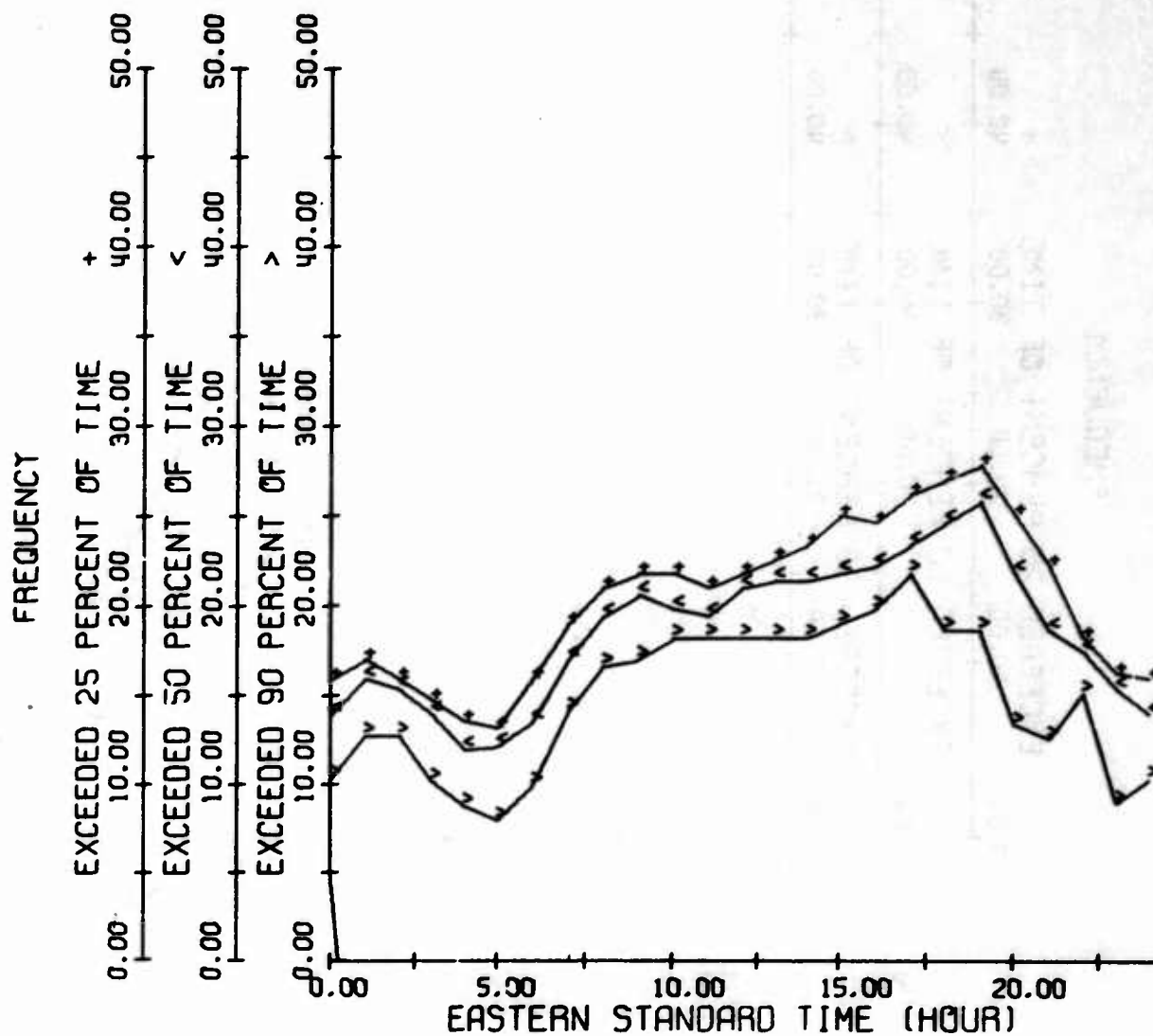


Figure 157. N Mode MOF Availability, Coco Solo Path, Summer 1966

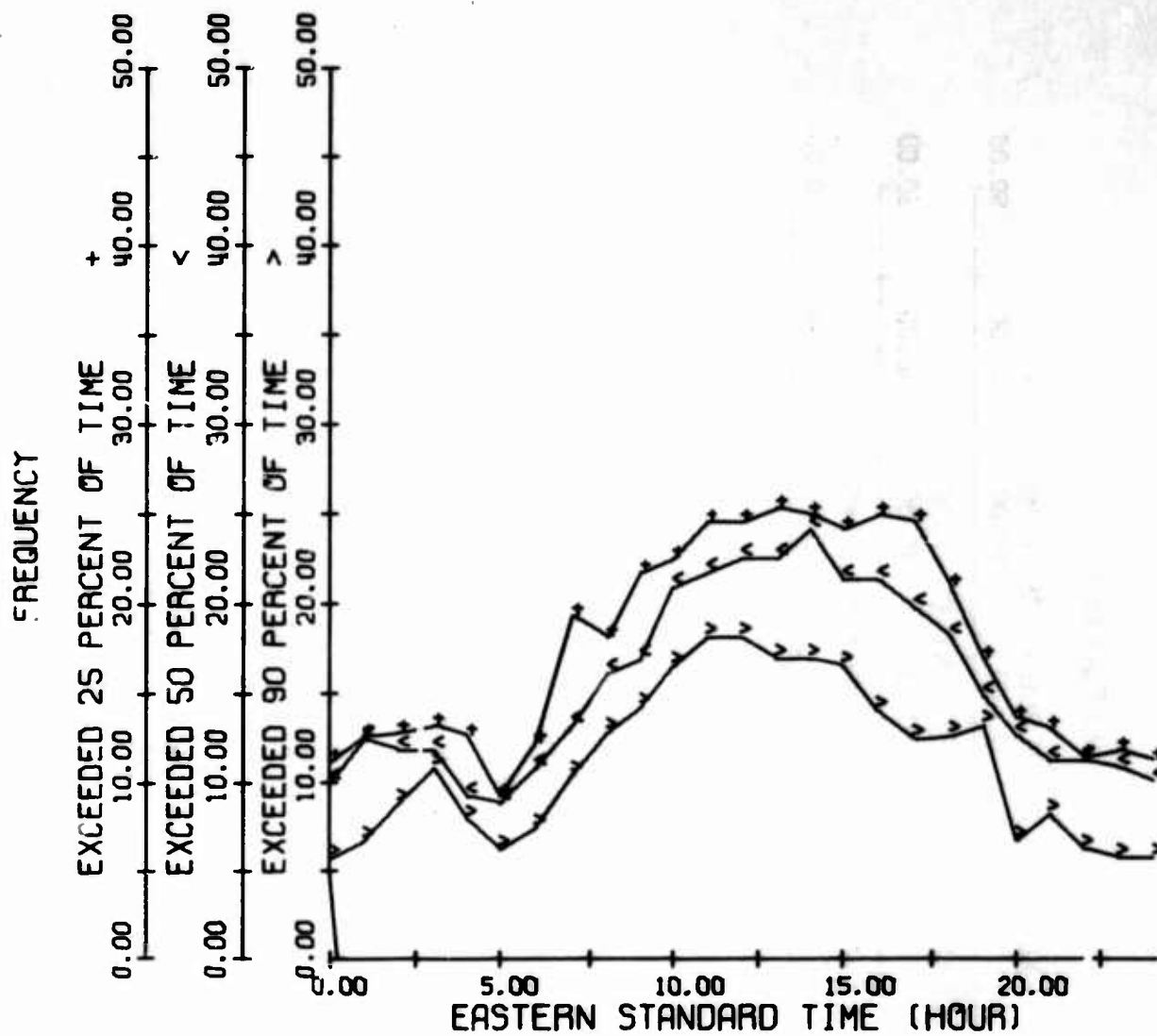


Figure 158. N Mode MOF Availability, Coco Solo Path, Autumn 1966

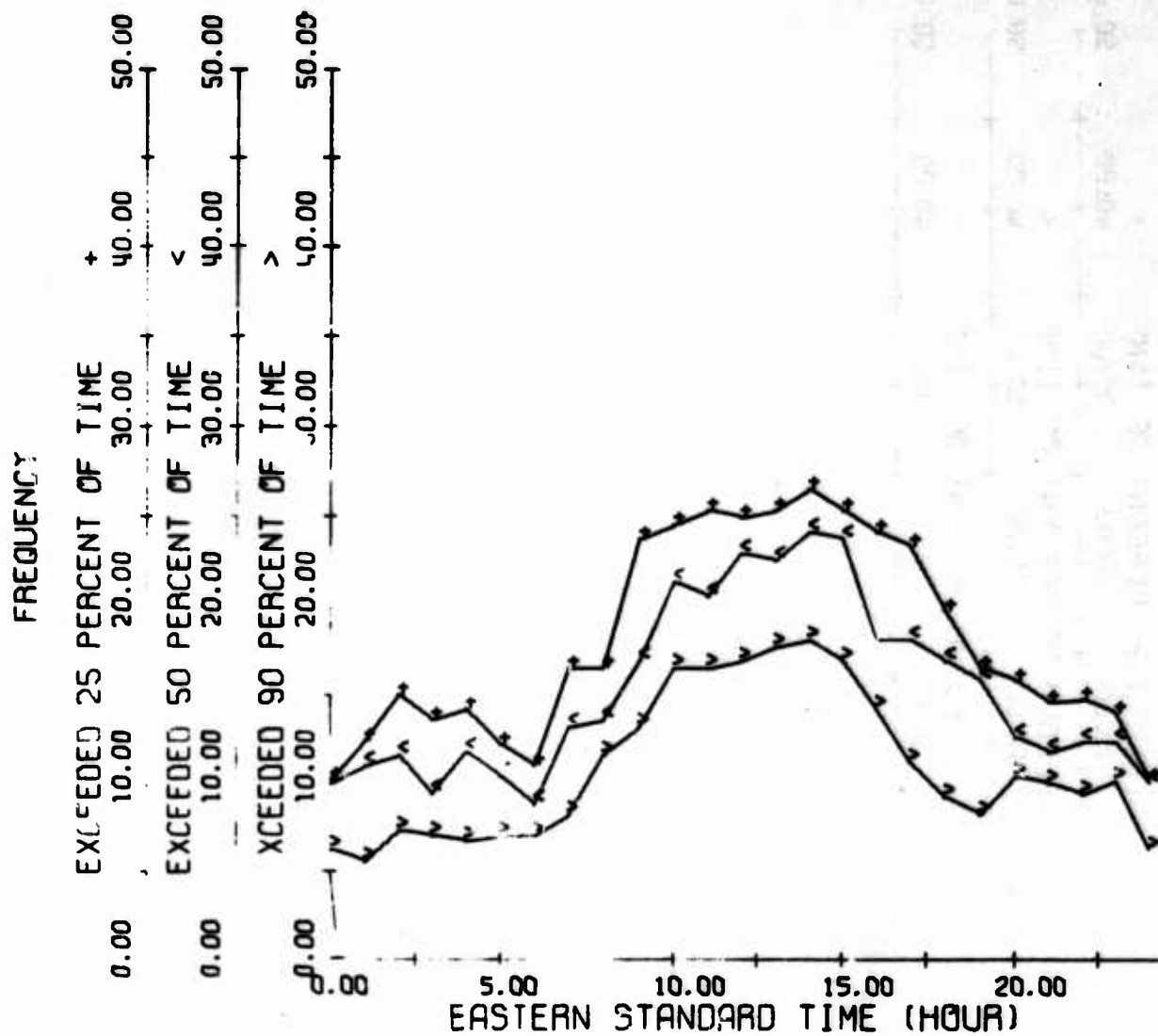


Figure 159. N Mode MOF Availability, Coco Solo Path, Winter 1967

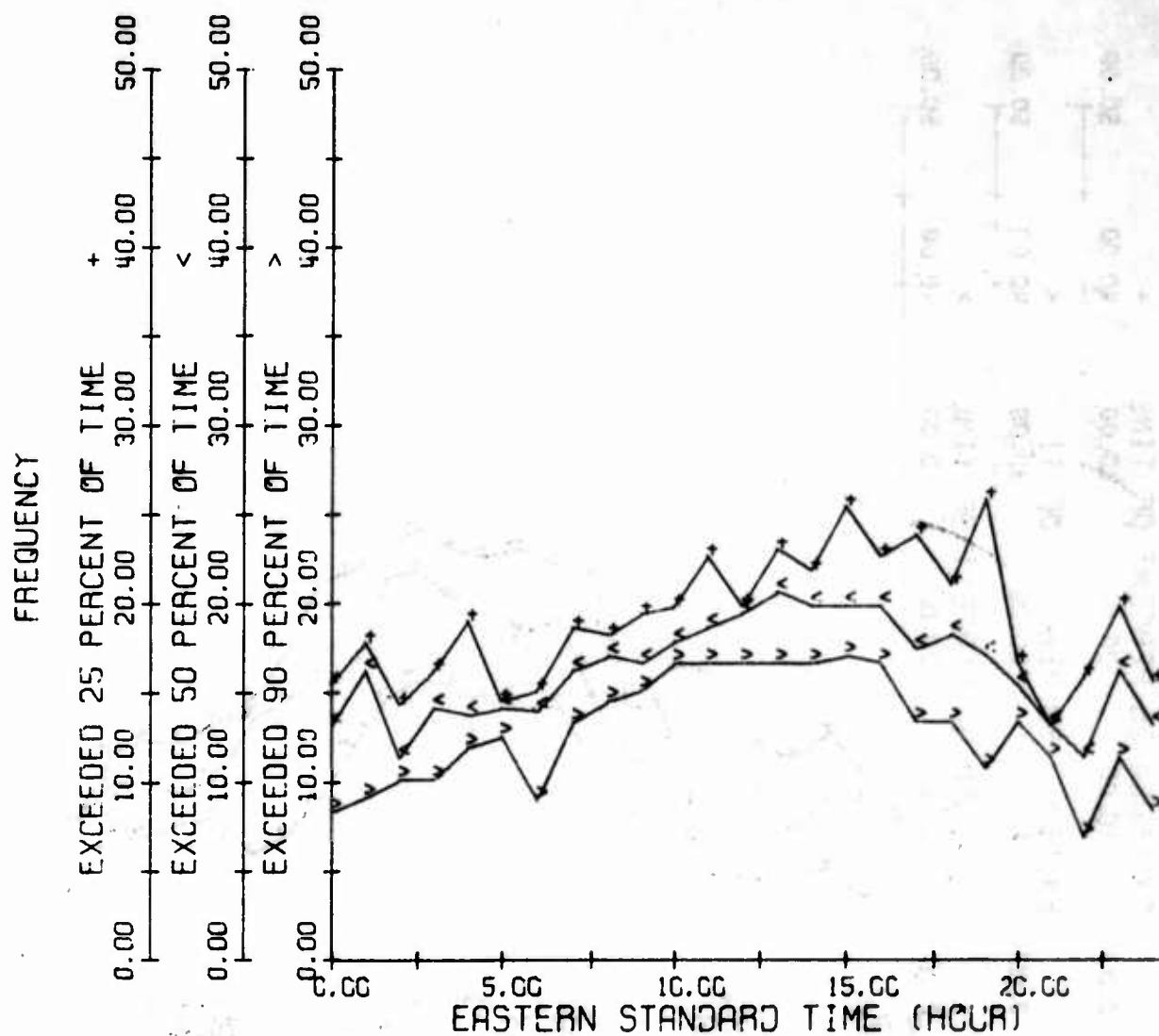


Figure 160. N Mode MOF Availability, Coco Solo Path, Spring 1967

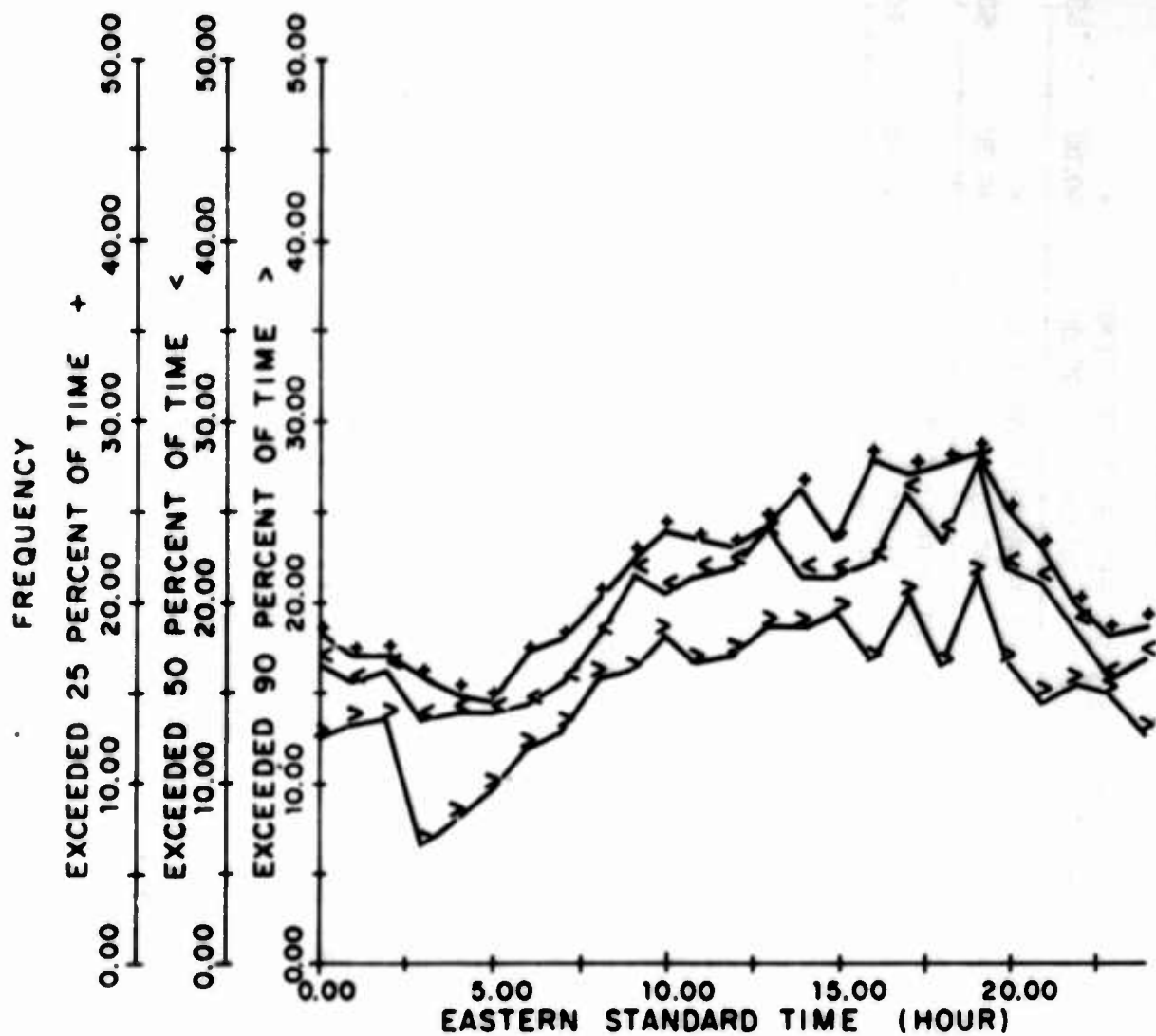


Figure 161. N Mode MOF Availability, Coco Solo Path, Summer 1967

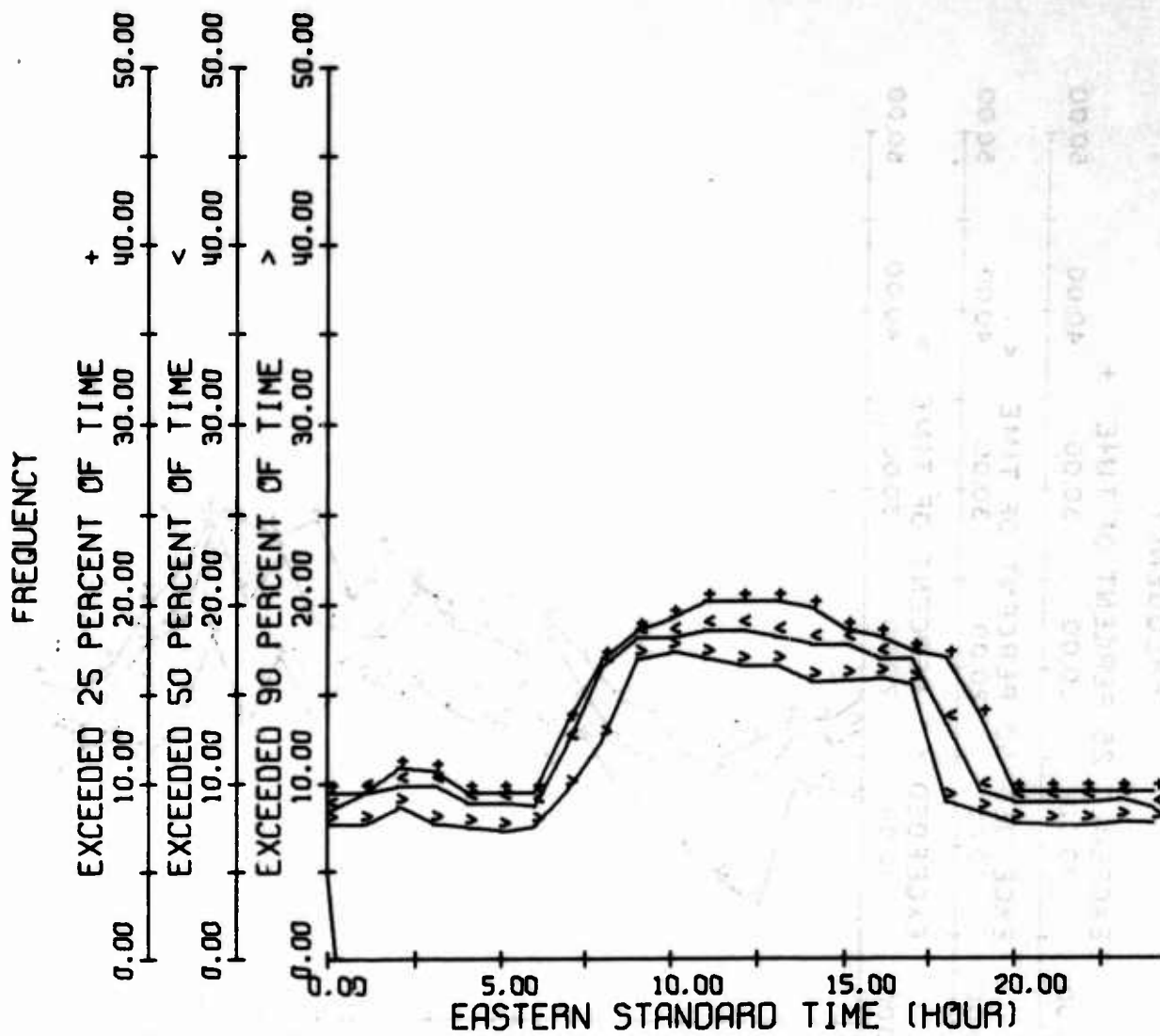


Figure 162. 2F2 Mode JF Availability, Coco Solo Path, Winter 1966

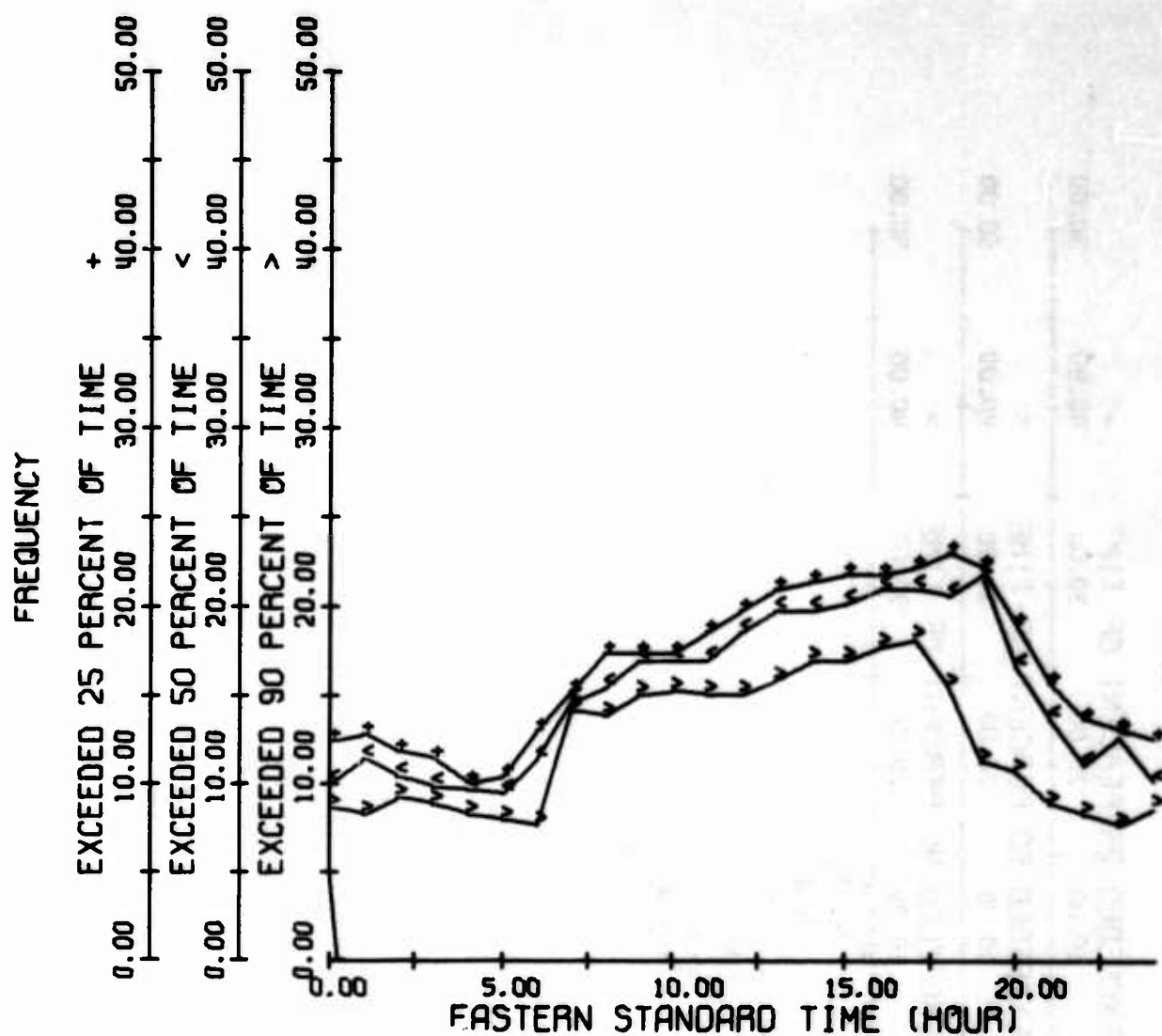


Figure 163. 2F2 Mode JF Availability, Coco Solo Path, Spring 1966

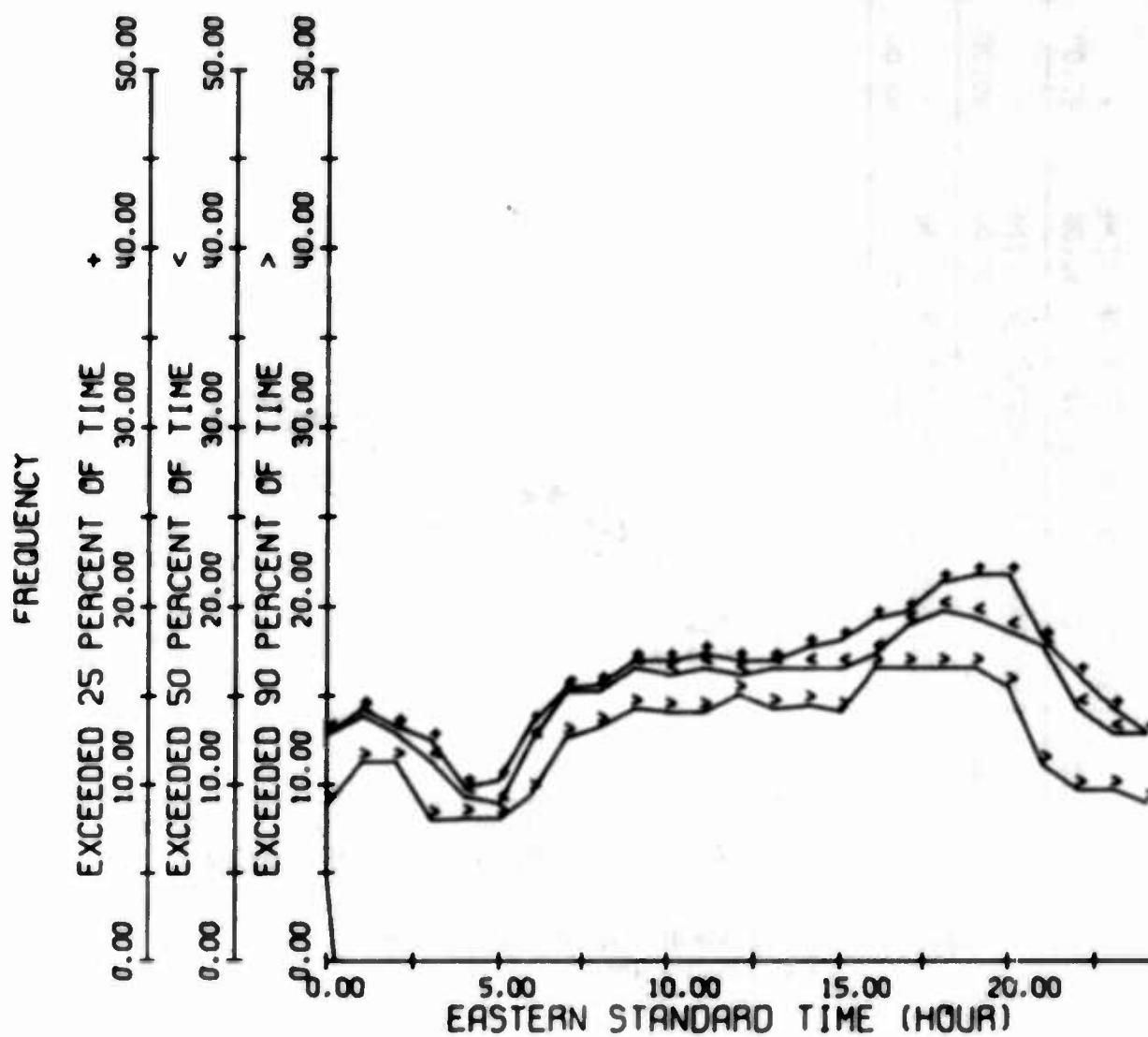


Figure 164. 2F2 Mode JF Availability, Coco Solo Path, Summer 1966

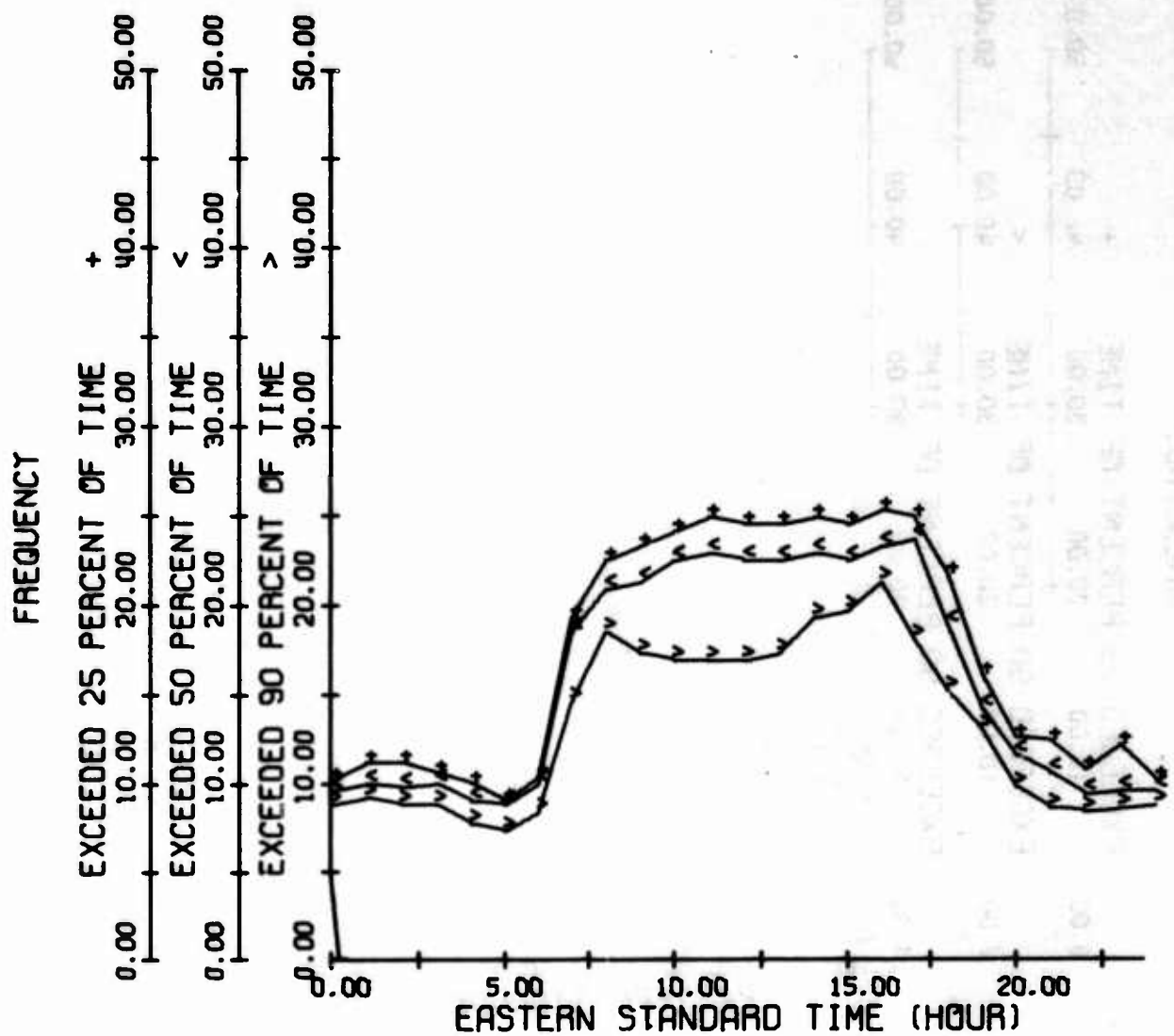


Figure 165. 2F2 Mode JF Availability, Coco Solo Path, Autumn 1966

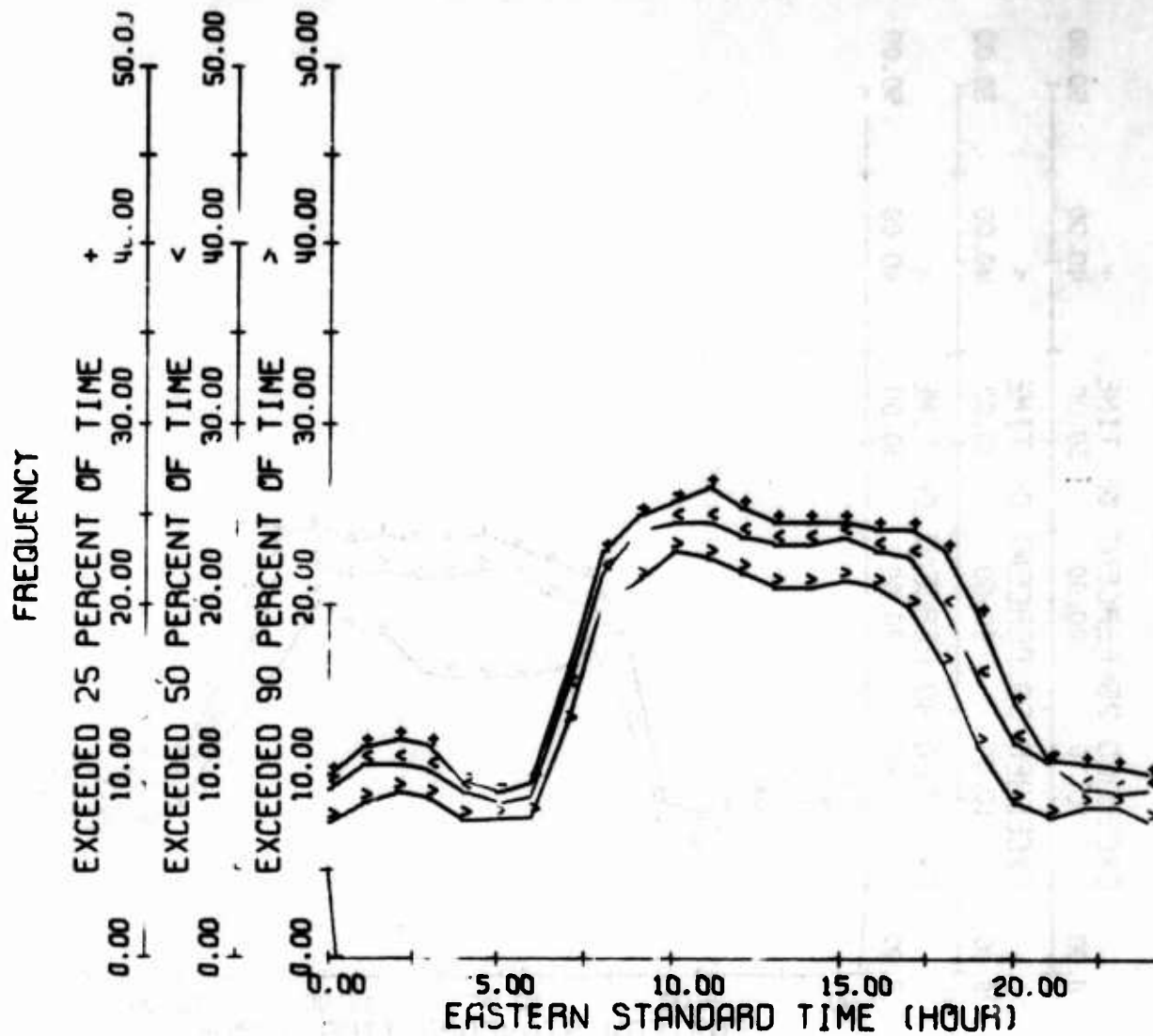


Figure 166. 2F2 Mode JF Availability, Coco Solo Path, Winter 1967

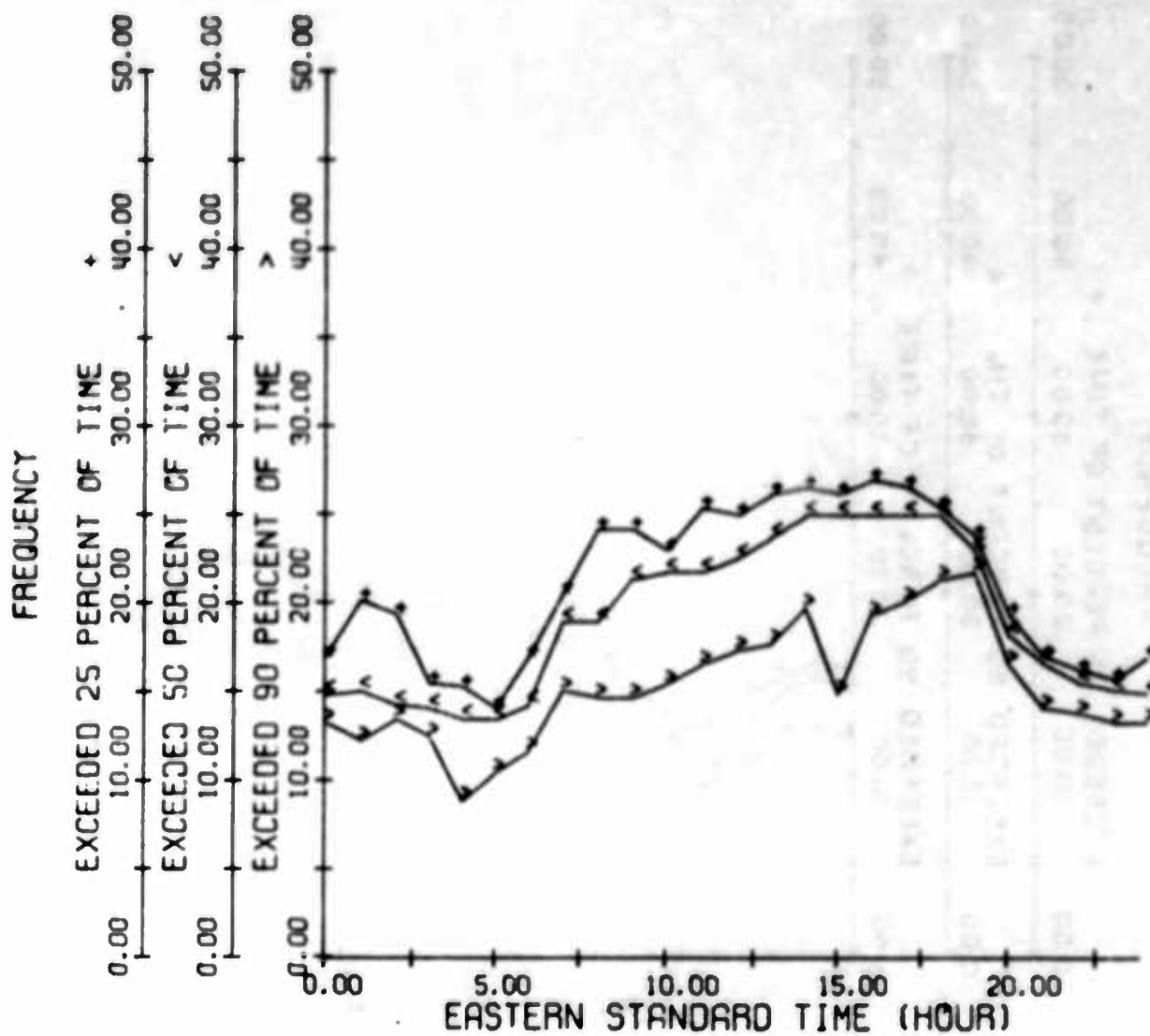


Figure 167. 2F2 Mode JF Availability, Coco Solo Path, Spring 1967

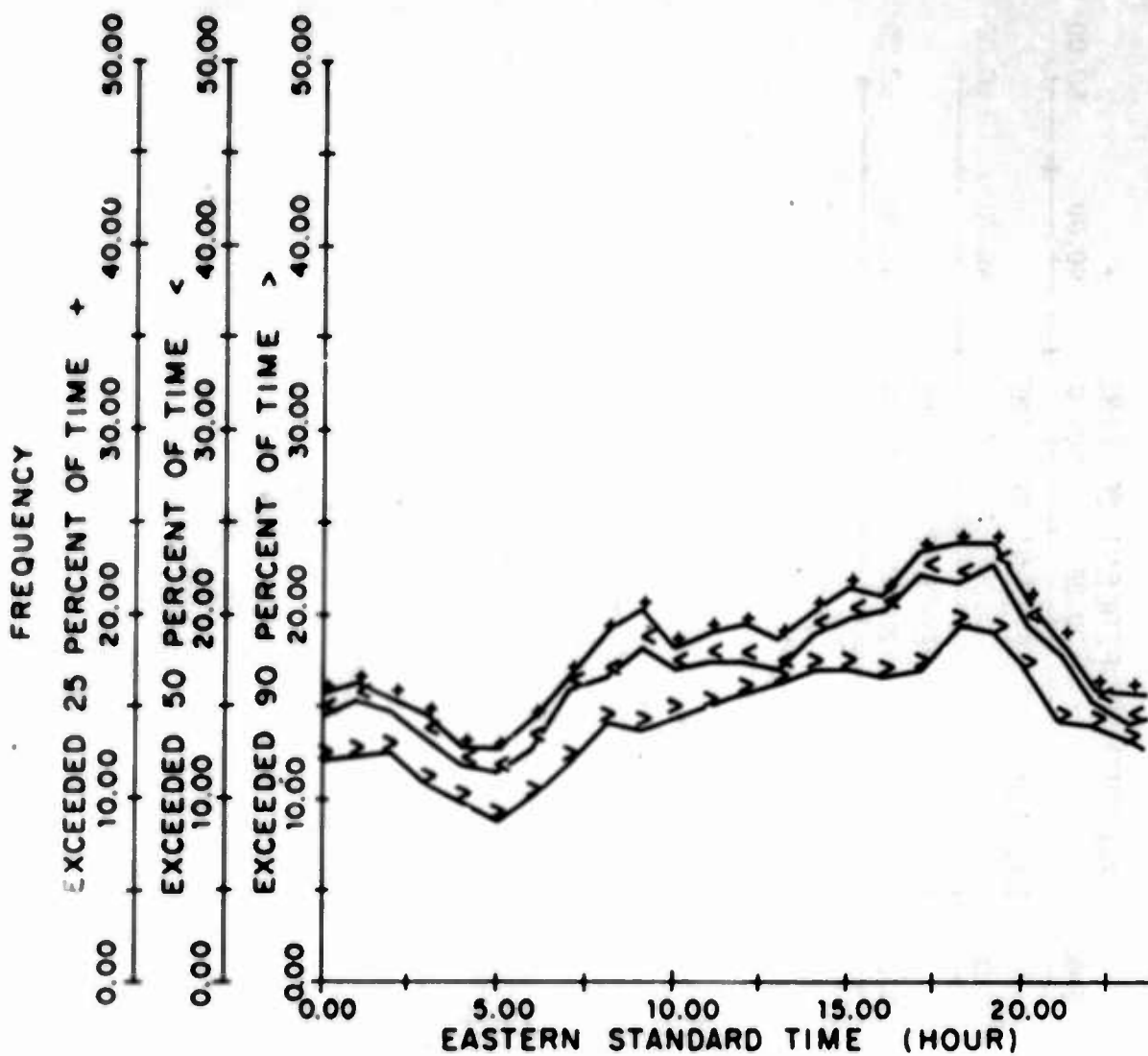


Figure 168. 2F2 Mode JF Availability, Coco Solo Path, Summer 1967

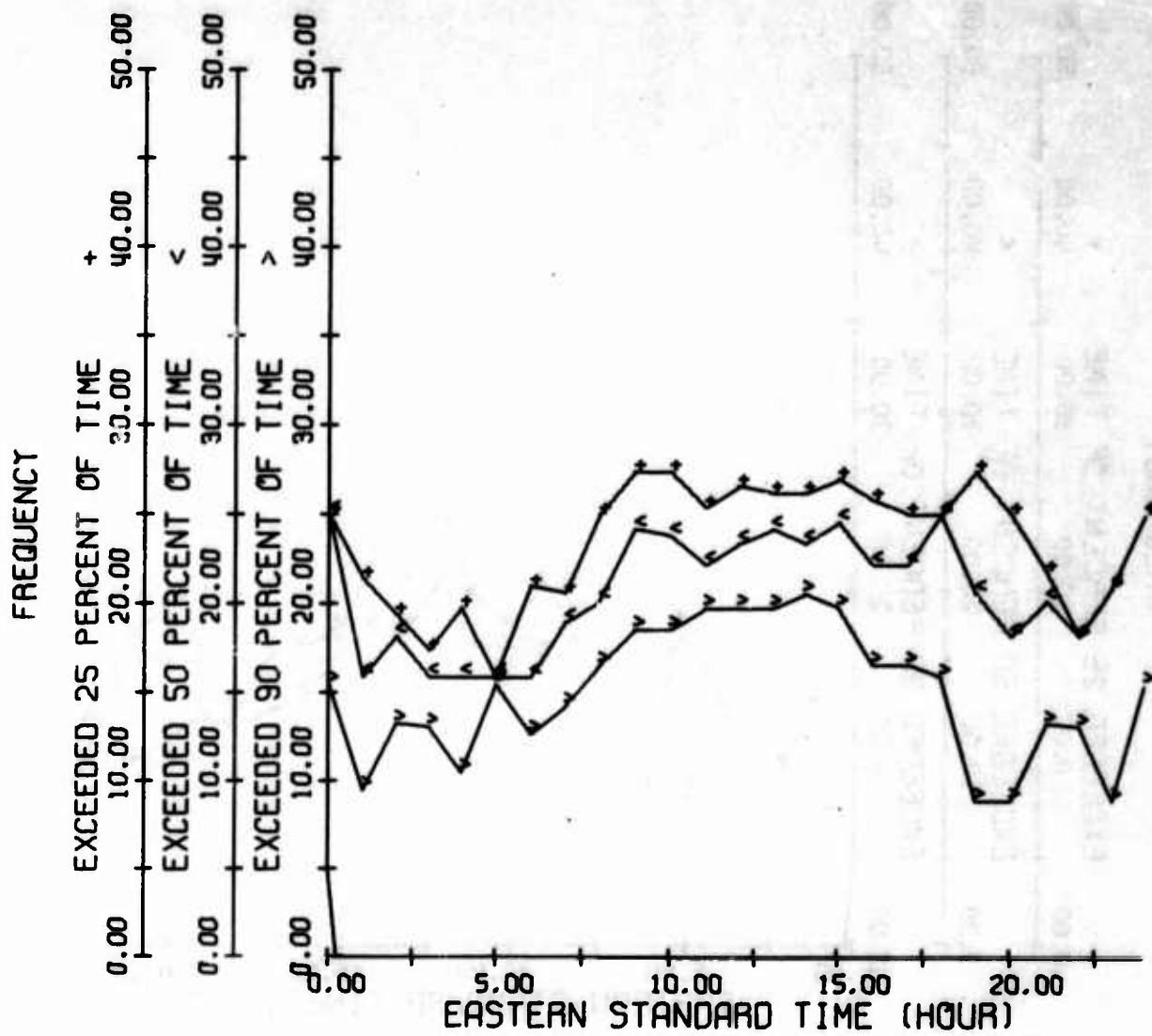


Figure 169. 2E Mode MOF Availability, Coco Solo Path, Summer 1966

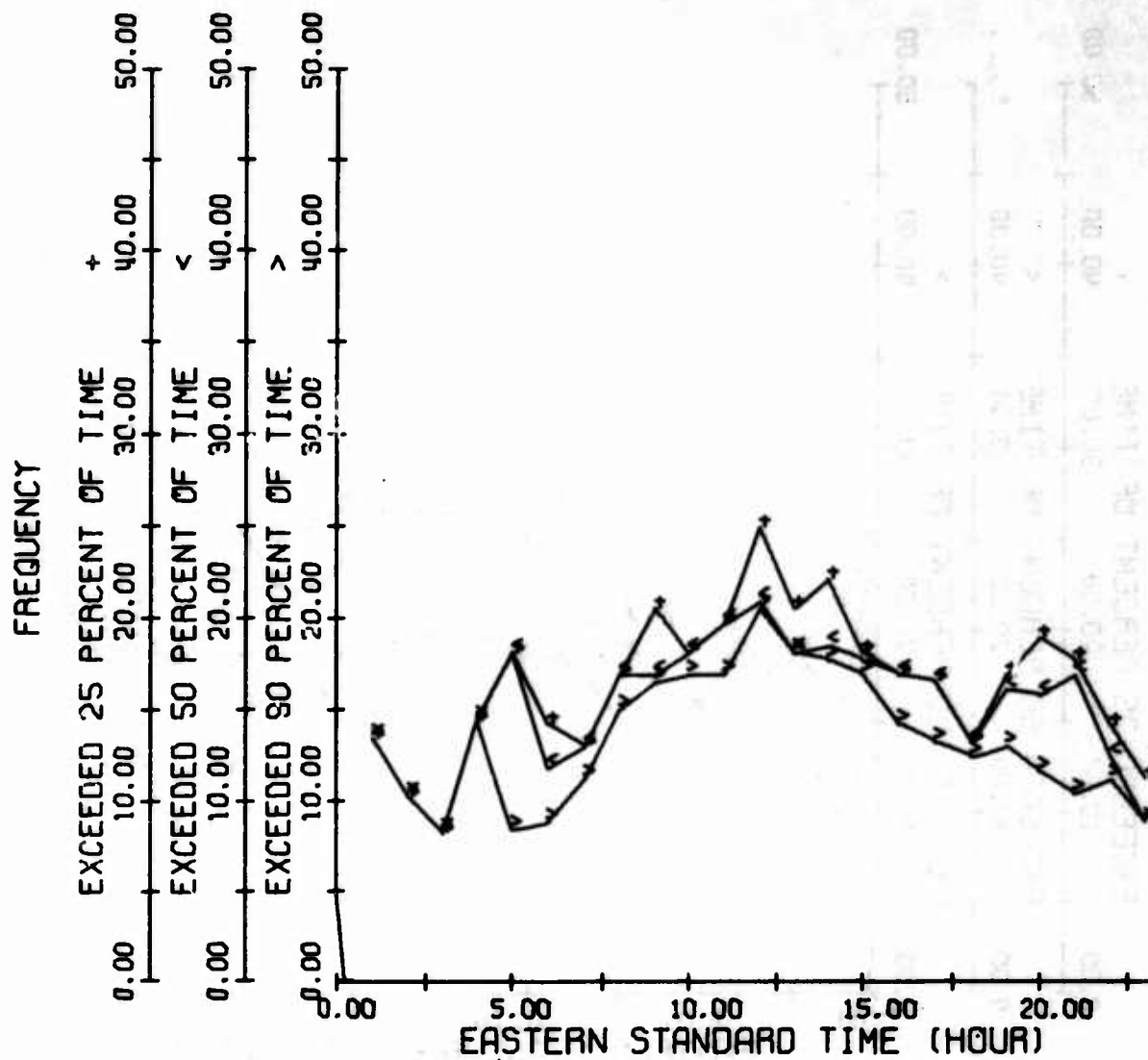


Figure 170. 2E Mode MOF Availability, Coco Solo Path, Autumn 1966

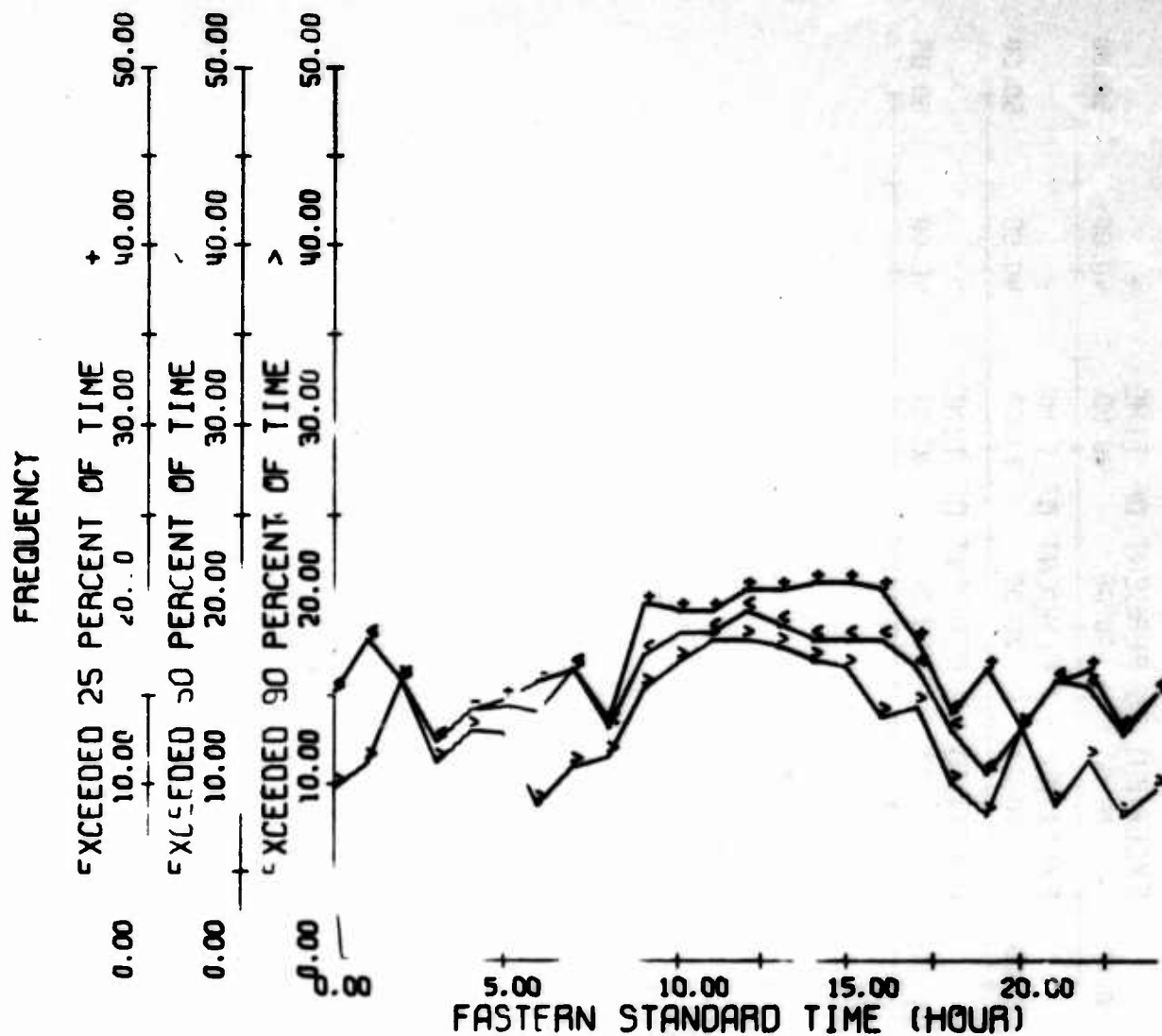


Figure 171. 2E Mode MOF Availability, Coco Solo Path, Winter 1967

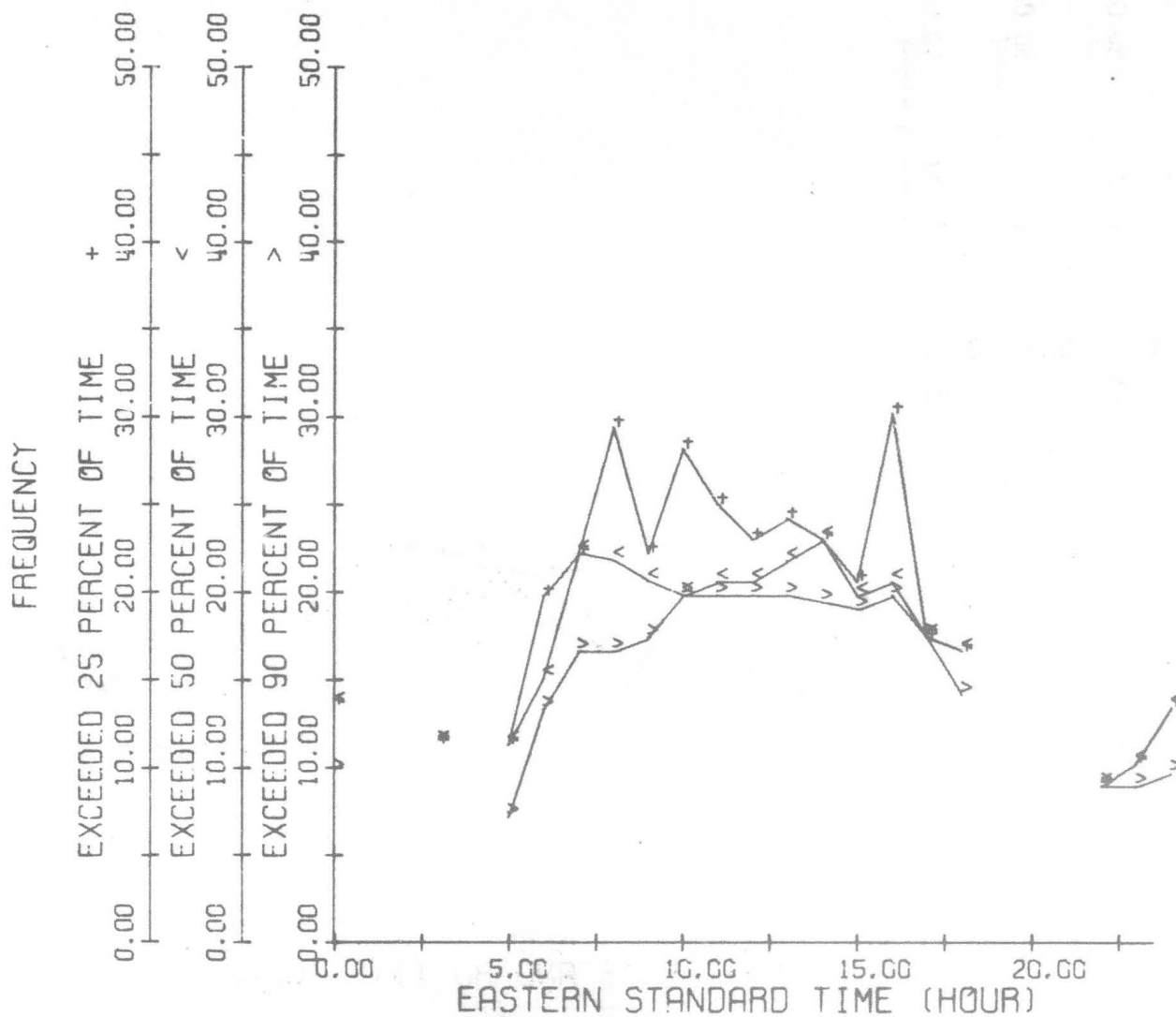


Figure 172. 2E Mode MOF Availability, Coco Solo Path, Spring 1967

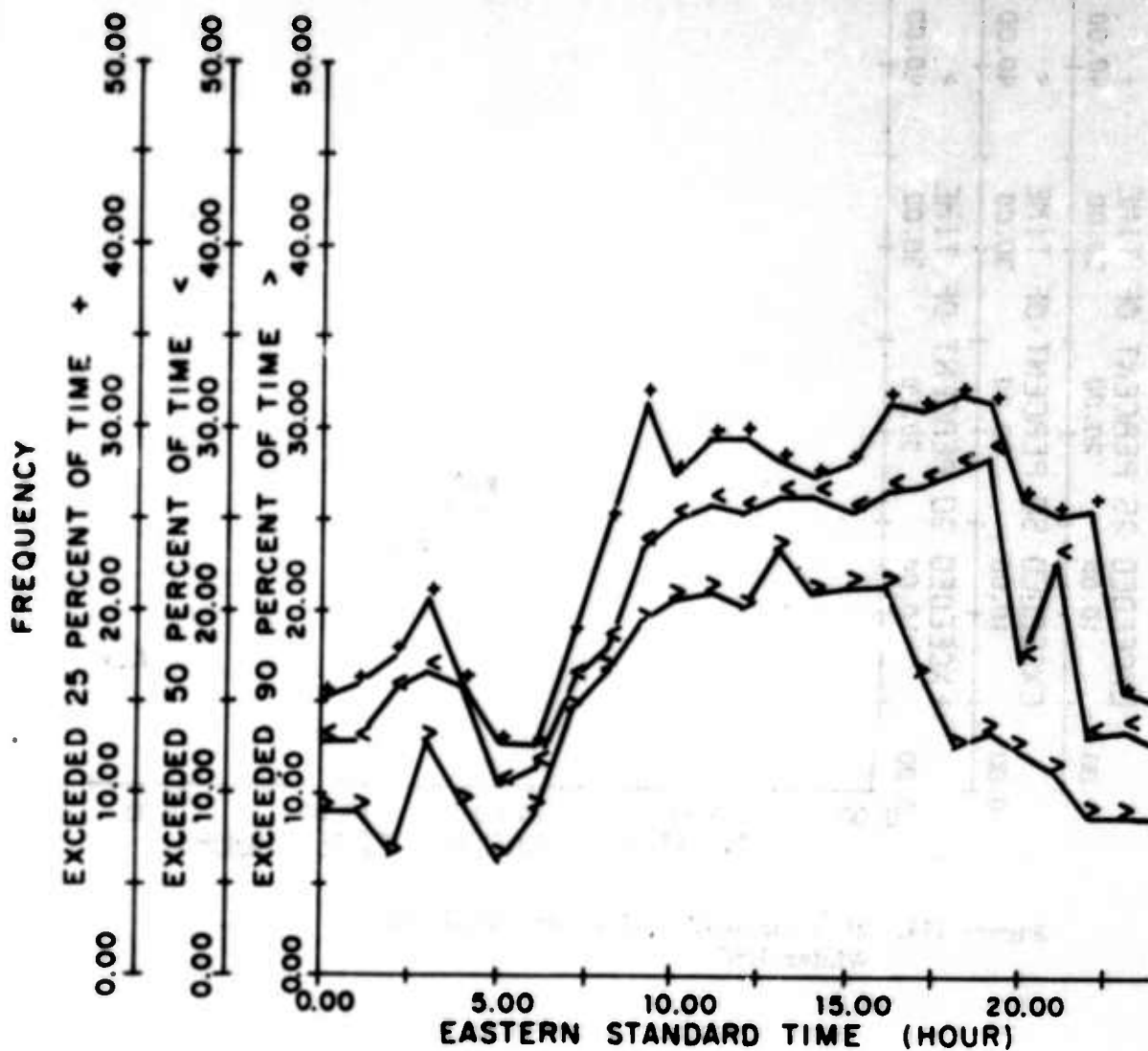


Figure 173. 2E Mode MOF Availability, Coco Solo Path, Summer 1967

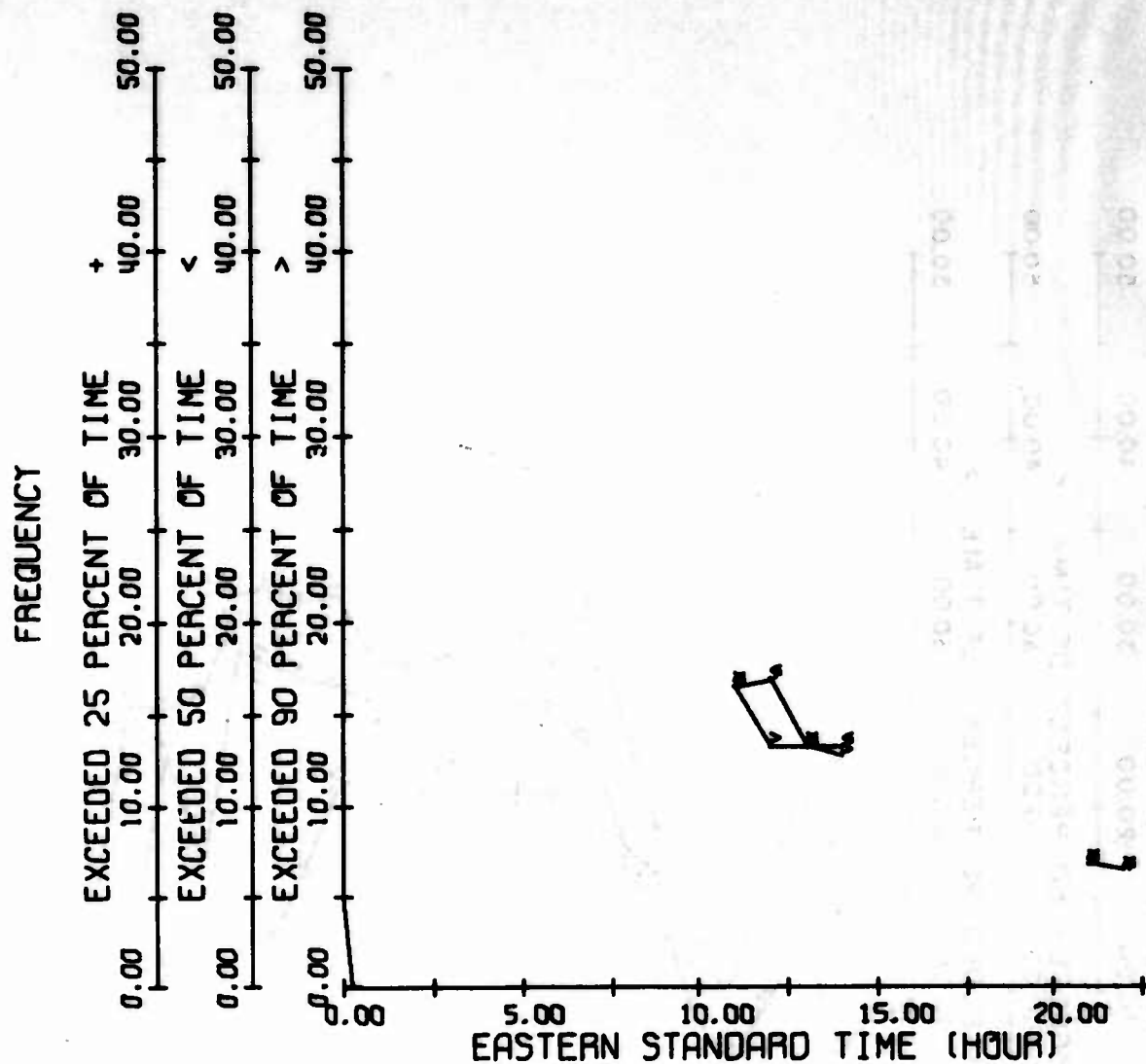


Figure 174. 2E Mode MOF Availability, Thule Path, Winter 1967

8. MOF-JF AVAILABILITY -- THULE TO STOCKBRIDGE/STARR HILL

The move to Starr Hill, as stated previously, was not made until the end of the winter; hence, the winter data are based on measurements made on the Thule to Stockbridge path. The 2E mode MOF availability results (Figures 174 and 175) actually show little of consequence in the winter due to a limited amount of data; however, results are quite normal during the daytime for the spring of 1967. The 1F2 mode JF availability (Figures 176 and 177) indicates that the 1F2 mode would be a very usable mode throughout the winter of 1967. It ranges from nighttime and dusk frequencies of 10 MHz for the 90 percent JF availability to spot frequencies of 30 MHz during the daytime. The nighttime frequencies are somewhat higher for the spring of 1967, but daytime frequencies never reach the levels that were achieved during the winter. The N mode MOF availability (Figures 178 and 179) shows creditable daytime frequencies for both winter and spring as also is the situation for the 2F2 mode (Figures 180 and 181). The 2E_s mode MOF availability (Figures 182 and 183) shows only a few spots of availability either during winter or spring.

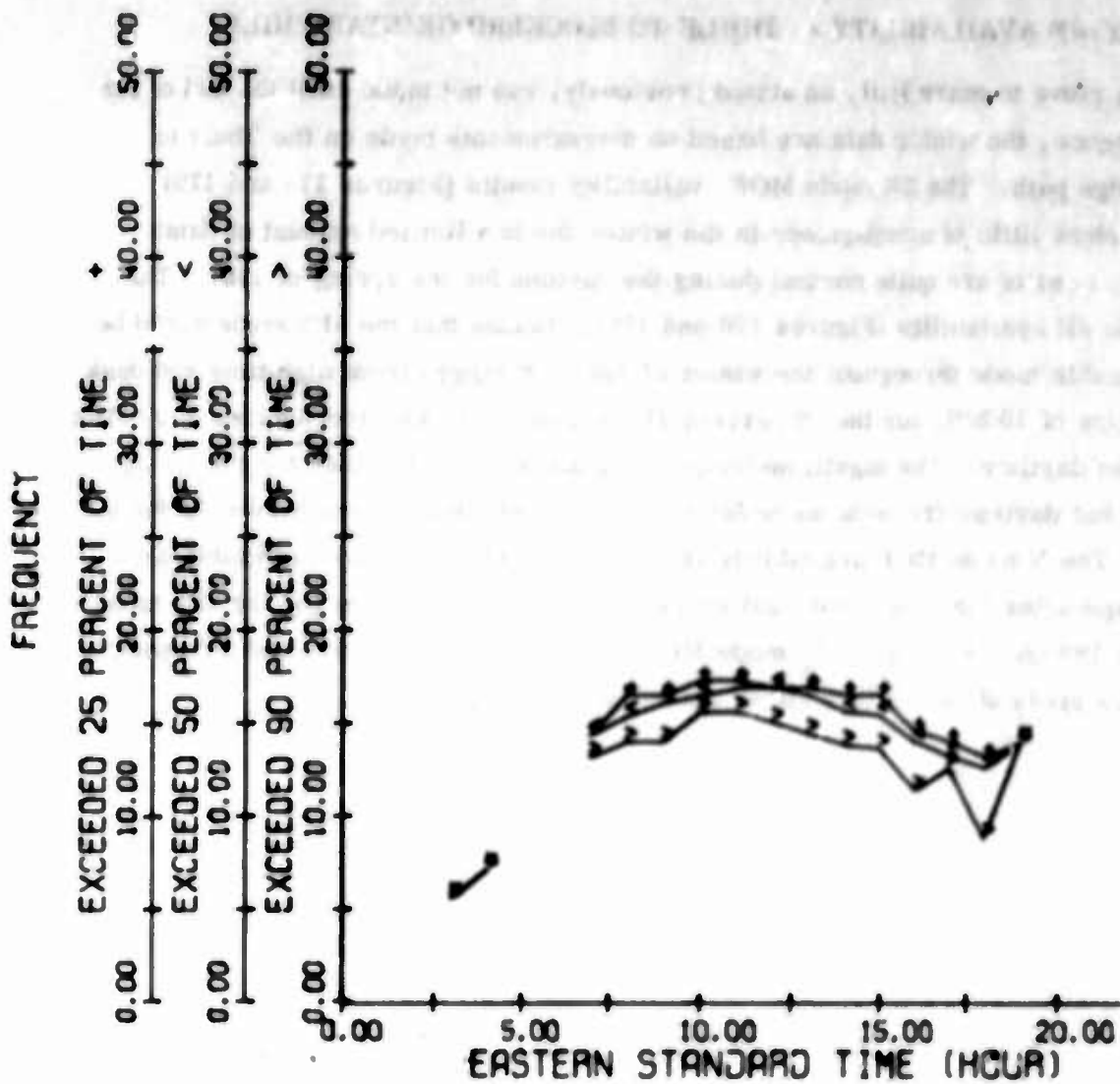


Figure 175. 2E Mode MOF Availability, Thule Path, Spring 1967

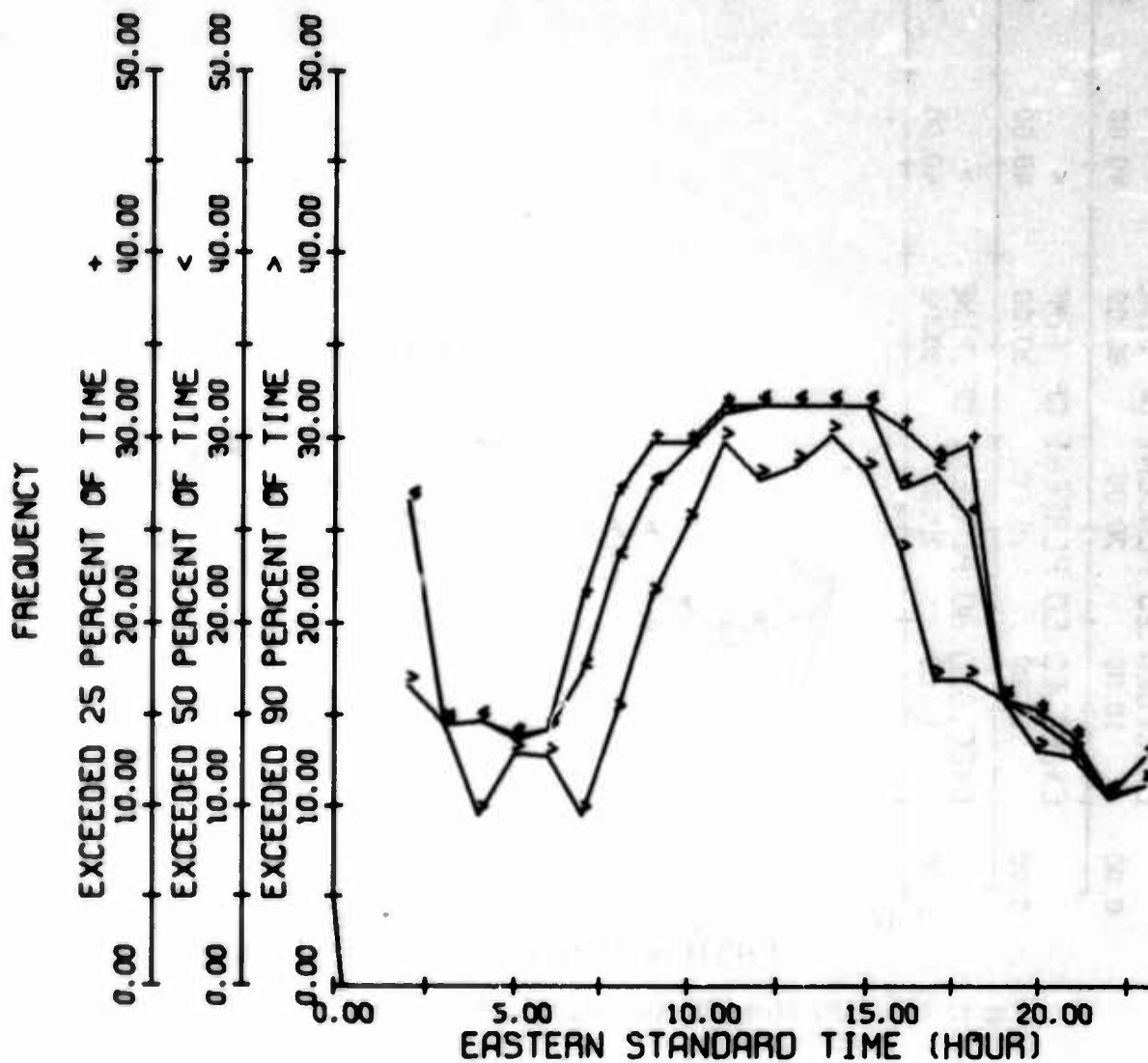


Figure 176. 1F2 Mode JF Availability, Thule Path, Winter 1967.

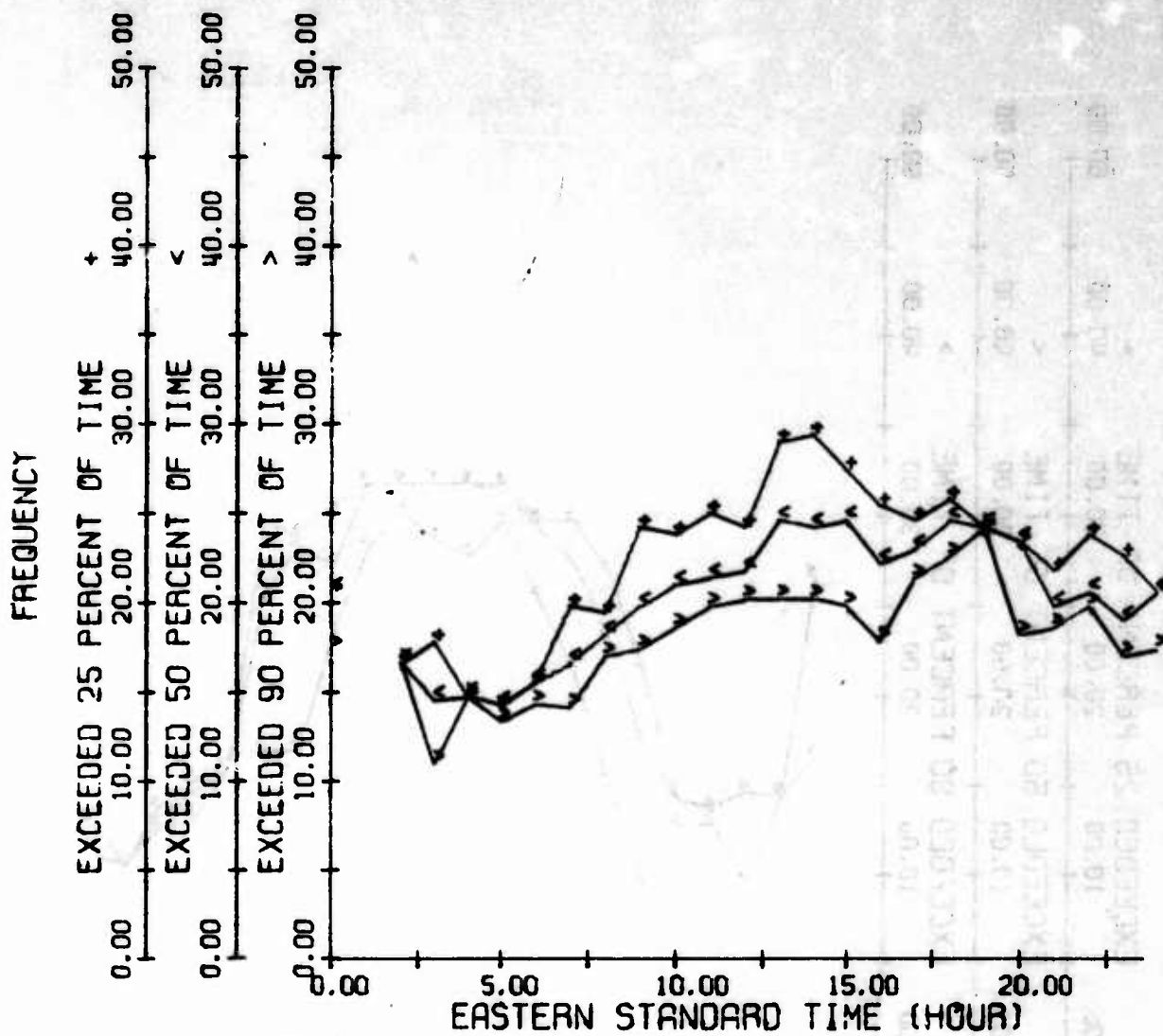


Figure 177. 1F2 Mode JF Availability, Thule Path, Spring 1967

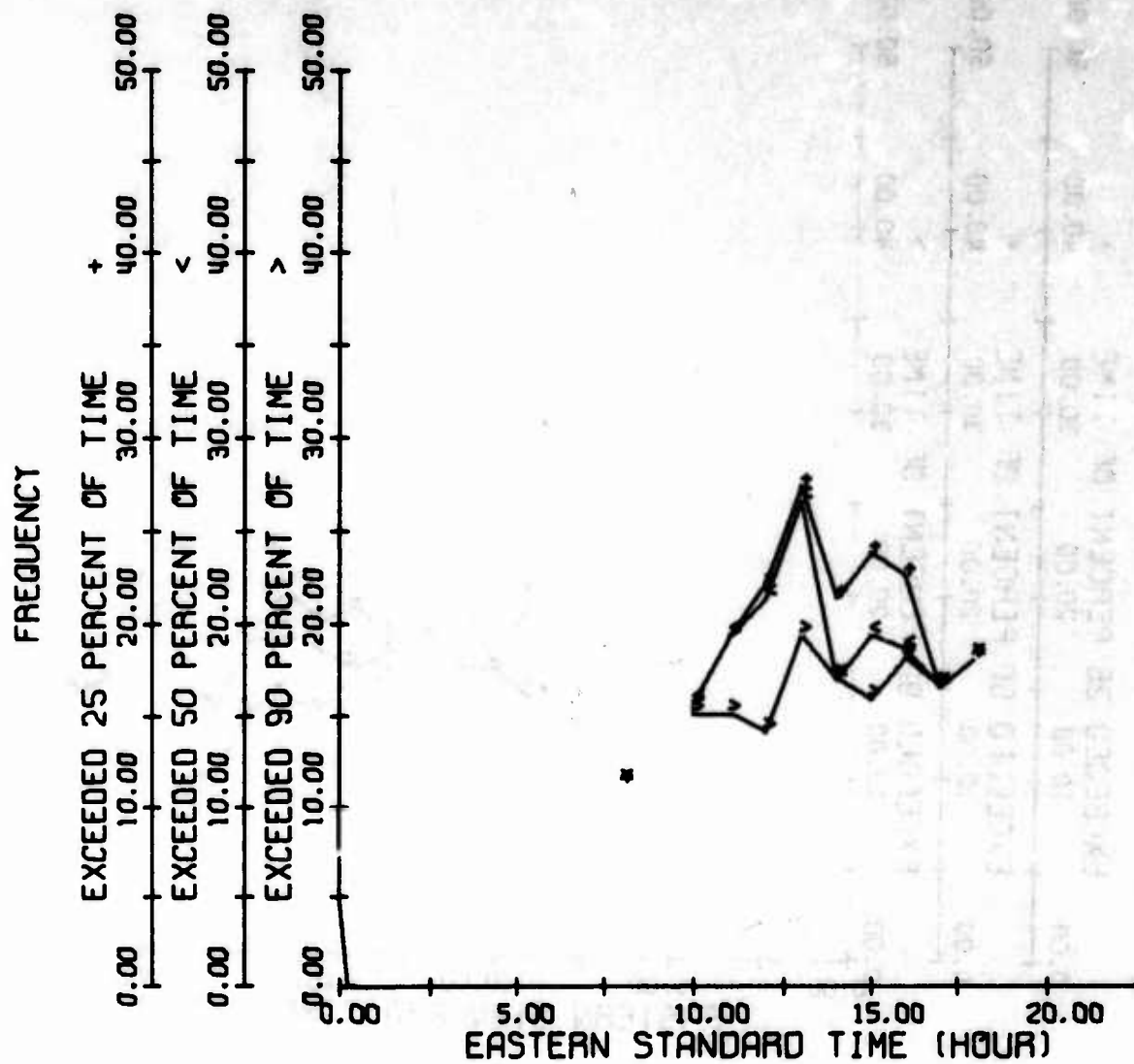


Figure 178. N Mode MOF Availability, Thule Path, Winter 1967

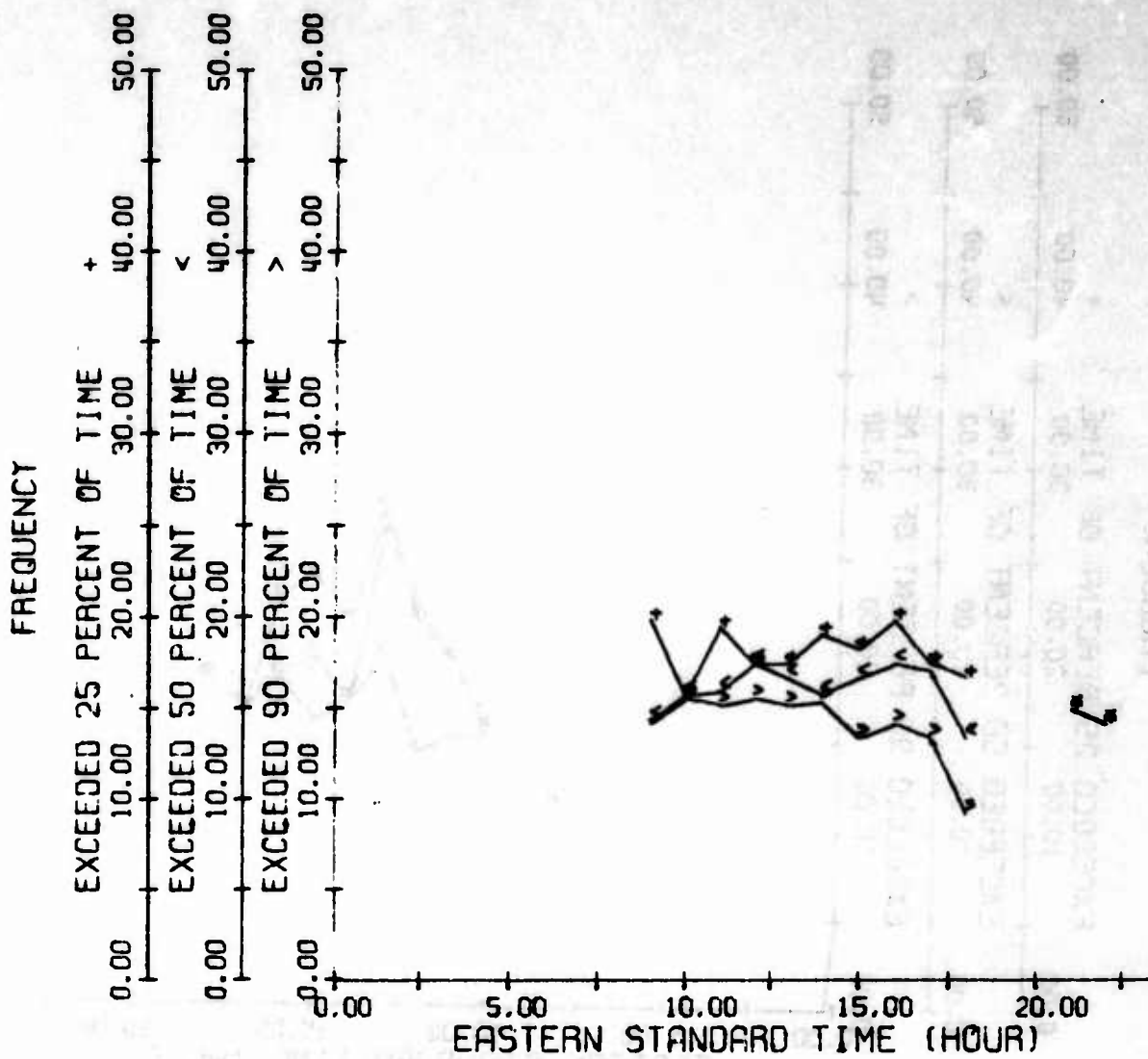


Figure 179. N Mode MOF Availability, Thule Path,
Spring 1967

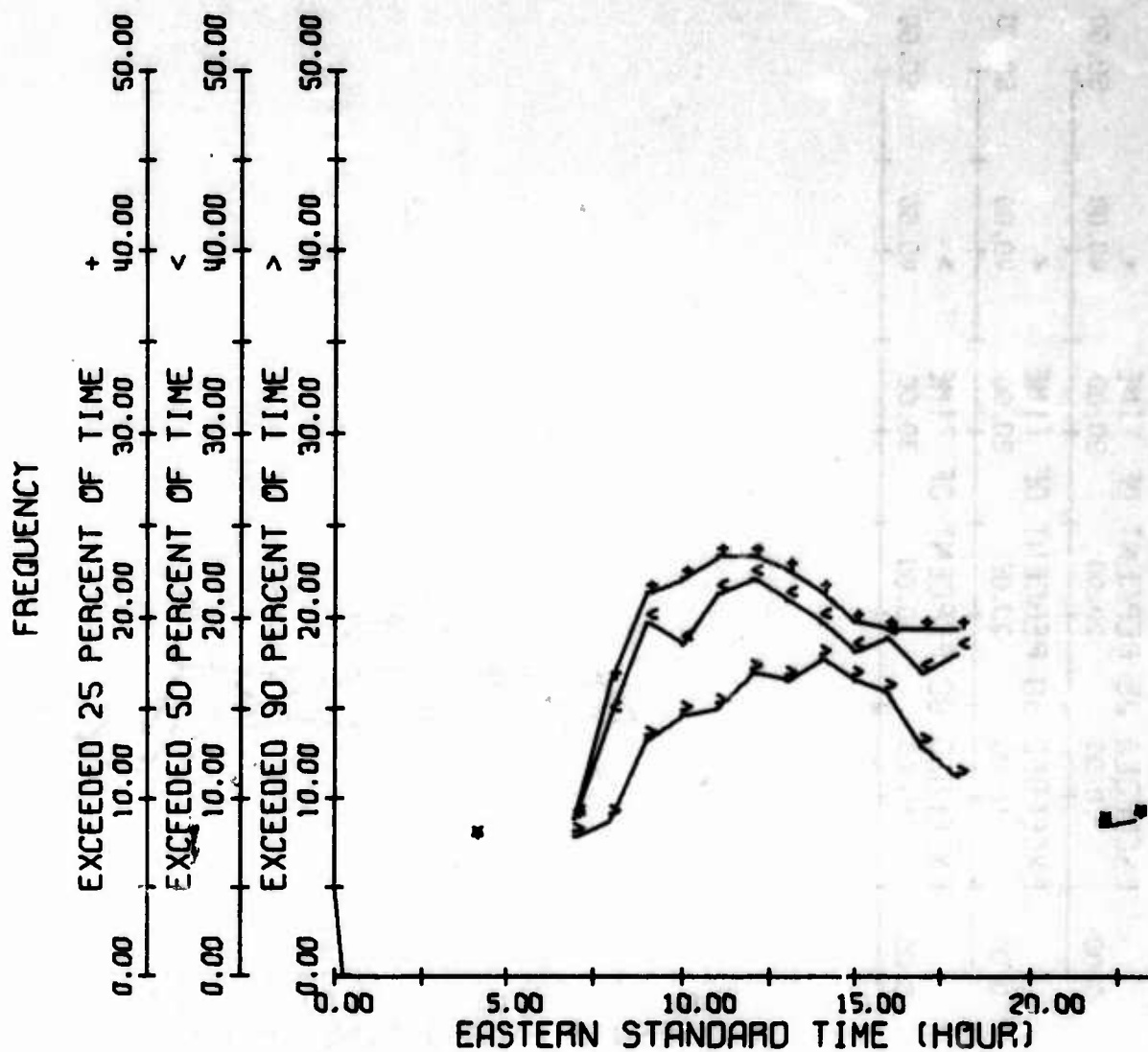


Figure 180. 2F2 Mode JF Availability, Thule Path, Winter 1967.

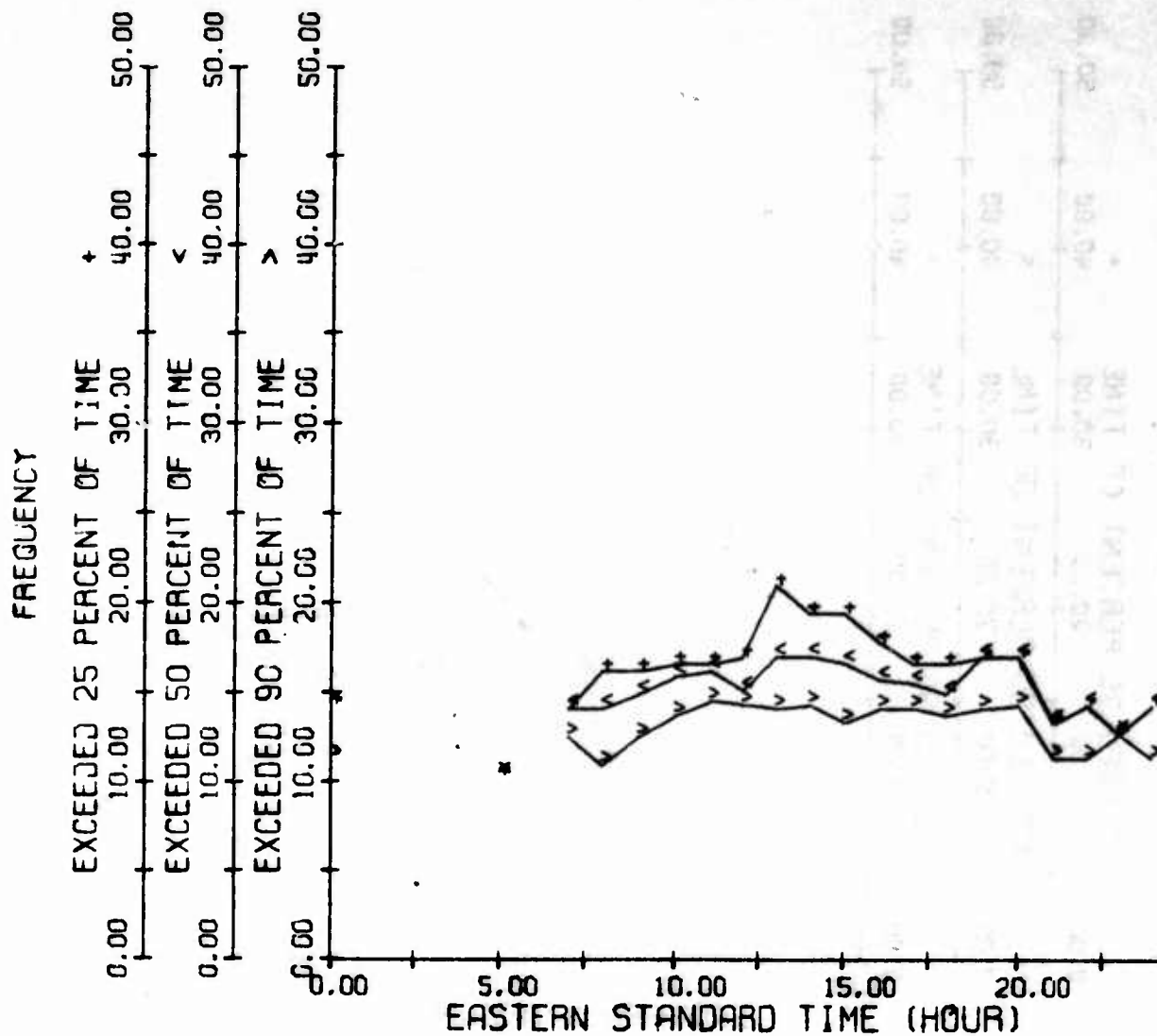


Figure 181. 2F2 Mode JF Availability, Thule Path, Spring 1967

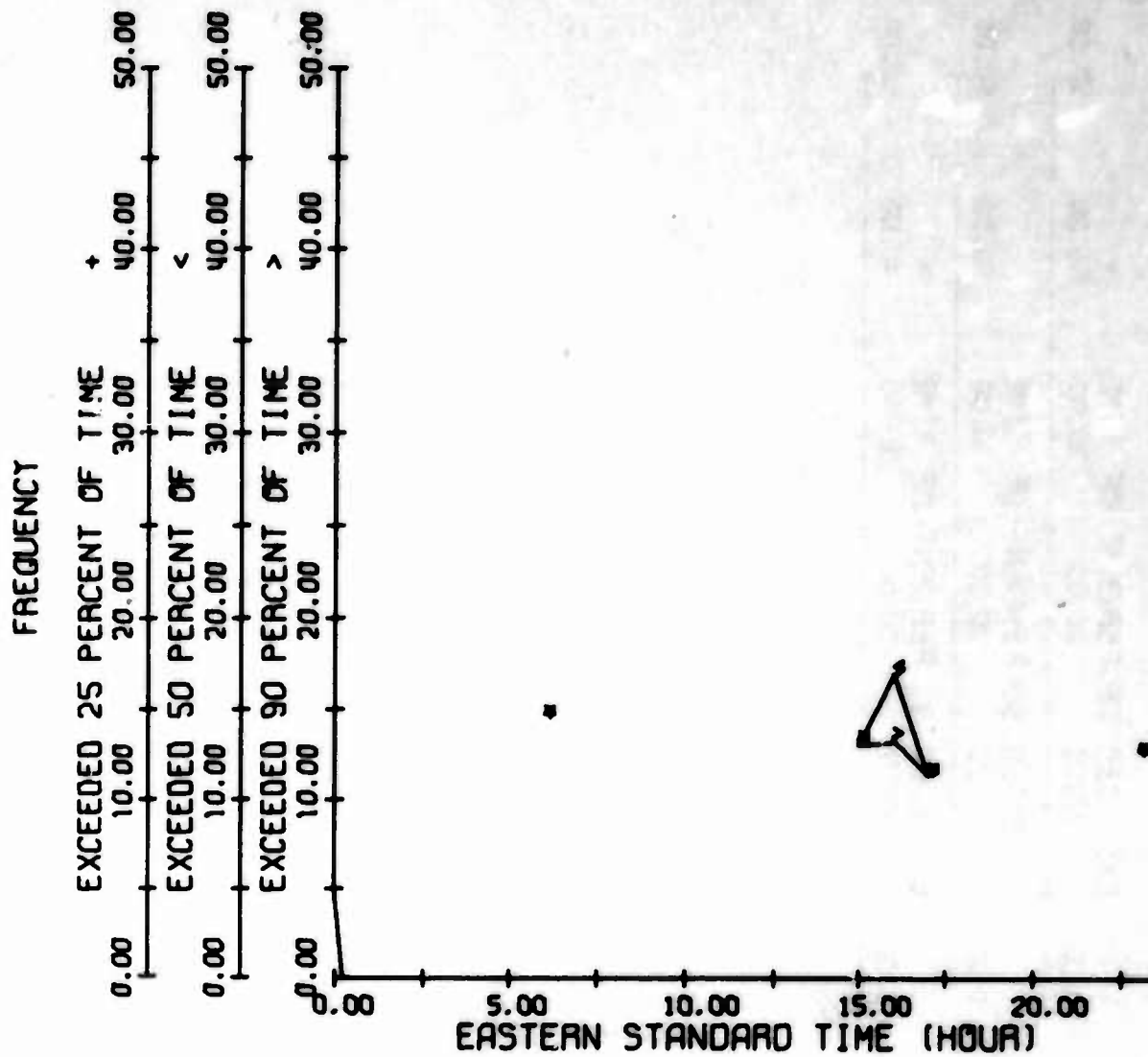


Figure 182. 2E Mode MOF Availability, Thule Path, Winter 1967

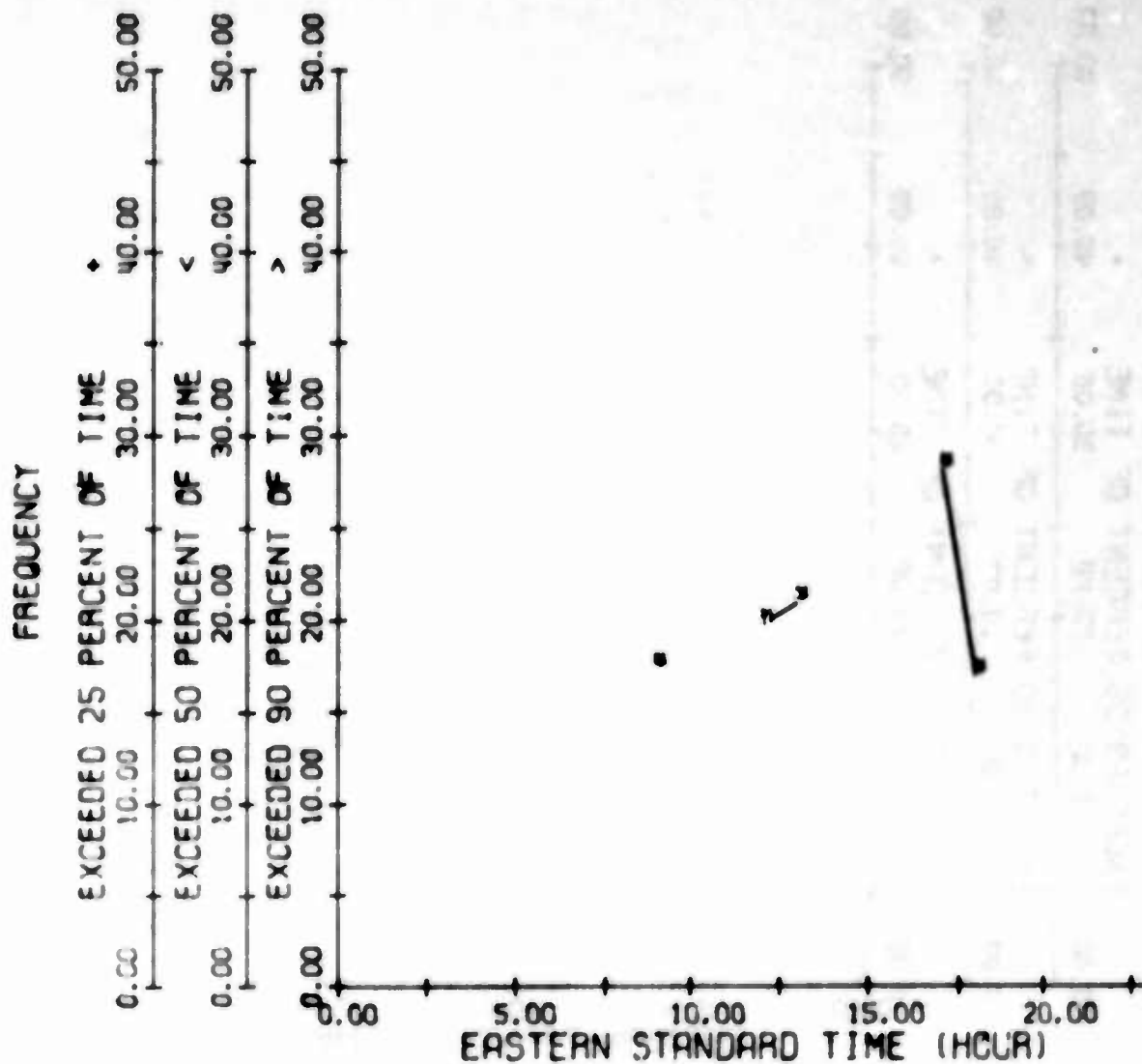


Figure 183. 2E, Mode MOF Availability, Thule Path, Spring 1967

9. DOWNTIME -- COCO SOLO TO STOCKBRIDGE/STARR HILL

For each individual mode previously shown, the time that the mode is not available is obviously 100 percent minus the percent of mode availability. In order to determine the overall mode availability for propagation over the Coco Solo path, various combinations of modes were considered (Table XII). Here the percentages of downtime for the combinations of 2E and 1F2 modes, 1F2 and 2F2 modes, and 2E, 1F2, and 2F2 modes are tabulated. A detailed examination of the downtime for the three-mode combination indicates that it was always zero for the seven seasons covered, which means that there was always one mode available for propagation over the Coco Solo path; also, there are no situations when both of the two-mode combinations showed downtimes for the same time and season. This again indicates the very high availability of at least one mode of propagation over the Coco Solo path. The N mode has not been included in the presentation since 100 percent availability existed without it. While the data base is in some cases small enough that as much as a 15 percent availability statistical variation should be expected in the data on a monthly basis, it is noted that these data cover a total of 21 months and are analyzed on a seasonal, rather than a monthly, basis.

It is interesting to note from Table XII that the 2E/1F2 combination shows some downtime at 0500 EST for six out of the seven seasons for which data are available.

TABLE XII

DOWNTIME (PERCENT)

Hour EST	Winter 66			Spring 66			Summer 66			Fall 66			Winter 67			Spring 67			Summer 67			Hour EST
	2E 1F2 1F2	2E 1F2 2F2	2E 1F2 2F2	2E 1F2 2F2	2E 1F2 2F2	2E 1F2 2F2	2E 1F2 2F2	2E 1F2 2F2	2E 1F2 2F2	2E 1F2 2F2	2E 1F2 2F2	2E 1F2 2F2	2E 1F2 2F2	2E 1F2 2F2	2E 1F2 2F2	2E 1F2 2F2	2E 1F2 2F2	2E 1F2 2F2	2E 1F2 2F2	2E 1F2 2F2	2E 1F2 2F2	
1																						1
2																						2
3	5																					3
4																						4
5																						5
6																						6
7																						7
8																						8
9																						9
10																						10
11																						11
12																						12
13																						13
14																						14
15																						15
16																						16
17																						17
18																						18
19																						19
20																						20
21																						21
22																						22
23																						23
24																						24

10. STATISTICAL SUMMARY

The graphical presentations that have been provided earlier for the mode reliability experiment are, in effect, the output from this experiment. Discussions of these graphs were designed to point out to the reader important trends and salient points in the data. The reader can utilize this information for detailed decisions that require knowledge of the mode propagation effects as a function of time of year, time of day, sunspot number, and other factors that affect high frequency propagation. There are times, however, when more gross decisions have to be made and more general summaries of information are needed. The following statistical summaries of the data gathered during the period from the winter of 1966 through the summer of 1967 on the Coco Solo path provide a quicker means for examination and assimilation of this information. Since only a limited amount of data was collected on the Thule path, no statistical summary is provided for the information gathered on that path.

a. Mode Availability

The most important factor for any communications or radar system is the requirement for a usable propagation path. In the following pages the means and standard deviations that are presented indicate the availability of the respective dominant modes for the seven seasons that are covered in this report for the Coco Solo path. These means and standard deviations are calculated utilizing all the data available for each mode.

(1) Seasonal Means

It can be seen, in Figure 184, that by comparing seasonal results for different years the 2E mode appears to lose in availability as the sunspot number has increased. The availability for the winter of 1967 is more than 30 percent below that for the winter of 1966 in mean, and in spring of 1967 is about 10 percent below the spring of 1966. For the one complete calendar year shown, winter was highest and fall was the lowest. The sequence seems to be from winter to spring down, and from spring to summer up slightly, and from summer to fall down; but, instead of coming up again in winter, the change in sunspot cycle appears to put this second winter farther down. Interestingly enough, it is up again in the spring of 1967, apparently exceeding the downward sunspot cycle trend that exists for the 2E mode.

The 1F2 mode availability seems to be highest consistently in spring and summer, and consistently lowest in winter and fall. No apparent effect of the sunspot cycle shows in the full day averages. The N mode availability appears to more nearly follow that of the 2E mode than of the F modes. The 2F2 mode availability has such small deviations throughout the entire time that there seems to be doubtful merit in trying to make any comparisons. The data available for the 2E_s mode availability indicate the highest availability in the summer of 1967, lowest in the winter, and up a little in the spring of 1967.

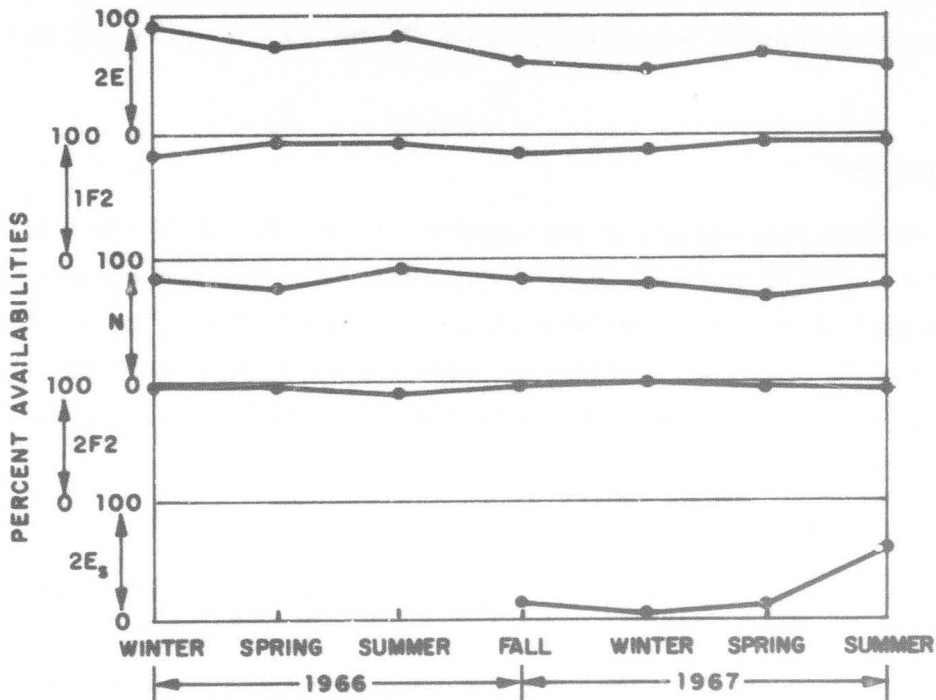


Figure 184. Mean Mode Availability, Coco Solo Path

(2) Seasonal Statistics by Time of Day

For the presentation of seasonal results as a function of time of day, the following time divisions are made: daytime - 0900 to 1600 EST, dusk - 0500 to 0800 EST and 1700 to 2000 EST, and nighttime - 2100 to 0400 EST. The time period included as dusk covers sunrise and sunset periods and obviously some also from daytime and nighttime. In general, the dusk may be described as a hybrid of the day and night with larger standard deviations. The previous presentation of seasonal means (Figure 184) covers an entire day and is in effect a summary of the three means to be presented in the material to follow. In each of the subsequent graphs, while the dusk data are included for study, a reasonably clear-cut understanding of the characteristics of the mode appears possible by discussion of the day and night statistics only.

During the day there is an increase for the 2E mode from winter to spring to summer and then a drop again in the fall and a further drop in the winter (Figure 185); however, the increase in the spring is not enough to bring it back to the level which existed the previous spring. The level for the summer of 1967 is about the same as for spring of 1967. It should be noted that the period covered represents a time of increasing sunspot number. The nighttime data show a strong downward variation for the seven seasons covered, even neglecting the winter data of 1966, when the two-hop sporadic-E mode was included with the 2E mode data and is very likely responsible for the large percentage of availability indicated.

The 1F2 mode results (Figure 186) show more distinctly opposing trends of day and night availability both with respect to season and sunspot number. The nighttime data show a somewhat general improvement of nighttime availability with respect to the increasing sunspot activity except for the winter of 1967.

The N mode (Figure 187) shows its usual completely confused and erratic picture (as expected).

The 2F2 mode data (Figure 188) show for daytime that the mode availability for the summers is the lowest for any season; fall and winter are 100 percent and spring a little under 100 percent. A slight improvement in both spring and summer with respect to the sunspot cycle is noted. For nighttime everything is 100 percent or almost 100 percent.

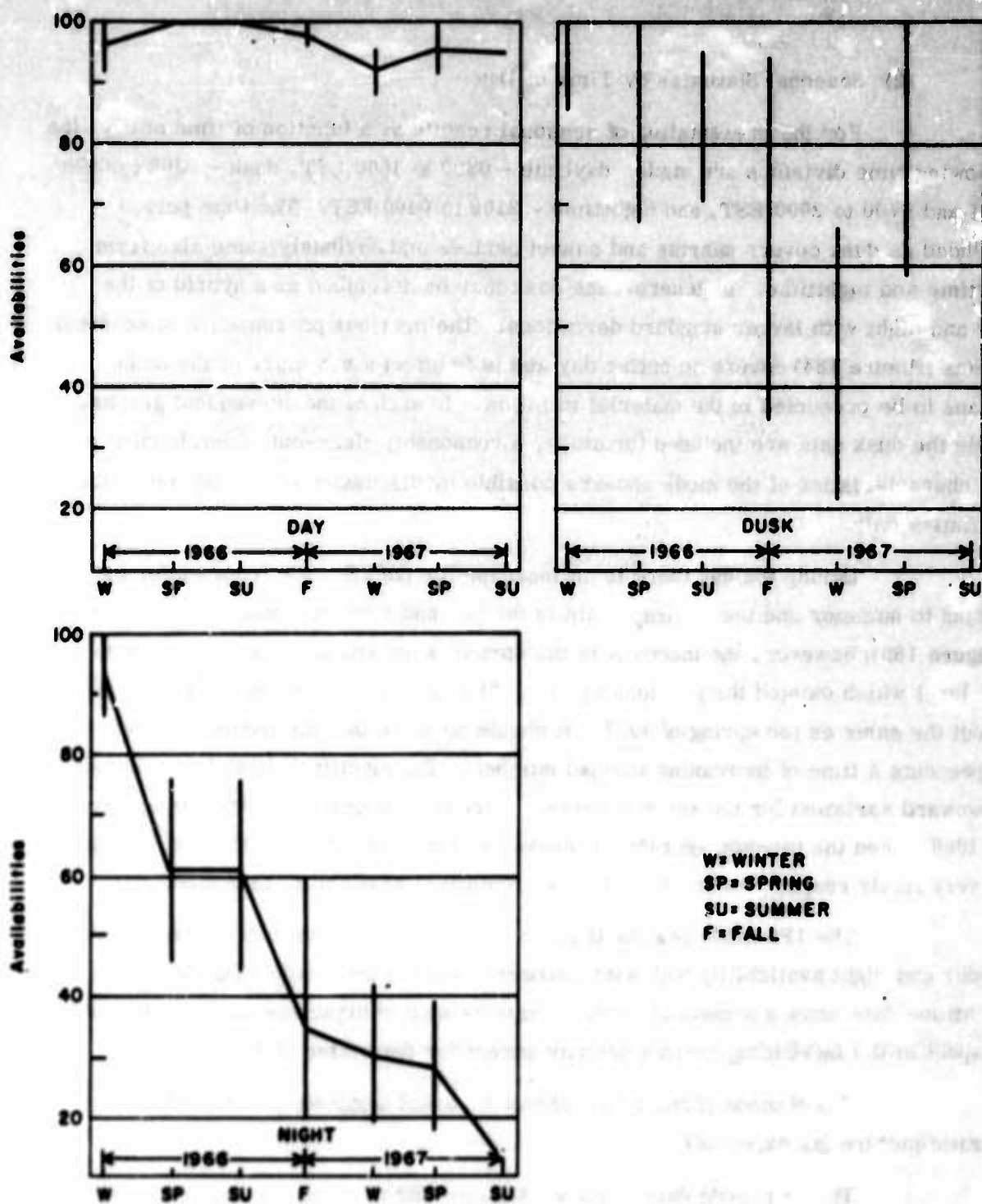


Figure 185. 2E Mode Availability, Coco Solo Path

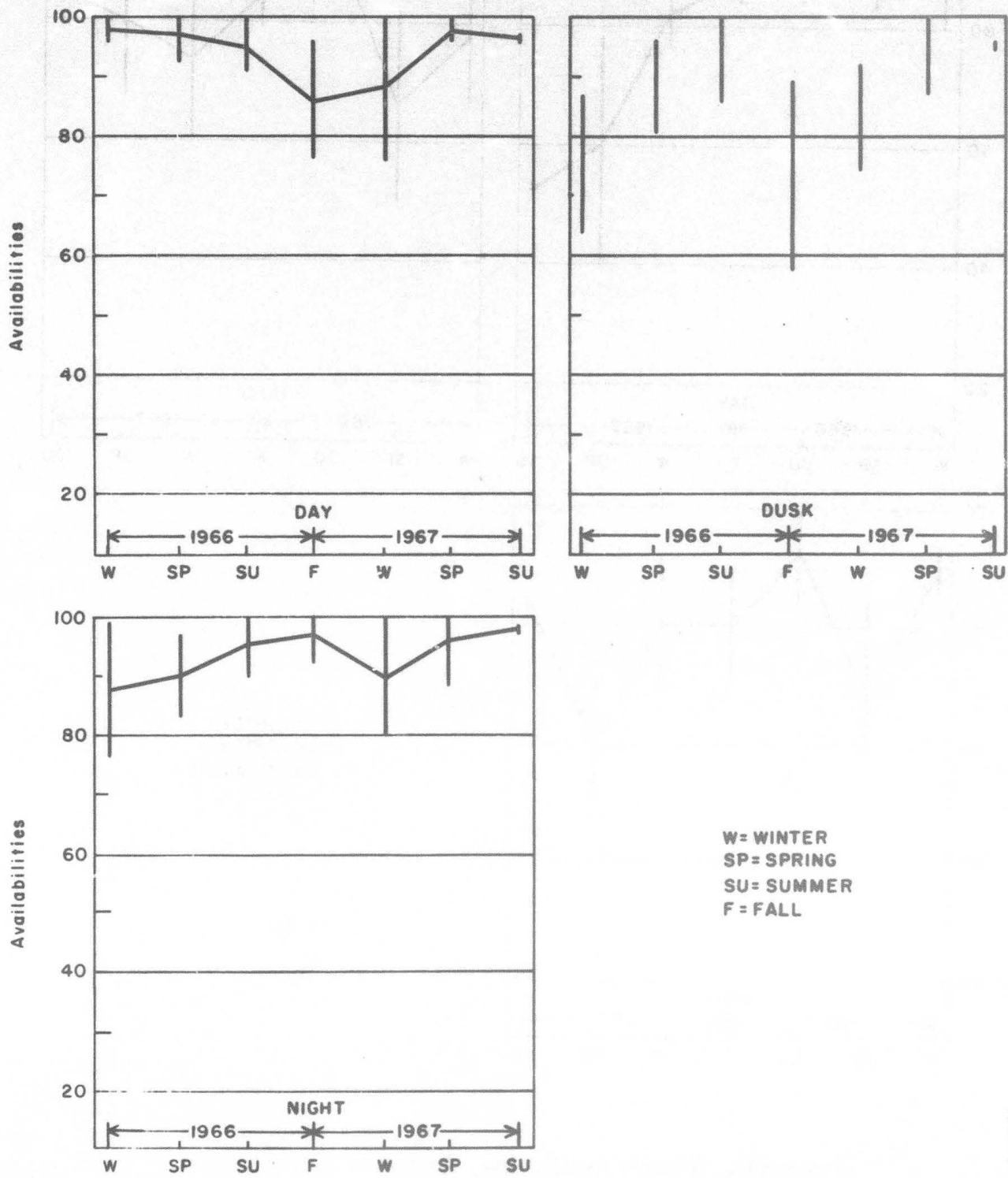


Figure 186. 1F2 Mode Availability, Coco Solo Path

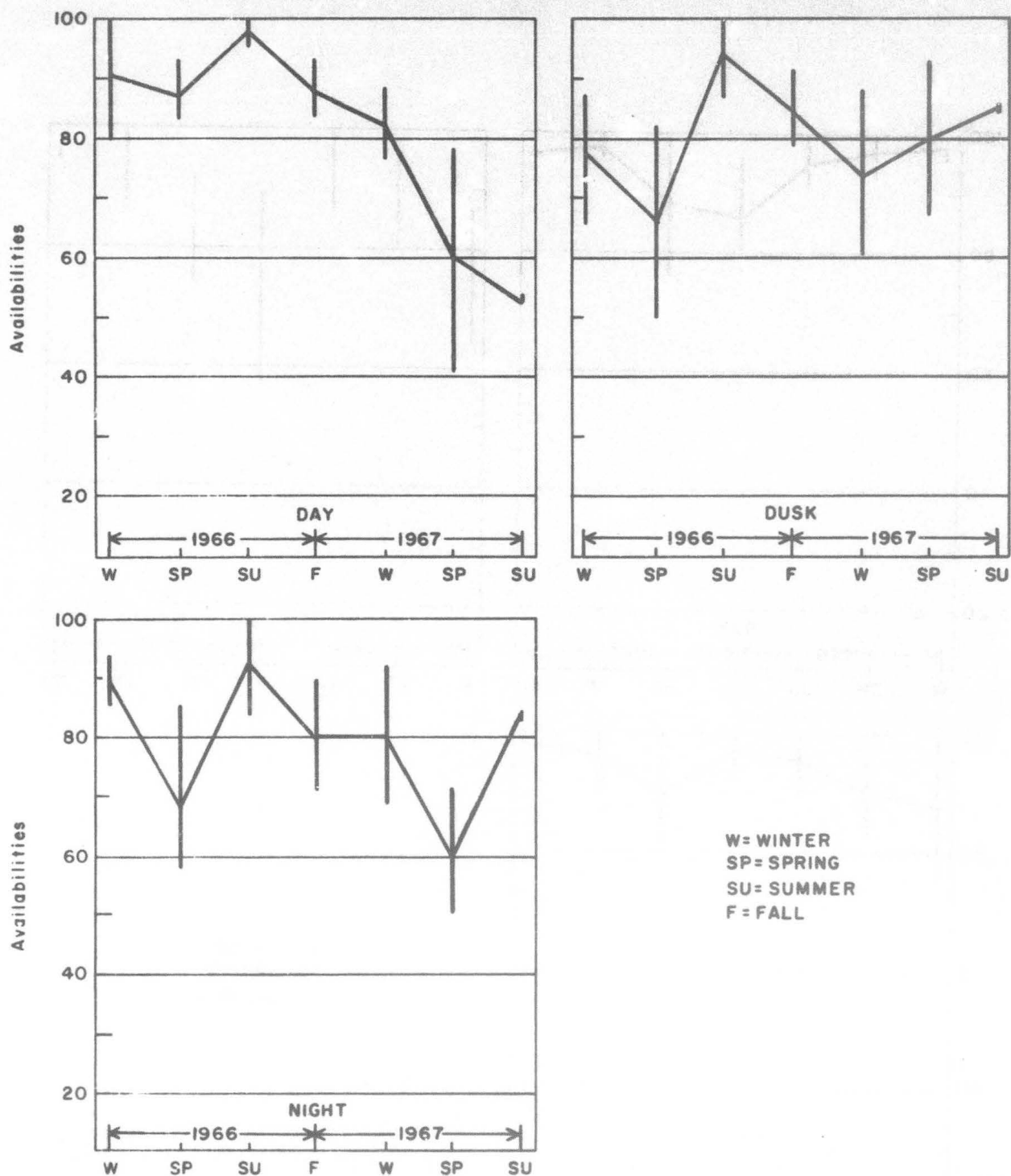


Figure187. N Mode Availability, Coco Solo Path

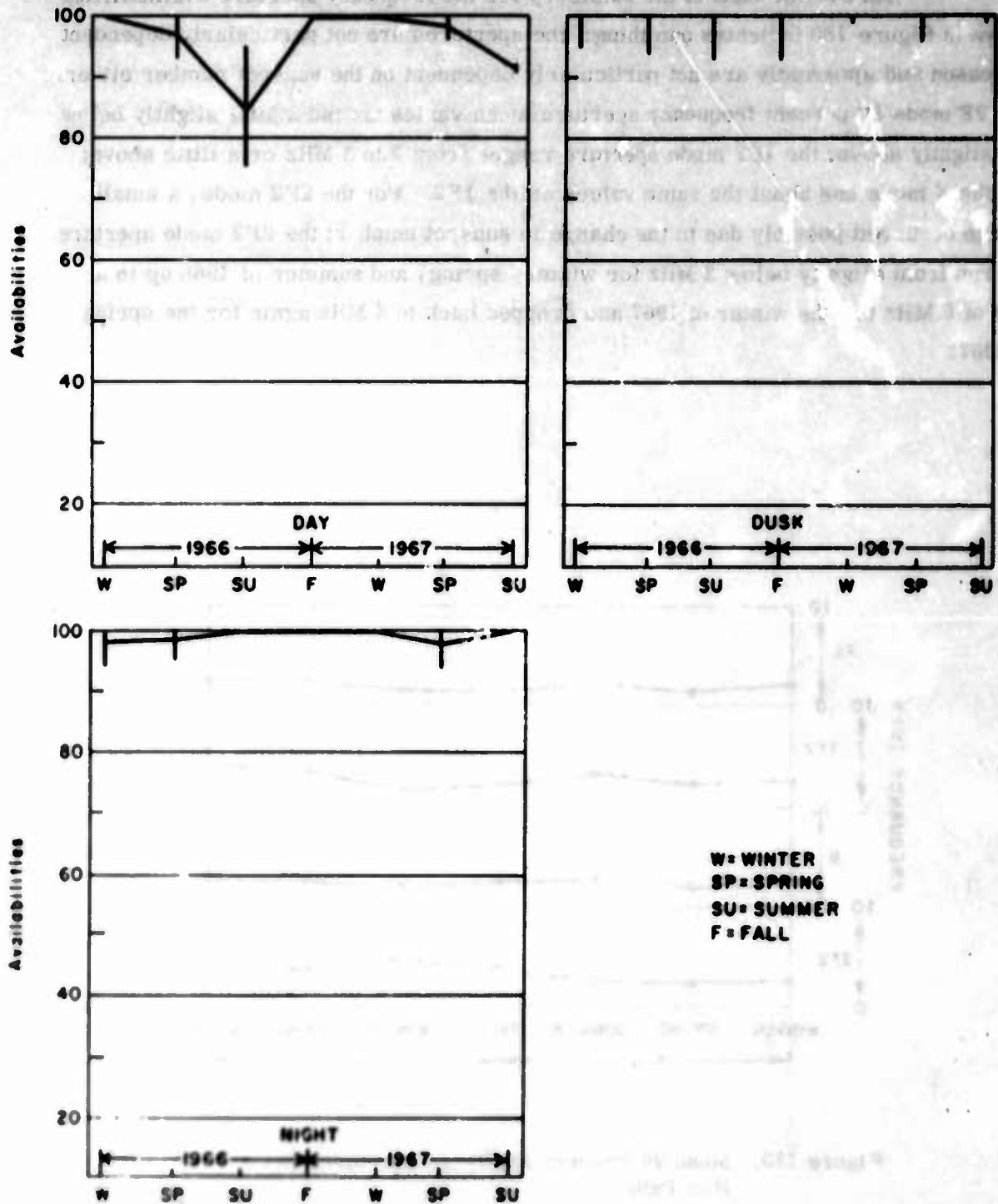


Figure 188. 2F2 Mode Availability, Coco Solo Path

b. Frequency Aperture Availability

(1) Seasonal Means for 90 Percent Availability

An overall view of the summary for the frequency aperture availabilities shown in Figure 189 indicates one thing: the apertures are not particularly dependent on season and apparently are not particularly dependent on the sunspot number either. The 2E mode 90 percent frequency aperture mean varies around 2 MHz slightly below and slightly above; the 1F2 mode aperture ranges from 2 to 3 MHz or a little above; and the N mode has about the same values as the 1F2. For the 2F2 mode, a small change occurred possibly due to the change in sunspot number; the 2F2 mode aperture has run from slightly below 2 MHz for winter, spring, and summer of 1966 up to a high of 5 MHz for the winter of 1967 and dropped back to 4 MHz again for the spring of 1967.

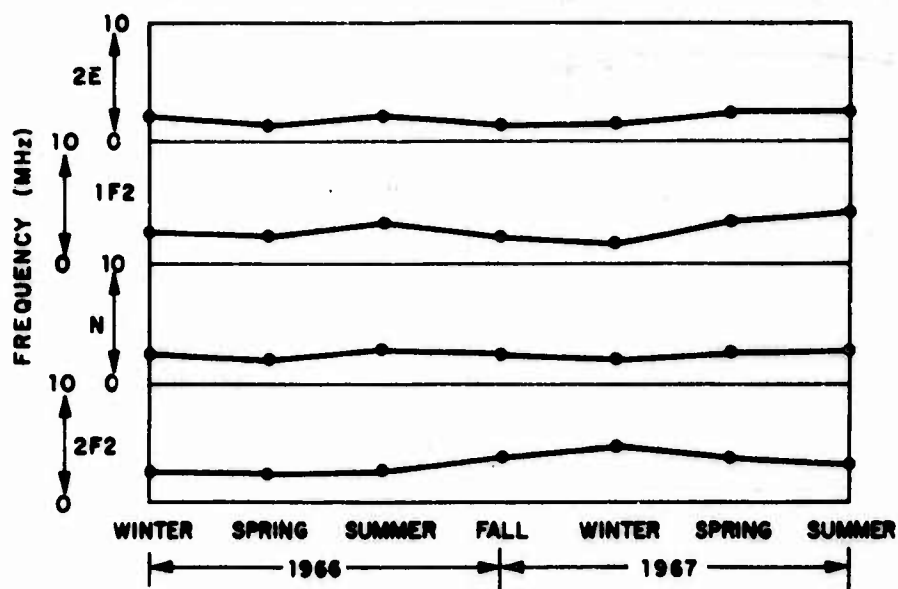


Figure 189. Mean 90 Percent Available Aperture, Coco Solo Path

(2) Seasonal Statistics by Time of Day

For the 2E mode (Figure 190) there appear to be no consistent trends except that the daytime aperture availability is much better than the nighttime availability, and the frequency aperture was increasing for the last two seasons covered in this report.

The 1F2 mode aperture availability (Figure 191) shows the same trends for both day and night: slight increases starting with spring of 1966 and summer of 1966, then a decrease in the fall, and in the daytime a further slight decrease in the winter. A distinct increase occurred in the summer nighttime aperture; during the daytime a distinct increase occurred in both the spring and summer.

The N mode (Figure 192) shows better consistency of aperture than of availability. There is first a drop from winter to spring, and increase in the summer, a drop to fall, little change between fall and winter, then an increase in spring for the nighttime and a further increase in the summer for the nighttime. For the daytime a decrease for spring of 1967 is followed by a significant increase in the summer of 1967.

The 2F2 mode (Figure 193) shows not only the best mode availability for all modes examined, but also the largest frequency apertures. It exhibited a consistency between day and night for the first four months examined: namely, from winter to spring--in summer a slight drop and an increase in the fall. At night, however, the winter of 1967 approximately parallels fall, while for daytime there is a distinct increase at this time. Then for springtime at night there is an increase while for daytime there is a decrease. In the summer of 1967 the aperture increased during both the daytime and nighttime.

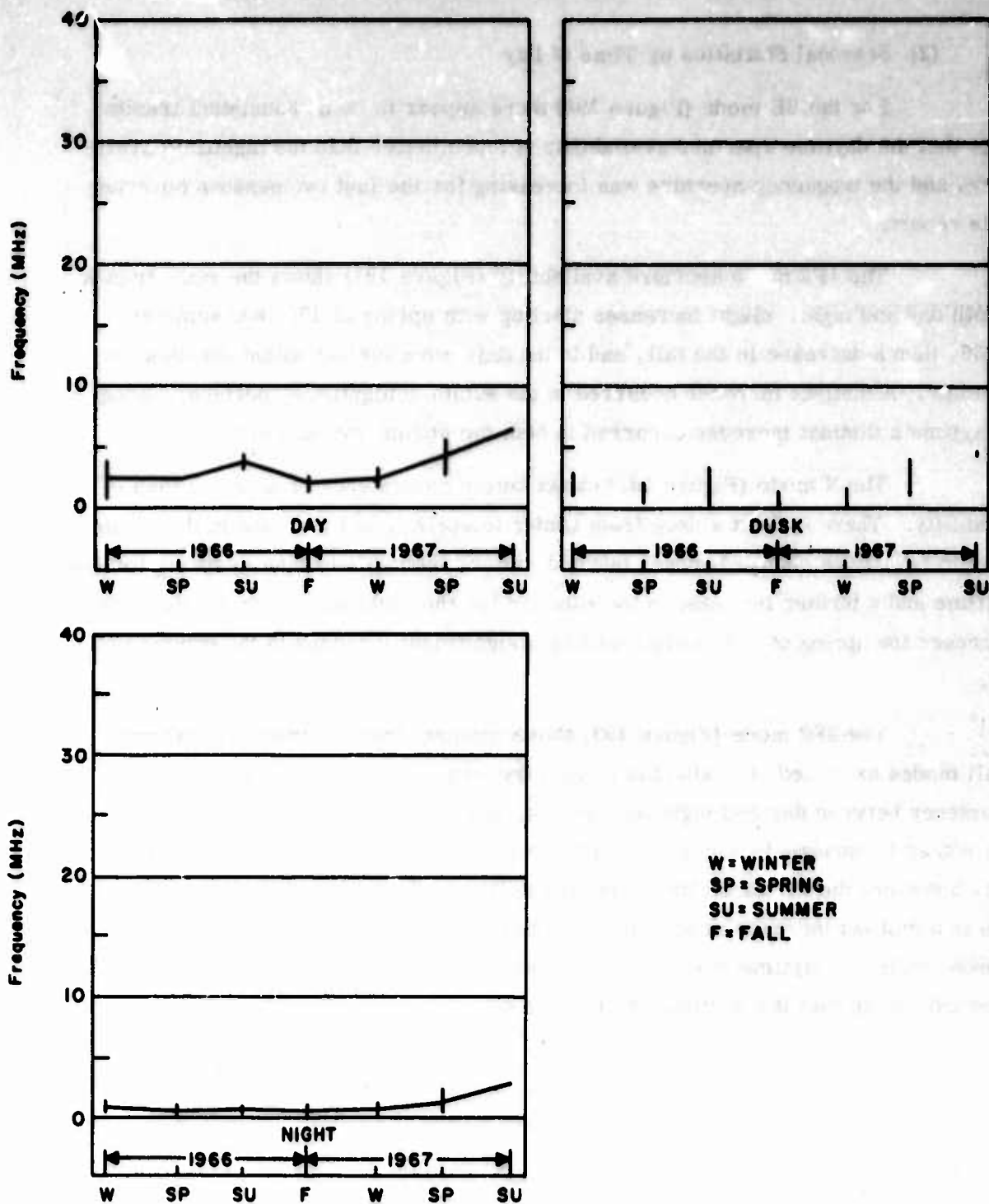


Figure 190. 2E Mode Mean Aperture, Coco Solo Path

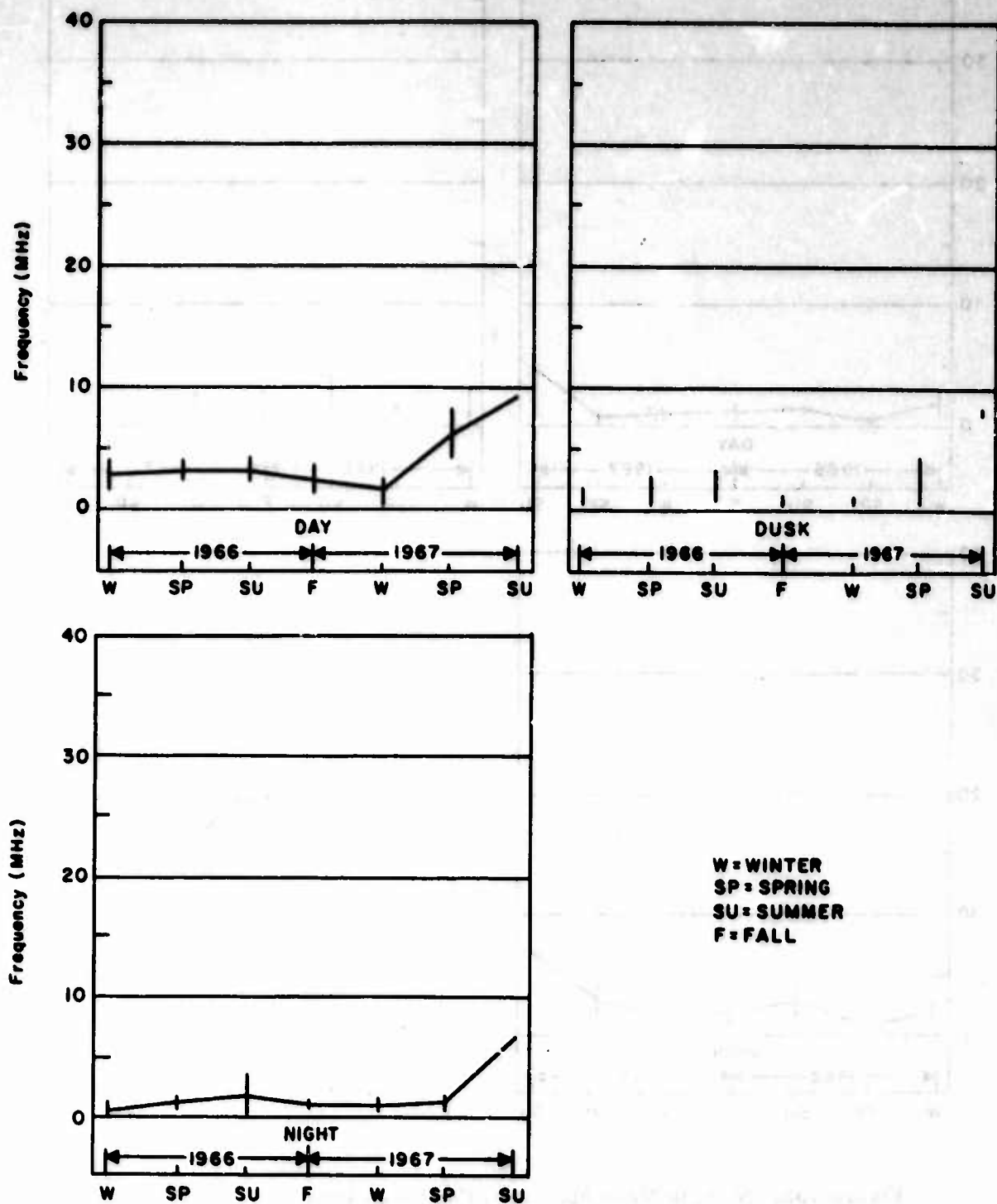


Figure 191. 1F2 Mode Mean Aperture, Coco Solo Path

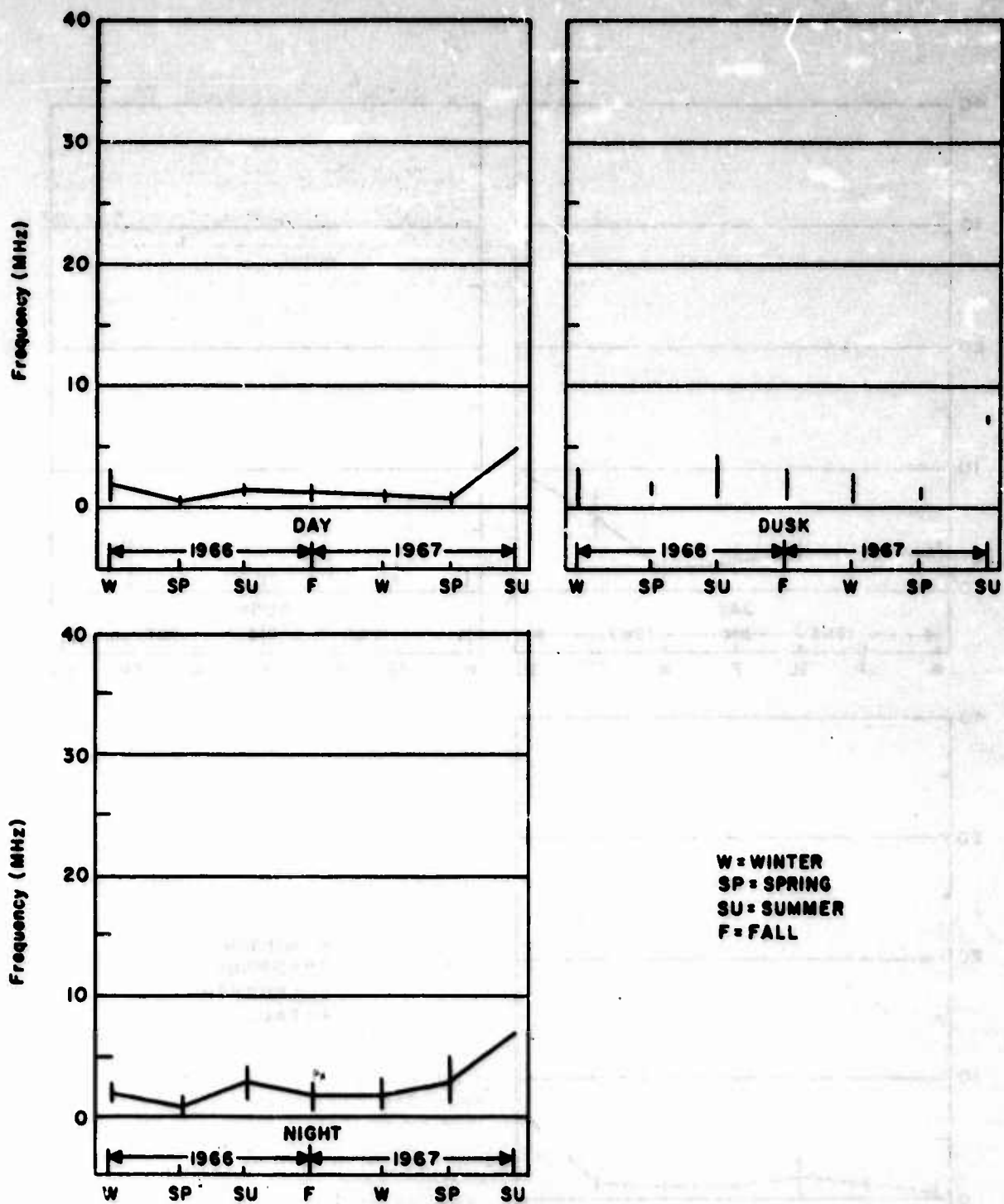


Figure 192. N Mode Mean Aperture, Coco Solo Path

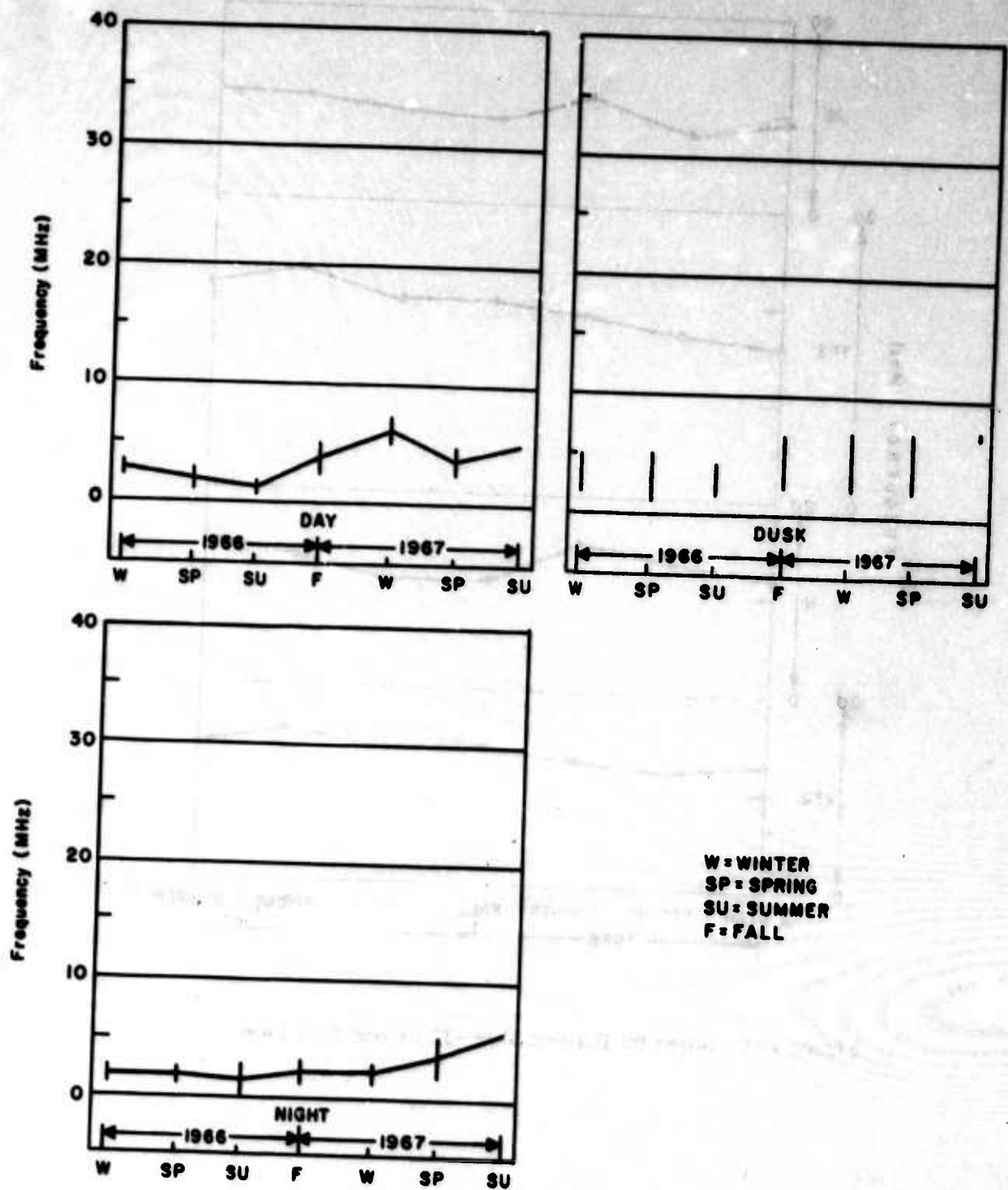


Figure 193. 2F2 Mode Mean Aperture, Coco Solo Path

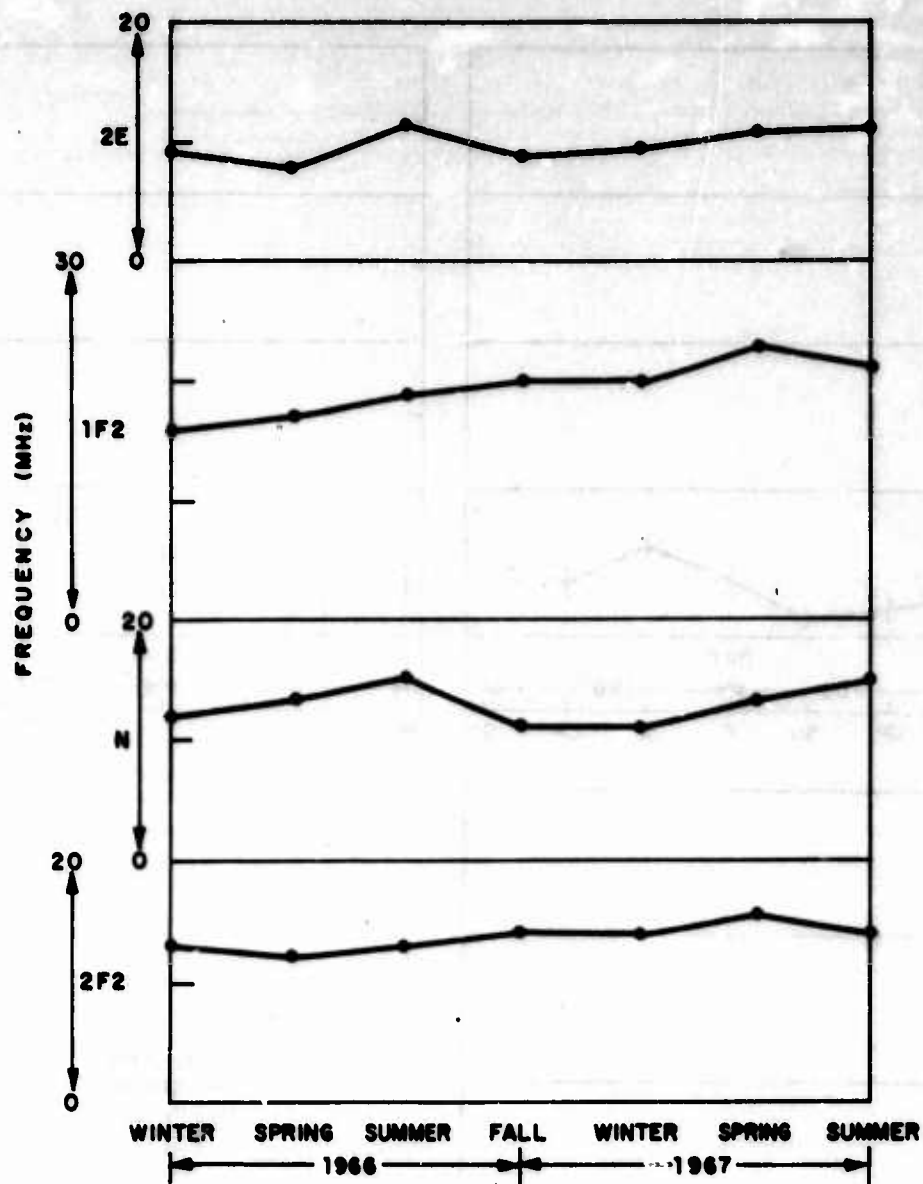


Figure 194. Mean 90 Percent MOF-JF, Coco Solo Path

c. MOF-JF Availability

The order of importance for OHR system design of the results of the mode reliability experiment is (1) the mode availability, (2) the extent of the mode's frequency aperture (if the mode is available) in order to answer the question as to whether the available frequency bandwidth is great enough to fill the needs of an OHR system, and (3) the maximum frequency available. For this case the junction frequency (JF) is used for the 1F2 and the 2F2 modes and the maximum observed frequency (MOF) for the 2E and N modes. The order of observation of the information has been (1) is the mode available, (2) what is its maximum frequency, and (3) after having determined the lowest observed frequency below the maximum frequency that presents an unbroken spectrum, what is the frequency aperture? Both the maximum frequency and lowest frequency have been determined on the basis of an observed mode and, hence, an availability of some frequency spectrum must exist. It is noted that a stronger correlation exists between the MOF or JF and (1) season of the year and (2) sunspot activity than exists for either mode availability or aperture availability and these factors.

(1) Seasonal Means

There is strong evidence in Figure 194 of the steady upward trend that exists as a result of increasing solar sunspot activity during this time. For the 2E and 2F2 modes, the first step, however, is a drop in the 90 percent MOF-JF availability, followed, in the case of the 2E mode, by a step upward in the summer of 1966 while the 2F2 mode makes a steady increase from spring of 1966 through 1967. The 1F2 mode shows a steady increase except that the fall of 1966 and winter of 1967 have identical means and there is a considerable increase from the winter of 1967 to the spring of 1967. The N mode availability goes steadily upward during the winter, spring, and summer of 1966, drops back in the fall of 1966, remains the same for the winter of 1967, and starts its uphill climb again in the spring of 1967.

(2) Seasonal Statistics by Time of Day

For the 2E mode (Figure 195) it is first noted that the daytime MOF's are much higher than the nighttime ones. Second, for daytime the trend is an increase for winter to spring, almost the same for summer, a drop in the fall, and a drop again in winter to a point only slightly greater than the winter of the year before (although a considerable increase in sunspot number has occurred).

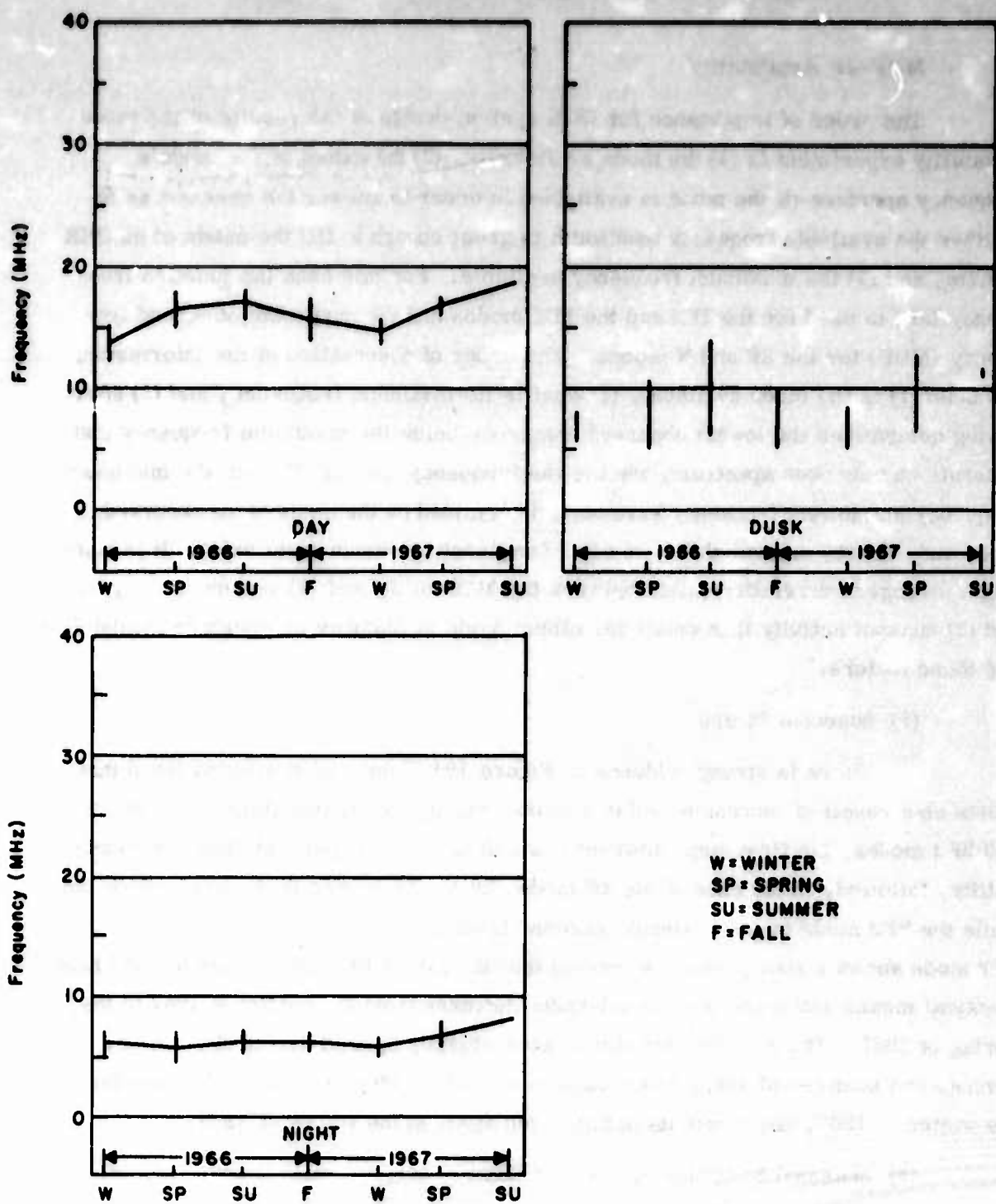


Figure 195. 2E Mode MOF, Cooo Solo Path

The increase to spring and then to summer shows again for 1967. At nighttime the first five seasons shown have very little change, but then an increase occurred in the spring during the winter of 1967, and this is followed by a further increase during the summer.

The 1F2 mode (Figure 196) may be the most important mode for the OHR systems under consideration. This is because of two factors:

1. It almost always has the highest junction frequency or maximum observed frequency, and
2. Since it passes through the highly attenuated portion of the ionosphere only twice instead of four times as for the other dominant modes, its absorption is generally less.

During the daytime both in 1966 and 1967 there is a decrease from winter to spring; however, there is an increase in 1967 from spring to summer compared to 1966 when there was a decrease for the 1F2 mode JF availability.

The N mode (Figure 197) shows nothing spectacular or unusual except in the summer of 1967, when a large increase occurs in the MOF both during the daytime and nighttime.

The results for the 2F2 mode (Figure 198) conform almost exactly to those for the 1F2, but with slightly lower frequencies throughout (as expected).

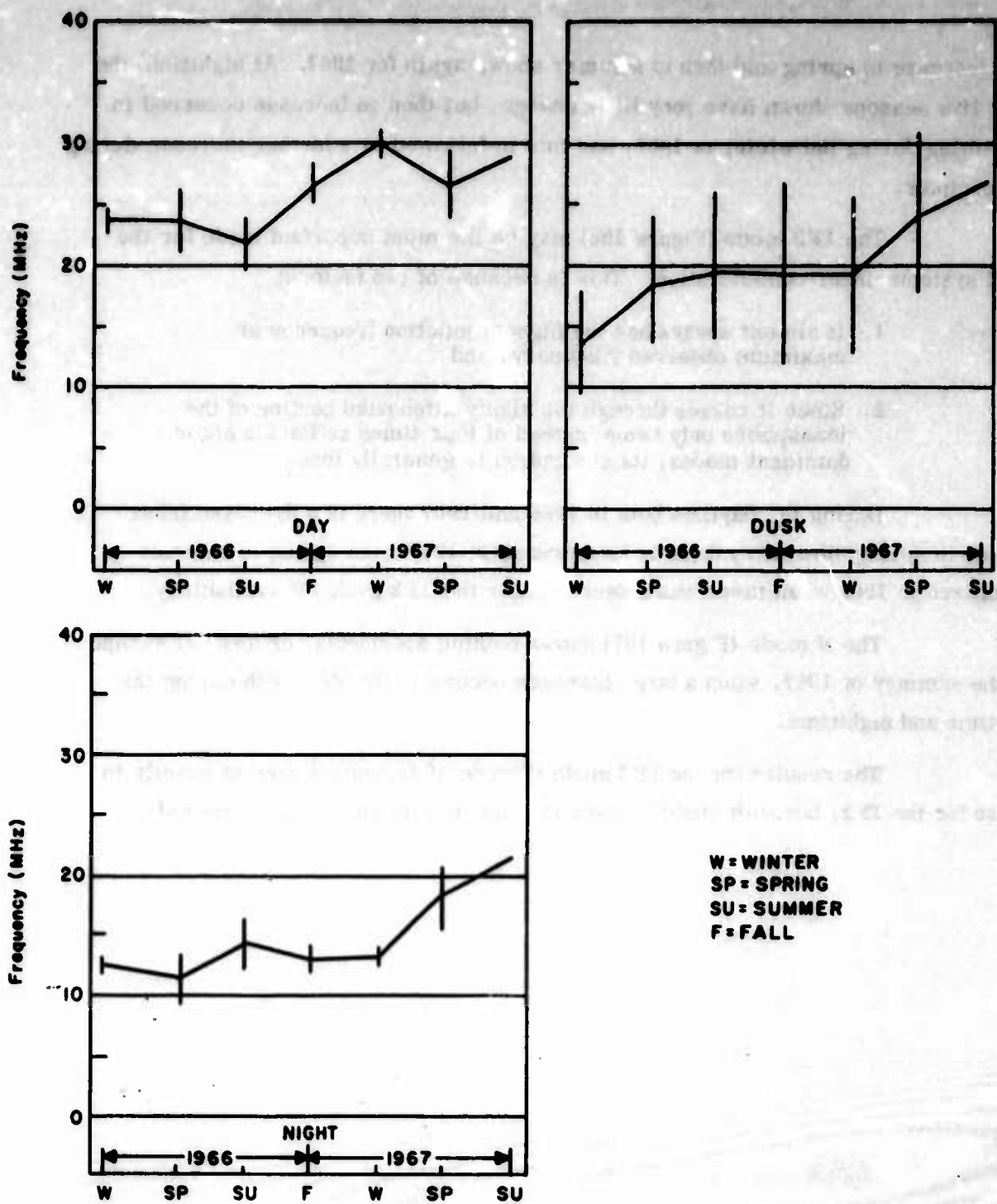


Figure 196. 1F2 Mode JF, Coco Sclo Path

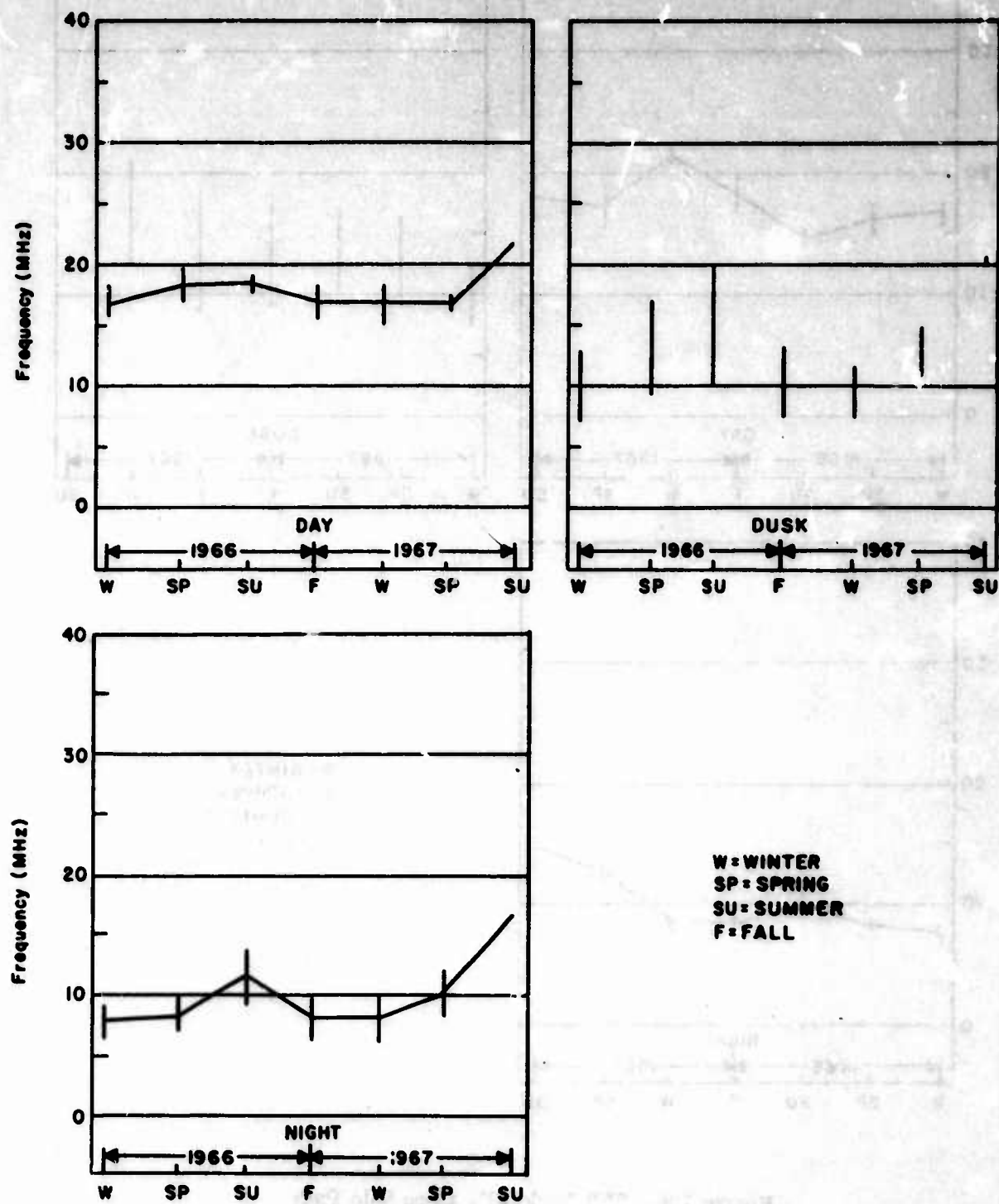


Figure 197. N Mode MOF, Coco Solo Path

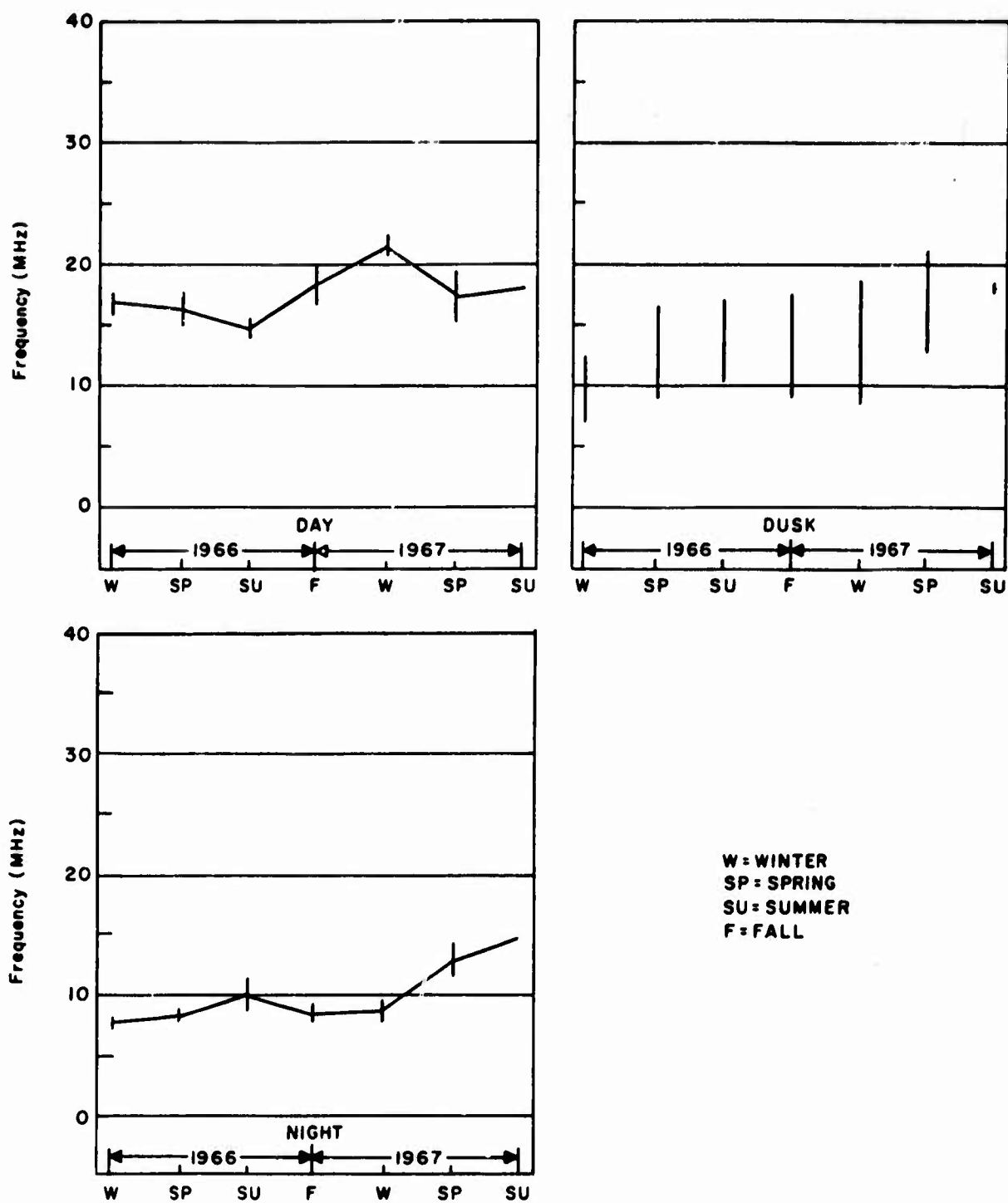


Figure 198. 2F2 Mode JF, Coco Solo Path

11. THE EFFECTS OF SOLAR DISTURBANCES ON PROPAGATION AS OBSERVED OVER THE COCO SOLO PATH

a. Introduction

There are two distinct results of solar disturbances which produce sufficiently large changes in the ionosphere to affect long range ionospherically propagated signals. First, when a solar flare occurs, prompt x-rays and gamma rays are radiated. These intercept the earth approximately 3.5 minutes later and increase the electron density of the ionosphere throughout the portion of the ionosphere that is exposed to the sun. For that portion most nearly facing the sun, the lower ionosphere, or D-layer, appears to be ionized more strongly than the upper ionosphere. On the edges of the exposed portion, where the upper ionosphere receives the direct radiation the longest and receives this quite obliquely, the upper ionosphere remains ionized to a greater extent than the lower ionosphere; thus, the electron densities increase more at midday in the lower than in the upper ionosphere, while immediately before sunrise and immediately after sunset the upper portion increases in electron density more due to a solar disturbance than the lower portion.

The second major effect from solar disturbances results from ionized material that is thrown out from the sun and travels to the earth at a much slower rate, actually reaching the earth sometime on the order of a day to a day and a half after the visual sighting of the flare. This ionized mass, sweeping across the earth, distorts the magnetic field and produces variations in magnetic intensity. These magnetic variations in turn affect the ionosphere, distorting and in extreme cases rather thoroughly mixing it.

Indications of the first effect are given by the optical observation of flares, their intensity, and the area of the sun that they cover. These are cataloged at stations throughout the world. The magnetic disturbances are also observed at various points throughout the world and their average is reported as the planetary three-hour range magnetic index K_p that varies from 0 through 9. Many other effects of solar disturbances are cataloged for special purposes, but flares and K_p 's are fundamental and will be used in the subsequent comparisons. A long term indication of solar activity is given by the value of the 12-month smoothed sunspot number. This in itself is a somewhat awkward tabulation, and not fully representative of the activity of the sun, but it has been in use for about 200 years and undoubtedly will

be retained for many years more. It is also available as a daily number, and as such does indicate solar activity which, in turn, can produce ionospheric disturbances and so will be compared with the propagation results over the indicated path. The two observed items that may most conveniently be correlated with these disturbances are the mode availability and the MOF-JF. To normalize these factors, comparisons are made on the basis of each month as a reference and hourly on the basis of available data. The values of the MOF-JF are given in terms of its standard deviation (σ) referenced to the mean value of the MOF-JF for the month. This serves to normalize all of the data involved regardless of the specific MOF's-JF's as they vary with time of day, season, and sunspot number. Actual values are tabulated in the range from minus three standard deviations to plus three standard deviations; this appears to adequately cover the actual ranges encountered. Availability of the mode can only be given in terms of available or not available. If it is available, the sigma value of the MOF-JF is within the range previously described. If it is not available, the minus five standard deviation point is used as a graphical indicator of this fact. The lack of information for a given time is indicated by the absence of any mark for the time in question.

b. Comparisons of Natural Factors and Recorded Signals

(1) Tabular Presentation

The extent of work required to copy all of the graphical presentations of the natural factors versus mode availability and MOF-JF availability statistics has limited the graphical presentation to that for two months. A simpler, if less spectacular presentation, is provided by Tables XIII through XXX. In these, the information is provided in monthly groupings by date in vertical columns and by hour horizontally. Each day-hour presentation includes in order: (1) mode availability and MOF using a standard deviation scale for the 2E mode, (2) mode availability and JF using a standard deviation scale for the 1F2 mode, (3) K_p , (4) sunspot number, and (5) flares.

The 2E mode is coded as follows:

I--3
-3-J--2
-2-K--1
-1-L- 0
0-M- 1
1-N- 2
2-~~O~~- 3
3-P

The 1F2 mode is coded as follows:

S--3
-3-T--2
-2-U--1
-1-V- 0
0-W- 1
1-X- 2
2-Y- 3
3-Z

K_p values from level 4 through 9 only are included.

Sunspot numbers are designated as follows:

0	0 to 20	5	101 to 120
1	21 to 40	6	121 to 140
2	41 to 60	7	141 to 160
3	61 to 80	8	161 to 180
4	81 to 100	9	above 180

Flares of importance 2, 3, and 4 are so listed.

If an observation was made and no signal seen, the designation in columns 1 and 2 is 0.

(2) Comparison of Natural Factors with Mode Availability and MOF-JF Availability

In the following paragraphs, each table will be discussed in terms of comparison and trends of mode availability and MOF-JF availability with respect to the basic natural factors that have been selected: flares, K_p 's, and sunspot numbers.

In December 1965 (Table XIII) no flares of level 2 or above are noted. The magnetic disturbances (K_p 's), with one exception on 1 December, did not cover a period of ELIDA data collection. In this case the K_p was a level 4 and covered an extensive period that overlapped the records obtained on this date. Nothing particularly unusual was noted in the 1F2 record. A drop to zero availability at 1000 EST cannot definitely be laid to the magnetic disturbance which extended across the quite normal 2E observation.

In January 1966 (Table XIV) a level 2 flare starting about 1900 EST on 17 January was accompanied by a quite high value of the MOF for the 2E mode and followed by a dropout of the 1F2 mode; however, similar values for each mode are noted elsewhere without flares. There is a coincidence, however, in that all three occurred together. Sunspot numbers here are on the order of 60.

In February 1966 (Table XV) the only flares observed that even approximated any importance were those in the early hours of 11 February, but the subsequent recordings of MOF for the 2E and JF for 1F2 do not appear abnormal. Overlaps of a level 4 K_p and recordings on 4 February also failed to make any change in pattern. The magnetic disturbance that overlapped recordings on 22 February in midday appeared to cause no particular changes. Level 5 K_p 's that overlapped the recordings in the early morning hours of 23 February matched dropout of the 2E mode at 0600 EST.

In March 1966 (Table XVI) the first disturbance to match is a level 4 flare in the morning of 16 March. This might have been expected to increase the electron density for that day but, while the record is quite good for both the 2E and the 1F2 modes, it should be noted that on 9 March, for exactly the same period of time, an almost identical record was obtained. On 18 March a level 2 flare also appears ineffective. On 23 March, the magnetic disturbances varying from level 5 to 7 and back to level 4 throughout the day and the level 2 flare at the end of recording time are matched with the dropouts for both the 2E and the 1F2 mode. On 28 March, an all-day set of magnetic disturbances followed by a level 2 flare at the end of the day are matched and followed with some dropouts for both modes.

TABLE XIII
NATURAL FACTORS, DECEMBER 19

	11	30	12	1	12	2	12	3	12	4	12	5	12	6	12	7	12	8	12	9	12	10	12	11	12	12	12	13	12	14	12	15	12	16	12	17	12	18
1			0		0		0		0		0		0		0		0		0		0		0		0		0		0	LV	0		1		1		1	
2			0		0		0		0		0		0		0		0		0		0		0		0		0		0	LU	0		1		1		1	
3			0		0		0		0		0		0		0		0		0		0		0		0		0		0	MU	0		1		1		1	
4			0		0		0		0		0		0		0		0		0		0		0		0		0		0	LV	0		1		1		1	
5			0		0		0		0		0		0		0		0		0		0		0		0		0		0	KU	0		1		1		1	
6			0		0		0		0		0		0		0		0		0		0		0		0		0		0	KV	0		1		1		1	
7			0		0		0		0		0		0		0		0		0		0		0		0		0	LU	0		0		1		1		1	
8			40		0		0		0		0		0		0		0		0		0		0		0		0	LW	0		0		1		1		1	
9			40		0		0		0		0		0		0		0		0		0		0		0		0	LW	0		0		1		1		1	
10		[OX40 MW40 MX40 NX40 40 NX40]	0		0		0		0		0		0		0		0		0		0		0		0		0	OX	0		0		1		1		1	
11	MW40		0		0		0		0		0		0		0		0		0		0		0		0		0	MW	0		0		1		1		41	
12	MX40		0		0		0		0		0		0		0		0		0		0		0		0		0	MW	0		0		1		1		41	
13	NX40		0		0		0		0		0		0		0		0		0		0		0		0		0	NX	0		0		1		1		41	
14	40		0		0		0		0		0		0		0		0		0		0		0		0		0	MW	0		0		1		1		41	
15		NX40	0		0		0		0		0		0		0		0		0		0		0		0		0	MW	0		0		1		1		41	
16		40	0		0		0		0		0		0		0		0		0		0		0		0		0	MW	0		0		1		1		41	
17		40	0		0		0		0		0		0		0		0		0		40		0		0		0	MO	0		0		1		1		1	
18		40	0		0		0		0		0		0		0		0		0		0		0		0		0	SV	0		0		1		1		1	
19		40	0		0		0		0		0		0		0		0		0		40		0		0		0	N	0		0		1		1		1	
20	0		0		0		0		0		0		0		0		0		0		0		0		0		0	M	0		1		1		1		0	
21	0		0		0		0		0		0		0		0		0		0		0		0		0		0	N	0		1		1		1		0	
22	0		0		0		0		0		0		0		0		0		0		0		0		0		0	M	0		1		1		1		0	
23	0		0		0		0		0		0		0		0		0		0		0		0		0		0	M	0		1		1		1		0	
24	0		0		0		0		0		0		0		0		0		0		0		0		0		0	MY	0		1		1		1		0	

TABLE XIII

AL FACTORS, DECEMBER 1965

13	12	14	12	15	12	16	12	17	12	18	12	19	12	20	12	21	12	22	12	23	12	24	12	25	12	26	12	27	12	28	12	29	12	30	12	31
0	0	LV 0	1		1		1	1	0	0	0	KU 0	0	0	0	40	1	1	3	KV 3	2	1														
0	0	LU 0	1		1		1	0	0	0	KO 0	0	0	0	0	41	1	3	KU 3	2	1															
0	0	MU 0	1		1		1	0	0	0	KU 0	0	0	0	0	41	1	3	00 3	2	1															
0	0	LV 0	1		1		1	0	0	0	KU 0	0	0	0	0	41	1	3	KV 3	2	1															
0	0	KU 0	1		1		1	0	0	0	KU 0	0	0	0	0	51	1	3	3	2	1															
0	0	KV 0	1		1		1	0	0	0	KU 0	0	0	0	0	51	OU 1	3	3	2	1															
0	0	0	1		1		1	0	0	0	KV 0	0	0	0	0	51	LV 1	3	3	2	1															
0	0	0	1		1		1	0	0	0	LX 0	0	0	0	0	41	LO 1	3	3	2	1															
0	0	0	1		1		1	0	0	0	0	0	0	0	0	41	MW 1	3	3	2	1															
0	0	0	1		1		1	0	0	0	0	0	0	0	0	41	MO 1	3	3	2	1															
0	0	0	1		1		41	0	0	0	0	0	0	0	0	0	1	OX 1	43	3	2	1														
0	0	0	1		1		41	0	0	0	0	0	0	0	0	0	1	MX 1	43	3	2	1														
0	0	0	1		1		41	0	0	0	0	0	0	0	0	0	1	MW 1	43	3	2	1														
0	0	0	1		1		41	0	0	0	0	0	0	0	0	0	1	MW 1	3	3	2	1														
0	0	0	1		1		41	0	0	0	0	0	0	0	0	0	1	MW 1	3	3	2	1														
0	0	0	1		1		41	0	0	0	0	0	0	0	0	0	1	LW 1	3	3	2	1														
0	0	0	1		1		1	0	0	MW 0	0	0	0	0	0	40	0	41	KV 1	3	3	2	1													
0	0	0	1		1		1	0	0	NV 0	0	0	0	0	0	50	0	41	1	LO 3	3	2	1													
0	M 0	0	1		1		1	0	0	LU 0	0	0	0	0	0	50	0	41	1	L 3	3	2	1													
0	M 0	1	1		1		1	0	40	0	NU 0	0	0	0	0	40	1	1	3	LO 3	2	1														
0	N 0	1	1		1		1	0	40	0	MV 0	0	0	0	0	40	1	1	3	LV 3	2	1														
0	M 0	1	1		1		1	0	40	0	MV 0	0	0	0	0	40	1		3	KV 3	2	1														
0	M 0	1	1		1		1	0	0	0	LV 0	0	0	0	0	40	1	1	3	KV 3	2	1														
0	MV 0	1	1		1		1	0	0	0	KV 0	0	0	0	0	40	1	1	3	KV 3	2	1														

TABLE XIV
NATURAL FACTORS, JANUAR

	1	1	1	2	1	3	1	4	1	5	1	6	1	7	1	8	1	9	1	10	1	11	1	12	1	13	1	14	1	15	1	16	1	17	1
1				0		0	LV 0		0		0		0		0		0		0	LV 0		0		0		1		1		2		2	K0		
2				0		0	KV 0		0		0		0		0		0		0	LU 0		0		0		1		1		2		2	KV		
3				0		0	KV 0		0		0		0		0		0		0	LU 0		0		0		1		1		2		2	KV		
4				0		0	LV 0		0		0		0		0		0		0	LU 0		0		0		1		1		2		2	LV		
5				0		0	KV 0		0		0		0		0		0		0	KU 0		0		0		1		1		2		2	K0		
6				0		0		0	MV 0		0		0		0		0		0		0	K0 0		0		1		1		2		2			
7				0		0		0		0		0		0		0		0		0		0	KV 0		0		1		1		2		23		
8				0		0		0	LO 0		0		0		0		0		0		0		0	LW 0		0		1		1		2		23	
9				0		0		0	MX 0		0		0		0		0		0		0		0		0		1		1		2		2		
10				0		0		0		0		0		0		0		0		0		0		0		0		1		1		2		2	
11				0		0		0	MX 0		0		0		0		0		0		0		0	NX 0		0		1		1		2		2	
12				0		0		0	MW 0		0		0		0		0		0		0		0	MW 0		0		1		1		2		2	
13				0		0		0	MX 0		0		0		0		0		0		0		0	W 0		0		1		1		2		2	
14				0		0		50	MX 0		0		0		0		0		0		0		0	MW 0		0		1		1		2		2	
15				0		0		50		0		0		0		0		0		0		0	0	MW 0		0		1		1		2		2	
16				0		0		50	MW 0		0		0		0		0		0		0		0	MX 0		0		1		1		2		2	
17				0		0		0	LO 0		0		0		0		40		0		0		0	K0 0		0		1		1		2		2	
18				0		0		0		0		0		0		0		40		0	LV 0		0	LV 0		0		1		1		2		2	
19				0		0	LO 0		0		0		0		0		0		40		0	KU 0		0		0		1		1		2		2	
20			0	40		0	KU 0		0		0		0		0		0		0		0		0	MO 0		0		1		1		2		2	
21			0	40		0	MU 0		0		0		0		0		0		0		0		0	LO 0		0		1		1		2		2	
22			0	40		0	NV 0		0		0		0		0		0		0		0		0	LO 0		0		1		1		2		2	
23			0	0		0	NV 0		0		0		0		0		0		0		0		0	MU 0		0		1		1		2		2	
24			0	0		0	MV 0		0		0		0		0		0		0		0		0	MV 0		0		1		1		2		2	

22
 32
 3

TABLE XIV

L FACTORS, JANUARY 1966

14	1 15	1 16	1 17	1 18	1 19	1 20	1 21	1 22	1 23	1 24	1 25	1 26	1 27	1 28	1 29	1 30	1 31
1	1	2	2	K0 3	3	1	2	2	1	2	KV 1	0	0	0	0	1	0
1	1	2	2	KV 3	3	1	2	52	1	2	L0 1	0	0	0	0	1	0
1	1	2	2	KV 3	3	1	2	52	1	2	OV 1	0	0	0	0	1	0
1	1	2	2	LV 3	3	1	2	52	1	2	LV 1	0	0	0	0	1	0
1	1	2	2	K0 3	3	1	2	42	1	2	LU 1	0	0	0	0	1	0
1	1	2	2	3	LU 3	1	2	42	1	2	LU 1	KU 0	0	0	0	1	0
1	1	2	23	3	LV 3	1	2	42	1	2	1	K0 0	0	0	0	1	0
1	1	2	23	3	MW 3	41	42	52	1	2	1	MW 0	0	0	0	1	0
1	1	2	2	3	MX 3	41	42	52	1	2	1	MW 0	0	0	0	1	0
1	1	2	2	3	MX 3	41	42	52	1	2	1	MX 0	0	0	0	1	0
1	1	2	2	3	NX 3	41	2	42	1	42	41	MX40	0	0	0	1	0
1	1	2	2	3	NW 3	41	2	42	1	42	41	MX40	0	0	0	1	0
1	1	2	2	3	MX 3	41	2	42	1	42	41	MX40	0	0	02	1	0
1	1	2	2	3	MX 3	41	52	42	1	2	1	0	0	0	0	1	0
1	1	2	2	3	3	41	52	42	1	2	1	MW 0	0	0	0	1	0
1	1	2	2	3	3	41	52	42	1	2	1	LW 0	0	0	0	1	0
1	1	2	2	3	3	1	2	42	1	2	1	K040	0	40	0	1	0
1	1	2	2	3	3	1	2	42	1	NV 2	1	K 40	0	40	0	1	0
1	1	2	2	3	3	1	2	42	1	NV 2	1	40	0	40	0	1	0
1	2	2	2	L0 32	3	1	2	42	1	42	MV 1	0	0	0	0	1	0
1	2	2	2	L0 3	3	1	2	42	1	42	MU 1	0	0	0	0	1	0
1	2	2	2	3	3	1	2	42	1	42	M 1	0	0	0	0	1	0
1	2	2	2	LU 3	3	1	2	2	1	2	LV 1	0	0	0	0	1	0
1	2	2	2	LU 3	3	1	2	2	1	2	LV 1	0	0	0	0	1	0

NATURAL FACTORS, FEBR

	2	1	2	2	2	3	2	4	2	5	2	6	2	7	2	8	2	9	2	10	2	11	2	12	2	13	2	14	2	15	1		
1		0		0		1		0		0		0		0	KU	0		0		0		0		0		0		0		0			
2		0		0		1		0		0		0		0	KU	0		0		0		0		0		0		0		0			
3		0		0		1		0		0		0		0	KU	0		0		0		0		0		0		0		0			
4		0		02		1		0		0		0		0	KU	0		0		0		02		0		0		0		0			
5		0		0		1		0		40		0		0		0		0		02		02		0		0		0		0			
6		0		0		1	KU	0		40		0		0		0	KU	0		0		0		0		0		0		0	KU		
7		0		0		1	KV	0		40		0		0		0	KV	0		0		0		0		0		0		0	KV		
8		0		0		41	LW	0		40		0		0		0	LW	0		0		0		0		0		0		0	LW		
9		0		0		41	MW	0		40		0		0		0	MW	0		0		MW	0		0		0		0		0	MW	
10		0		0		41	NW	0		40		0		0		0	MW	0		02		MW	0		0		0		0		0	MW	
11		0		0		1	MW	0		0		0		0		0	MW	0		02		MW	0		0		0		0		0	MW	
12		0		0		1	MW	0		0		0		0		0	MX	0		02		NW	0		0		0		0		0	MW	
13		0		0		1	MW	0		0		0		0		0	YX	0		02		NX	0		0		0		0		0	MW	
14		0		0		41	MW	0		40		0		0		0	NW	0		02		NX	0		0		0		0		0	MW	
15		0		0		41	NV	0		40		0		0		0	MW	0		02		MW	0		0		0		0		0	MW	
16		0		0		41	LW	0		40		0		0		0	MW	0		02		0		0		0		0		0		0	MW
17		0		0		1	KW40			0		0		0		0	LV	0		02		0		0		0		0		0		0	LW
18		0		0		1	LW40			0		0	K0	0		0	L0	0		02		0		0		0		0		0		0	MW
19		0		0		1	40			0		0	K0	0		0	0			02		0		0		0	0V	0		0		0	
20		0		1		0		0		40		0	LU	0		0	0			02		0		0		0	KU	0		0		0	
21		0		1		0		0		40		0	KU	0		0	0			02		0		0		0	LU	0		0		0	
22		0		1		0		0		40		0		0		0	0			0		0		0		0	M0	0		0		0	
23		0		1		0		0		0		0	LU	0		0	0			0		0		0		0	KU	0		0		0	
24		0		1		0		0		0		0	KU	0		0	0			0		0		0		0	KU	0		0		0	

TABLE XV

TURAL FACTORS, FEBRUARY 1966

11	2 12	2 13	2 14	2 15	2 16	2 17	2 18	2 19	2 20	2 21	2 22	2 23	2 24	2 25	2 26	2 27	2 28
0	0	0	0	0	0	0	1	1	41	2	2	92	42	KU 1	1	1	1
0	0	0	0	0	0	0	1	1	41	2	2	92	42	KU 1	1	1	1
0	0	0	0	0	0	0	1	1	41	2	2	92	42	KU 1	1	1	1
02	0	0	0	0	0	0	1	1	41	2	2	92	42	KU 1	1	1	1
02	0	0	0	0	0	0	1	1	41	2	2	92	42	KU 1	1	1	1
0	0	0	0	0	KU 0	0	1	1	41	2	2	92	42	KU 1	1	1	1
0	0	0	0	0	KU 0	0	1	1	41	2	2	92	42	KU 1	1	1	1
0	0	0	0	0	LW 0	0	1	1	41	2	2	92	42	KU 1	1	1	1
0	0	0	0	0	MW 0	LW 0	MW 1	1	1	41	2	92	42	KU 1	1	1	1
0	0	0	0	0	MW 0	MW 0	MW 1	1	1	41	2	92	42	KU 1	1	1	1
0	0	0	0	0	MW 0	MW 0	MW 1	41	1	41	2	92	42	KU 1	1	1	1
0	0	0	0	0	MW 0	MW 0	MW 1	41	1	41	2	92	42	KU 1	1	1	1
0	0	0	0	0	MW 0	MW 0	MW 1	41	1	41	2	92	42	KU 1	1	1	1
0	0	0	0	0	MW 0	MW 0	MW 1	41	1	41	2	92	42	KU 1	1	1	1
0	0	0	0	0	MW 0	MW 0	MW 1	41	1	41	2	92	42	KU 1	1	1	1
0	0	0	0	0	MW 0	MW 0	MW 1	41	1	41	2	92	42	KU 1	1	1	1
0	0	0	0	0	MW 0	MW 0	MW 1	41	1	41	2	92	42	KU 1	1	1	1
0	0	0	0	0	LW 0	0	1	1	1	2	42	MW 2	2	1	1	1	1
0	0	0	0	0	MW 0	0	1	1	1	2	42	2	MW 2	1	1	1	1
0	0	0	0	0	0	0	1	1	1	2	42	2	MV 2	1	1	1	1
0	0	0	0	0	0	0	1	1	41	2	2	2	2	KU 1	41	1	1
0	0	0	0	0	0	0	1	1	41	2	2	2	2	KU 1	41	1	1
0	0	0	0	0	0	0	1	1	41	2	2	2	2	KU 1	41	1	1
0	0	0	0	0	0	0	1	1	41	2	2	92	42	LU 1	1	1	1
0	0	0	0	0	0	0	1	1	41	2	2	92	42	LU 1	1	1	1

NATURAL FACTORS, MA

	Date																																				
	2	20	3	1	3	2	3	3	3	4	3	5	3	6	3	7	3	8	3	9	3	10	3	11	3	12	3	13	3	14	3	15	3	16	3	17	3
1			KU	1		0		0		0		0		0		0	KU	0		0		0		0		0		0		70	J0	0		1		2	
2			KU	1		0		0		0		0		0		0	OU	0		0		0		0		0		0		70	J?	0		1		2	
3			OU	1		0		0		0		0		0		0	KU	0		0		0		0		0		0		70	OT	0		1		2	
4			OU	1		0		0		0		0		0		0	KU	0		0		0		0		0		0		70	OT	0		1		2	
5			KU	1		0		40		0		0		0		0	OU	0	OU	0		0		0		0		0		40	KY	0		14		2	
6			1	KU	0		40		0		0		0		0		OU	0	KU	0		0		0		0		0		40	KU	0		JU	1		2
7			1	KW	0		40		0		0		0		0		0	K0	0		0		0		0		0		40		0		KV	1		2	
8			1	LV	0		0		0		0		0		0		0	LW	0		0		0		0		0		90		0		LV	1		2	
9			1	MW	0		0	MV	0		0		0		0		0	MW	0	MW	0	MV	0		0		0		90		0		MW	1	MW	2	MW
10			1	MW	0		0	MV	0		0		0		0		0	MV	0	MW	0	MW	0		0		0		90		0		MW	1	MW	2	MW
11			1	MW	0		0	MW	0		0		0		0		0	MW	0	MW	0	MW	0		0		0		90		0		MW	1	MW	2	MW
12			1	MW	0		0	MW	0		0		0		0		0	PW	0	MW	0	MW	0		0		0		90		02		MW	1	MW	2	MW
13			1	MW	0		MV	0	MW	0		0		0		0		M4	0	MW	0	MW	0		0		0		90		0		MW	1	MW	2	MW
14			1	MW	0		MW	0	MW	0		0		0		0		MW	0	MX	0	MW	0		0		0		0		0		MW	1	MV	2	MX
15			1	MW	0		M0	0	MW	0		0		0		0		MW	0	LX	0	MW	0		0		0		0		0		MW	1	MW	2	MW
16			1	M0	0		L0	0	MX	0		0		0		0		MW	0	LW	0	MW	0		0		0		0		0		MW	1	MW	2	M0
17			1	LW	0		0	40		0		0		0		0		LW	0	0	LW	0		0		0		40		0		0		LW	1		2
18			1		0		0	40		0		0		0		0		K0	0	0	MW	0		0		0		40		KU	0	0	KW	1		2	
19			1		0		0	40		0		0		0		0		00	0	0	0	0		0		0		40		00	0	0		1		2	
20		1		0	0		0	0		0		0		0		0		00	0	0	0	40		0		0		40		00	0	1		2		2	
21		1		0	0		0	0		0		0		0		0		OU	0	0	0	40		0		0		40		OU	0	1		2		2	
22		1		0	0		0	0		0		0		0		0		LU	0	0	0	40		0		0		40		OU	0	1		2		2	
23		1		0	0		0	0		0		0		0		0		K0	0	0	0	0		0		0		70		KY	0	1		2		2	
24		1		0	0		0	0		0		0		0		0		KU	0	0	0	0		0		0		70		J0	0	1		2		2	

FACTORS, MARCH 1966

5	3 16	3 17	3 18	3 19	3 20	3 21	3 22	3 23	3 24	3 25	3 26	3 27	3 28	3 29	3 30	3 31	
1	2	2		1	2F	2	2	OV 2	2	1	1	0	0	0	OU91	2	2
1	2	2		2	32	2	2	KV 2	92	1	1	0	0	40	OU 1	2	2
1	2	2		3	32	2	2	00 2	92	1	1	0	0	40	00 1	2	2
1	2	2		4	32	2	2	OU 2	92	1	1	0	02	40	00 1	2	22
14	2	2		5	432	2	22	OU 2	72	1	1	0	0	40	00 1	2	2
JU 1	2	2		6	432	2	22	JU 2	0072	1	1	0	0	40	00 1	KU 2	2
KV 1	2	2		7	432	2	2	22	KV72	1	1	0	0	40	1	LV 2	2
LV 1	2	2		8	32	2	2	2	LV72	1	1	60	0	90	1	OW 2	2
MW 1	MW 2	MW 22		9	32	2	2	2	MV72	MW 1	1	60	0	90	1	W 2	MV 2
MW 1	MW 2	MW 2		10	32	2	2	2	MW72	MX 1	MW 1	60	0	90	1	MW 2	MV 2
MW 1	MW 2	MW 2		11	32	2	2	2	MW62	MW 1	MW41	40	0	90	1	2	MV 2
MW 1	MW 2	MW 2		12	32	2	2	2	MX62	MX 1	MX41	40	0	90	1	2	MW 2
MW 1	MX 2	MW 2		13	32	2	2	2	MX62	MX 1	MX41	40	0	90	1	2	MW 2
MW 1	MV 2	MX 2		14	932	2	2	2	MV72	W 1	MX 1	0	0	70	1	PX 2	MX 2
MW 1	MW 2	MW 2		15	932	2	2	2	MV72	MO 1	MX 1	0	0	70	1	PX 2	KW 2
MW 1	MW 2	MO 2		16	932	2	2	2	MO72	MX 1	MX 1	0	0	70	1	MX 2	MX 2
LW 1	2	2		17	932	2	LW 2	2	L042	1	1	0	0	90	1	LW 2	2
KW 1	2	2		18	9J2	2	LW 2	2	KV42	1	1	0	0	K090	1	LW 2	2
1	2	2		19	932	2	MV 2	2	422	1	1	0	0	L090	1	2	2
2	2	3		20	22	42	V 2	2	1	1	02	0	0	MV41	22	2	3
2	2	3		21	2	42	OV 2	2	1	1	0	0	0	KU412	2	2	3
2	2	32		22	2	42	JV 2	2	13	14	0	0	0	OU41	2	2	3
2	2	27		23	2	2	OV 2	2	13	14	0	0	0	OU91	2	2	3
2	2	27		24	2	2	LU 2	2	1	1	0	0	02	OU91	2	2	3

In April (Table XVII) a K_p of 4 on 1 April is matched by a dropout of the 1F2 mode at 1100 EST. A flare occurring shortly after noon during the time of the same level of K_p is now matched by a quick increase of the 1F2 that holds until the end of the recording time for the day at about 1600 EST. The only other match between the recordings and natural factors occurs on 15 April when an early morning flare is followed by observations that start at 0800 EST and show no abnormal characteristics.

In May (Table XVIII) an importance 2 flare on the morning of the 2nd preceding recording which show nothing distinctive for the 1F2, but there was a higher-than-normal 2E mode a few hours later. Again, it should be noted that at several other times in the same month similar slightly higher-than-normal 2E mode values show up without flares. The next coincidence of recordings and natural factors occurred on 26 May when K_p 's ranging from 4 to 7 appear to have no effect on either mode. On 31 May the K_p values of 5 in the late afternoon are followed by higher-than-normal nighttime 2E mode MOF's.

In June 1966 (Table XIX) the first occurrence of a natural factor that was coincident with a data collection period is on the 23rd. Here, K_p 's of level 4 apparently have had no effect of importance. Two flares shortly before noon on 27 June and again at about sunset are followed by improved 1F2 level and then by a drop, respectively. A somewhat clean-cut termination of the 2E mode at sunset also occurs.

A flare occurring on the morning of 1 July appears to have had no effect on either mode (Table XX). A magnetic disturbance on the morning of 8 July is accompanied by a dropout of the E, but a level 2 flare during the forenoon appears to have no effect. The magnetic disturbance on 27 July has also had no effect.

In August 1966 (Table XXI) a magnetic disturbance of K_p 4 on the 5th is accompanied by a 2E mode dropout and the flare during the forenoon is, in turn, accompanied by a 1F2 mode dropout. The fact that the 2E mode had come back up and the 1F2 mode has dropped at this point may be significant. A K_p of 4 on 9 August appears to have made no significant change. A flare on 16 August is accompanied by a slight drop in the 1F2 mode. The magnetic disturbance that covers midnight between 18 and 19 August is followed by a slight drop. The level 4 magnetic disturbance at the same time is followed by an immediate dropout of the 2E mode and later of the 1F2. The same level of magnetic disturbance showed no effect at 1100 to 1300 EST. Regrettably, other natural occurrences during the remainder of the month were not matched by any records.

In September 1966 (Table XXII) no matching records exist until the afternoon of the 15th when a level 4 magnetic disturbance apparently has no effect; however, on 19 September a disturbance of the same level was followed by a dropout of both the 1F2 and the 2E modes. A flare at about noon on 20 September followed a magnetic disturbance. The flare is accompanied by a dropout of the 2E mode and no change in the 1F2 mode. A flare and a magnetic disturbance at noon on 23 September, however, surprisingly shows no effect on either mode. The magnetic disturbances that exist on 26 September are accompanied by one dropout of the 1F2 mode and by a long dropout of the 2E during the evening that strangely enough is followed by an unusually high level of 2E mode at night. The magnetic disturbance on 28 September apparently caused no effect; similarly on the 29th, but on 30 September there is a dropout of the 2E mode.

In October 1966 (Figure 199 and Table XXIII) the magnetic disturbances on 4 and 5 October are accompanied by dropouts of both the 1F2 and the 2E modes with the exception that the 2E mode did not drop out on the 5th. On 6 October the combination of the magnetic disturbance and the flare in the vicinity of the noon hours has caused very little variation in the normal signal. Magnetic disturbances on 24 and 25 October and a flare on the 24th are noted. The only significant result, however, is several dropouts of the 1F2 mode on the 24th and again on the 25th, but a magnetic disturbance on the 26th does not match any dropouts. On 31 October, however, the 1F2 drops out for a combination of the magnetic disturbance and the flare in the early afternoon. Possibly the flare may have held up the 2E, offsetting the effect of the magnetic disturbance.

In November 1966 (Table XXIV) dropouts exist for the 1F2 mode accompanying a level 5 K_p on the first. It is questionable whether the zero value of the 2E at this point is a normal nighttime lack of 2E or a result of the magnetic disturbance. The effect of the flare of level of importance 2 is somehow lost in the picture. The magnetic disturbances on 3 November are followed by several dropouts of both modes. On 14 November an importance 3 flare is followed by a dropout of the 1F2 and then by a reasonably high level of both modes. The flare on 17 November is accompanied by a drop of the 1F2 and a complete dropout of the 2E mode. Magnetic disturbances on the 28th were preceded by a 1F2 mode dropout and followed by 2E; while on the 30th, the 2E mode dropout occurred soon after the disturbance and later returned to normal.

NATURAL FACTORS, APRIL

	4	1	4	2	4	3	4	4	4	9	4	6		4	7	4	8	4	9	4	10	4	11	4	12	4	13	4	14	4	15	4	16	
1		3		92		3		3		2		2		4		3		3		2		1		1		1		1		1		1		
2		3		2		3		3		2		2		2		3		3		2		1		1		1		1		1		1		
3		3		2		3		32		2		2		3		3		3		2		1		1		1		1		1		1		
4		3		2		3		3		2		2		4		3		3		2		1		1		1		1		1		1		
5		3		2		3		3		2		2		5		3		32		2		1		1		1		1		1		1		
6		3		2		3		3		2		2		6		3		3		2		1		12		1		1		13		1		
7		3		2		3		3		2		2		7		3		3		2		1		1		1		1		1		1		
8		43		2		3		3		2		2		8		3		3		2		1		1		1		1		1		1		
9	LV43		2		3		3		2		2			9	MV	3		3		2		1	LV	1		MV	1		1		LV	1		
10	MV43		2		3		3		2	MW	2			10	MV	3		MV	3		2		1	MV	1		MV	1		MV	1		1	
11	M043		2		3		3		2	MW	2			11	MV	3		MV	3		2		1	MV	1		MV	1		MV	1		1	
12	M43		2		3		3		2	MW	2			12		3		MV	3		2		1	MW	1		MW	1		MW	1		1	
13	X432		2		3		3		2	MX	2			13		3		MW	3		2		1	MW	1		MW	1		MX	1		1	
14	MX432		2		3		3		2	MX	2			14		3		MW	3		2		1	MW	1		MW	1		MX	1		1	
15	WX43		2		3		3		2	MX	2			15		MV	3		MV	3		2		1	MW	1		MW	1		MX	1		1
16	LX43		2		3		3		2	MW	2			16		LV	3		LV	3		2		1	MX	1		MW	1		LX	1		1
17	93		2		3		3		2		2			17		3		3		2		1		1		1		1		1		1		
18	93		2		3		3		2		2			18		3		3		2		1		1		1		1		1		1		
19	90		2		3		JW	3		2		2		19		3		3		2		1		1		1		1		1		1		
20	42		3		3		JV	2		2		3		20		93		22		1		1		1		1		1		1		1		
21	422		3		3		JU	2		2		3		21		93		2		1		1		1		1		1		1		1		
22	42		3		3		JT	2		2		3		22		93		2		1		1		1		1		1		1		1		
23	92		3		3		OT	2		2		3		23		3		2		1		1		1		1		1		1		1		
24	92		3		3		OT	2		2		3		24		3		2		1		1		1		1		1		1		1		

TABLE XVII

NATURAL FACTORS, APRIL 1966

4 11	4 12	4 13	4 14	4 15	4 16	4 17	4 18	4 19	4 20	4 21	4 22	4 23	4 24	4 25	4 26	4 27	4 28	4 29	4 30
1	1	1	1	1	1	2	2	1	JU 1	2	2	43	2	2	2	JU 2	2	2	2
1	1	1	1	1	1	2	2	1	OU 1	2	2	43	2	2	2	OU 2	2	2	2
1	1	1	1	1	1	2	2	1	JU 1	2	2	43	2	2	2	JU 2	2	2	2
1	1	1	1	1	1	22	2	1	OT 1	2	2	43	2	2	2	OT 2	OU 2	2	2
1	1	1	1	1	1	2	2	1	OU 1	2	2	3	2	2	2	OT 2	OU 2	2	2
12	1	1	1	13	1	2	2	1	JV 1	JU 2	2	3	2	2	2	2	JV 2	2	2
1	1	1	1	1	1	2	2	1	1	KW 2	2	3	2	2	2	2	OW 2	2	2
1	1	1	1	1	1	2	2	1	1	LW 2	2	3	2	2	2	2	LV 2	2	2
V 1	MV 1	1	1	LV 1	1	2	MV 2	1	1	MW 2	MU 2	3	2	MW 2	2	2	MV 2	MV 2	2
IV 1	MV 1	MV 1	1	MV 1	1	2	MW 2	1	1	MW 2	MU 2	3	2	MV 2	2	2	MV 2	MV 2	2
IV 1	MV 1	MV 1	MV 1	MV 1	1	2	MX 2	1	1	MW 2	MV 2	3	2	MV 2	2	2	MW 2	MV 2	2
IV 1	MW 1	MW 1	MW 1	MW 1	1	2	MX 2	1	1	MW 2	2	3	2	MW 2	2	2	MW 2	MW 2	2
IV 1	MW 1	MX 1	1	MW 1	1	2	MW 2	1	1	MX 2	2	3	2	MX 2	2	2	MW 2	MW 2	2
IV 1	MW 1	MX 1	MW 1	MW 1	1	2	MW 2	1	1	MX 2	MV 2	3	2	MX 2	2	2	MW 2	MW 2	2
IV 1	MW 1	MX 1	LW 1	MW 1	1	2	MW 2	1	1	MX 2	MW 2	3	2	MX 2	2	2	MW 2	MW 2	2
IX 1	MW 1	LX 1	LW 1	1	1	2	LW 2	1	1	LX 2	LW 2	3	2	2	LW 2	2	LW 2	2	2
1	1	1	1	1	1	2	2	1	1	LX 2	2	3	2	2	LX 2	2	LW 2	2	2
1	1	1	1	1	1	2	2	MX 1	1	LX 2	2	3	2	2	MX 2	2	2	2	2
1	1	1	1	1	1	2	2	MX 1	1	2	2	3	2	2	LX 2	2	2	2	2
1	1	1	1	1	2	2	2	1	LW 1	2	2	43	2	2	2	MW 2	2	2	2
1	1	1	1	1	2	2	2	1	OU 1	2	2	43	2	2	2	LV 2	2	2	2
1	1	1	1	1	2	2	2	1	OU 1	2	2	43	2	2	2	JU 2	2	2	2
1	1	1	1	1	2	2	2	1	OU 1	2	2	43	2	2	2	JU 2	2	2	2
1	1	1	1	1	2	2	2	1	1	OU 2	2	43	2	2	2	JU 2	2	2	2

TABLE XVIII

NATURAL FACTORS, MAY 19

	1	2	3	4	5	6	7	8	9	10	11	12	13	14	15	16	17	18
1	2	2	2	LU 3	1	1	0	0	0	0	KU 0	0	1	2	2	2	1	OV 1
2	2	2	2	JU 3	1	1	0	0	0	0	OU 0	0	1	2	2	2	1	OV 1
3	2	2	2	OT 3	1	1	0	0	0	0	LU 0	0	1	2	2	2	1	OV 1
4	2	22	2	OT 3	OT 1	1	0	0	0	0	LU 0	0	1	2	2	2	1	OU 1
5	2	2	2	OT 3	JT 1	1	0	0	0	0	LU 0	LU 0	1	2	2	2	1	KU 1
6	2	2	2	3	LV 1	1	0	0	0	0	0	MV 0	1	2	2	2	1	1
7	2	2	2	3	LW 1	1	0	0	0	0	0	NV 0	1	2	2	2	1	1
8	2	LV 2	2	3	LV 1	LV 1	0	0	LV 0	0	0	NV 0	LV 1	2	2	MW 2	1	1
9	2	MV 2	2	3	LV 1	MV 1	0	0	LV 0	0	0	MV 0	LV 1	2	2	NW 2	1	1
10	2	MW 2	2	3	MV 1	LV 1	0	0	MV 0	0	0	MV 0	LV 1	2	2	MV 2	1	1
11	2	MW 2	2	3	MW 1	MV 1	0	0	MV 0	0	0	MW 0	MV 1	2	2	MW 2	1	1
12	2	NX 2	2	3	NW 1	MV 1	0	0	NX 0	0	0	MW 0	MV 1	2	2	MW 2	1	1
13	2	NX 2	2	3	NX 1	MW 1	0	0	LW 0	0	0	LX 0	MV 1	2	2	MW 2	1	1
14	2	MW 2	2	3	LX 1	MW 1	0	0	LW 0	0	0	LX 0	MV 1	2	2	MW 2	1	1
15	2	LW 2	2	3	LX 1	1	0	0	NW 0	0	0	LX 0	LW 1	2	2	NW 2	1	1
16	2	2	2	3	LX 1	1	0	0	0	LW 0	0	LX 0	1	2	2	2	MW 1	1
17	2	2	LW 2	3	LW 1	1	0	0	0	LW 0	40	LX 0	1	2	2	2	LW 1	1
18	2	2	KV 2	3	1	1	0	0	0	LW 0	40	0	1	2	2	2	KX 1	1
19	2	2	KV 2	3	1	1	0	0	0	NX 0	40	0	1	2	2	2	JW 1	1
20	2	2	KV 3	1	1	0	0	0	0	NW 0	0	1	2	2	2	1	KW 1	1
21	2	2	0 3	1	1	0	0	0	0	NV 0	0	1	2	2	2	1	LV 1	1
22	2	2	OU 3	1	1	0	0	0	0	NU 0	0	1	2	2	2	1	OV 1	1
23	2	2	3	1	1	0	0	0	0	MU 0	0	1	2	2	2	1	OV 1	1
24	2	2	OU 3	1	1	0	0	0	0	LU 0	0	1	2	2	2	1	OV 1	1

TABLE XVIII

L FACTORS, MAY 1966

	5 15	5 16	5 17	5 18	5 19	5 20	5 21	5 22	5 23	5 24	5 25	5 26	5 27	5 28	5 29	5 30	5 31
	2	2	1	OV 1	1	2	4	3	3	3	KU 3	3	3	3	1	2	92
	2	2	1	OV 1	1	2	4	3	3	3	KU 3	43	3	3	1	2	92
	2	2	1	OV 1	1	2	4	3	3	3	JU 3	43	3	3	1	2	92
	2	2	1	OU 1	1	2	4	3	3	3	JU 3	43	3	3	1	2	92
	2	2	1	KU 1	JU 1	2	4	3	3	3	OU 3	73	3	3	1	2	42
	2	2	1	1	JV 1	2	4	3	3	3	3	73	3	3	1	2	42
	2	2	1	1	LV 1	2	4	3	3	3	32	LU73	3	3	1	2	42
	2	MW 2	1	1	LW 1	MV 2	4	3	LW 3	3	3	LU73	LU 3	3	1	2	42
	2	NW 2	1	1	LW 1	MW 2	4	3	LV 3	3	3	LV73	MW 3	3	1	2	42
	2	MV 2	1	1	LV 1	MW 2	4	3	NV 3	3	3	LW73	MW 3	3	1	2	42
	2	MW 2	1	1	MV 1	MW 2	4	3	NW 3	3	3	63	MW 3	32	1	2	62
	2	MW 2	1	1	NW 1	MX 2	4	3	NW 3	3	3	MV63	NW 3	32	1	2	62
	2	MW 2	1	1	MX 1	NX 2	4	3	MX 3	3	3	MW63	NX 3	32	1	2	62
	2	MW 2	1	1	MW 1	NX 2	4	3	MX 3	3	3	MX73	3	3	1	2	62
	2	NW 2	1	1	LW 1	NX 2	4	3	NX 3	3	3	MW73	3	3	1	2	62
	2	2	MW 1	1	MW 1	2	4	3	3	MW 3	3	LW73	3	3	1	2	LW62
	2	2	LW 1	1	LX 1	2	4	3	3	NW 3	3	LW73	3	3	1	2	LW92
	2	2	KX 1	1	1	2	4	3	3	NX 3	3	73	3	3	1	2	KX92
	2	2	JW 1	1	1	2	4	3	3	NX 3	3	73	3	3	1	2	KX92
	2	1	KW 1	1	2	4	3	3	3	NW 3	3	3	43	1	2	2	JX 3
	2	1	LV 1	1	2	4	3	3	3	LV 3	3	3	43	1	2	2	JW 3
	2	1	OV 1	1	2	4	3	3	3	MV 3	3	3	43	1	2	2	LW 3
	2	1	OV 1	1	2	4	3	3	3	LU 3	3	3	3	1	2	92	KW 3
	2	1	OV 1	1	2	4	3	3	3	LU 3	3	3	3	1	2	92	3

TABLE XIX

NATURAL FACTORS, JUNE 1966

	0	1	6	2		6	3	6	4	6	5	6	6	6	7	6	8	6	9	6	10	6	11	6	12	6	13	6	14	6	15	6	16	6	17	6	18				
1		3		3		1		2		3		2		2		1	KV	1		1		1		2		1		1		1	JU	1		2		2		1			
2		3		3		2		2		3		2		2		1	KV	1		1		1		2		1		1		1	JV	1		2		2		1			
3		3		3		3		2		3		2		2		1	KU	1		1		1		2		1		1		1	JU	1		2		2		1			
4		3		3		4		2		3		2		2		1	JT	1		1		1		2		1		1		1	Y	1		2		2		1			
5		3		3		5		2		3		2		2		1		KY	1		1		2		12		1		1		Y	1	JT	2		2		1			
6		32		3		6		2		3		2		2		1		LU	1		1		2		1		1		1		1	OT	2		2		1				
7		3		3		7		2		3		2		2		1		LV	1		1		2		1		1		1		1	HU	2		2		1				
8		3		3		8		2		3		2		2		1		LW	1		1		2		1	LW	1		1		1	LU	2	LV	2		1				
9		3	MW	3		9		MW	2		3		2	MV	2		1		LW	1		NX	1		2		1	MW	1		1	LU	2	LV	2		1				
10		3	MV	3		10		LW	2		3		2	MW	2		1		LV	1		MW	1		2		1		1		1	LV	2	LW	2		1				
11		3	MV	3		11		MW	2		3		2	MV	2		1		MV	1		MV	1		2		1	MV	1		1	LV	2	MW	2		1				
12		3	MV	3		12		MW	2		3		2	MV	2		1		NV	1		MW	1		2		1	MW	1		1	MW	2	MW	2		1				
13		3	MV	3		13		MW	2		3		2	MW	2		1		NV	1		MW	1		2		1	NX	1		1	MW	2	MW	2		1				
14		3	MW	3		14		MW	2		3		2	MW	2		1		MV	1		MW	1		2		1	NX	1		1	MW	2	MW	2		1				
15		3	MW	3		15		NX	2		3		2		2		1		MW	1		MW	1		2		1	MW	1		1	MW	2	MW	2		1				
16		3	MW	3		16			2		3		2		2	NX	1		MW	1			1		2		1		1	MW	1		1	MW	2		2		1		
17		3		3		17			2		3		2		2	LX	1			1		NX	1		1		2		1		1	LW	1		1	LW	2		2		1
18		3		3		18			2		3		2		2	LX	1			1		1		1		2		1		1	LX	1		1		2		2		1	
19		3		3		19			2		3		2		2	KX	1		1		1		1		2		1		1		1	OX	1		1		2		2		1
20		93		2		20			3		2		2		2	1	KO	1		1		1		2		1		1		1	KW	1		2		2		1		1	
21		93		2		21			3		2		2		2	1	KO	1		1		1		2		1		1		1	KV	1		2		2		1		1	
22		93		2		22			3		2		2		2	1	KV	1		1		1		2		1		1		1	JU	1		2		2		1		1	
23		3		2		23			3		2		2		2	1	KU	1		1		1		2		1		1		1	JU	1		2		2		1		1	
24		3		2		24			3		2		2		2	1	JV	1		1		1		2		1		1		1	KU	1		2		2		1		1	

TABLE XIX

URAL FACTORS, JUNE 1966

	6 13	6 14	6 15	6 16	6 17	6 18	6 19	6 20	6 21	6 22	6 23	6 24	6 25	6 26	6 27	6 28	6 29	6 30
	1	1	JU 1	2	2	1	1	2	1	1	2	OV 3	4	3	3	2	2	2
	1	1	JV 1	2	2	1	1	2	1	1	2	JU 3	4	3	3	2	2	2
	1	1	JU 1	2	2	1	1	2	1	1	2	JT 3	4	3	3	2	2	2
	1	1	Y 1	2	2	1	1	2	1	1	2	JT 3	4	3	3	2	2	2
	1	1	Y 1	JT 2	2	1	1	2	1	1	42	JT 3	4	3	3	2	2	2
	1	1	1	OT 2	2	1	1	2	1	1	42	LV 3	4	3	3	2	2	2
	1	1	1	MU 2	2	1	1	2	1	1	42	LV 3	4	3	3	2	2	2
LM 1	1	1	1	LU 2	LV 2	1	1	2	1	1	LU 2	MU 3	4	3	3	2	2	2
NM 1	1	1	1	LU 2	LM 2	1	1	2	1	MV 1	MV 2	MV 3	4	3	3	2	2	2
	1	1	1	LV 2	LM 2	1	1	2	MV 1	MU 1	MV 2	MV 3	4	3	3	2	MV 2	MV 2
NV 1	1	1	1	LM 2	NM 2	1	1	MV 2	MV 1	MV 1	MW 2	MW 3	42	3	32	MV 2	MV 2	MU 2
NW 1	1	1	1	NM 2	NM 2	1	1	MV 2	MU 1	NX 1	MW 2	MW 3	4	3	MW 3	MW 2	MW 2	MV 2
MX 1	1	1	1	NM 2	NM 2	1	1	MV 2	MV 1	NX 1	MW 2	MW 3	4	3	MW 3	MW 2	MW 2	MV 2
MX 1	1	1	1	NM 2	NM 2	1	1	MU 2	NM 1	NM 1	MX42	MW3	4	3	MX 3	MW 2	MW 2	MW 2
NW 1	1	1	1	NM 2	NM 2	1	1	MV 2	MX 1	NM 1	MX42	53	4	3	MX 3	MW 2	MW 2	MV 2
1	NM 1	1	NM 2	2	1	1	NM 2	MX 1	LX 1	1	42	53	4	3	MX 3	LM 2	LM 2	2
1	LM 1	1	LM 2	2	1	1	LM 2	LX 1	1	1	42	43	4	3	LM 3	LX 2	2	2
1	LX 1	1	2	2	1	1	LX 2	1	1	1	42	43	4	3	LM 3	2	2	2
1	OX 1	1	2	2	1	1	KX 2	1	1	1	42	43	4	3	KX 3	2	2	2
1	KW 1	2	2	1	1	2	KW 1	1	2	2	3	4	53	3	JW 22	2	2	2
1	KV 1	2	2	1	1	2	KV 1	1	2	2	3	4	53	3	OV 2	2	2	2
1	JU 1	2	2	1	1	2	KU 1	1	2	2	3	4	53	3	OV 2	2	2	2
1	JU 1	2	2	1	1	2	KU 1	1	2	2	3	4	3	3	OV 2	2	2	2
1	KU 1	2	2	1	1	2	KU 1	1	2	2	OV 3	4	3	3	2	2	2	2

TABLE XX

NATURAL FACTORS, JULY 1966

	7	1	7	2	7	3	7	4	7	5	7	6	7	7	7	8	7	9	7	10		7	11	7	12	7	13	7	14	7	15	7	16	7	17				
1	JU	2		2		2		2		2		2		2		KU	3	62	42		1		2		43		2		1		1		2		2				
2	LU	2		2		2		2		2		2		2		OV	43	62	92		2		2		43		2		1		1		2		2				
3	HO	2		2		2		2		2		2		2		OT	43	62	922		3		2		43		2		12		1		2		2				
4	KU	2		2		2		2		2		22		2		JT	43	62	92		4		2		43		22		1		1		2		2				
5	KU	22		2		2		2		2		2		2		KT	43	42	92		5		24		3		22		1		1		2		2				
6	KU	2		2		2		2		2		2		2		KU	43	42	92		6		2		LV	3		2		1		1		2		2			
7	LV	2		2		2		2		2		2		2		LW	43	42	92		7		LV	2		3		LW	2		1		1		2		2		
8	LW	2		2		2		2		2		2		2		LW	32	2	42		8		MV	2		3		2		1		1		2		2			
9	LV	2		2		2		2		2		2		MW	2	MW	3	2	42		9		MV	2		3		2		1		1		2		2			
10	MW	2		2		2		2		2		NV	2	MW	2	MW	3	2	42		10		LV	2		3		MW	2		1		MV	1		2		2	
11	MV	2		2		42		MO	2	NV	2	MX	2	MV	3	MV	3	42	2		11		MV	2		3		MW	2		1		MV	1		2		2	
12	MV	2		2		42		MW	2	MV	2	MW	2	MU	3	MU	3	42	2		12		MU	2		3		MX	2		1		MV	1		2		2	
13	MW	2		2		42		NV	2	NV	2	MW	2	MV	3	MV	3	42	2		13		MV	2		3		2		1		MV	1		2		2		
14	MX	2		2		2		NV	2	MW	2	MW	2	MV	3	MV	3	2	2		14		MU	2		MX	3		MW	2		1		MW	1		2		2
15		2		2		2		MW	2	MW	2	LV	2		3			2	2		15		MU	2		MW	3		MW	2		1		MX	1		2		2
16		2		2		2		MX	2		2		2		3			2	2		16			2		MX	3		2		1		1		2		2		
17		2		2		2		LX	2		2		2		63			2	2		17			2		3		2		1		41		2		2			
18		2		2		2		LX	2		2		2		63			2	2		18			2		3		2		1		41		2		2			
19		2		2		2			2		2		2		63			2	2		19			2		3		2		1		41		2		2			
20		2		2		2			2		2		22		3			92	42	2	20			3		2		1		1		2		2		2			
21		2		2		2			2		2		22		3			92	42	2	21			3		2		1		1		2		2		2			
22		2		2		2			2		2		2		3			92	42	2	22			3		2		1		1		2		2		2			
23		2		2		2			2		2		2		3			623	42	2	23			43		2		1		1		2		2		2			
24		2		2		2			2		2		2		3			62	42	2	24			43		2		1		1		2		2		2			

TABLE XX

L FACTORS, JULY 1966

	7 14	7 15	7 16	7 17	7 18	7 19	7 20	7 21	7 22	7 23	7 24	7 25	7 26	7 27	7 28	7 29	7 30	7 31
1	1	1	2	2	2	1	3	2	3	2	3	3	3	2	3	JU 3	3	3
2	1	1	2	2	2	1	3	2	3	2	3	3	3	2	3	JU 3	3	3
3	12	1	2	2	2	1	3	2	3	2	3	3	32	2	3	JU 3	3	3
12	1	1	2	2	2	1	3	2	3	2	3	3	3	2	3	JT 3	3	3
12	1	1	2	2	2	1	3	2	3	2	3	3	3	2	3	JU 3	3	3
1	1	1	2	2	2	1	3	2	3	2	3	3	3	2	3	OU 3	3	3
1	1	1	2	2	2	1	3	2	3	2	3	3	3	2	3	OV 3	3	3
1	1	1	2	2	2	1	3	2	3	2	3	3	3	42	LW 3	LW 3	3	3
1	1	1	2	2	2	1	3	2	MV 3	2	3	3	3	MV42	3	M0 3	3	3
1	MV 1	1	2	2	2	1	3	2	M0 3	2	3	3	MW 3	MV42	3	M0 3	3	3
1	MV 1	1	2	2	2	1	3	2	M0 3	2	3	MV 3	MW 3	MV42	3	M0 3	3	3
1	MV 1	1	2	2	2	1	3	MX 2	MW 3	2	3	MV 3	MW 3	MV42	3	MW 3	3	3
1	MV 1	1	2	2	2	1	3	MX 2	MW 3	2	3	MV 3	MX 3	MW42	3	MW 3	3	3
1	MW 1	1	2	2	2	1	3	42	MW 3	2	3	MV 3	MX 3	MX 2	3	3	3	3
1	MX 1	1	2	2	2	1	3	42	3	2	3	MW 3	MX 3	MX 2	3	3	3	3
1	1	1	2	2	2	1	3	42	3	2	3	MW 3	L0 3	MX 2	3	3	3	3
1	41	1	2	2	2	1	3	2	3	2	3	LW 3	OX 3	2	3	3	3	3
1	41	1	2	2	2	1	3	2	3	2	3	LX 3	3	2	33	3	3	3
1	41	1	2	2	2	1	3	2	3	2	3	MX 3	3	2	3	3	3	3
1	2	2	2	2	1	3	2	43	42	3	3	JX 3	2	3	3	3	3	3
1	2	2	2	2	1	3	2	43	42	3	3	OW 3	2	3	3	3	3	3
1	2	2	2	2	1	3	2	43	42	3	3	JV 3	2	3	3	3	3	3
1	2	2	2	2	1	3	2	3	2	3	3	OV 3	2	3	3	3	3	3
1	2	2	2	2	1	3	2	3	2	3	3	3	2	3	32	3	3	3

TABLE 1
NATURAL FACTORS

	0	1	0	2	0	3	0	4	0	5	0	6	0	7	0	8	0	9	0	10	0	11	0	12	0	13	0	14	0	15
1		3		3		3		2	OV	2		2		1		0		0		0		0	OV	1		1		1		2
2		3		3		3		2	JV	42		2		1		02		0		0		0	JV	1		1		1		2
3		3		3		3		2	JV	42		2		1		0		0		0		0	OU	1		1		1		2
4		3		3		3		2	OU	42		22		1		0		0		0		0	JV	1		1		1		2
5		3		3		3		2	OU	2		2		1		0		0		0		0	OT	1		1		1		2
6		3		3		3		2	OV	2		2		1		0		0		0		0	KT	1		1		1		2
7		3		3		3		2	LV	2		2		1		0		0	LX	0		0	LU	1		1		1		2
8		3		3		3	LW	2	LW	22		2		1		0		0		0		0	LV	1		1		1		2
9		3		3	MV	3	MW	2	MV	22		2		1		0		0		0		0	NV	1		1		1		2
10		3	MV	3	MV	3	MW	2	MW	22		2		1		0	MV	0	M	0		0	MW	1		1		1		2
11		3	MV	3	MV	3	MV	2	MV	2		2		1	MV	0	MV	0		0		0	MW	1		1		1	MW	2
12	MU	3	MW	3		3	MW	2	MW	2		2		1	MV	0	MW	0		0	MW	0	MW	1		1		1	MW	2
13	MV	3	MW	3	MW	3	MX	2	MW	2		2		1	MW	0	MV	0		0	MW	0	MW	1		1		1	MX	2
14		3	MW	3	MX	3	MX	2		2		2		1	MX	0	MW	0		0	MX	0		1		1		1	MX	2
15	MV	3	MW	3	MX	3	MX	2		2		2		1	MX	0	MW	0		0	MW	0		1		1			MX	2
16	MW	3	LW	3	LX	3		2		2		2		1	MX	0	LW	0		0		0		1		1		1	LW	2
17	LW	3	LW	3		3		2		2		2		1	LX	0	LX	0		0		40		1		1		1	LW	2
18	LW	3		3		3		2		2		2		1	OV	0		0		0		40		1		1		1	OV	2
19	MW	3		3		3		2		2				1	LW	0		0		0		40		1		1		1	OV	2
20	MW	3		3		2		2		2		1		0	JV	0		0		40		1		1		1		2	JV	1
21	MU	3		3		2		2		2		1		0	OV	0		0		40		1		1		1		2	JV	1
22	OU	3		3		2		2		2		1		0	JV	0		0		40		1		1		1		2	OT	1
23	OU	3		3		2		2		2		1		0	OU	0		0		0		1		1		1		2	OU	1
24	OU	3		3		2		2		2		1		0	OU	0		0		0		1		1		1		2	OT	1

TABLE XXI

URAL FACTORS, AUGUST 1966

0 13	0 14	0 15	0 16		0 17	0 18	0 19	0 20	0 21	0 22	0 23	0 24	0 25	0 26	0 27	0 28	0 29	0 30	0 31
1	1	2	1	1	1	1	OU41	1	1	1	3	3	4	4	4	4	42	93	3
1	1	2	1	2	1	1	OU 1	1	1	1	3	3	4	4	4	4	4	3	3
1	1	2	1	3	1	1	OT 1	1	1	1	3	3	4	4	4	4	4	3	3
1	1	2	1	4	1	1	OO 1	1	1	1	3	32	4	4	4	4	4	3	3
1	1	2	1	5	12	1	OO 1	1	12	1	43	432	4	4	4	4	4	93	3
1	1	2	1	6	12	1	KT 1	1	1	1	432	432	4	4	4	4	4	93	3
1	1	2	1	7	1	1	LU 1	1	1	1	43	432	4	4	4	4	4	93	3
1	1	2	1	8	1	1	LV 1	1	1	1	43	432	4	4	4	4	44	93	43
1	1	2	1	9	NW 1	NW 1	NW 1	1	1	1	43	432	4	4	4	4	44	93	43
1	1	2	NV 1	10	NV 1	NW 1	NV 1	1	1	1	43	43	4	4	4	4	44	93	43
1	1	NW 2	NV 12	11	NV 1	NW 1	NV41	1	1	1	43	3	4	4	4	44	4	63	43
1	1	NW 2	NV 1	12	NV 1	NW 1	NW41	1	1	1	43	3	4	4	4	4	4	63	43
1	1	NX 2	NW 1	13	NW 1	NW 1	NW41	1	1	1	43	3	4	4	4	4	4	63	43
1	1	NX 2	NX 1	14	NW 1	NX 1	1	1	1	1	43	3	4	42	4	4	4	73	43
1	1	NX 2	LX 1	15	NX 1	NX 1	1	1	1	1	43	3	4	42	4	4	4	73	43
1	1	LW 2	NX 1	16	NX 1	1	1	1	1	1	43	3	4	4	4	4	4	73	43
1	1	LW 2	LW 1	17	1	1	1	1	1	12	43	3	4	4	4	4	4	73	3
1	1	OW 2	1	18	1	1	1	1	1	1	43	3	4	4	4	4	4	73	3
1	1	OW 2	1	19	1	1	1	1	1	1	43	3	4	4	4	4	4	73	3
1	2	JV 1	1	20	1	1	1	1	1	3	3	44	4	4	4	4	73	3	92
1	2	JU 1	1	21	1	1	1	1	1	3	3	44	4	4	4	4	73	32	92
1	2	OT 1	1	22	1	1	1	1	1	3	3	44	4	4	4	4	732	3	92
1	2	OU 1	1	23	1	41	1	1	1	3	3	4	4	4	4	4	93	3	2
1	2	OT 1	1	24	1	41	1	1	1	3	3	4	4	4	4	4	93	3	2

TABLE XXII
NATURAL FACTORS, SEPTEMBER

	9	1	9	2	9	3	9	4		9	5	9	6	9	7	9	8	9	9	9	10	9	11	9	12	9	13	9	14	9	15	9	16	9	17
1			23		1		.00		1		1	91	41	91		1	41	2	1	1	1	41	2	1	1	1	1	41	2	3					
2	2		23	41	70				2		1	41	1	91		1	1	2	1	1	1	1	1	1	1	1	1	1	1	2	3				
3	2		23	41	70				3		1	41	1	91		1	1	2	1	1	1	1	1	1	1	1	1	1	1	2	3				
4	2		23	41	70				4		1	41	1	91		1	1	2	1	1	1	1	1	1	1	1	1	1	1	2	3				
5	92		23	61	60				5		1	91	1	61		1	1	2	12	1	1	1	1	1	1	1	1	1	1	2	3				
6	92		2	61	60				6		1	91	1	61		1	1	2	1	1	1	12	1	1	1	1	1	1	1	2	3				
7	92		2	61	60				7		12	91	1	61		1	1	2	1	1	1	12	1	1	1	1	1	1	1	2	3				
8	2		2	61	60				8		41	41	1	91		1	1	2	1	1	1	1	1	1	1	1	1	1	1	2	3				
9	2		2	61	60				9		41	41	1	91		1	1	2	1	1	1	1	1	1	1	1	1	1	1	1	2	3			
10	2		2	61	60				10		41	41	1	91		1	1	2	MV 1	MV 1	LV 1	LV 1	MV 2												
11	2		2	61	40				11		41	41	1	91	41	1	2	MV 1	LV 1	LV 1	LV 1	MV 2													
12	2		2	61	40				12		41	41	1	91	41	1	2	MV 1	MV 1	MV 1	MV 1	MV 2													
13	2		2	61	40				13		41	41	1	91	41	1	2	1	MV 1	LV 1	1	MV 2													
14	92	42	71	0					14		1	1	1	41	1	1	2	1	MV 1	1	MV 41	0N 2													
15	92	12	71	0					15		1	1	1	41	1	1	2	1	MV 1	MV 1	MV 41	MV 2													
16	92	1	71	0					16		1	1	1	41	1	1	2	1	1	1	1	41	2												
17	2		2	91	0				17		1	1	1	91	41	1	2	1	1	1	41	41	2												
18	2		2	91	0				18		1	1	1	91	41	1	2	1	1	1	41	41	2												
19	2		2	91	0				19		1	1	1	91	41	1	2	1	1	1	41	41	2												
20	2		1	00	1				20		1	1	41	1	41	2	1	1	1	1	91	2	43												
21	2		1	00	1				21		1	1	41	1	41	2	1	1	1	1	91	22	43												
22	2		1	00	1				22		1	1	41	1	41	2	1	1	1	1	91	2	43												
23	2		1	00	1				23		91	41	91	1	41	2	1	1	1	1	41	2	3												
24	2		1	003	1				24		91	41	91	1	41	2	1	1	1	1	41	2	3												

TABLE XXII

TURAL FACTORS, SEPTEMBER 1966

	9 12	9 13	9 14	9 15	9 16	9 17	9 18	9 19	9 20	9 21	9 22	9 23	9 24	9 25	9 26	9 27	9 28	9 29	9 30
1																			
2	1	1	1	41	2	3	4	43	3	4	4	3	3	43	2	42	51	42	1741
2	1	1	1	1	2	3	4	3	43	4	4	10 3	3	43	2	2	1	42	1741
2	1	1	1	1	2	3	4	3	43	4	4	0T 3	3	43	2	2	1	42	1741
2	1	1	1	1	2	3	4	3	43	4	4	0T 3	3	43	2	2	1	42	0T41
2	12	1	1	1	2	34	4	3	3	42	4	1T 3	3	3	2	42	1	2	0T 1
2	1	1	12	1	2	3	4	3	3	4	4	JU 3	3	3	2	42	1	2	0T 1
2	1	1	12	1	2	3	4	3	3	4	4	KV 3	3	3	2	42	1	2	LV 1
2	1	1	1	L0 1	2	3	4	32	43	4	LW 4	LW 3	3	3	42	2	1	LV 2	LW 1
2	1	1	1	L0 1	LV 2	3	4	3	MW43	MW 4	MW 4	MW 3	3	3	42	LV 2	MW 1	MW 2	LW 1
2	MV 1	MV 1	LV 1	LV 1	MV 2	3	4	3	LW43	MW 4	MW 4	MW 3	3	3	42	MW 2	MW 1	MV 2	MW 1
2	MW 1	LV 1	LW 1	LV 1	MV 2	3	4	3	LW43	MW 4	4	MW432	3	3	MW42	MW 2	MW41	42	MW 1
2	MV 1	MV 1	MV 1	MV 1	MW 2	3	4	MW 3	MW43	MW 4	4	MW43	3	3	MW42	MW 2	MW41	MW42	MW 1
2	1	MV 1	LV 1	1	MW 2	3	4	MW 3	0W432	LW 4	MW 4	MW43	3	3	MW42	MW 2	MW41	MW42	MV 1
2	1	MW 1	1	MW41	0W 2	3	4	MW 3	0W 32	MW 4	MW 4	MW43	3	3	MW42	MX 2	MW 1	MW42	MV 1
2	1	MW 1	MW 1	MW41	MW 2	3	4	MW 3	32	MW 4	MW 4	43	3	3	MX42	MW 2	LW 1	MW42	1
2	1	1	1	41	2	3	4	LW 3	L0 32	LW 4	4	43	3	3	LW42	LW 2	LV 1	42	1
2	1	1	41	41	2	3	4	LW43	L0 3	4	4	3	3	3	L0 2	L0 2	41	2	41
2	1	1	41	41	2	3	4	0W43	3	4	4	3	3	3	0X 2	2	41	2	41
2	1	1	41	41	2	3	4	0043	3	4	4	3	3	3	0V 2	2	41	2	41
1	1	1	51	2	43	4	3	3	44	4	3	3	43	2	0T42	41	2	1	2
1	1	1	51	22	43	4	3	0U 3	44	4	3	3	43	2	0T42	41	2	1	2
1	1	1	51	2	43	4	3	0U 3	44	4	3	3	43	2	JS42	41	2	1	2
1	1	1	41	2	3	4	43	0U 32	4	4	3	3	43	2	JU42	51	42	41	2
1	1	1	41	2	3	4	43	0U 3	4	4	3	3	43	2	0U42	51	42	41	2

NATURAL FACTORS, OCTOBER 1966

	10	1	10	2	10	3	10	4	10	5	10	6	10	7	10	8	10	9	10	10	10	11	10	12	10	13	10	14	10	15	10	16	10	17	10	18	10	19	10	20						
1	2	2	2	2	1	92	52	JU	2	2	3	3	2		3	3	3	43	3	3	3			3	3	3	3	43	3	3	3	3	3	3	3	3	3	3	3	3	3	3				
2	2	2	2	2	1	42	42	JU	2	2	3	3	2		OU	2	3	3	43	3	3	3			OU	2	3	3	43	3	3	3	3	3	3	3	3	3	3	3	3	3	3			
3	2	2	2	2	1	42	42	JU	2	2	3	3	2		OU	3	3	3	43	3	3	3			OU	3	3	3	43	3	3	3	3	3	3	3	3	3	3	3	3	3	3	3		
4	2	2	2	2	1	42	42	JU	2	2	3	3	2		OU	3	3	3	43	3	3	3			OU	3	3	3	43	3	3	3	3	3	3	3	3	3	3	3	3	3	3	3		
5	2	2	2	2	1	92	2	OT	2	2	23	3	3	2		OU	3	3	3	43	3	3	3			OU	3	3	3	43	3	3	3	3	3	3	3	3	3	3	3	3	3	3		
6	2	2	2	2	1	92	2	JU	2	2	23	3	3	2		JO	3	3	3	43	3	3	3			JO	3	3	3	43	3	3	3	3	3	3	3	3	3	3	3	3	3	3		
7	2	2	2	2	1	92	2	KO	2	2	23	3	3	22		KV	3	OM	3	3	43	3	3	3			KV	3	OM	3	3	43	3	3	3	3	3	3	3	3	3	3	3			
8	2	2	2	2	1	2	42	LV	2	2	2	3	3	2		LW	3	3	3	53	3	3	3			LW	3	3	3	53	3	3	3	3	3	3	3	3	3	3	3	3	3			
9	2	2	2	2	1	MO	2	MV	42	MW	2	2	2	3	3	2		MW	3	32	3	53	3	3	3			MW	3	32	3	53	3	3	3	3	3	3	3	3	3	3	3			
10	2	2	2	2	MW	1	MW	2	MW	42	MW	2	2	2	3	3	2		MW	3	3	3	53	3	3	MW	3	3	3	53	3	3	3	3	3	3	3	3	3	3	3	3	3	3		
11	2	2	2	MW	2	MW	41	MW	52	MW	22	MW	2	2	2	3	3	2		MW	3	3	43	43	3	3	MW	3	3	43	43	3	3	3	3	3	3	3	3	3	3	3	3	3		
12	2	2	2	MW	2	MW	41	MV	52	MW	22	MW	2	2	2	MW	3	MW	3	2					MW	3	3	43	43	3	3	3	3	3	3	3	3	3	3	3	3	3	3	3		
13	2	2	2	MW	2	MW	41	MV	52	MW	22	MW	2	2	2	MW	3	MW	3	2					MW	3	3	43	43	3	3	3	3	3	3	3	3	3	3	3	3	3	3	3	3	
14	2	2	2	MW	2	MW	51	92	MW	2	MW	2	2	2	2	MW	3	MW	3	2					MW	3	3	43	3	3	3	3	3	3	3	3	3	3	3	3	3	3	3	3		
15	2	2	2	MW	2	LV	51	MW	52	MW	2	2	2	2	2	MW	3	MO	3	2					3	3	43	2	3	3	3	3	3	3	3	3	3	3	3	3	3	3	3	3		
16	2	2	2	LV	2	LW	51	LO	52	2	2	2	2	2	2	LW	3	LO	3	2					3	3	43	2	3	3	3	3	3	3	3	3	3	3	3	3	3	3	3	3		
17	2	2	2	LW	2	00	61	2	2	2	2	2	2	2	2	LO	3	LO	3	2					3	3	43	3	3	3	3	3	3	3	3	3	3	3	3	3	3	3	3	3		
18	2	2	2	OM	2	61	2	2	2	2	2	2	2	2	2	JO	3	3	2					3	3	43	3	3	3	3	3	3	3	3	3	3	3	3	3	3	3	3	3	3		
19	2	2	2	OU	2	61	2	2	2	2	2	2	2	2	2	KU	3	3	2					3	3	43	3	3	3	3	3	3	3	3	3	3	3	3	3	3	3	3	3	3		
20	2	2	2	00	1	92	2	2	2	2	2	2	2	2	2	3	OU	3	2	3					3	3	3	3	3	3	3	3	3	3	3	3	3	3	3	3	3	3	3	3	3	
21	2	2	2	00	1	92	2	2	2	2	2	2	2	2	2	3	OU	3	2	3					3	3	3	3	3	3	3	3	3	3	3	3	3	3	3	3	3	3	3	3	3	
22	2	2	2	OU	1	92	2	2	2	2	2	2	2	2	2	3	OU	3	2	3					3	3	3	3	3	3	3	3	3	3	3	3	3	3	3	3	3	3	3	3	3	
23	2	2	2	OU	1	92	92	2	2	2	2	2	2	2	2	3	3	2	3					3	3	43	3	3	3	3	3	3	3	3	3	3	3	3	3	3	3	3	3	3	3	3
24	2	2	2	OU	1	92	92	2	2	2	2	2	2	2	2	3	3	2	32					3	3	43	3	3	3	3	3	3	3	3	3	3	3	3	3	3	3	3	3	3	3	3

TABLE XXIII

L FACTORS, OCTOBER 1966

10	14	17	15	10	16	10	17	10	18	10	19	10	20	10	21	10	22	10	23	10	24	10	25	10	26	10	27	10	28	10	29	10	30	10	31
3	3	43	3	3	3	3	4	4	4	3	3	2	OU42	1	1	1	1	91																	
3	3	63	3	3	3	3	KU 4	4	4	3	3	42	JU 2	1	1	1	1	41																	
3	3	63	3	3	3	3	JU 4	4	4	3	3	42	OU 2	1	1	1	1	41																	
3	3	63	3	3	3	3	OU 4	4	4	3	3	42	OU 2	1	1	1	1	41																	
3	3	43	3	3	3	3	OU 4	OU 4	4	3	3	42	OU 2	1	1	1	1	41																	
3	3	43	3	3	3	3	JU 4	OU 4	4	3	3	KV42	OU 2	1	1	1	1	41																	
ON 3	3	43	3	3	3	3	LO 4	KV 4	4	3	3	KO42	KO 2	1	1	1	1	41																	
3	3	93	3	3	3	3	MU 4	4	4	3	3	LU42	LU 2	1	1	1	1	91																	
32	3	93	3	3	3	3	MU 4	4	4	3	3	LM 3	MU42	MU 2	1	1	1	1	91																
3	3	93	3	3	3	3	MU 3	MU 4	MO 4	4	3	3	MU42	MO 2	1	1	1	1																	
3	43	43	3	3	3	3	MU 3	MU 4	MU 4	4	3	MU43	MX 2	MU42	MU 1	1	1	41	MU41																
3	43	43	3	3	3	3	MU 3	MU 4	4	4	3	MU43	MU 2	MU42	MU 1	MU 1	1	41	MX41																
3	43	43	3	3	3	3	MU 3	MU 4	4	4	3	MU432	MU 2	MU42	MX 1	MX 1	1	41	MU41																
3	43	3	3	3	3	3	MX 3	MU 4	4	4	3	MX 3	42	MV 2	MO 1	MU 1	1	1	MU91																
3	432	3	3	3	3	3	MX 3	4	4	4	3	MO 3	42	2	MO 1	MO 1	1	1	MX912																
3	432	3	3	3	3	3	LX 3	4	4	4	3	MO 3	42	2	LO 1	1	1	1	LU91																
3	43	3	3	3	3	3	4	4	4	4	3	LM 3	42	2	LM 1	1	1	91	LX41																
3	43	3	3	3	3	3	4	4	4	4	3	MX 3	42	2	MO 1	1	1	91	JO41																
3	43	3	3	3	3	3	4	4	4	4	3	MO 3	42	2	JO 1	1	1	91	JV41																
3	3	3	3	3	3	3	4	4	4	3	3	2	ON2	1	OU 1	1	1	91	42																
3	3	3	3	3	3	3	4	4	4	3	3	2	ON2	1	V 1	1	1	91	42																
3	3	3	3	3	3	3	4	4	4	3	3	2	ON2	1	L 1	1	1	91	42																
3	43	3	3	3	3	3	4	4	4	3	3	2	42	1	OU 1	1	1	91	42																
3	43	3	3	3	3	3	4	4	4	3	3	2	42	1	KU 1	1	1	91	42																

TABLE XXIV
NATURAL FACTORS, NOVEMBER 1966

	11	1	11	2	11	3	11	4	11	5	11	6	11	7	11	8	11	9	11	10	11	11	11	12	11	13	11	14	11	15	11	16	11	17	11	18	11	19						
1	42	KV	2		1		1		1		1		1	2		2	OU	2		3		3		4		3		3		3	OU	2		2		2		3						
2	92	KU	2	41		1		1		1		1		2		2	OU	2		3		3		4		3		3		3	JU	2		2		2		3						
3	92	KU	2	41		1		1		1		1		22		2	OU	2		3		3		4		3		3		3	KV	2		2		2		3						
4	92	OU	2	41		1		1		1		1		2		2	OU	2		3		3		4		3		3		3	KU	2		2		2		3						
5	OU92	OU	2	41		1		1		1		1		2		2	OU	2		3		3		4		3		3		3	OU	2		2		2		3						
6	KU922	KU	2	41		1		1		1		1		2	OU	2	OU	2		3		3		4		3		3	OU	3	OU	2		2		2		3						
7	KV92	KW	2	41		1		1		1		1		2	KU	2	KV	2		3		3		4		3		3	KO	3	KV	2		2		2		3						
8	LO92	LO	2		1		1		1		1		1	2	LO	2	LW	2		3		3		4		3		33	LO	3	LW	2		2		2		3						
9	M092	MW	2		1		1		1		1		1	MW	2	HX	2	M0	2		3		3		4		3		M0	3	LW	3	MW	2		2		2		3				
10	MW92	HX	2		1		1		1		1		1	MX	2	M0	2	M0	2		3		3		4		3		LO	3	LW	3	MW	2		2		2		3				
11	M092	MV	2	41		1		1		1		1		MW	2	MW	2	MW	2		M0	3		3		4		3		HX	3	MW	3	MW	2		MW	2	42		3			
12	M092	MW	2	HX41		1		1		1		1		MW	2	MW	2	MW	2		HX	3		HX	3		4		3		HX	3	MW	3	MW	2		MW	2	MW42		3		
13	M092	MW	2	HX41		1		1		1		1		MW	2	HX	2	MW	2		HX	3		MW	3		4		3		OU	3		3	MW	2		MW	2	MW42		3		
14	2	MW	2	MW	1		HX	1		1		1		MW	2		2	MW	2		MW	3		MW	3		4		3		MW	3		3	MW	2		MW	2	MW	2		3	
15	2	2	2	M0	1		1		1		1		1	MX	2		2		2		LW	3		MW	3		4		3		LW	3		3		2		MW	2		MW	2		3
16	2	2	2	LW	1		1		1		1		1	LW	2		2		2		LW	3		3		4		3		LW	3		3		2		LW	2		2		3		
17	2	2	2	OW	1		1		1		1		1	KO	2		2		2		OW	3		3		4		3		KO	3		3		2		LW	2		42		3		
18	2	2	2	0	1		1		1		1		1	KO	2		2		2		OV	3		3		4		3		KO	3		3		2		OW	2		42		3		
19	2	2	2	OU	1		1		1		1		1	OU	2		2		2		KV	3		3		4		3		KO	3		3		2		OU	22		42		3		
20	2	41	41	OU	1		1		1		1		2		2		2		3		OU	3		4		3		3		3		3		2		2		OU	2		3		3	
21	2	41	41	OU	1		1		1		1		2		2		2		3		OU	3		4		3		3		3		3		2		2		OU	2		3		3	
22	2	41	41	OU	1		1		1		1		2		2		2		3		OU	3		4		3		3		3		3		2		2		OU	2		3		3	
23	2	1	1	OU	1		1		1		1		2		2		2		3		OU	3		4		3		3		3		3		2		2		OU	2		3		3	
24	2	1	1	OU	1		1		1		1		2		2		2		3		OU	3		4		3		3		3		3		2		2		2		2		3		3

TABLE XXIV

FACTORS, NOVEMBER 1966

1	19	11	16	11	17	11	18	11	19		11	20	11	21	11	22	11	23	11	24	11	25	11	26	11	27	11	28	11	29	11	30
3	OU	2		2		2		3		1	3	3	4	KU	3		3	3	3		2	2		1	KU	1						
3	JU	2		2		2		3		2	3	3	4	OU	3		3	3	3		2	2		1	KU	51						
3	KV	2		2		2		3		3	3	3	4	OU	3		3	3	3		2	2		1	KU	51						
3	KU	2		2		2		3		4	3	3	4	JU	3		3	3	1		2	22		1	OU	51						
3	OU	2		2		2		3		5	3	3	4	OU	3		3	3	3		2	2		KU	1	OU	41					
U	3	OU	2		2		2	3		6	3	3	4	OU	3		3	3	3		2	2		JU	1	KU	41					
0	3	KV	2		2		2	3		7	3	3	4	KW	3		3	3	3		2	2		KW	1	LV	41					
0	3	LW	2		2		2	3		8	3	3	4	LO	3		3	3	3		2	2		LW	1	LW	41					
W	3	MW	2		2		2	3		9	3	3	M0	4	LO	3		3	3	3		2	M0	2	LW	1	MW	41				
W	3	NW	2		2		2	3		10	3	3	LO	4	MW	3		3	3	3		2	LO	2	MW	1	MW	41				
W	3	NW	2	MW	2		42	3		11	3	OU	3	MW	4	MW	3		3	3	3		2	MW	42	MX	1	MW	51			
W	3	NW	2	MW	2		MW	42	3		12	3	MW	3	MW	4	MW	3		3	3	3		2	OU	42	NW	1	MW	51		
3	NW	2	MW	2		MW	42	3		13	3	MW	3	MW	4	MW	3		3	3	3		2	MW	42	MW	1	MW	51			
3	MW	2	MW	2		MW	2	3		14	3	MW	3	MW	4	MW	3		3	3	3		2	MW	52		1	MX	1			
3		2	MW	2		MW	2	3		15	3	LW	3	M	4		3	3	3	3		2	MW	52		1		1				
3		2	LW	2			2	3		16	3	LW	3	M	4		3	3	3	3		2	LW	52		1		1				
3		2	LW	2		42		3		17	3	KW	3		4		3	3	3	3		2	LW	2		1	41					
3		2	OU	2		42		3		18	3	JV	3		4		3	3	3	3		2	LW	2		1	41					
3		2	OU	22		42		3		19	3	OV	3		4		3	3	3	3		2	JV	2		1	41					
2		2	OU	2		3		3		20	3	KU	4		3		3	3	3	42		2		1	51	41						
2		2	OU	2		3		3		21	3	KV	4		3		3	3	3	42		2		1	51	41						
2		2	OU	2		3		3		22	3	OU	4		3		3	3	3	42		2		1	51	41						
2		2	OU	2		3		3		23	3	KV	4		3		3	3	3	2		2		1	1	41						
2		2		2		3		3		24	3		4		3		3	3	3	2		2		1	1	41						

On 1 December 1966 (Table XXV) a level 4 K_p is followed by several dropouts of both modes. On 5 December level 4 and 5 magnetic disturbances are followed by or accompanied by dropouts of the 1F2 and the 2E. On 13, 14, and 15 December K_p levels ranging from 4 to 7 are accompanied by slightly increased dropouts and variations of both modes. Magnetic disturbance across midnight of the 20th are followed the next day by several dropouts that include both modes. Similarly, on 22 December and the large set of disturbances on the 26th and the 27th have roughly eliminated both modes.

At this point, it is well to note that the sunspot numbers have increased quite materially and are in turn accompanied by increases in the number of natural factors observed. It should be noted, however, that with the exception of a greater increase in MOF during the day (with respect to night), as the sunspot number increases no major increase in MOF is shown, because all values of MOF are normalized monthly to mean and standard deviations.

It is noted for January 1967 (Table XXVI) that a level 2 flare on the 9th is accompanied only by a drop in the 1F2 JF, but interestingly enough it is both preceded and accompanied by a dropout of the 2E mode.

In February 1967 (Table XXVII) a flare on the 7th is accompanied by a dropout of the 2E mode and apparently has little effect on the 1F2 mode. Magnetic disturbances on 8 February and a flare the same morning are accompanied by some dropout, and apparently a matching increase of the 2E mode with the occurrence of the flare. The flare of level 4 on 13 February appears to have no effect on the 1F2 mode but is followed by a dropout of the 2E mode. The small data existing on the 16th for the 2E mode shows a dropout accompanying some quite strong magnetic disturbances. Flares on 22 February have apparently had no effect on the 1F2 mode, but there are a number of dropouts for the 2E mode. On the 23rd, with one flare early in the morning and a magnetic disturbance in the afternoon, there are at least an equal number of dropouts. The flare right after noon on 27 February is followed much later by dropouts by both the 1F2 and the 2E modes.

In March 1967 (Table XXVIII) it can be seen that the magnetic disturbance in the late afternoon of the 20th shows no effect on the data. On 23 March a level 2 flare in midafternoon shows no distinctive effects. On the 27th another level 2 flare at approximately noon does not appear to be effective.

In April 1967 (Table XXIX) a magnetic disturbance in the forenoon on the 4th resulted in a complete dropout of the 2E mode. A flare just after noon on 14 April appears to have had no effect and the flare in the late afternoon of the 20th may have held the 2E mode up slightly longer after sunset than would otherwise have resulted. The magnetic disturbance on 19 April that started in the evening of the 18th shows no early morning 2E mode. This may or may not have been a dropout of the 2E mode. On the 24th a magnetic disturbance of the same level running through the noon hour shows no effect.

In May 1967 (Figure 200 and Table XXX) a magnetic disturbance on the afternoon of the 1st results in a 2E mode dropout. A flare and a magnetic disturbance on 2 May in the early morning show no distinctive effect on the 1F2 mode and it leaves a question whether the zero value in the morning for the 2E mode results from either. On 3 May, however, a dropout of the 1F2 mode and later for the 2E mode is noted that may well be credited to the flare and/or the magnetic disturbance with a K_p of 7. Flares on the 8th preceded record taking, but the results of both modes appeared quite normal. The flare on the 10th in the forenoon shows no distinctive effect of either mode. It should be noted that, in the middle of this month, the sunspot number is quite low, but towards the latter part of the month, particularly on 28 May, it has exceeded the 180 level indicated on this record. On the 25th a very strong magnetic disturbance was preceded by many small flares, only one of level 2 being noted in the forenoon. While on this record a midnight dropout of the 1F2 mode and an evening dropout of the 2E mode do not look particularly impressive, a very wide range of variations in the mode structure that occurred resulted in literally smearing together all of the modes in late afternoon and into the evening, showing many interesting effects that can only be documented by the oblique ionograms themselves. Some small magnetic disturbances on the 31st may or may not have been responsible for the 2E mode dropout and its fluctuations.

TABLE XXV

NATURAL FACTORS, DECEMBER 19

	12	1	12	2	12	3	12	4	12	5	12	6	12	7	12	8		12	9	12	10	12	11	12	12	12	13	12	14	12	15	12	16	12	17	12	18
1	41		1		1		2	43				3	OU 3			4	1	4		5		6		6	45	OU45		5		5		3		2			
2	41		1		1		52	43				3	OU 3			4	2	4		5		6		6	45	OV 5		5		5		3		2			
3	41		1		1		52	43				3	OU 3			4	3	4		5		6		6	45	OV 5		5		5		3		2			
4	41		1		1		52	43				3	OU 3			4	4	4		5		6		6	45	OV 5		5		5		32		2			
5	1		1		12		42	3				3	OU 3			4	5	42		5		6		6	5	OU 5		5		5		3		2			
6	1		1		1		42	3				OU 3	OU 3			4	6	4		5		6		6	OU 5	OU 5		5		5		3		2			
7	1		1		1		42	3				OU 3	OU 3			4	7	4		5		6		6	OU 5	KV 5		5		5		3		2			
8	1		1		1		2	3				LW 3	LW 3			42	8	4		52		6		6	LW45	LW65		5		5		3		2			
9	1		1		1		2	MO 3				LW 3	MO 3			4	9	4		5		6		MM 6	MO45	MO65		5		5		3		2			
10	1		1		1		2	MX 3				MO 3				4	10	4		5		6		MM 6	MO45	MO65		5		5		3		2			
11	MM 1		1		1		2	MM 3				MM 3	MO 3			MM 4	11	4		5		6		MM 6	MM55	MX75	MX45		5		3		2				
12	MM 1		MM 1		1		2	MM 3				LW 3	MM 3			MM 4	12	MM 4		5		6		MM 6	MM55	MX75	NW45		5		3		2				
13	MM 1		MM 1		1		2	MX 3				MM 3	MM 3			MM 4	13	MM 4		5		6		MM 6	MO55	MX75	NX45		5		3		2				
14	41		MM 1		1		2	MM53				3	LW 3			MM 4	14	MM 4		5		6		MM 6	5	MY55	MX 5		5		3		22				
15	LW41		LW 1		1		2	MX53				3				MM 4	15	MM 4		5		6		LW 6	5	55	MX 5	LX 5		3		3		2			
16	LW41		1		1		2	MM53				3				LW 4	16	MM 4		5		6		LW 6	5	55	LX 5	LW 5		3		3		2			
17	OW 1		1		1		42	OW 3				3				OW 4	17		4		5		6		OW 6	5	55	KW 5		5		43		2			
18	JV 1		1		1		42	OV 3				3				OU 4	18		4		5		6		OV 6	5	55	JV 5		5		43		2			
19	1		1		1		42	3				3				JU 4	19		4		5		6		6	52	55	OU 5		5		43		2			
20	KO 1		1		2		43	3				3				KU 4	20		5		6		6		5	5	5	OU55		3		2		2			
21	OU 1		1		2		43	3				3				OU 4	21		5		6		6		5	5	5	55		3		2		2			
22	JU 1		1		2		43	3				3				OU 4	22		5		6		6		5	5	5	55		3		2		2			
23	OU 1		1		2		43	3				3				OU 4	23		5		6		6		45	45	5	5	3		2		2		2		
24	OU 1		1		2		43	3				3				OU 4	24		5		6		6		45	45	5	5	3		2		2		2		

TABLE XXV

FACTORS, DECEMBER 1966

12 14 12 15 12 16 12 17 12 18 12 19 12 20 12 21 12 22 12 23 12 24 12 25 12 26 12 27	12 28 12 29 12 30 12 31
OU45 5 5 3 2 2 1 KU41 1 1 2 3 3 52	OU 2 2 3 3
OV 5 5 5 3 2 2 1 JU 1 1 1 42 3 3 42	OU 2 2 3 3
OV 5 5 5 3 2 2 1 JU 1 1 1 42 3 3 42	2 2 3 3
OV 5 5 5 32 2 2 1 OU 1 1 1 42 3 3 42	2 2 3 3
OU 5 5 5 3 2 2 OU 1 OU 1 1 1 2 3 43 42	2 2 3 3
OU 5 5 5 3 2 2 JU 1 OU 1 1 1 2 3 43 42	2 2 3 3
KV 5 5 5 3 2 2 K0 1 KV 1 1 1 2 32 43 K042	2 2 3 3
LW65 5 5 3 2 2 LV 1 LO 1 1 1 2 3 43 52	2 2 3 3
M065 5 5 3 2 LW 2 MW 1 M0 1 1 1 2 3 43 MW52	2 2 3 3
M065 5 5 3 2 MW 2 MW 1 00 1 1 1 2 3 43 52	2 2 3 3
MX75 MX45 5 3 2 MW 2 MW 1 MW 1 MW 1 1 2 3 53 42	2 2 3 3
MX75 MW45 5 3 2 M0 2 MW 1 MW 1 MW 1 OM 1 2 3 53 42	2 2 OM 3 3
MX75 NX45 5 3 2 MW 2 MW 1 MW 1 1 MW 1 2 3 53 N042	2 2 OM 3 3
MY55 MX 5 5 3 22 MW 2 1 LW 1 MW 1 MW 1 2 3 43 42	22 MW 2 MW 3 3
55 MX 5 LX 5 3 2 LW 2 1 1 MW 1 M0 1 2 3 43 42	2 LW 2 MW 3 3
55 LX 5 LW 5 3 2 LW 2 1 1 LW 1 1 2 3 43 42	2 LW 2 3 3
55 KW 5 5 43 2 OM 2 1 1 0W41 1 2 43 43 42	2 K0 2 3 3
55 JV 5 5 43 2 00 2 1 1 K041 1 2 43 43 42	2 JW 2 3 3
55 OU 5 5 43 2 OU 2 1 1 41 1 2 43 43 42	2 00 2 3 3
5 0U55 3 2 2 1 1 1 1 2 3 3 142 2	2 OU 3 3 3
5 55 3 2 2 1 1 1 JU 1 2 3 3 142 2	2 OU 3 3 3
5 55 3 2 2 1 1 1 JU 1 2 3 3 142 2	2 OU 3 3 3
5 5 3 2 2 1 41 1 KU 1 2 3 3 52 2	2 OU 3 3 3
5 5 3 2 2 1 41 1 1 2 3 3 52 2	2 3 3 3

TABLE XXVI
NATURAL FACTORS, JANUARY 19

	1	1	1	2	1	3	1	4	1	5	1	6	1	7	1	8	1	9	1	10	1	11	1	12	1	13	1	14	1	15	1	16	1	17	1	18	1	19
1	3		4		6	KU	7		7		7		6	75		45		5	OT	5		4		4		64		2		2		2	OU	3		4		
2	3		4		6	KU	7		7		7		6	65		5		5		5		4		4		64		2		2		2	OU	3		42		
3	3		4		6	OU	7		7		7		6	65		5		5	OU	5		4		4		64		2		2		2		3		4		
4	3		4		6	KU	7		7		7		6	45		5		5		5		4		4		64		2		2		2	OU	3		4		
5	3		4	OU	6	KU	7		7		7		46	65		5		5	OT	5		4		4		54		2		2		2	OU	3		4		
6	3		4	KU	6	KU	7		7		7		46	65		5		5		5		4		4		54		2		2	OU	2	KU	3		4		
7	3		4	LU	6	KO	7		7		7		46	65		5	KV	5		5		4		4		54		2		2	KV	2		3		4		
8	3		4	OW	6	LW	7		7		7		46	45		5	LW	5	OO	5		4		64		4		2		2	LW	2		3		4		
9	3		4	OW	6	MW	7		7		7		46	45		NO	5	MW	5	MO	5		4		64		4		2		MW	2	MW	2	MW	3		4
10	3		4	MO	6	MW	7		7		7		46	45		5	MW	5	MW	5		4		64		4		2		MW	2	MW	2	MW	3		4	
11	3		4	NO	6	MW	7		7		7		56	55		NO	5	MW	5	W45	NW	4		4		4		2		2	MW	2		3		4		
12	3		4	NW	6	NW	7		7	MW	7		56	55		MW	5	OW	5	45	NW	4		4		42		2		2	MW	2		3		4		
13	3		4	MW	6	MW	7		7	OW	7		56	55		NW	5	MW	5	45	MW	4		4		42		2		2	MW	2		3	MW	4		
14	3		4		6	MW	7	MW	7	OW	7		56	5		W	5		5	5	MW	4		44		4		2		2		2	MW	3	LW	4		
15	3		4		6		7	MW	7	OW	7		56	5		MW	5		5	5	MW	4		44		4		2		MW	2		2		3	MW	4	
16	3		4		6		7	MW	7	OW	7		56	5		LW	5		52	5	LW	4		44		4		2		LW	2		2		3	MW	4	
17	3		4		6		7	MW	7		7		56	5		OW	5		5	5	OO	4		64		4		2		OW	2		2		3	OO	4	
18	3		4		6		7	V	7		7		56	5		KW	52		5	5	OO	4		64		4		2		2		2		3	KW	4		
19	3		4		62		7	KV	7		7		56	5		OV	5		5	5		4		64		4		2		2		2			KV	4		
20	4		6		72		7	KV	7		6		65	5		5		5		4		4		74		2		2		2		3		4	OU	4		
21	4		6		72		7	KU	7		6		65	5		5		53		4		4		74		2		2		2		3		4	KU	4		
22	4		6		72		7	KU	7		6		65	5		5		53		4		4		74		2		2		2		3		4	JO	4		
23	4		6		72		7	KU	7		6		75	45		5		5		4	KU	4		64		2		2		2		3		4	OO	4		
24	4		6		7		7	KU	7		6		75	45		5		5		4		4		64		2		2		2		3		4	KU	4		

BLE XXVI

TORS, JANUARY 1967

16	1 17	1 18	1 19		1 20	1 21	1 22	1 23	1 24	1 25	1 26	1 27	1 28	1 29	1 30	1 31
2	2	OU 3	4	1	4	5	6	7	6	6	6	6	46	6	6	9
2	2	OU 3	42	2	4	5	6	7	6	OU 6	6	6	46	6	6	9
2	2	3	4	3	4	5	6	7	6	OU 6	6	6	46	6	6	9
2	2	OU 3	4	4	4	5	6	7	6	OU 6	6	6	46	6	6	9
2	2	OU 3	4	5	4	5	6	7	OU 6	OU 6	6	6	6	6	6	9
2	OU 2	KU 3	4	6	4	5	6	7	OU 6	OU 6	6	6	6	6	6	9
2	UV 2	3	4	7	4	5	6	7	UV 6	UV 6	6	6	6	6	62	UV 9
2	LM 2	3	4	8	4	5	6	7	LM 6	LM 6	6	6	6	6	LM 6	LM 9
2	MM 2	MM 3	4	9	4	5	6	7	MM 6	MM 6	6	6	6	6	MM 6	MM 9
2	MM 2	MM 3	4	10	4	5	6	7	LO 6	MM 6	MM 6	6	6	6	MM 6	MM 9
2	MM 2	3	4	11	MM44	5	6	7	MM 6	MM 6	MM 6	6	6	6	MM 6	MM 9
2	MM 2	3	4	12	MM44	5	6	7	MM 6	MM 6	MM 6	MM 6	6	62	MM 6	MM 9
2	MM 2	3	MM 4	13	MM44	5	6	7	MM 6	MM 6	6	MM 6	6	6	MM 6	MM 9
2	2	MM 3	LM 4	14	LM 4	5	6	7	6	MM 6	MM 6	MM 6	6	6	MM 6	9
2	2	3	MM 4	15	MM 4	5	6	7	6	6	MM 6	MM 6	6	6	MM 6	9
2	2	3	MM 4	16	MM 4	5	6	MM 7	6	6	MM 6	LM 6	6	6	MM 6	9
2	2	3	30 4	17	LM 4	52	6	MM 7	6	6	MM 6	6	6	6	MM 6	9
2	2	3	MM 4	18	MM 4	5	6	7	6	6	MM 6	6	6	6	MM 6	9
2	2	3	UV 4	19	MM 4	5	6	7	6	6	UV 6	6	6	6	UV 6	9
2	3	4	OU 4	20	MM 5	6	7	6	6	6	OU 6	6	6	6	9	4
2	3	4	KU 4	21	UV 5	6	7	6	6	6	6	6	6	6	9	4
2	3	4	JO 4	22	5	6	7	6	6	6	OU 6	6	6	6	12	4
2	3	4	OU 4	23	5	6	7	6	6	6	OU 6	46	6	6	4	4
2	3	4	KU 4	24	5	6	7	6	6	6	OU 6	46	6	6	9	4

TABLE XXVII
NATURAL FACTORS, FEBRUARY 1967

	2	1	2	2	2	3	2	4	2	5	2	6	2	7
1	OT	4				4		5		3		4		6
2	OT	4				4		5		3		4		6
3	OU	4				4		5		3		4		6
4	OT	4				4		5		3		4		6
5	OU	4				4		5		3		4		OU 6
6	OT	4				4		5		3		4		OU 62
7	OU	4				4		5		3		4		OU 6
8	OU	4				4		5		3		4		LM 6
9	OU	4				4		5		3		4		LM 6
10	MO	4				4		5		3	MO	4		MW 6
11	MW	4	OU	4		4		5		43		4		MW56
12	MW	4	OU	4	MW	4		52		43		4		MW56
13	MW	4	OU	4	MW	4		52		43		4		MW56
14	MW	4	LM	4	MW	4		52		3		42		66
15		4	MW	4	MW	4		5		3	MW	42		66
16		4	LM	4	MW	4		5		3	MW	4		66
17		4	OU	4		4		49		3	LM	4		66
18		4	OU	4		4		49		3	OU	4		66
19		4	OU	4		4		49		3	OU	4		66
20		4	OU	4		5		3		94		6		69
21		4	OU	4		5		3		94		6		69
22		4	OU	4		5		3		94		6		69
23		4	OU	42		5		3		4		6		69
24		4	OU	4		5		3		4		6		OU69

	2	8	2	9	2	10	2	11	2	12	2	13	2	14	2	15	2	16	2	17	
1	OU65				5		4	44		3		3		2	OU	2		3		43	
2	OU55				5		4	44		3		3		2	OU	2		93		3	
3	KU55				5		4	44		3		3		2	OU	2		93		3	
4	JU552				5		4	44		3		3		2	OU	2		93		3	
5	JT55				5		4	4		3		3		2	OU	2		83		3	
6	OT55				5		4	4		3		3		OU	2	JO	2	83		3	
7	KV55				5		4	4		3		3		2	KV	2		83		3	
8	LM55				5		4	4		3		OU	3	LM	2	LM	2	73		3	
9	MW55				5		4	4		32		LM	3	MW	2	LM	2	73		3	
10	MO55				5		4	4		3		MX	3	MW	2	MW	2	0073		3	
11	MV45				MW	5		4		3		MW	3	MW	2	MW	2	M043		MW	3
12	MX45				MW	5		4		3		MV	3	MX	2	MW	2	43		MW	3
13	MW45				MW	5		4		3		OU	3		2	MW	2	43		MW	3
14	MW55				MW	5		MW	4		3		MW	34		2		53		MW	3
15	55				MW	5		MW	4		3		MW	34		2		53		MW	3
16	55				MW	5		4		3		LM	34		2		2	93		MW	3
17	45				LM	5		4		3		LM	34		2		52	43		3	
18	45				LM	5		4		3		OU	3		?	52	43		3		
19	45				5		4	4		3		3		2		52	43		3		
20	5				OU	4		4		3		3		2		2	3	43		3	
21	5				OU	4		4		3		3		2		2	3	43		3	
22	5				OT	4		4		3		3		2		2	3	43		3	
23	5				OT	4		44		3		3		2		2	3	43		3	
24	5				4		44	3		3		3		2	OU	2		3		43	3

TABLE XXVII

AL FACTORS, FEBRUARY 1967

11	2 12	2 13	2 14	2 15	2 16	2 17	2 18	2 19	2 20	2 21	2 22	2 23	2 24	2 25	2 26	2 27	2 28
14	3	3	2 0U 2		3	43	3	2	3	3 0U 4	4	5	45	6	9	8	
14	3	3	2 0U 2		53	3	3	2	3	3 JU 4	4	5	5	6	9	8	
14	3	3	2 0U 2		53	3	3	2	3	3 JU 4	4	52	5	6	9	8	
14	3	3	2 00 2		53	3	3	2	3	3 4	43	5	5	6	9	8	
4	3	3	2 00 2		83	3	3	2	3 0T 3	0T 4	4	5	5	6	9	0T 8	
4	3	3	0U 2 J0 2		83	3	3	2	3 KU 2	0U 4	4	5	5	6	9	0U 8	
4	3	3	2 KV 2		83	3	3	2	3 KV 3	KV 4	4	5	5	6	9	KV 8	
4	3	0W 3	LW 2	LW 2	73	3	3	2	LW 3	LW 3	LW 4	4	5	5	6	9	LW 8
4	32	LW 3	MW 2	LW 2	73	3	3	2	LW 3	MW 3	LW 4	4	5	5	6	9	MW 8
4	3	MX 3	MW 2	MW 2	0073	3	3	2	MW 3	MW 3	0W 42	MW 4	5	5	6	9	MW 8
4	3	MW 3	MW 2	NW 2	M043	MW 3	3	2	NW 3	NW 3	NW 42	0W 4	MW 5	5	6	9	MW 8
4	3	MV 3	NX 2	NW 2	43	NW 3	3	2	MW 3	MW 3	0W 4	NW 4	0W 5	5	6	92	NW 8
4	3	0W 3	2	MW 2	43	NW 3	3	2	MW 3	3	0W 4	MW 4	0X 5	5	6	92	8
4	3	MW 34	2	2	53	MW 3	3	2	NW 3	3	4	NW44	0W 5	5	6	9	8
4	3	MW 34	2	2	53	MW 3	3	2	LW 3	3	4	MW44	MX 5	5	6	9	8
4	3	LW 34	2	2	53	MW 3	3	2	L0 3	3	4	L044	5	5	6	0W 9	82
4	3	LW 34	2	52	43	3	3	2	LW 3	3	4	LW 4	5	5	6	LW 9	8
4	3	0W 3	2	52	43	3	3	2	KW 3	3	4	0W 4	5	5	6	00 9	8
4	3	3	2	52	43	3	3	2	3	3	4	J0 4	5	5	6	9	8
3	3	2	2	3	43	3	2	3	3	4	4	JV 5	52	6	49	8	8
3	3	2	2	3	43	3	2	3	3	4	4	JU 5	5	6	49	8	8
3	3	2	2	3	43	3	2	3	3	4	4	JU 5	5	6	49	8	8
3	3	2	2	3	43	3	2	3	3	4	4	JU 5	45	6	9	8	8
3	3	2	00 2	3	43	3	2	3	3	4	4	5	45	6	9	8	8

TABLE XXVIII
NATURAL FACTORS, MARCH 1967

	3	1	3	2	3	3	3	4	3	5	3	6	3	7	3	8	3	9	3	10	3	11	3	12	3	13	3	14	3	15	3	16	3	17	3	18	3
1	OT	0	0	9	0	0	0	7	6	4	4	4	4	3	3	2	2	2	2	3	43	4															
2	OT	0	0	9	0	0	0	7	6	4	4	4	4	3	3	2	2	2	2	3	3																
3	OT	0	0	9	02	0	0	7	6	4	4	4	4	3	3	2	2	2	2	3	3																
4	OT	0	0	9	0	0	0	7	6	4	4	4	4	3	3	2	2	2	2	3	32																
5	OO	0	0	9	0	0	0	7	6	4	4	4	4	3	3	2	2	2	2	3	3																
6	OT	0	0	9	0	0	0	7	6	4	4	4	4	3	3	2	2	2	2	3	3																
7	JV	0	0	9	0	0	0	7	6	4	4	4	4	3	3	2	2	2	2	3	3																
8	KV	0	0	9	0	0	0	7	6	4	4	4	4	3	3	2	2	2	2	3	3																
9	MV	0	0	9	0	0	0	72	6	4	4	4	4	3	3	2	2	2	2	3	3																
10	0	0	0	9	02	0	0	7	6	4	4	4	4	3	3	2	2	2	2	3	3																
11	0	02	0	9	0	0	0	7	6	4	4	4	4	3	3	2	2	2	2	3	63	92															
12	0	0	0	9	0	0	0	7	6	4	4	4	4	3	3	2	2	2	2	3	63	92															
13	0	0	0	9	0	0	0	7	6	4	4	4	4	3	3	2	2	2	2	3	63	92															
14	0	0	0	9	0	0	0	7	6	4	4	4	4	3	3	2	2	2	2	3	3	42															
15	0	0	0	9	0	0	0	7	6	4	4	4	4	3	3	2	2	2	2	3	3	42															
16	0	0	0	9	0	0	0	7	6	4	4	4	4	3	3	2	2	2	2	3	3	42															
17	0	0	0	9	0	0	0	7	6	4	44	4	4	3	3	2	2	2	2	3	3	92															
18	02	0	0	9	0	0	0	7	6	4	44	4	4	3	3	2	2	2	2	3	3	92															
19	02	0	0	9	0	0	0	7	6	4	44	4	4	3	3	2	2	2	2	3	3	92															
20	0	9	0	0	0	7	6	4	4	4	43	3	2	2	2	2	2	2	3	3	42	3															
21	0	9	0	0	0	7	6	4	4	4	43	3	2	2	2	2	2	2	3	3	42	3															
22	0	9	0	0	0	7	6	4	4	4	43	3	2	2	2	2	2	2	3	3	42	3															
23	0	9	0	0	0	7	6	4	4	4	3	3	2	2	2	2	2	2	3	43	42	3															
24	0	9	0	0	0	7	6	4	4	4	3	3	2	2	2	2	2	2	3	43	42	3															

RURAL FACTORS, MARCH 1967

[illegible]

TABLE XXIX

NATURAL FACTORS, APRIL 1967

4	1	4	2	4	3	4	4	4	5		4	6	4	7	4	8	4	9	4	10	4	11	4	12	4	13	4	14	4	15	4	16	4	17	4	18		
1	9		3		2		42		3		1	OT 3		3		5		3		3		3		2		3		2		2		1		42		2		
2	9		J		2		2		3		2	OT 3		3		5		3		3		3		2		3		2		2		1		2		2		
3	9		3		2		2		3		3	OU 3		3		5		3		3		32		2		3		2		2		1		2		2		
4	9		32		2		2		3		4	OU 3		3		5		3		3		3		2		3		2		2		1		2		2		
5	49		43		2		2		3		5	OU 3		3		5		3		3		3		2		3		2		2		1		2		2		
6	49		43		2		2		JV 3		6	OU 3		3		5		3		J		3		2		3		2		2		1		2		KT 2		
7	49		43		2		2		KW 3		7	KV 3		3		5		3		3		3		2		3		2		2		1		2		LU 2		
8	49		43		2		52		MW 3		8	LV 3		3		5		3		3		3		LV 2		3		2		2		1		2		LU 2		
9	49		43		2		52		MW 3		9		3		3		5		3		3		MW 3		MW 2		3		2		2		1		2		MU 2	
10	49		43		2		52				10		3		3		5		3		MW 3		MW 3		MW 2		MW 3		MW 2		2		1		MW 2		MU 2	
11	9		3		2		OW 2				11		3		3		5		3		MW 3		MW 3		MW 2		MW 3		MW 2		2		1		MW 2		MV 2	
12	9		3		2		OW 2				12		3		3		5		3		MW 3		MX 3		MW 2		MX 3		NW 2		2		1		MW 2		MW 2	
13	J		3		2		OW 2		MV 3		13	OX 3		3		5		3		MW 3		MX 3		MX 2		NX 3		NW 22		2		1		MW 2		MW 2		
14	99		3		2		OX 2		MW 3		14	OX 3		MX 3		5		3		MW 3				3	MX 2		NW 3		MW 2		2		1		MW 2		2	
15	99		3		2		OX 2				15	MW 3		MW 3		5		3		LW 3		3		2		MW 3				2		2		1		MW 2		2
16	99		3		2		2				16	MX 3		MW 3		5		3		LX 3		3		2		MW 3				2		2		1		MW 2		2
17	49		3		2		LX 2				17	LW 3		3		5		3		LX 3		3		2		LW 3				2		2		1		LW 2		2
18	49		3		2		2				18	KW 3		3		5		3		W 3		3		2		LW 3				2		2		1		KW 2		2
19	49		3		2		2				19	KW 3		3		5		3		3		3		2		KW 3				2		2		1		KW 2		2
20	3		2		2		3				20	KV 3		3		5		3		3		3		2		3		V 2		2		1		42		2		42
21	3		2		2		3				21	U J		5		3		3		3		3		2		3		OU 2		2		1		42		2		42
22	3		2		2		3				22	U 3		5		3		3		3		3		3		3		OU 2		2		1		42		2		42
23	3		2		42		3				23	U 3		5		3		3		3		3		2		3		OU 2		2		1		42		2		42
24	3		2		42		3		OU 3		24	JO 3		5		3		3		3		3		2		3		OU 2		2		1		42		2		42

TABLE XXIX

L FACTORS, APRIL 1967

13	4 14	4 15	4 16	4 17	4 18	4 19	4 20	4 21	4 22	4 23	4 24	4 25	4 26	4 27	4 28	4 29	4 30
3	2	2	1	42	2	OU42	2	3	3	4	93	3	OV 3	2	3	3	3
3	2	2	1	2	2	42	2	3	93	4	3	3	3	2	3	3	32
3	2	2	1	2	2	OU42	2	3	93	4	3	3	T 3	2	3	3	3
3	2	2	1	2	2	JT42	2	3	93	4	3	3	T 3	2	3	3	3
3	2	2	1	2	2	JT42	2	3	43	4	43	3	T 3	2	3	3	3
3	2	2	1	2	KT 2	KT42	2	3	43	4	43	K 3	JT 3	2	3	3	3
3	2	2	1	2	LU 2	LV42	2	3	43	4	43	LM 3	JV 3	2	3	3	3
3	2	2	1	2	LU 2	MV 2	2	3	3	4	43	LM 3	OV 3	2	3	3	3
3	2	2	1	2	MU 2	MV 2	2	MV 3	3	4	MW43	MW 3	MV 3	2	3	3	3
3	MW 2	2	1	MW 2	MU 2	MV 2	MW 2	MV 3	3	4	MW43	MW 3	MW 3	2	3	3	3
3	MW 2	2	1	MW 2	MV 2	MV 2	2	MW 3	3	54	MW43	MW 3	MV 3	2	MW 3	3	3
3	MW 2	2	1	MW 2	MW 2	MW 2	2	MW 3	3	54	MW43	MW 3	MW 3	2	MW 3	3	3
3	NW 22	2	1	MW 2	MW 2	MW 2	2	MW 3	3	54	MX43	MX 3	MW 3	2	MW 3	3	3
3	MW 2	2	1	MW 2	2	MW 2	2	MW 3	3	54	MX43	3	MV 3	2	MW 3	3	3
3	2	2	1	MW 2	2	2	MW 2	MW 3	3	54	MW43	3	3	2	MW 3	3	3
3	2	2	1	MW 2	2	2	MW 2	MW 3	3	54	MW43	3	3	2	3	3	3
3	2	2	1	LW 2	2	2	MW 22	3	3	4	LW 3	3	3	2	3	3	3
3	2	2	1	KW 2	2	2	LX 2	3	3	4	LW 3	3	3	2	3	3	3
3	2	2	1	KW 2	2	2	JW 2	3	3	4	M 3	3	3	2	3	3	3
2	2	1	42	2	42	2	JV 3	3	44	93	3	3	2	3	3	3	3
2	2	1	42	2	42	2	JU 3	3	44	93	3	3	2	3	3	3	3
2	2	1	42	2	42	2	JU 3	3	44	93	3	3	2	3	3	3	3
2	2	1	42	2	42	2	U 3	3	4	93	3	3	2	3	3	3	3
2	2	1	42	2	42	2	3	3	4	93	3	V 3	2	3	3	3	3

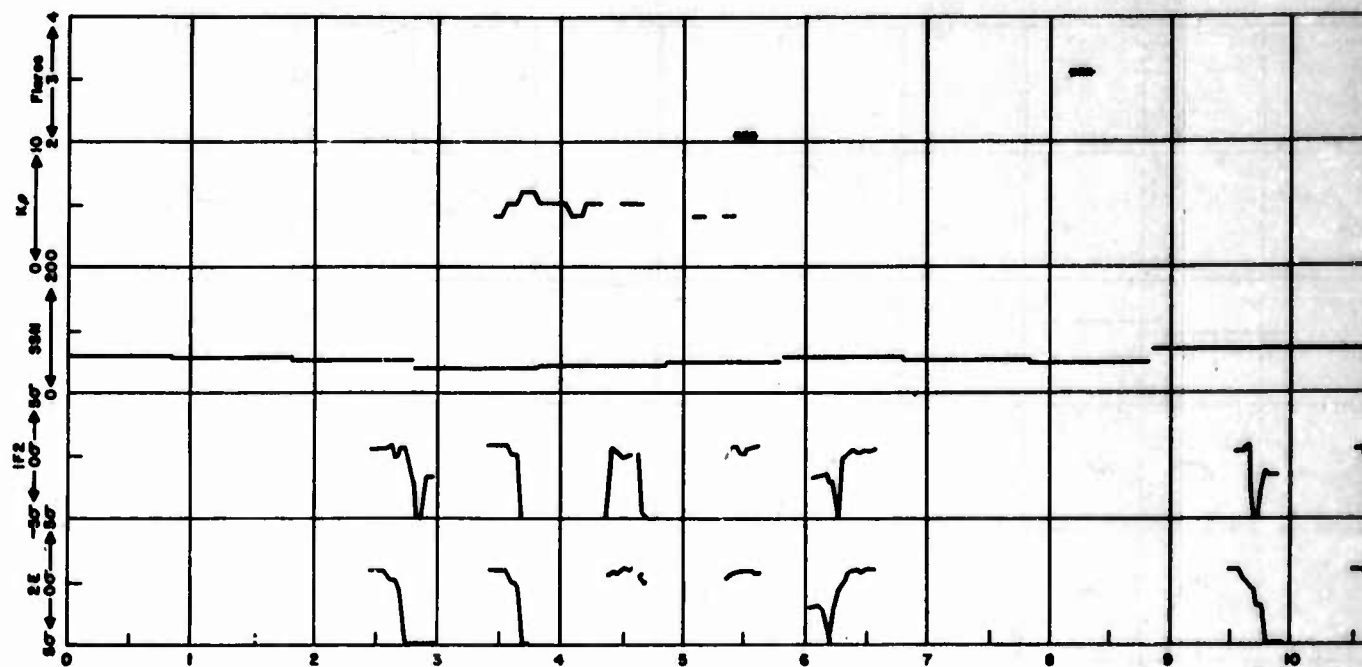
TABLE XXX
NATURAL FACTORS, MAY 1967

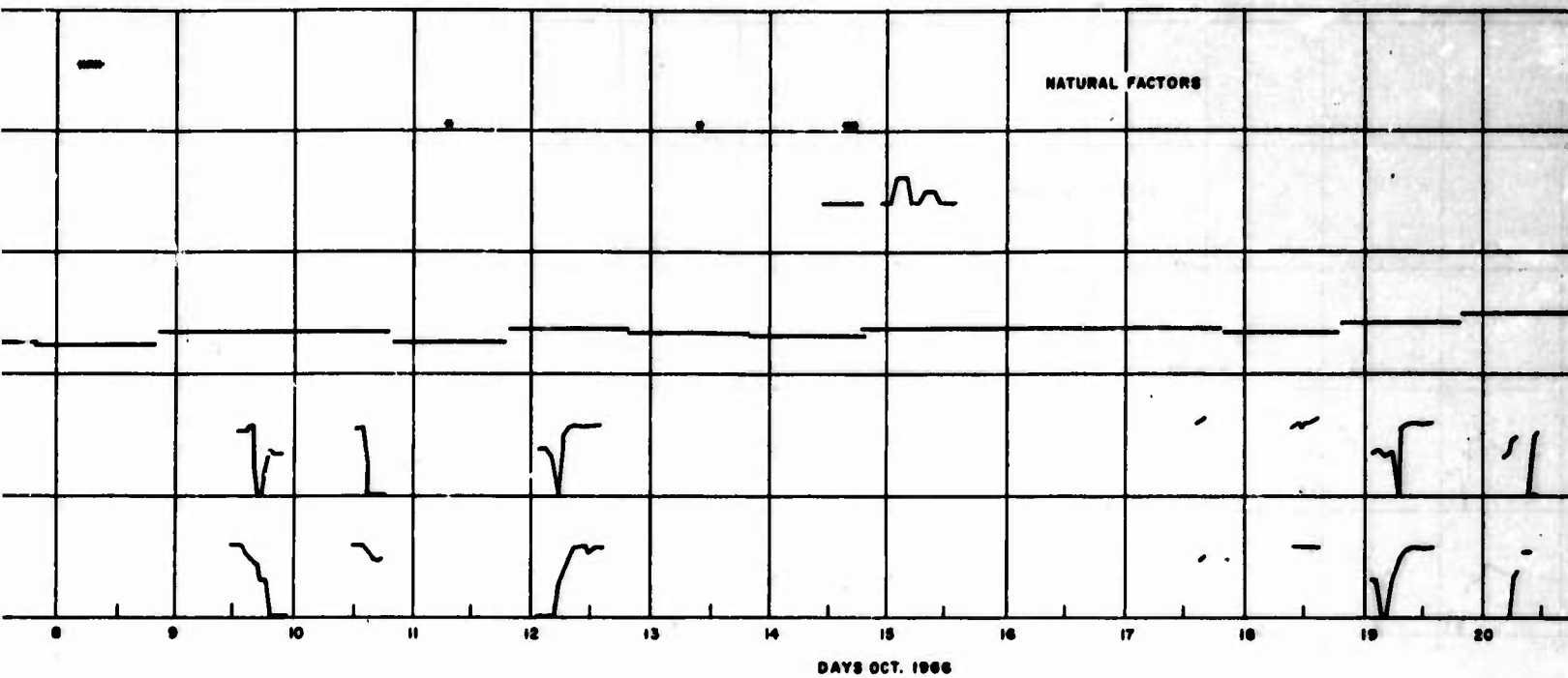
	1	5	2	5	3	5	4	5	5	5	6	5	7	5	8	5	9	5	10	5	11	5	12	5	13	5	14	5	15	5	16	5	17	5	18	5	19	5	20
1	3	3	72	43	3	2	52	0	1	OU 0	1	41	51	1	1	1	1	1	1	2	3	3																	
2	3	3	52	3	3	2	52	0	1	OU 0	1	1	1	1	1	1	1	1	1	2	3	3																	
3	3	3	52	3	3	2	52	0	1	OU 0	1	1	1	1	1	1	1	1	1	2	3	3																	
4	3	32	52	3	3	2	52	0	1	OU 0	1	1	1	1	1	1	1	1	1	22	32	3																	
5	3	OU532	72	3	3	2	2	0	JU 1	OU 0	1	1	1	1	13	1	1	22	32	3																			
6	3	JU53	KU72	3	3	2	2	0	LV 1	OV 0	1	1	1	1	1	1	2	3	3																				
7	3	KU53	LO72	3	33	2	2	03	LW 1	LV 0	1	1	1	1	1	LV 1	LV 1	2	LV 3	3																			
8	3	LV 3	72	3	3	2	2	03	MW 1	LV 02	1	1	1	1	4U 1	1	MU 1	MU 2	MU 3	3																			
9	32	MV 3	72	3	3	2	2	KT 03	MW 1	MV 0	1	1	1	1	4U 1	1	MU 1	2	MV 3	3																			
10	3	3	M072	3	3	22	2	MV 0	MW 1	MV 0	1	1	1	1	4V 1	1	MV 1	2	MV 3	3																			
11	3	MX43	72	3	3	2	2	MV 0	MW 1	0	MV 1	MU 1	1	1	4V 1	1	MV 1	MV 2	NV 3	32																			
12	3	LW43	72	OV 3	MW 3	2	2	MW 0	MW 1	0	MV 1	LV 1	1	1	1	1	NV 1	MV 2	3	3																			
13	3	LW43	72	3	MW 3	2	2	MW 0	MX 1	0	MW 1	OV 1	1	1	1	1	MW 1	OW 1	MV 2	3	3																		
14	53	43	OW52	MW 3	MW 3	2	2	MX 0	1	0	MW 1	LV 1	1	1	1	1	MW 1	MW 1	NV 2	3	3																		
15	43	43	52	MW 3	MW 3	2	2	MX 0	1	0	MX 1	MW 1	1	1	1	1	MW 1	MV 1	2	3	3																		
16	53	43	52	MW 3	MW 3	2	2	MX 0	1	MY 0	MX 1	1	1	1	1	4W 1	MW 1	MW 1	2	3	3																		
17	43	53	2	MW 3	3	2	2	LW 0	1	LX 0	LX 1	1	1	1	1	LW 1	LW 1	LW 1	LW 2	3	3																		
18	KW43	53	2	MW 3	3	2	2	KW 0	1	MW 0	LW 1	1	1	1	1	1	1	LW 1	KW 2	3	3																		
19	OW43	53	2	3	3	2	2	0	1	LX 0	LW 1	1	1	1	1	1	1	1	2	3	3																		
20	3	62	43	KV 3	2	2	0	1	0	JV 1	LO41	1	1	1	1	1	2	3	3	4																			
21	3	62	43	OV 3	2	2	0	1	0	1	OU41	1	1	1	1	1	2	3	3	4																			
22	3	62	43	OU 3	2	2	0	1	0	1	JU41	1	1	1	1	1	2	3	3	4																			
23	3	72	43	OU 3	2	52	0	1	0	1	JU41	51	1	1	1	1	2	3	3	4																			
24	3	72	43	OU 3	2	52	0	1	0	1	OU41	51	1	1	1	1	2	3	3	4																			

TABLE XXX

L FACTORS, MAY 1967

5 15	5 16	5 17	5 18	5 19	5 20	5 21	5 22	5 23	5 24	5 25	5 26	5 27	5 28	5 29	5 30	5 31	12 31
1	1	1	2	3	3	4	5	6	OV 7	7	98	9	9	77	6	KW66	
1	1	1	2	3	3	4	5	6	JV 7	7	78	9	493	67	6	JV56	
1	1	1	2	3	3	4	5	6	KU 7	7	78	9	49	67	6	JV56	
1	1	1	22	32	3	4	5	6	KU 7	7	78	9	49	67	6	JV56	
13	1	1	22	32	3	4	5	6	KV 7	57	78	9	69	47	6	OW 6	
1	1	1	2	3	3	4	5	KV 6	K 7	572	78	9	69	47	6	V 6	
1	LV 1	LV 1	2	LV 3	3	4	5	LW 6	LW 7	572	78	9	69	47	6	LW 6	
4U 1	1	MU 1	MU 2	MU 3	3	4	5	MW 6	MW 7	87	78	9	69	57	66	MW 6	
4U 1	1	MU 1	2	MV 3	3	42	5	MW 6	MW 7	87	78	9	69	57	66	6	
4V 1	1	MV 1	2	MV 3	3	4	MV 5	MW 6	MW 7	87	78	9	69	NU572	66	6	
4V 1	1	MV 1	MV 2	OV 3	32	4	MW 5	NW 6	MW 7	NW77	48	9	79	MU 7	66	46	
1	1	NV 1	MV 2	3	3	4	NW 5	MX 6	MX 7	NX77	48	9	79	NU 7	66	46	
1	MW 1	OW 1	MV 2	3	3	4	NW 5	MV 6	MX 7	MX77	48	9	79	NU 7	66	NX46	
1	MW 1	MW 1	OV 2	3	3	4	NW 5	463	MY47	NW87	MU48	49	69	NU 7	66	MX46	
1	MW 1	MV 1	2	3	3	4	NW 5	46	47	NW87	MU48	49	69	MO 7	66	46	
4W 1	MW 1	MW 1	2	3	3	4	MW 5	46	47	MW87	48	49	69	MO 7	66	46	
LW 1	LW 1	LW 1	LW 2	3	3	4	MW 5	6	7	LW97	58	49	59	7	66	6	
1	1	LW 1	KW 2	3	3	4	LW 5	6	7	KX97	58	49	59	7	66	6	
1	1	1	2	3	3	4	KV 5	6	7	OW97	58	49	59	7	66	6	
1	1	2	3	3	4	52	6	7	7	JW98	9	49	67	6	76	3	
1	1	2	3	3	4	5	6	7	7	98	9	49	67	6	76	3	
1	1	2	3	3	4	5	6	7	7	OT982	9	49	67	6	76	3	
1	1	2	3	3	4	5	6	7	7	OT982	9	9	77	6	66	3	
1	1	2	3	3	4	5	6	7	7	0098	9	9	77	6	66	3	





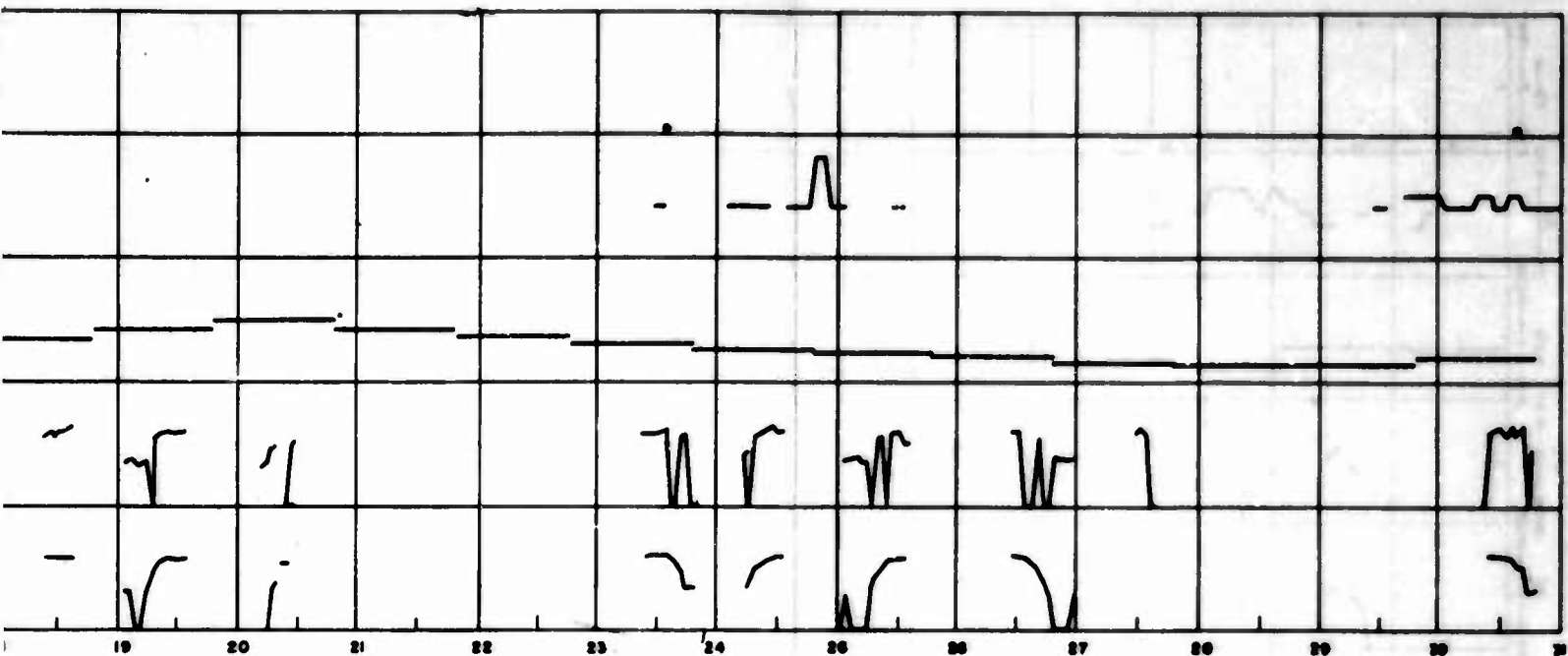


Figure 199. Natural Factors, October 1

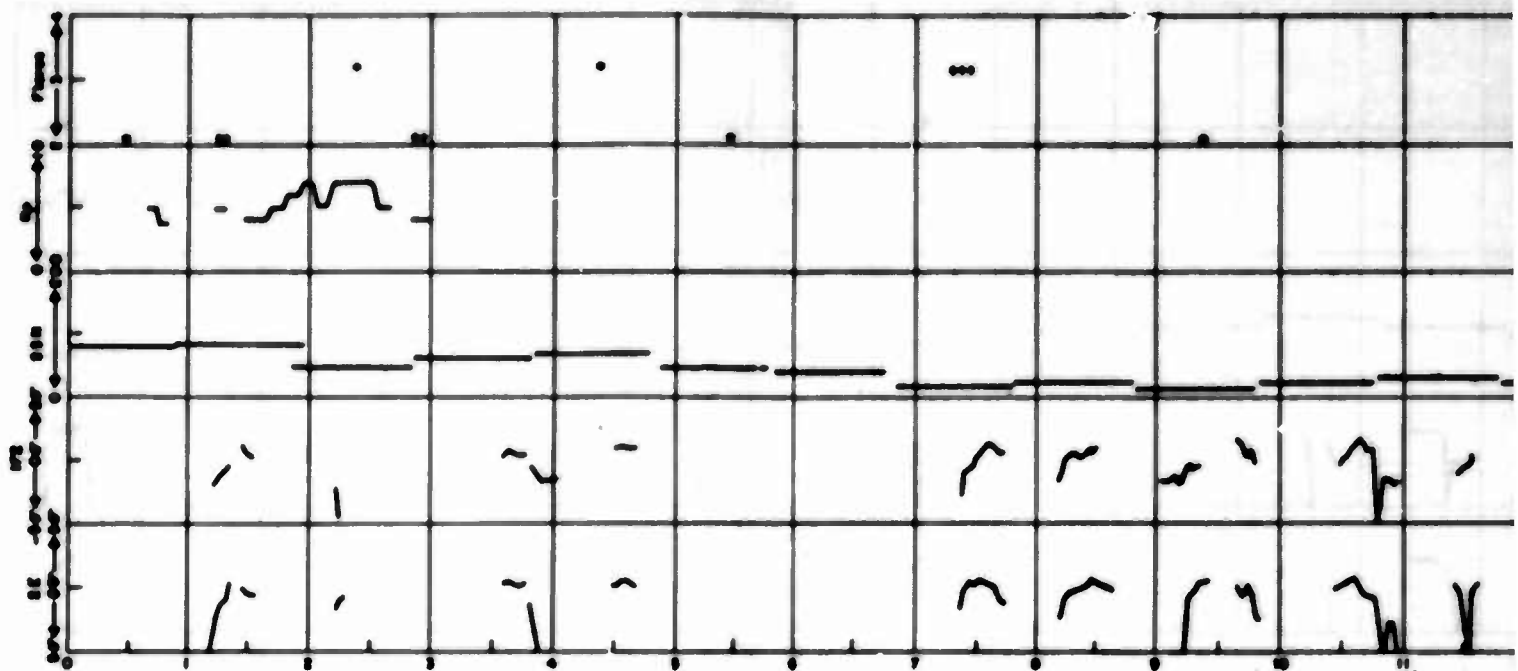
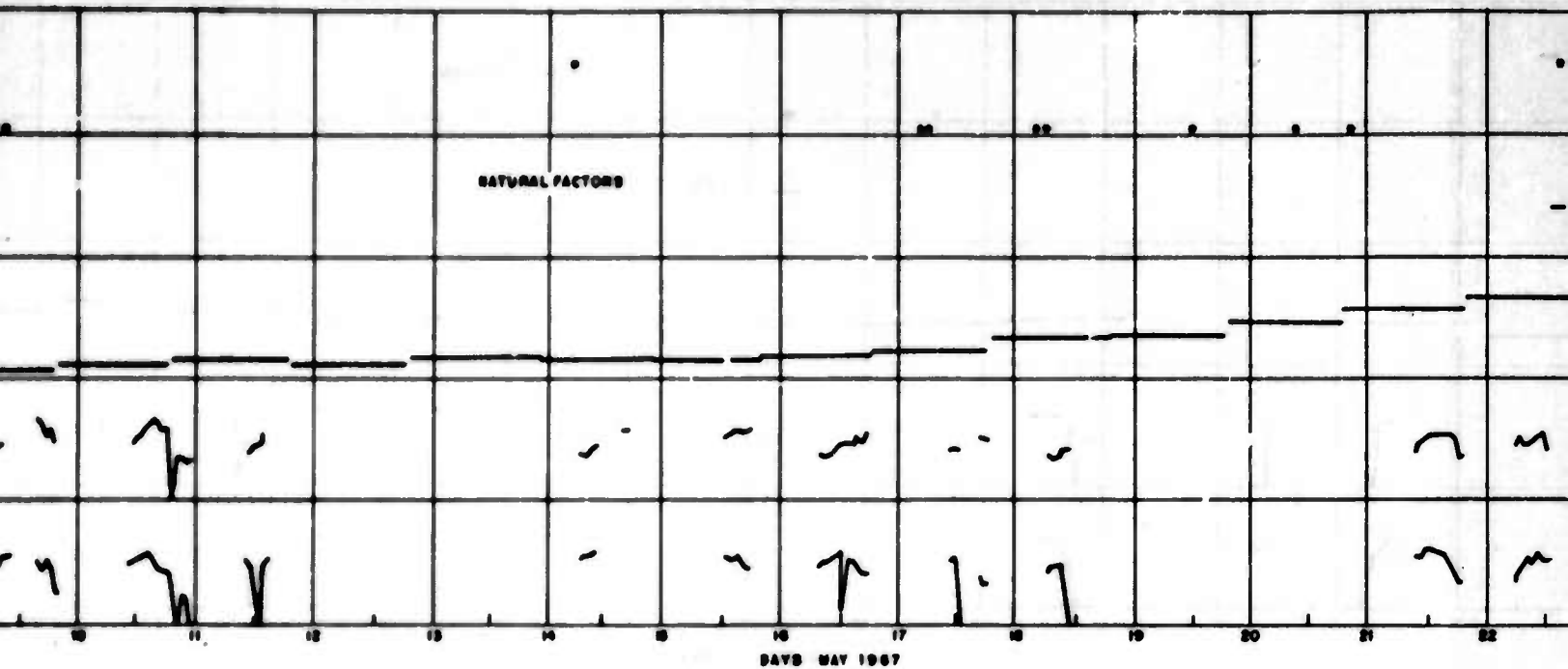
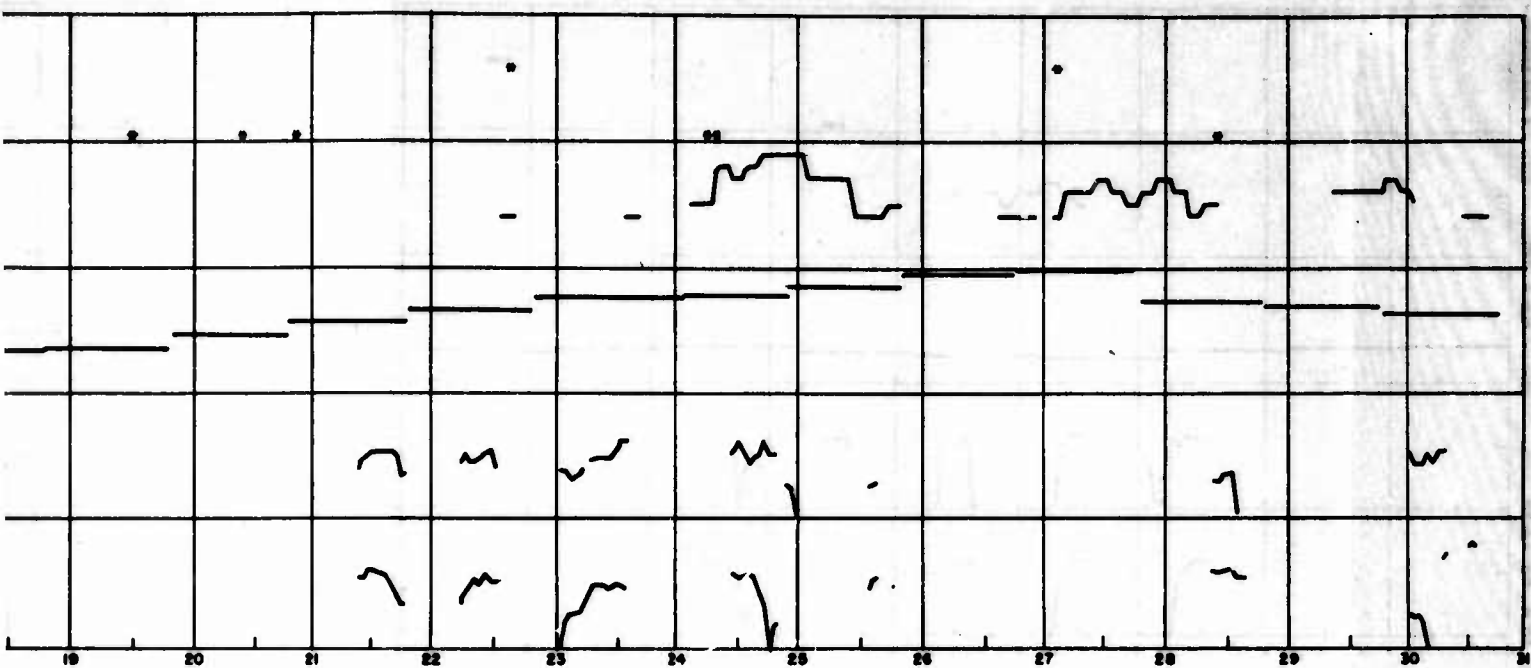


Figure 200. Natural Factors, May 1967





SECTION IV

MODE LOSS EXPERIMENT

No mode loss data for the Coco Solo path have been reduced and analyzed for the time after March 1967. The mode loss results for this path have been published in previous reports (Refs. 2, 4, and 6) covering the period from October 1965 to February 1967. There are a number of reasons for this situation: (1) the receiving site was moved during the early part of March 1967 from the RADC facility at Stockbridge to a new one at the RADC Starr Hill Test Annex which is near Remsen, New York, and (2) the primary emphasis during this period of time was placed on the checkout of digital equipment which would allow a more thorough and complete analysis of mode loss results received on two orthogonal antennas to be performed.

An additional-loss term (AL_{2E}) (which is equivalent to the excess loss) has been described* that would allow more accurate predictions to be made for the absorption loss for 2E mode propagation, based on measurements made on the Coco Solo path. In view of the measurement corrections reported in reference 6 (pages 121-123), the equation for AL_{2E} has been modified using the average of the reported values for February through May 1966 (11 dB). The new expression for AL_{2E} is

$$AL_{2E} = 37.3 \left[\frac{1.13f}{MUF} - 1 \right] \quad (\text{dB}) \quad (22)$$

where

f is the measurement frequency in MHz

MUF is the predicted maximum usable frequency for the 2E mode in MHz using the method described in reference 11

It should be pointed out that AL_{2E} should be used in conjunction with the reference 8 absorption loss equation without the 8.4-dB factor to predict the total ionospheric loss as defined in Figure 201.

* Reference 4, pp. 102-111

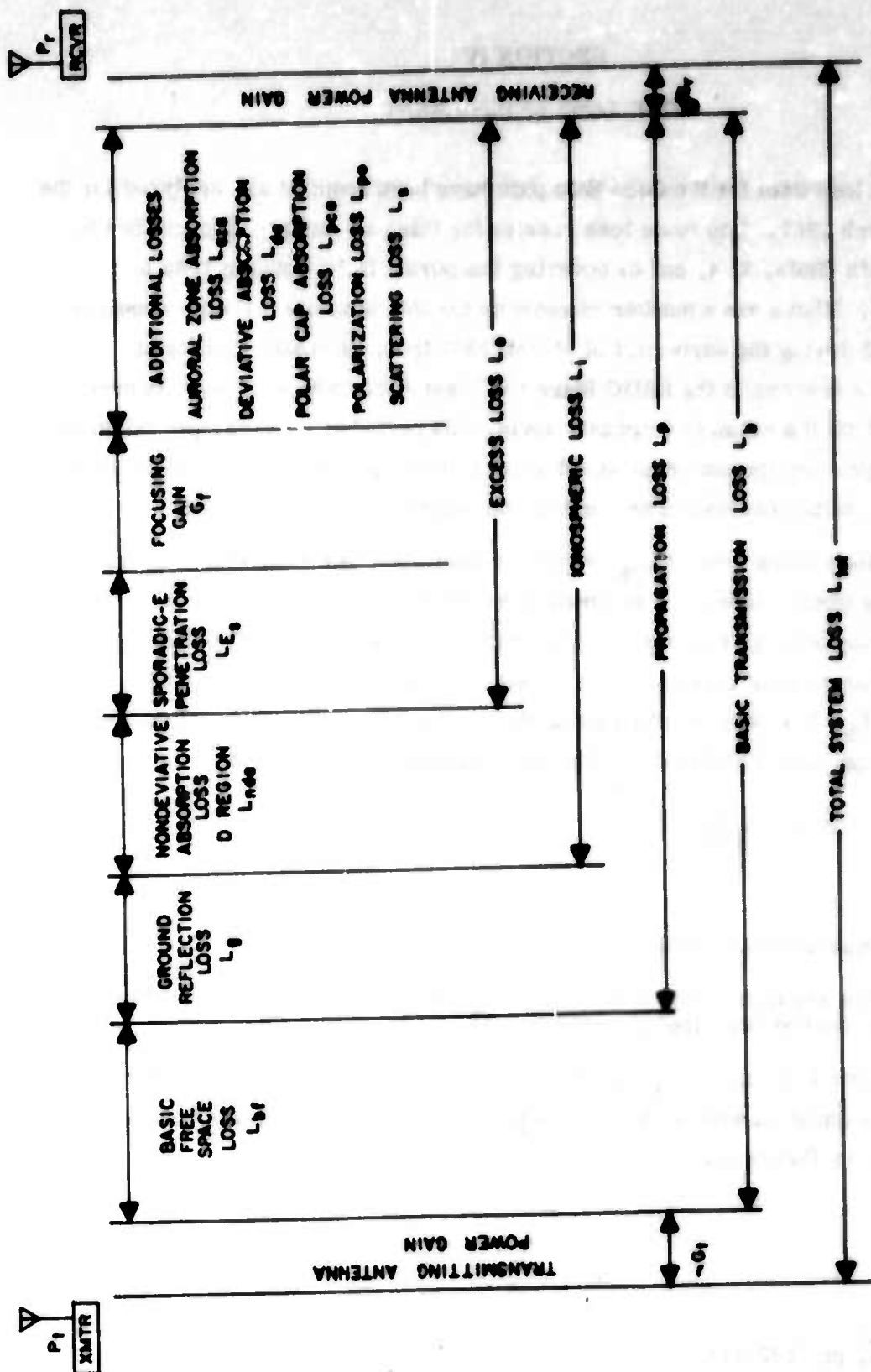


Figure 201. Loss Nomenclature

Using the data collected from February 1966 to February 1967 over the Coco Solo to Stockbridge path on both the mode reliability and mode loss experiments, a data bank of punched cards was prepared that could be employed for more detailed statistical analysis of the mode loss results. Due to time and funding considerations, a complete investigation of factors affecting the mode loss using this data bank was not possible; however, an example of the type analysis that can be performed using this information is depicted in Figure 202. The excess loss measured for 2E mode propagation at 11.3 MHz is plotted against the ratio f/MOF where f is the measurement frequency (11.3 MHz for this example) and MOF is the maximum observed frequency for the 2E mode as determined from the oblique ionogram taken at approximately the same time as the mode loss data. The numbers 1 through 9 in this plot represent the number of events at the particular point in question. A letter "A" stands for numbers greater than 9. The jagged line represents the average value of the excess loss as determined from all the appropriate data points collected over a 13-month period. The straight line represents the excess loss (AL_{2E}) as expressed by Equation (22) which is based on four months of 2E mode loss data at 11.3 MHz. A careful examination of these two curves in Figure 202 indicates a very good agreement between them and a confirmation of the previous investigation.

The antenna gain patterns for the antennas employed for the mode loss experiment of both the RADC Stockbridge facility and at the Coco Solo transmitting site are shown in Appendix IV. Included are the patterns for both arrays that were used at Coco Solo.

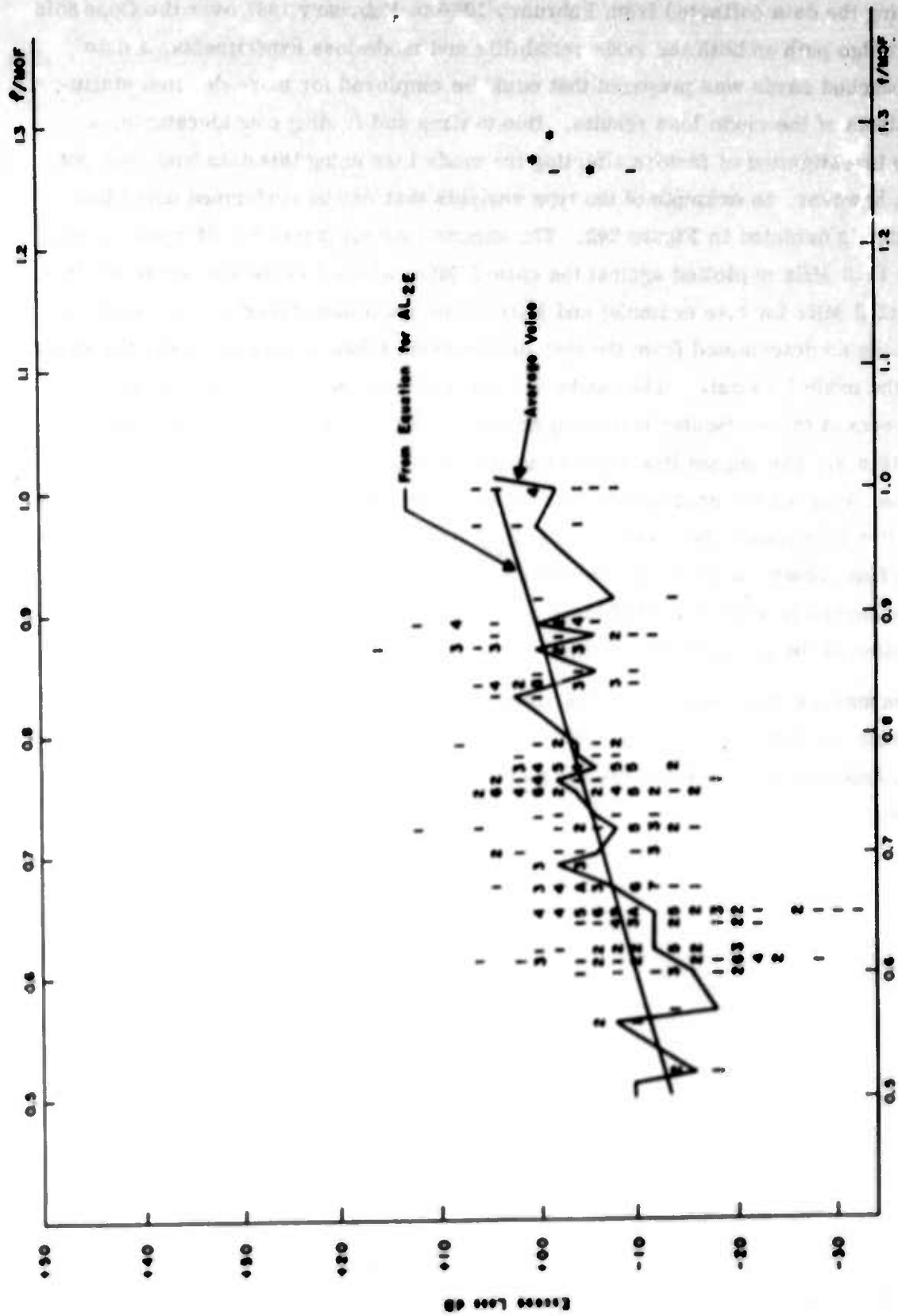


Figure 202. Excess Loss VS. $1/MOF$ For 2E Mode At 11.3 MHz (No. of Points 431, Daytime Only)

SECTION V

SPECTRUM EXPERIMENT

1. INTRODUCTION

The purpose of the spectrum experiment is to ultimately determine the effect of the ionosphere and other variables on signal coherence, signal doppler, and signal spectral shape. The OHR system designer must have a knowledge of these three outputs in order that he might determine the optimum processing format, the radar's capability in a doppler processing mode (i.e., one can easily envision the desirability of detecting targets which have an extremely low relative velocity), and the back-scatter results to be expected from forward propagation measurements, respectively.

On this program almost all of the effort on this experiment has been aimed at obtaining signal coherence information because it was felt that the doppler resolution capability of the measuring system was not fine enough to give desirable enough signal doppler and signal spectral shape information. Recently instrumented modifications to the measurement system now make it feasible to obtain doppler shifts to an accuracy on the order of 0.01 Hz; therefore, subsequent data collection should be aimed at obtaining doppler as well as signal coherence information. The fine doppler resolution capability of the modified system will make it feasible to determine whether the signal spectral shape is really gaussian as has been assumed in the work to date.

Signal coherence data obtained on this experiment for the period 23 September 1966 through 7 July 1967 will be presented in this report. Coco Solo to Central New York data are available for the entire period, while Thule to Starr Hill data are available for the period 26 April through 7 July 1967. System configuration changes since the last experimental report* will also be discussed. The coherent integration loss factor, L_1 , associated with coherently integrating a received pulse train of partially incoherent pulses will be discussed and used to show that the definition of signal coherence as numerically equal to one-half the half-amplitude width of the normalized signal autocorrelation function is indeed an adequate and desirable measure of signal coherence. Results for the processing gain obtained using various types of signal integration for an example OHR system will also be discussed.

* Reference 6

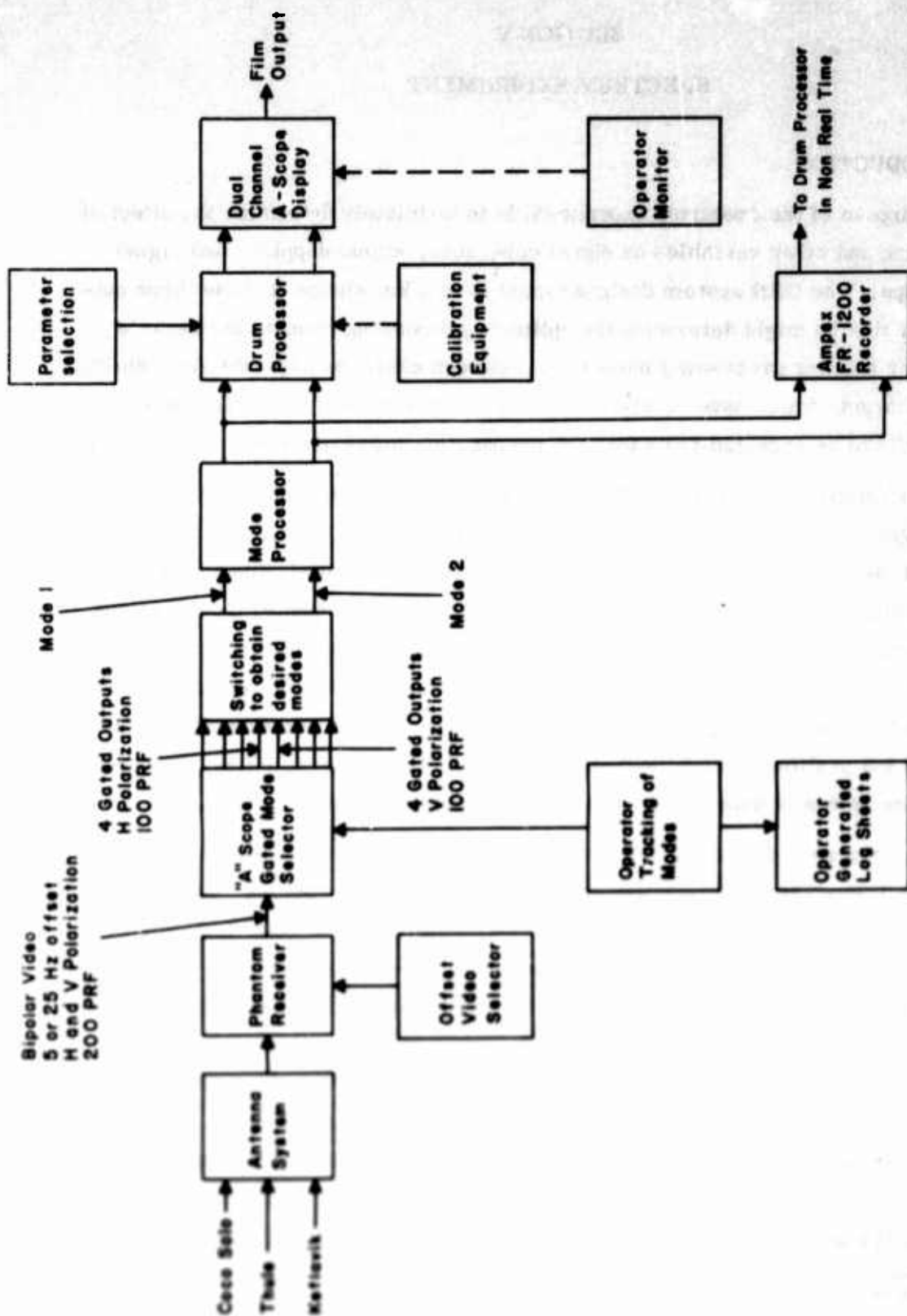


Figure 203. Data Collection for the Spectrum Experiment

2. EQUIPMENT AND EXPERIMENTAL PROCEDURES

The basic instrumentation setup employed for the spectrum experiment for data gathered through 7 July 1967 is shown in reference 6, Figure 108. For this basic setup, data taking was generally restricted to the real time processing of any combination of two of up to four gated modes received using one of the horizontally polarized antennas. The drum processor was limited to 100 or 200 steps of the scanning oscillator with two nominal 20-kHz bandwidth analysis filters (single 3.5-kHz and 30.0-kHz bandwidth analysis filters were also available). As shown in reference 6, the equipment placed an upper bound on the measurement of signal coherence time of about 6.5 seconds. Finally, the requirement of processing the chosen mode returns in real time required that the following parameters be selected by the operator without knowing the nature of the output to be expected:

1. Video offset frequency (i.e., 5.0 or 25.0 Hz).
2. Step mode of the scanning oscillator (100 or 200),
3. Drum processor frequency resolution (high, 0.1 Hz; or low, 0.50 Hz), and
4. Drum processor storage time (10 or 200 seconds in the high resolution mode; 2 or 200 seconds in the low resolution mode).

To alleviate these restrictions the spectrum experiment configuration of Figure 108 of reference 6 was modified to that of Figure 203. With this new configuration, the restriction of real time processing has been removed by the addition of the Ampex tape recorder. The restriction of simultaneously processing only two modes still exists because the mode processor is limited to two channels; however, these two modes can be chosen from the eight gated modes possible considering both the horizontally and vertically polarized receive antennas (i.e., four possible for each polarization). This allows a comparison of the same mode on both polarizations to determine whether mode spectral characteristics are a function of polarization. The switching is set up such that any combination of two of the four possible modes from the horizontal antenna may be selected in place of one mode of each polarization. Finally, the parameter selection possibilities for the spectrum analyzer (magnetic drum processor) have been increased to the extent that:

1. Either a 100-, 200-, 400-, or 800-step mode for the scanning oscillator may be selected; therefore, it is now possible to choose frequency step sizes of 0.09, 0.045, 0.0225, and 0.01125 Hz in the high resolution drum

processor mode or 0.45, 0.225, 0.1125, and 0.05625 Hz in the low resolution mode. Using the analysis from reference 6 for a half-cosine modulation function, the theoretical upper limit in the determination of signal coherence time, assuming impulse sampling by the drum processor, is $0.393 (\Delta f)^{-1}$ second where Δf is given above for each frequency step size; thus, for 100-, 200-, 400-, and 800-step scan oscillator modes, the theoretical upper bound on determining τ_0 is 4.37, 8.75, 17.5, and 35.0 seconds, respectively, for the high resolution drum processor mode and 0.87, 1.75, 3.50, and 7.0 seconds, respectively, for the low resolution drum processor mode.

2. The drum processor frequency resolution versatility has been increased by the addition of 5-kHz analysis filters such that in the high resolution mode, frequency resolutions of 0.025 or 0.10 Hz are possible; while in the low resolution mode frequency resolutions of 0.125 or 0.50 Hz are possible.
3. Storage time on the drum processor has been made much more versatile in that the data on the instrumentation recorder may be played back at a speed other than that used for recording.
4. The addition of the tape instrumentation recorder removes the restriction of having to choose the correct spectral processing parameters (frequency sampling interval, frequency resolution, and integration or storage time on the drum processor) on a real time basis; thus, the data bank for the spectrum experiment should grow at a significantly faster pace in the future since improper results caused by processing over nonstationary time intervals, equipment malfunctions (in the processing and recording equipment), and operator error may be corrected by reprocessing the tape recorded data at a later date. The effect of ionospheric and other disturbances may in the future be more thoroughly investigated because of the ability to process data after the disturbances have been identified.

3. DATA REDUCTION AND PROCESSING

a. Format and Handling

The reduction of voltage spectrum magnitude data was handled in the same manner for this report as described in reference 6.

b. Computer Program

The computer program used to process the reduced mode spectrum values is the same as that utilized for the data presented in reference 6 because the system block diagram of Figure 203 was not finalized until 1 August 1967 after the data collection for this experiment had been completed. No attempt was made to mathematically compensate for the nonimpulsive nature of the sampling process in the analyzer section of the drum processor because of the present installed capability of processing future data of much greater signal coherence times.

4. RESULTS

a. Coco Solo to Central New York Path

Histograms of the one-way signal coherence results for the 1F2, 2E, 2F2, 3E, and 2E_g modes propagated over the Coco Solo path using data obtained on both channels of the drum processor during the period 23 September 1966 to 5 July 1967 are shown in Figure 204. The Central New York receiving station was located at Stockbridge for data collection until 1 March 1967, after which it was at Starr Hill (the first reducible data for this path were obtained on 26 April 1967). The histograms of Figure 204 represent a combination of the data for the whole period while Figure 205 shows the separate histograms for the primary modes (1F2, 2E, and 2F2) for data collected utilizing each respective receiving site. The total measurement time (TMT) that each mode was observed and the number of different measurement days (NMD) that the data analyzed were obtained on are shown in both Figures 204 and 205. Figure 206 is a plot of signal coherence time versus time of day (GMT) for 2E and 1F2 mode data obtained on 25 and 26 May 1967 when a significant auroral event occurred. The 2E mode data for Figure 206 were obtained from 2205 through 2328 GMT at a 22.4-MHz operating frequency with the drum processor in its high resolution 10-second storage time mode. The 1F2 data of Figure 206 were obtained from 0213 through 0422 GMT at a 13.0-MHz operating frequency with the drum processor in its low resolution two-second storage time mode. It should be noted that the 1F2 data of Figure 206 have not been included in the results of Figures 204 and 205.

b. Thule to Starr Hill Path

The histograms of Figure 207 represent the one-way signal coherence time for the 1F2 and 2E modes using data obtained on both channels of the drum processor during the period 26 April through 5 July 1967 on the Thule to Starr Hill path. The

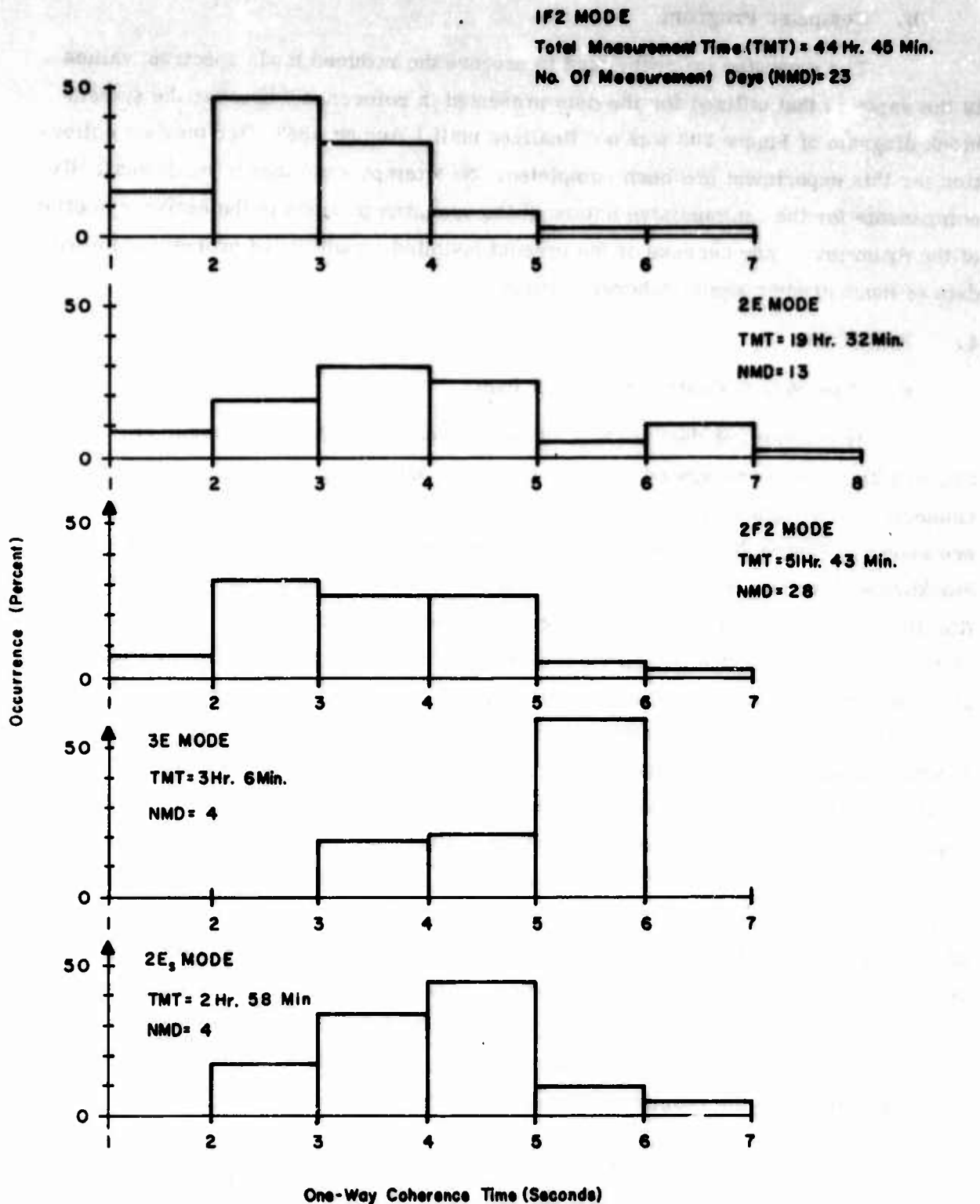


Figure 204. One-Way Signal Coherence Time for Various Modes, Coco Solo to Starr Hill and Stockbridge Paths. Drum Processor Integration Time = 200 Seconds.

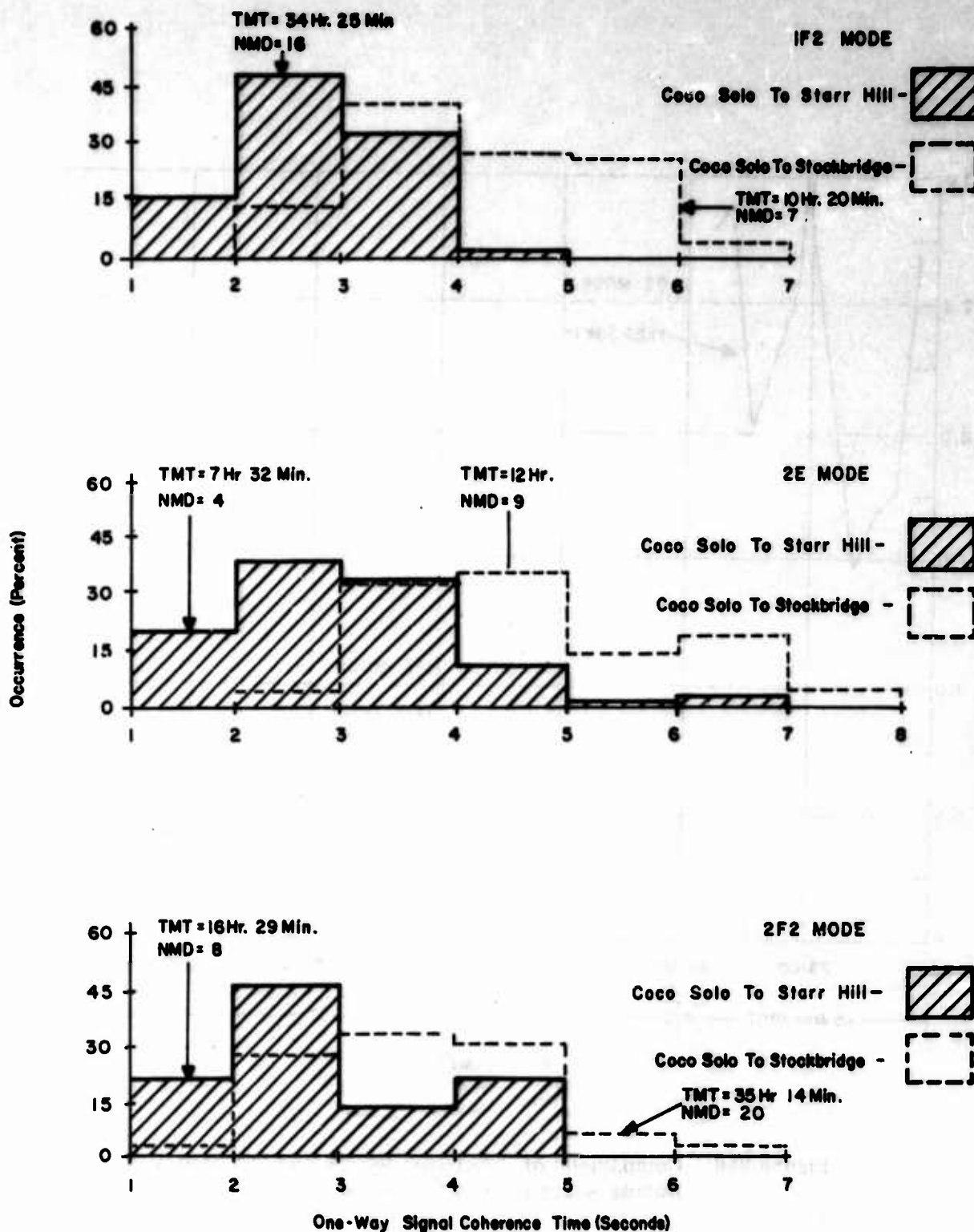


Figure 205. Comparison of One-Way Signal Coherence Values for Various Modes, Coco Solo to Starr Hill and Stockbridge Sites. Drum Processor Integration Time = 200 Seconds

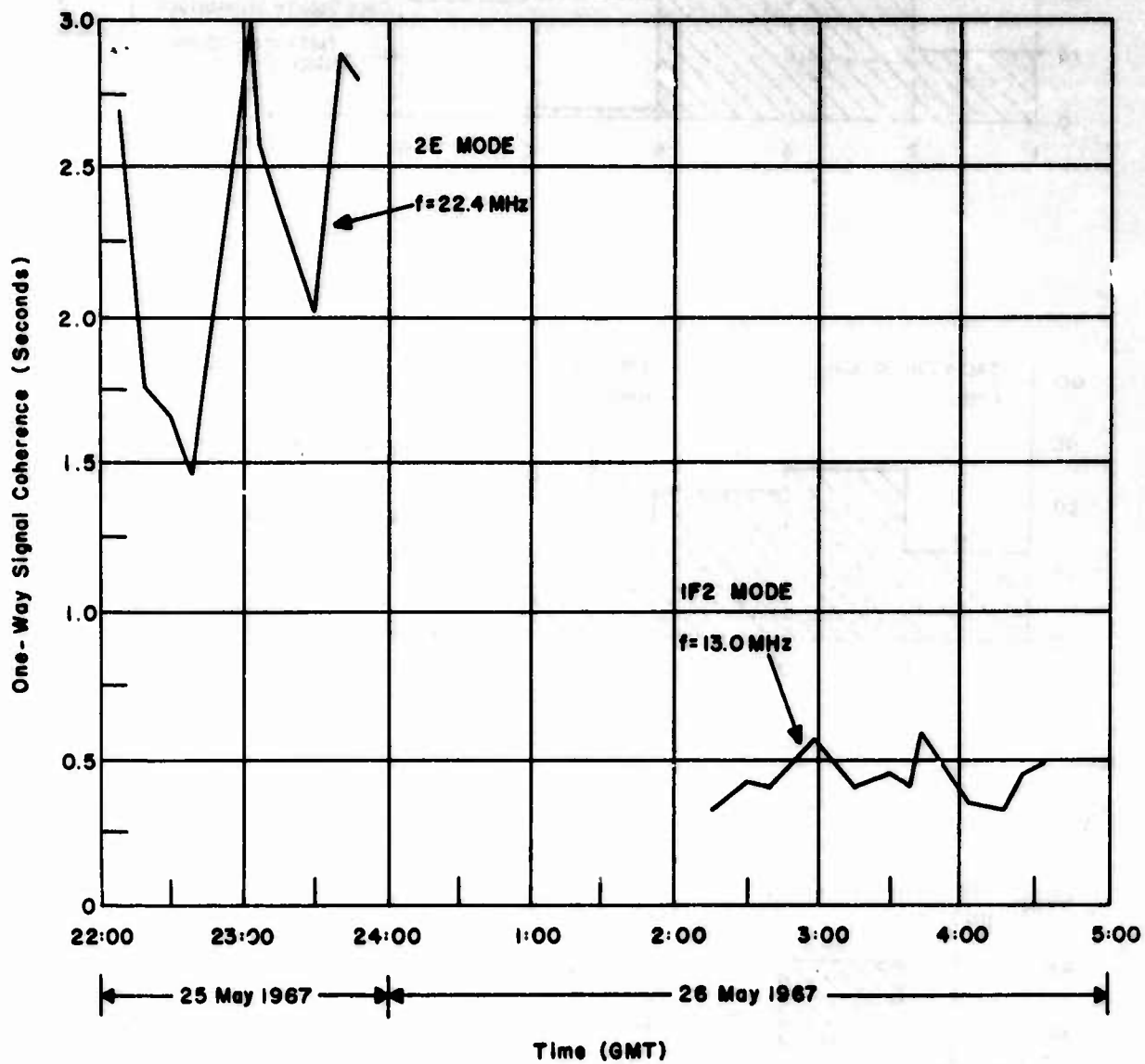


Figure 206. Comparison of Coherence for 2E and 1F2 Modes During Aurora, Coco Solo to Starr Hill Path

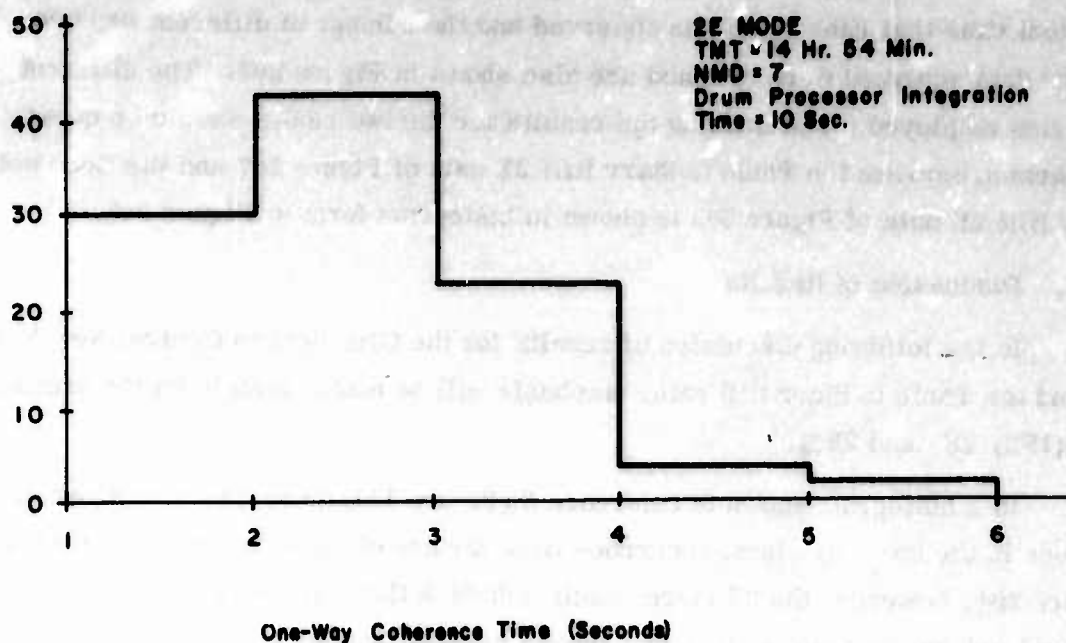
total actual time that each mode was observed and the number of different days on which the data analyzed were obtained are also shown in Figure 207. The different time scales employed for presenting the results for the two modes should be noted. A comparison between the Thule to Starr Hill 2E data of Figure 207 and the Coco Solo to Starr Hill 2E data of Figure 205 is shown in histogram form in Figure 208.

c. Discussion of Results

In the following discussion of results for the Coco Solo to Central New York paths and the Thule to Starr Hill path, emphasis will be placed mainly on the primary modes (1F2, 2E, and 2F2).

In a histogram shown in reference 6 (Figure 111) there was no noticeable difference in the one-way signal coherence time for any of the three primary modes. In Figure 204, however, the 2E mode result indicates that, on the average, its one-way signal coherence time is about one second greater than for either of the F2 layer modes. From Figure 205, the same comparison exists if only the Coco Solo to Starr Hill data are evaluated; the 2E one-way coherence time for the north-south midlatitude path is about one second greater than for either the 1F2 or 2F2 modes.

The results of Figure 205 indicate another interesting comparison: the Coco Solo to Stockbridge one-way signal coherence time is much greater than the Coco Solo to Starr Hill values for each of the three primary modes. Operating frequency and time of day have to be discounted as affecting variables, because the data on each path were obtained at operating frequencies nearly the same percentage of the MOF for each mode and at the same time of day as a percentage of the total time observed. Because about 90 percent of the Coco Solo to Stockbridge results were obtained during October, November, and December of 1966, and all of the Coco Solo to Starr Hill results were obtained between 24 May and 5 July 1967, it might be concluded that signal coherence is seasonally dependent. After a close look at the Coco Solo to Starr Hill data, it was found that a discrete doppler of from 0.2 to 0.5 Hz occurred in a somewhat random fashion every few minutes. Because a 200-second integration time was utilized on the drum processor for all of the Coco Solo data, a discrete doppler would cause the voltage spectrum output of the drum processor to spread out by the amount of the doppler shift with a resultant decrease in the calculated signal coherence time. The origin of the doppler shift is somewhat in doubt although it is probably not ionospherically induced because of the discrete nature of



Occurrence (Percent)

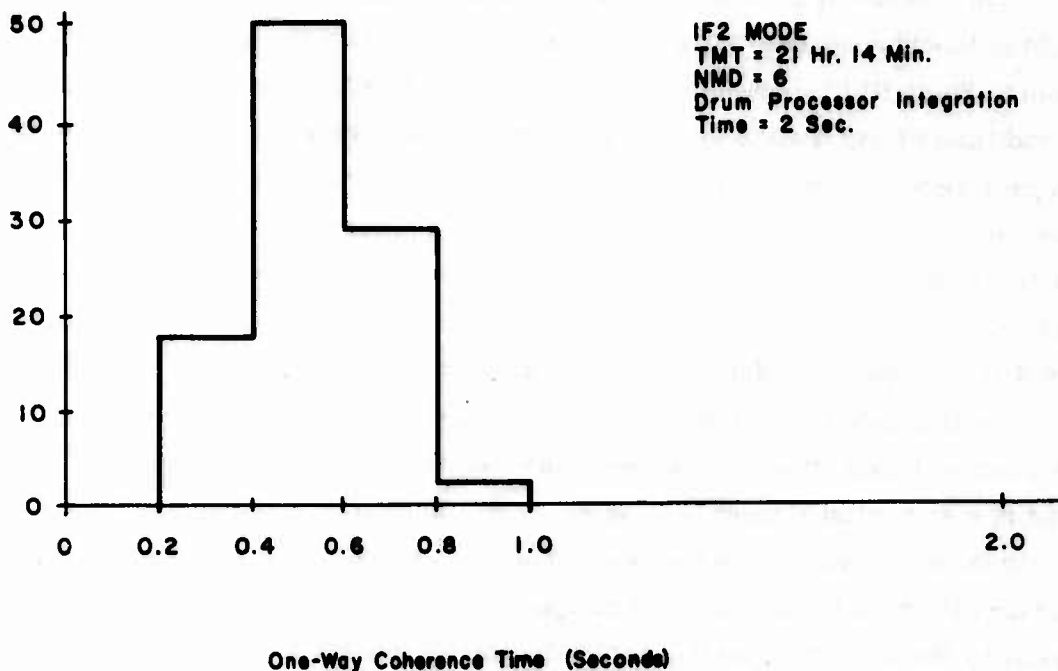


Figure 207. Coherence Time Occurrence for 2E and 1F2 Modes, Thule to Starr Hill Path

the change (the doppler shift is discrete to the extent that for drum processor voltage spectrum displays recorded on 35-mm film at 30-second increments, the shift would occur somewhere within the 30-second interval). The drum processor and the Starr Hill frequency synthesizer have been discounted because this frequency shifting was not apparent on Thule to Starr Hill data taken at approximately the same time. It would, therefore, appear that the difficulty is due to equipment malfunction at the Coco Solo transmitting site. Until this matter can be investigated more fully, it is inappropriate to draw any pertinent conclusions at this time as to the seasonal dependence of the signal coherence time. It should also be mentioned that it is possible to subtract out the effect of the previously mentioned frequency changes on the Coco Solo to Starr Hill data if one assumes that the signal coherence is constant during the time that the change affects the data; however, past data which were uncorrupted by any frequency changes indicate that this may not be a good assumption to make.

The results in Figure 206 represent what may be expected during the occurrence of an auroral disturbance. The two major points of interest are the reduction in signal coherence for the 1F2 mode compared to the normal range of values and the large difference in signal coherence between the 1F2 and 2E modes for the Coco Solo to Starr Hill path. It should also be noted that the 2E signal coherence is reduced by a factor of about two compared to the results of Figure 205, but this reduction is nowhere near the reduction evident for the 1F2 mode. It should be noted that the comparison between the 1F2 and 2E modes indicates that the Coco Solo to Starr Hill 2E mode is not greatly affected by the auroral occurrence; however, until such time as 2E and 1F2 mode data can be taken together during auroral activity, the fact that the 2E data of Figure 206 were obtained nearly four hours before the 1F2 data somewhat clouds the probability that the E layer is much less affected by auroral activity than the F2 layer (from a signal coherence standpoint). During the period over which the 1F2 mode information was obtained, ionograms indicate a spreading phenomenon whereby no identification of modes is possible because of the energy spread in time. This spreading of the energy causes the A-scope display of the modes to represent what appears to be a single mode with a great deal of multipath, similar in all respects to the general behavior of Thule to Starr Hill F2 layer modes under "normal" conditions of propagation on this path. No data on Thule to Starr Hill path modes are available during this auroral occurrence because no contact was possible with Thule from about 1000 GMT on 24 May through 2100 GMT on 26 May 1967 when data taking

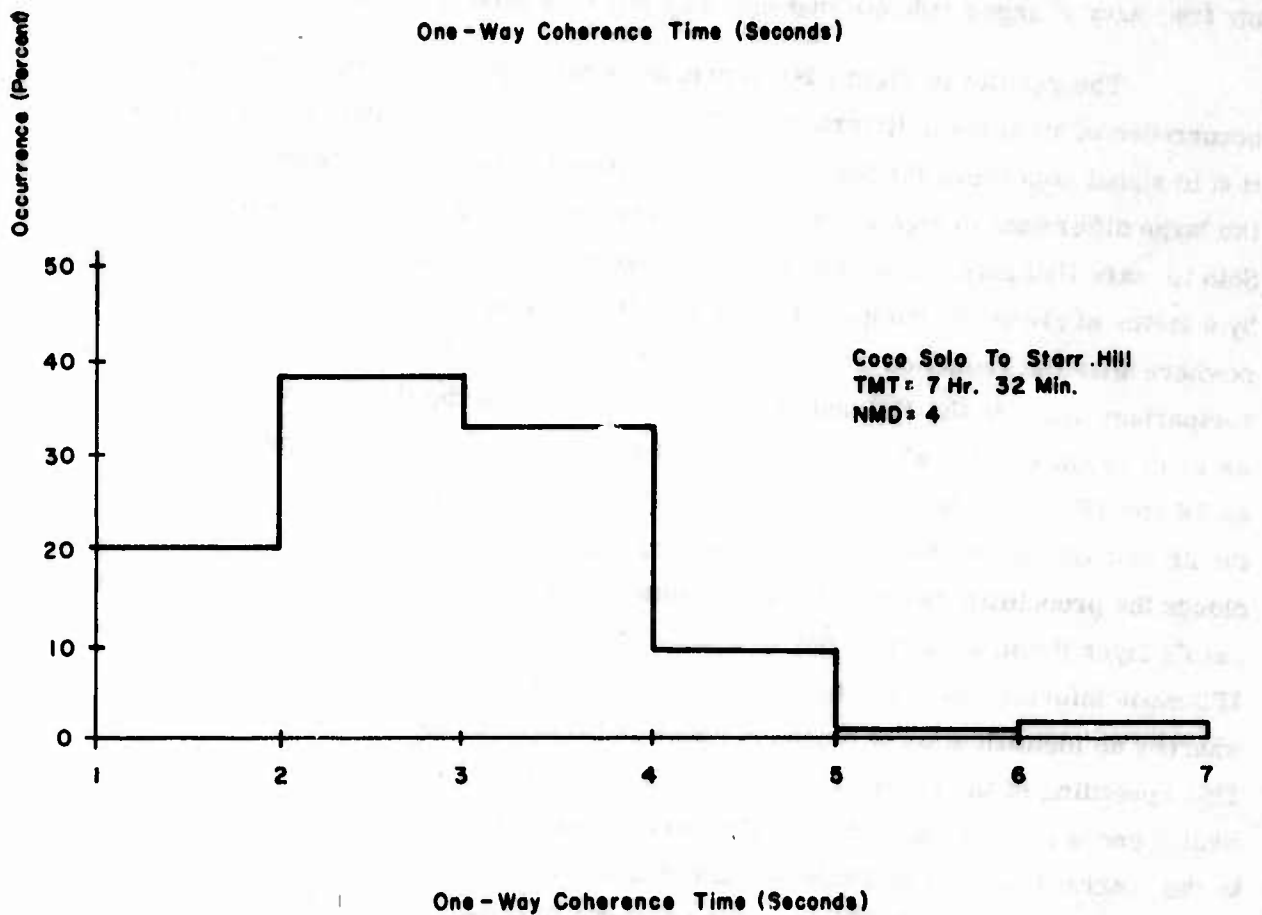
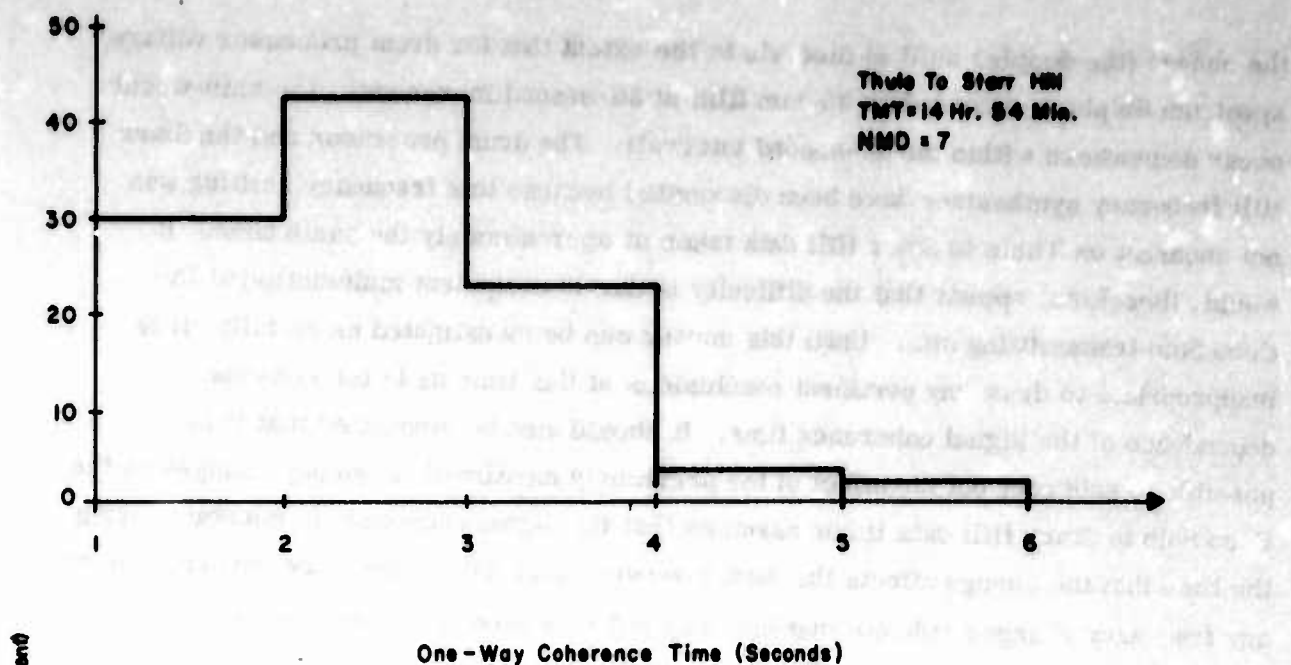


Figure 208. Signal Coherence Time for 2E Mode, Coco Solo and Thule to Starr Hill Paths

was terminated at the usual time for the weekend shutdown. The significant point about the effect of this auroral event is that it did markedly affect the coherence time. When a quantitative measure of auroral activity becomes available, it would appear that the relative effect on the E and F2 layers may be determined. From the presently available E and F2 layer mode data on the Thule to Starr Hill path and the results of Figure 206, it would appear that the first hypothesis to test would be that aurora affects the signal coherence time for the E layer modes much less than for the F2 layer modes.

From the Thule to Starr Hill results of Figure 207 it is obvious that the 2E mode signal coherence time is much greater than for the 1F2 mode. Although the data bank for these two modes is still somewhat small to provide any absolute comparisons (i.e., it is certainly possible that F2 layer modes may at times exhibit a much greater coherence than that so far observed), it is apparent to date that the 2E mode is on the order of four times more coherent than the 1F2 mode on this northern path.

The results of Figure 208 bear out further the comparison that the expected value of signal coherence for 2E mode propagation on a north-south auroral path is only about one second less than on an equal length north-south temperate path; thus, 2E mode signal coherence appears to be somewhat insensitive to path location.

One final result which has not been previously discussed is the polarization sensitivity of signal coherence. Spectrum experimental data were taken on a few days in June 1967 for a given mode received on the horizontally and vertically polarized antennas and fed to the separate (and identical) channels of the drum processor. 1F2 mode Coco Solo to Starr Hill dual polarization data were gathered on 6 June 1967 from 1219 to 1401 GMT at an operating frequency of 17.8 MHz and on 7 June 1967 from 0832 to 0955 GMT at an operating frequency of 9.0 MHz; the voltage spectral displays were identical (and thus the signal coherence time). 2E mode Thule to Starr Hill dual polarization data were gathered on 26 June 1967 from 1648 to 1809 GMT and again no spectral difference was noted; thus, as is to be expected, the signal coherence time is not strongly dependent on the received polarization.

d. Discussion of Sources of Error

(1) Error Sigma

The error sigma discussed in Section IV-2b of reference 6 and given in general form in Equation (25) of Appendix I of that document indicates the following error for the signal coherence.

$$\sigma_{\tau_0} = \frac{0.872\tau_0}{\sqrt{T'/\tau_0}} \quad (23)$$

where

T' = integration time on the magnetic drum processor

τ_0 = is obtained from the condition that $\rho(\tau_0) = 0.5$

$\rho(\tau)$ = the normalized autocorrelation function for a particular mode of propagation

The evaluation of Equation (23) for the results obtained to date will be deferred to the next section where the two-way signal coherence (τ_0') is obtained from the one-way results presented so far. It will be shown that, in general, there is a much greater spread in the measured values about the mean value than there is error as indicated by Equation (23); however, if longer integration times are possible within the bounds of stationarity limitations, the decrease in error by a $\sqrt{2}$ factor for each doubling of the integration time would certainly be desirable.

(2) Incorrect Mode Identification

For the Coco Solo path, the histogram of Figure 204 shows that incorrect mode identification is not too critical a factor since the coherence results do not appear to be very mode dependent. On the Thule path, however, it appears that the E and F2 layer modes vary in coherence quite markedly. The only logical way to reduce this error factor is to take great care in identifying modes -- which has been done -- and to be especially critical of questionable results. This procedure was followed for the results presented in this report.

(3) Nonimpulsive Sampling on the Drum Processor

Due to the nonimpulsive nature of the sampling on the drum, the practical upper bound on the determination of signal coherence is lower than the theoretical limit; for example, with the drum processor in its high resolution mode, 200-second storage, and 200-step scan oscillator mode, the theoretical upper bound on the determination of τ_0 for a cosine modulation function (gaussian-like autocorrelation function) is 8.75 seconds. Using a nominal 20-kHz bandwidth analysis filter (actual bandwidth referred to the drum processor input is approximately 0.105 Hz), the practical upper bound was shown in reference 6 to be about 6.5 seconds; thus, when a measured/calculated coherence result is near the practical maximum obtainable, it

is very probable that the actual value is much greater. From the data processed to date it is apparent that the nonimpulse filtering error probably occurs mainly in the 2E mode Coco Solo to Central New York data. Any erroneous measured/calculated results, however, are conservative in that the actual coherence time is possibly much greater than is indicated by the results.

(4) Too Long a Drum Sampling Interval

This would allow a doppler frequency change to cause an apparent spectral spreading and, thus, a decrease in correlation time. In general, past data have not been greatly affected by this mechanism because the layer acceleration required to produce the doppler change does not often occur. There are cases, however, where the accelerations are significant. In these cases, care has been taken in the data reduction operation to take the doppler change into account.

(5) Signal Integration over Nonstationary Time Periods

It is not possible at this time to specify the magnitude of this error mechanism.

5. INTEGRATION CONSIDERATIONS FOR OVER-THE-HORIZON RADARS UTILIZING SPECTRUM RESULTS

a. Introduction

Reeve (Ref. 12) has shown that the output signal-to-noise ratio (SNR) for an OHR system utilizing signal integration is related to the integration time, T , and an integration loss factor, L_i , by

$$\text{SNR}_{\text{output}} \propto 10 \log_{10} \frac{T}{T_r} - L_i \quad (\text{dB}) \quad (24)$$

where T_r = pulse repetition period

It is assumed in Equation (24) that the result must be applied separately to each ionospheric mode. It is the purpose of this section to show how the integration loss factor, L_i , is related to the one-way signal coherence time measured on the spectrum experiment; why the one-way signal coherence time (τ_o) is a desirable measure of signal coherence for a backscatter OHR; and that the per mode signal coherence results obtained indicate that a considerable coherent integration gain is available for use in an OHR system.

b. Some Useful Analytical Results

Some analytical results which pertain to the evaluation of the integration loss factor, L_i , are presented without proof (with an indication of where their derivation may be obtained).

(1) Evaluation of L_i for Coherent Integration Only

It has been shown that the loss associated with coherently integrating a pulse train of L partially phase incoherent pulses is

$$L_{ic} = L - 1 - \frac{2}{L} \sum_{j=1}^{L-1} (L-j) \rho^j \quad (25)$$

where L_{ic} = integration loss factor assuming coherent integration alone

$$\rho = \exp \left[-2.776 (T_r/\tau_1)^2 \right]$$

τ_1 = 3-dB width of an assumed normalized gaussian signal autocorrelation function, $\rho(\tau) = (-\tau^2/2\sigma^2)$

$$= 2 \tau_0 \text{ where } \rho(\tau_0) = 0.5$$

(2) Evaluation of L_i for the Case of Optimum Combination of Coherent and Noncoherent Integration

Bauer (Ref. 13) has shown that attempts to coherently integrate pulse trains which are long compared with the width of their autocorrelation functions will result in a loss in performance over simple noncoherent processing; therefore, a method of processing is suggested whereby the total pulse train length, LM , of partially phase incoherent pulses is divided into a number, M , of subtrains, each of length L . The pulse trains of length L are coherently integrated and the resulting M outputs are integrated noncoherently. The loss associated with this process is

$$L_{it} = LM - 1 - \frac{2}{L} \sum_{j=1}^{L-1} (L-j) \rho^j - L_m \quad (26)$$

where

ρ is the same as for Eq. (25)

L_m is the integration gain associated with the noncoherent integration of the M subgroups (each assumed independent), as derived by Marcum (Ref. 14)

(3) Determination of Two-Way (Backscatter) Signal Coherence Time from the One-Way (Forward Scatter) Result

Nelson (Ref. 15) has shown that for the normalized gaussian one-way signal autocorrelation function, and assuming reciprocity in the propagation path, the two-way signal coherence time, τ'_0 , is related to the one-way signal coherence time, τ_0 , by the following equation.

$$\tau'_0 = 0.707 \tau_0 \quad (27)$$

c. Use of Integration in a Typical OHR Application

To illustrate the application of the previously discussed analytical results and the significance of the experimentally obtained one-way signal coherence time, the signal processing gains obtainable using coherent integration alone, an optimum combination of coherent and noncoherent integration, and noncoherent integration alone will be discussed.

Assume, for the example to follow, that the integration gain for an OHR of 2000-nmi unambiguous range (a pulse repetition rate of 40 pps is utilized to satisfy this requirement) must be such as to obtain a probability of detection of 0.90 and a false alarm rate of 10^{-5} . From the data presented in Figure 205 assume that the one-way signal coherence times for F2 and E layer north-south temperate path modes are 3.5 and 4.0 seconds, respectively. From the data presented in Figure 207 assume that the one-way signal coherence times for the F2 and E layer north-south auroral path modes are 0.5 and 2.5 seconds, respectively. The drum processor integration times used to obtain these results are given in the appropriate figures. Using the one-way coherence results and the applicable integration times, the two-way signal coherence and standard deviations for each one-way signal coherence time on each path are

$$\tau'_0 \text{ (F2 - Temperate)} = \tau'_0 \text{ (F2T)} = 2.48 \text{ seconds}$$

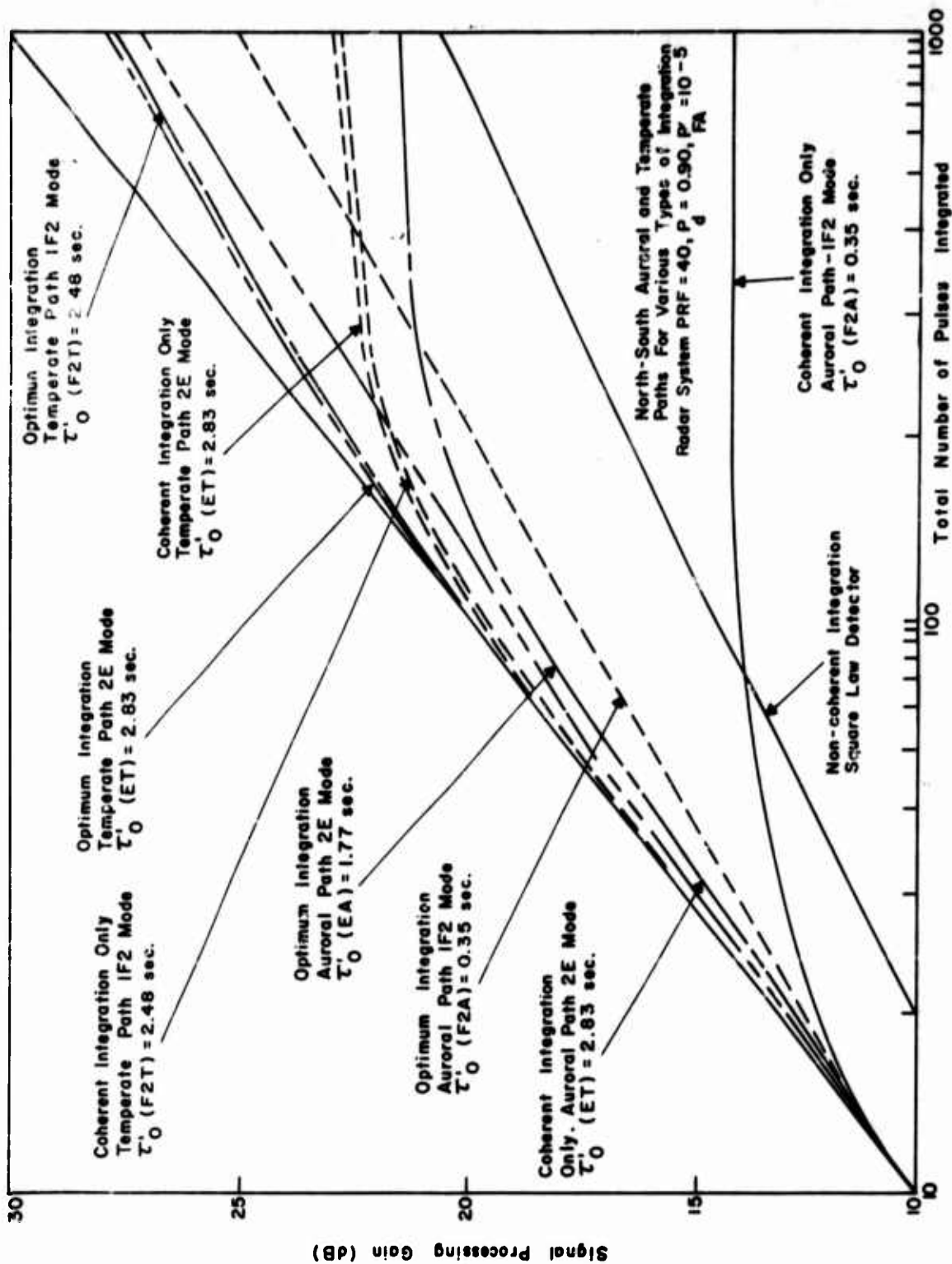


Figure 209. Signal Processing Gain vs. Number of Pulses Integrated

$$\sigma_{\tau_0'}(\text{F2T}) = 0.24 \text{ second}$$

$$\tau_0'(\text{E - Temperate}) = \tau_0'(\text{ET}) = 2.83 \text{ seconds}$$

$$\sigma_{\tau_0'}(\text{ET}) = 0.29 \text{ second}$$

$$\tau_0'(\text{F2 - Auroral}) = \tau_0'(\text{F2A}) = 0.35 \text{ second}$$

$$\sigma_{\tau_0'}(\text{F2A}) = 0.127 \text{ second}$$

$$\tau_0'(\text{E - Auroral}) = \tau_0'(\text{EA}) = 1.77 \text{ seconds}$$

$$\sigma_{\tau_0'}(\text{EA}) = 0.65 \text{ second}$$

Figure 209 shows the signal processing gain of Equation (24) obtainable for each type of integration under consideration (for each mode-path combination) as a function of the number of pulses integrated. The curves for coherent integration alone were obtained with the aid of Figure 210, which shows the coherent integration loss as a function of the ratio of integration time, T , to the two-way signal coherence time, τ_0' , for the 40-prf radar in question; (i.e., Figure 210 is an evaluation of Equation (25)). The gain curve for noncoherent integration was obtained from Marcum (Ref. 14) for a square law detector with $P_d = 0.90$ and $P_{FA} = 10^{-5}$. The optimum combination of coherent/noncoherent integration curves for Figure 209 was obtained with the aid of Figure 211, which essentially shows that for the general cases of interest, the optimum coherent integration time is equal to the two-way coherence time τ_0' . Defining the two-way signal coherence time, τ_0' , from $\rho(\tau_0') = 0.5$ is therefore a desirable measure of signal coherence since it amounts to the optimum coherent processing interval where a combination of pre- and postdetection integration is employed.

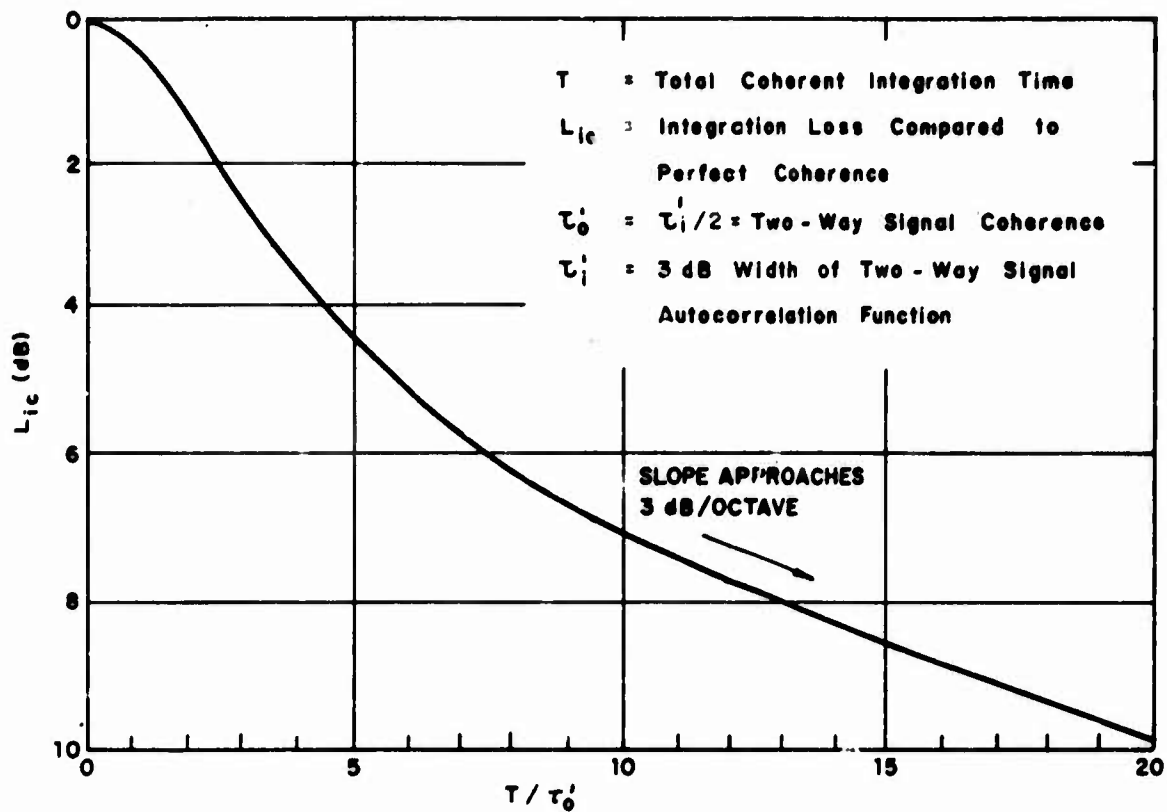


Figure 210. Coherent Integration Loss for a 40-prf Radar due to Signal Decorrelation

One result based on the curves shown in Figure 209 is that the integration gain achievable with an OHR system is dependent on mode, path, and type of processing format. If it eventually turns out that the coherence time for the 2E mode is not azimuthal dependent (as discussed in Section V-4), then the curves of Figure 209 indicate that the use of a coherent processor with an OHR system will make it possible to achieve 4 to 6 dB gain improvement over noncoherent performance assuming that integration times on the order of three seconds are utilized. It should also be noted for OHR systems employing long integration times (greater than 10 seconds) that instrumenting an optimum coherent/noncoherent integration capability will in general allow several dB of gain improvement over noncoherent processing alone. Finally, the data in Figure 209 indicate that coherent processing should definitely be considered in future OHR systems.

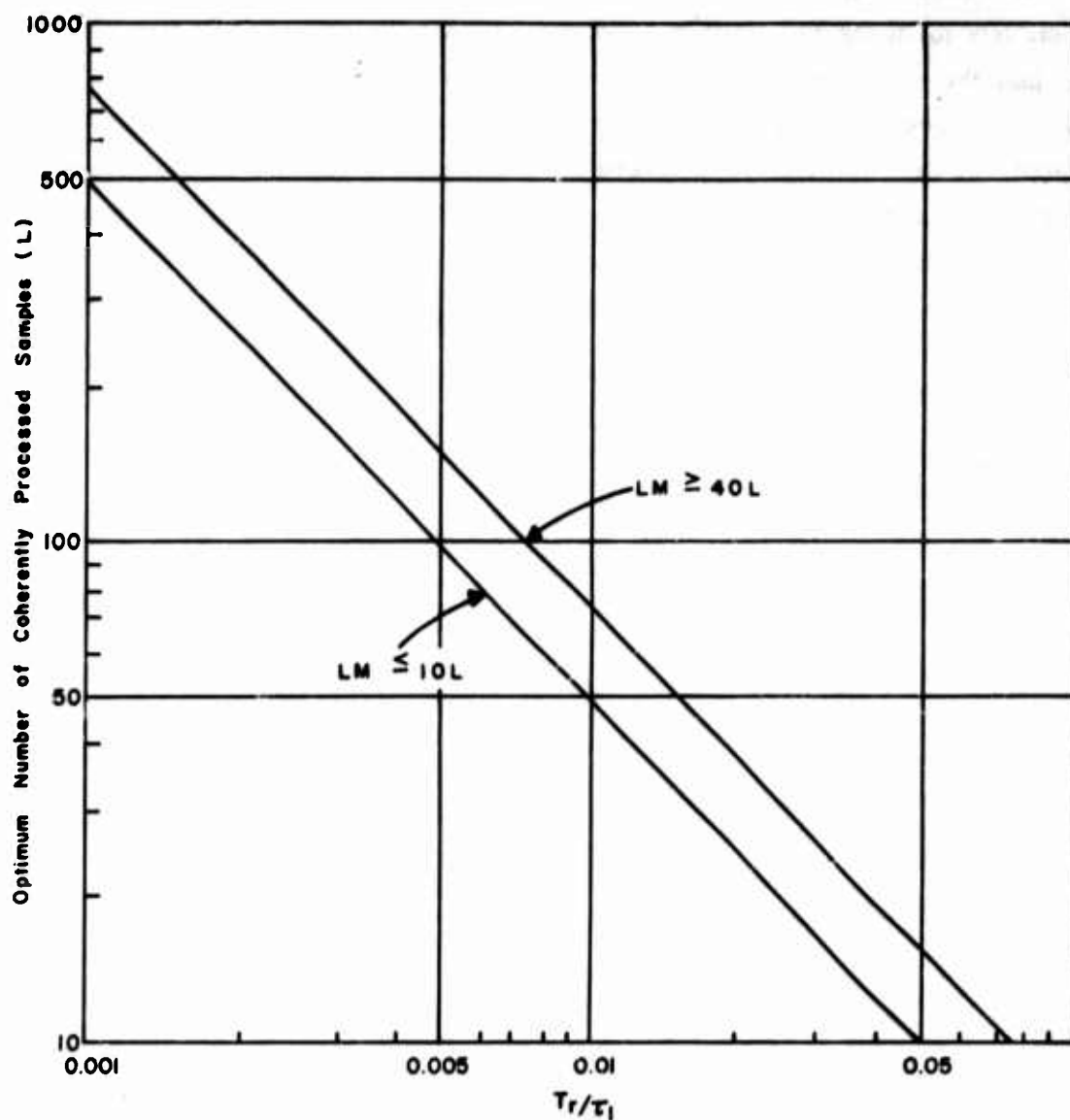


Figure 211. Optimum Length of Coherently Processed Train as a Function of the Ratio of Pulse Repetition Period to the 3-dB Width of the Signal Autocorrelation Function

SECTION VI

AZIMUTH OF ARRIVAL EXPERIMENT

1. INTRODUCTION

During the early part of January 1968 and the middle part of February some on-the-air tests were conducted using the modified azimuth of arrival (AOA) equipment described in references 5 and 7. Since these were the first actual tests using a signal transmitted from one of the remote ELIDA field sites, some equipment and calibration problems were encountered; however, these were of a relatively minor nature and allowed useful data to be obtained on the received bearing for signals received via the 1F2 and 2F2 modes of propagation over the 3792-km path from Coco Solo to the RADC Starr Hill Test Annex.

It was not possible in the time available to perform a complete and thorough analysis of the AOA measurements obtained on 2, 3, and 4 January, and 12 and 14 February 1968 using transmissions from the remote site at Coco Solo; however, it is felt that something can be gained from a description and discussion of some of the measurements that were recorded. The tests were performed using pulse compression, which allowed nominal separation of rays more than $10\mu\text{s}$ apart in time; hence, data could be gathered quite easily on "individual" modes of propagation such as the 1F2L, 1F2H, and 2F2, and this was done quite often. It should be pointed out that most of the time there was not one $10\text{-}\mu\text{s}$ pulse that faded in and out, but rather a number of pulses spread over maybe a $30\text{-}\mu\text{s}$ period* for propagation via the low ray of the 1F2 mode over the Coco Solo path. For the Thule path it has not been uncommon to see the signal spread out continuously over a $70\text{-}\mu\text{s}$ interval for 1F2 propagation.

For transmissions on the Coco Solo path it is generally possible to track in time the position of the peak of a nominal $10\text{-}\mu\text{s}$ pulse; however, the pulse will frequently break up into two separate pulses with neither one occurring at the same time as the original pulse. When this occurred during these tests, it sometimes happened that the received bearing recorded before and after the split would be different.

*This is a nominal value which depends greatly on location of path, mode of propagation, ionospheric conditions, etc., and is a matter which deserves further study.

To calibrate the AOA equipment a test signal (identical to that transmitted at the remote sites) was inserted in place of the two signals from the interferometer and its phase at the two inputs varied by employing different lengths of cable. Previously, the two transmission lines from the main building to the two vertical arrays had been adjusted to practically identical electrical lengths and the complete array had been built with its boresight on the great circle bearing to Coco Solo. Aircraft calibration tests have not as yet been performed to measure the actual boresight of the antenna/transmission line combination. They are scheduled to be conducted on a follow-on contract. From a review of the data recorded and to be presented there appears to be a difference of a few degrees between the calibrated 0° (or on-boresight position) and the actual received boresight position; hence, in the discussion to follow the emphasis in interpreting the AOA results will be on the relative bearing of the received signal and its variation. The automatic marginal detection alarm (AMDA) designed to be used with the AOA equipment was not available for any of the tests to be described. The amplitude of the combined vertical signal for the tests conducted in February was recorded in addition to the azimuth of arrival. This signal was not available for the measurements made in January.

2. DISCUSSION OF MEASUREMENTS

The data of major interest recorded on the dates mentioned earlier at the RADC Starr Hill Test Annex will now be discussed in detail. All of the data to be described were obtained between 0300 and 2000 EST with the majority in the afternoon. Frequencies employed for these tests were 23.6, 25.5, 27.9, and 30.1 MHz, with no one transmission at any of these frequencies lasting longer than one hour. Oblique soundings were also obtained during these tests so that the mode of propagation for each signal that was measured could be identified. All of the measurements were made on either the 1F2L, 1F2H, or 2F2 mode. It was not possible in the time available to distinguish between the low and high ray for the 2F2 mode in many cases.

On the afternoon of 2 January 1968, the first on-the-air tests were conducted with the modified AOA equipment between 1200 and 1500 EST. Permanent measurements of the received bearing were obtained using an eight-channel Sanborn recorder. Due to the way the equipment was aligned, the 0° bearing position is not usually the same as the position with noise only as the input to the AOA equipment. This can be observed in most of the records to be presented in this section. It can also be observed

in the records of received bearing when the AOA signal transmissions ceased at the remote site to permit the sounding signal to be transmitted. Each individual sounding lasted for 12.8 seconds and a group of these soundings occurred every 10 minutes. A Sanborn record taken between 1327 and 1332 EST, when the transmit frequency was 30.1 MHz, is shown in Figure 212*. Gate 1 was tracking a weak 1F2 mode and the second gate was on the 2F2 mode. Since the 1F2 mode was quite weak, judging from the Sanborn trace, the 1F2 bearing varied between the 0° position as determined using the test signal generator and the noise-only position (which is indicated by a broken line). The gate 2 data show considerably larger bearing deviations for the 2F2 mode than for the 1F2 mode, which was generally the case for the data obtained during this test period. It will be noticed that the bearing variation becomes quite small a minute or so before the start of the soundings. During the previous minute there were some rapid bearing changes in a short period of time. During part of this time the SNR was quite high as indicated by the lack of noise on the Sanborn trace.

The next record shown (Figure 213) was obtained from 1404 EST to 1412 EST while still transmitting at 30.1 MHz. Again data for both the 1F2 and 2F2 modes of propagation were obtained. It is believed that the 1F2 information was for low ray propagation while the 2F2 data were taken quite close to the JF for this mode of propagation. What is extremely interesting to notice is the different arrival angles for the 2F2 mode depending on the time position of the gate which cannot be determined from the Sanborn records. At this instance, the 2F2 mode consisted of a number of 10- μ s pulses and the gate was moved from one to another with the result shown. There appears to be an angle of arrival bearing difference of about 15°. It is interesting to note that received bearing was about 10° to the east side of the 0° position (set using the test signal generator). At about 1410 EST the signal level is very strong and the received bearing is slightly to the west.

From the AOA records taken on 3 January 1968 three examples will be shown which were obtained at 1425, 1550, and 1850 EST. These are shown in Figures 214, 215, and 216, respectively. The first one is an example of the bearing obtained when simultaneously tracking the 1F2, 2F2L, and 2F2H modes. It can be seen from an examination of this figure that the 1F2 bearing is closer to the 0° position than either of the other two. Generally speaking, the wide fluctuations have occurred when the received vertical signal level is almost equal to the noise level; i.e., when the signal is in a fade.

*Disregard the designation of direction in Figures 212-223.

An example of the received bearings for three separated rays that comprise the 2F2 mode is shown in Figure 215. The operating frequency for this set of data was 27.9 MHz which was very close to the JF for the 2F2 mode existing at this time. Some wide fluctuations can be noticed for the signal tracked by gate 2.

A Sanborn record taken between 1846 and 1858 EST on 3 January 1968 is shown in Figure 216. The modes tracked were the 1F2L, 1F2H, and a second 1F2H. The operating frequency was 23.6 MHz and the initial time separation between the modes was 330 and 80 μ s respectively; this changed to 250 and 100 μ s at the end of this period. A better signal level was obtained at this time via the 1F2H rays than via the 1F2L mode. An examination of this figure will reveal that a very steady received bearing exists throughout this period. From this record it can be seen that the 1F2L mode is closer to the established 0° position than either 1F2H rays. This might be due to variation in the antenna boresight with elevation angle, especially for signals arriving near the horizon.

Two Sanborn records from the measurements made on 4 January 1968 will be presented. The first is shown in Figure 217 when the operating frequency was 30.1 MHz and was for the time between 1215 and 1226 EST. For this record there was no distinguishable difference between the noise-only position and the 0° position determined using the test signal generator. The SNR was very adequate for the main 1F2L signal judging by the size of the bearing trace.

The gate 1 1F2L signal is generally to the east (or above the 0° position), but there are times when the received bearing is below the 0° position. It is noted that at times the signal split up into two or more pulses with a change in bearing. There appears to be a number of preferred bearing positions as can be seen from an examination of Figure 217. The change in bearing is usually very gradual with a few abrupt changes in received bearing in evidence.

Between 1222 and 1225 EST gate 2 was placed on a second 1F2 mode pulse which was separated by 20 μ s from the main pulse. Its received phase was generally quite steady except for some initial fluctuations at 1223 EST.

Additional Sanborn traces for the 1F2L mode from 1245 to 1255 EST are shown in Figure 218. The operating frequency was 30.1 MHz the same as for the previous figure. The two traces shown are for two closely spaced pulses that make up part of

the 1F2 mode. During the early part of the period shown the main component as depicted by the top trace is very steady and close to the 0° position. Around 1246 EST the difference in received bearing when gate 1 is moved from one pulse to another may be seen. After 1253 EST the received bearing for the main component deviates more from the 0° position--up to 15° in spots.

The signal represented by gate 2 varied more than that followed by gate 1 as can be seen from Figure 218.

The Sanborn record obtained between about 0930 and 0940 EST on the morning of 14 February 1968 is shown in Figure 219. The operating frequency was 30.1 MHz and the 1F2 JF was approximately 32 MHz at this time. The oblique inogram taken at 0940 EST indicated the presence of an N mode which extended to about 29 MHz and a faint trace for the 1F2 high ray. This last statement is borne out by the amplitude level measured for the 1F2H ray using gate 2. It should be pointed out that in all the Sanborn records to be presented for 14 February 1968 the position for no input signal (marked "noise-only output" on the recordings) is considerably removed from the 0° bearing position established using the test signal generator. This is believed due to a change in the power supply for the mode processor which took place after the data were collected on 12 February 1968. This difference between the no-signal position and the 0° position with a strong signal must be considered when analyzing and interpreting the records presented. No fixed frequency transmissions are possible when the sounding takes place; this is the reason for the four noise positions every 10 minutes.

For the Sanborn record shown in Figure 219 the level of the received 1F2H signal was generally quite low so no useful information could be obtained except for about a minute around 0939 EST. Then a signal was received about the 0° position. Of major interest is the variation in bearing position as a function of where the sampling gate was set if more than one 10- μ s pulse was received for the 1F2 mode of propagation. Most of the abrupt changes in received bearing are due to moving the gate from one pulse to another one which is also present at that time. This is true for the data taken around 0933 and 0936 EST. It is seen that the resulting change in bearing is from 5° to 10° for a change of 10 to 20 μ s in gate position (which corresponds to another pulse). There were times when this change in sampling time was made due to the presence of two or more pulses without a noticeable change in received bearing.

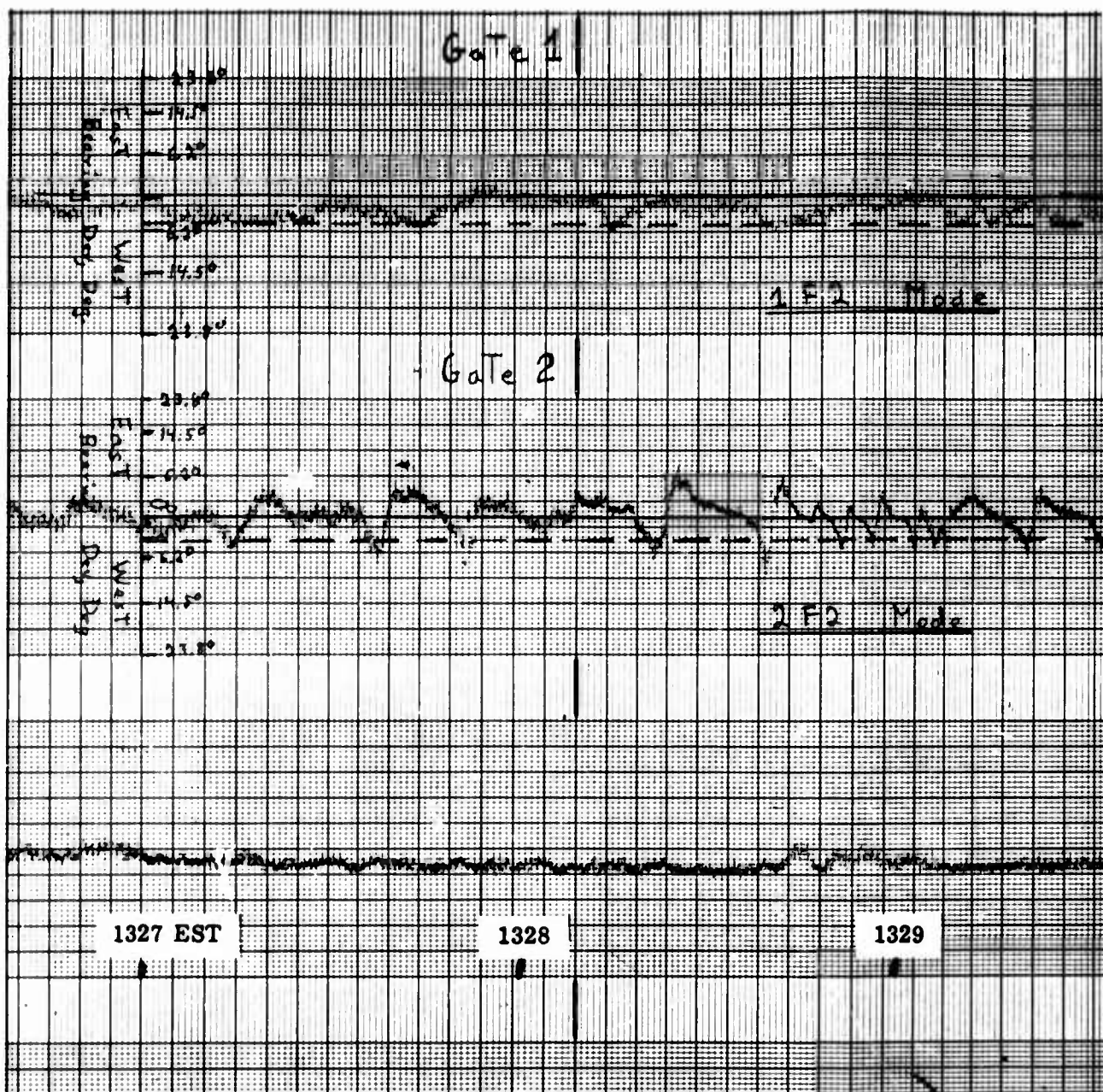
The next Sanborn record (Figure 220) shows similar variations in received bearing depending on gate position at the point marked "front" which referred to the first of two pulses that were being tracked. Again there is an indication of about a 5° change in received bearing for a 1F2L mode; the operating frequency was 30.1 MHz. Starting at about 1010 EST a considerable change in the received bearing occurred over a period of about one minute. What is immediately obvious is a change of about 25°, but due to the characteristic of the phase detector employed it appears that a foldover in the bearing data has occurred. After the soundings the received bearing fluctuations do not seem as great as before. These appear to be a number of received bearing positions that are favored during this period of time with a given one lasting for about a minute or so. Also, the "mean" boresights for these different positions appear to differ by 5° to 10°.

This last point is well exemplified in Figure 221, which is for the 1F2L mode at an operating frequency of 27.9 MHz. The record shown extends over a period of 24 minutes and the received 1F2L signal level is quite good as can be seen by examining the amplitude trace for this period. The bearing variations are generally quite gradual in this record and again a number of preferred bearings are indicated at 2°, 5°, and possibly 10° for a short period of time around 1043 EST. The two abrupt changes in the received bearing before the sounding at 1040 EST correspond to a fade in signal amplitude as can be determined from an examination of the two traces.

Another record for the 1F2L mode taken around 1100 EST on 14 February is shown in Figure 222; the operating frequency was 27.9 MHz. For this recording only, the antenna connections to the AOA equipment were reversed and the received bearings now generally fall below the 0° position where previously they usually were above the line. As mentioned earlier, the complete receiving array used as the interferometer has not yet been calibrated and it is believed that there is a small boresight error which is responsible for the bias in the received bearing which has appeared in the data. This record again illustrates the point that the received bearing varies over about a 10° range.

The last record to be shown for 14 February 1968 is shown in Figure 223, taken around 1140 EST. At this time it was possible to receive both the 1F2L and 2F2L modes using an operating frequency of 25.5 MHz. The 1F2 JF was about 40 MHz when this

record was made. At the beginning of this record it is indicated where the attenuator to the mode loss receiver was increased by 20 dB to take care of a large signal level. Shown in this record is an example of two different bearings for a 2F2L mode made up of "two" pulses separated by 25 μ s. The difference in bearing for the two pulses is about 5°. The arrival time difference between the 1F2L and 2F2L modes was approximately 450 μ s.



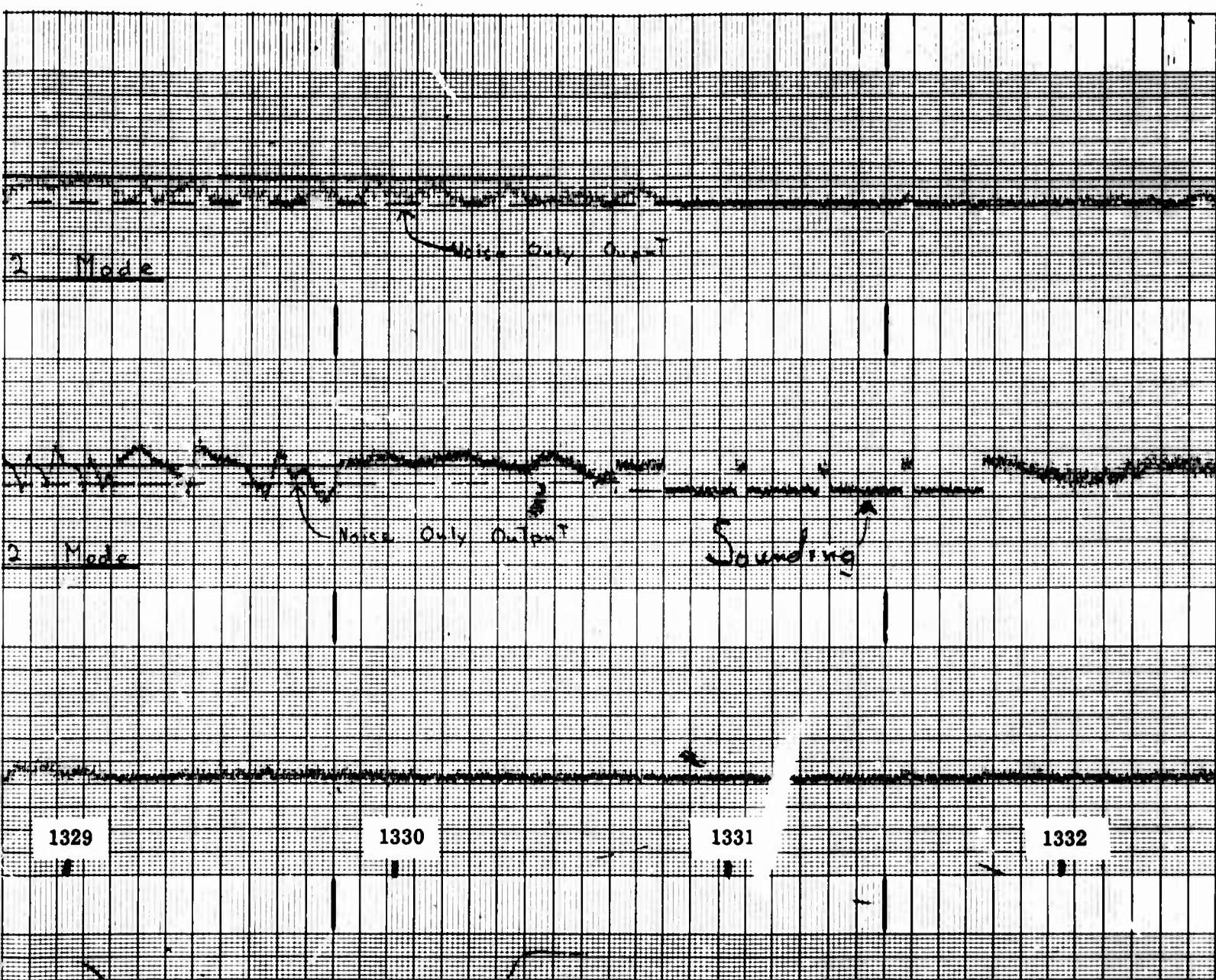


Figure 212. AOA Records for 2 January 1968 around 1330 EST

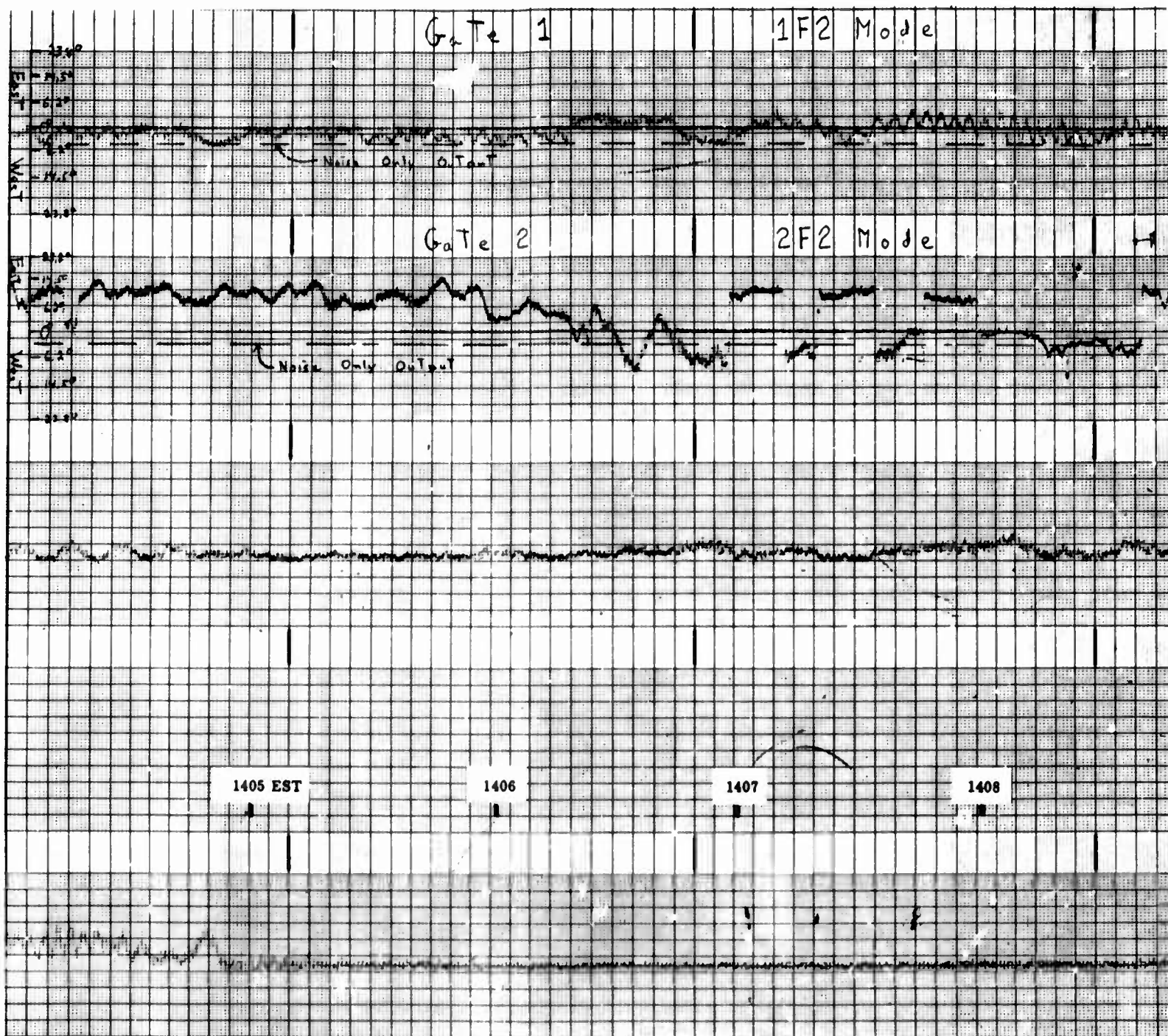
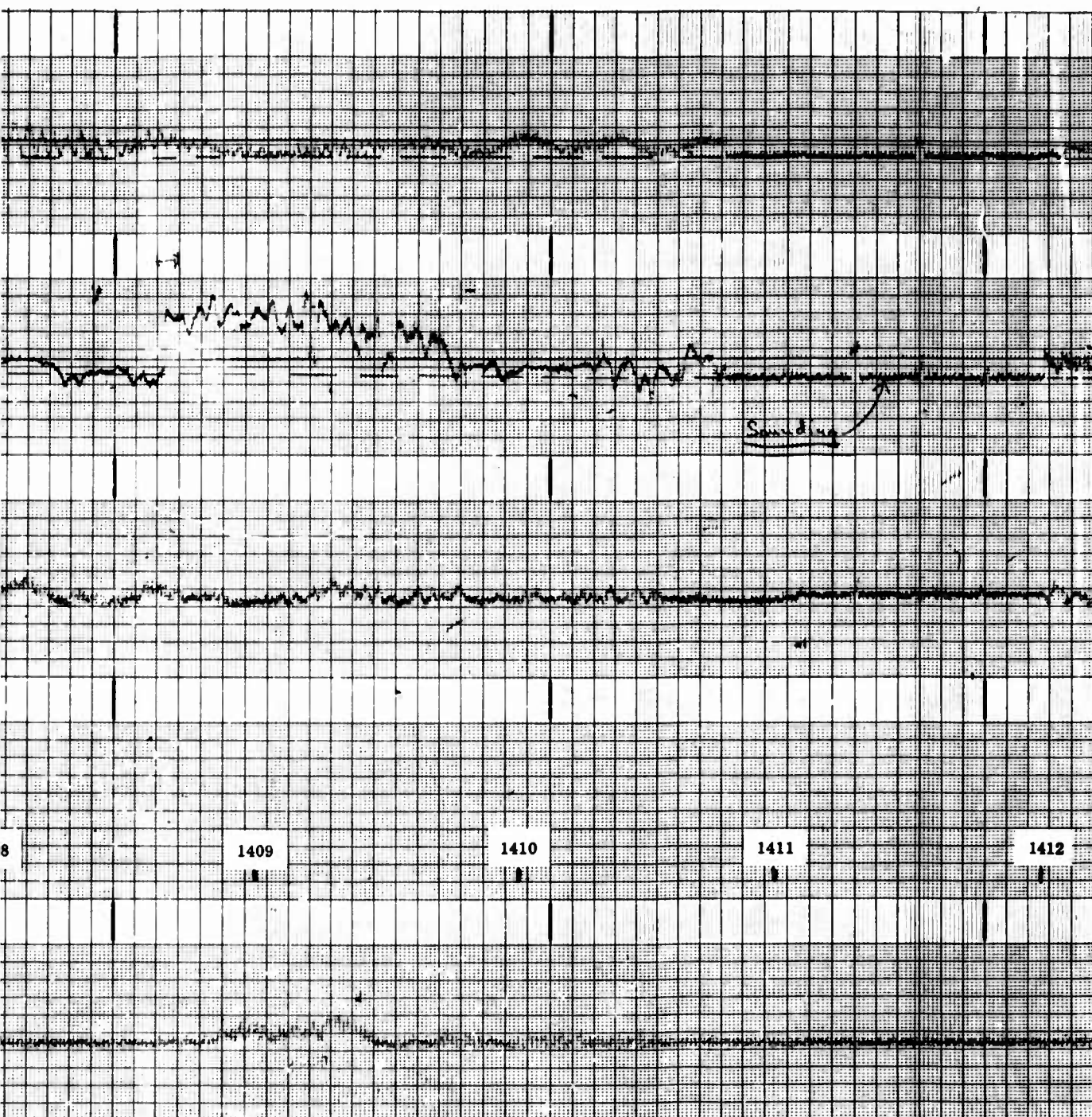
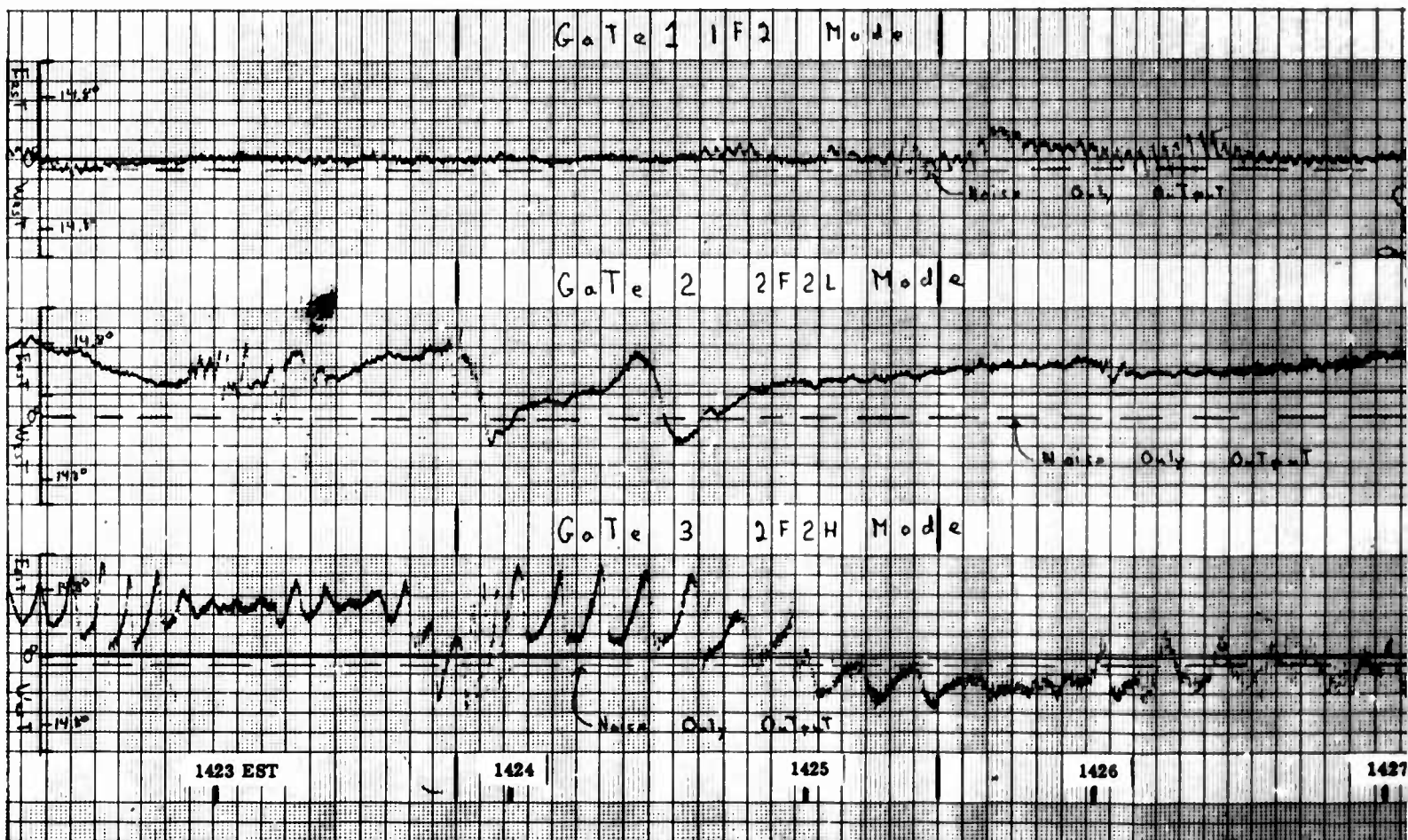


Figure 213. AOA Record for 2 January
1968 around 1405 EST





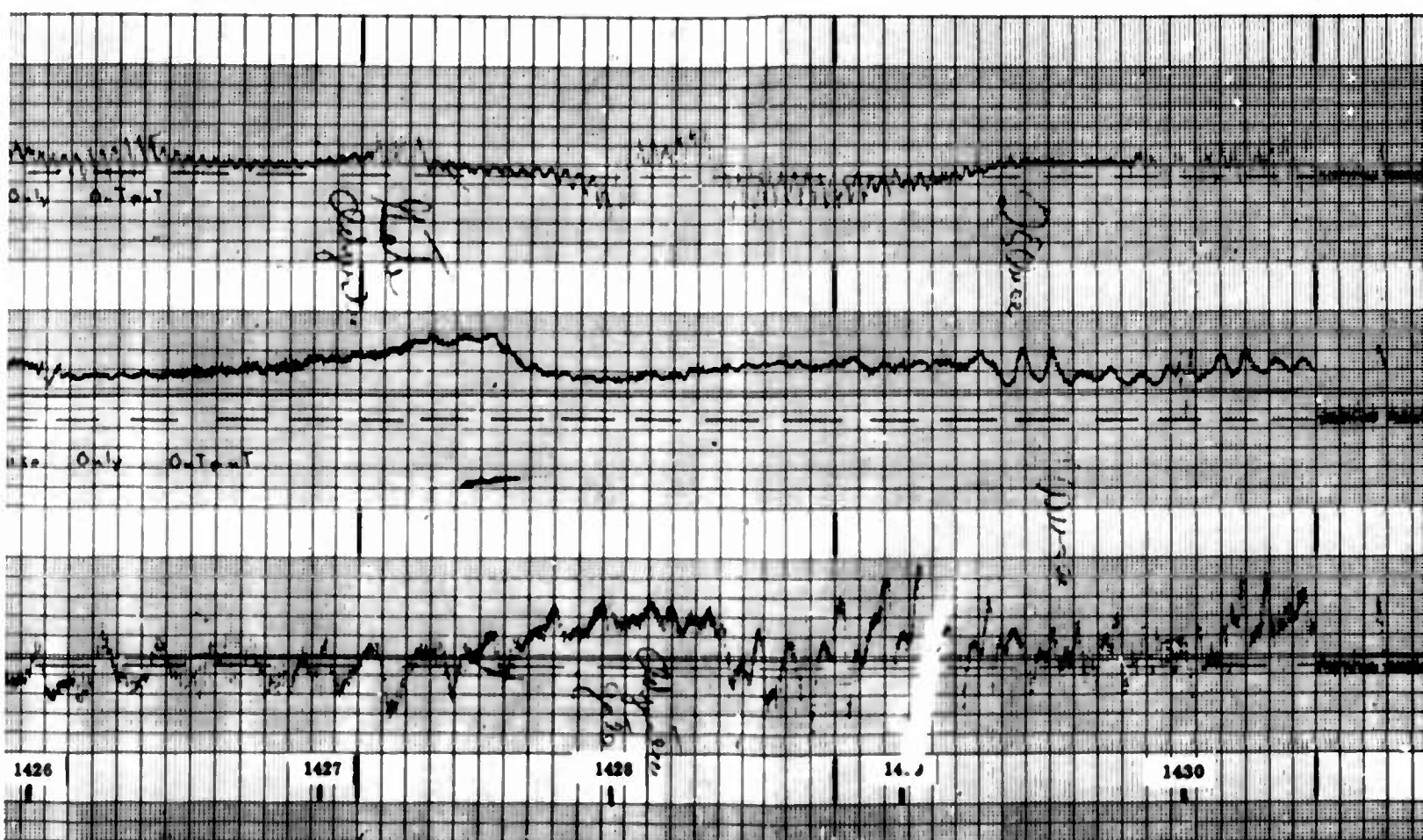


Figure 214. AOA Record for 3 January 1968 around 1425 EST

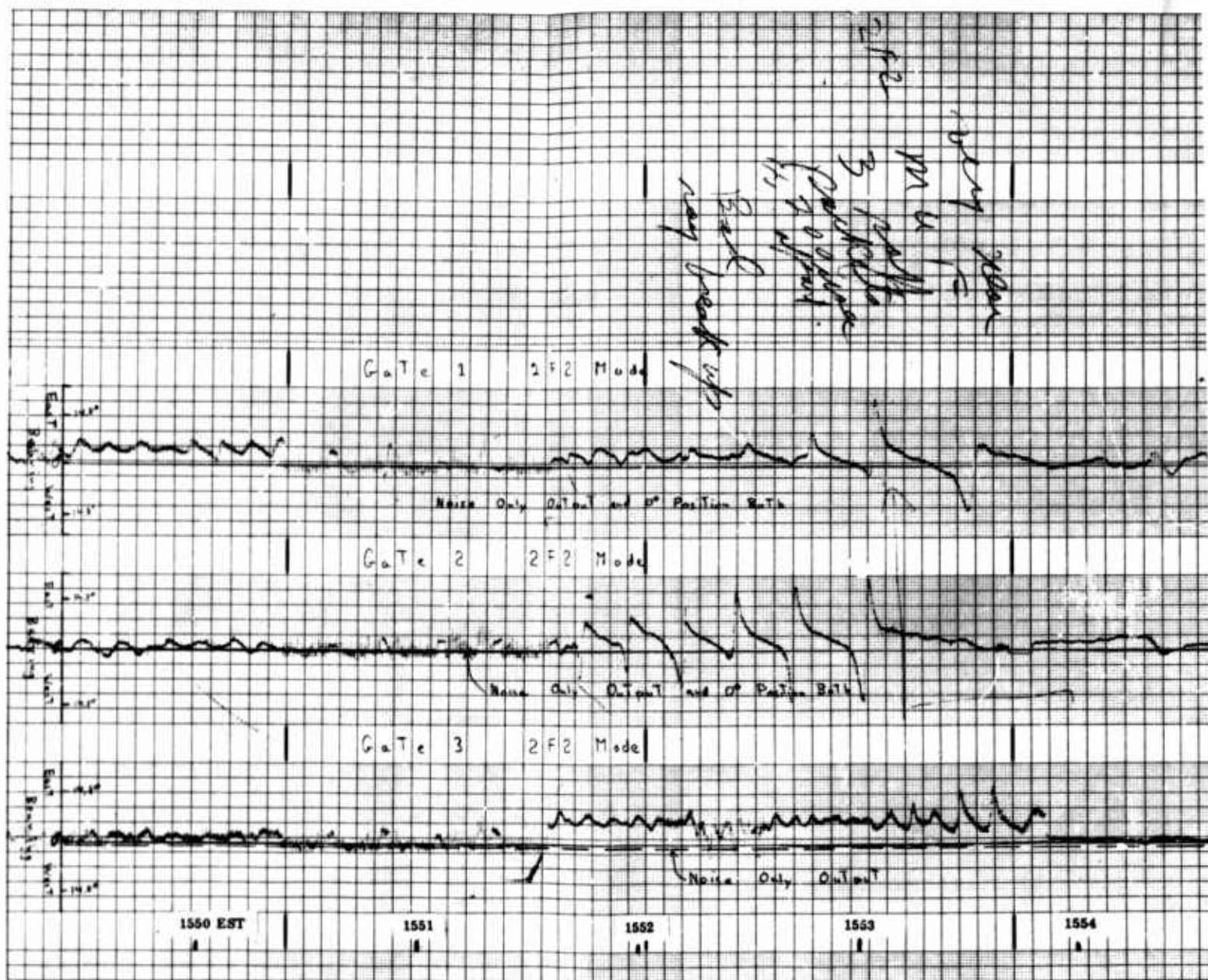
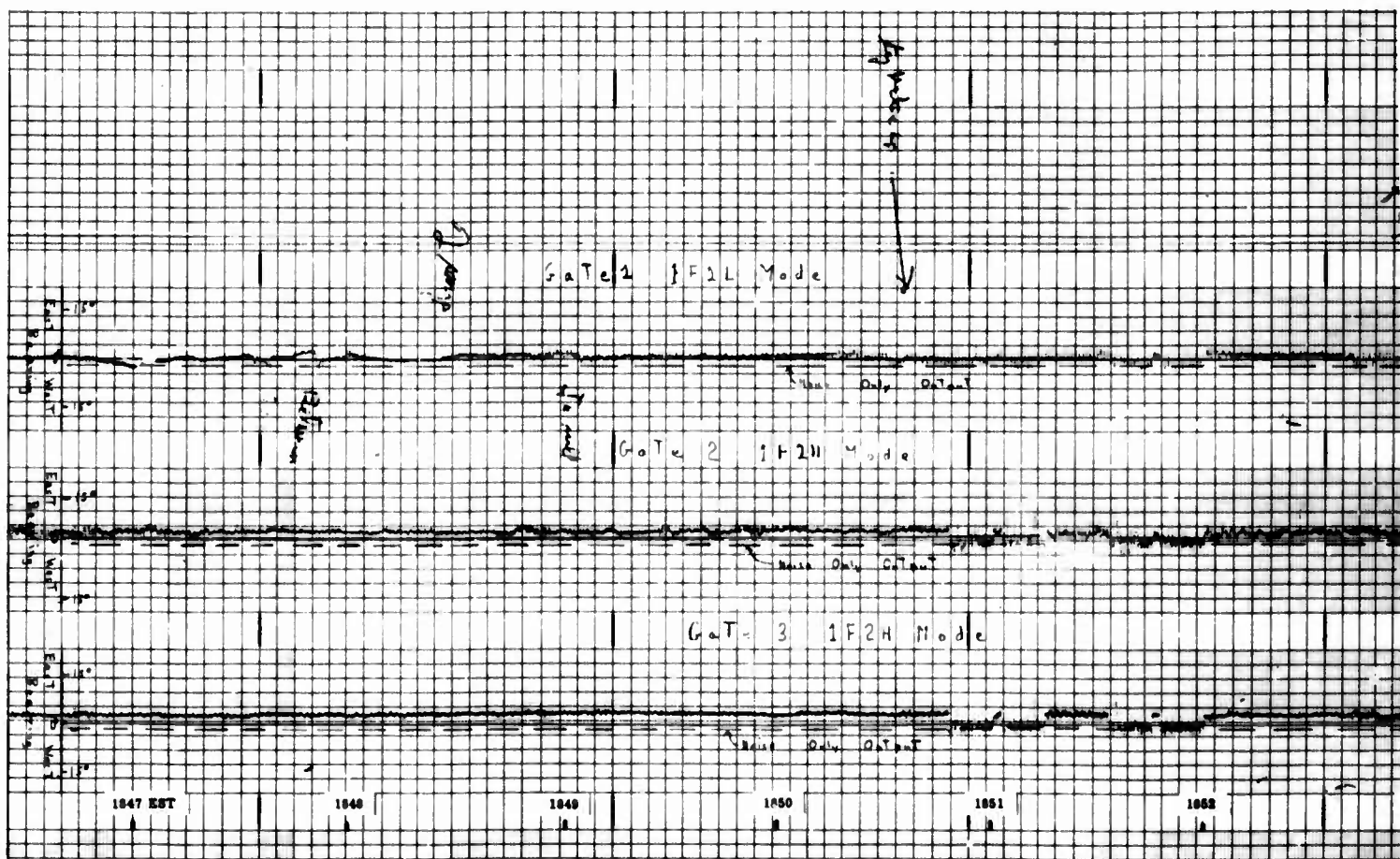


Figure 215. AOA Record for 3 January
1968 around 1550 EST





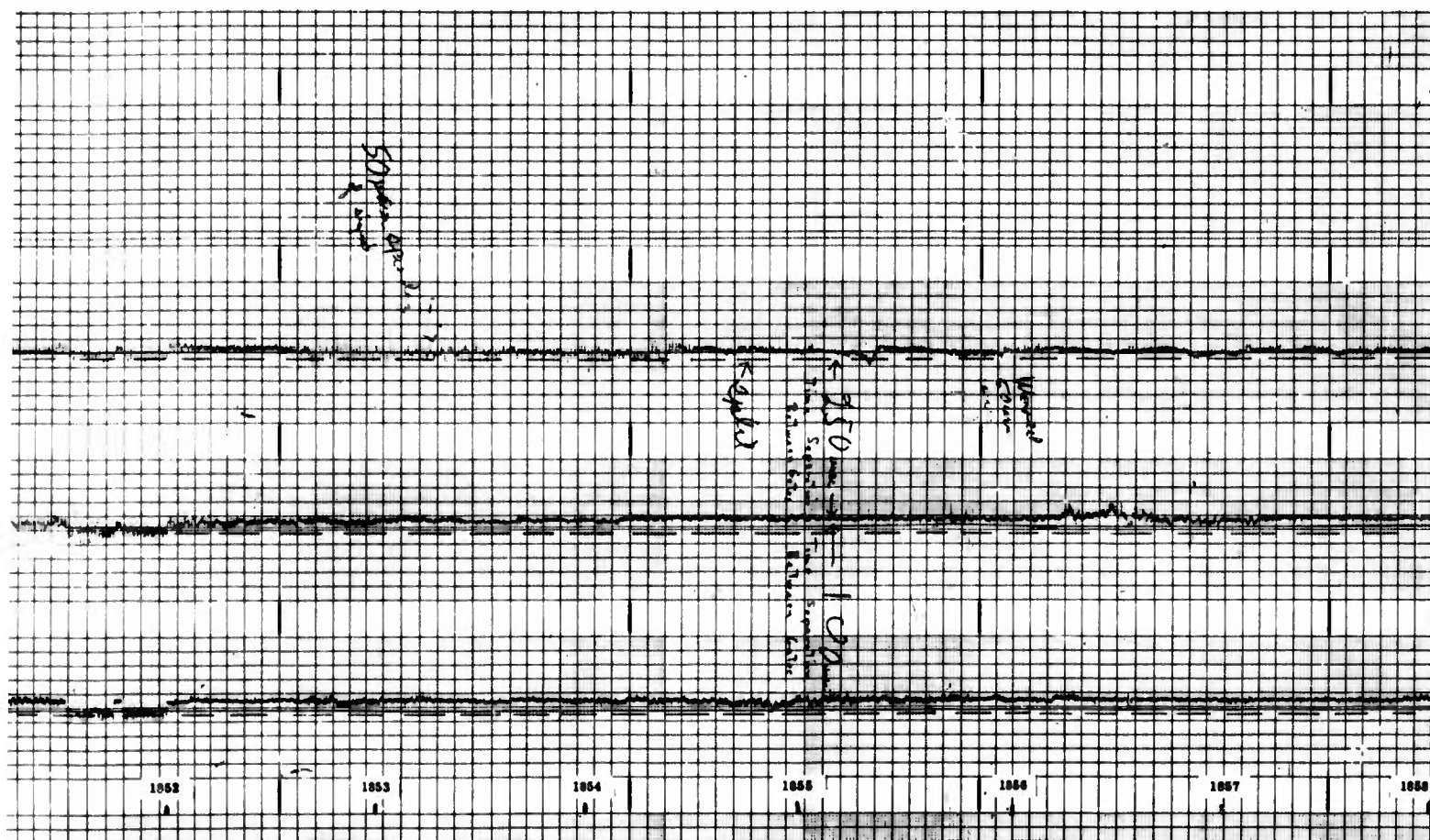


Figure 216. AOA Record for 3 January 1968 around 1850 EST

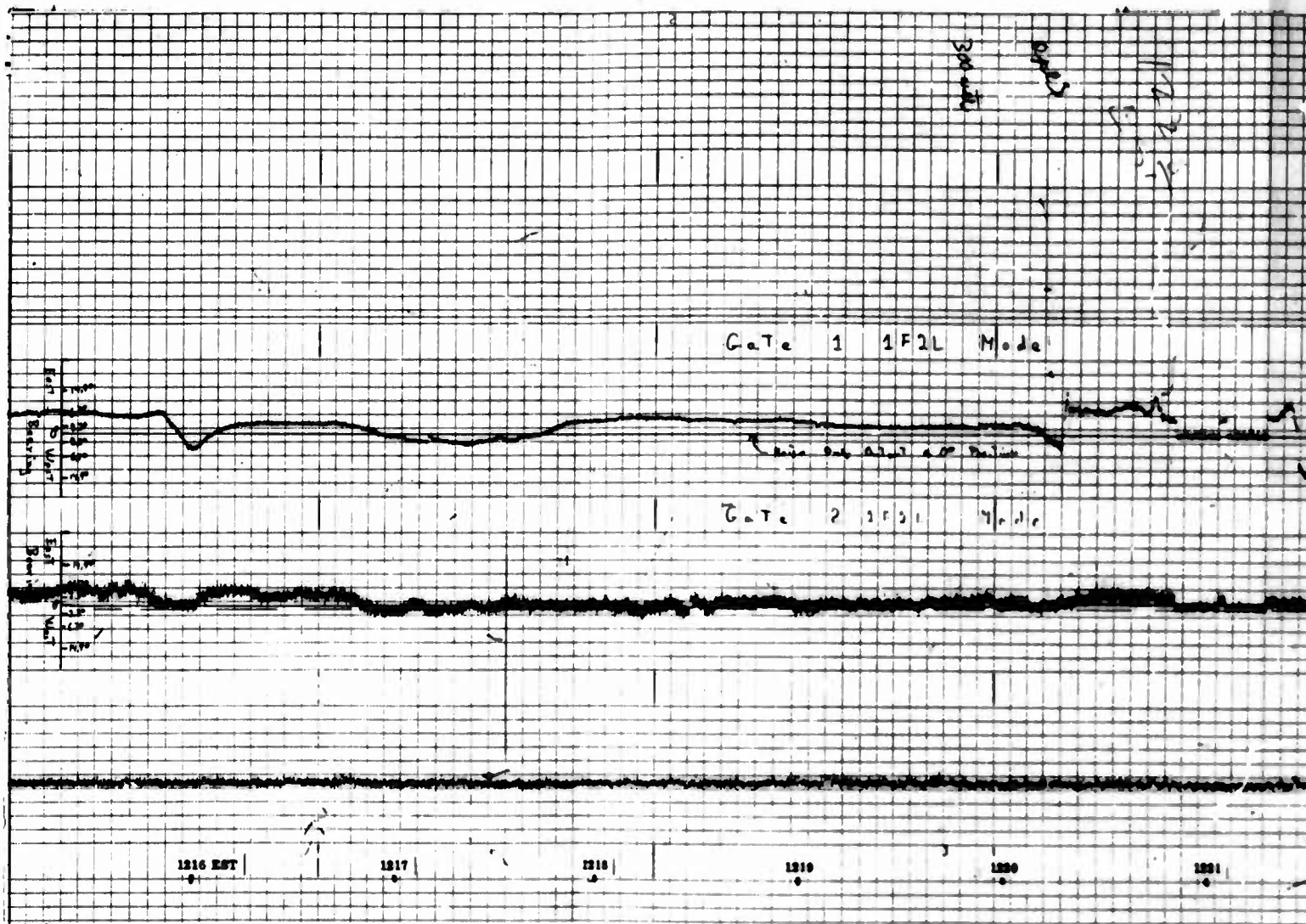


Figure 217. AOA Record for 4 January
1968 around 1220 EST

175
GMA

Western

175
GMA

175
GMA

175
GMA

175
GMA

175
GMA

175
GMA

175
GMA

175
GMA

generally water

175
GMA

1246

1247

1248

1249

1250

1251

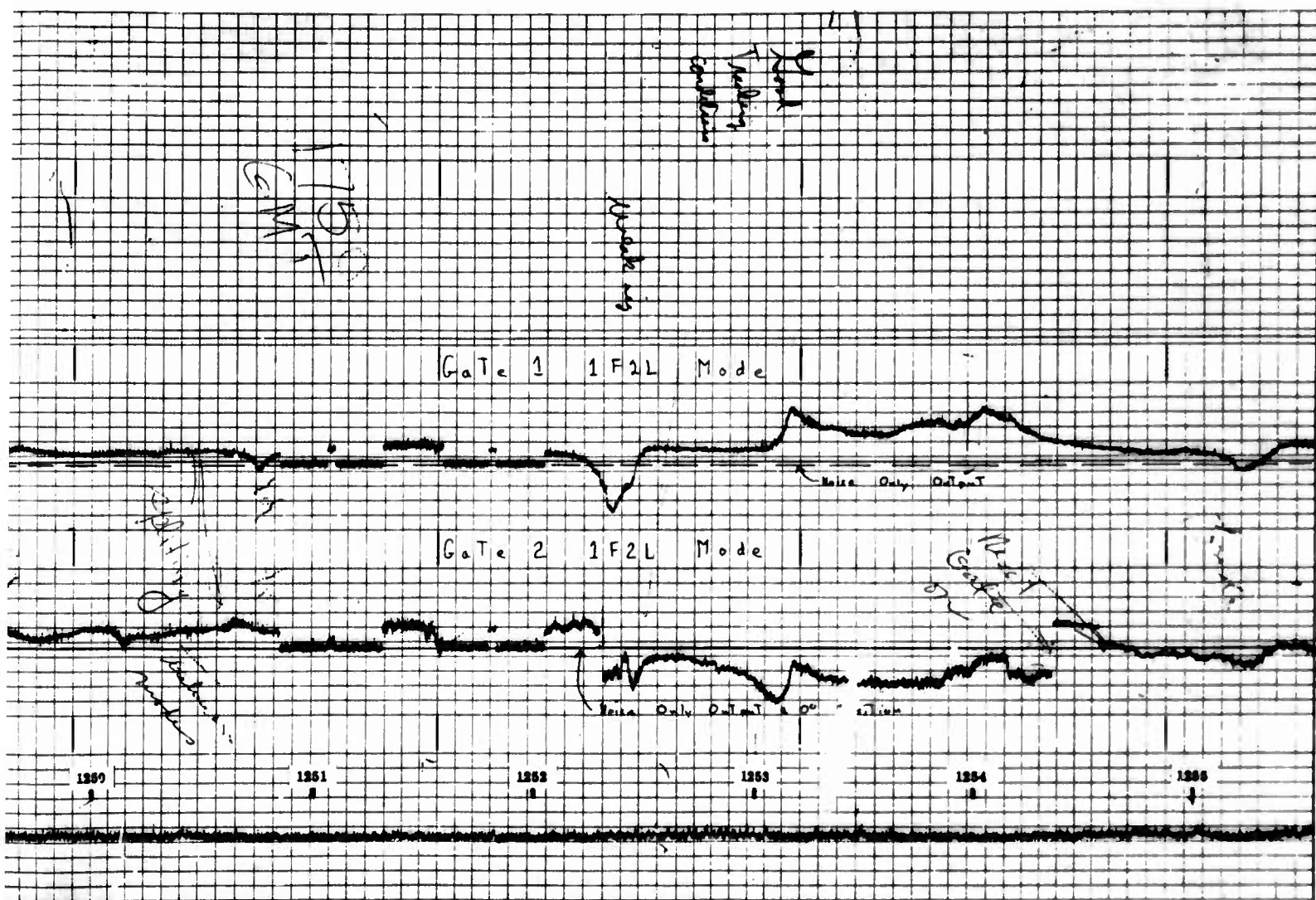


Figure 218. AQA Record for 4 January 1968 around 1250 EST

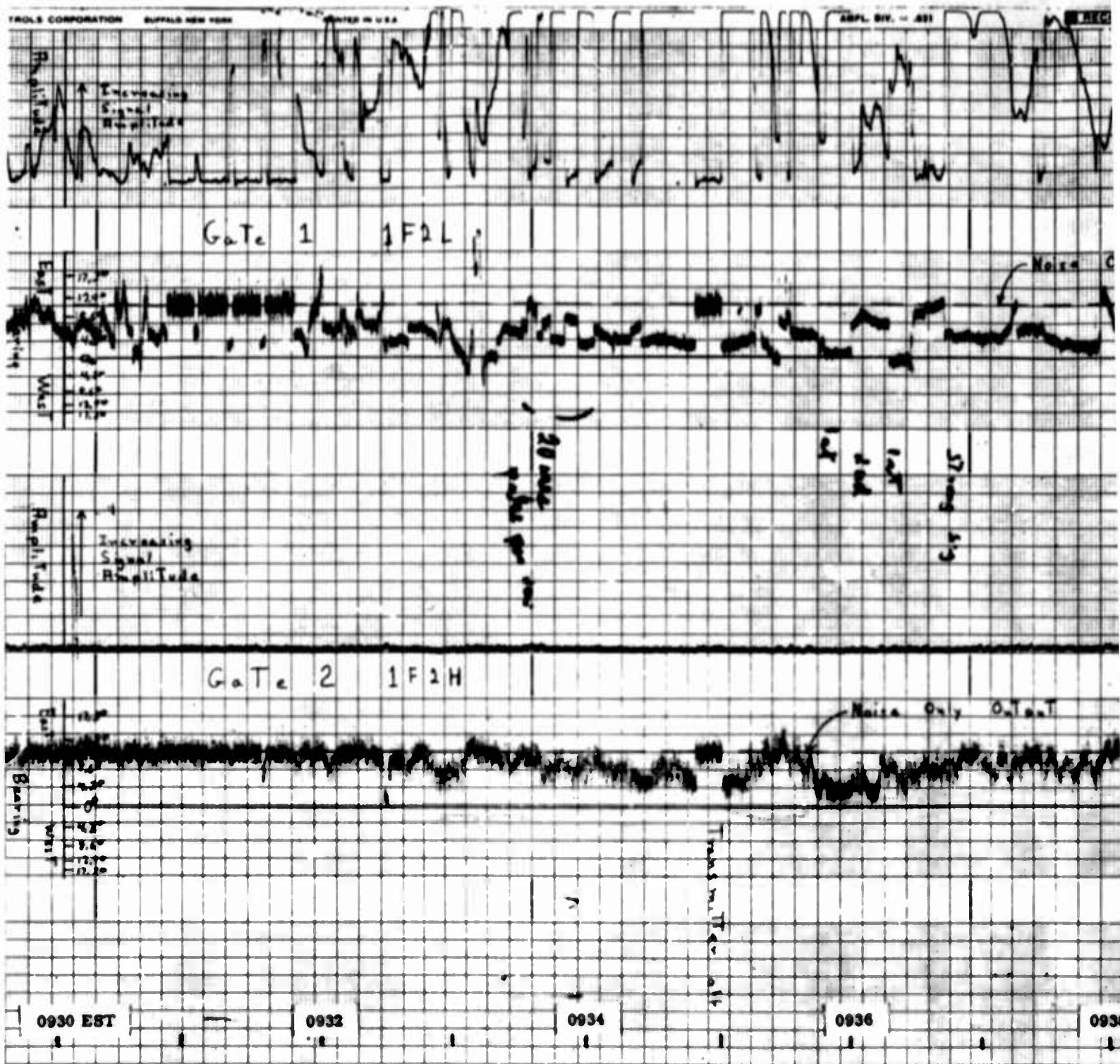
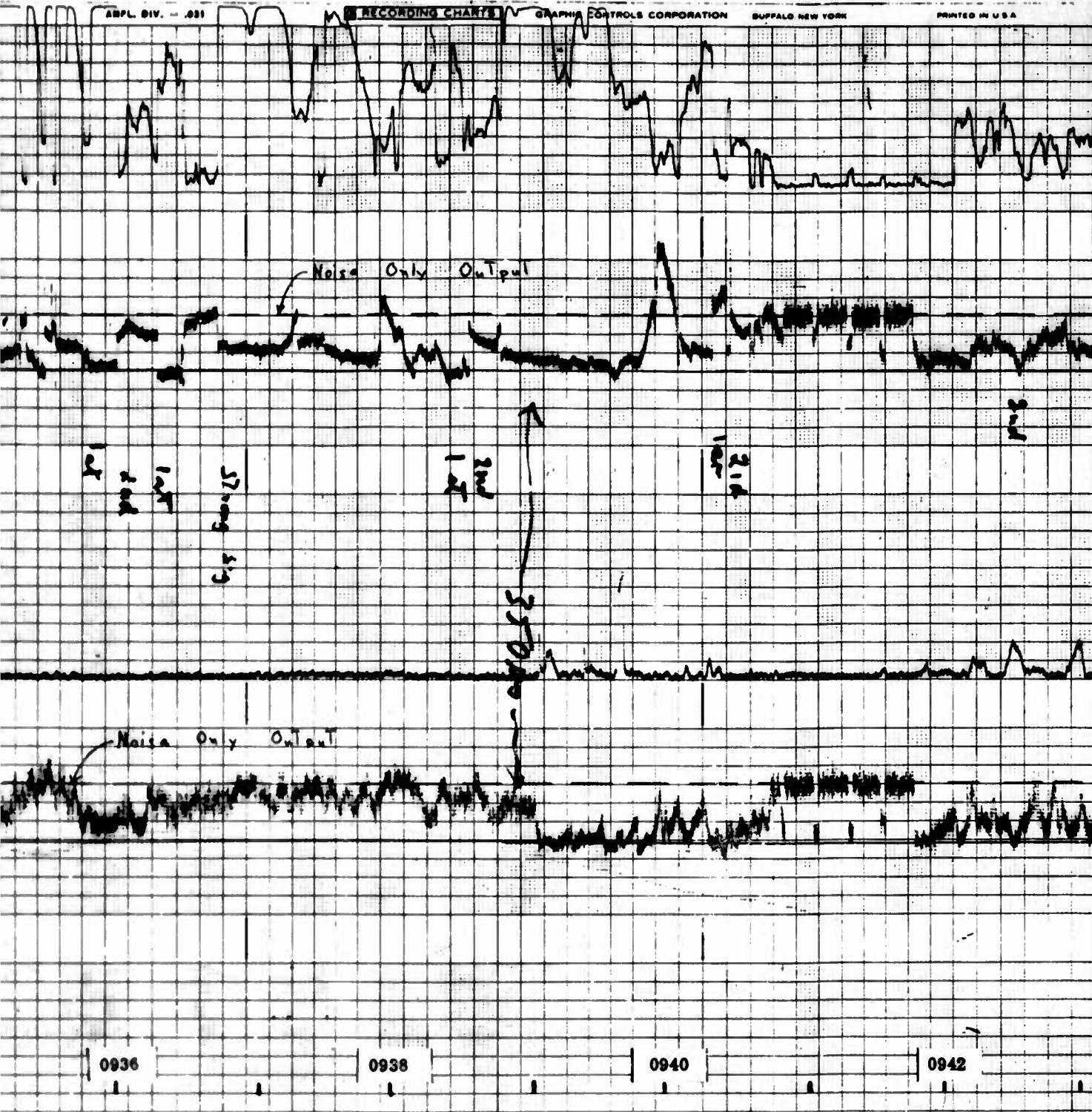


Figure 219. AOA Record for 14 February
1968 after 0930 EST



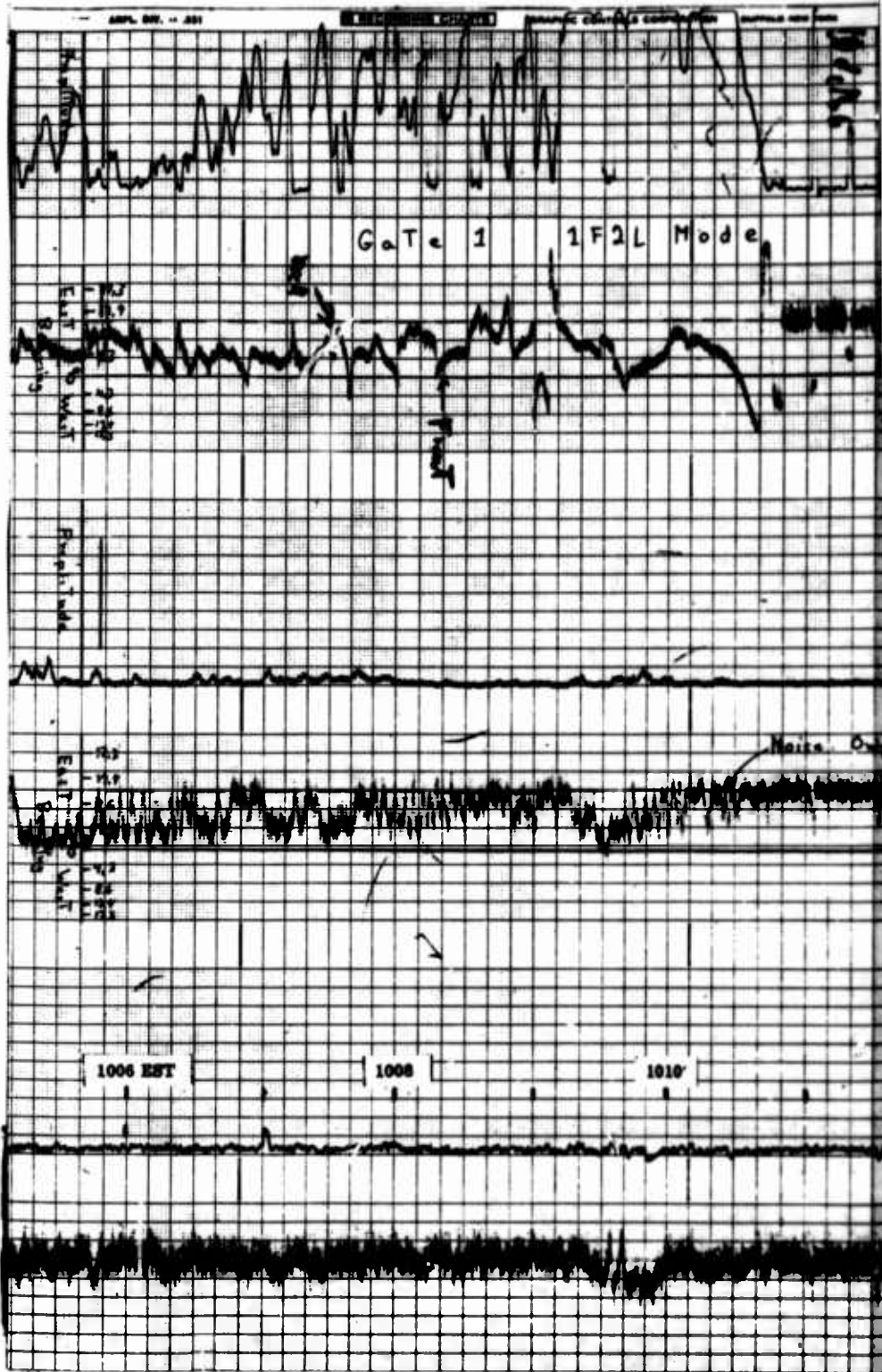
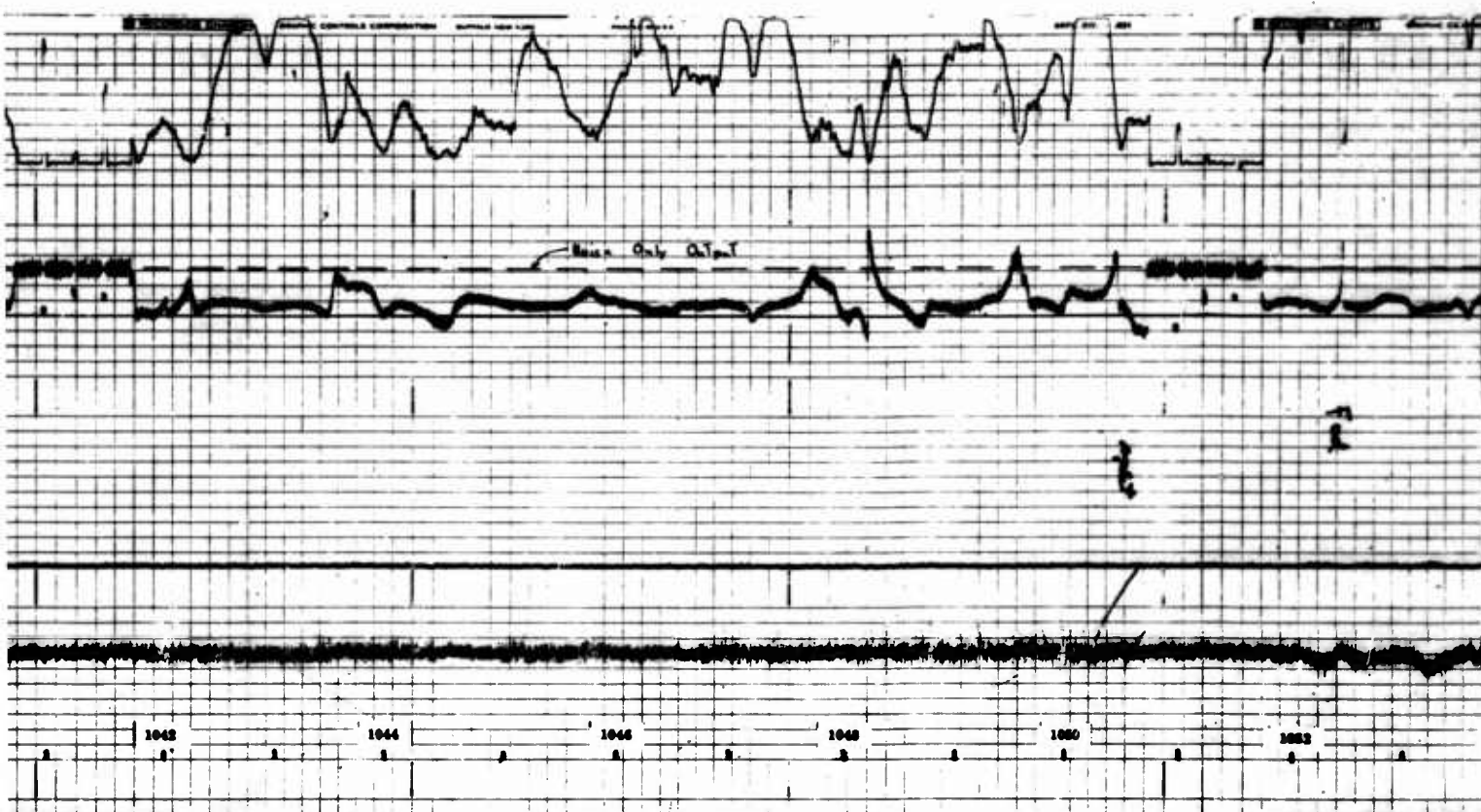


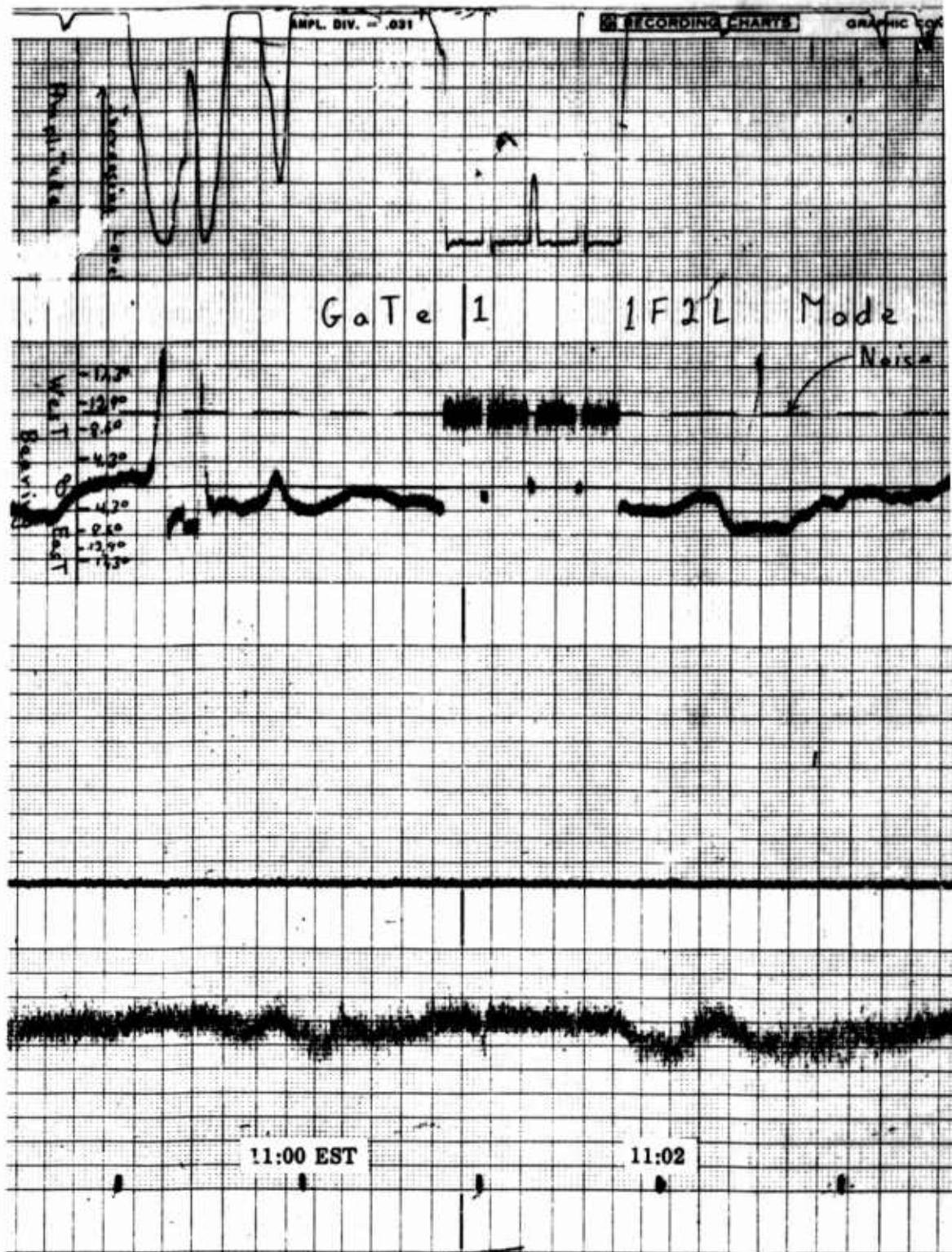


Figure 220. AOA Record for 14 February 1968 around 1010 EST



Figure 221. AOA Record for 14 February 1968 around 1040 EST





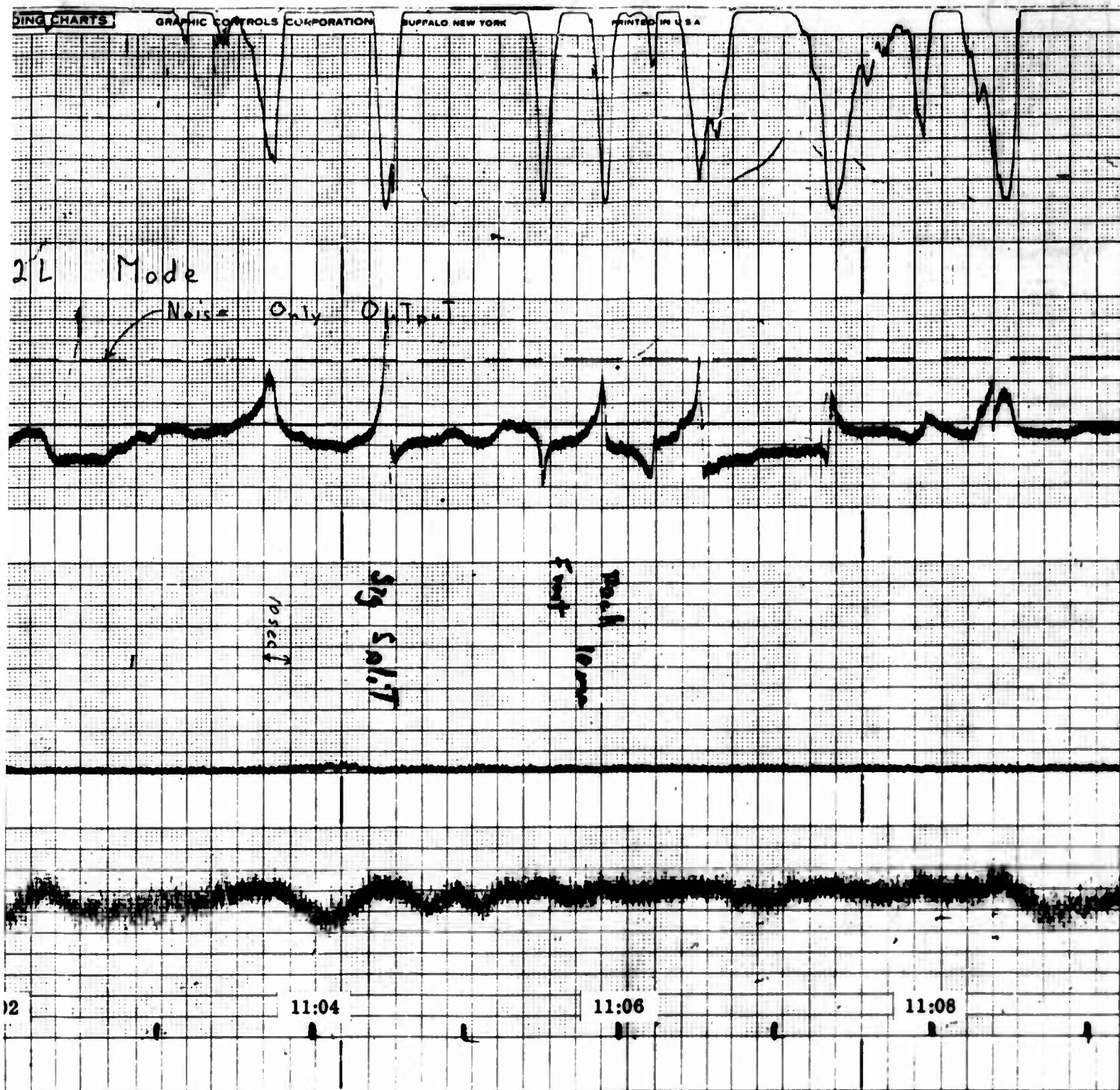


Figure 222. AOA Record for 14 February 1968 around 1100 EST

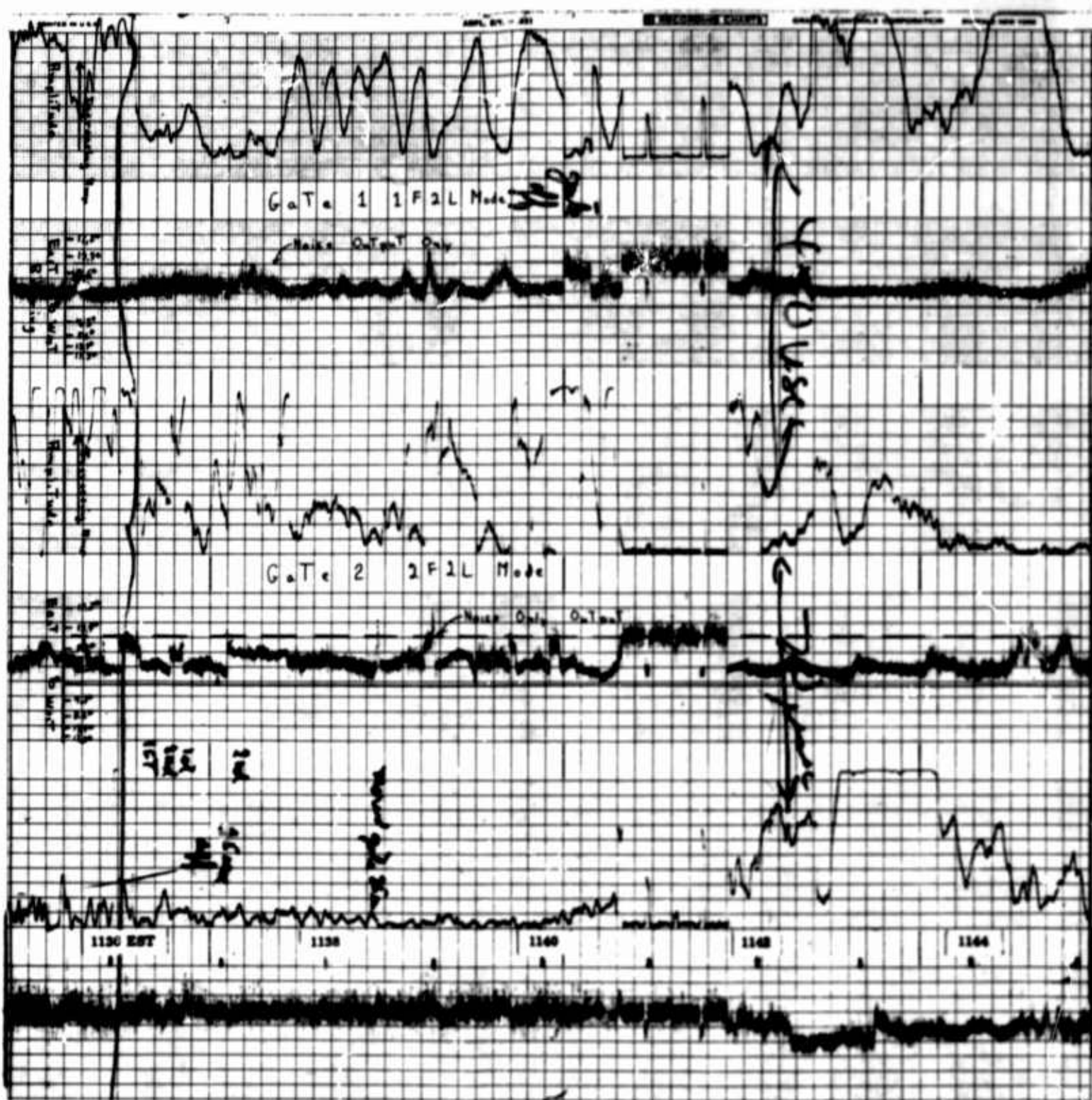


Figure 223. AOA Record for 14 February 1968 around 1135 EST

SECTION VII

NOISE/INTERFERENCE EXPERIMENT

1. INTRODUCTION

This section describes the noise/interference (N/I) experiment in terms of the measurement objectives, instrumentation facilities, and experimental results.

2. EXPERIMENT DESIGN CONSIDERATIONS

a. Experimental Objective

Within the context of the Expanded Little IDA objective, which is to improve the knowledge of HF propagation for over-the-horizon radar (OHR) applications, the noise/interference (N/I) experimental objective is to advance the knowledge of the N/I environment in order to permit economical OHR system design and operation and more accurate system performance prediction. So far as this experiment is concerned, the N/I environment includes communication and radar station RF emissions as well as atmospheric, galactic, and random man-made noise in the 4- to 40-MHz band.

b. Experimental Motivation

An important environmental factor in OHR system design is the N/I level with which an operational OHR system must contend. Since the radar design is based, in part, on achieving a certain SNR (and, hence, a certain target detection probability), the N/I level directly affects output power level considerations for the OHR system. An accurate assessment of the noise and interference environment will lead to economically optimum OHR system design and operational performance. On the other hand, significant quantitative uncertainty in characteristics of noise and interference may lead to overspecification of OHR system power output requirements which may result in unjustified, if not prohibitive, system cost. Alternately, underspecification of radar output power will result in unsatisfactory detection performance because of unfavorable SNR's; hence, it is extremely important to accurately characterize the N/I environment over the frequency range that the OHR system requires and in terms of parameters useful to the OHR system designer.

To date, CCJR Report 322 (Ref. 8) which is based on data collected on a world-wide basis over a four-year period of time, is the primary source for predicting noise levels. This report indicates the atmospheric and galactic noise levels that would be collected by a short vertical whip antenna.

Since an OHR system will likely utilize a highly directive antenna and operate on channels that may be contaminated, not only by atmospheric noise, but also by signals from other HF users, there is reason to question the validity of the direct use of the CCIR 322 results for OHR system synthesis. A summary of the weaknesses of the available data in the literature with respect to the N/I problem is as follows.

Virtually all organized data have been taken using a short vertical monopole antenna over ground. What little data are available using directive antennas are somewhat inconclusive as exact antenna performance is not known. The azimuthal and elevation angle gain differences of directive antennas over omnidirectional antennas may cause significantly different N/I readings.

The HF noise literature generally does not report interference from other HF stations, which may be the limiting factor in achieving the required margin in SNR.

While the ambient noise level over the frequency band of interest may be known, the availability of a percentage of channels at the ambient noise level is not known. The statistics associated with clear channel availability will govern OHR operational procedures such as noise environment monitoring rates, frequency search rates, and power level requirements.

The effects of polarization (as would be observed with linearly polarized antennas) on N/I reception are not well known. Any significant polarization sensitivity of noise and interference could influence OHR system design.

There are many modifications to be made to apply existing data to any given site; frequency, bandwidth, and location are but a few. To apply existing data would force a designer to add a costly safety factor with the result that the OHR system may be overdesigned. If this is not done, the system may fail to perform its prescribed function with the required reliability.

In view of these existing shortcomings in the available literature and the importance of the accurate prediction of the N/I level to be expected by an OHR system, it was deemed highly desirable to perform a number of experiments to obtain some of the needed information.

c. Information Needs

The selection of specific N/I measurements is governed by the type of N/I information required by the OHR system designer. In order to identify legitimate N/I information needs, any postulated information should satisfy the following criteria:

1. The information would potentially affect OHR system design philosophy,
2. The information would potentially improve the performance and/or operation of an OHR system, and
3. The information advances the state of the knowledge (i.e., CCIR 322).

While the stated criteria are reasonably restrictive, it was still possible to identify information needs that, in total, would require an excessive measurement program; however, the major N/I information needs that were judged to satisfy the listed criteria and were consistent with the stated objective of the Expanded Little IDA program were as follows:

1. Validity of CCIR noise predictions to OHR design,
2. Polarization and elevation angle sensitivity,
3. Geographical area sensitivity,
4. Frequency and diurnal variation of interference,
5. Clear channel availability,
6. Temporal stationarity of interference, and
7. Correlation with signal loss and geophysical phenomena.

The ability to perform the experiments to address the above information needs and the quality of the measurement data is ultimately constrained by the instrumentation available. Accordingly, it is appropriate at this point to review the instrumentation involved in N/I measurements.

d. Instrumentation Configuration

The N/I experiment is characterized by passive operation so that the N/I instrumentation (all located at Starr Hill) is described, for the most part, by the antennas and receivers. The N/I receiving system is operationally divided into two distinct receiving networks. One receiving network consists of a short vertical monopole antenna and an Environmental Science Services Administration (ESSA) noise receiver (having the designation "ARN-2") and is identical to the HF portion of the world-wide ESSA noise measuring stations. This receiving network is depicted at the top of Figure 224. The second receiving network, illustrated in the remainder of

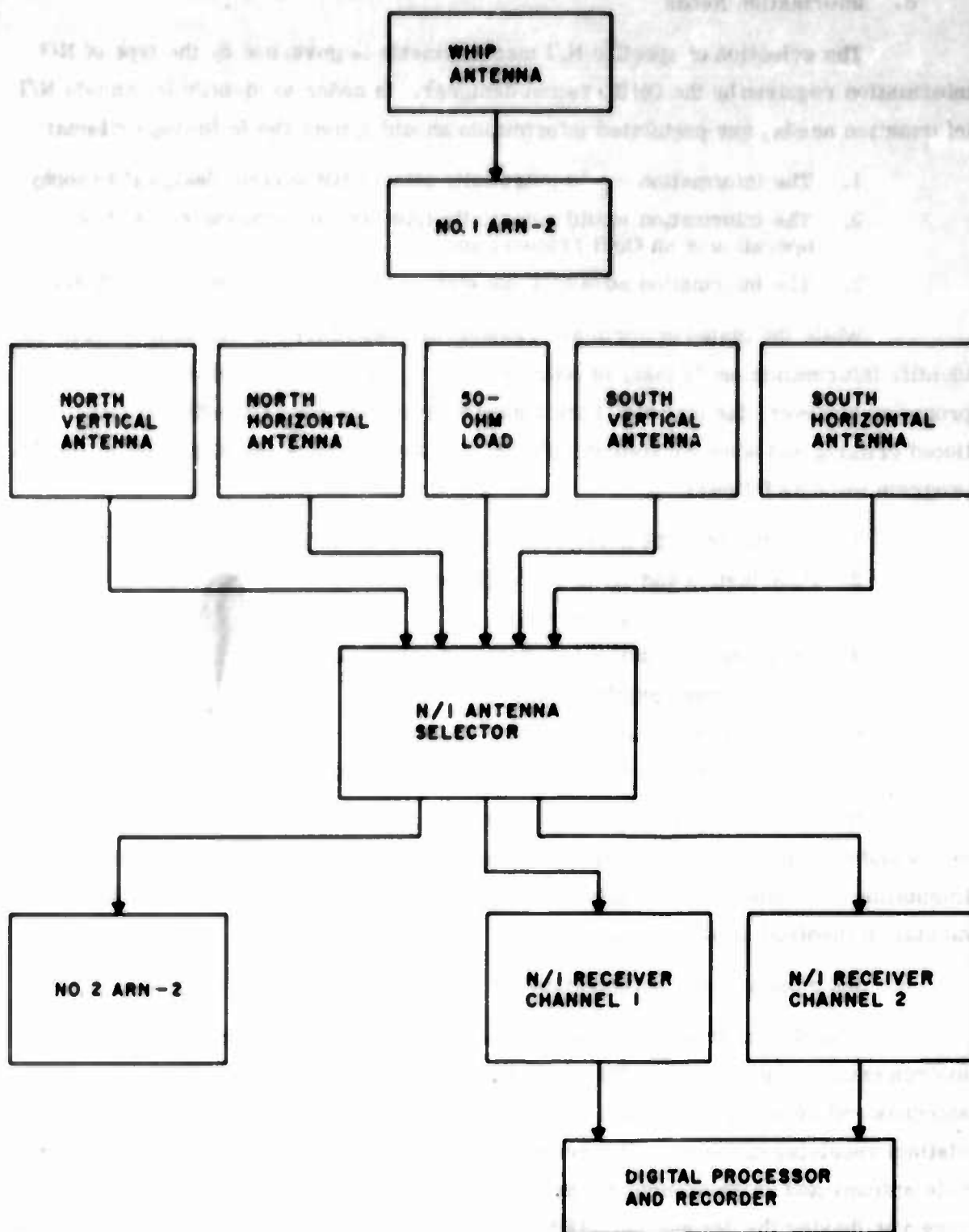


Figure 224. Noise/Interference Experiment Instrumentation Representation

this figure, utilizes the cross-polarized, log-periodic antennas (common to the other ELIDA experiment), another ARN-2 receiver, and a dual-channel, General Electric fabricated N/I receiver.

Under normal operating procedures the vertical monopole or whip antenna is connected to the No. 1 ARN-2 receiver for continuous data connection. The No. 2 ARN-2 is connected to one of the array antennas, also for continuous data collection, if the selected antenna is not required for the N/I receiver or another experiment. The N/I receiver has two complete receiver channels, each of which may be connected to an array antenna. Furthermore, in the multiplex mode, one receiver channel may be operated in a multiplex fashion, switching between two antennas, so that three antennas in total may be utilized by the N/I receiver for one measurement cycle.

Insofar as data recording is concerned, two recording processes are utilized. The ARN-2 noise receivers have self-contained Esterline-Angus paper chart recorders which operate unattended.

The output of the N/I receiver is stored in the digital processor for a short period of time and is then recorded on magnetic tape using an incremental digital recorder. The N/I data are "unpacked" and further processed using a digital computer with the data from the other experiments collected and recorded using the digital processing equipment.

3. NOISE MEASUREMENTS WITH ARN-2 RECEIVERS

a. Measurement Technique

An atmospheric radio noise receiver (designation ARN-2), on loan from ESSA, was in operation at the Starr Hill Test Annex from February through October 1967. As mentioned previously, the Starr Hill ARN-2 configuration may be considered to consist of two independent receivers, one receiver being connected to a whip antenna and the other receiver to one of the directional antennas located at the site.

The ARN-2 measures and records the integrated noise power as seen by the selected antenna. The frequencies on which the noise environment is measured are generally free from radio signals, and, therefore, provide a measure of strictly atmospheric, galactic, and random man-made noise. In particular, the ARN-2 listening frequencies are within the guard band of WWV, the ESSA radio station.

The ARN-2 receiver at Starr Hill used with the whip antenna is constrained to operate only on 2.5, 5, 10, and 20 MHz, while the modified ARN-2 receiver employed with one of the directional antennas operates on only 5.0, 10.0, and 20.0 MHz.

In actual operation, the ARN-2 listens for 15 minutes on each frequency, and thereby provides a measurement on each frequency once per hour.

The parameter measured is the average noise power over a 500-second integration period within the 15-minute listening period. The ARN-2 receiver is capable of measuring the noise power with a 100-dB dynamic range and utilizes a 200-Hz bandwidth. Special self-contained calibration equipment permits the ARN-2 receivers to directly record the effective antenna noise figure defined as the noise power available from an equivalent lossless antenna relative to kT_0 . A summary of the ARN-2 receiver characteristics is presented in Table XXXI.

The auxiliary equipment for the ARN-2 receiver, also in operation at Starr Hill, is for the purpose of measuring the deviation (V_d) of the average voltage and the average logarithm (L_d) of the voltage with respect to the average power. The purpose of measuring these additional parameters of the noise is that, according to ESGA, they permit construction of the average amplitude probability distributions of the noise voltage. The statistical significance of the measured parameters will be discussed later.

TABLE XXXI
ARN-2 RECEIVER CHARACTERISTICS

Nominal Operating Frequencies	Receiver 1	Receiver 2
T = 00 to T = 1. minutes	2.5 MHz	Not used
T = 15 to T = 30	5 MHz	5 MHz
T = 30 to T = 45	10 MHz	10 MHz
T = 45 to T = 60	20 MHz	20 MHz
Dynamic Range	100 dB	
Integration Period	500 seconds	
Bandwidth	200 Hz	
Noise Figure	7 dB	

b. Data Output Format

The integrated noise power is recorded on Esterline-Angus chart paper, a section of which has been reproduced in Figure 225. Four frequencies have been recorded for 15 minutes every hour and the indicated power level at the end of each 15 minutes is read to the nearest dB.

There are two additional strip chart recorders which, concurrently with the power measurement, record the log deviation and voltage deviation parameters.

Two sets of the three chart recorders are utilized, one set for each ARN-2 receiver.

The chart readings are edited and summarized on a monthly basis in four-hour time blocks as will be seen in the results to follow.

c. Results

The results of the ARN-2 noise measurements are directly comparable to the CCIR Report 322 noise levels inasmuch as these are based on noise measurements obtained primarily with ARN-2 receivers. Accordingly, the CCIR Report 322 values will be taken as a reference and comparisons made with the measurements obtained at the Starr Hill site.

(1) Median Noise Power

The median noise power (F_{am}) is the median level of noise in dB above kT_b where the median value is taken from a time-block of hourly readings. CCIR 322 uses a time-block consisting of the readings in a four-hour period every day for a three-month period that comprises a season.

Illustrated in Figures 226 through 229 are the CCIR seasonal predictions (P) with the corresponding Starr Hill measurements (M) for the winter, spring, summer, and autumn seasons where the seasons normally consist of the following months:

Winter	Spring	Summer	Autumn
December January February	March April May	June July August	September October November

The figures depict the frequency variation of the median noise power in each of the six four-hour blocks of the day. The curves representing the measured data for the

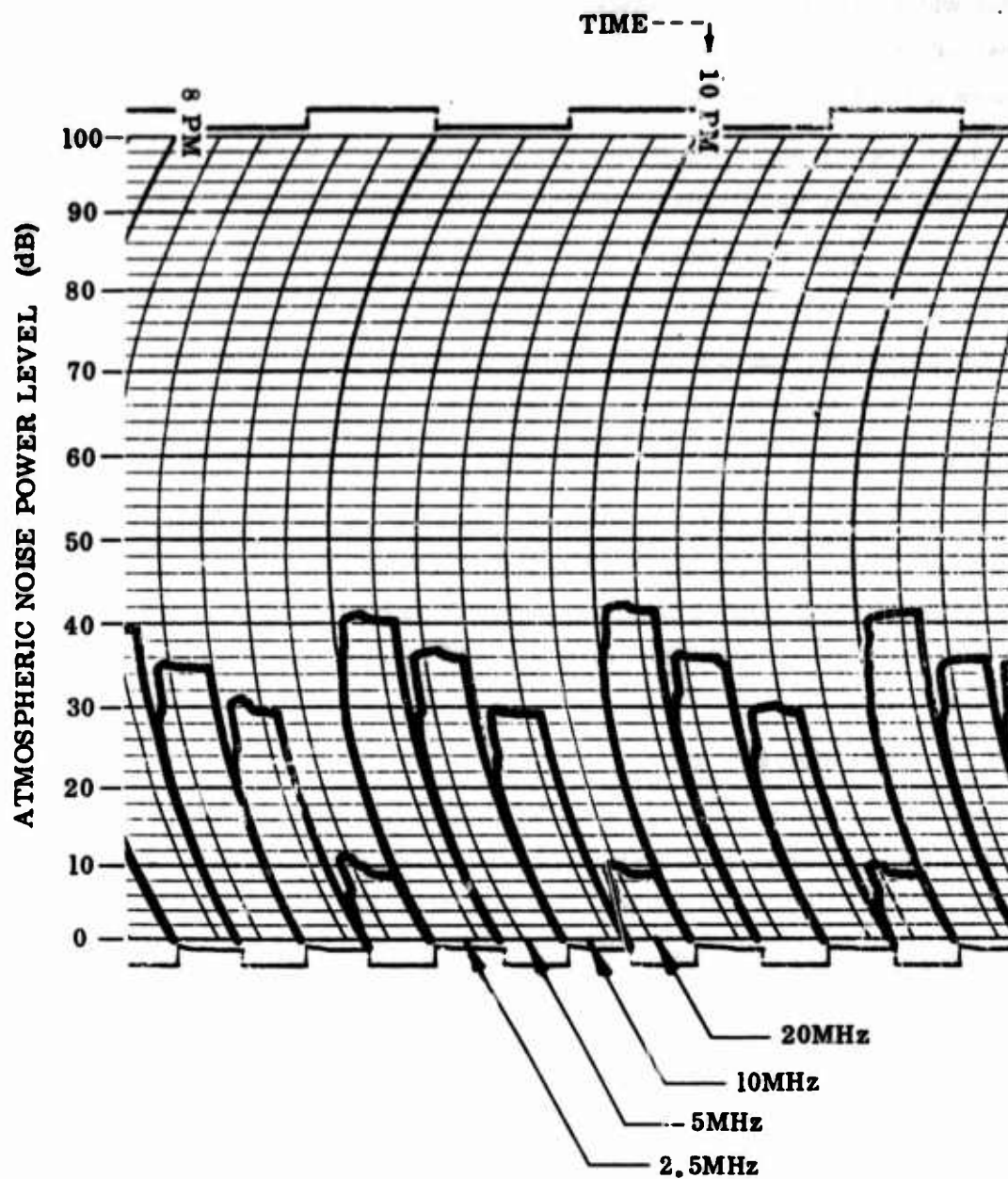


Figure 225. ARN-2 Receiver Output Format

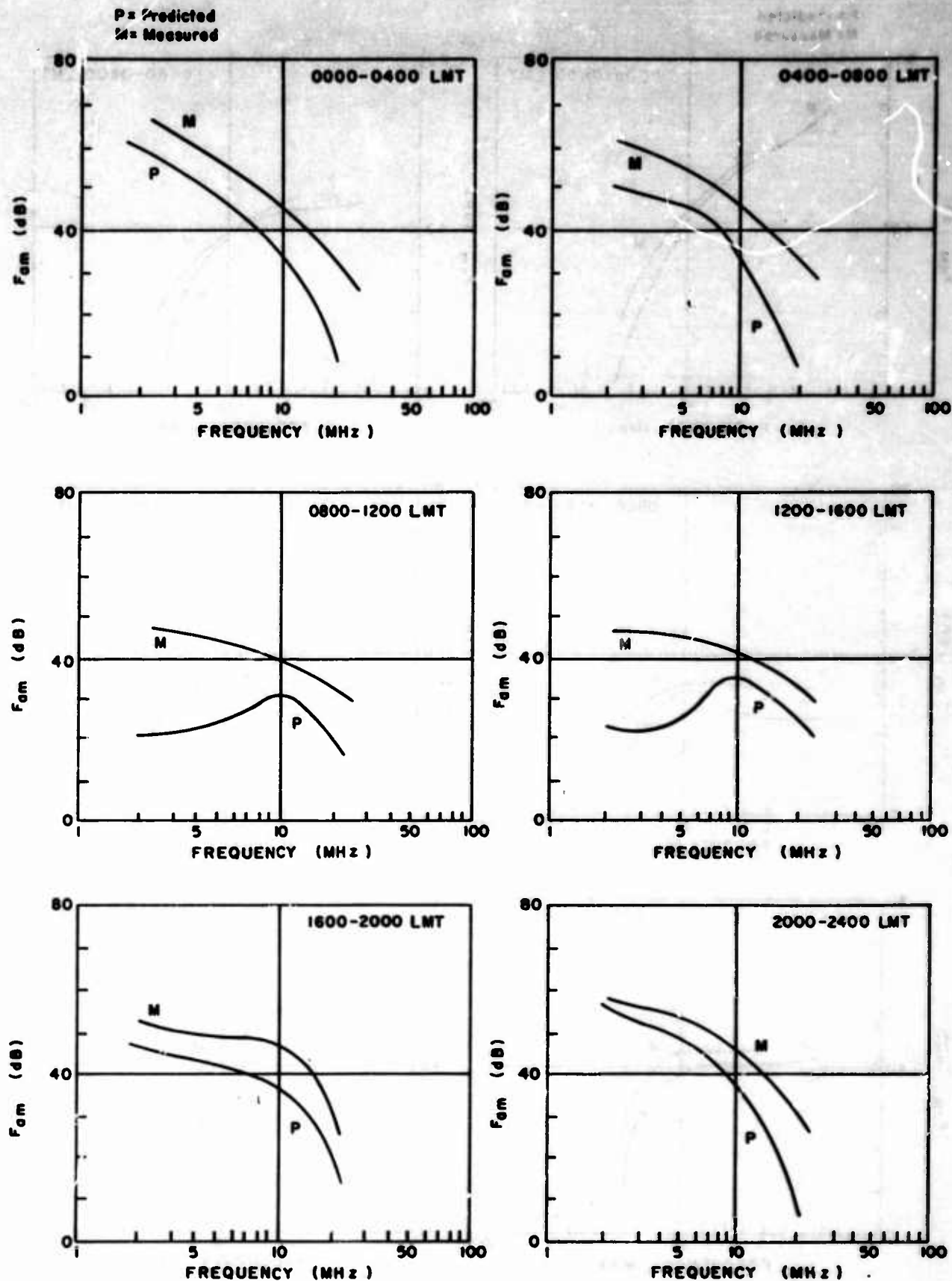


Figure 226. Seascam Median Noise Power, Omnidirectional Antenna
Starr Hill, Winter 1967

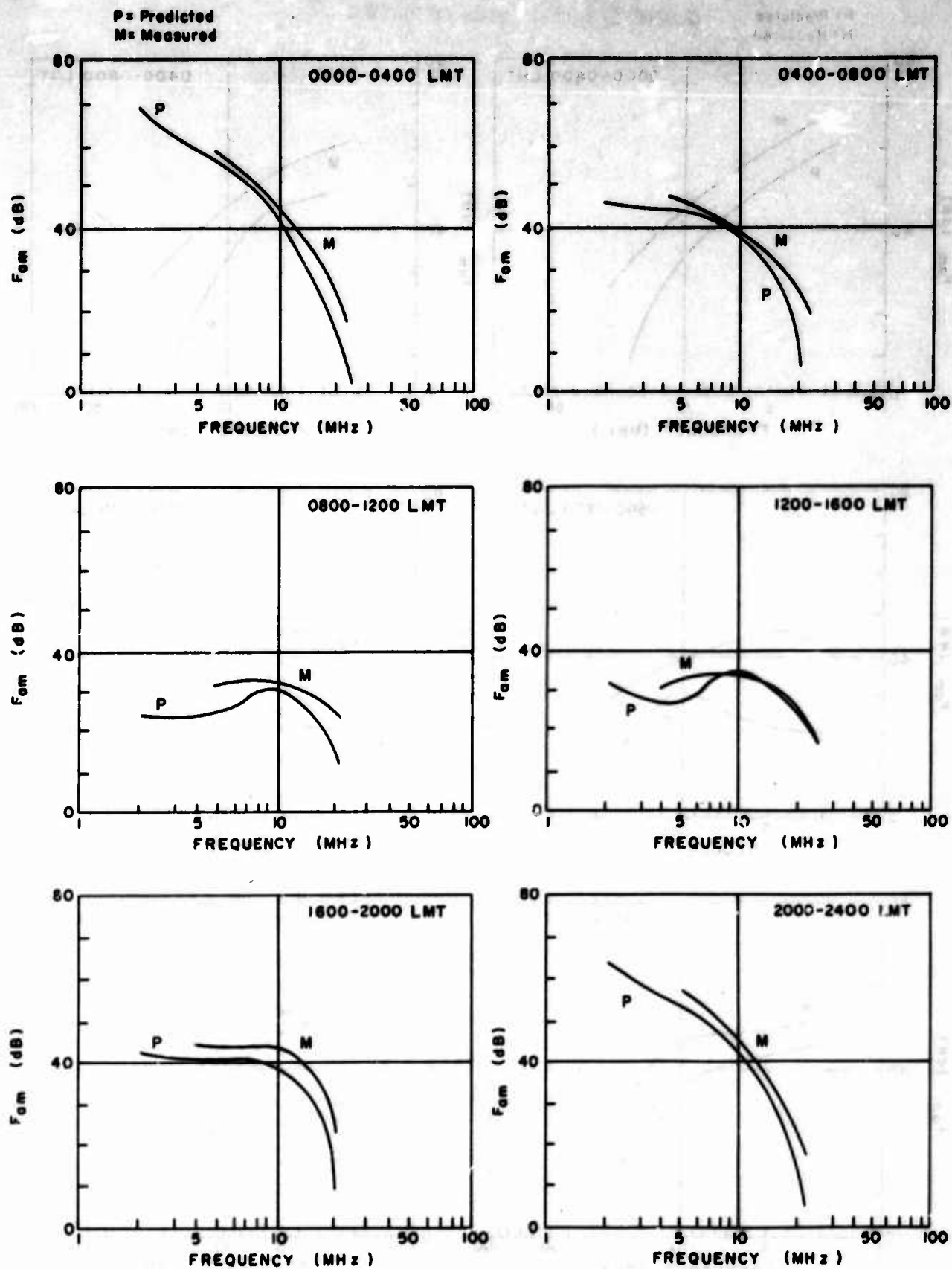


Figure 227. Season Median Noise Power, Omnidirectional Antenna, Starr Hill, Spring 1967

winter season contain only February data inasmuch as February 1967 was the first full month of ARN-2 data collected at the Starr Hill site. The autumn season contains only September 1967 data.

It should be pointed out that the curves of predicted values are strictly the atmospheric noise estimates whereas the curves for the measured values include both atmospheric and galactic noise. This difference will be evident at the measurement frequencies of 10 and 20 MHz since, at those frequencies, the galactic noise tends to be higher than the atmospheric noise.

The agreement between the predicted and measured noise levels is within the expected variability of the median noise power. With the knowledge that the predicted seasonal medians are reasonably closely verified by these measurements at Starr Hill, it is of interest to examine a smaller time interval. Consider the monthly medians shown in Figures 230 through 235. Note that even the measured monthly medians compare favorably with the seasonal predictions.

(2) Decile Values

While the time block median noise levels provide meaningful indications of the general diurnal and frequency variation of noise, it is also desirable to know the variability of the hourly values of atmospheric and galactic noise about the median. One such measure of the variability is the decile values; that is, the 10 and 90 percent exceedence levels, expressed relative to the median or 50 percent exceedence level, provide an indication of the statistical variation of hourly values of noise.

Figures 236, 237, and 238 depict the seasonal decile values of noise power for the winter, spring, and summer seasons as a function of frequency and time of day. A comparison of the measured and predicted values shows that the observed noise variability is similar to the predicted variability.

(3) Other Statistics

The auxiliary equipment associated with the ARN-2 noise receivers is designed to directly record additional noise parameters identified as the log deviation and the voltage deviation. These parameters are defined as follows:

$$L_d = 20 \log \frac{e_{rms}}{e_{log}}$$

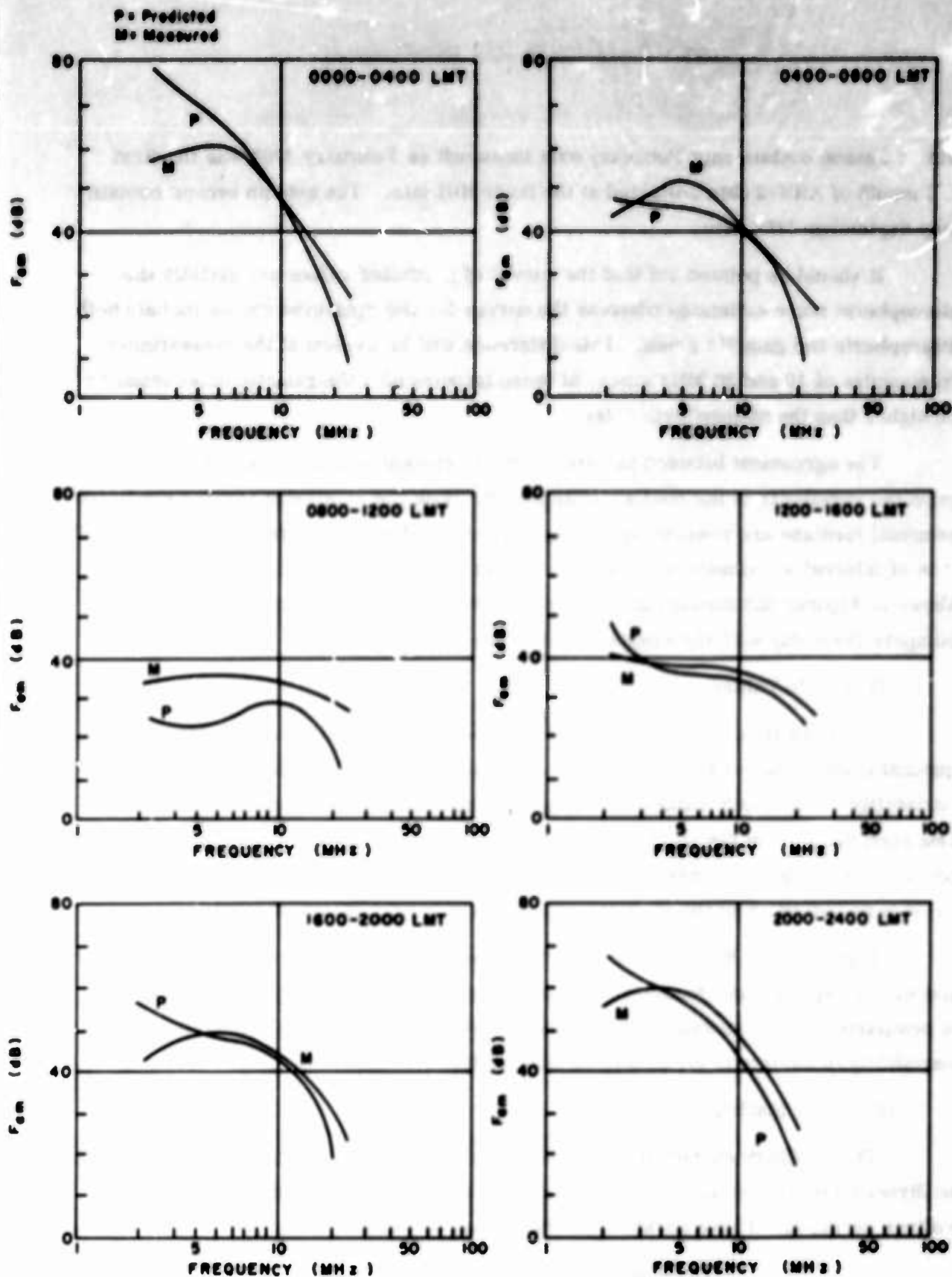


Figure 228. Season Median Noise Power, Omnidirectional Antenna
Starr Hill, Summer 1967

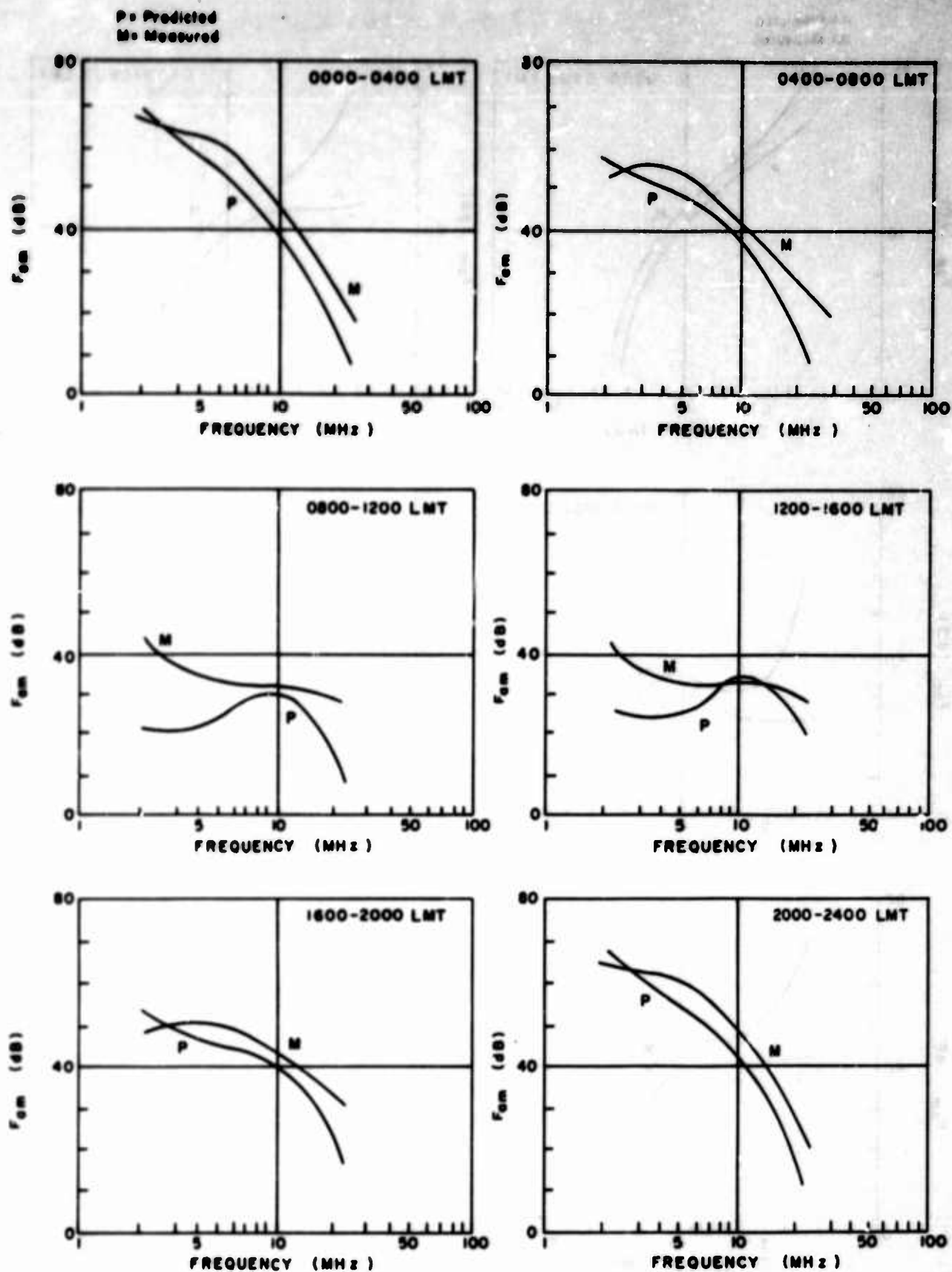


Figure 229. Season Median Noise Power, Omnidirectional Antenna
Starr Hill, Autumn 1967

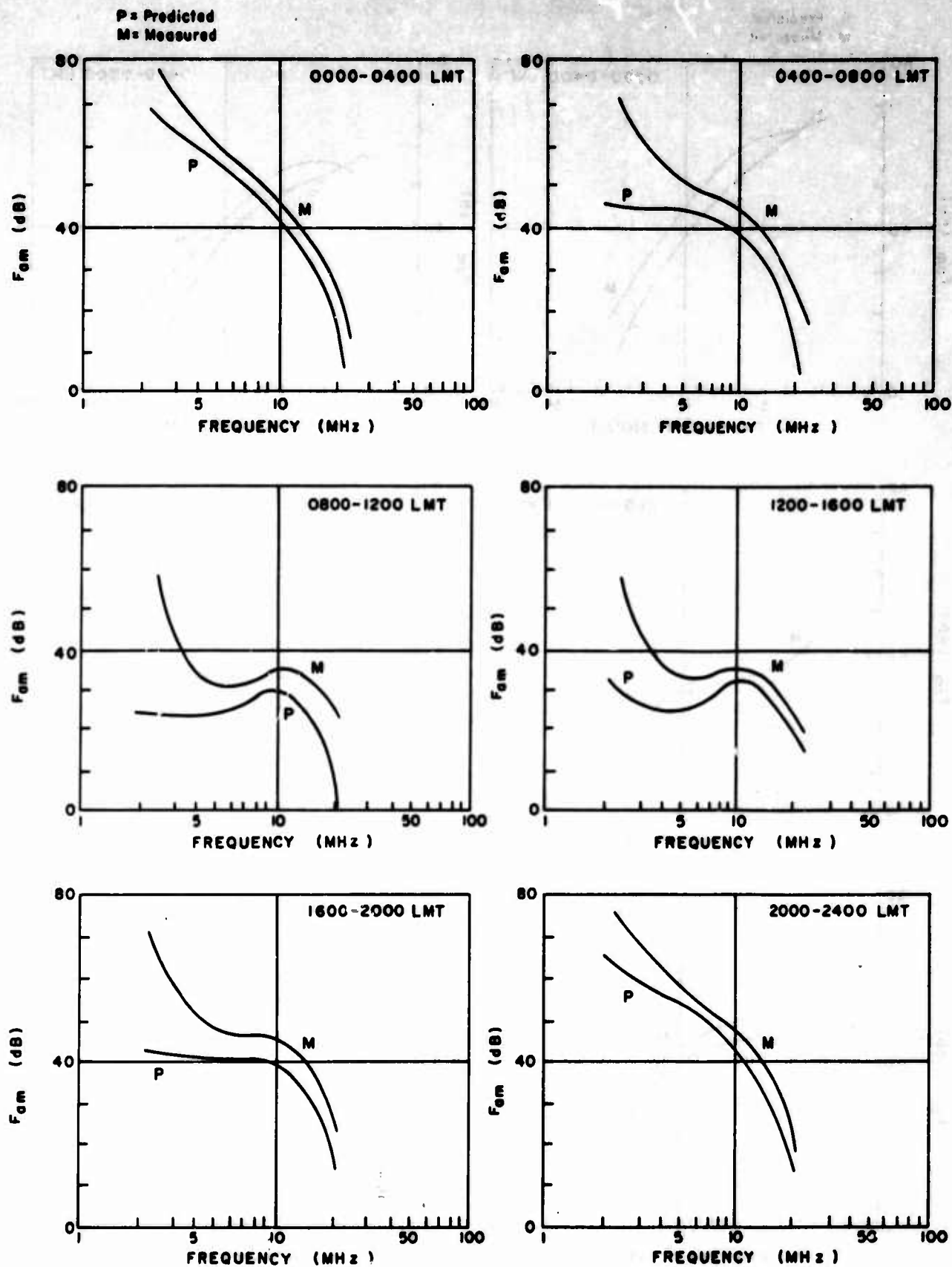


Figure 230. Monthly Median Noise Power, Omnidirectional Antenna
Starr Hill, March 1967

$$V_d = 20 \log \frac{e_{rms}}{e_{avg}}$$

where L_d = logarithm of the voltage deviation below mean noise power (F_n)

V_d = the voltage deviation in decibels below mean noise power (F_n)

e_{rms} = rms noise voltage

e_{log} = antilog of the mean log noise voltage

e_{avg} = average noise voltage

ESSA has shown how these parameters may be utilized to construct the amplitude probability distributions of atmospheric noise.

The results of measurement of L_d and V_d are presented in Tables XXXII through XLV for the months of February through August 1967. In some cases data are reported as collected with a directional antenna. This means that measurements were collected using the log-periodic antennas and the No. 2 ARN-2. It is interesting to note that the parameter values obtained using different antennas are within 1 dB, indicating that L_d and V_d are more or less independent of direction.

Since it may be of interest to examine the monthly variation of the decile values, Figures 239 through 243 are included, illustrating the noise deciles of the months during the spring and summer seasons.

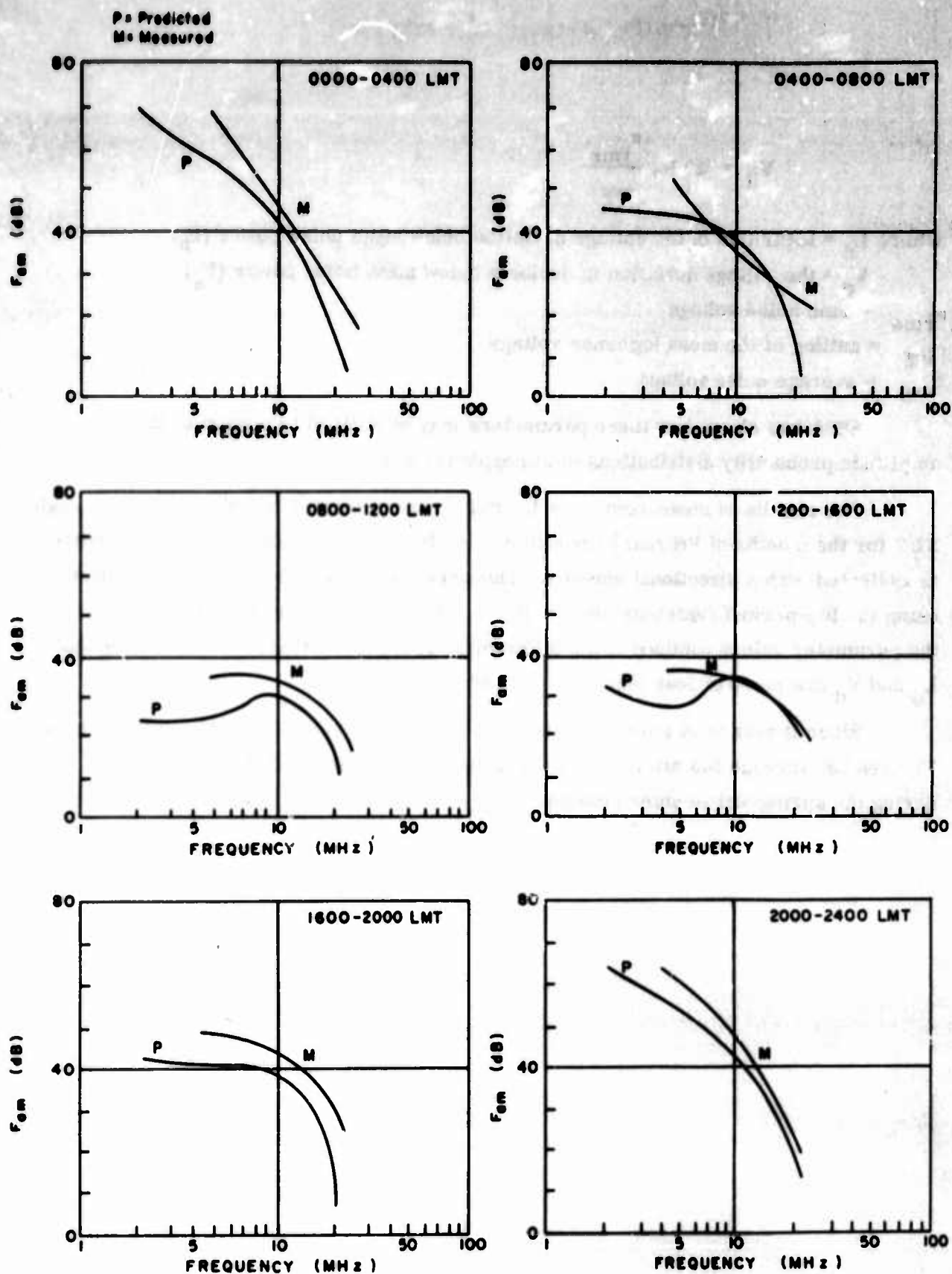


Figure 231. Monthly Median Noise Power, Omnidirectional Antenna
Starr Hill, April 1967

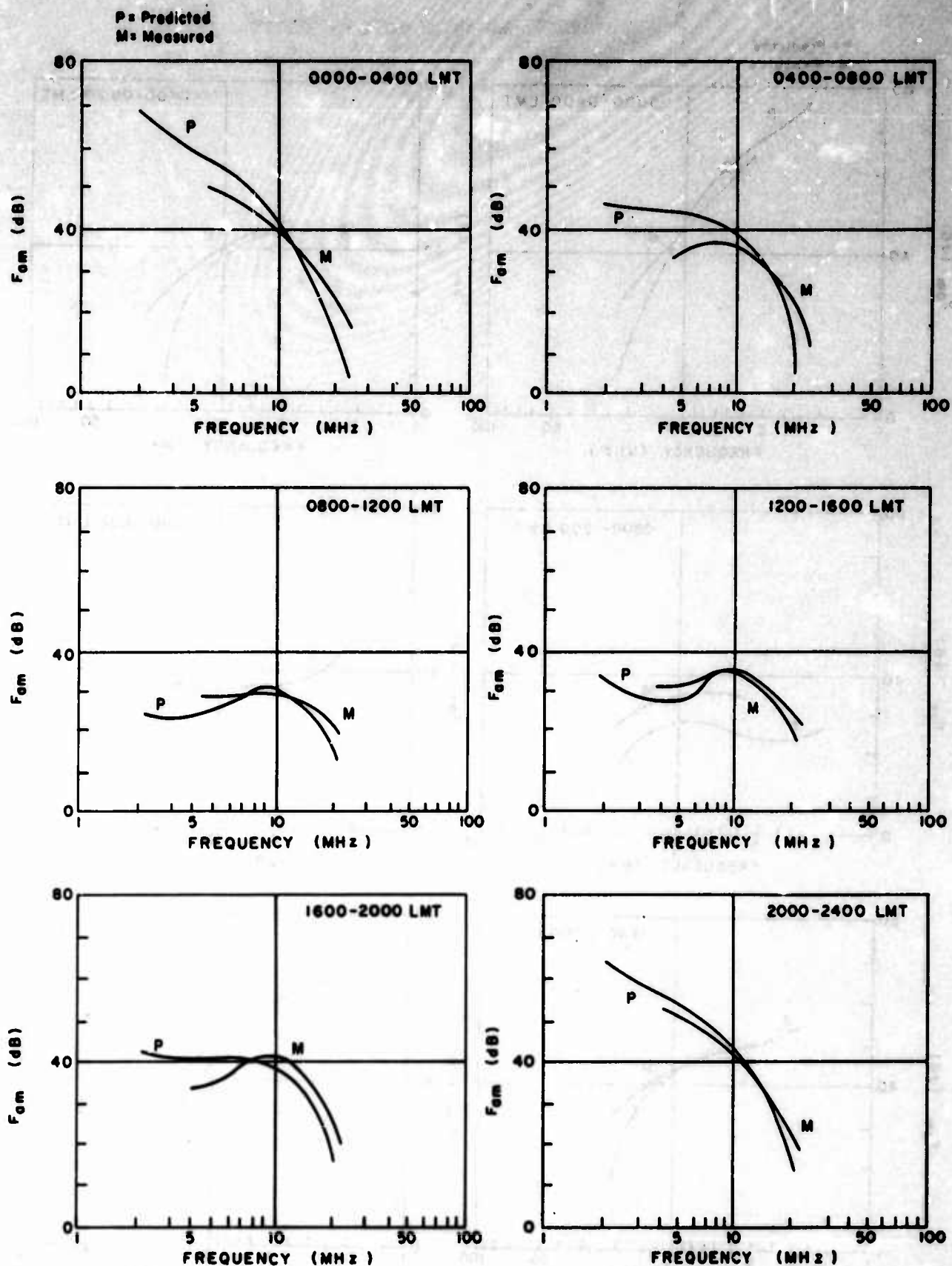


Figure 232. Monthly Median Noise Power, Omnidirectional Antenna
Starr Hill, May 1967

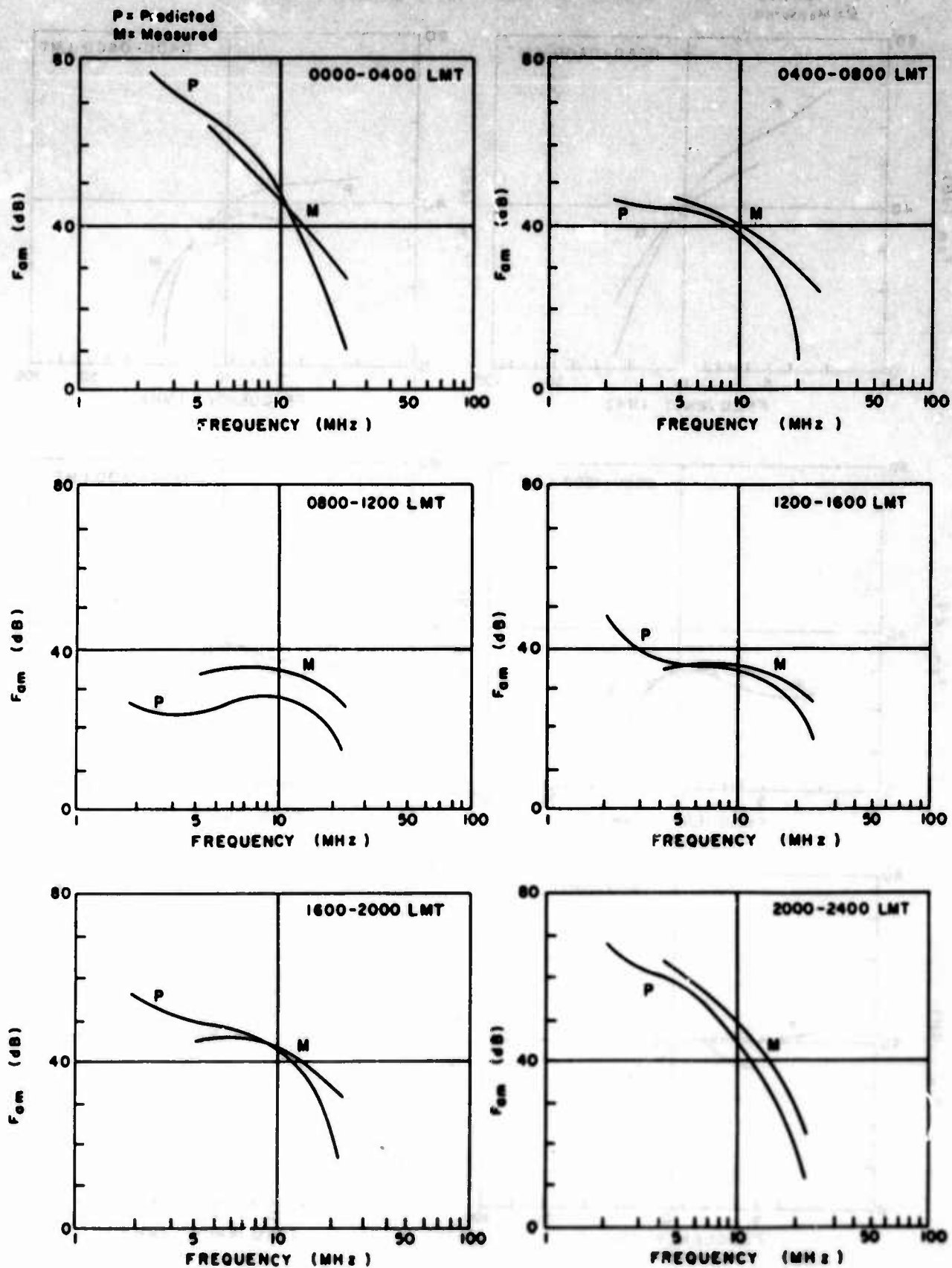


Figure 233. Monthly Median Noise Power, Omnidirectional Antenna
Starr Hill, June 1967

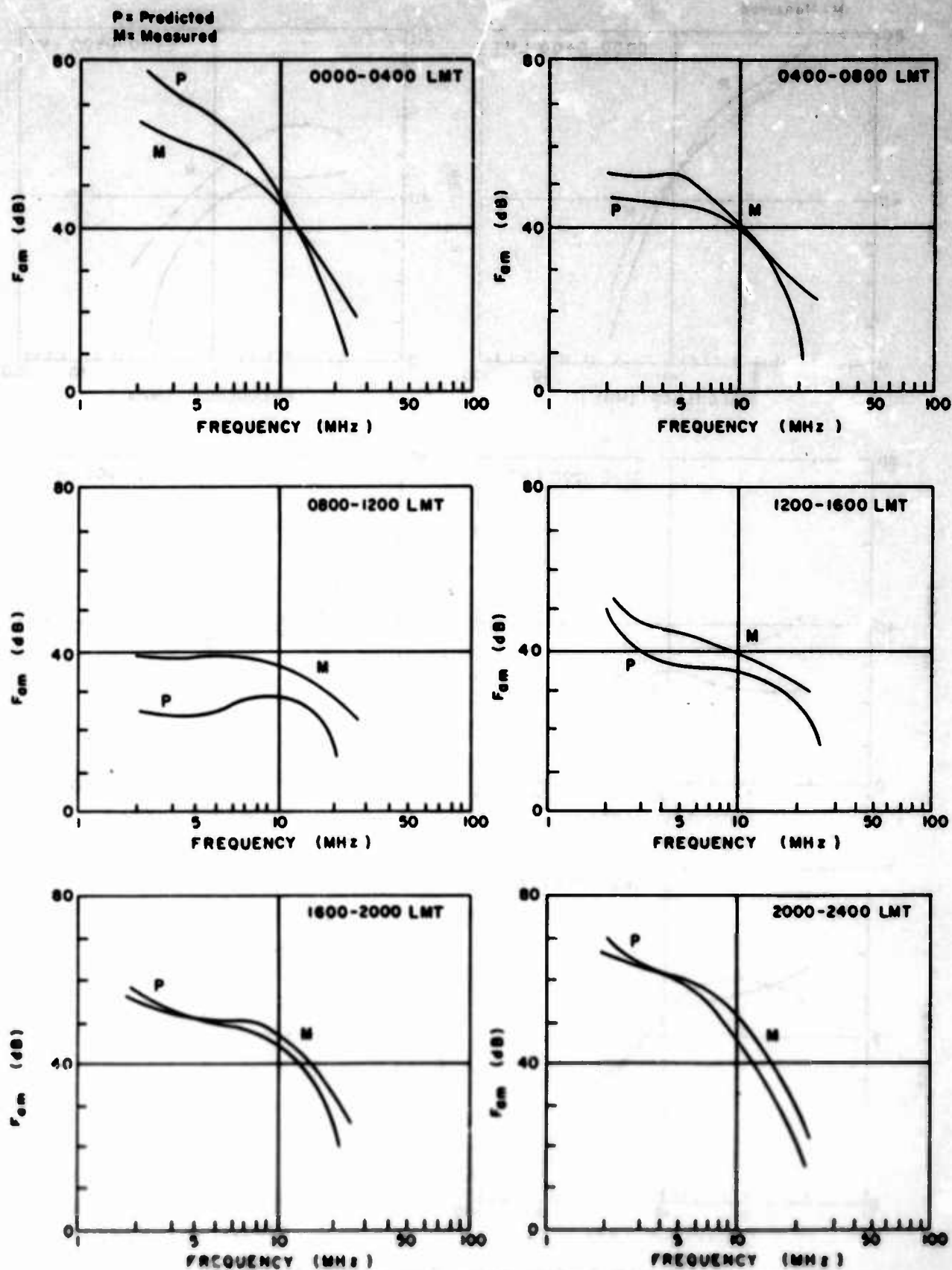


Figure 234. Monthly Median Noise Power, Omnidirectional Antenna
Starr Hill, July 1967

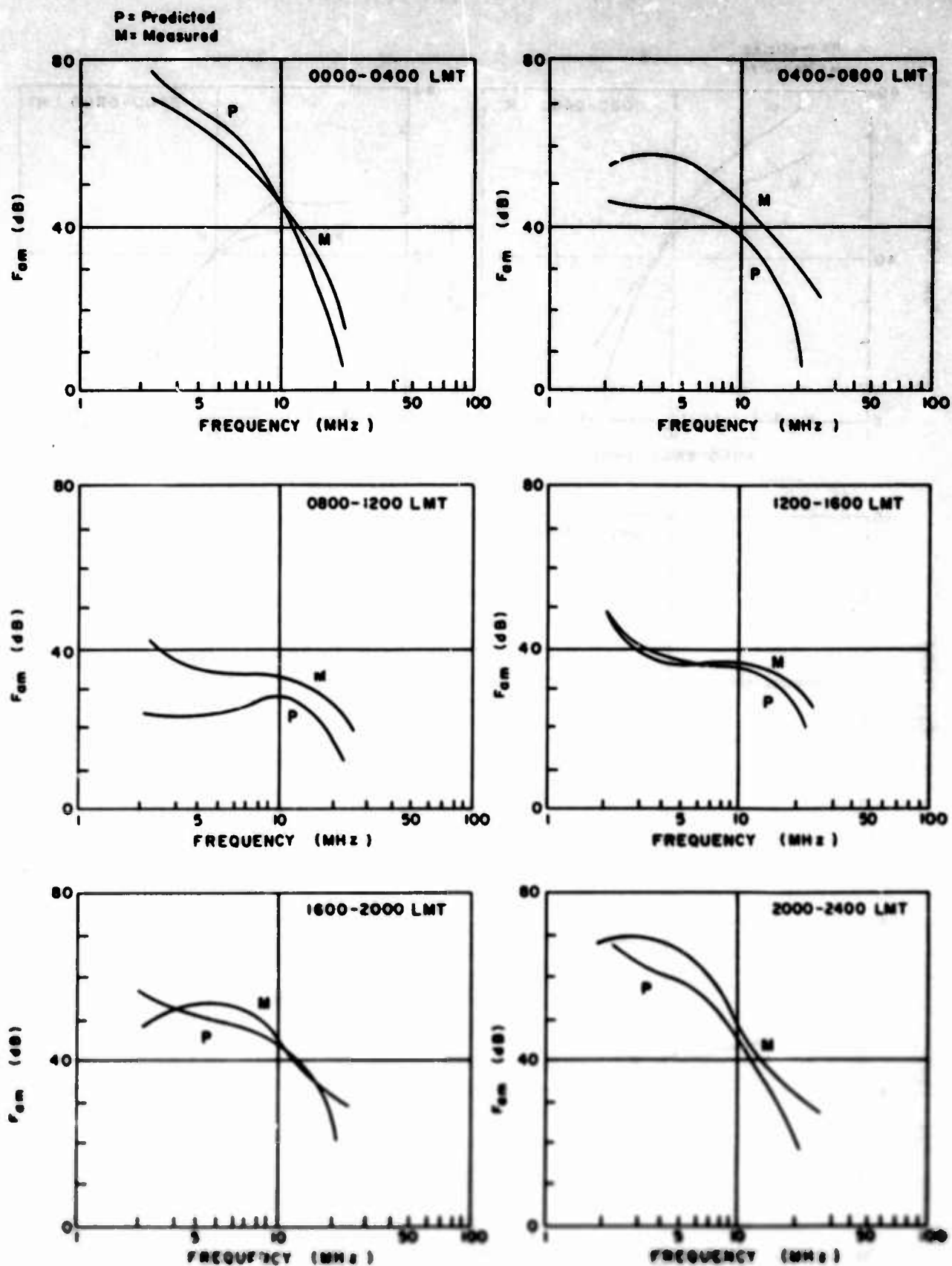


Figure 235. Monthly Median Noise Power, Omnidirectional Antenna
Starr Hill, August 1967

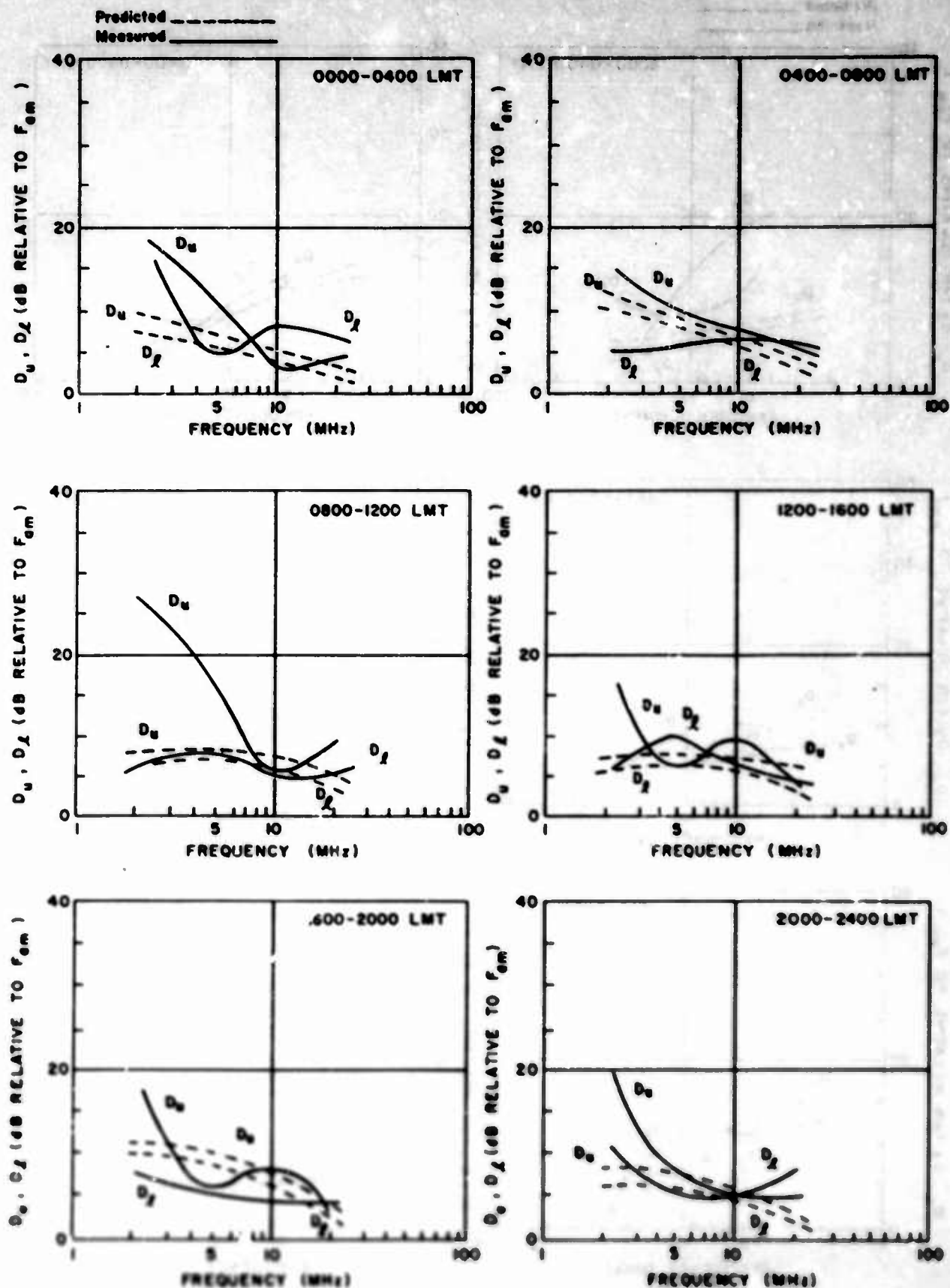


Figure 136. Season Noise Power Deciles, Omnidirectional Antenna
Starr Hill, Winter 1967

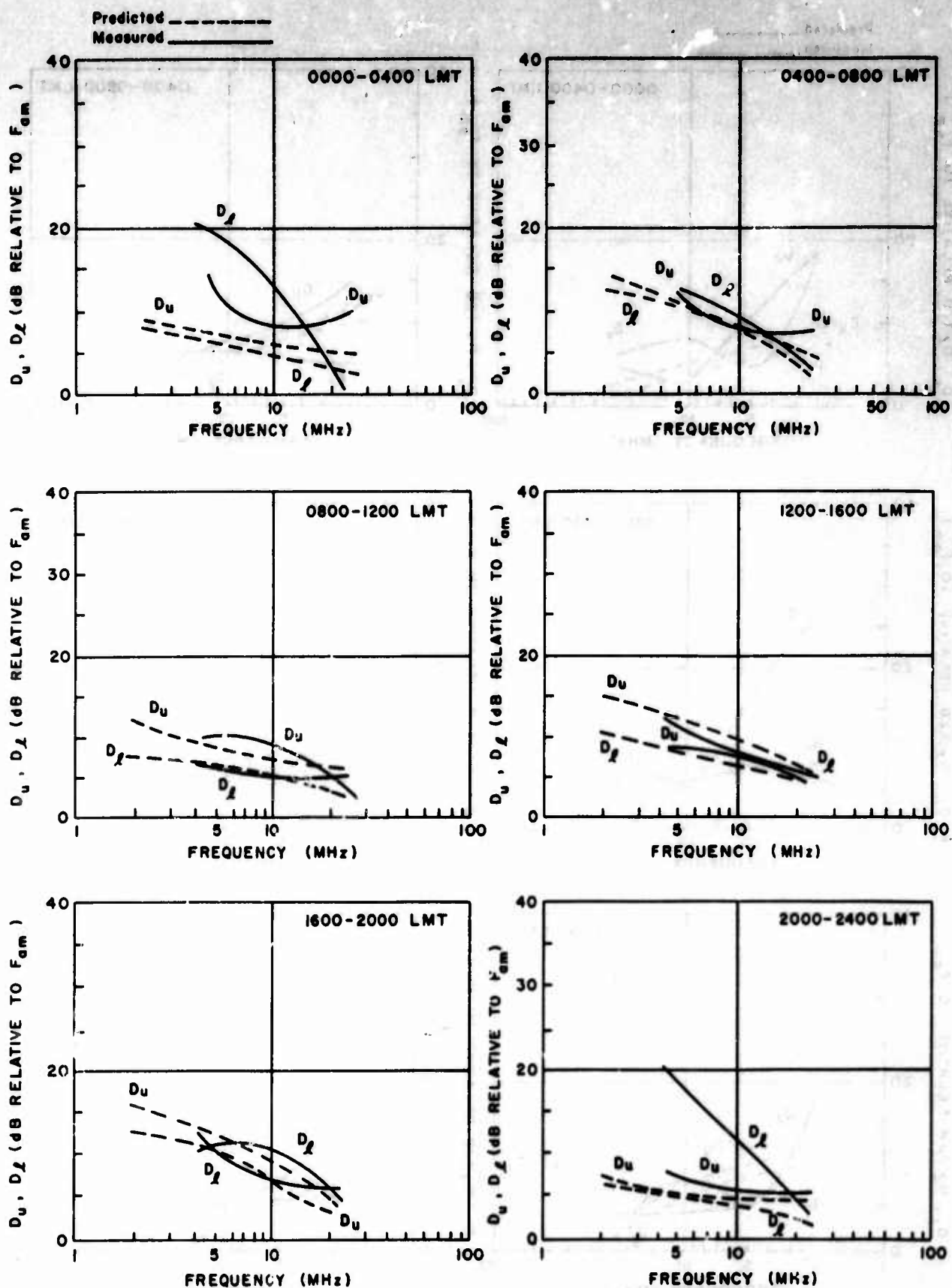


Figure 237. Season Noise Power Deciles, Omnidirectional Antenna
Starr Hill, Spring 1967

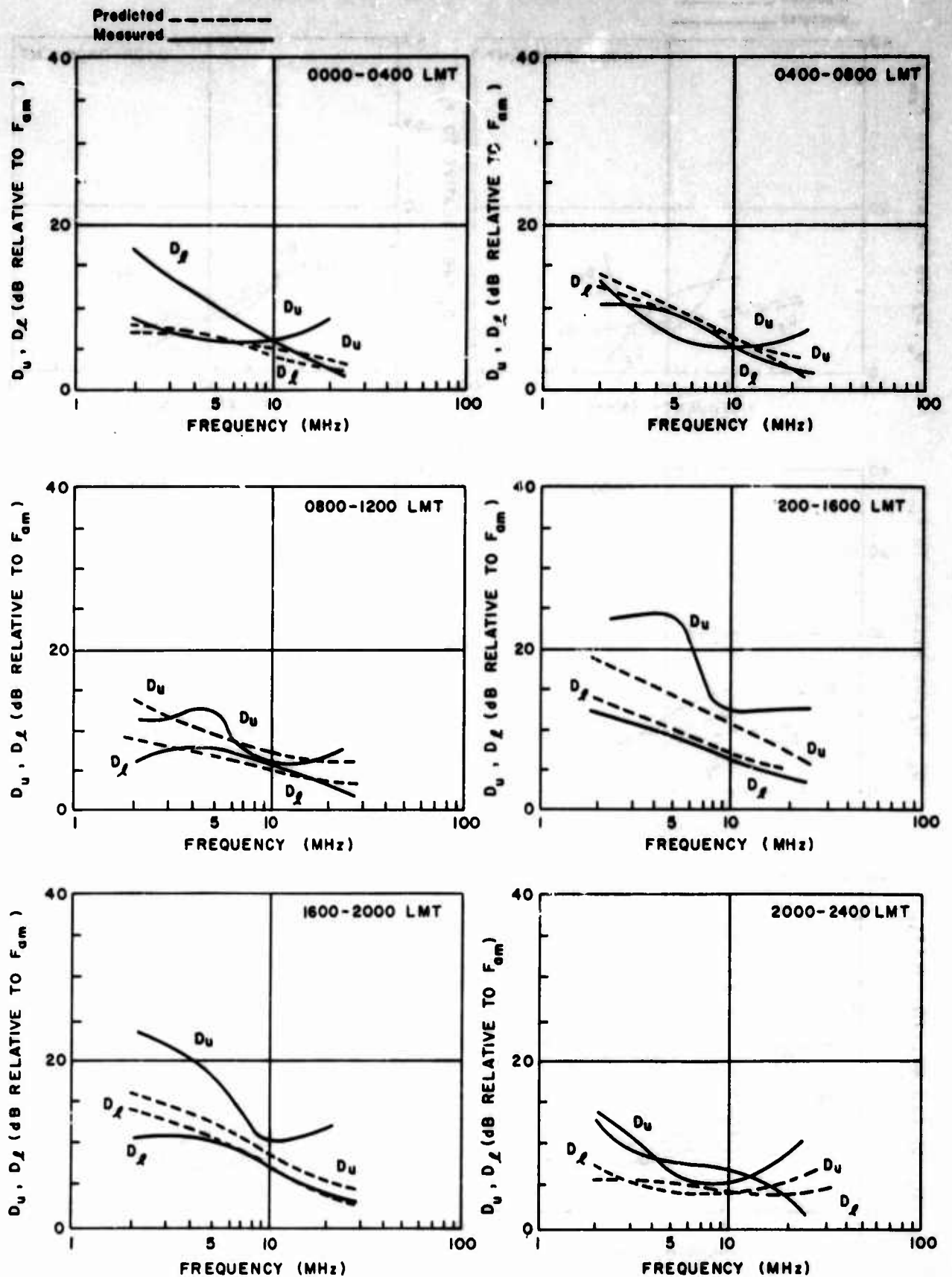


Figure 238. Season Noise Power Deciles, Omnidirectional Antenna
Starr Hill, Summer 1967

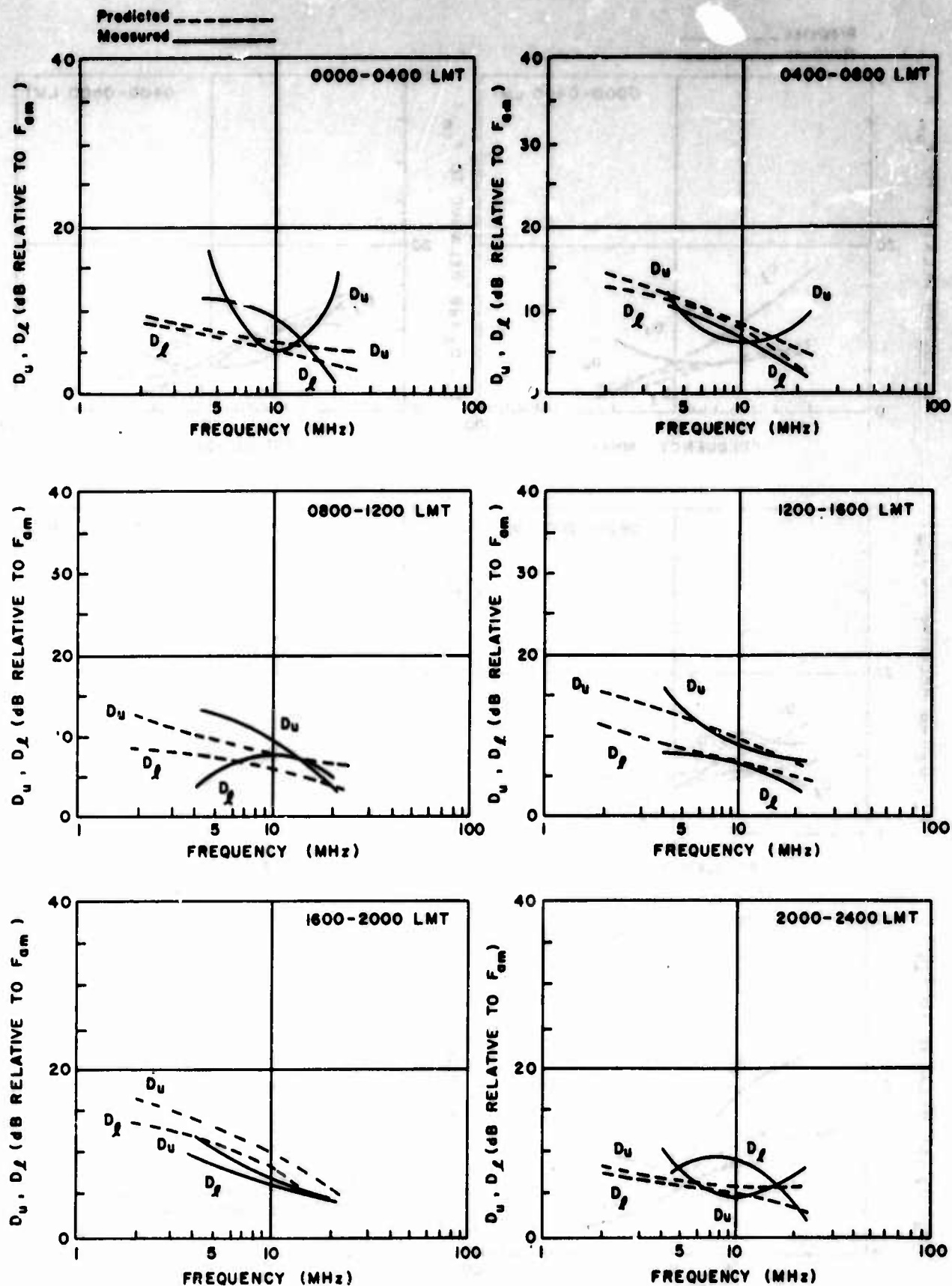


Figure 239. Monthly Noise Power Deciles, Omnidirectional Antenna
Starr Hill, March 1967

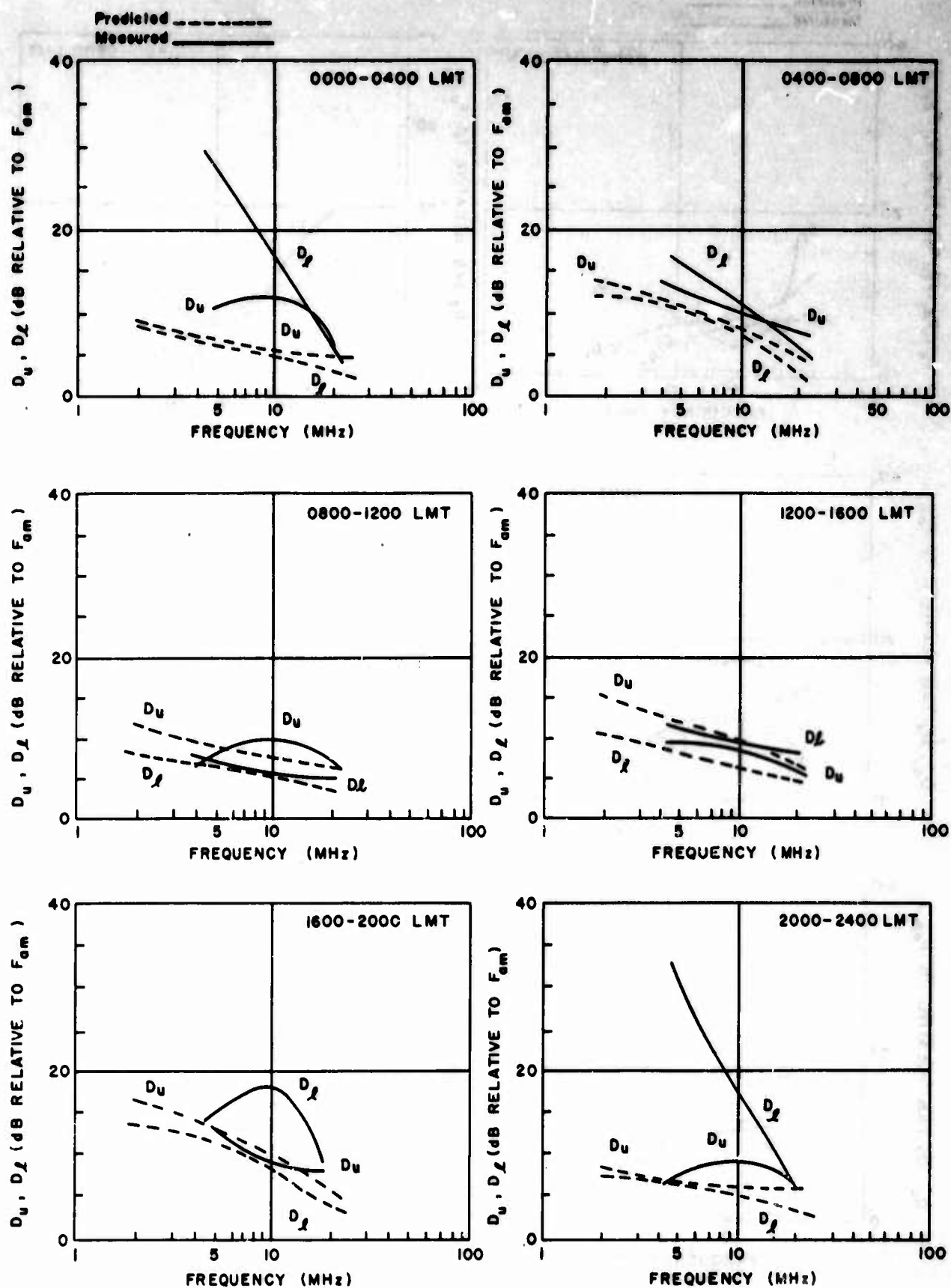


Figure 240. Monthly Noise Power Deciles, Omnidirectional Antenna
Starr Hill, May 1967

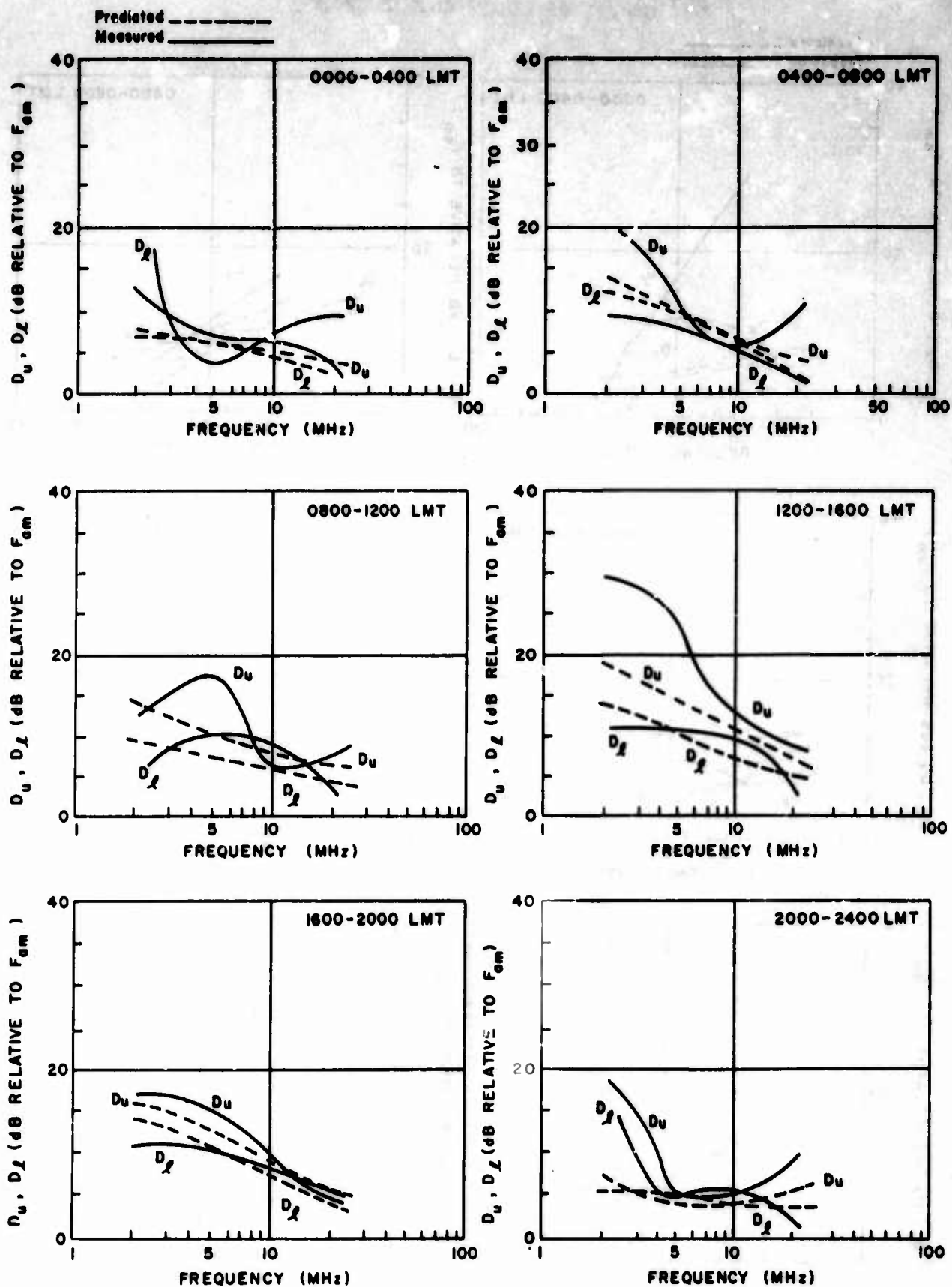


Figure 241. Monthly Noise Power Deciles, Omnidirectional Antenna
Starr Hill, June 1967

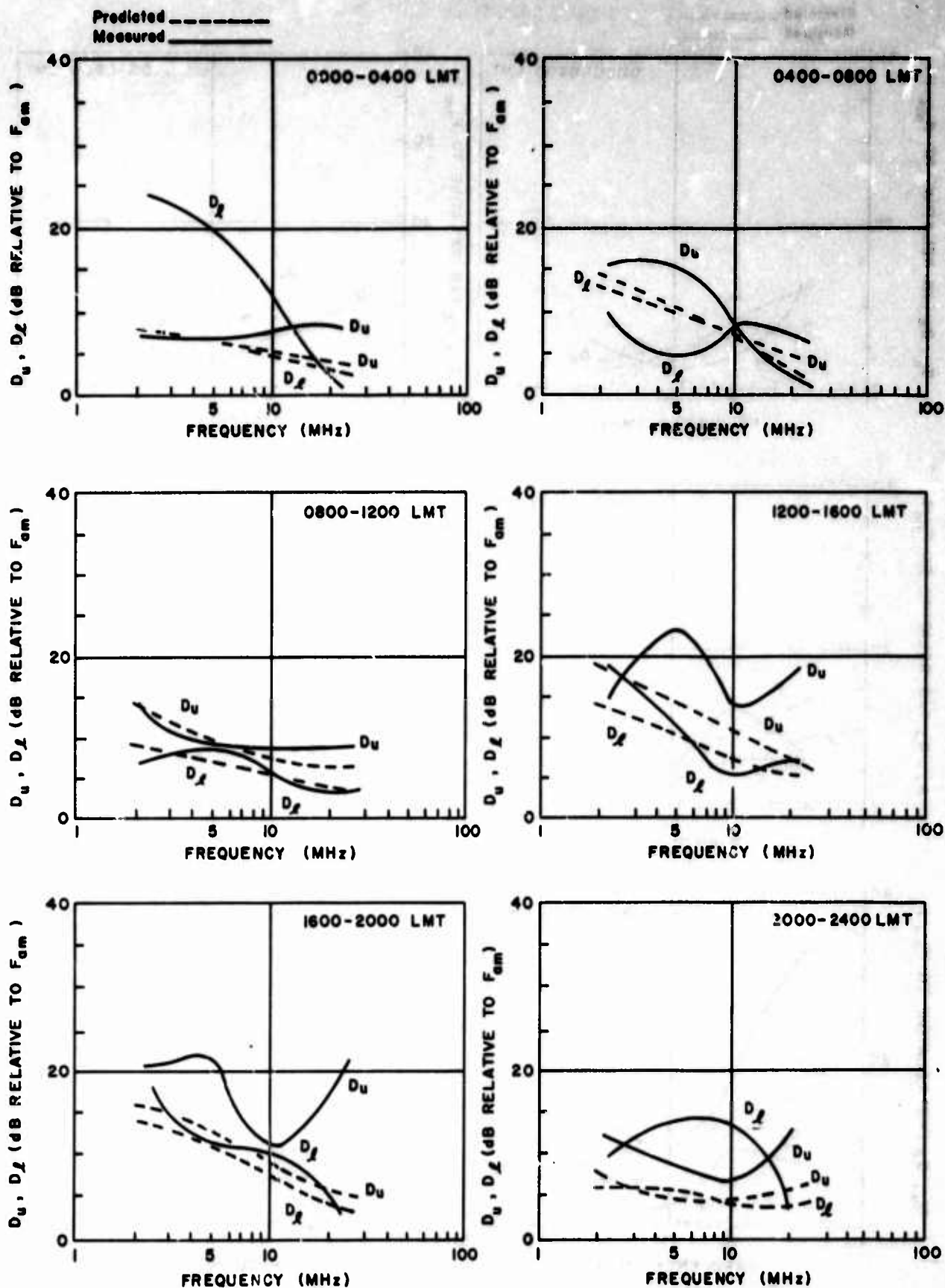


Figure 242. Monthly Noise Power Deciles, Omnidirectional Antenna
Starr Hill, July 1967

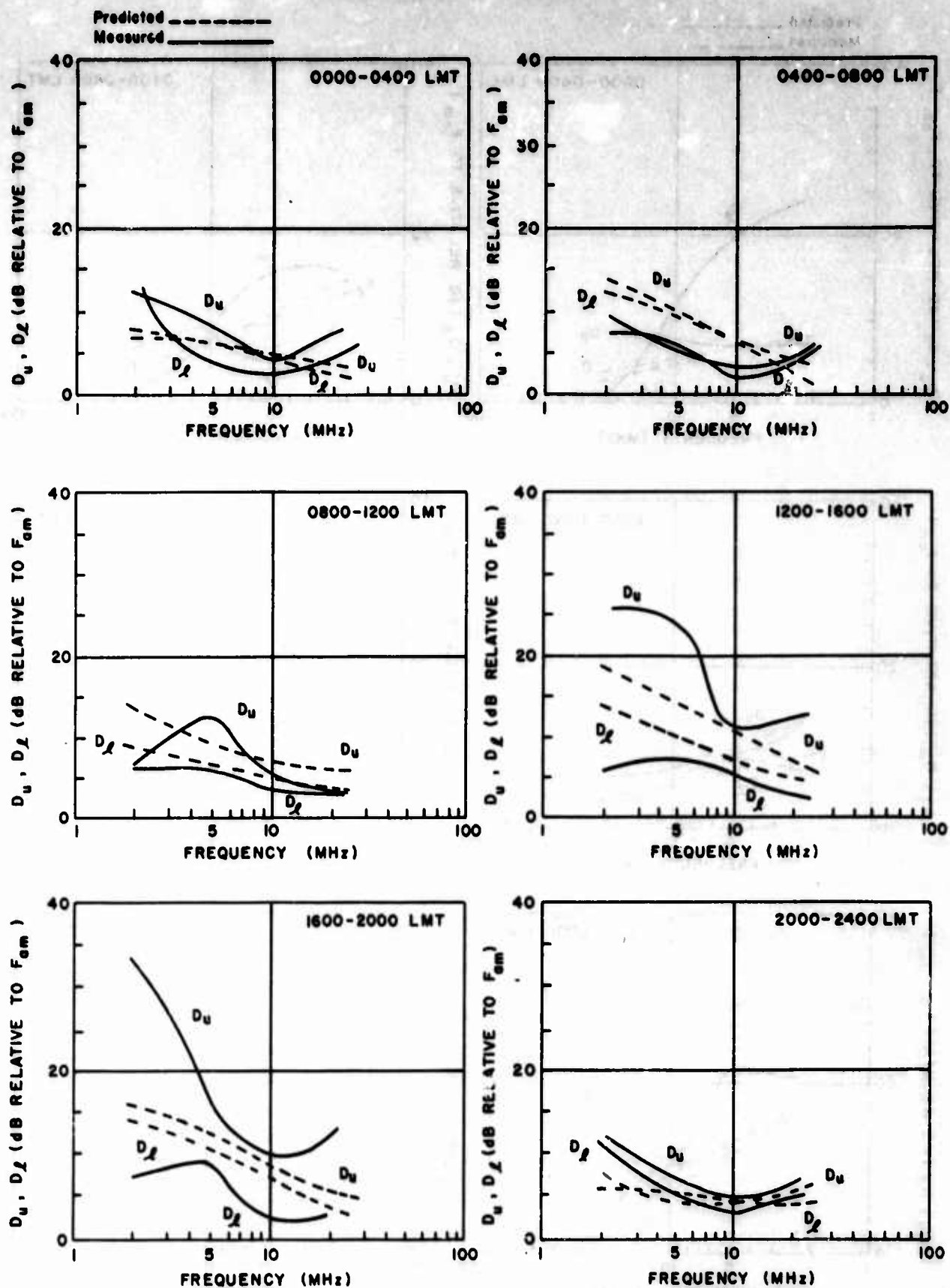


Figure 243. Monthly Noise Power Deciles, Omnidirectional Antenna
Starr Hill, August 1967

TABLE XXXII

LOG DEVIATION (L_d) IN DECIBELS BELOW F_a

FEBRUARY 1967

Omnidirectional Antenna

Frequency (MHz)	Local Mean Time					
	0000- 0400	0400- 0800	0800- 1200	1200- 1600	1600- 2000	2000- 2400
2.5	4.3	6.6	4.1	4.0	4.6	5.6
5	8.7	7.9	4.7	4.6	6.4	7.1
10	4.9	5.2	4.3	5.0	5.7	5.9
20	3.9	4.0	4.0	4.0	4.2	3.9

TABLE XXXIII

VOLTAGE DEVIATION (V_d) IN DECIBELS BELOW F_a

FEBRUARY 1967

Omnidirectional Antenna

Frequency (MHz)	Local Mean Time					
	0000- 0400	0400- 0800	0800- 1200	1200- 1600	1600- 2000	2000- 2400
2.5	2.3	9.2	2.2	2.0	2.5	3.4
5	5.7	4.9	2.2	2.0	3.9	4.7
10	2.7	3.0	2.2	2.3	3.1	3.2
20	2.0	2.2	2.0	2.2	2.5	3.0

TABLE XXXIV
LOG DEVIATION (L_d) IN DECIBELS BELOW F_a

MARCH 1967

Omnidirectional Antenna

Frequency (MHz)	Local Mean Time					
	0000- 0400	0400- 0800	0800- 1200	1200- 1600	1600- 2000	2000- 2400
2.5	6.5	4.8	3.1	3.6	4.6	4.9
5	9.0	9.6	5.6	4.1	7.4	8.4
10	6.2	6.0	6.6	4.8	5.5	5.9
20	3.0	3.2	4.8	4.6	4.2	3.7

TABLE XXXV
VOLTAGE DEVIATION (V_d) IN DECIBELS BELOW F_a

MARCH 1967

Omnidirectional Antenna

Frequency (MHz)	Local Mean Time					
	0000- 0400	0400- 0800	0800- 1200	1200- 1600	1600- 2000	2000- 2400
2.5	3.4	2.3	1.8	2.2	2.5	2.6
5	5.1	5.5	3.5	2.5	4.3	4.9
10	3.8	3.4	3.7	3.0	3.1	3.5
20	1.5	1.9	2.9	2.8	2.3	2.1

TABLE XXXVI
LOG DEVIATION (L_d) IN DECIBELS BELOW F_a

APRIL 1967

Omnidirectional Antenna

Frequency (MHz)	Local Mean Time					
	0000- 0400	0400- 0800	0800- 1200	1200- 1600	1600- 2000	2000- 2400
2.5	8.2	3.8	3.0	2.8	3.0	4.6
5	10.7	8.5	4.2	6.2	9.4	9.4
10	8.0	10.0	5.4	5.4	6.3	5.8
20	3.5	3.9	4.9	4.1	4.9	4.8

TABLE XXXVII
VOLTAGE DEVIATION (V_d) IN DECIBELS BELOW F_a

APRIL 1967

Omnidirectional Antenna

Frequency (MHz)	Local Mean Time					
	0000- 0400	0400- 0800	0800- 1200	1200- 1600	1600- 2000	2000- 2400
2.5	3.5	2.1	1.6	2.0	1.3	2.3
5	5.5	4.7	3.0	2.7	0.5	6.1
10	4.7	7.0	4.0	3.2	3.8	4.0
20	1.9	2.0	2.7	2.6	2.9	2.6

TABLE XXXVIII

LOG DEVIATION (L_d) IN DECIBELS BELOW F_a

MAY 1967

Omnidirectional Antenna

Frequency (MHz)	Local Mean Time					
	0000- 0400	0400- 0800	0800- 1200	1200- 1600	1600- 2000	2000- 2400
2.5	8.1	7.0	3.5	3.9	4.4	6.2
5	7.9	5.5	5.4	4.5	6.1	5.8
10	6.1	7.7	6.1	5.7	6.2	5.8
20	3.1	3.0	4.3	5.0	4.1	3.1

TABLE XXXIX

VOLTAGE DEVIATION (V_d) IN DECIBELS BELOW F_a

MAY 1967

Omnidirectional Antenna

Frequency (MHz)	Local Mean Time					
	0000- 0400	0400- 0800	0800- 1200	1200- 1600	1600- 2000	2000- 2400
2.5	4.5	2.6	2.6	2.6	2.9	2.4
5	4.0	4.0	2.4	2.4	3.5	3.8
10	4.1	6.1	4.6	4.6	4.7	3.9
20	1.8	2.4	3.2	2.5	2.5	2.2

TABLE XL
LOG DEVIATION (L_d) IN DECIBELS BELOW F_2

JUNE 1967

Omnidirectional Antenna

Frequency (MHz)	Local Mean Time					
	0000- 0400	0400- 0800	0800- 1200	1200- 1600	1600- 2000	2000- 2400
2.5	7.6	6.1	4.8	5.2	8.9	7.7
5	7.6	7.9	6.5	8.0	8.8	5.8
10	5.9	7.6	7.7	8.1	6.8	4.0
20	3.8	4.7	5.3	5.4	5.3	4.3

Directional Antenna

Frequency (MHz)	Local Mean Time					
	0000- 0400	0400- 0800	0800- 1200	1200- 1600	1600- 2000	2000- 2400
5	6.3	5.9	3.8	6.7	10.4	6.5
10	4.4	6.6	5.7	8.1	7.3	5.5
20	2.8	2.7	4.1	5.6	4.1	3.7

TABLE XLI

VOLTAGE DEVIATION (V_d) IN DECIBELS BELOW F_a

JUNE 1967

Omnidirectional Antenna

Frequency (MHz)	Local Mean Time					
	0000- 0400	0400- 0800	0800- 1200	1200- 1600	1600- 2000	2000- 2400
2.5	3.8	2.6	2.3	3.2	4.0	3.5
5	4.0	4.5	2.9	4.5	4.7	3.1
10	3.3	4.1	4.4	4.5	3.8	3.0
20	1.9	2.7	2.7	3.3	3.1	2.1

Directional Antenna

Frequency (MHz)	Local Mean Time					
	0000- 0400	0400- 0800	0800- 1200	1200- 1600	1600- 2000	2000- 2400
5	3.8	3.3	2.2	3.6	6.7	3.8
10	2.4	3.9	3.7	4.7	4.1	3.1
20	1.6	1.5	2.0	2.8	2.7	2.2

TABLE XLII
LOG DEVIATION (L_d) IN DECIBELS BELOW F_a

JULY 1967

Omnidirectional Antenna

Frequency (MHz)	Local Mean Time					
	0000- 0400	0400- 0800	0800- 1200	1200- 1600	1600- 2000	2000- 2400
2.5	7.2	8.7	6.5	10.2	7.7	7.7
5	15.7	15.7	14.5	15.7	19.0	17.7
10	5.0	6.0	7.7	8.7	7.5	5.2
20	3.7	4.2	5.0	6.5	6.0	4.0

TABLE XLIII
VOLTAGE DEVIATION (V_d) IN DECIBELS BELOW F_a

JULY 1967

Omnidirectional Antenna

Frequency (MHz)	Local Mean Time					
	0000- 0400	0400- 0800	0800- 1200	1200- 1600	1600- 2000	2000- 2400
2.5	4.0	5.0	2.2	3.5	4.0	5.5
5	3.5	5.0	5.0	9.0	6.0	3.0
10	2.0	3.0	4.2	5.2	4.0	2.7
20	1.0	1.7	2.2	4.2	3.2	2.0

TABLE XLIV

LOG DEVIATION (L_d) IN DECIBELS BELOW F_a

AUGUST 1967

Omnidirectional Antenna

Frequency (MHz)	Local Mean Time					
	0000- 0400	0400- 0800	0800- 1200	1200- 1600	1600- 2000	2000- 2400
2.5	10	9	5	4	9	9
5	8	9	6	7	9	6
10	7	8	9	10	7	6
20	3	4	5	5	5	4

Directional Antenna

Frequency (MHz)	Local Mean Time					
	0000- 0400	0400- 0800	0800- 1200	1200- 1600	1600- 2000	2000- 2400
5	9	9	5	8	10	8
10	6	9	10	12	9	6
20	4	4	6	6	6	4

TABLE XLV
VOLTAGE DEVIATION (V_d) IN DECIBELS BELOW F_a
AUGUST 1967

Omnidirectional Antenna

Frequency (MHz)	Local Mean Time					
	0000- 0400	0400- 0800	0800- 1200	1200- 1600	1600- 2000	2000- 2400
2.5	5	5	3	2	6	5
5	5	5	4	5	5	3
10	4	5	6	6	4	3
20	2	2	3	3	3	2

Directional Antenna

Frequency (MHz)	Local Mean Time					
	0000- 0400	0400- 0800	0800- 1200	1200- 1600	1600- 2000	2000- 2400
5	5	5	3	5	6	4
10	3	5	6	7	4	3
20	2	2	3	3	3	2

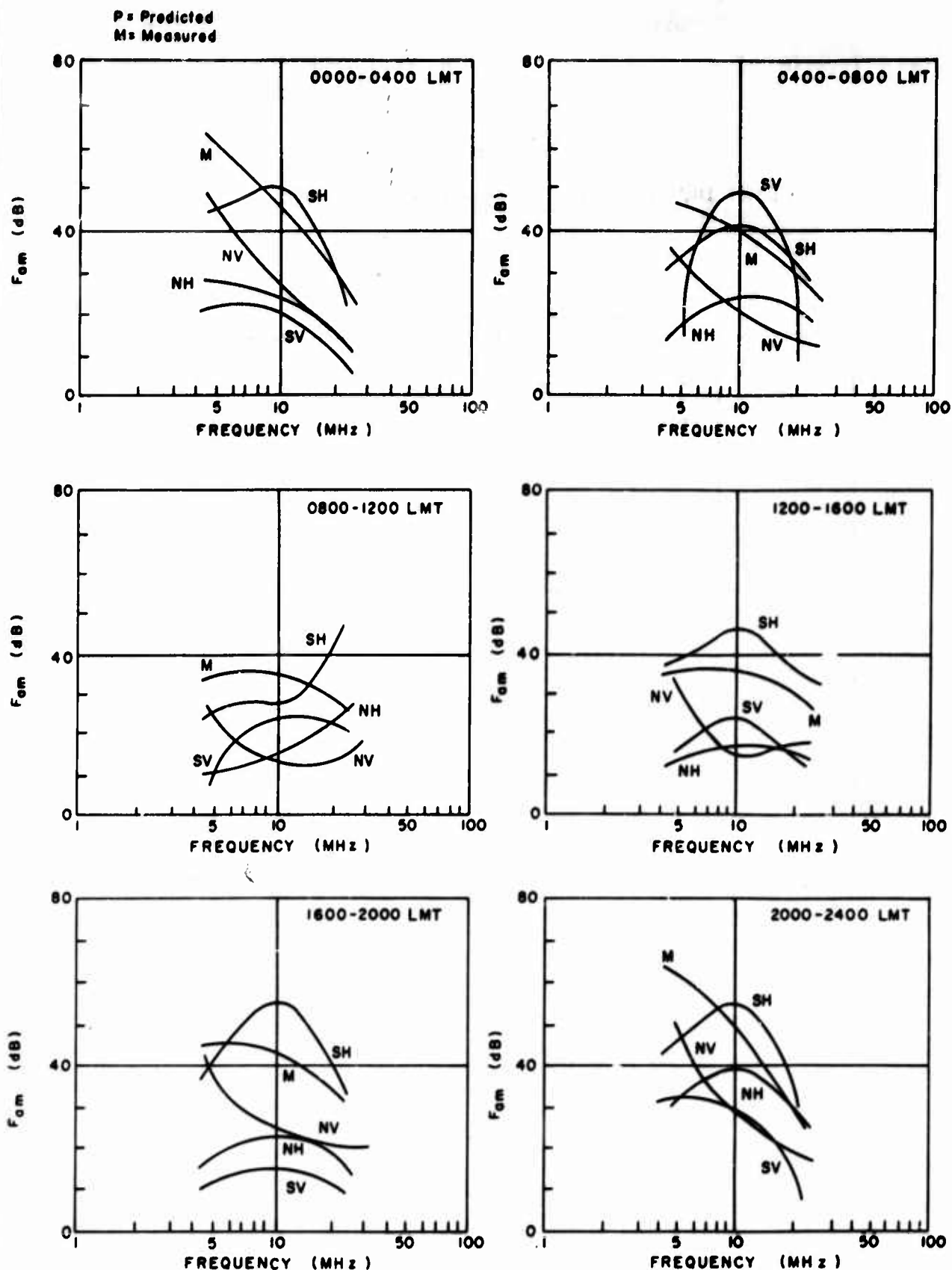


Figure 244. Monthly Median Noise Power, Directional Antenna
Starr Hill, June 1967

(4) Directional Antenna Comparison

Three complete months (June, August, and September 1967) of data were obtained using the No.2 ARN-2 receiver connected to a directional antenna. It is of interest to compare the received noise levels as collected using the different antennas including the whip antenna; also, considering the directional antennas as one group and the whip antenna separately, further conclusions may be drawn pertaining to the use of CCIR Report 322 for OHR system design.

Figures 244, 245, and 246 illustrate the monthly median noise power results for the six four-hour time blocks as a function of frequency. The identifications used on the curves are as follows:

- M = Measured with whip antenna
- NH = Measured with north horizontal antenna
- NV = Measured with north vertical antenna
- SH = Measured with south horizontal antenna
- SV = Measured with south vertical antenna

It should be pointed out that the nominal range for both horizontal arrays located at Starr Hill is from 8 to 64 MHz while the nominal range for the vertical arrays is from 4 to 64 MHz. It is presently postulated that this is the reason for the decrease in atmospheric noise recorded at 5 MHz using the horizontal arrays.

Since only one directional antenna could be connected to the No.2 ARN-2 at one time, the direct comparison of all five curves in Figures 244, 245, and 246 may be criticized as being invalid. Accordingly, the difference between the directional antenna and the whip antenna on an hour-by-hour basis is presented in Figure 247, where all three months of data were utilized as a data base. The variation of differences appeared virtually independent of time of day.

4. N/I MEASUREMENTS, GENERAL ELECTRIC RECEIVER

a. Measurement Technique

The dual channel N/I receiver measures HF noise and interference by discretely scanning (in 4-kHz steps) across a 1-MHz band. The scanning is performed automatically between integer frequencies where the starting frequency is selectable from 4 to 38 MHz. The receiver "listens" with a 120-dB dynamic range for a selectable 0.3- or 3.0-second integration time on each 4-kHz frequency increment.

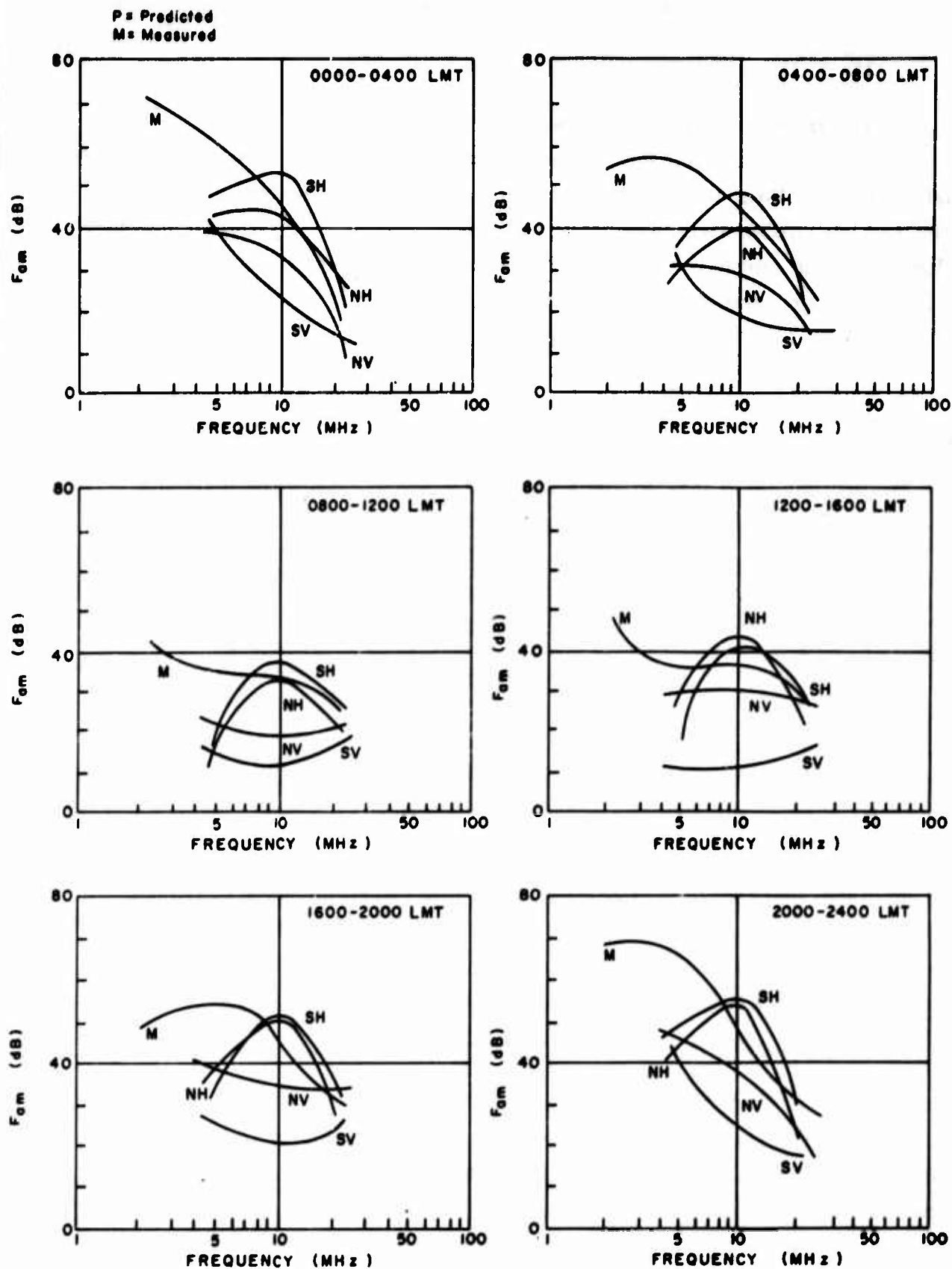


Figure 245. Monthly Median Noise Power, Directional Antenna
Starr Hill, August 1967

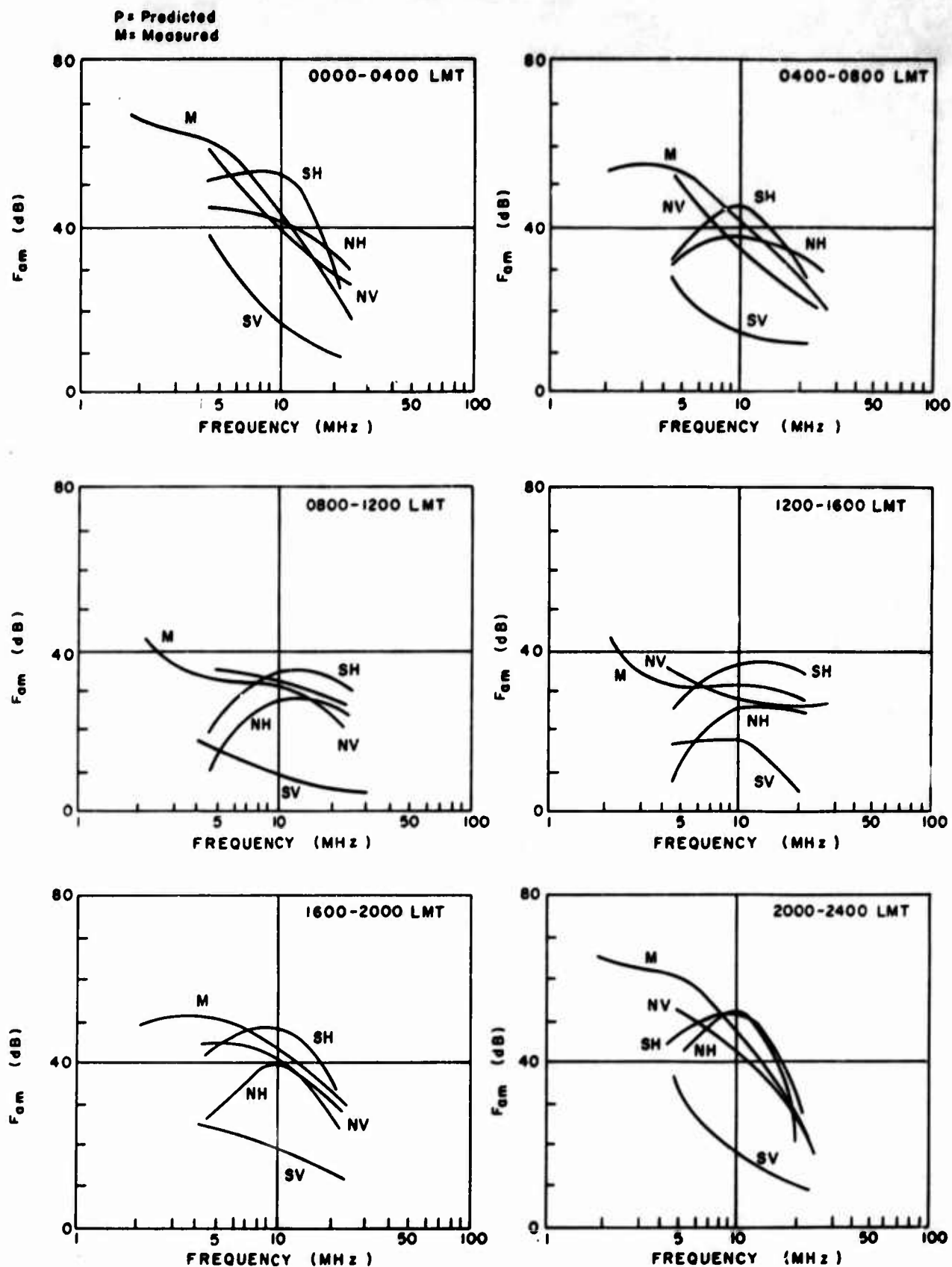


Figure 246. Monthly Median Noise Power, Directional Antenna
Starr Hill, September 1967

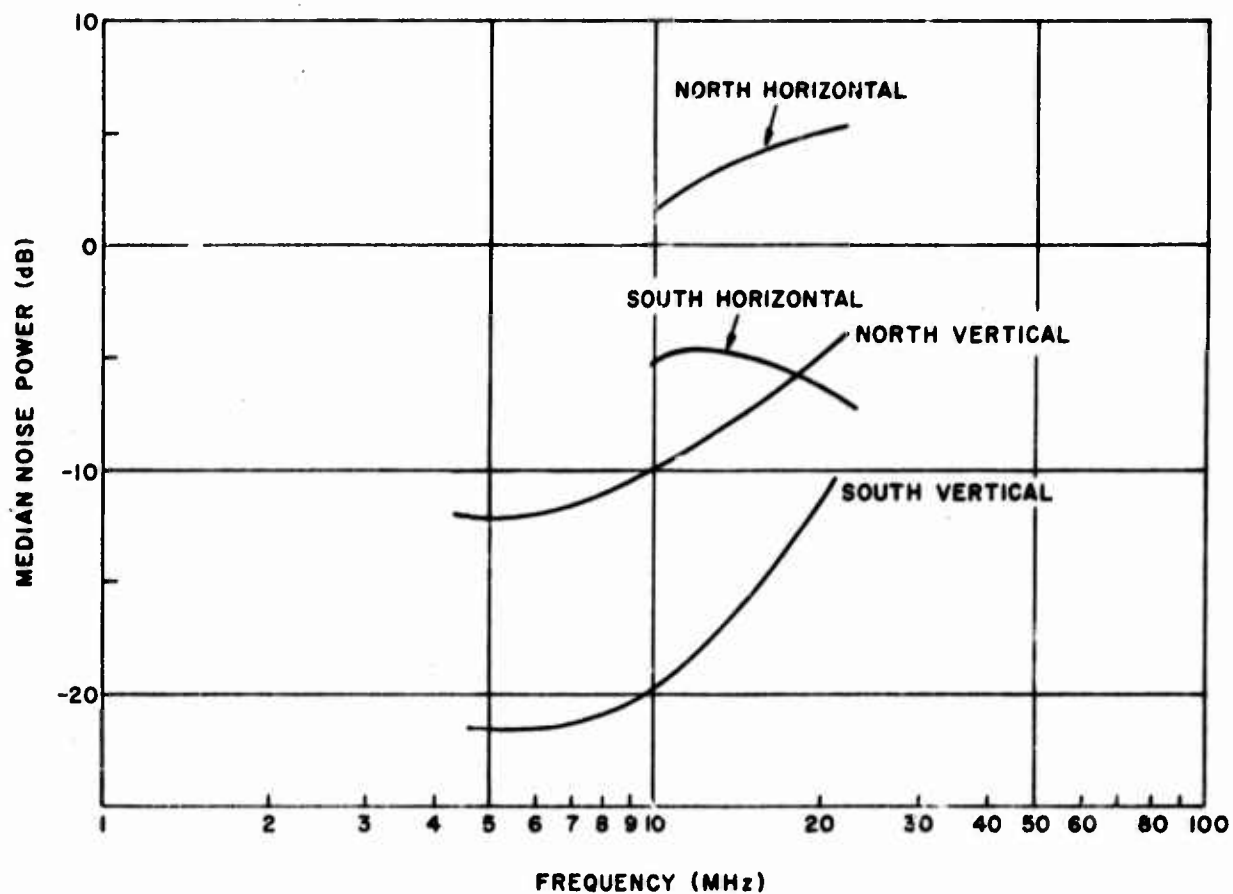


Figure 247. Median Noise Power, Directional Antenna
Relative to Omnidirectional Antenna
Starr Hill, 1967

Operationally, the N/I receiver has two complete receiver channels and is normally connected to two of the four directional antennas at a given time. The usual operating procedure is to initiate a 75-second (250 4-kHz channels x 0.3 second per channel) cycle using two antennas on a given frequency band (or groups of frequencies) and then to initiate a second 75-second cycle utilizing the remaining two antennas, again at the same frequency (or groups of frequencies). In this manner all combinations of azimuthal "look" direction and antenna polarization are employed at approximately the same time.

The parameter that is measured is the integrated power level in each 4-kHz channel. The 250 power level measurements obtained on one cycling of the receiver are quantized with 3-dB granularity, and a power distribution histogram is constructed using this information. What is actually recorded at the site is the density histogram. Because of the dual-channel nature of the receiver, two cumulative distributions are usually generated each time that the receiver is cycled. A multiplex mode of operation is also possible where three distributions are obtained on each cycle.

The measured gain versus frequency characteristic of the receiver is accounted for in processing the data, to an rms accuracy of ± 1.3 dB.

The integrated signal on each channel is converted to digital form, quantized in 3-dB steps. This digital number is used to select the address of a word in core storage, and the count stored in this word is incremented by 1. The result after all 250 channels have been sampled, is a probability density distribution, giving the number of 4-kHz channels carrying signals in each particular 3-dB range for an overall dynamic range of 120 dB. The distribution is transferred from core storage to magnetic tape, and the cores cleared to zero, before the next 1-MHz scan.

The receiver can be connected to any one of four antennas. Two of the antennas point north (azimuth 3°) and two point south (azimuth 188°). One antenna of each pair is horizontally polarized; the other is vertically polarized. The four antennas are designed NH, NV, SH, and SV to indicate azimuth and polarization. The azimuthal beamwidth of each of these antennas is approximately 60° . In elevation, the half-power points are at approximately 0° and 20° .

Measurements have been made of VSWR of the antennas (Ref. 5). For the horizontally polarized antennas the VSWR rises very rapidly below 7 MHz. The vertically polarized antennas remain below 2.5:1 down to 3.5 MHz.

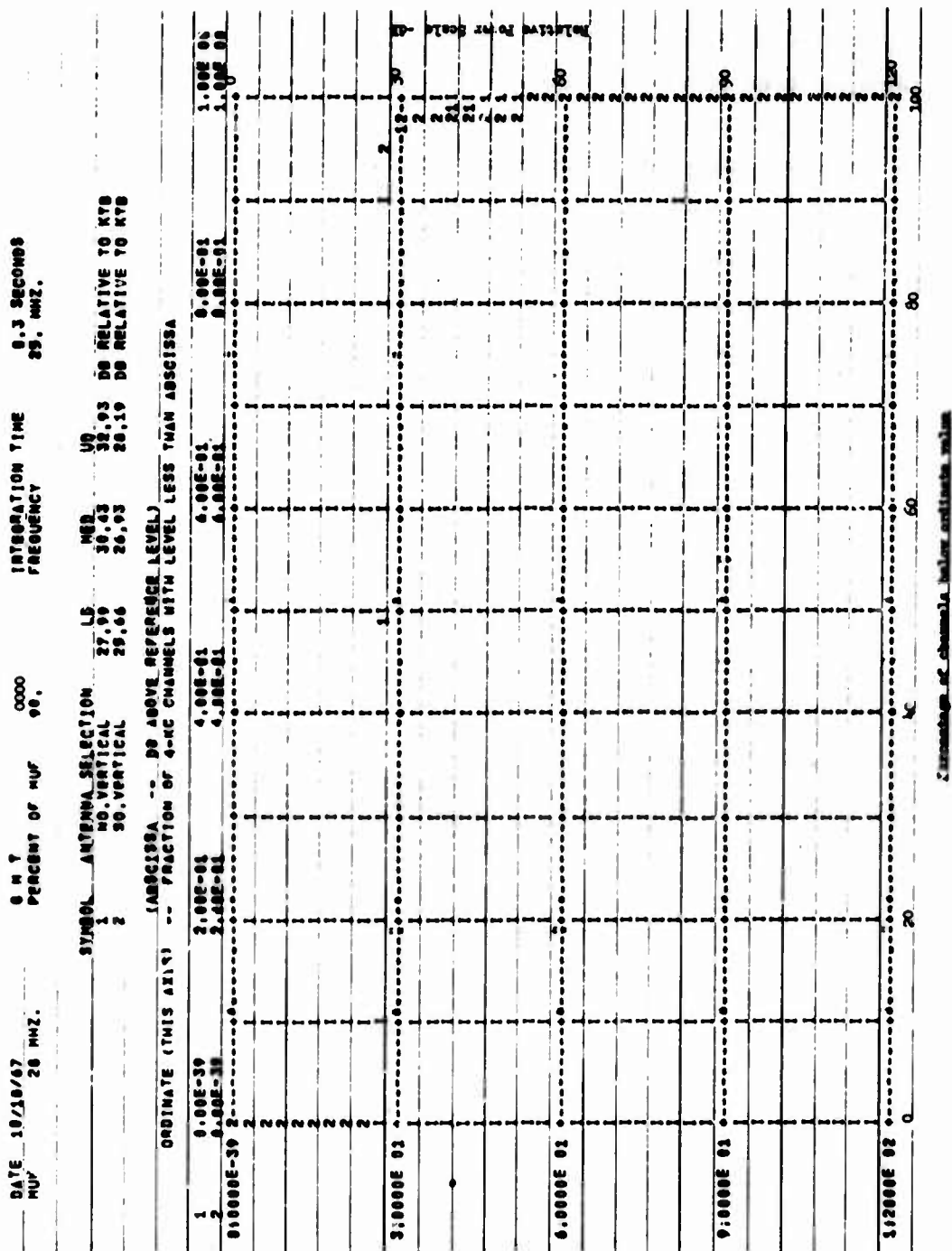


Figure 248. N/I Receiver Output Format, 90 Percent of MUF

In processing the data, the computer determines the median and decile signal levels; i.e., the levels which are exceeded in 10, 50, and 90 percent of the 250 channels. These levels are expressed as dB above kT_0 which is taken as 168 dB below one watt.

b. Data Output Format

The normal method of processing the N/I receiver output which is recorded on magnetic tape is to use a computer program to determine the cumulative distribution function and then to print the resulting distribution. Photoreductions of actual computer listings are illustrated in Figures 248 through 251.

Each page of computer listing represents one scan through a 1-MHz band with both channels of the receiver. At the top of each page is identification information regarding the key parameters plus the summary statistics. The parametric information includes the date, time, integration time, MUF, percentage of MUF utilized, the actual frequency used (approximately MUF x percentage), and the antennas employed on receiver channels 1 and 2. The summary statistics of the histogram that are tabulated are the lower deciles (LD), median (MED), and the upper decile (UD) in dB above kT_0 .

The graph (like Figure 248) shows the actual distribution of power levels in a 1-MHz band in a cumulative distribution form; i.e., one axis represents the N/I level in dB above kT_0 while the other axis identifies the fraction of the channels below the indicated power level. The curve constructed with the symbol "1" denotes the measurements from receiver channel 1, and correspondingly for the symbol "2." In cases where the "1" and "2" curves are coincident, the "2" symbol only is printed.

In the receiver scan represented by Figure 248 the curves would be interpreted as follows: no channels are below the 30 dB appropriate level shown, 20 percent of the channels are below about 40 dB, 60 percent are below 54 to 60 dB, etc. The summary statistics are based upon this distribution curve, except that system correction factors are reflected in the summary statistics.

The N/I distribution curves are useful for qualitative observations of the N/I environment. General indications of N/I "floor level," median value, general spread of N/I power, and the maximum interference level may all be derived from an inspection of these distributions. The computer listings also provide a rapid, visual indication of proper receiver and digital processor performance. In general, however, the total amount of information contained in the distribution curves exceeds the requirements for data needed to analyze the N/I environment.

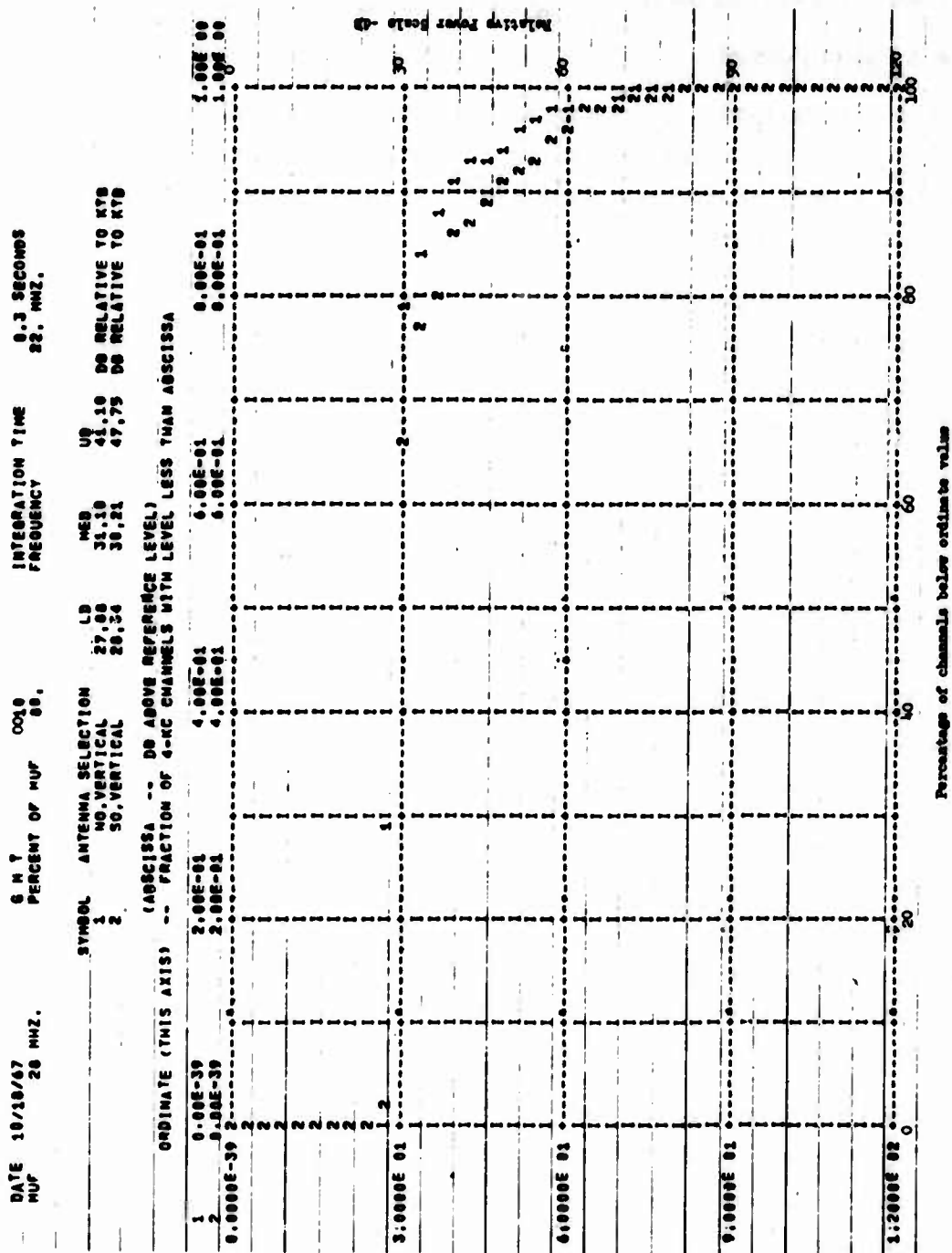


Figure 249. N/I Receiver Output Format, 80 Percent of MUF

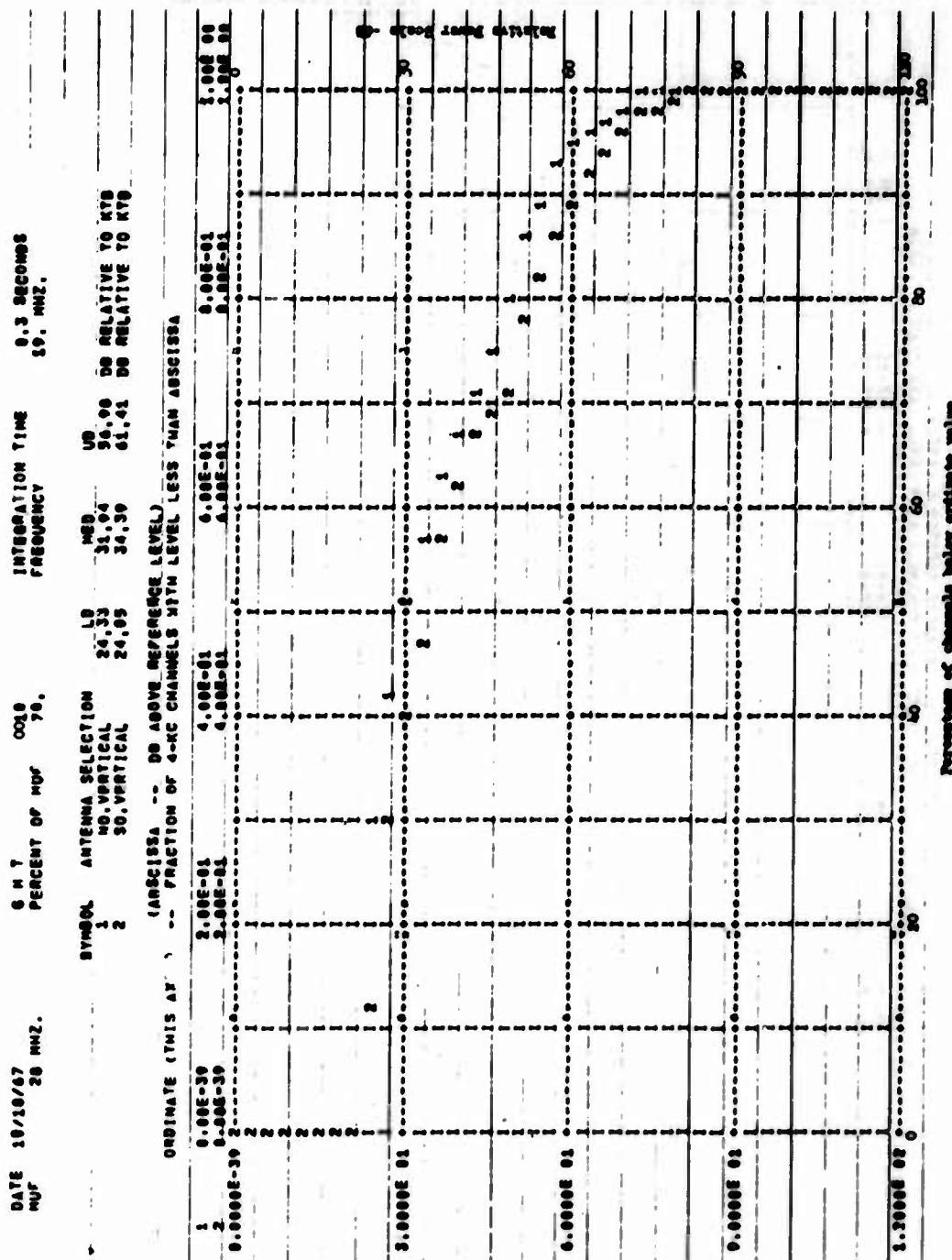


Figure 250. N/I Receiver Output Format, 70 Percent of MUF

Figure 251. N/I Receiver Output Format, 50 Percent of MUF

For the computation of statistical trends, the summary statistics and parameter information of each computer page are recorded on punched cards (one card per receiver channel per computer page) for further computer processing as illustrated in Figure 252. With the summary statistics on punched cards it is possible to group these statistics by frequency, azimuthal direction, time of day, etc. The grouped statistics are further averaged and reduced to yield the results presented in the following section.

c. Results

(1) The Data

The data analyzed for this report were gathered during the months of September and October 1967 at the RADC Starr Hill Test Annex and consist of a total of 2170 punched cards, each derived from one 1-MHz scan. Each card contains the median and decile levels, together with the frequency, time of day, and antenna. When divided into four groups according to the antenna used, the distribution of the data is:

Antenna	NH	NV	SH	SV
Number of points	492	538	519	621

There is very little data for the lower frequencies—below 15 MHz—during the daytime period of 1200 to 1900 GMT (0700 to 1400 EST, local time at the receiving site); likewise, there is an absence of higher-frequency data, above 19 MHz, during the nighttime hours 0800 to 1000 GMT (0300 to 0500 EST). Except for these two voids, the data are fairly well distributed in time and frequency.

The data were gathered during a shakedown period when this and other associated equipment were being installed, modified, and debugged at the receiving site. A variety of equipment difficulties, particularly in the digital circuitry, introduced errors in the data cards which were subsequently corrected by hand when the difficulties were traced. The overall calibration of system sensitivity was done as carefully as possible, but it is possible that the accuracy is not as great as the equipment will be capable of when installation and calibration are complete.

(2) Frequency Dependence

The most conspicuous variation in the interference level is that due to frequency. This variation is illustrated in Figure 253. The plotted level at each frequency is the average of all the measured medians at that frequency, including all four antennas and all times of day.

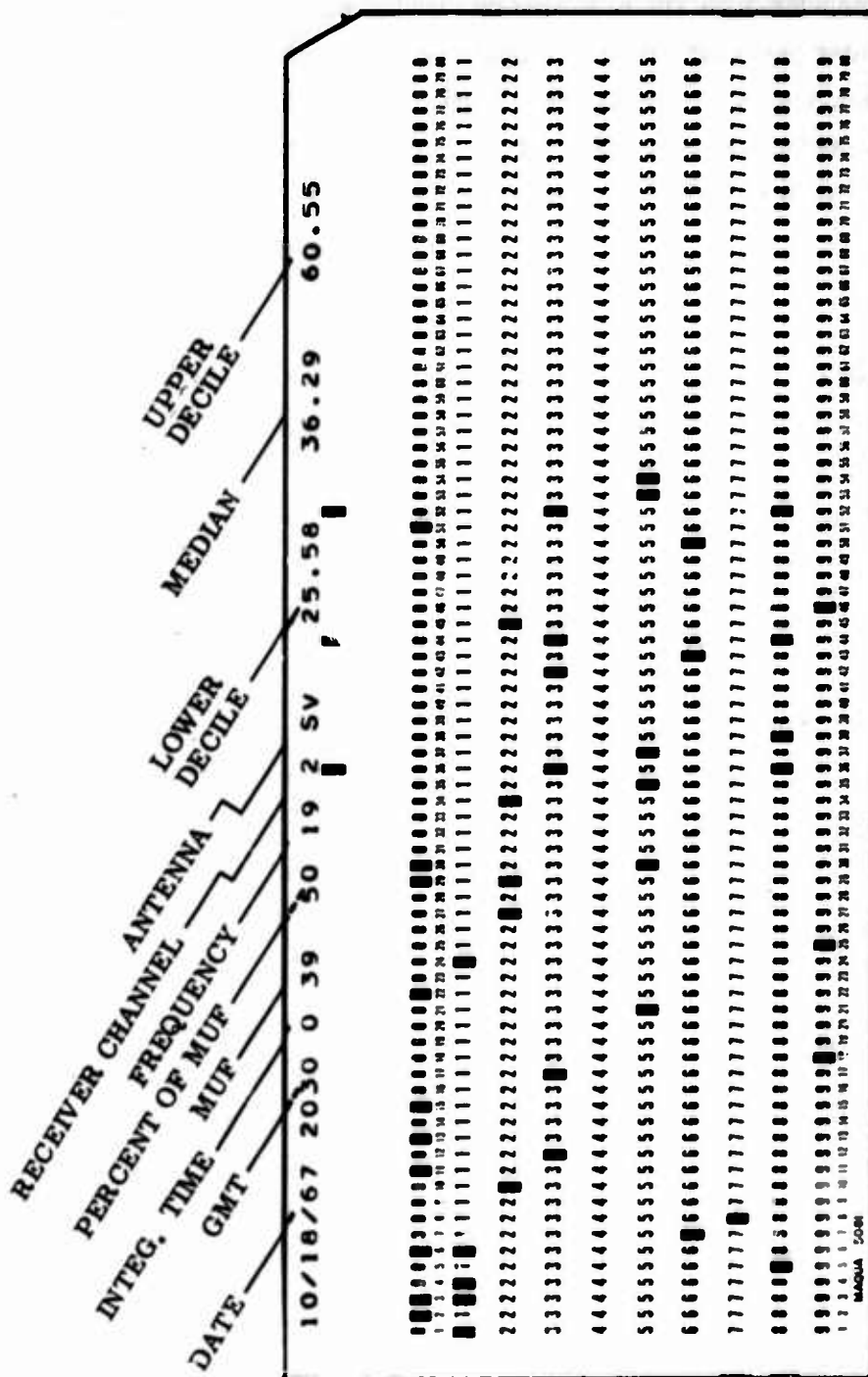


Figure 252. N/I Receiver Summary Statistics

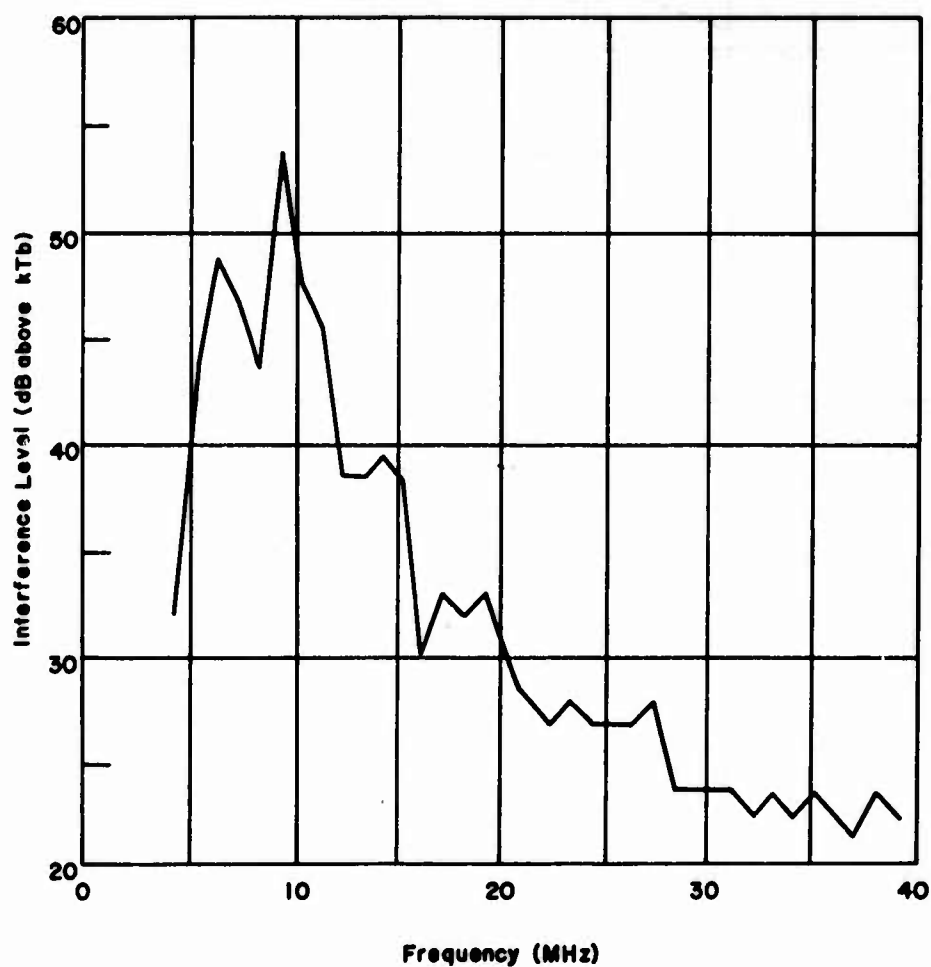


Figure 253. Interference Level vs. Frequency

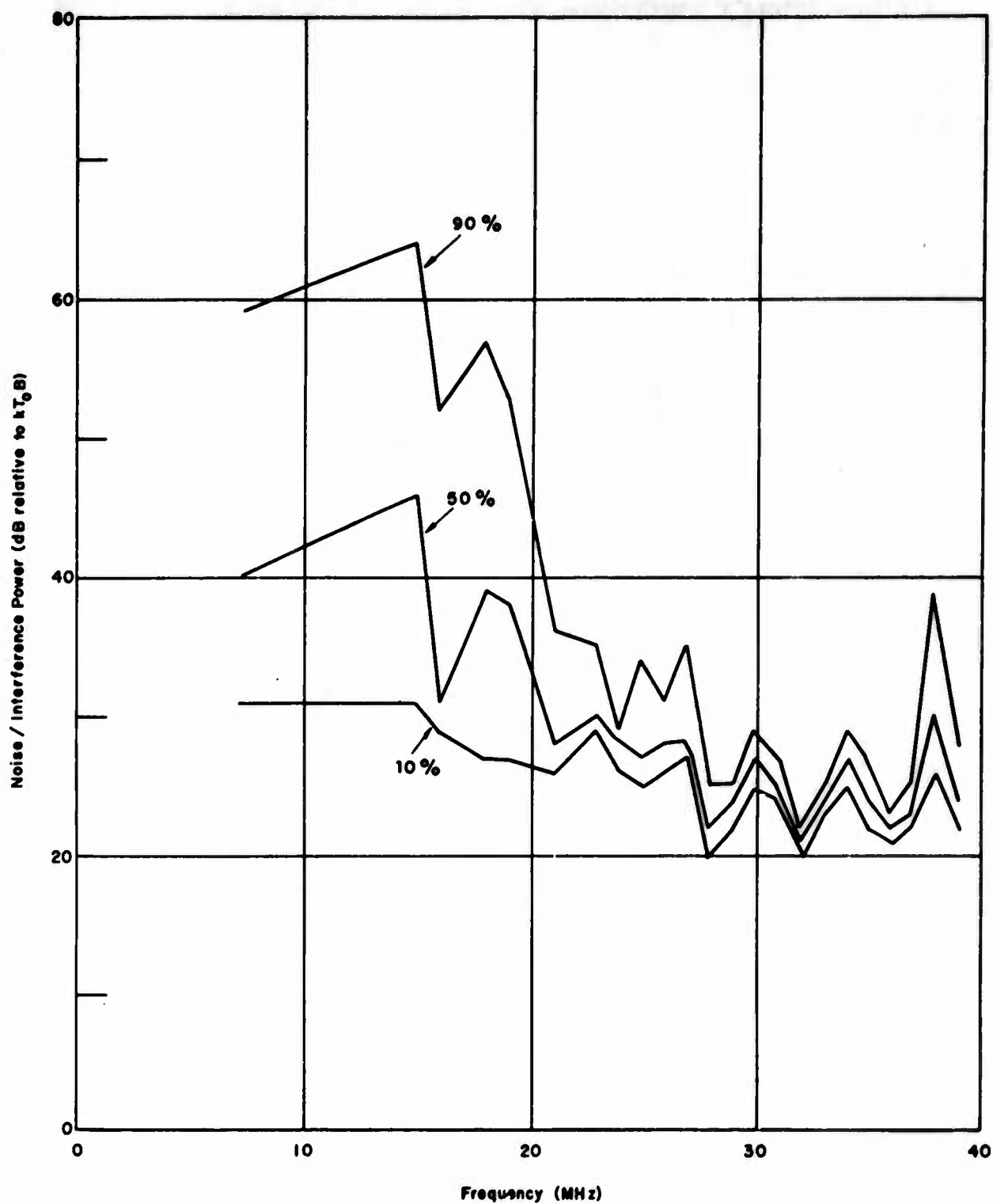


Figure 254. Noise/Interference Power for North Horizontal Antenna, Autumn 1967, Daytime

The low level in the 8- to 9-MHz band, and the high level in the adjacent 9- to 10-MHz band, cannot be traced to antenna or receiver characteristics. It appears that these are true features of the occupancy of these frequencies. The decrease at higher frequencies is expected because of inability of the ionosphere to reflect signals above some upper limit.

(3) Dependence on Azimuth and Polarization

For further analysis the data were divided according to the receiving antenna used, which gives two polarizations (horizontal and vertical) at each of two azimuthal directions (north and south). The data were then further divided into day and night, giving a total of eight categories of data. Each category contains between 100 and 200 points at various frequencies. The sorting, averaging, and plotting were done by machine, and the resulting curves are given in Figures 254 through 259. Each of these plots shows the lower decile, median, and upper decile levels versus frequency for one of the eight categories. The frequency scale is in terms of the lower edge of each 1-MHz band.

The "day" data are all the data taken in the eight-hour interval from 1330 to 2130 GMT. To the nearest hours, this is 1400 to 2100 GMT, inclusive. The "night" data are for 0200 to 0900 GMT, inclusive. Data taken in the two four-hour transitional periods are not used. These day and night periods were chosen on the basis of predicted ionosphere characteristics, namely the predicted MUF's for the paths approximately 4000 km long, extending in the boresight directions for the two antenna groupings. Figure 260 shows the predicted diurnal MUF curves for these two paths and the chosen day and night intervals.

The polarization dependence can be examined by comparing Figure 254 with 256 and Figure 255 with 257. Allowing for the shortage of low frequency data in Figure 254 there is no essential difference between the two polarizations in the north direction. To the south, however, levels received on the vertical antenna are generally higher than on the horizontal antenna, apparently due to an intermittent problem with the antenna switching network associated with the south horizontal antenna. For this reason, no separate figures for this antenna are included in this report. The three nighttime illustrations provided (Figures 255, 257, and 259) are seen to be very nearly alike. The three daytime illustrations (Figures 254, 256, and 258) are also similar, except below 15 MHz where data are scarce and the curves poorly defined.

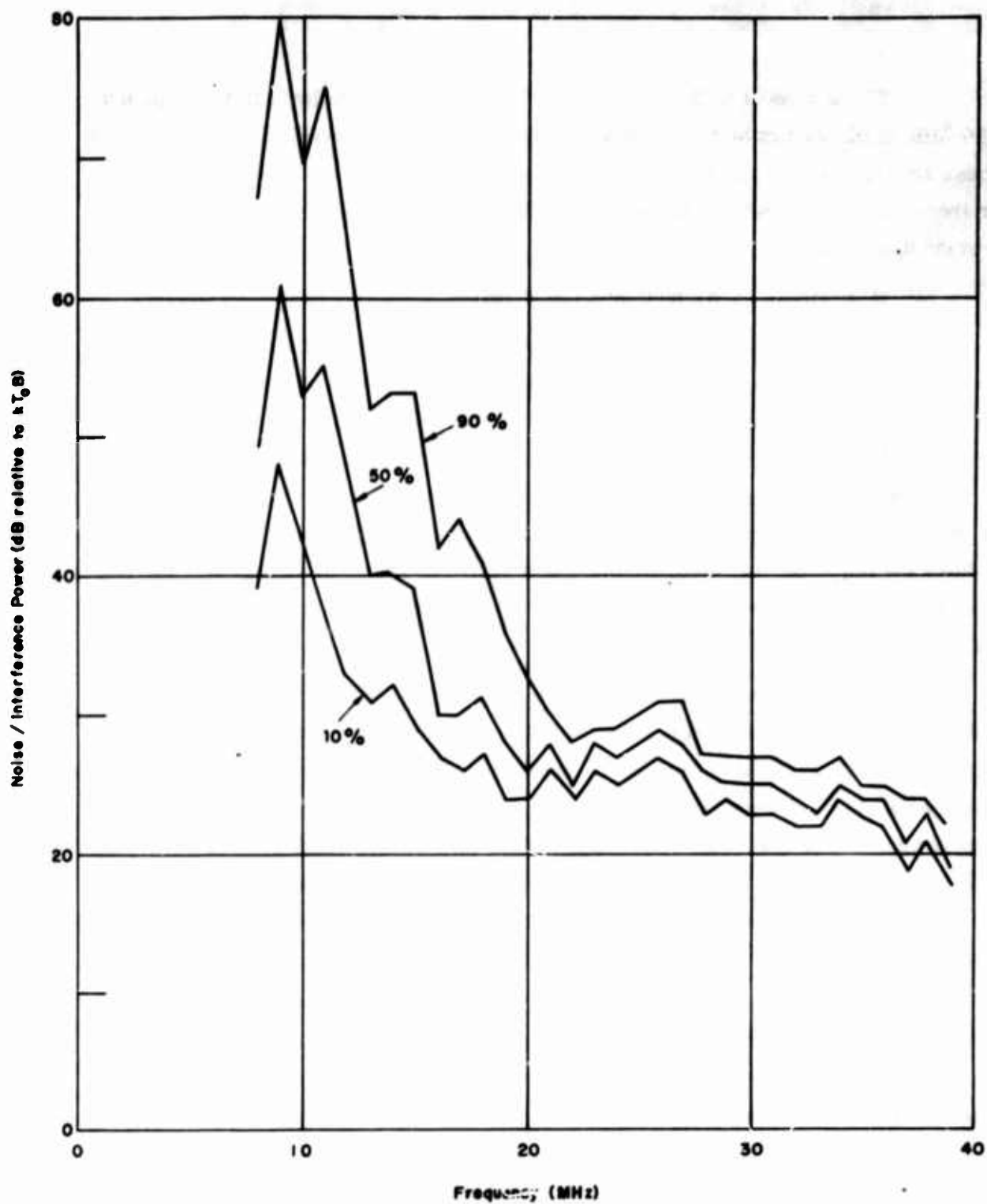


Figure 255. Noise/Interference Power for North Horizontal Antenna, Autumn 1967, Nighttime

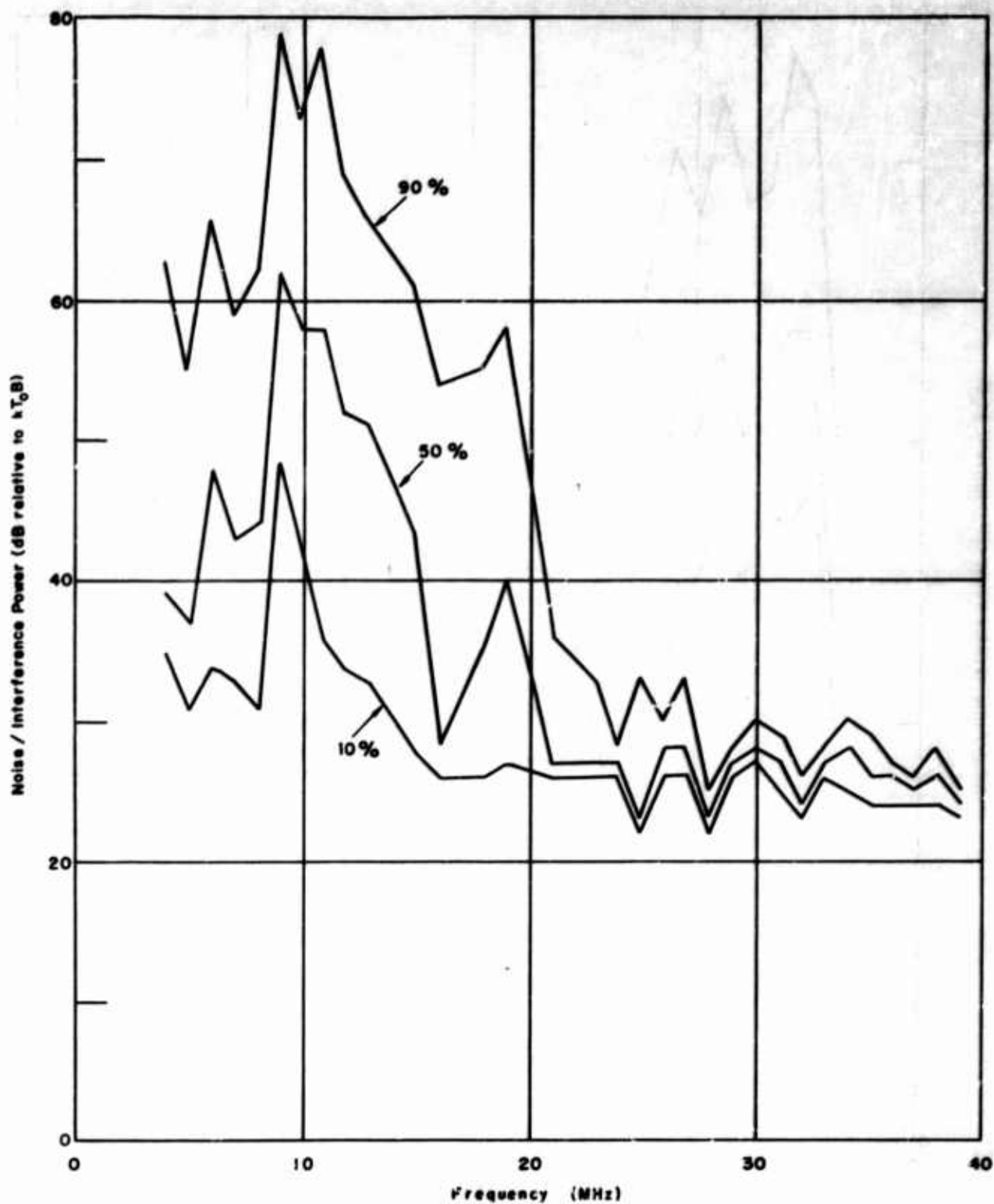


Figure 256. Noise/Interference Power for North Vertical Antenna, Autumn 1967, Daytime

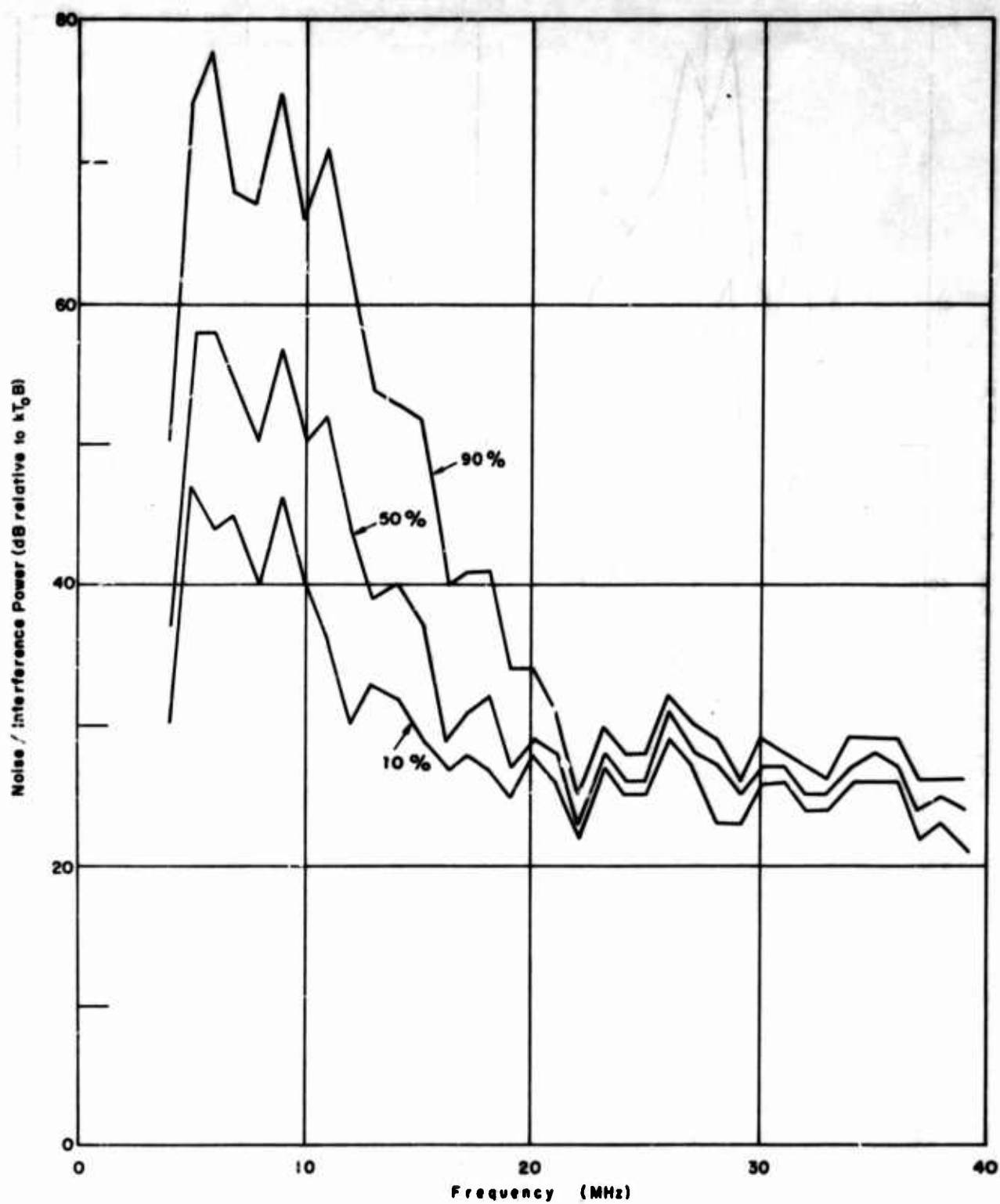


Figure 257. Noise/Interference Power for North Vertical Antenna, Autumn 1967, Nighttime

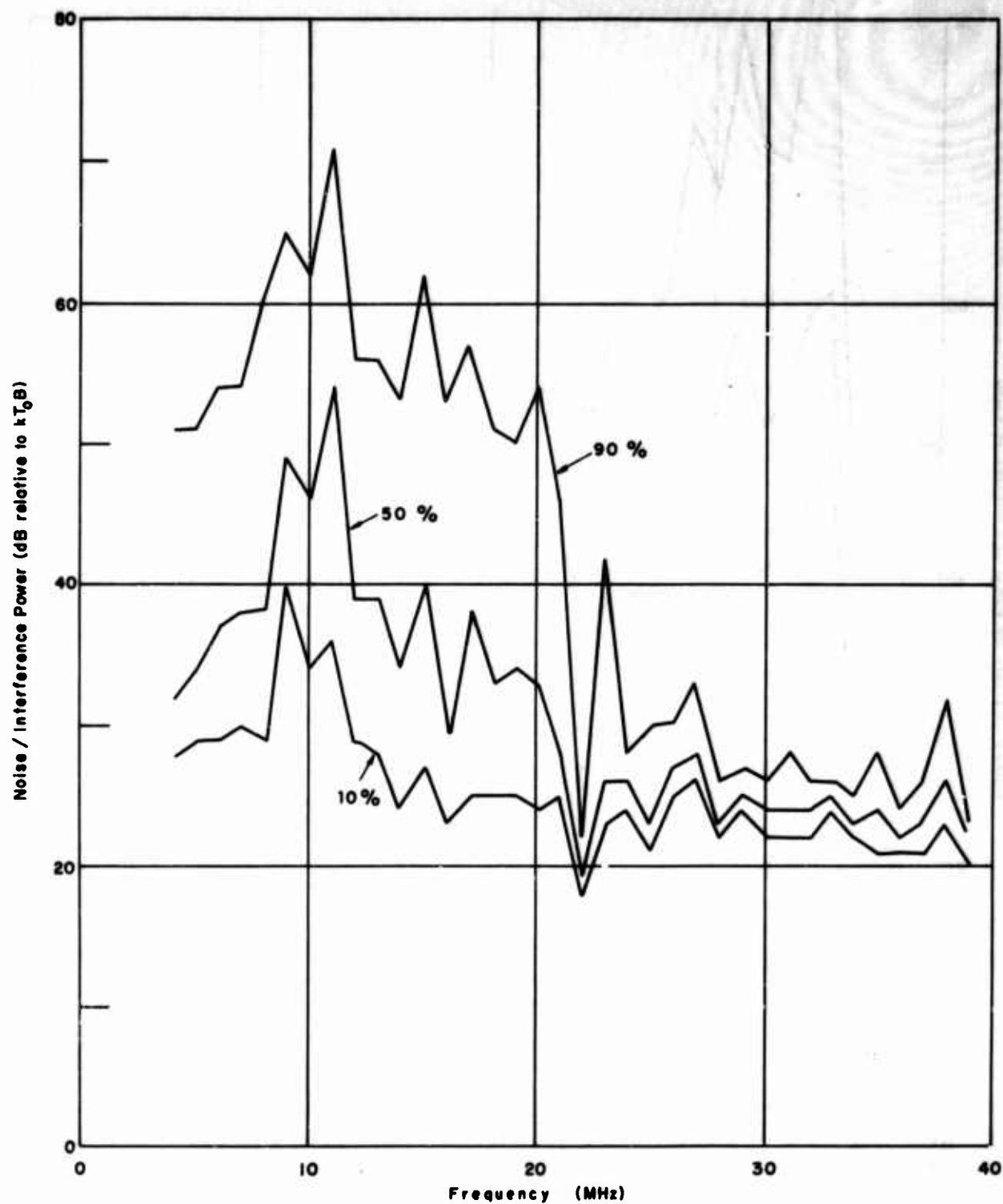


Figure 258. Noise/Interference Power for South Vertical Antenna, Autumn 1967, Daytime

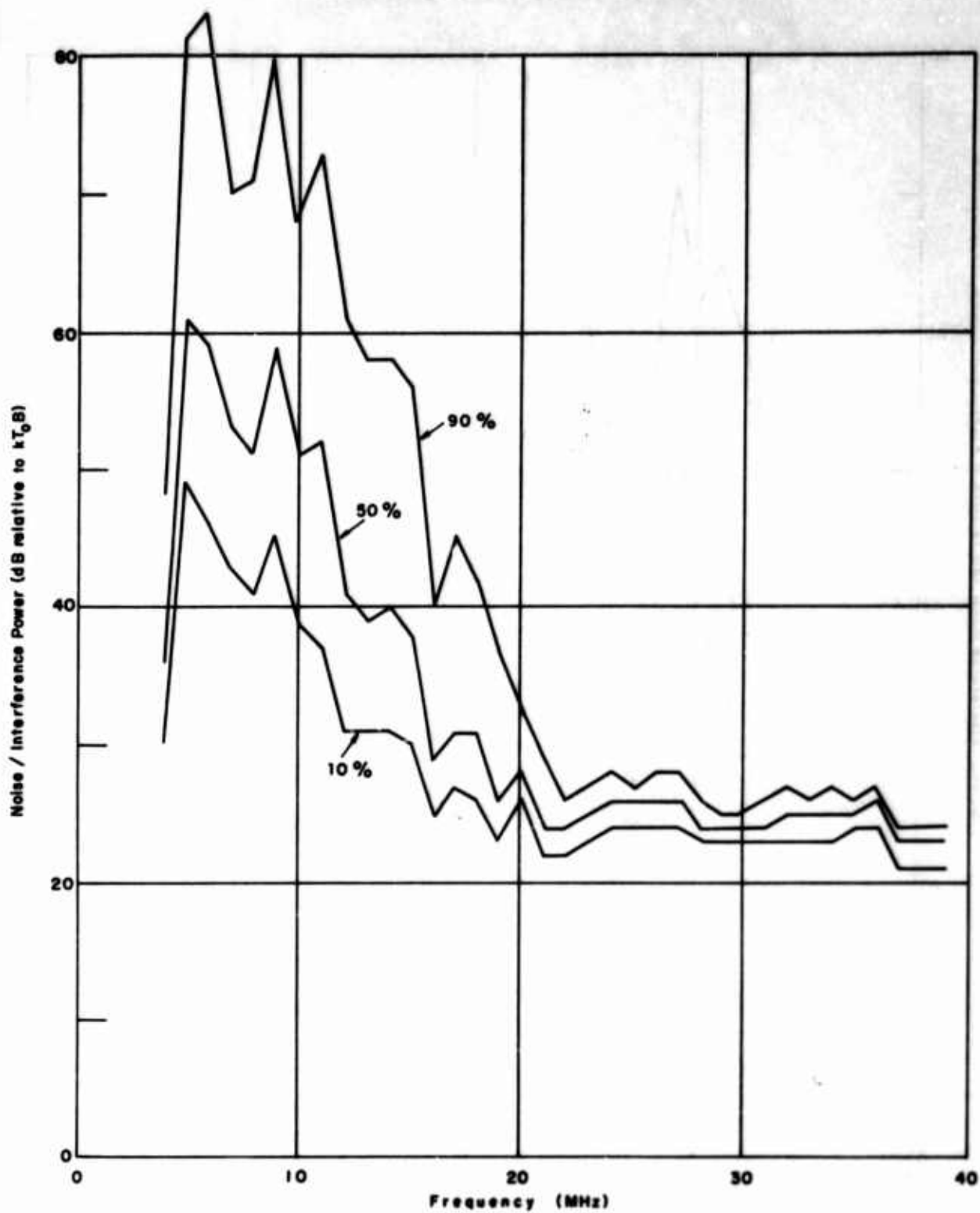


Figure 259. Noise/Interference Power for South Vertical Antenna, Autumn 1967, Nighttime

The table below gives overall average levels for the three azimuth/polarization combinations that are considered in this report.

Antenna	Overall Average (dB)	
	Day	Night
NH	28.8	37.3
NV	31.8	38.0
SV	29.7	37.1

(4) Diurnal Variations

The principal difference between the day and night plots is that the peak interference levels which are found around 10 MHz are slightly smaller during the day, but then persist to higher frequencies.

To show typical diurnal variations in more detail, hourly averages for three selected frequency ranges are plotted in Figure 261. These data are from the south vertical antenna, and each curve is the average of all the measured median levels in three adjacent 1-MHz bands. Such grouping of several bands was necessary to have enough points to define the curve.

At the lower frequencies the interference level reaches a minimum during daytime hours. This corresponds to the daytime increase in D-region absorption. At high frequencies the E and F regions of the ionosphere will support long range propagation more often during the day, as seen on the MUF curves of Figure 260; thus, the interference level would be expected to rise slightly during the day.

(5) Clear Channel Probability

A question of practical importance related to the level of interference which is present is the chance of finding a clear channel at or near a desired operating frequency. In order to obtain this sort of information, let the clear channel probability be defined as the number of clear 4-kHz channels in a 1-MHz band, divided by the total number of channels in the band, 250.

Next it is necessary to define a clear channel. Subjectively, by a clear channel is meant one which contains no interference. Such a channel would still contain noise, at a level determined by either external noise of natural origin or internal receiver noise. A clear channel could be defined objectively as one in which the total

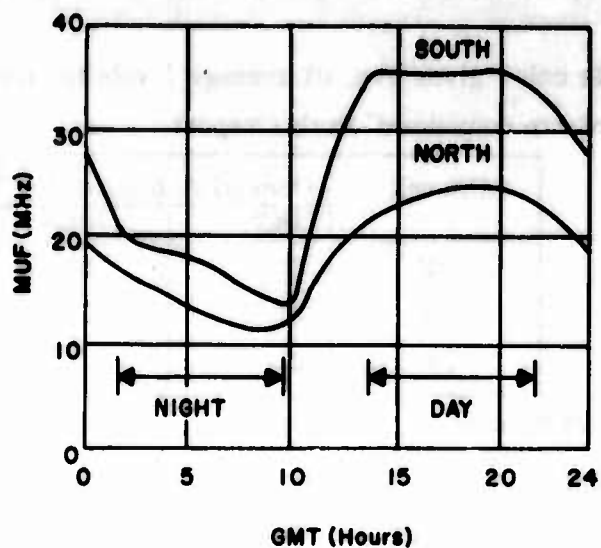


Figure 260. Predicted MUF, September and October 1967

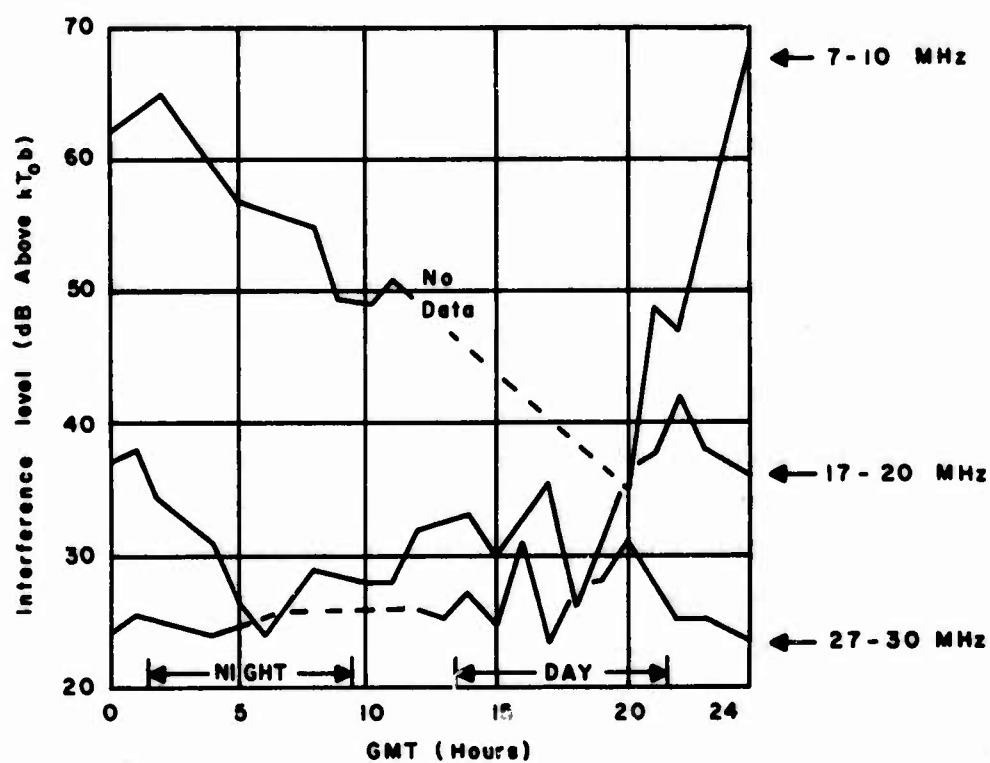


Figure 261. Diurnal Variations of Interference Level, SV Antenna

level is equal to the natural or receiver noise level. A small margin would have to be provided to allow for statistical variations in the noise level. The N/I data do not distinguish between noise and interference, so the noise level must be estimated by some means.

Figure 262 is a cumulative distribution plot in which the abscissa is interference level, X , and the ordinate is the percent of channels containing signal below the level X . Assume a total absence of interfering signals over some 1-MHz band. If the receiver is nearly flat over the band, each of the 250 channels would contain about the same noise level and the cumulative distribution curve would look like curve A, nearly vertical. Next, assume that there is no noise, but that all 250 channels contain interference at varying levels. The distribution would be a curve like B, of unknown shape, but extending down to levels below the noise level of A. With both noise and interference present, curve C is obtained. If the clear channel level is defined as any level below X_A , there are no clear channels. If the clear channel level is defined slightly above X_A , the number or percent of clear channels is very sensitive to the exact defining level chosen.

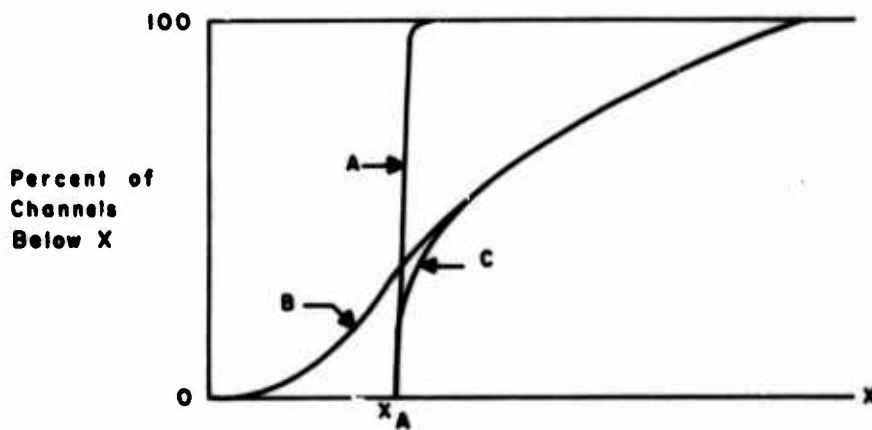


Figure 262. Cumulative Distribution Curves of Noise and Interference

SECTION VIII

CONCLUSIONS

1. MODE RELIABILITY EXPERIMENT

Availability of the four principle modes--2E, 1F2, N, and 2F2--has been such that during the period of approximately 15 months covered in this report, one or more of these modes was always available over the Coco Solo to central New York path. For the Thule to New York path some uncertainties exist, but even on this path availability of at least one mode existed for almost 100 percent of the time.

The 1F2 mode appears to be the most useful of all in that its junction frequency is the highest. The 2F2 mode appears to be the most dependable of all modes considered, but has a lower junction frequency than the 1F2 mode. The 2E mode fills in well during the daytime. The N mode has, if any merit, the capability of filling in when the E_s layer blanks the other usable modes at one or both ends of the path. The 2E_s mode, while capable of supporting suitable propagation when present, is more often a nuisance than a help.

Examination of frequency aperture availability for all modes shows that the apertures are usually quite narrow. This is partially due to the method of determining the LOF in the data reduction process used for the oblique ionograms. The LOF is taken at the first major break in the mode trace below the MOF-JF unless there is a long strong occurrence below this break. Since almost all of the oblique ionograms observed show only patchy sections below the recorded LOF, the apertures are usually narrow. The 90 percent available frequency apertures range from 1 MHz to between 4 and 5 MHz throughout the period. The preceding information was for the Coco Solo to New York path. The Thule to New York path was not as good; however, the data base is quite small over the Thule path.

During the period covered, the MOF's or JF's increased steadily with respect to the solar cycle and followed the usual variations as a function of time of year. One general item that has not been stressed previously is the fact that peak values during the summer and early fall tend to lag the midday by a much larger amount as the season progresses and as early fall begins. In the winter, on the other hand, the maximum JF's or MOF's effectively match the period covered by the sunlight hours.

During the lower values of the sunspot cycle, an almost perfect match occurred between predicted and measured 50 percent MOF or JF's, but as the sunspot cycle increased, the match with predictions has decreased slightly.

Data analysis of the mode reliability data has been computerized to a large extent, thus removing the burden of a large amount of manual calculations. The most pressing problem remaining is interpretation of the results of these calculations and the correlation of these with other geophysical data.

2. MODE LOSS EXPERIMENT

The measurement results for the mode loss experiment, covering the period from October 1965 to February 1967, and the analyses made using these results have been discussed in Section IV and in earlier reports on this program (references 2, 4, and 6). A summary of the more important conclusions drawn from these mode loss investigations is provided below.

1. For 2E propagation over the Coco Solo to Stockbridge path, the reference 17 loss predictions without the 8.4-dB factor agree well with the measured losses when the operating frequency is in the neighborhood of 0.9 of the 2E MOF.

When the operating frequency increases toward the MOF, as was the case during sunrise and sunset measurement periods at 11.3 MHz and around noontime at 16.6 MHz, the measured 2E ionospheric loss minus the estimated loss (which is the predicted loss using measured elevation angles) in decibels increases almost linearly with f/MOF for $f/\text{MOF} > 0.6$.

The empirical mathematical expression derived using four months of data measured during periods of low E_s activity, which predicts the additional or excess loss over the predicted propagation loss for the range $0.6 < f/\text{MUF} < 1.0$ is given by

$$AL_{2E} = 37.3(1.13 f/\text{MUF} - 1) \quad (\text{dB})$$

When this term is added to the reference 17 prediction equation (without the 8.4-dB factor) the resulting losses are in good agreement with the measured 2E propagation losses for both the 11.3- and 16.6-MHz measurements.

It is, therefore, believed that the predictions made using the reference 17 techniques without the 8.4-dB factor provide a good measure of the propagation losses for 2E propagation if the ratio f/MUF is in the neighborhood of 0.9. Above a value of 0.6 in addition to nondeviate absorption, another loss mechanism becomes important. This other loss mechanism may be due to a combination of deviative absorption, partial reflection, and divergence.

2. A statistical analysis of the 2E measured losses in "excess" of those predicted (using reference 17 without the 8.4-dB term or ground reflection loss) has clearly indicated that these additional propagation losses are a function of operating frequency. These results support the conclusion stated above that an additional factor is needed for use with the reference 17 equation which will account for the position of the operating frequency relative to the MOF of the 2E mode. For the F2-layer modes of propagation it appears that the effects of the lower layers must also be taken into consideration, perhaps by another function dependent on the lower layer MOF-JF and thickness/height factor in addition to a term which is a function of the F2 JF; hence, it is very likely that an improved loss prediction formula will consist of a linear combination of several independent functions, where the type of functions required for loss prediction will depend on the mode of propagation under consideration.
3. A comparison of the measured 2E MOF's and LOF's for the 1F2 and 2F2 modes was made using the data collected during May 1966 over the Coco Solo to Stockbridge path. The purpose of this investigation was to determine if the F2-layer mode LOF was primarily dependent on the value of the 2E MOF. The resulting data showed no decisive confirmation of the expected relationship between these two quantities; instead, it indicated that there are number of factors involved in determining the LOF's for F2-layer modes over a path of this length.
4. The main features of the difference or excess losses were presented on two different levels in Section III of reference 6. First, the highlights of the loss distributions by months were given; it was noticed that the monthly medians for the difference (excess) losses were not always identical and their variations usually betrayed no seasonal pattern. The random variations in the monthly median difference levels whenever these occurred can be

ascribed generally to one cause: the low number of samples that make up the distribution. When the monthly data are put together, the number of samples increases considerably and the objection of an insufficient sample size is effectively removed. Highlights of the loss distributions based on the data for all months constitute the second level of presentation.

Basing the arguments only on this firmer statistical ground, the overall conclusions about the mode median difference (excess) losses can be summarized as follows:

1. The median difference losses appear mode dependent.
2. The median difference losses appear frequency dependent; that is, well exemplified by the results for the 2E, 2E_g, and (to a lesser degree) the 2F2 modes.
3. The median difference losses appear day- and night-dependent; again, this is evident from the results for the 2E_g, N, and 2F2 modes.
4. The median difference losses appear high and low ray dependent. The difference is very significant for the 1F2 mode at all frequencies and for the 2F2 at 11.3 MHz.
5. The spread of the distributions is mode dependent. Here, it is noticed that the 1F2 deciles are almost twice those for the 2E and 2F2 modes. The deciles for the 2E and the N modes are also higher. A wider spread in the distribution implies that the desired signal level has to be obtained at a higher cost in terms of the transmitted power if a high percentage of reliability is to be maintained.
6. The median difference loss of the semi-empirical absorption loss formula (SEALF) is 8.4 dB based upon the interpretation used in reference 17. It is a constant that does not depend either on mode, frequency, or time of day. Since items 1 to 5 indicate that the observed median difference losses are dependent on these and other parameters, it is concluded that the SEALF should be modified to include these effects.

It should be noted that the best agreement between the 8.4 dB of the SEALF and the observed median difference loss occurs for the 2F2 mode and for the 1F2 mode at higher frequencies.

3. SPECTRUM EXPERIMENT

The results shown in Figure 204 for the Coco Solo to central New York path indicate that, on the average, the 2E mode one-way signal coherence time is about one second greater than that for either the 1F2 or 2F2 mode. The median value of the 2E one-way signal coherence time is between three and four seconds.

From the Thule to Starr Hill results depicted in Figure 207, it is obvious that the 2E mode signal coherence time is much greater than that for the 1F2 mode for this path. Although the data for these two modes are limited in quantity, it is apparent to date that the 2E mode propagation is on the order of four times more coherent than that for the 1F2 mode on this northern path. The median value of the signal coherence time for the 1F2 mode is approximately 0.5 seconds.

The data shown in Figure 208 indicate that the expected value of signal coherence for propagation via the 2E mode on a north-south auroral path is only about one second less than on an equal length north-south temperate path; thus, 2E mode signal coherence appears to be somewhat insensitive to path location.

4. AZIMUTH OF ARRIVAL EXPERIMENT

In view of the fact that actual data from the azimuth of arrival experiment only became available for a few days at the end of the program, while the AOA equipment was undergoing final testing, it was not felt advisable to draw any conclusions from the limited data collected.

5. NOISE/INTERFERENCE EXPERIMENT

a. Noise Measurements with ARN-2

Reviewing the data presented in Figures 226 through 229 for the measured atmospheric noise level (using a standard ARN-2 with a whip antenna) on a seasonal basis compared with the appropriate values contained in CCIR Report 322, it is apparent that for most time blocks the measured value is higher than the predicted value. This is also true, as would be expected, for the monthly atmospheric noise results presented in Figures 230 through 235 covering the months of March through August 1967. The winter results shown in Figure 226 were for the month of February 1967 only; likewise, Figure 229 contains the autumn data for the month of September 1967 only. It is believed that one reason for the apparent difference between the measured and predicted values is that the measured value includes both atmospheric and galactic noise, while the predicted values shown are for atmospheric noise only. Where this will have the most effect on the predicted level is at 20 MHz for all time blocks and for the overall predicted level for the 0800 to 1200 LMT and 1200 to 1600 LMT time blocks.

The results obtained when the second ARN-2 noise receiver is connected to the directional antennas located at the RADC Starr Hill Test Annex are shown in Figures 244, 245, and 246. These data are for the months of June, August, and September 1967. Also depicted in these figures are the corresponding monthly median results obtained from the standard ARN-2 noise measuring set. It must be remembered when examining these figures that the nominal frequency range for both horizontal arrays is 8 to 64 MHz, while the corresponding range for the vertical arrays is from 4 to 64 MHz; also, the directional ARN-2 measurements are taken at only three frequencies: 5, 10, and 20 MHz. The measurements made at 5 MHz using either horizontal array are thus subject to question and may be the reason for the decrease in atmospheric noise shown at 5 MHz for the horizontal antenna compared to those at 10 MHz using the same antennas.

From a study of Figures 244, 245, and 246 it can be seen that the lowest noise levels are generally recorded on the south vertical array. This is especially true for the September data depicted in Figure 246. A brief examination of the logs revealed no problem with the antenna preamplifiers during this month that would explain the lower levels recorded using the south vertical array.

b. Noise/Interference Measurements

The N/I distributions shown in Figures 248 through 251 indicate the difference that exists in the distributions as a function of the MUF. At the time that these measurements were taken (0010 GMT) the predicted median MUF (4000) F2 in a northerly direction from Starr Hill is 19 MHz and in a southerly direction is 28 MHz. No actual measurements of the JF over the Thule and Coco Solo Paths are available for this period, but based upon past experience on the mode reliability experiment (see references 4 and 6) the 1F2 MUF's and JF's have usually agreed quite closely.

Figure 248, which is the N/I distribution at 25 MHz (actually from 25.0 to 26.0 MHz); as measured using the north and south vertical antennas indicates that there are many 4-kHz channels at the noise level set by the natural environment or receiver noise figure; however, Figure 251 (which is the N/I distribution at 14 MHz taken a few minutes after the preceding one) shows that there are interfering signals in practically all the channels. This is indicated by the shape of the distribution which does not rise steeply from the natural-environment/noise-figure floor level. Also, the interference extends over about a 60-dB range.

The most obvious variation in the N/I level is that due to frequency and is illustrated by the results depicted in Figure 253. There was no essential difference between the results obtained on the two orthogonally polarized arrays pointed in a northern direction. The data obtained on the two vertical arrays located at Starr Hill are likewise very similar.

SECTION IX

ABBREVIATIONS AND SYMBOLS

A_{Fr}	- Fredericksburg Magnetic Observatory daily index of magnetic activity on a linear scale
AL_{2E}	- Additional 2E propagation loss above that predicted in decibels
b	- bandwidth in hertz
CCIR	- International Radio Consultative Committee
CRPL	- Central Radio Propagation Laboratory (now ITSA)
D_l	- value of the average noise power exceeded for 90 percent of the hours within a time block (dB below the median value for the time block)
D_u	- value of the average noise power exceeded for 10 percent of the hours within a time block (dB above the time block median)
dB	- decibel(s)
E_s	- sporadic E
ELIDA	- Expanded Little IDA
ESSA	- Environmental Science Services Administration
EST	- Eastern Standard Time
F_{am}	- Median of the hourly values of F_a (effective antenna noise-factor) within a time block in dB
f	- operating frequency
f_{oE}	- ordinary wave critical frequency of the E layer
FOT	- optimum working frequency
GMT	- Greenwich Mean Time
HF	- high frequency
Hz	- hertz
ITSA	- Institute for Telecommunication Sciences and Aeronomy
JF	- junction frequency
k	- Boltzmann's constant
K_{Fr}	- Fredericksburg Magnetic Observatory three-hour range magnetic index
K_p	- planetary three-hour range magnetic index

kHz	- kilohertz
km	- kilometer(s)
LOF	- lowest observed frequency
LUF	- lowest usable frequency
ms	- millisecond(s)
MHz	- megahertz
MOF	- maximum observed frequency
MUF	- maximum usable frequency
mV	- millivolts
NH	- north horizontal (antenna)
NV	- north vertical (antenna)
N/I	- noise/interference
NMD	- number of measurement days
nmi	- nautical mile(s)
OHD	- over-the-horizon detection
OHR	- over-the-horizon radar
P	- clear channel probability
pps	- pulses per second
prf	- pulse repetition frequency
RADC	- Rome Air Development Center
RF	- radio frequency
SEALF	- Semi-empirical absorption loss formula of reference 17
SH	- south horizontal (antenna)
SNR	- signal-to-noise ratio
SSN	- sunspot number
SV	- south vertical (antenna)
SWF	- shortwave fadeout
T₀	- reference temperature at 288° Kelvin
TCF	- time compression factor
TMT	- total measurement time
μs	- microsecond(s)
2F2L	- the two-hop F2 layer low ray
2F2H	- the two-hop F2 layer high ray

APPENDIX I

TRANSFORMATION OF PROBABILITY DENSITY FUNCTIONS FOR $Z = XY$

Given:

Statistically independent random variables x and y for which the probability density functions, $p_x(x)$ and $p_y(y)$, respectively, are known.

Find:

The probability density function $p_z(z)$ where z is related to x and y by

$$z = xy \quad (28)$$

x and y are gaussian distributed random variables with the following probability density functions

$$p_x(x) = \frac{1}{\sqrt{2\pi}\sigma_x} e^{-\frac{1}{2}\left[\frac{x-\bar{x}}{\sigma_x}\right]^2} \quad (29)$$

$$p_y(y) = \frac{1}{\sqrt{2\pi}\sigma_y} e^{-\frac{1}{2}\left[\frac{y-\bar{y}}{\sigma_y}\right]^2} \quad (30)$$

The probability density of z is given by*

$$p_z(z) = \int_{-\infty}^{\infty} \frac{1}{x} p_{xy}\left[x, \frac{z}{x}\right] dx \quad (31)$$

where

$p_{xy}(x, \frac{z}{x})$ is the joint probability density of x and y where $\frac{z}{x}$ has been substituted for y .

Since x and y are independent,

$$p_{xy}(x, y) = p_x(x) p_y(y) \quad (32)$$

*Papoulis, A., Probability, Random Variables, and Stochastic Processes, McGraw Hill, 1965, pp. 205.

therefore, by substituting $\frac{z}{x}$ for y

$$p_{xy}(x, \frac{z}{x}) = \frac{1}{2\pi \sigma_x \sigma_y} e^{-\frac{1}{2} \left[\frac{x - \bar{x}}{\sigma_x} \right]^2 - \frac{1}{2} \left[\frac{\frac{z}{x} - \bar{y}}{\sigma_y} \right]^2} \quad (33)$$

finally

$$p_z(z) = \frac{1}{2\pi \sigma_x \sigma_y} \int_{-\infty}^{\infty} \frac{1}{x} e^{-\frac{1}{2} \left[\frac{x - \bar{x}}{\sigma_x} \right]^2 - \frac{1}{2} \left[\frac{\frac{z}{x} - \bar{y}}{\sigma_y} \right]^2} dx \quad (34)$$

Equation (34) can be integrated by numerical techniques. Computer programs for doing this exist and details of such computations are discussed in Appendix II.

APPENDIX II

COMPUTATION OF PROBABILITY CONVOLUTIONS

1. MATHEMATICAL DESCRIPTION

Assume a function of the form

$$z = f(w, x, y)$$

where w , x , and y are random variables. The cumulative probability, $P(z \leq Z)$, which is the probability of the variable z being less than some specified value Z , may be expressed in terms of the joint probability density function of w , x , and y as

$$P(z \leq Z) = \iiint p(w, x, y) dw dx dy$$

where $z = f(w, x, y) \leq Z$

The above expression, a definition, states that this cumulative probability is equal to the joint cumulative probability of w , x , and y lying in ranges such that $z \leq Z$ when they are substituted into the functional relationship $f(w, x, y)$.

The above expression is the foundation for the computation of probability convolutions and will now be manipulated into a more tractable form to illustrate a useful computational approach. First assume the variables are independent so that the joint probability density is equal to the product of the individual probability densities. Then

$$P(z \leq Z) = \iiint p(w) p(x) p(y) dw dx dy$$

This may now be put into a form amenable to digital computer computation. The three probability densities above are continuous functions. The integrations may be carried out in a piecewise fashion and then summed. These piecewise integrations of probability densities are true probabilities of a variable lying within a specified increment. Representing the increment by its mean value

$$P(z \leq Z) = \sum_{i=1}^I \sum_{j=1}^J \sum_{k=1}^K P(w_i) P(x_j) P(y_k)$$

where $f(w, x, y) \leq Z$

Here the variable w is divided into I increments, each increment being represented by its mean, w_i . Similar descriptions apply to x and y .

The significance and implementation of the above expression can now be offered. It should be possible to divide each of the three distributions w , x , y into a number of values, each of which can be expected to occur with a specific probability. It is recognized that the product

$$P(w_i) P(x_j) P(y_k)$$

in the expression above is the probability of a specific combination of w_i , x_j , and y_k values. Then the above expression merely states that the cumulative probability of z being less than a specific value Z is equal to the sum of the probabilities of all combinations of w_i , x_j , and y_k which produce values of z which do not exceed Z . The extension of the above concepts to implementation is obvious. It is merely necessary to compute the function z for each combination of w_i , x_j , and y_k , along with the probability of each combination, order in ascending order of z , and accumulate the probabilities.

2. PRACTICAL DIFFICULTIES AND THEIR SOLUTION

The following computational difficulties arise if the above procedure is followed exactly:

1. The distributions for some variables are extremely nonuniform and the number of samples required to adequately represent the data can become large, and
2. The amount of data to be sorted increases exponentially with the number of variables, resulting in storage limitation problems.

These problems can be alleviated in the following manner. The difficulty with distributions that have extremely long tails can be overcome by using equiprobable values for the independent variable. This is especially suited for continuous variables, but can be used for discrete variables if necessary. This approach is shown in Figure 263. Only 10 sample points were taken here, resulting in appreciable quantization errors. But 20 sample points lead to very practical results. If for some reason there is considerable interest in the extreme values there is no reason why smaller intervals should be avoided in one area; for example, if probability of detection is being investigated and extremely high values are of interest, a set of 14 values could be used which occur at cumulative probabilities of 5(10)85; 91(2)99. With discrete distributions, if the number of discrete values is reasonably small (less than 20), the actual values

should probably be used. With a greater number of values it might be best to approximate by a continuous function and use equiprobable values, or to form groups of discrete values so that the group have almost equal probabilities and then represent the group by the group mean.

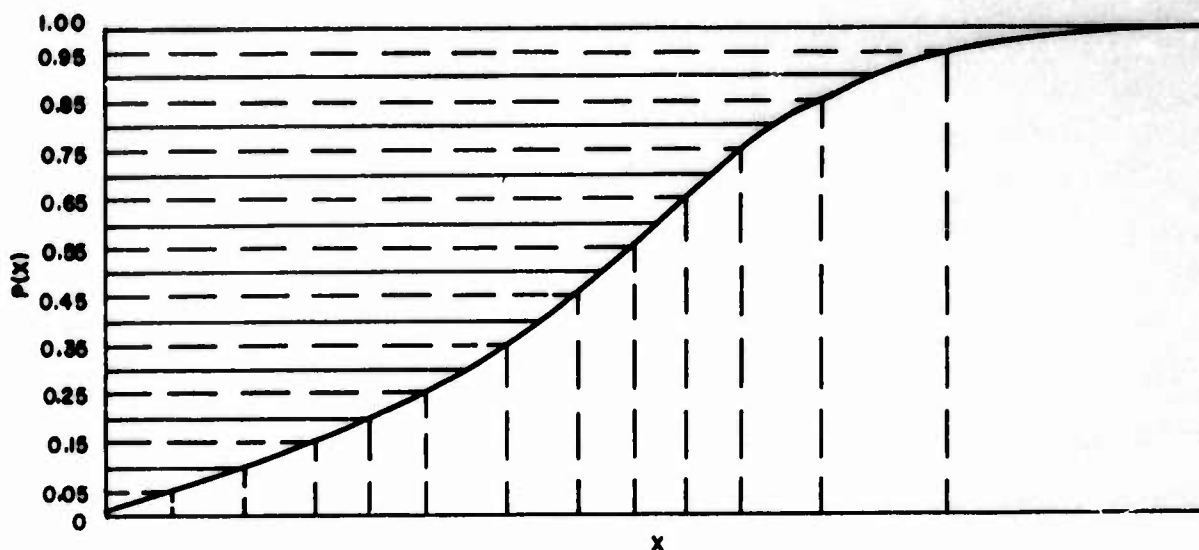


Figure 263. Equiprobable Value Approximation to Continuous Distribution

The difficulty with large quantities of data can be minimized by representative sampling; for example, if 20 values are used for each of three variables, there would be 8000 points at which to evaluate the dependent variable and which would have to be sorted. Specifically considering $z(w, x, y)$, the 8000 points are

$$z_{ijk} = z(w_i, x_j, y_k) \text{ for } 1 \leq i, j, k, \leq 20$$

To reduce the sorting process the following can be done. Compute the 400 points $z(w_1, x_j, y_k)$ and their respective probabilities. Sort and calculate the cumulative probabilities. Select 20 representative values to typify the data for $w = w_1$. This process is now repeated for each value of w . The resulting 20 representative values for each of the 20 values of w can be merged and sorted and, if desired, again represented by 20 typical values. This simplification involves 21 sorts on sets of 400 values rather than one sort of 8000. For four independent variables the reduction is from one

sort of 160,000 to 43 sorts of 400 values. This is the same philosophy used in standard sort and merge programs. The specific advantage achieved here is to keep the storage requirements to a reasonable limit. In addition, by having the output representation in the same form as the input, standard subroutines can be built up to handle complex cases.



APPENDIX III

NUMERICAL CALCULATION OF CONFIDENCE LIMITS

The Tchebysheff inequality as used in Equation (21) is of the form

$$P \left[|\hat{Z} - Z| \geq \epsilon \right] \leq \frac{1}{N\epsilon^2} \left\{ [1+x] y [1-y] + y x [1-x] \right\} \quad (35)$$

where

$$Z = P(\text{usable mode}); \hat{Z} = \hat{P}(\text{usable mode})$$

$$x = \hat{P}(\text{SNR} < M)$$

$$y = P(x \text{ exists})$$

Since x , y , and z represent probabilities, they can have values from 0 to 1. Before actual confidence limits can be calculated, values for x and y are required; however, if values for these two quantities are chosen, then some idea of the confidence limit that can be achieved will be available. In order to present a worst case type of example, the term which forms the upper bound on the confidence limit will be maximized; thus, it is desired to maximize

$$\omega = (1+x) y (1-y) + y x (1-x) \quad (36)$$

N and ϵ are not included in the function to be maximized because they are independent of x and y .

In order to maximize ω , the conditions are (Ref. 16)

$$\frac{\partial \omega}{\partial x} = \frac{\partial \omega}{\partial y} = 0 \text{ at point P} \quad (37)$$

and

$$\frac{\partial^2 \omega}{\partial x^2} < 0, \quad \frac{\partial^2 \omega}{\partial x^2} \frac{\partial^2 \omega}{\partial y^2} > \frac{\partial^2 \omega}{\partial x y} \text{ at P} \quad (38)$$

The necessary derivatives are

$$\begin{aligned}\frac{\partial \omega}{\partial x} &= y(1-y) + y(1-x-x) \\ &= y(2-y-2x)\end{aligned}\quad (39)$$

$$\begin{aligned}\frac{\partial \omega}{\partial y} &= (1+x)(1-y-y) + x(1-x) \\ &= (1+x)(1-2y) + x(1-x)\end{aligned}\quad (40)$$

$$\frac{\partial^2 \omega}{\partial x^2} = -2y \quad (41)$$

$$\frac{\partial^2 \omega}{\partial y^2} = -2(1+x) \quad (42)$$

$$\begin{aligned}\frac{\partial^2 \omega}{\partial x \partial y} &= 2-y-2x-y \\ &= 2(1-y-x)\end{aligned}\quad (43)$$

Equation (37) requires that

$$y = 2 - 2x \text{ from Equation (39)}$$

and

$$y = \frac{1 + 2x - x^2}{2 + 2x} \text{ from Equation (40)}$$

Simultaneous solution of the above yields

$$3x^2 + 2x - 3 = 0$$

or

$$x = 0.723, -1.39$$

The solution $x = -1.39$ is disregarded for it lies outside the range 0 to 1. The value of y corresponding to $x = 0.723$ is

$$y = 2 - 2(0.723) = 0.554$$

Thus, the point P is (0.723, 0.554).

In order to check Equation (38)

$$\left. \frac{\partial^2 \omega}{\partial x^2} \right|_P = -2y = -1.108 < 0$$

$$\left. \frac{\partial^2 \omega}{\partial x^2} \right|_P \left. \frac{\partial^2 \omega}{\partial y^2} \right|_P > \left. \frac{\partial^2 \omega}{\partial x \partial y} \right|_P$$

$$-1.108 [-2 (1.723)] > 2 (1 - 0.554 - 0.723)$$

$$3.82 > -0.554 \text{ which checks.}$$

Therefore, P = (0.723, 0.554) is indeed a maximum for ω . ω_{\max} , then, is

$$\omega_{\max} = \omega|_P =$$

$$(1.723) (0.554) (0.446) + (0.554) (0.723) (0.277)$$

$$= 0.537$$

(44)

The worst-case confidence interval becomes

$$P \left[\left| \hat{P} (\text{usable mode}) - P (\text{usable mode}) \right| \geq \epsilon \right]$$

$$\leq \frac{0.537}{N \epsilon^2}$$

(45)

The expression given in Equation (45) can be used to obtain an upper bound confidence limit on the estimate of P (usable mode; e.g., if the estimate is to be within 0.1 of the true value, then $\epsilon = 0.1$, and

$$\frac{0.537}{N \epsilon^2} = \frac{53.7}{N}$$

If N = 100, the probability that the estimate differs from the true value by more than 0.1 is 53.7 percent. For N = 1000 the probability is 5.37 percent. Various ϵ 's and N's can be used as indicated.

APPENDIX IV

COCO SOLO LPV ANTENNA PATTERNS

The 4- to 32-MHz antenna curtain that was employed at the beginning of the Expanded Little IDA program at the site in Coco Solo was replaced by a new, longer, logarithmically-periodic vertical dipole array with a frequency range of 4 to 64 MHz. The antenna installation was completed in August 1966 and its patterns were then measured by a team of RADC and General Electric personnel. The measurement antenna which is a model LPV 12-A array manufactured by AL-Products Company is of wire and dielectric-support construction, suspended between a rear tower and a front pole. The lower ends of the elements are attached to a cable catenary several inches above the level of the earth. The entire site is a swampy area about one foot above sea level. A tide range of only about nine inches exists, so flooding is normally not a problem. The VSWR of the antenna has been measured to be under 2 : 1 between 4 and 64 MHz.

An extensive measurement program was conducted to determine the gain of the new LPV array as a function of frequency and bearing. Eight measurement frequencies were selected that covered the expected frequency range to be employed for the mode loss and azimuth of arrival experiments: 8 to 30 MHz. These numbers were derived considering expected propagation conditions and frequency limitations imposed by the Phantom equipment and the horizontally polarized antenna at the RADC Starr Hill Test Annex.

Shown in Table XLVI are the actual antenna pattern measurement frequencies that were employed for these tests at the Coco Solo site. Listed also are the losses that were measured for the transmission line and balun that provide the link between the transmitter located in the operations room at the Coco Solo site and the actual LPV array.

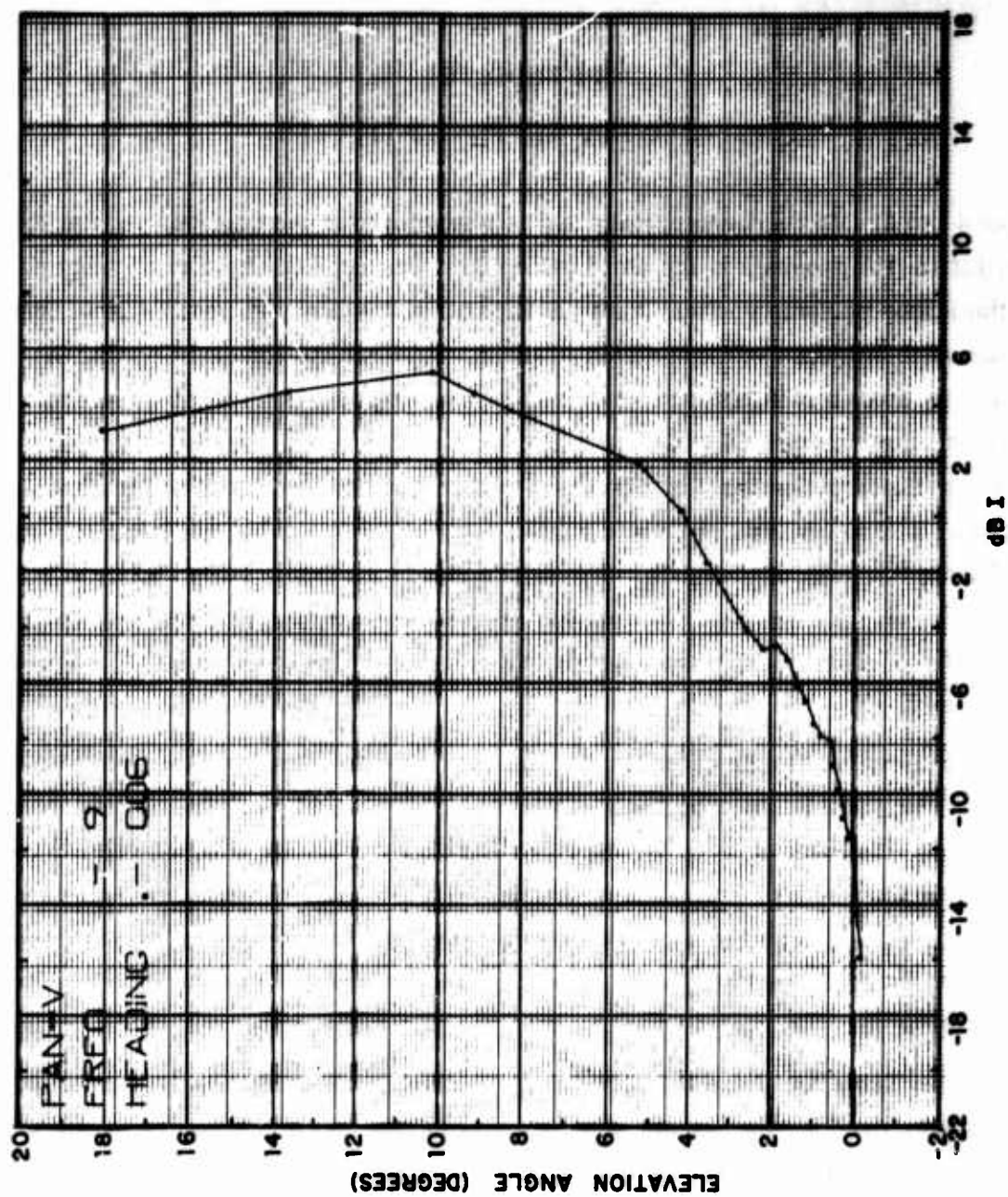


Figure 264. LPV Antenna Gain Pattern, 9.104 MHz

TABLE XLVI**COCO SOLO LPV MEASUREMENTS**

Measured Frequency (MHz)	Transmission Line Loss (dB)
9.104	2.3
11.399	2.7
13.989	3.0
16.459	3.2
19.0	3.4
22.0	3.8
26.1	4.1
30.0	4.3

The resulting on boresight antenna power gain patterns with respect to an isotropic antenna in free space for the new Coco Solo LPV array are shown in Figures 264 through 270. The gain patterns shown for 11.399, 16.459, and 22.0 MHz were used to obtain the mode loss results reported in reference 6 for the months of September 1966 through February 1967.

It should be pointed out that a very consistent increase in gain as a function of bearing was observed at most frequencies due to the effects of the local surroundings at the Coco Solo site. This statement is based on measurements which were made at $\pm 5^\circ$ and $\pm 10^\circ$ off boresight, with the maximum gain at a bearing of 356° with respect to north. The bearing to Starr Hill from Coco Solo is approximately 6° .

For reference, the antenna pattern gains employed for the Stockbridge receiving antenna (at the three measurement frequencies: 11.3, 16.0, and 22.3 MHz) to determine the mode loss results are shown in Figure 271, 272, and 273. Shown also in these figures are the interpolated and extrapolated values for the power gain patterns of the previous LPV array located at Coco Solo. The combined transmitting and receiving antenna power gains used for the mode loss data collected before September 1966 on the Expanded Little IDA program are also shown in these figures.

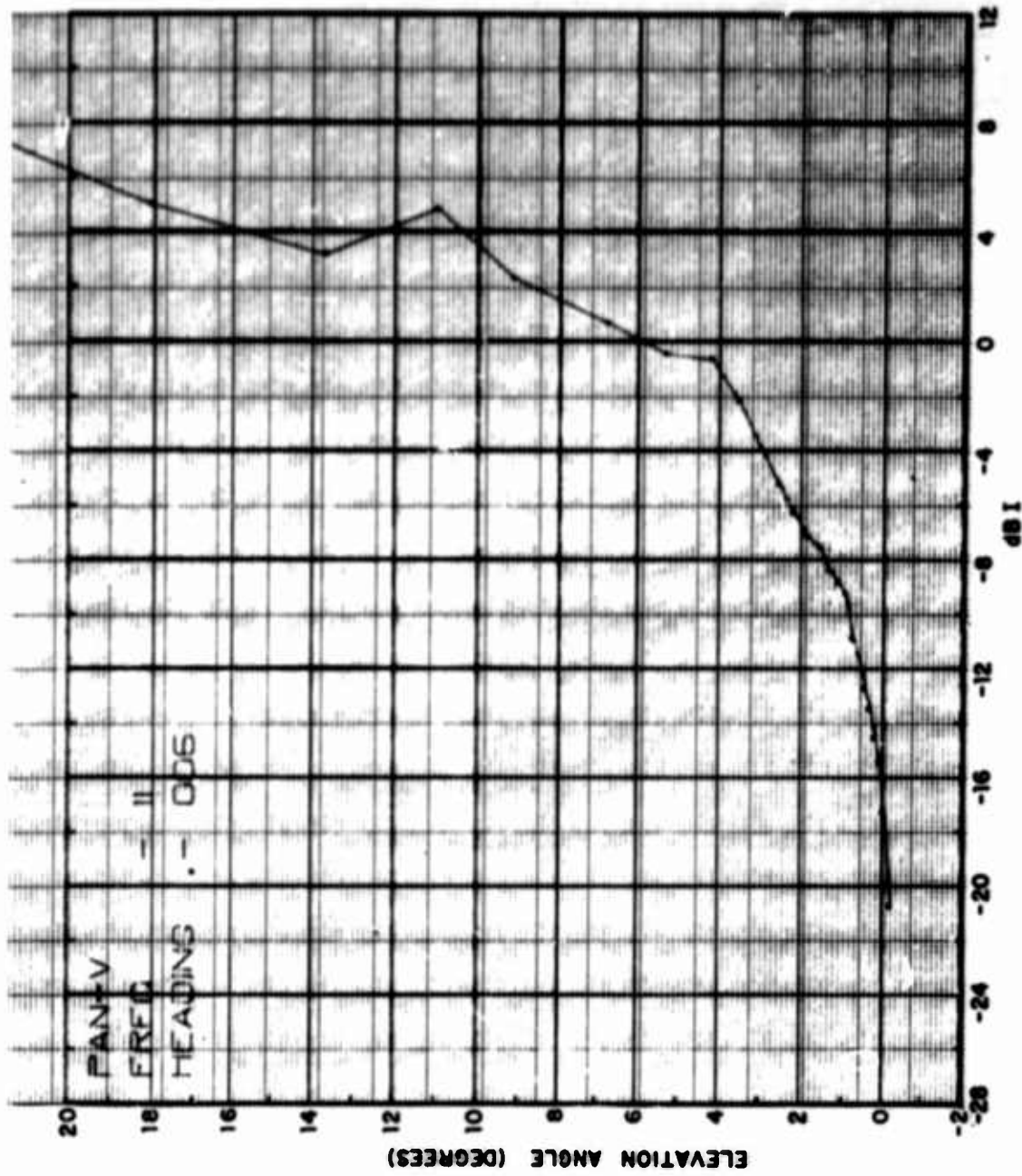


Figure 265. LPV Antenna Gain Pattern, 11.399 MHz

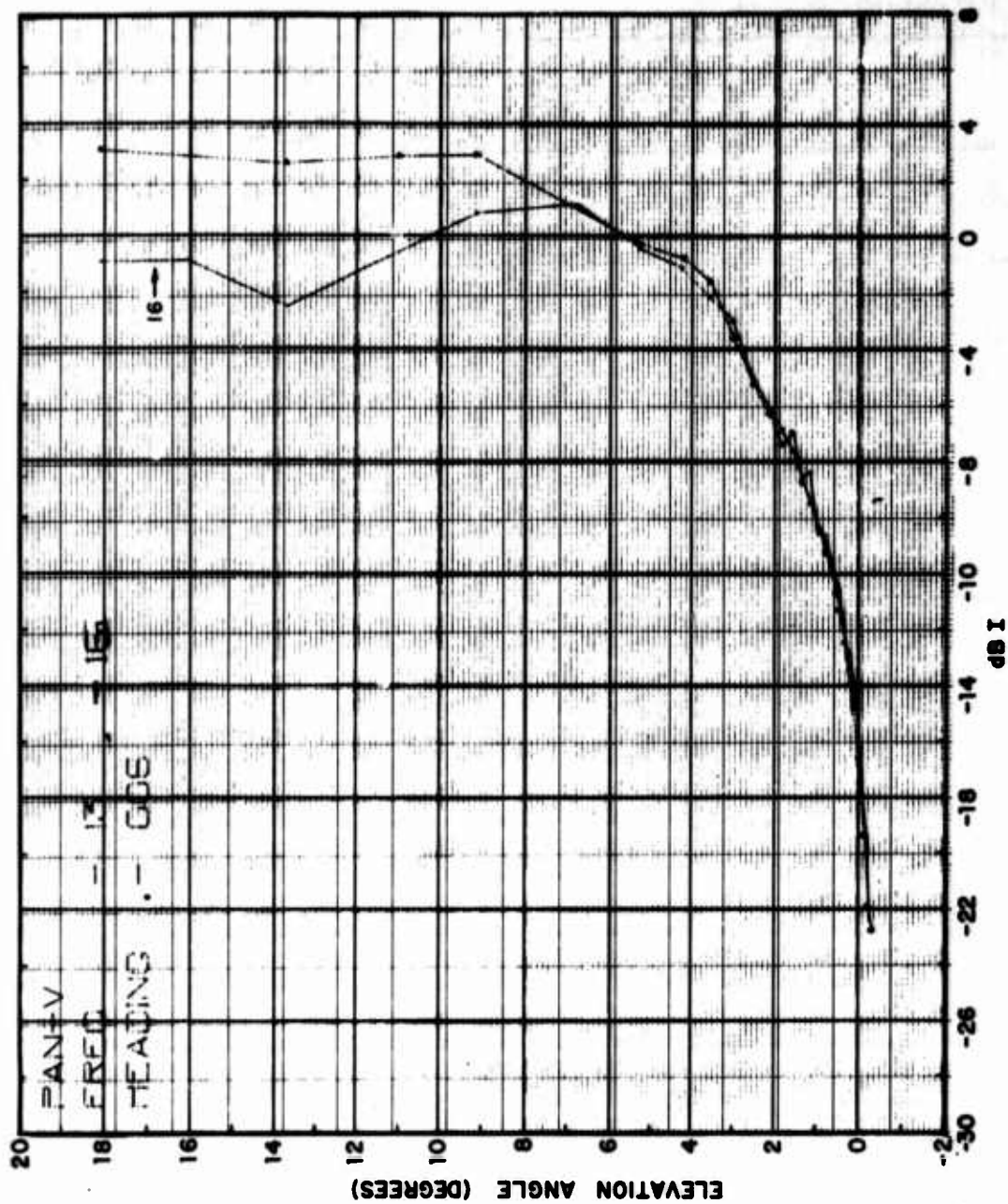


Figure 266. LPV Antenna Gain Pattern, 13.989 and 16.459 MHz

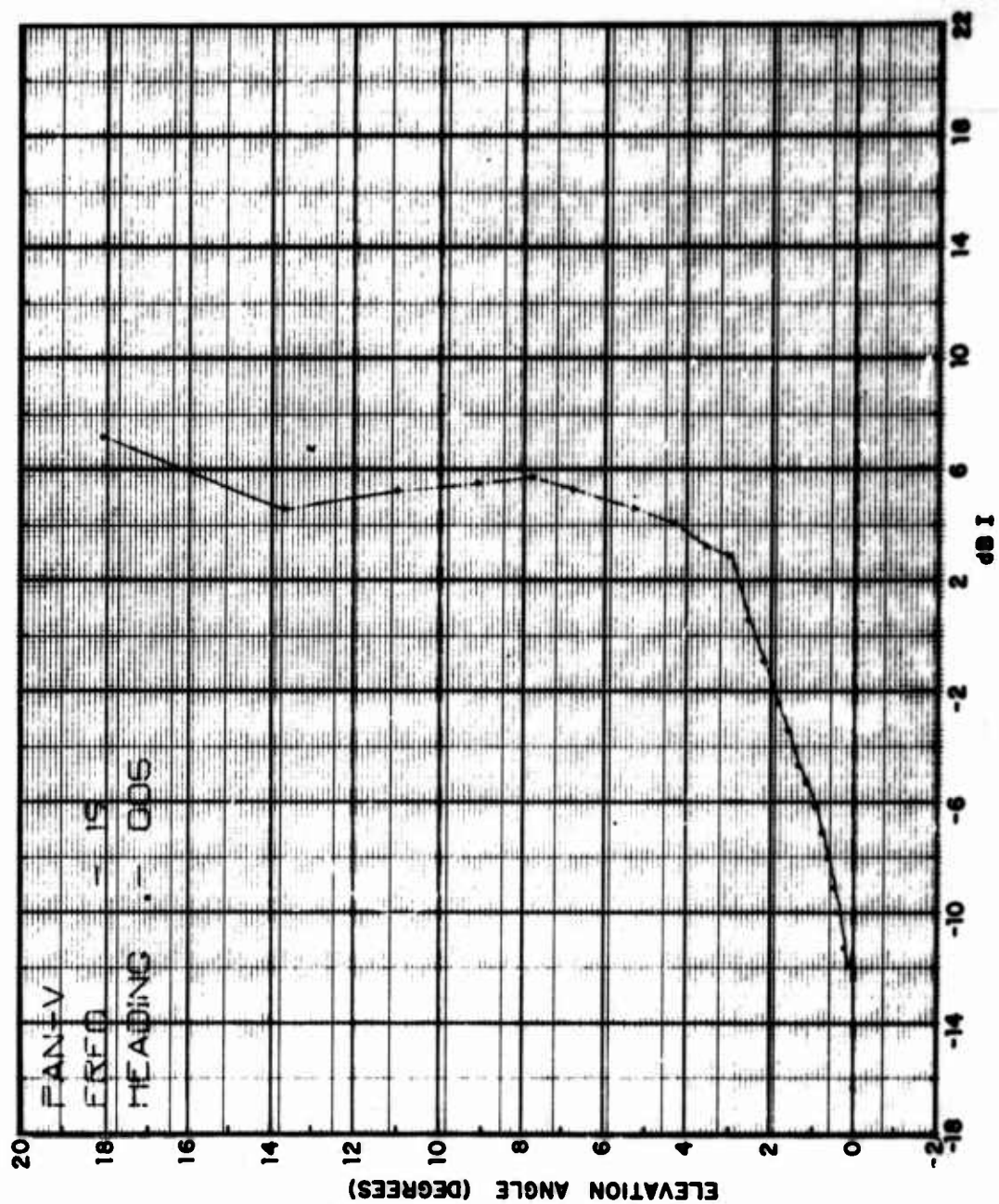


Figure 267. LPV Antenna Gain Pattern, 19 MHz

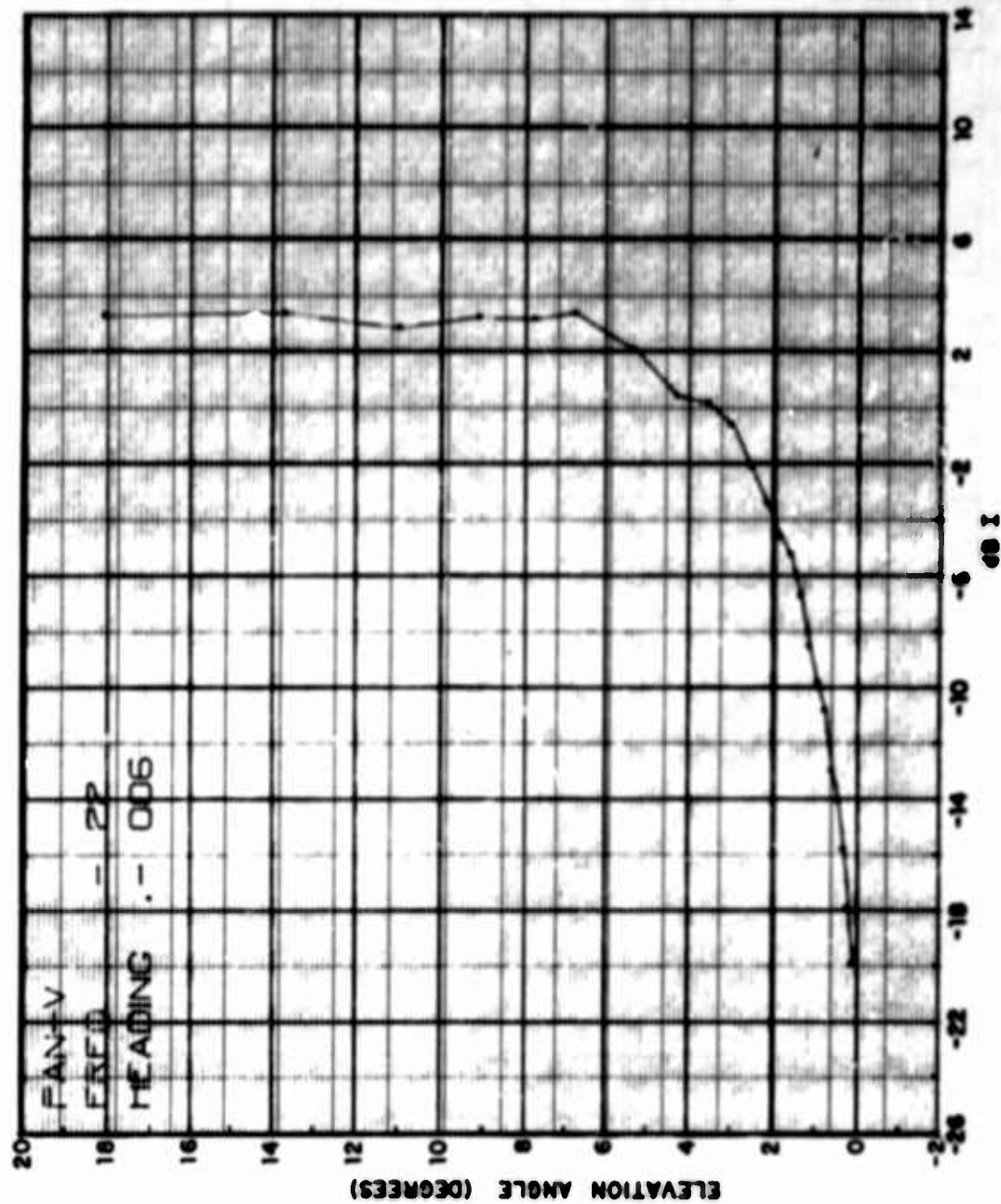


Figure 268. LPV Antenna Gain Pattern, 22 MHz

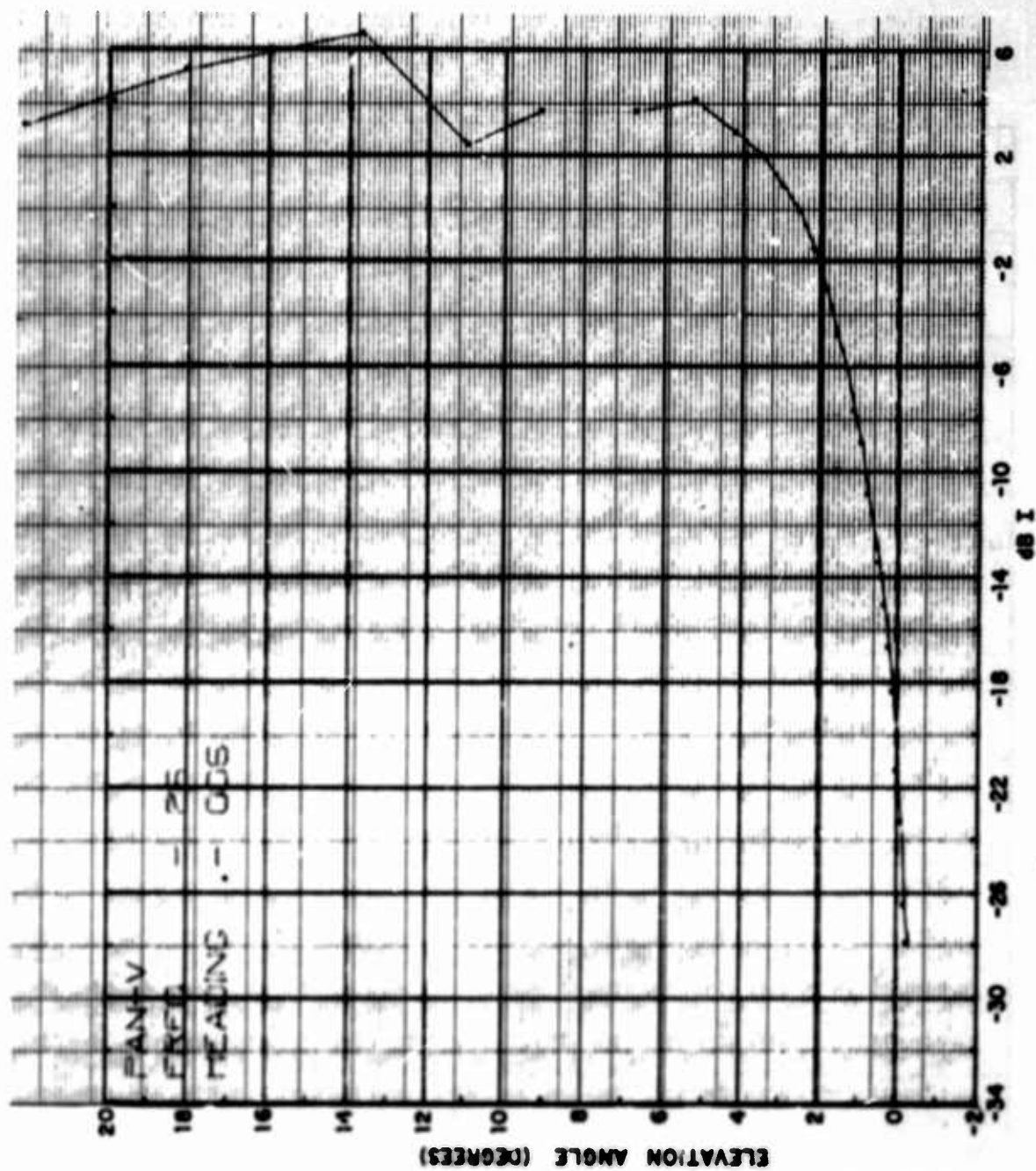


Figure 269. LPV Antenna Gain Pattern, 26.1 MHz

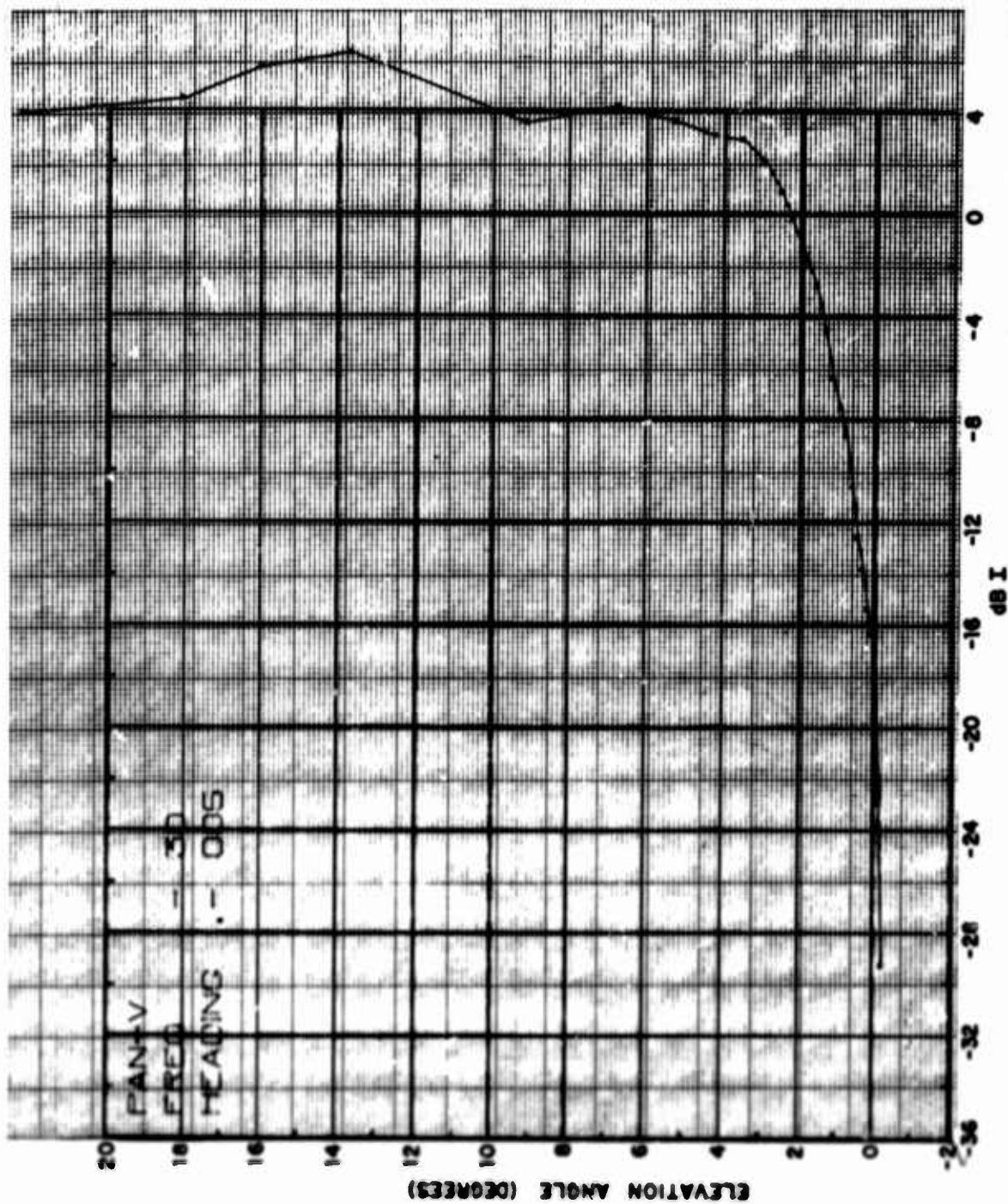


Figure 270. LPV Antenna Gain Pattern, 30 MHz

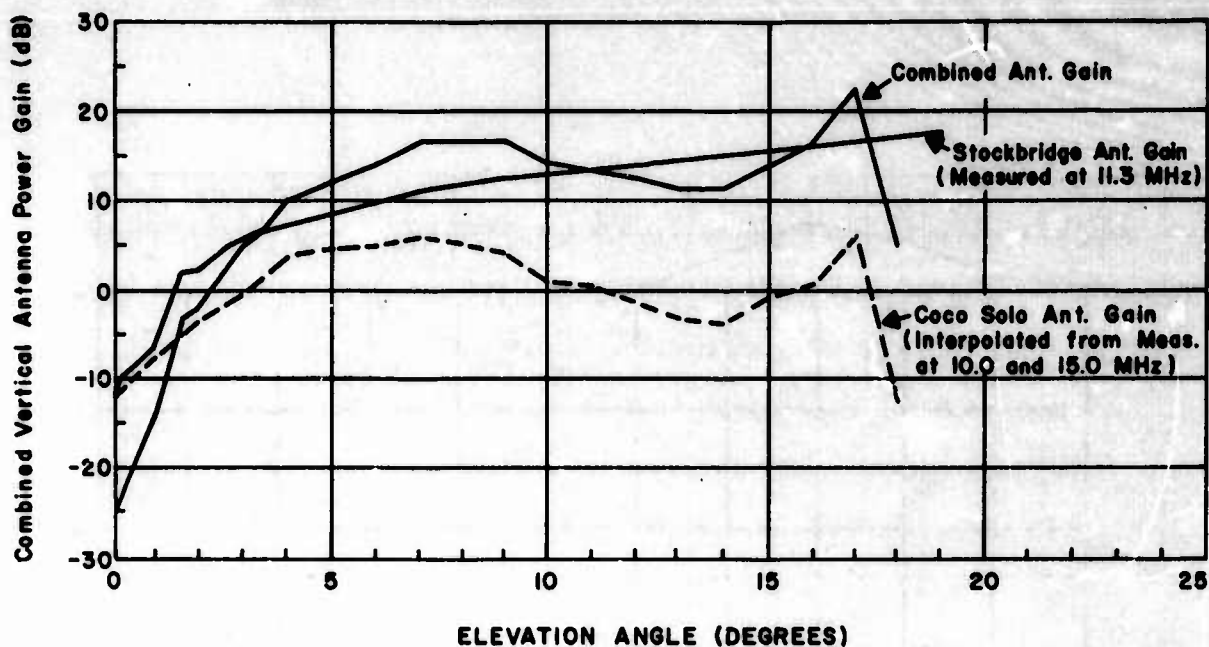


Figure 271. Combined Antenna Patterns for Mode Loss Experiment at 11.3 MHz.

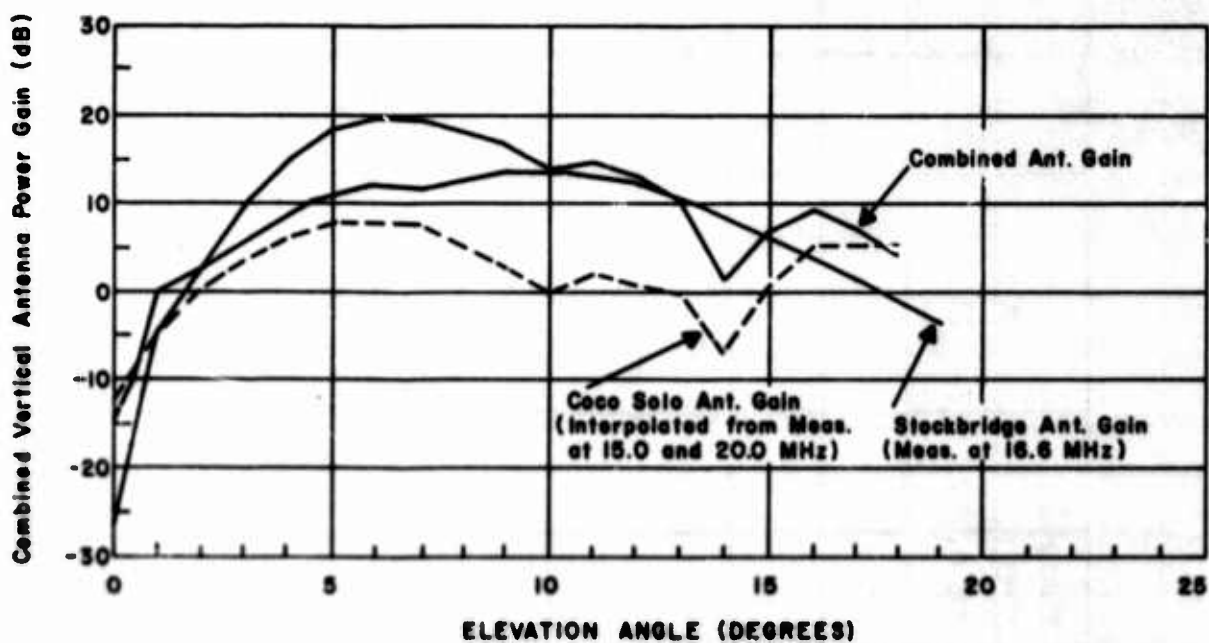


Figure 272. Combined Antenna Patterns for Mode Loss Experiment at 16.6 MHz

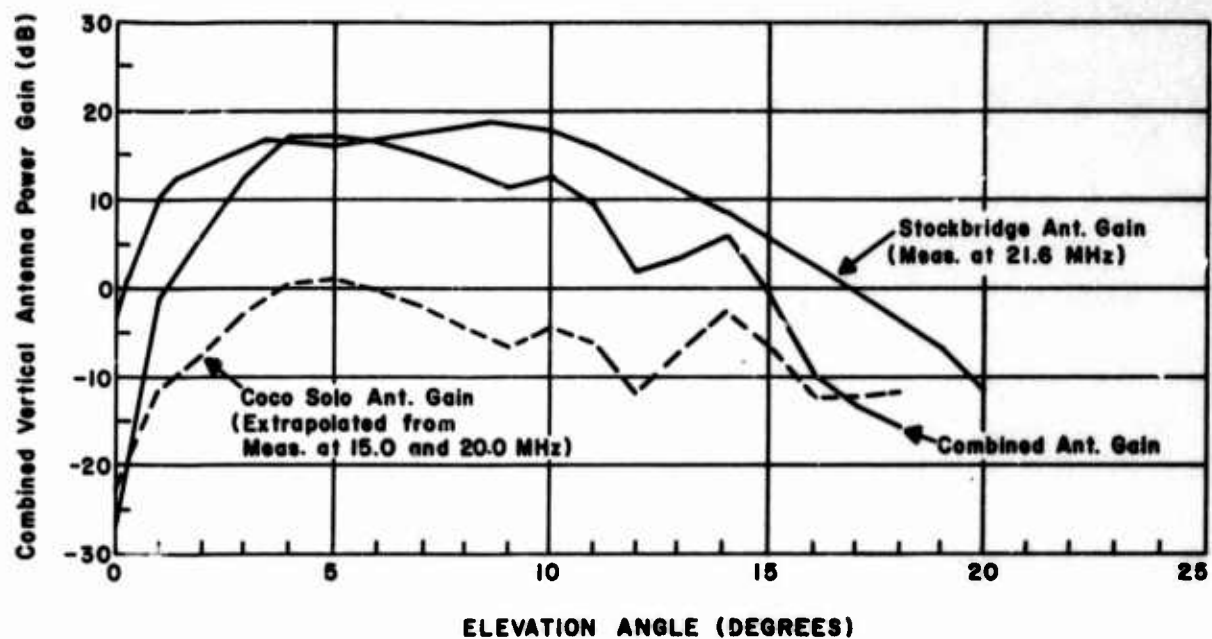


Figure 273. Combined Antenna Patterns for Mode Loss Experiment at 22.3 MHz.

APPENDIX V

GEOGRAPHICAL DATA ON ELIDA FIELD SITES

Geographical information on the transmitting and receiving sites employed on the Expanded Little IDA program is given in Table XLVII. Also listed are the calculated great circle ground distances and bearings between the remote transmitting sites and the central receiving sites for the paths of interest. These were determined employing a computer program (EEE02--Loran-C Baseline and Azimuth Computation Using the Sodano Fifth Method) developed by personnel of the United States Coast Guard to aid in their analysis of Loran-C operation. To obtain the results shown in Table XLVII, the Clarke (1866) spheroid was employed which has gained wide acceptance as a model for the northern Western Hemisphere.

TABLE XLVII

GEOGRAPHICAL INFORMATION ON THE EXPANDED LITTLE IDA FIELD SITES*

	North Latitude	West Longitude
Starr Hill	43° 20' 43"	75° 15' 3"
Coco Solo	9° 21' 45"	79° 53' 45"
Thule	76° 24' 15"	68° 44' 34"
Keflavik	63° 57' 31.3"	22° 43' 29.1"
Stockbridge	43° 01' 57"	75° 39' 05"

From Starr Hill to	Bearing	Distance		
		km	nmi	smi
Coco Solo	188° 11' 0" (6° 1' 53")	3792.43	2047.75	2356.50
Thule	2° 47' 52" (188° 40' 15")	3695.59	1995.46	2296.33
Keflavik	36° 36' 8" (260° 35' 48")	3991.93	2155.47	2480.46

*These calculations for distance and bearing are based upon the Clarke (1866) spheroid.

TABLE XLVII (concluded)

From Stock- bridge to	Bearing	Distance		
		km	nmi	smi
Coco Solo	187° 32' 30" (5° 35' 17")	3753.56	2026.76	2332.35
Thule	2° 56' 37" (189° 10' 24")	3731.92	2015.08	2318.90

REFERENCES AND BIBLIOGRAPHY

A. REFERENCES

1. RADC-TR-66-309, Expanded Little IDA Program - Instrumentation, Interim Report No. 1, General Electric Company, HMED, Syracuse, New York, August 1966. AD #803283
2. RADC-TR-66-492, Expanded Little IDA Program, Experimental Program and Results, Interim Report No. 2, General Electric Company, HMED, Syracuse, New York, September 1966. AD #800284
3. RADC-TR-66-719, Expanded Little IDA Program - Instrumentation, Interim Report No. 3, General Electric Company, HMED, Syracuse, New York. AD #812269
4. RADC-TR-67-75, Expanded Little IDA, Experimental Program and Results, Interim Report No. 4, General Electric Company, HMED, Syracuse, New York, January 1967. AD #813993L
5. RADC-TR-67-502, Expanded Little IDA, Instrumentation, Interim Report No. 5, General Electric Company, HMED, Syracuse, New York, July 1967. AD #822008
6. RADC-TR-67-618, Expanded Little IDA, Experimental Results, Interim Report No. 6, General Electric Company, HMED, Syracuse, New York, October 1967.
7. RADC-TR-68- , Expanded Little IDA, Instrumentation, Final Report, General Electric Company, HMED, Syracuse, New York, January 1968.
8. CCIR, Documents of the Xth Plenary Assembly, World Distribution and Characteristics of Atmospheric Radio Noise, Report 322, Geneva, New York, 1963.
9. Davenport and Root, Random Signals and Noise, McGraw Hill, 1958.
10. Lindgren and McElrath, Introduction to Probability and Statistics, MacMillan, New York, 1959.
11. Ostrow, S.M., Handbook for CRPL Ionospheric Predictions Based on Numerical Methods of Mapping, NBS Handbook 90, December 21, 1962.

12. Reeve, J.A., OTH Radar System Synthesis on the Expanded Little IDA Program with Some Current Results on Signal Processing Gain Obtainable Using Coherent Integration, paper presented at 673A Technical Review Meeting, RADC, 13 September 1967.
13. Bauer, L., Comparison of Processor Gain Performance For the Detection of Signals from Correlated Phase Coherent Diversity Channels, Technical Information Series Report R65EMH27, General Electric Company, Syracuse, New York, August 1965.
14. Marcum, J.I., "A Statistical Theory of Target Detection by Pulsed Radar", Mathematical Appendix, Trans. IRE, Vol IT-6, pp. 145-267, April 1960.
15. Nelson, G.R., Measurements of the "One-Way" Spectrum of a One-Hop Propagated HF Signal, an unclassified paper published in the Over-the-Horizon-Radar Proceedings of June 1966, Sponsored by the Advanced Research Projects Agency.
16. Hildebrand, F., Advanced Calculus For Applications, Prentice-Hall, Inc., 1965, p. 351.
17. Laitinin, P.O., and Haydon, G.W., Analysis and Predictions of Sky-Wave Field Intensities in the High Frequency Band, U.S. Army Signal Radio Propagation Agency, Technical Report No. 9, Revised October 1962.

B. BIBLIOGRAPHY

1. Aarons, J., Radio Astronomical and Satellite Studies of the Atmosphere; Jules Aarons, pp. 535-8; North Holland Publishing Company; 1963.
2. Balser, M., and Smith, W.B., "Some Statistical Properties of Pulsed Oblique HF Ionospheric Transmissions", Journal of Research of NBS-D Radio Propagation, 66D, #6, pp. 721-730, November-December, 1962
3. Condon, E.U., and Odishow, H., Handbook of Physics, "Elements of Probability", Eisenhart, C. and Zelin, M., pg. 1-151, McGraw Hill, 1958.

4. Crichlow, W.Q., Spaulding, A.D., Roubique, C.J., and Disney, R.T., Amplitude Probability Distributions for Atmospheric Radio Noise, National Bureau of Standards Monograph 23, Issued November 4, 1960.
5. Davies, K., Ionospheric Radio Propagation, National Bureau of Standards Monograph 80, 1965.
6. HF2 and HF charts, Canadian Ionospheric Data from Resolute, Churchill, Kemora, St. Johns, and Ottawa, Telecommunications and Electronics Branch, Department of Transport
7. Ionospheric Predictions, Environmental Science Services Administration (ESSA), Supt. of Documents, U.S. Govt. Printing Office, Washington, D.C. 20402
8. Journal of Geophysical Research, Geomagnetic and Solar Data, (K_p , K_{fr} , $ProV$, Rz)
9. Lucas, D.L., and Haydon, G.W., Predicting Statistical Performance Indexes for High Frequency Ionospheric Telecommunication Systems, ESSA Technical Report IER 1-ITSA 1, ITSA, Boulder, Colorado, August 1966.
10. Nelson, G.R., Measurements of the "One-Way" Spectrum Of A One-Hop Propagated HF Signal, an unclassified paper published in the Over-The-Horizon-Radar Proceedings, Sponsored by the Advanced Research Projects Agency, June 1966.

UNCLASSIFIED

Security Classification

DOCUMENT CONTROL DATA - R & D

(Security classification of title, body of abstract and indexing annotation must be entered when the overall report is classified)

1. ORIGINATING ACTIVITY (Corporate author) General Electric Company Heavy Military Electronics Division Syracuse, New York 13206		2a. REPORT SECURITY CLASSIFICATION UNCLASSIFIED	
		2b. GROUP N/A	
3. REPORT TITLE EXPANDED LITTLE IDA - EXPERIMENTAL RESULTS			
4. DESCRIPTIVE NOTES (Type of report and inclusive dates) Final Report			
5. AUTHOR(S) (First name, middle initial, last name) R.W. Swanson T.C. Matsumoto D.T. Olmsted			
6. REPORT DATE August 1968	7a. TOTAL NO. OF PAGES 422	7b. NO. OF REFS 17	
8a. CONTRACT OR GRANT NO. AF 30(602)-3946	9a. ORIGINATOR'S REPORT NUMBER(S)		
b. PROJECT NO. 5582			
c. Task 558202	9b. OTHER REPORT NO(S) (Any other numbers that may be assigned this report) RADC-TR-68-180		
d.			
10. DISTRIBUTION STATEMENT Each transmittal of this document outside the Department of Defense must have prior approval of RADC (EMASA), GAFB, NY 13440.			
11. SUPPLEMENTARY NOTES		12. SPONSORING MILITARY ACTIVITY Rome Air Development Center (EMASA) Griffiss Air Force Base, New York 13440	
13. ABSTRACT This report discusses the effort performed on Contract AF 30(602)-3946 in the areas of data collection, reduction, and analysis involving five major HF propagation experiments. These experiments were concerned with determining HF propagation mode reliability, mode loss, azimuth of arrival and spectrum characteristics of individual modes. In addition a noise/interference measurement experiment was performed. Under this effort three propagation circuits were instrumented with transmitting terminals located at Thule, Greenland; Keflavik, Iceland; and Coco Solo, Panama and central receiving sites situated at the Stockbridge/Starr Hill Test Annexes, Griffiss Air Force Base, New York. Experimental results discussed herein are primarily based on data collection over the Coco Solo, Panama to central New York path. A limited amount of data collected over the Thule path are discussed. Delays encountered in both instrumentation and site acquisition resulted in achieving only a small data sample over the Thule path and no data sample over the Iceland path.			

DD FORM 1 NOV 65 1473

UNCLASSIFIED

Security Classification

UNCLASSIFIED

Security Classification

14.	KEY WORDS	LINK A		LINK B		LINK C	
		ROLE	WT	ROLE	WT	ROLE	WT
	HF Propagation Ionosphere Absorption Polarization Spectrum Noise/Interference						

UNCLASSIFIED

Security Classification